

Synthesis and Characterisation of New Schiff Base Chelates of Platinum Group Metals

Submitted in fulfilment of the requirements for the degree of

DOCTOR OF PHILOSOPHY

By

Rosanne C. Salmond

BSc. (MSc.) (UKZN)

September 2011

School of Chemistry
University of KwaZulu-Natal
Pietermaritzburg

Declaration

I hereby certify that this research is as a result of my own investigations which has not already been accepted in substance for any degree and is not submitted in candidature for any other degree.

Signed.....

Rosanne C. Salmond

I hereby certify that this statement is correct.

Signed.....

Professor O. Q. Munro

Supervisor

School of Chemistry
University of KwaZulu-Natal
Pietermaritzburg

September 2011

Acknowledgments

I would like to thank my supervisor: **Prof Orde Q. Munro**, for providing this acquiescent topic; and for his help and contributions. I would particularly like to thank him for his assistance at the end of my work when he made my thesis a priority due to my time limit, despite his own ailments. I wish him well on his path to recovery.

I would also like to take this opportunity to thank:

Craig Grimmer: for recording and helping to interpret my NMR spectra; as well as for his patient assistance whenever needed.

Caryl Janse Van Rensberg: for running and helping to interpret my LC-MS data, and for her input and ideas.

Shawn Ball and Hashim Desai: for their efficiency and willingness to help.

Paul Forder and Clarence Mortlock: for all my new and repaired glassware.

Raj, Fazel, Irene, Prudence and Bheki: for their help and invaluable assistance in the laboratory.

Michelle Francis: for her help and support throughout my postgrad years.

From the Inorganic Research Lab: Savannah & Malcolm for their help and pleasantness.

The Warren Organic Laboratory Researchers: for their help whenever required.

Prof J. S. Field: for his valid counsel and contributions.

Dr Vincent Smith and Prof Len Barbour: for the successful collection of X-ray data, despite the time limitations.

Alex Fageson (Prof. Mark T. Muller's group, College of Medicine, University of Central Florida, USA): for performing Topoisomerase II kinetoplast DNA (kDNA) decatenation assays on my metal complexes.

Dr Desigan Reddy: for his invaluable assistance and counsel, as well as his help with reading and checking my Experimental.

Kristy-Lyn Barry: thank you for being there no matter what the situation, your contributions and support have been invaluable to me.

Santham Govender Chetty: my solid rock; without whom teas, lunches, meetings and my PhD on the whole, would have been very hollow. Thank you for the help, understanding and support.

Carmen Changoo: for her support and friendship and for going out of her way to always help me. *Also, a BIG thank you to her for taking the burden of printing, copying and binding this Thesis while I was away, without her I don't know how I would've made it.*

André van der Hoven, Madira L., Zimbili M., Kerry Smith, Kirsty Stewart, Sandra K., Muvhango R., Ashwin and Vineet: although some have moved on you have all played a positive role in my life during my postgrad years – for this I thank you all.

Those who gave me support; and advised and empathised from far: **Ylenia, Janine S., Lynette, Venashree, Kuveshnee, Eloïse and Phil.**

As well as: **Jo, Lindsay, Janine G., Gabz, Belinda, Helen, Mark, Cass, Vonnie, Karin, Sarah W., Monika, Nick, Melani, Jem, Suzanne, Breetjie, Jessica R., Caz, Sarah S., Amy, Kelly, Cath, Chippies, Morag, Donna, Candice, Casey, Tracey, Mish, Shelly, Gretha, Sonja,**

P, Wb, O and Lh: may you always get what you deserve from life!

Piled Higher & Deeper©: thanks to Jorge Cham for the laughs and the constant reminder that I was not alone against the PhD!

Desigan, Hilary, Mum and Kristy-Lyn: for their proof reading of this work, despite the time constraints.

Mintek: for the *in vitro* cytotoxicity studies that were carried out on my samples and for project funding at the end of my work.

The financial assistance of the National Research Foundation (NRF) towards this research is hereby acknowledged. Opinions expressed and conclusions arrived at, are those of the author and are not necessarily to be attributed to the NRF.

Clyde and Hilary Wilson: thank you for all you have done for me over the last five years, I am eternally grateful for your support, help and generosity.

Sheryn, Dylan, Jers, Jorja & 'Froo': thank you for your support and for all that you did to make these last few years easier. Thank you for getting me through the worst and for being there to celebrate the best; I am lucky to call you all my siblings (and niece).

My Wonderful Parents: thank you for your support (in all the different ways you provided it) and for your continuous love and encouragement. Many times, knowing I had your backing made it possible for me to continue. *Without you, this would **never** have been possible!*

Neil: thank you for your encouragement and understanding. Thank you for always helping me through the next trial or obstacle with words of assistance (even when you didn't understand). Your love and continuous support have been so important to this work and invaluable to me.

Finally, I would like to dedicate this work to four amazing people. Although some of them are no longer with us, their memory will always live on:

William F. & Valerie A. Salmond

and

D. Roy & Mollie F. Thornhill

List of Abbreviations and Symbols

2D	Two Dimensional
Å	Angstrom
AgPF ₆	Silver hexafluorophosphate
BC	Before Christ
CDCl ₃	Deuterated chloroform
CD ₃ CN	Deuterated acetonitrile
CD ₃ OD	Deuterated methanol
cisplatin	<i>cis</i> -Diaminedichloroplatinum(II)
¹³ C NMR	Carbon Magnetic Resonance
CSD	Cambridge Structural Database
CT	Charge-transfer
CT-DNA	Calf thymus DNA
d	Doublet
DCM	Dichloromethane
DFT	Density Functional Theory
DMF	<i>N, N</i> -dimethylformamide
DNA	Deoxyribonucleic acids
ε _a	Extinction coefficient
ε _b	Extinction coefficient for the free metal complex
ε _f	Extinction coefficient for the metal complex in the fully bound form
esd	Estimated Standard Deviation
eV	Electron volts
FDA	Food and Drug Administration
FMO	Frontier molecular orbital
FT	Fourier transform
fw	Formula Weight
GGA	Generalised Gradient Approximation
HF	Hartree-Fock
¹ H NMR	Proton Magnetic Resonance
HOMO	Highest Occupied Molecular Orbital
HPLC	High Performance Liquid Chromatography

HR-ESI-MS	High Resolution Electron Spray Mass Spectrum
Int.	Intensity
IR	Infrared
IUCR	International Union of Crystallography
<i>J</i>	Coupling constant
<i>K_b</i>	Binding Constant
L1	<i>N,N</i> -bis[(pyridin-2-yl)methylene]1,2-diaminoethane
L2	<i>N,N</i> -bis[(pyridin-2-yl)methylene]1,3-diaminopropane
L3	<i>N,N</i> -bis[(pyridin-2-yl)methylene]1,3-diaminopropan-2-ol
L4	<i>N,N</i> -bis[(pyridin-2-yl)methylene]1,3-diamino-2,2-dimethylpropane
L5	<i>N,N</i> -bis[(pyridin-2-yl)methylene]1,2-diaminocyclohexane
L6	<i>N,N</i> -bis[(pyridin-2-yl)methylene]1,2-diaminophenylene
L1b	<i>N,N</i> -bis[phenyl(pyridin-2-yl)methylene]1,2-diaminoethane
L2b	<i>N,N</i> -bis[phenyl(pyridin-2-yl)methylene]1,3-diaminopropane
L3b	<i>N,N</i> -bis[phenyl(pyridin-2-yl)methylene]1,3-diaminopropan-2-ol
L4b	<i>N,N</i> -bis[phenyl(pyridin-2-yl)methylene]1,3-diamino-2,2-dimethylpropane
L5b	<i>N,N</i> -bis[phenyl(pyridin-2-yl)methylene]1,2-diaminocyclohexane
L6b	<i>N,N</i> -bis[phenyl(pyridin-2-yl)methylene]1,2-diaminophenylene
L1bh	2-(2-phenylimidazolidin-2-yl)pyridine
L2bh	2-phenyl-2-pyridin-2-ylhexahydropyrimidine
L2h	2-pyridin-2-yl-1,4,5,6-tetrahydropyrimidine
L4bh	5,5-dimethyl-2-phenyl-2-pyridin-2-ylhexahydropyrimidine
L6h	2-pyridin-2-yl-1 <i>H</i> -benzimidazole
L1m	<i>N,N</i> -bis[(pyridin-2-yl)ethylene]1,2-diaminoethane
L2m	<i>N,N</i> -bis[(pyridin-2-yl)ethylene]1,3-diaminopropane
L3m	<i>N,N</i> -bis[(pyridin-2-yl)ethylene]1,3-diaminopropan-2-ol
L4m	<i>N,N</i> -bis[(pyridin-2-yl)ethylene]1,3-diamino-2,2-dimethylpropane
L5m	<i>N,N</i> -bis[(pyridin-2-yl)ethylene]1,2-diaminocyclohexane
L6m	<i>N,N</i> -bis[(pyridin-2-yl)methylene]1,2-diaminophenylene
LR-ESI-MS	Low Resolution Electron Spray Mass Spectrum
L(S)DA	Local (Spin) Density Approximation
LUMO	Lowest Unoccupied Molecular Orbital
m	Multiplet
MDR	Multidrug resistance

MgSO ₄	Magnesium sulfate
MHz	Megahertz
ml	Millilitres
μL	Microlitres
MLCT	Metal to Ligand Charge Transfer
mmol	Millimoles
mM	Millimolar
MOs	Molecular Orbitals
MP2	Møller-Plesset perturbation theory
MRI	Magnetic resonance imaging
m/z	mass per charge ratio
N _i	Imine Nitrogen atom
NLO	Non-linear optical
NMR	Nuclear Magnetic Resonance
N _p	Pyridine Nitrogen atom
nM	Nanomolar
ON	Oxygen, nitrogen
PGM	Platinum group metals
ρ	Electron density
RMSD	Root mean square deviation
RNA	Ribonucleic Acid
s	Singlet
s	Binding site size
Salen	Salicylethylenediamine
SCF	Self-consistent field
t	Triplet
THF	Tetrahydrofuran
TLC	Thin layer chromatography
UV	Ultraviolet
vis	Visible
XRD	X-ray Diffraction

Abstract

The principal goal of this work was to synthesise and fully characterise a range of platinum group metal chelates of bis(pyridine-imine) ligands. These four-nitrogen donor Schiff base ligands are underdeveloped relative to their *salen* (ONNO donor) counterparts. The purified metal complexes were to be tested for their cytotoxicity against cancer cell lines and their mode of interaction (expected to be intercalation) studied.

The syntheses, spectroscopic and structural properties of some novel and some already known bis(pyridine-imine) ligands are described. Furthermore, UV-Vis, IR and NMR spectroscopy, as well as electrospray ionisation mass spectrometry, have been used to characterize the ligands and comparisons were made with relevant literature. Fifteen Schiff base ligands were successfully condensed from a 2-formyl or 2-ketopyridine starting material and a diamine bridging group, while the attempted syntheses of a further three are described. Literature methods or variations thereof were employed in the syntheses of these derivatives, which generally resulted in good yields. X-ray quality crystals were obtained and X-ray structures were determined for four novel ligands and five unexpected cyclised hexahydropyrimidine- and imidazole-containing bidentate ligands, of which three were novel structures.

The series of bicationic palladium and platinum complexes synthesised here were analysed by NMR, IR and UV-Vis techniques, as well as X-ray crystallography when possible. The complexes were prepared by reacting the free ligands with platinum group metal salts in refluxing acetonitrile. The complexes exhibit infrared bands for the imine C=N stretch between 1604–1670 cm^{-1} ; around 15–40 cm^{-1} lower than the free ligands. The ^1H NMR spectra in the CH=N chemical shift region also display shifts (0.1 to 0.8 ppm for the palladium complexes or 0.4 to 0.9 ppm for the platinum complexes) which are consistent with metallation.

X-ray crystal structures were obtained for eight novel metal complexes, which all crystallised in the monoclinic crystal system. The solid state analysis shows changes in the free ligands upon introduction of the metal ions, caused by the coordination process.

Metallation of the free ligands led to twisting of the ligands due to size effects and the spatial restrictions of the coordination geometry of the central metal ions. The structures were generally solved by direct methods and refined to $R_1 = 0.0729$ or less. Single-crystal X-ray diffraction analysis confirmed that the mononuclear complexes exhibit a distorted square planar coordination sphere composed of the four donor nitrogen atoms (two imine and two pyridyl nitrogen atoms) from the Schiff base ligands. The complexes were generally very stable and differed by the type of metal ion (platinum(II) or palladium(II)) and the diamine bridging group (2-carbon or 3-carbon linking chain with various substituted groups). A range of unconventional F...H-C contacts is revealed to play an important role in the overall bonding and crystal packing of many complexes.

To better understand our measured data and to separate the intrinsic properties of our molecules from intermolecular interactions, theoretical calculations at the DFT (B3LYP) level were carried out. These calculations predict the structural and spectroscopic properties for the free ligands and their metallated counterparts. DFT simulations were performed for the fifteen synthesised ligands (B3LYP functional, 6-31G** basis set), as well as three projected ligands that could not be synthesised, and for all proposed thirty-six metal complexes (B3LYP functional, SDD basis set). DFT simulations were used to obtain theoretical IR frequency data which was compared to the literature and used to prove the location of a local minimum energy structure in the geometry optimisation rather than a transition state. Our results collectively showed the B3LYP level of theory to be useful in the prediction of IR frequencies for these Schiff base ligands as well as the platinum(II) and palladium(II) complexes.

Geometry optimisations performed using density functional theory for the free ligands and metal complexes were compared, where possible, with X-ray data. For the free ligands the main structural differences were observed for the position of the pyridyl-imine "arms" of the ligands with relatively good agreement between the two structures for the bridging groups. On the other hand, the metal complexes showed greater discrepancies for the bridging groups rather than for the pyridine rings. These differences were also affected by the length of the carbon bridge; the longer the carbon bridge, the less variation was observed. The trends in the variation of bond distances and angles with the metal ion identity and ligand structure delineated by DFT simulations were matched by similar trends in the X-ray data.

Differences between the gas phase calculated geometries and those determined by X-ray diffraction were attributed to packing effects in the solid state and intermolecular interactions not being accounted for during DFT computations. The impressive similarity observed between the structures obtained from X-ray crystallography and computed by DFT shows the applicability of these computations at the B3LYP level of theory. They were able to accurately predict structural and spectroscopic properties for the ligands and complexes presented in this work.

The *in vitro* cytotoxicities of some of the metal complexes were evaluated against two mouse cancer cell lines. The compounds tested had lower than expected cytotoxicity towards the cell lines studied with IC_{50} values $> 100 \mu\text{M}$. The interaction of the complexes with calf thymus DNA has been explored by using absorption studies. From the observed changes in absorption possible modes of binding to DNA have been proposed for the metal complexes. Significant changes were observed in the absorption spectra upon interaction of the complexes with DNA, from which large binding constants were determined. The changes were, however, not as intense as expected nor were the spectral variations typical of intercalating drugs. There were also no bathochromic shifts nor any isobestic points observed for most of the metal complexes, except one. For the cationic PGM chelates studied, the lack of shift in the wavelength of the visible range MLCT band maximum and small changes in the band intensity were more indicative of weak electrostatic interactions. Our spectral data were thus interpreted as being consistent with non-intercalative binding; either simple electrostatic adduct formation or major/minor groove binding.

The binding constant values (K_b) of the metal complexes estimated from the titration with calf thymus DNA monitored by absorption spectroscopy were all in the range of 10^5 M^{-1} . This is within the range of those reported for other platinum(II) and palladium(II) metal complexes that have shown intercalation and/or groove binding. With the lack of inhibition of growth of the selected cancer cell lines it is possible that the compounds do not reach nuclear DNA in living cells or that such compounds are possibly substrates for efflux transporters. All the metal complexes in this work were determined to not be pure DNA intercalators as had been expected; however, in some cases partial intercalation cannot be ruled out from the spectral data.

Contents

Acknowledgements	III
List of Abbreviations and Symbols	VI
Abstract	IX
CHAPTER 1 – Introduction	1
1.1 Introduction	1
1.1.1 The Quandary	1
1.1.2 The Solution	1
1.2 Schiff bases	2
1.2.1 Background	2
1.2.2 This work	6
1.3 Metal-based pharmaceutical drugs	11
1.3.1 Background	11
1.3.2 Drug actions against cancer	12
1.3.3 DNA Intercalation	14
1.4 The metals	16
1.4.1 Platinum(II)	16
1.4.2 Palladium(II)	17
1.5 Drug Discoveries	18
1.5.1 Cisplatin	18
1.5.2 Platinum-based Drugs	19
1.5.3 Examples of Other Cancer Drugs	19
1.6 Feasibility and Objectives	22

CHAPTER 2 – Experimental	24
2.1 General Information	24
2.2 Instrumentation	24
2.3 Schiff Base free Ligands	25
2.3.1 Synthesis of <i>N,N'</i> -bis[(pyridin-2-yl)methylene] <i>diamine</i>	25
2.3.2 Synthesis of <i>N,N'</i> -bis[(pyridin-2-yl)methylene] 1,3diamino-propan-2-ol (L3)	27
2.3.3 Synthesis of <i>N,N'</i> -bis[(pyridin-2-yl)methylene]1,3- diamino-2,2-dimethylpropane	27
2.3.4 Synthesis of <i>N,N'</i> -bis[(pyridin-2-yl)methylene]1,2- diaminophenylene (L6)	28
2.3.5 Synthesis of <i>N,N'</i> -bis[(pyridin-2-yl)ethylene] <i>diamine</i>	28
2.3.6 Synthesis of <i>N,N'</i> -bis[(pyridin-2-yl)ethylene] 1,3- diamino-propan-2-ol (L3m)	29
2.3.7 Synthesis of <i>N,N'</i> -bis[(pyridin-2-yl)ethylene]1,3- diamino-2,2-dimethylpropane (L4m)	30
2.3.8 Synthesis of <i>N,N'</i> -bis[(pyridin-2-yl)methylene]1,2- diaminophenylene (L6m)	30
2.3.9 Synthesis of <i>N,N'</i> -bis[phenyl(pyridin-2-yl)methylene]- <i>diamine</i>	31
2.3.10 Synthesis of <i>N,N'</i> -bis[phenyl(pyridin-2-yl)methylene] <i>diamine</i>	32
2.3.11 Synthesis of <i>N,N'</i> -bis[phenyl(pyridin-2-yl)methylene]- 1,2-diaminocyclohexane (L5b)	33
2.3.12 Synthesis of <i>N,N'</i> -bis[phenyl(pyridin-2-yl)methylene]- 1,2-diaminophenylene (L6b)	34
2.3.13 Characterisation data for the cyclised hexahydro- pyrimidine- and imidazole-containing bidentate ligands	34
a) 2-pyridin-2-yl-1,4,5,6-tetrahydropyrimidine (L2h)	35
b) 2-pyridin-2-yl-1 <i>H</i> -benzimidazole (L6h)	35
c) 2-phenyl-2-pyridin-2-ylhexahydropyrimidine (L2bh)	35

d) 5,5-dimethyl-2-phenyl-2-pyridin-2-ylhexahydropyrimidine (L4bh)	36
e) 2-phenyl-2-pyridin-2-yl-octahydro-1-benzimidazole (L5bh)	36
2.4 Platinum Group Metal complexes	37
2.4.1 Metallation with PGMs	37
2.4.2 Template Metallation	37
2.4.3 Characterisation of the metal complexes	38
2.5 Discussion of the methods and characterisation	42
CHAPTER 3 – X-ray Crystallography	46
3.1 Introduction	46
3.2 Objectives	60
3.3 Methodology	61
3.4 Results and Discussion	62
3.4.1 General	62
3.4.2 X-ray data for the free ligands	65
3.4.3 X-ray structures of the Schiff base ligands	68
3.4.4 X-ray data for the platinum(II) and palladium(II) complexes	77
3.4.5 X-ray structures of the metal complexes	80
3.4.5.1 Molecular structures	81
3.4.5.2 Crystal Packing	93
CHAPTER 4 – Density Functional Theory	101
4.1 Introduction	101
4.2 Functionals	108
4.2.1 Local Density Methods	108
4.2.2 Gradient Methods	109
4.2.3 Hybrid Functionals	110

4.3 Performing a calculation	111
4.4 DFT and Schiff Base Ligands	112
4.4.1 Choosing the Functionals and Basis Sets	115
4.4.2 Computational Methods	120
4.5 Objectives	121
4.6 Results and Discussion	122
4.6.1 Introductory remarks	122
4.6.2 Geometry Optimisations	124
4.6.3 Molecular Orbitals	139
4.6.4 IR	151
Chapter 5 – DNA Binding Studies	160
5.1 Introduction	160
5.2 Objectives	171
5.3 Experimental	171
5.3.1 Materials and Chemicals	171
5.3.1.1 Biological screening	171
5.3.1.2 DNA Binding	171
5.3.1.3 Topoisomerase II kinetoplast DNA (kDNA) decatenation assay	172
5.3.2 Physical Measurements	172
5.3.2.1 Biological screening	172
5.3.2.2 DNA Binding	172
5.3.2.3 Topoisomerase II kinetoplast DNA (kDNA) decatenation assay	173
5.4 Results and Discussion	173
Chapter 6 – Conclusion	187
References	191

APPENDIX A	212
A1 – Crystallographic data tables for L1	214
A2 – Crystallographic data tables for L4	218
A3 – Crystallographic data tables for L5	222
A4 – Crystallographic data tables for L2h	226
A5 – Crystallographic data tables for L1bh	230
A6 – Crystallographic data tables for L2bh	234
A7 – Crystallographic data tables for L4b	238
A8 – Crystallographic data tables for L4bh	242
APPENDIX B	246
B1 – Crystallographic data tables for PtL1	248
B2 – Crystallographic data tables for PdL1	252
B3 – Crystallographic data tables for PtI2	256
B4 – Crystallographic data tables for PdL2	260
B5 – Crystallographic data tables for PtL4	264
B6 – Crystallographic data tables for PdL4	269
B7 – Crystallographic data tables for PdI4m	275
B8 – Crystallographic data tables for PdL4b	280
APPENDIX C	285
C1 – Conversions	286
C2 – Data for the metal complexes computed by DFT	287
APPENDIX D	288
D1 – Absorption spectra of metal complexes with subsequent CT-DNA additions	289
D2 – Plots of $(\epsilon_a - \epsilon_f) - \epsilon_f$ against [DNA base pairs] for the metal complexes	291
APPENDIX E (CD)	
E1 – DFT Output Files	
E2 – Structure Factor Tables	
E3 – Crystallographic Data Tables	
E4 – CIF Files	
E5 – DNA Binding Spectra	

CHAPTER 1 – Introduction

1.1 Introduction

1.1.1 The Quandary

South Africa is a developing country with its economy classified as one of the major emerging markets in the world. A significant problem is that although this emerging market has a high potential for growth, it will eventually reach a limit due to the fact that the economy is mainly resource based. Mining is a common and well-recognised industry in South Africa.¹ South Africa is known throughout the world for its mineral resources due to its significant proportion to the world reserves: platinum metals (90%), manganese (80%), chrome (73%), vanadium (45%) and gold (41%). Some experts believe that although South Africa does not have crude oil and bauxite, there may be other world-class deposits waiting to be discovered.¹

The raw materials mined in South Africa (minerals and fossil fuels) are exported to other countries as crude products. This means that other countries then have the opportunity to use those crude products and develop them into something with an improved value and application. These products are then bought back by South Africa at an elevated price resulting in financial losses for the South African economy. To make sure that the economy can continue to grow there needs to be some way of continuing to find potential for those resources that are available.

1.1.2 A Solution

South Africa is fortunate to have an abundance of these natural resources (especially precious metals), but they will not be infinitely available. Effort therefore needs to be made now to discover and develop new technology and new materials (so that value may be added to these primary resources), as well as new industries and market opportunities in order to benefit the economy and people. By doing this (e.g. by processing raw materials into secondary or tertiary goods that can be sold at a higher price than the primary form) the economy will be secured for a longer period of time, allowing further growth. Without this type of change South Africa will continue to sell all its resources to developed countries, making the other countries richer and South Africa poorer.

South Africa is the largest producer of platinum and a major producer and supplier of palladium.² These are therefore a good choice of metals to be used and developed in this study. These metals can be used to develop novel metal-based pharmaceutical drugs for the treatment of cancer, malaria, and life-threatening viral infections, resulting in not only a positive contribution to the South African economy, but also to South Africa itself.

1.2 Schiff Bases

1.2.1 Background

Schiff base ligands were first recognised when they were prepared and characterised by a German chemist, Hugo Schiff, in 1864.³ Hugo Schiff (1834–1915) studied in Germany with Friedrich Wohler, but spent most of his more than 60 year career in Italy.⁴ There are earlier reports that Ettling had synthesised similar complexes in 1840;⁵ however, it was Schiff's name that came to represent this class of compounds from around 1869. Schiff bases are imines that have a hydrocarbon substituent group (alkyl or aryl, but not hydrogen) on the nitrogen atom. An azomethine is a Schiff base that has a hydrogen atom on the carbon of the imine bond. (Thus most of the ligands in this work are more correctly azomethines; however, they are more commonly referred to in the literature as Schiff base ligands.) Schiff base ligands are relatively stable; however, owing to the imine group in these compounds they are susceptible to hydrolysis and transamination by nucleophiles,⁶ as shown by Holanda *et al.*⁷

There has been a great deal of research and many publications devoted to Schiff bases due to their inexpensive and simple syntheses, stability, structural differences and wide-ranging denticities, as well as the variety of their possible applications.^{8,9,10,11,12,13} Schiff base ligand synthesis usually employs the use of a high boiling point volatile organic solvent (however, solventless methods have been proposed¹⁴). The coordination of metals to Schiff base ligands takes place through the imine nitrogen and another group, which is connected to the aldehyde used to form the ligand. There are a vast number of publications showing the development of coordination chemistry using Schiff bases and their metal complexes including pure synthetic work as well as bio- and physiochemical studies.¹⁵

Schiff bases have been widely studied and employed in amongst other things: catalysis, molecular electronics, magnetism and photochemistry. Schiff base complexes have, in particular, become ubiquitous in the literature of catalysis. Ruthenium complexes have been known to act as catalysts^{16,17} for the activation of small molecules.¹⁸ Other Schiff base metal complexes that have shown catalytic activity include copper(II)^{19,20} and manganese(III)²¹ as well as uranium complexes of multidentate N-donor ligands.²² Manganese, cobalt, chromium and nickel Schiff base complexes have found application as catalysts for oxidation reactions.^{23,24,25} Chiral metal Schiff base complexes have shown catalytic activity towards the epoxidation of terminal olefins.²⁶ They have also been applied in different asymmetric catalysis reactions, for example: cyclopropanation,²⁷ aziridination²⁸ and hetero-Diels–Alder.²⁹ Schiff base ligands are still regularly prepared and some of these well-designed schiffs are referred to as “privileged ligands”.³⁰ These ligands have the ability to stabilise a range of metals in a range of oxidation states; this subsequently allows them to control the performance of the complex in catalytic transformations.

An interesting utilisation of Schiff base ligands is for metal ion transport due to their innate ability to bind with varying affinities to a wide range of metal ions. One example of this is oligosalicylaldehyde and its Schiff base oligomers, which are capable of forming polymer-metal complexes with metal salts. This allows the ligand to carry (and remove) metal ions from industrial waste waters.³¹ A range of Schiff bases have also been used as new lead(II) extracting agents to remove this toxic metal ion from the water carried by popular lead piping used in service pipes and household plumbing, etc.^{32,33} Elimination of toxic heavy metal contaminants from aqueous waste streams has become one of the most significant environmental problems being explored. In addition to the free ligands, cobalt(II) complexes of Schiff bases have also been studied for transportation, in this case, for the reversible process of O₂ transfer.³⁴ Schiff bases have also found application in materials chemistry; where they have shown photophysical, conducting and magnetic potentials.^{35,36,37} They have been used for reversible optical data storage³⁸ and have found application as non-linear optical (NLO) materials.^{39,40} Schiff base complexes have also found application in producing stereochemical models concerning main group and transition metal coordination chemistry.⁴¹

The potential for applications of Schiff base ligands and complexes also extends to biological behaviour and activities. This is due to the coordination behaviour of

polydentate ligands with transition metals sometimes modelling or even being able to mimic specific physical and chemical properties of numerous biological molecules.⁴² Schiff base compounds may operate as important intermediates in enzymatic reactions³⁰ or even inhibit enzymatic action.⁴³ In particular, the structural similarity of Schiff base compounds to biological systems has resulted in many studies. Some Schiff base compounds have shown pharmacological and antitumour activity,^{44,45} have been found to be good biological inhibitors^{46,47} or modeled or used in biological systems.^{48,49,50,51,52,53,54,55} Other complexes have shown resistance reversal (the ability to reverse multidrug resistance (MDR) in cancer patients) and the ability to slow the cell growth of leukemia,^{56,57} as well as *in vitro* antibacterial, antiviral and antitumoural activities.^{6,58} Some metallated Schiff base complexes were found to have antibacterial and antifungal activity,^{59,60,61,62} and some of these exhibited varying strengths of cytotoxicity as well^{59,61,62} (against various cancer cell lines). A few other complexes of Schiff base ligands have also been preliminarily screened as potential anticancer drugs.^{63,64,65,66}

In particular, Schiff base complexes with Co(II), Ni(II), Cu(II) and Zn(II) have already shown promising biological and antitumour activity.^{15,67} Certain Schiff base complexes, e.g. diorganotin(IV) complexes, have even shown higher anti-tumour activity (*in vitro* and *in vivo*) and lower toxicity than the well-known cisplatin (see Section 1.4).^{68,69,70,71} A series of Schiff bases derived from gossypol (a disesquiterpene extracted from cotton seeds) have shown antimalarial activity;⁷² while antibacterial activity has been seen for a range of novel Mn(II), Co(II), Ni(II), Cu(II), and Zn(II) complexes with vitamin K3-thiosemicarbazone.⁷³ Schiff base complexes have even been used in conjunction with ^{99m}Tc and ^{186/188}Re to form a new class of potential radiopharmaceuticals.⁷⁴

There are intensive studies for Schiff bases of *o*-hydroxy acylaromatics (ON-donors) in both the liquid and the solid state using UV techniques, NMR, neutron diffraction and X-rays.⁷⁵ However, a more common structure seen in the literature is that of the tetradentate derivative synthesised from salicylaldehyde and a diamine, known as a Salen derivative. These Salen structures (salicylethylenediamine) can be considered to be the prototype for N,N,O,O tetradentate Schiff base ligands. These Salen ligands are relatively stable due to their characteristic structural feature of intramolecular hydrogen bonding, common in these types of compounds.^{76,77,78} Another well-documented Schiff base compound is “acacen” (acetylacetonimine). Like Salen, it is a convenient

structural block for the creation of supramolecular structures. Nickel and copper complexes of *N,N'*-ethylene-bis(acetylacetonate) have been studied.^{79,80,81,82}

Schiff base complexes, particularly those of the salen-type are attractive due to the active role of the metal centre, the presence of charge-transfer (CT) transitions at low energies and their thermal stability.⁸³ Salens are quadridentate ligands that coordinate through two N and two O atoms to the central metal cation. If necessary a base will occupy one axial coordination site and dioxygen binds to the other. This particular type of chelating ligand has been examined at length in order to expand the understanding of the thermodynamics and kinetics of oxygen binding in these model systems.⁸⁴

One of the first Salen ligands with its copper complex was reported in 1889 by Combes *et al.*⁸⁵ Therefore these metal complexes subsequently became a fundamental class of compounds in coordination chemistry (with more than 2000 being characterised). Interest intensified in salen-type complexes after the preparation of salen complexes by the Jacobsen⁸⁶ and Katsuki⁸⁷ groups (applied in the early 1990s in epoxidation reactions). Since then, there have been many 3d transition metal complexes in the literature that involve N_2O_2 tetradentate Schiff base ligands. The specific properties of these complexes depend mainly on the nature and conformation of the ligand. For example, Salens have found remarkable application as anticorrosive materials; they inhibit the corrosion of mild steel.^{88,89}

Schiff bases, particularly those derived from aromatic *o*-hydroxyaldehydes (Salen), are examples of interesting compounds that have attracted a great deal of attention due to their interesting thermochromism and/or photochromism properties. The characteristics responsible for these properties are thought to be directly connected to the ground state and excited state proton transfer.^{90,91} Photochromism and thermochromism are phenomena exhibited in the solid state and in solution, and are caused by reversible colour changes induced by irradiation or by a change in temperature, respectively.^{92,93} Thermochromism in Salen systems has been explained by the intramolecular proton transfer reaction, while photochromism has been attributed to photo-induced proton transfer.⁹¹ Reports have shown that there seems to be a link between planarity and these chromic properties; i.e. molecules showing thermochromism are, in general, planar while those exhibiting photochromism are non-planar.^{94,95,96} It has, however, been

suggested that what determines thermochromic or photochromic behaviour is not the planarity, but instead the imino nitrogen atom's lone pair electron density.⁹⁷

In 1994 modifications to copper(II) complexes of Salen-type Schiff base compounds gave a series of DNA intercalators and groove-binders⁹⁸ and in 2004, a chromium-salen complex was found to have an inhibitory effect on the growth of *Shigella dysenteriae* (enteropathogens that may cause bacillary dysentery in humans and monkeys)⁹⁹. There is a great deal of literature for iron-salen complexes, both in the solid state and solution.^{100,101,102,103,104,105,106,107,108} They have demonstrated catalytic activity¹⁰⁷ as well as electron transfer reactions which imitate the catalytic functions of peroxidases.¹⁰⁸ Despite the considerable occurrence of iron in living systems less attention has been dedicated to the biological features of iron–Salen complexes. In their quest to find stable iron complexes that would interact powerfully with DNA in aqueous solutions, Silvestri and co-workers have reported on the interaction between Fe(Salen)Cl and native calf thymus DNA.¹⁰⁹ Zinc salen complexes have shown application as sensing materials^{110,111}, emissive materials (OLEDs)¹¹², and as building blocks for supramolecular structures.^{113,114}

Metallated bidentate Schiff base ligands^{115,116} with nitrogen donors are also present in the literature (with cobalt, nickel, iron palladium and platinum). The metallation of tridentate nitrogen donor ligands (pyridinaldazine with iron(II) and nickel(II)) were studied in a series of three papers by Stratton *et al.*^{117,118,119} Less literature exists for Schiff base ligands that have four nitrogen atom donors. However, the coordination chemistry of compounds with nitrogen donor atoms of varying denticity has been studied for many years. Some of the ligands to be presented in this work are not novel. Studies also exist for many of the ligands in this particular range as well as similarly structured Schiff base ligands that have been metallated. These metallations take place most commonly with copper,^{120,121,122,123,124} nickel,^{125,126} cobalt,¹²⁷ manganese^{128,129}, and iron^{130,131} as well as with lanthanide metals¹³² and ruthenium.¹³³

1.2.2 This Work

The particular series of neutral tetradentate (4-nitrogen) Schiff base ligand systems first chosen for this research have the standard structure of two pyridine fragments connected by different diamino bridges. The first type of ligand relating to these was

reported in 1915 with the synthesis of 2-pyridinaldazine.¹³⁴ The 2-Pyridinaldazine (Figure 1.1) is the simplest form of this type of ligand as it does not contain a particular hydrocarbon-bridging group, only the two imines, each with a pyridine ring. Since then many variations on these bis(pyridine-imine) ligands have been designed and synthesised. Some of the variations synthesised in this work have been previously synthesised **L1**^{123,124,125,126,129,130,132,133,135,136,137,138,139,140,141,142,143}, **L2**^{127,128,133,134,135,137,139,144,145,146}, **L3**^{126,128,147,148}, **L4**¹⁴⁹, **L5**^{138,150,151,152,153,154,155,156,157,158}, **L6**^{159,160,161,162,163,164,165,166}, **L1m**^{138,167,168,169,170,171,172,173,174}, **L2m**^{146,168,170,175,176,177,178,179}, **L3m**¹⁸⁰, **L4m**¹⁸¹, **L5m**¹⁸², **L6m**, **L1b**^{125,146,172,173,174,183,184,185,186,187,188,189}, **L2b**^{127,146,185,189,190,191,192,193}, **L3b**, **L4b**, **L5b** and **L6b**. Some of them have also been used as starting materials for the synthesis of a range of other ligands¹⁴ or metallated with a range of different metals (copper, iron, nickel, zinc, manganese, cadmium and some of the lanthanides).

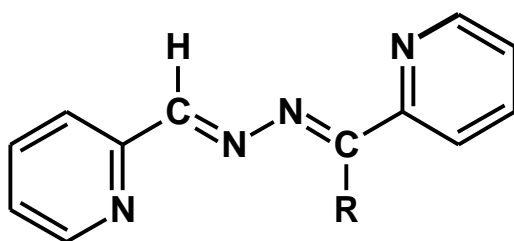


Figure 1.1: The structure of 2-pyridinaldazine.

After the synthesis of the original six ligands (**L1–L6**, Figure 1.2) it was decided to extend the range of ligands by changing the group on the imine carbon atom. In doing this it would also allow us to study the influence of this group, not only on the structure but also the effect it may have on the cytotoxicity of the complexes. It was decided to introduce bulk first in the form of a methyl substituent (**L1m–L6m**) and then a phenyl ring (**L1b–L6b**). The resulting range of complexes to be synthesised is shown in Figure 1.2. This work therefore aims to prepare a series of tetradentate bis(pyridine-imine) chelates and study their reactivity with some transition metals: platinum and palladium (Figure 1.2). The final complexes will be of interest for their technical application, molecular structures, spectroscopic properties, and their biochemical significance.

These Schiff base ligands form part of the symmetrical N_p, N_i, N_i, N_p type, where N_p and N_i are N(pyridine) and N(imine) donor centres, respectively. The N(imine) donor atoms are part of the bridge that connects the two pyridyl groups and the nature of this bridge

will be altered by using different diamine starting materials. This will produce an assortment of different ligands to determine the effect of the different attached groups. This range of neutral tetradentate Schiff base ligand systems which possesses two pyridine functional groups will be prepared by the one-pot reaction. This involves the condensation of 2-pyridinecarboxaldehyde, 2-acetylpyridine or 2-benzoylpyridine with the appropriate diamines (e.g. $\text{H}_2\text{N-X-NH}_2$, where X = a hydrocarbon bridging chain in Scheme 1.1) in a 2:1 mole ratio in dry ethanolic medium. This condensation is a rather simple, high-yielding and well-documented procedure. The reactants are structurally/conformationally predisposed in forming a ligand with no steric constraints and there is limited freedom for side reactions. Each of the ligands will be synthesised using an appropriate literature method or an adaptation thereof.

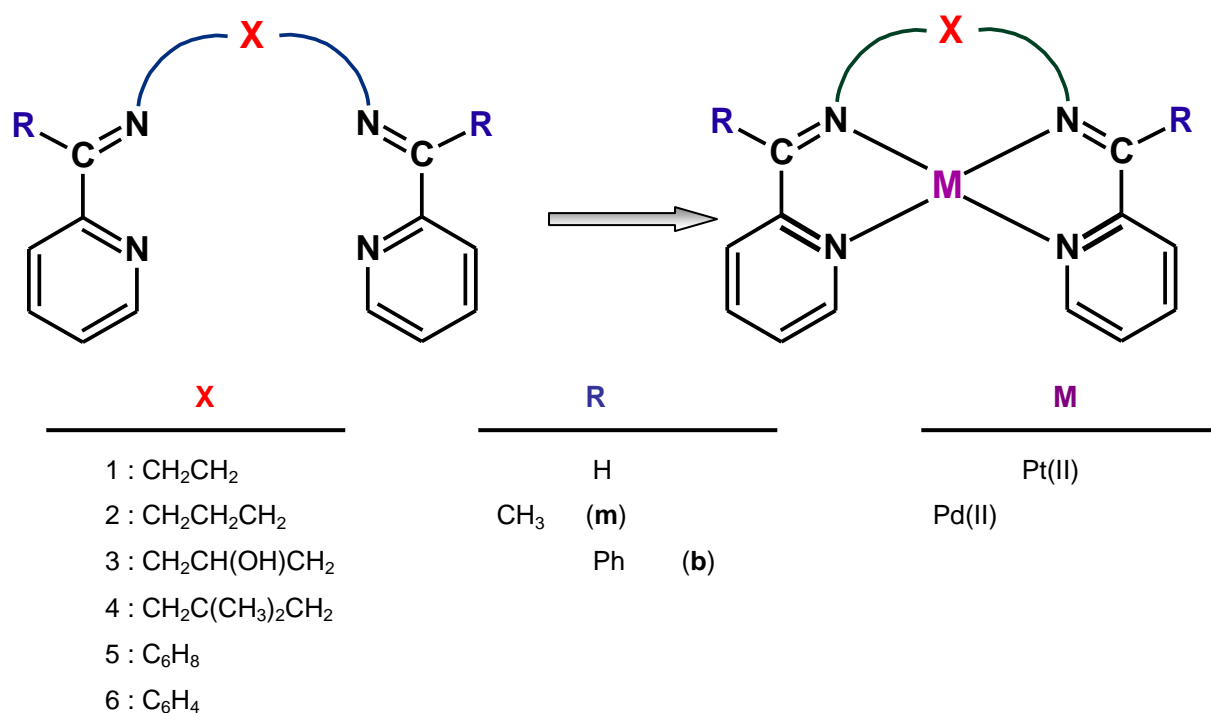
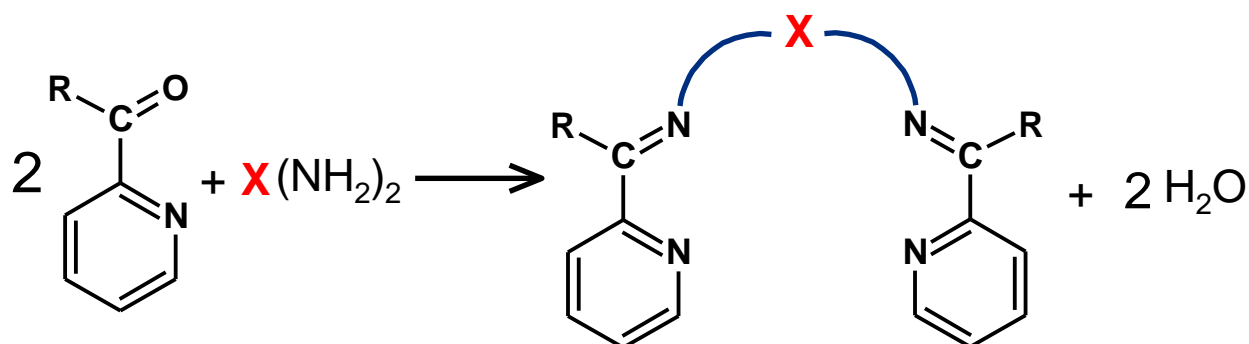


Figure 1.2: Structure of the *N,N*-bis-(2-pyridinecarboxaldimine) ligand systems and their metal complexes.



Scheme 1.1: The condensation for the synthesis of the Schiff base pyridyl ligands, *N,N*-bis-(2-pyridinecarboxaldimine).

The ligands must be capable of presenting the bonding donor atoms, which are members of the continuous chain, to a suitable metal atom (either with or without preliminary loss of protons). For a four-covalent metal ion (e.g. platinum, palladium) a quadridentate ligand must be spatially capable of offering the four donor atoms in order to form either a tetrahedron or a square shape so that they may bond readily to the metal ion. For a six-covalent metal ion (e.g. vanadium and iron) a quadridentate ligand must be capable of presenting its four donor atoms spatially so that two apices either in the *trans* position or in *cis* positions may be occupied by other atoms. Organic compounds which are capable of offering their four donor atoms to a metal atom to form a square ('planar quadridentates') are most often of the linear (open-chain) type, with the four donor atoms being members of the chain or on attached rings within the chain. These molecules are mostly flat, which is the orientation seen for their metal derivatives as well.

The four available nitrogen atoms in this range of ligands allow for tetrafunctional coordination to metals. The N_p atoms are easily accessible to metal ions due to the flexibility of the ligand and there is suitable separation between the two N_i atoms to allow for coordinating. The neutral ligand therefore coordinates via the two pyridine-nitrogen and the two imine-nitrogen atoms forming a N_4 square-plane around the metal ion. The range of ligands synthesised in this work differ by the spacer chain between the two picolinylaldimine fragments and the group on the imine carbon atom, we therefore expect to see similarities between the free ligands as well as their metal complexes.

Thus far no literature for the metallation or applications of any of these Schiff base ligands with platinum or palladium could be found. Indeed, a search of the Cambridge Structural Database¹⁹⁴ (CSD) reveals that there are numerous crystallographically characterised complexes for 4N donor Schiff base complexes containing transition group metal ions such as nickel and copper and a few were also found to contain zinc and iron. However, only one palladium structure could be found, PAKLOD (Figure 1.3), which had a similarly structured 4N donor Schiff base ligand to those of this work. This Schiff base complex synthesised by Kettunen *et al.* in 2005 differed by the structure of the extended bridge.

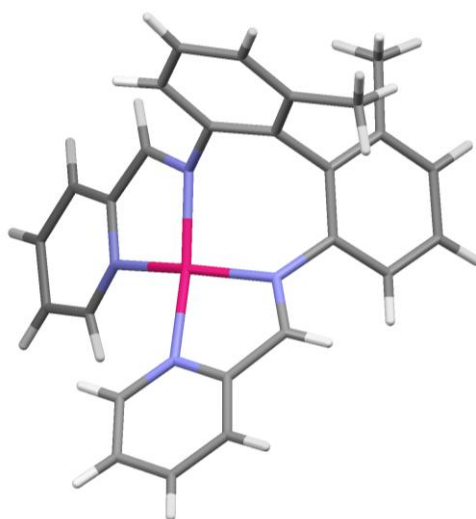
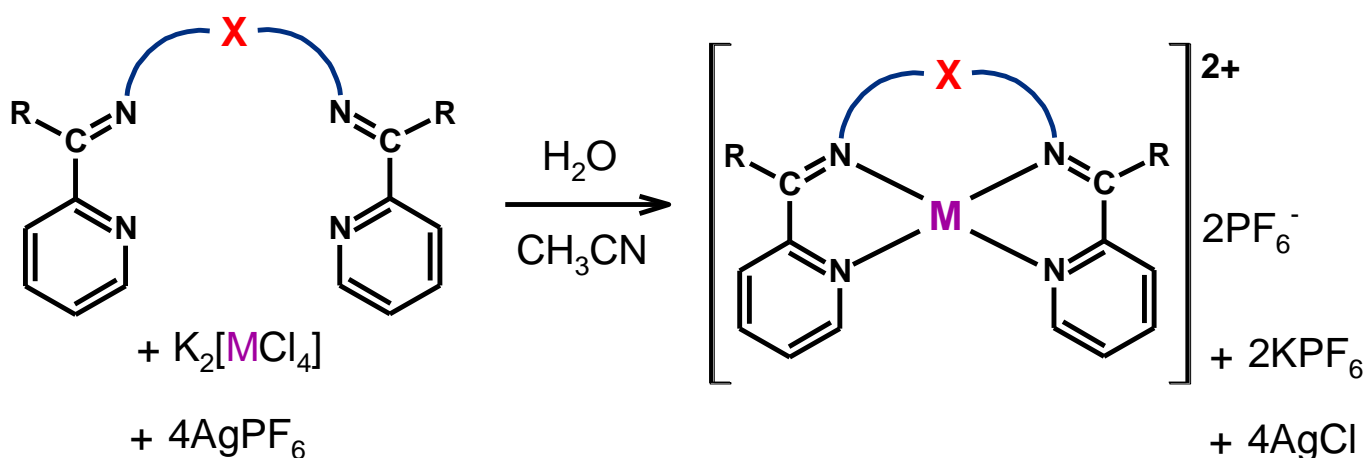


Figure 1.3: The structure of a palladium(II) 4N donor Schiff base complex comprising two pyridyl-imine chelating units, PAKLOD.¹⁹⁵

This proposed range of eighteen ligands in combination with these metals is therefore expected to produce novel complexes. These thirty-six complexes will hopefully present some interesting biological activity and, most importantly, possible cytotoxicity towards cancer cells. Due to the lack of literature for the metallation of this type of ligand with the metals chosen in this work, a new procedure was developed specifically for this. This method is shown in Scheme 1.2. Due to the slower kinetics of platinum(II) a greater time period is needed to obtain the Pt(II) derivatives in comparison to the Pd(II) derivatives. An attractive feature of these complexes is that they generate a much greater diversity of adjustable properties due to the coordinated metal centre or by the adaptation of the bridge and imine-groups for the ligands.



Scheme 1.2: A typical metallation reaction for the formation of platinum(II) and palladium(II) complexes of the Schiff base pyridyl ligands employed in this work.

1.3 Metal-based pharmaceutical drugs

1.3.1 Background

Metals may cause harm to the body, e.g. an over exposure to cadmium results in itai-itai disease and a deficiency of iron causes anaemia; however, metals used for medicinal purposes date back around 5000 years.¹⁹⁶ Many different metals have been used as treatments of a variety of ailments. Bismuth has been used to rehydrate infants with diarrhoea¹⁹⁷ and silver has been used as an antibiotic.¹⁹⁸ Copper has found application in treating, amongst other things: tuberculosis, burns, chronic wounds and seizures.¹⁹⁹ Although gadolinium has no known biological activity itself, it is used in the research techniques that examine biological systems, e.g. as an MRI (Magnetic Resonance Imaging) contrast agent.²⁰⁰ Gold compounds have been used clinically in the alleviation of various symptoms, particularly those normally associated with rheumatoid arthritis.²⁰¹

After the elucidation of the structure of the DNA double helix in 1953 by Watson and Crick²⁰² important insights into the structure of genes were exposed. This resulted in the investigation of how genes could be modified as this could help to develop new approaches in the treatment of various diseases. By developing gene therapy techniques the growth of malignant genes can be stopped and damaged genes repaired. Metal compounds have subsequently found useful application in this particularly important field. This has made inorganic chemistry a fast developing area with novel diagnostic and therapeutic metal drugs having a significant influence on the field.

The development of metal complexes as new drugs is not an easy undertaking. It is important that biodistribution and clearance of the metal complexes are considered, as an accumulation of metal ions in the body can have detrimental consequences. It is also necessary to investigate the drug's pharmacological specificity. Before a drug may be entered into clinical trials it is necessary to first show favourable physiological responses to *in vitro* (with targeted biomolecules and tissues) and *in vivo* (with xenografts and animal models) studies.^{203,204}

It is important to understand the mechanism of action that a metal complex uses to achieve its activities. This is imperative for the clinical success of the complex in addition to the logical planning for new compounds with improved potency.²⁰³ This also helps with the understanding of undesirable effects and helps to assess the risk the drugs may

have for humans. Positively charged metal centres are favoured for the binding to negatively charged biomolecules, e.g. proteins and nucleic acids. Consequently, numerous prospects exist for the use of metal complexes in the pharmaceutical discipline. A broad array of medicinal applications has thus been found for metal complexes and the number of complexes gaining wider acceptance is ever increasing.²⁰³

In order to investigate and produce new pharmaceutical drugs certain standards and criteria must also be taken into account. These drugs need to be designed so that they possess the appropriate structure and features. It is important that the drug has specificity, which can either be inherent or added onto the structure (e.g. monoclonal antibodies, targeting groups). The final drug needs to have a medium to high cytotoxicity ($LC_{50} < 10 \text{ mM}$; ideal ca. 10–100 nM) in order to be considered. Another important feature is the cost. The expense of making the new drug will need to be cheaper than the currently available drugs for it to become market-competitive. For metal drugs it is also important to take into account the possible accumulation of metals in the body as this may have detrimental effects.

The range of metal complexes to be synthesised for this work are expected to be planar structures of aromatic tetradentate (4-nitrogen donor) ligands based on pyridyl ring systems (Figure 1.1). The choice of metals for the complexes of these ligands has been made with biological activity in mind: platinum(II) and palladium(II). The metals selected have previously shown a range of bioactivity in literature, including anti-cancer activity (see Sections 1.4.1 and 1.4.2). These ions are capable of introducing a positive net charge to the neutral ligand and this coupled with the planar aromatic character of the ligand system is expected to afford an efficient DNA intercalator and thus a possible topoisomerase I/II inhibitor. The key objective of this research project is, therefore, to synthesise, fully characterise, and screen this range of novel metal complexes for their cytotoxicity against cancer.

1.3.2 Drug actions against cancer

There are three main treatments for cancer: 1) Surgery – which can be risky and often not possible, 2) Radiation therapy – involves treatment with high-energy X-rays and other types of radiation either externally or internally, and 3) Chemotherapy – uses drugs to

either inhibit the growth of tumours or to kill the cancer cells.²⁰⁵ The choice and particulars of a treatment is dependant on the type and stage of the cancer.

Drugs are classified according to an assortment of criteria: chemical structure, pharmacological action etc. It is necessary to differentiate between a drug's action and its effects. An action is the biochemical physiological mechanism and the effect is the observable consequence of this action. One common problem is the fact that no drug will cause a single consequence and therefore more than one effect will be observed. The main mode of action therefore needs to be selective toxicity; but this is not easy due to similarities between normal and abnormal cells. The anti-cancer drugs currently available have different mechanisms and hence produce different effects. It is impossible to find a "single cure" for cancer as more than 100 varieties exist.²⁰⁶

Metal ions have a known influence on cellular processes and have shown interesting effects on cell division and gene expression. However, they also affect non-natural processes, such as antitumour chemistry, carcinogenicity and toxicity. Treatment with cisplatin has been successful for a large number of patients and has been determined as a DNA cross-linking agent, as has Carboplatin (a successful cisplatin analogue). They bind covalently to DNA; favouring the N-7 position of adenine and guanine. Their ability to bind to two different sites on DNA causes a "cross-link", either to two separate DNA strands or within the same one. This then hinders the synthesis and transcription of DNA and hence impedes the growth of the cancerous cells.²⁰⁶ This has resulted in interest in the interaction between other metals and DNA, in particular, the way in which the metals binds to DNA.²⁰⁴

The main concern in chemotherapy is to kill the tumour cells without causing too much harm to the healthy cells. Drugs used stem from many different sources, some expected: from natural products such as plants, microbes and fungi; and some unexpected: from dyestuffs and chemical warfare agents.²⁰⁴ There is a possibility with these types of treatments that spontaneous (intrinsic) drug resistance may result for certain tumours. This may limit certain drug use; however, the resistance may be easily detected which allows new drugs to be screened without difficulty.²⁰⁴ A combination of drugs may then be used to overcome certain drug resistances. These drugs may operate by different approaches as a wide range of mechanisms exist by which cancer drugs may act.

Enzyme Inhibitors Some may directly inhibit enzymes and can be reversible or irreversible. A competitive inhibition means the drug will compete with the substrate for the active site on the enzyme. A noncompetitive inhibition occurs when the drug binds to the enzyme at a separate site, but stops the substrate from being able to bind at the active site.²⁰⁶

Suppression of Gene Function Suppression of gene function may take place in a number of the stages involved in protein synthesis or obstructing nucleic acid biosynthesis. The drugs inhibiting nucleic acid biosynthesis are not very selective and are therefore very toxic.²⁰⁶

Antimetabolites These drugs hold an extraordinary chemical similarity to a standard metabolite. This antimetabolite tricks an enzyme and subsequently produces an imitation metabolite which is then useless and cell growth is hampered.²⁰⁶

Stop or retard DNA replication The different modes of action involve blocking certain steps of the formation of nucleotides or deoxyribonucleotides which are essential for the production of DNA. Damage may be caused by disrupting the replication process which either completely stops replication or spoils it. Disruption may be caused to the formation of spindle cells that are essential for cell splitting.²⁰⁶

Another mechanism used by anti-cancer drugs is that of **DNA intercalation**.

1.3.3 DNA Intercalation

The main mode of action expected to be used by the target chelates of the platinum group metals in this work is that of DNA intercalation. The mechanism by which these compounds work is through insertion between the base pairs. The molecules that bind in this manner are therefore known as intercalators due to the way they “intercalate” into the compact array of stacked bases. They cause a change in the tertiary structure of the DNA helix²⁰⁷ mainly through non-covalent interactions. In the process the double helix is deformed and subsequently impedes DNA replication, repair, transcription or recombination. Intercalating agents are therefore often known as potent mutagens.

DNA has a double helix structure held together by hydrogen bonding between base pairs. The DNA helix has two grooves (major and minor) resulting from the way in which the two strands defined by the sugar-phosphodiester backbone (which run "antiparallel" to one another) are intertwined. There are several enzymes that are responsible for the replication of DNA as well as the repair of DNA.²⁰⁸ The ones that are of particular interest for this work would be topoisomerase I and II.

Briefly, most DNA is circular or supercoiled until it has to be replicated. It needs to be unwound for this process but it is not just a matter of unwinding the DNA as it is usually topologically linked or knotted. In order for it to be unwound, the DNA strand/s need to be cleaved and reannealed.²⁰⁸ This is where the topoisomerases come into play. Topoisomerase I only cleaves one strand and reanneals it, whereas topoisomerase II cleaves both strands and reanneals them both.²⁰⁸ This therefore allows supercoiled DNA to unwind and replicate.

Some drugs such as topotecan also H-bond to topoisomerase I at the DNA cleavage site and irreversibly arrest the enzyme or poison it. When DNA intercalators alter the tertiary structure of DNA, topoisomerases no longer recognise their normal substrate (undistorted DNA) and therefore are unable to perform their normal function of regulating DNA. The mode of action of many DNA intercalators is thus disruption of cell division and gene transcription. Inhibition or termination of the unwinding process prevents cell replication and initiates programmed cell death (apoptosis).²⁰⁸ This in turn stops the rapid rate at which cancer cells usually replicate.

Thus intercalating drugs have to slot in between DNA adjacent bases to impede this replication of the strands. When an intercalator binds to the helix the sugar-phosphate backbone of the DNA strand is distorted and the DNA is lengthened (as shown in Figure 1.3).²⁰⁹ This clearly alters the properties of the DNA significantly. This mechanism of DNA intercalation (insertion) takes place between the base pairs of the aforementioned minor or major grooves. An opening needs to be created by a degree of unwinding of the DNA strands, dependant on the intercalator. In turn the drug needs to be of a suitable size and chemical nature; the best ligands are usually polycyclic, aromatic and planar. The Schiff base ligand systems chosen for this work fit the above criteria.

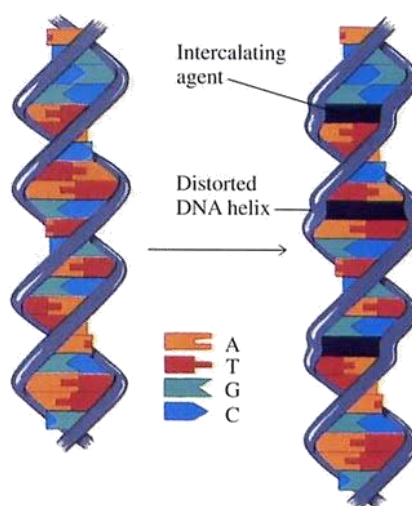


Figure 1.3. A structural view of how a DNA intercalator inserts itself and binds to the DNA helix causing deformation and subsequent interference with replication.²⁰⁹

1.4 The metals

1.4.1 Platinum(II)

Platinum has been found in the Egyptian tombs dating back as far as 1200 BC and in South America from around 100 BC.²¹⁰ Platinum's value today is due to its function in many industrial applications. There are two dominant uses for platinum: catalytic converters and fine jewellery, which together consume around 70% of the world's resources of platinum.²¹¹ Platinum is used worldwide in exhaust pipes as catalytic converters by converting harmful nitric oxide, hydrocarbons and carbon monoxide into harmless emissions. Its use for jewellery is favoured especially in conjunction with diamonds due to the clear, non-yellow shine that platinum allows. Other uses of platinum include catalysts, fuel cells, hard disks, electrodes, spark plugs, oxygen sensors, turbine engines and anticancer drugs.^{211, 212, 213}

The greatest impact on platinum-cancer chemistry was from the discovery of the antitumour activity of *cis*-diaminedichloroplatinum(II),²¹⁴ commonly known as cisplatin (see Section 1.5). It has been a little over 45 years since this discovery and various other drugs have since been tested, but those showing promising results are mostly cisplatin analogs. However, promising pharmacological character has also been seen for platinum complexes with distinctively different DNA binding modes from that of cisplatin.

Platinum(II) complexes have shown considerable biological activity as determined in cytotoxicity assays.²¹⁵ DNA binding properties of Pt(II) and Pd(II) complexes have been studied *in vitro*²¹⁶ and have shown cytotoxicity comparable to that of cisplatin.²¹⁷ Many of the well-known platinum anticancer complexes developed since cisplatin have amine ligands. We expect our platinum complexes with imine ligands will have a fundamentally different manner of binding to DNA than that of cisplatin. These molecules are most likely to be planar with only slight deviations from the plane which should make good examples of DNA intercalators.

1.4.2 Palladium(II)

Palladium was discovered and named by William Hyde Wollaston (6 August 1766 – 22 December 1828) in 1803.²¹⁸ As a member of the platinum group metals (PGMs), palladium shares many properties with platinum and therefore parallels some of platinum's uses. Palladium has also been used as an autocatalyst, as well as in electronics, jewellery (since 1939), fuel cells, coinage, oil refining, polyester, photography, water treatment, hydrogen purification and medicine.²¹⁹

Due to the results seen for complexes using platinum(II), attention has shifted to other platinum group metals. In particular, palladium(II) complexes have found great potential as antitumour agents.^{220,221,222} A strong interaction with DNA has been seen for Pt(II) and Pd(II) Schiff bases with pyrimidine rings.²²³ The DNA helicoidal structure is found to be destabilised after *in vitro* and *in vivo* studies of the interaction of palladium complexes with DNA.²²⁴ Ligand exchange has been revealed as a factor for the success with platinum drugs, but Pd(II) is known to undergo faster ligand exchange reactions than Pt(II). Palladium(II) therefore seems unlikely to follow the same mechanism as some of the original platinum(II)-based drugs on the market. Palladium(II) will, however, be a four coordinate square planer structure which is expected to have similar properties to that of some of the platinum complexes. Therefore appropriately designed palladium complexes may find use as DNA intercalators as well.

1.5 Drug Discoveries

1.5.1 Cisplatin

This compound was first described in 1845²²⁵, but its anticancer properties were only discovered in 1964. It has been found that cisplatin is able to enter cells by passive diffusion²²⁶ and also in a different manner, as more recently discovered, by active transport mediated by the copper transporter, Ctr1p^{227,228}, in yeast and mammals. The cytotoxicity of cisplatin has been shown to be due to its cross-linking binding to DNA that interferes with replication and transcription, in turn causing cell death.²⁰³

Cisplatin (Figure 1.4), marketed as Platinol®, showed incredible success by providing the first cure for small cell lung cancer and improving survival of patients with ovarian cancer in the advanced stages. It was also used for bladder, neck and head cancers and cured 80% of patients with testicular cancer.²²⁹ Unfortunately, side effects and drug resistance started to limit cisplatin's clinical applications. Biological carriers were then added to cisplatin to increase specificity which subsequently reduced side effects and drug resistance. Other drugs that are more effective with less toxic side effects, and possibly more favourable properties such as solubility in aqueous solution, were therefore required. Therefore since the early 1970s more than 3000 platinum complexes have been synthesised and tested.²³⁰

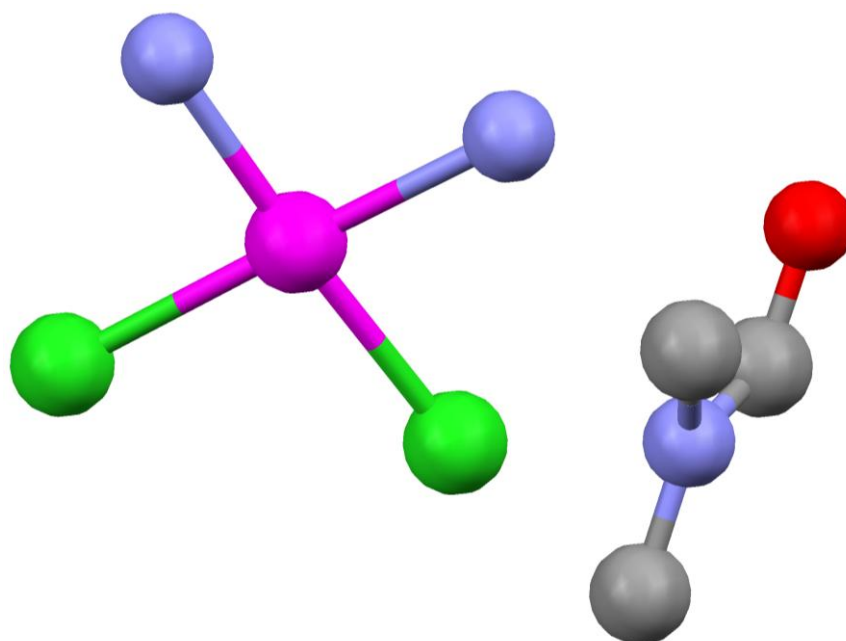


Figure 1.4: The structure of the dimethylformamide solvate of *cis*-diaminedichloroplatinum(II),²³¹ known as cisplatin (hydrogen atoms have been excluded for clarity).

1.5.2 Platinum-based Drugs

Even minor modifications to the structure of drugs can have an impact on their biological character including their antitumour activity and toxicity. Thus research efforts for platinum complexes that might produce more specific anticancer drugs with a broader range of antitumour activity have been investigated. Subsequently, a few more platinum-based drugs have been accepted by the Food and Drug Administration (FDA)²³²: Carboplatin (ovarian cancer)²³³, Satraplatin (hormone-refractory prostate cancer)²³⁴, Oxaliplatin (metastatic colorectal cancer)²³⁵, and Picoplatin (small-cell lung cancer)²³⁶ (Figure 1.5). Side effects have also been noted for some of these drugs: suppression of bone marrow activity by Carboplatin and peripheral nerve damage by Oxaliplatin.²³⁷

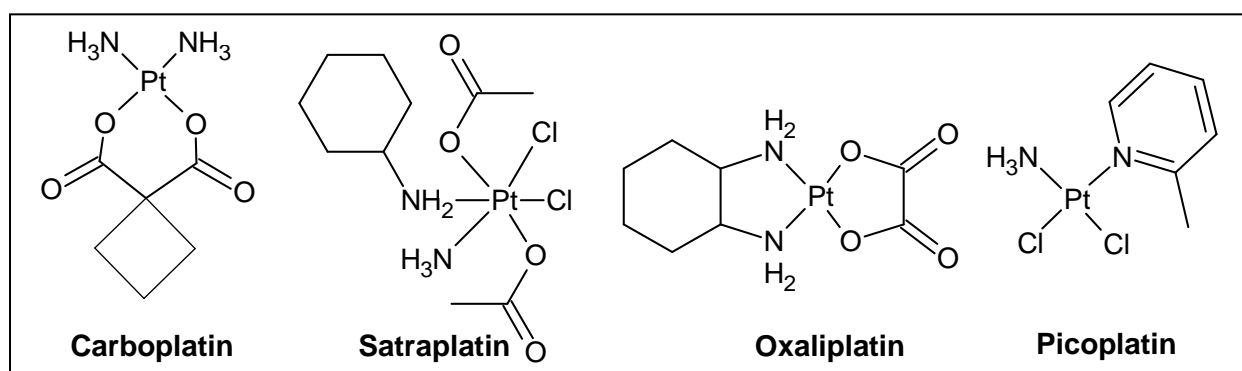


Figure 1.5: Some of the platinum-based drugs accepted by the Food and Drug Administration (FDA)²³² for clinical use in treating cancer.

1.5.3 Examples of Other Cancer Drugs^{238,239}

Methotrexate, marketed as Trexall™ (originally approved by FDA on 21 March 2001) is an antimetabolite used to treat epidermoid cancers of the head and neck, breast cancer and lung cancer (particularly squamous and small cell). It operates by competitive inhibition of folic acid reductase to interfere with DNA synthesis, repair and replication.

Carac® (originally approved by FDA on 27 October 2000) contains fluorouracil which is an antimetabolite and obstructs the methylation reaction of deoxyuridylic acid to thymidylic acid. It has found use on the skin treating pre-cancerous and cancerous skin growths.

Hydrea® (originally approved by FDA on 7 December 1967) is an antineoplastic agent, of which the mechanism cannot currently be described. It contains hydroxyurea which

affects cancer cells or sickled red blood cells in the body. It has been used to treat melanoma, primary squamous cell (epidermoid) carcinomas of the head and neck, chronic myelocytic leukemia and recurrent, metastatic, or inoperable carcinoma of the ovary.

Mercaptopurine is in a cancer medication sold as Purinethol™ (originally approved by FDA on 11 September 1953) and is also an antimetabolite. It inhibits the biosynthesis of adenine nucleotides and has been used to treat acute lymphatic leukemia or acute myelogenous leukemia.

Cerubidine® (originally approved by FDA on 3 February 1995) has antimitotic and cytotoxic activity owing to a number of proposed mechanisms of action, including inhibiting topoisomerase II. Its active ingredient is daunorubicin hydrochloride and it has shown an antitumour effect against a range of animal tumours.

Doxorubicin hydrochloride is the active ingredient in Doxil® (originally approved by FDA on 17 November 1995). It is an anthracycline topoisomerase inhibitor indicated for patients with ovarian cancer, where the disease has advanced or recurred after platinum-based chemotherapy.

Taxol® (originally approved by FDA on 29 December 1992) contains paclitaxel which is a novel antimicrotubule agent that promotes the assembly of microtubules from tubulin dimers and stabilises microtubules by preventing depolymerisation. It has been indicated as initial and ensuing therapy for the treatment of advanced carcinoma of the ovary, as well as breast cancer. In combination with cisplatin it has been used to treat non-small cell lung cancer.

Mitomycin® (originally approved by FDA on 19 April 1995) has an active ingredient of the same name. It is not recommended as a single-agent, but has shown usefulness in conjunction with other chemotherapeutic drugs in treating disseminated adenocarcinoma. It is a potent DNA cross-linker and has also been used for breast, oesophageal and bladder cancers.

Carmustine is the active ingredient in Gliadel® (originally approved by FDA on 23 September 1996), which is a nitrosourea oncolytic agent. It has been indicated for brain

tumours; producing an antineoplastic effect by alkylating DNA and RNA. It also found use in treating newly-diagnosed high grade malignant glioma and recurrent glioblastoma multiforme.

Camptosar® (originally approved by FDA on 14 June 1996) contains irintecan which is a derivative of cemptothecin. Its cytotoxicity has been shown to be caused by double-strand DNA damage created during DNA synthesis when replication enzymes interact with the ternary complex. This drug has found use for metastatic carcinoma of the colon or rectum; either as combination first-line therapy or when the disease has recurred or progressed.

Recently, the discovery that a metal compound does not have to be extremely cytotoxic to have effective anti-cancer properties was made. Some promising discoveries have been made for the metals gallium²⁴⁰ and ruthenium²⁴¹ (which have mainly anti-metastatic effects – prevent the spreading of cancers or are discriminatory for metastases), as well as for gold²⁴² (Figure 1.6).

Even though some complexes have successfully been through Phase I and II human clinical trials, the mechanisms of their action are still often (but not always) unknown. The combination of different drugs that have varying modes of action often synergises their effects. Thus there is continued interest in the various metallopharmaceutical mechanisms due to the anticipation that together they might provide an even wider range of successful chemotherapeutic agents.²⁴³

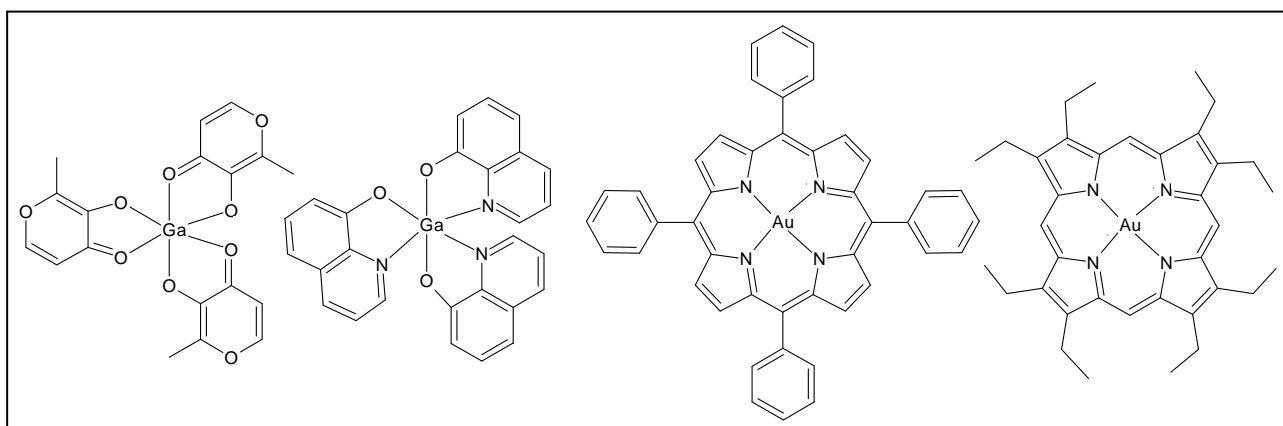


Figure 1.6: Structures of oral gallium complexes²⁴⁰ (left) and gold(III)–porphyrin complexes²⁴² (right) that have been used for cancer treatment.

1.6 Feasibility and Objectives

The metals chosen for this research have all shown some kind of bioactivity, particularly as anticancer drugs. The biological activity of various drugs containing platinum is well documented^{203,204,244} and palladium has also found bioactive applications.^{220,221,222}

The best ligands for DNA intercalators are usually polycyclic, aromatic and planar. The ligand systems synthesised as the basis of this work fit the above criteria, and in combination with the bioactive metals, result in complexes that are likely to present some interesting activity towards cancer cells. Our work is also novel as very little literature concerning the metallation of Schiff base ligands (particularly those similar in structure to our choice of ligands) could be found with platinum or palladium.

In planning the present study, we anticipated that the complexes of interest would function well as DNA intercalators due to several key design criteria. The overall positive charge on the complex will effectively target the negatively charged DNA double helix electrostatically and bind by π - π stacking with pyrimidine and purine bases. This results in their mode of action in most cases being to inhibit topoisomerase II. We have already seen positive results for similar ligands (patent pending) and therefore expect that the slightly larger aromatic rings and extended π -electron system in pyridine-based ligands should enhance the DNA-binding affinity of the compound relative to related N-heterocycle analogues. With the total charge of the cation being +2 we anticipate improved cytotoxicity due to improved electrostatic contributions to the recognition of DNA. The literature also shows other agents with similar metals and ligands that have already displayed biological activity (as discussed).

The principal objectives for this work were to:

- (1) synthesise a range of free Schiff base ligands (some novel and some currently known);
- (2) fully characterise all these free ligands using UV-Vis, IR and liquid chromatography mass spectrometry (LC-MS), as well as ^1H and ^{13}C NMR spectroscopy;
- (3) metallate these free ligands with platinum(II) and palladium(II);
- (4) fully characterise the resulting metal complexes using UV-Vis, IR and ^1H , ^{13}C and ^{195}Pt NMR spectroscopy;

- (5) obtain X-ray crystal structures for the free ligands and metal complexes, where possible;
- (6) perform DFT computational studies for each of these free ligands and their respective metallated derivatives;
- (7) observe and investigate the similarities and differences between DFT simulation data and X-ray structures;
- (8) screen the metal complexes against a range of cancer cells to determine their bioactivity; and
- (9) perform titrations of the metal complexes with DNA using electronic absorption spectroscopy in order to determine equilibrium constants.

CHAPTER 2 – Experimental

2.1 General Information

Solvents were obtained from Merck and were used as received, unless otherwise stated. Hexane was dried by distillation over pressed sodium wire. Tetrahydrofuran (THF) was dried by distillation over Na/K alloy and absolute ethanol was dried using activated molecular sieves (3 Å). Acetonitrile was dried using an Innovative Technology PurSolv solvent purification system.

The six diamines: 1,2-diaminoethane ($\geq 99.5\%$), 1,3-diaminopropane (99%), 1,3-diaminopropan-2-ol (95%), 1,3-diamino-2,2-dimethylpropane (99%), *cis*-1,2-diaminocyclohexane (97%) and 1,2-diaminophenylene (99.5%); and the metal precursors potassium tetrachloroplatinate ($K_2[PtCl_4]$, 99.99%) and potassium tetrachloropalladate ($K_2[PdCl_4]$, 98%), were all used as received from Aldrich.

2-Pyridinecarboxaldehyde (99%, Aldrich) was stored at 6 °C until use. 2-Acetylpyridine ($\geq 99\%$, Aldrich) and 2-benzoylpyridine ($\geq 99\%$, Aldrich) were stored at room temperature. Silver hexafluoroantimonate ($AgSbF_6$, 98%), silver tetrafluoroborate ($AgBF_4$, 98%) and silver hexafluorophosphate ($AgPF_6$, 98%) were obtained from Aldrich and stored and dispensed under inert conditions.

2.2 Instrumentation

Electronic UV-Vis spectra were recorded using a UV-1800 Shimadzu spectrophotometer. FT-IR spectra were obtained on a Bruker Alpha-P spectrometer with a diamond ATR crystal (36 scans, spectral resolution $\geq 2.0\text{ cm}^{-1}$).

1H , ^{13}C and ^{195}Pt NMR spectra of solutions of the ligands and complexes were recorded using either a Bruker Avance 500 (11.7 T Oxford magnet) or Bruker Avance 400 (9.4 T Bruker magnet) equipped with a 5 mm BBO-Z probe. The proton and carbon NMR spectra were assigned with the use of DEPT and 2D COSY and HSQC data. Coupling

constants are reported as averages calculated from peak separations measured with SpinWorks.²⁴⁵

Molecular weights, for the ligands and metal complexes, were obtained using electrospray ionisation in the positive and negative modes (sample specific) on a Waters LCT Premier mass spectrometer.

2.3 Schiff base free ligands

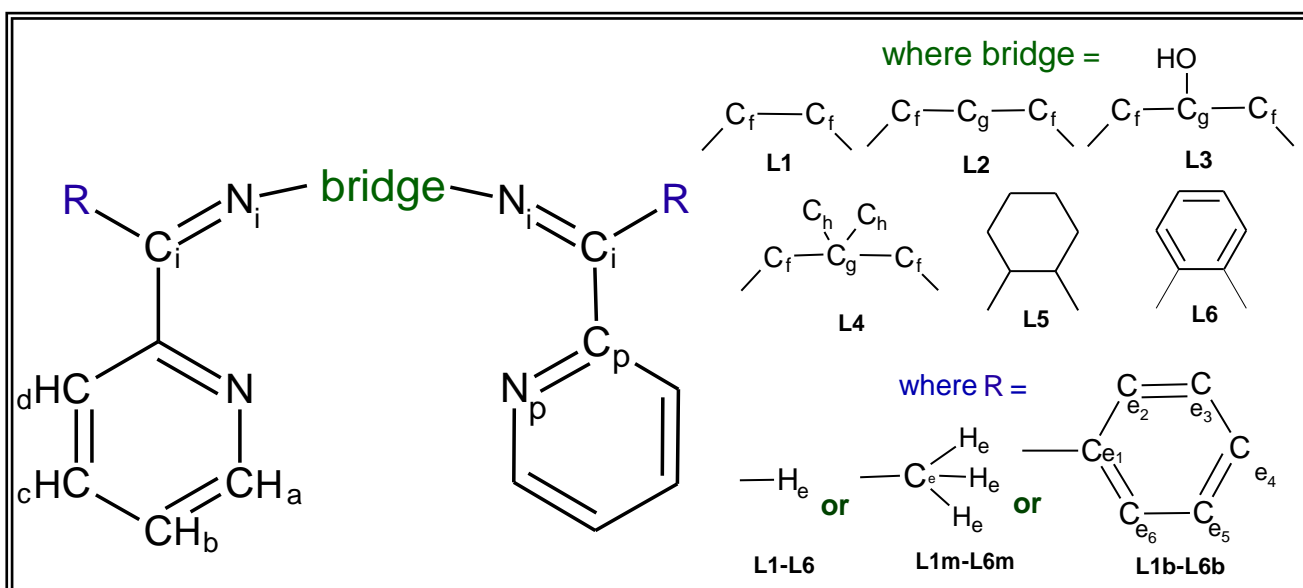


Figure 2.1: A basic framework of the Schiff base structure showing the notation used for labelling the atoms for each free ligand.

2.3.1 Synthesis of *N,N*-bis[(pyridin-2-yl)methylene]diamine

Where *diamine* = 1,2-diaminoethane (**L1**),^{129,139} 1,3-diaminopropane (**L2**)^{127, 129, 146} or *cis*-1,2-diaminocyclohexane (**L5**).^{152,158}

To a solution of 2-pyridinecarboxaldehyde (1.50 mL, 15.8 mmol) in absolute ethanol (15 mL) at 40 °C, was added dropwise the respective diamine (7.90 mmol). The resulting solution was heated at reflux for a period of 6 hours and thereafter the resulting solution was cooled to room temperature. The solution was dried by the addition of anhydrous MgSO₄, which was subsequently removed by filtration. The filtrate was then passed through a column of aluminium oxide with dichloromethane (DCM) as the eluting solvent to remove any traces of starting material. The yellow/orange liquid was concentrated to

afford an oil from which the product either precipitated as a yellow-orange solid (**L1** and **L5**) upon standing, or remained as an oil (**L2**).

L1: Yield: 1.244 g, 66%. UV-Vis (CH_3OH ; λ_{max} , nm): 235.0, 272.5. ^1H NMR (500 MHz, CD_3OD) [δ , ppm]: 8.55 (d of q, $J = 40.7$, 2H, H_a), 8.38 (s, 2H, H_e), 7.97 (d, $J = 7.8$, 2H, H_d), 7.78 (t of d, $J = 7.7$, 1.6, 2H, H_c), 7.36 (m, 2H, H_b), 4.04 (s, 4H, H_f) ^{13}C NMR (125 MHz, CD_3OD) [δ , ppm]: 163.5 (C_i), 153.7 (C_p), 149.0 (C_a), 137.2 (C_c), 125.3 (C_b), 121.6 (C_d), 60.9 (C_f). IR $\nu(\text{cm}^{-1})$: 3051, 3007, 2903, 2866, 2842, 1648, 1585, 1567, 1465, 1435, 1348, 1283, 1226, 1197, 1152, 1092, 1044, 1022, 991, 977, 957, 871, 796, 772, 742, 663, 617, 518, 470, 406. HR-ESI-MS: m/z 261.1119 [$\text{M}+\text{Na}$] $^+$ calculated for $\text{C}_{14}\text{H}_{14}\text{N}_4\text{Na}$ 261.1116.

L2: Yield: 1.674 g, 84%. UV-Vis (CH_3OH ; λ_{max} , nm): 235.5, 272.5. ^1H NMR (400 MHz, CD_3OD) [δ , ppm]: 8.63 (d of d, $J = 4.8$, 2H, H_a), 8.41 (s, 2H, H_e), 7.99 (d, $J = 8.1$, 2H, H_d), 7.72 (t of d, $J = 7.7$, 1.7, 2H, H_c), 7.29 (m, 2H, H_b), 3.79 (s, 4H, H_f), 2.16 (p, $J = 6.9$, 2H, H_g). ^{13}C NMR (125 MHz, CD_3OD) [δ , ppm]: 162.2 (C_i), 153.9 (C_p), 148.9 (C_a), 137.3 (C_c), 125.2 (C_b), 121.4 (C_d), 58.5 (C_f), 31.2 (C_g). IR $\nu(\text{cm}^{-1})$: 3400, 3296, 3279, 3053, 3009, 2925, 2886, 2841, 1647, 1586, 1567, 1467, 1435, 1333, 1293, 1227, 1147, 1044, 1022, 991, 974, 860, 770, 742, 654, 616, 501, 405. HR-ESI-MS: m/z 275.1274 [$\text{M}+\text{Na}$] $^+$ calculated for $\text{C}_{15}\text{H}_{16}\text{N}_4\text{Na}$ 275.1273.

L5: Yield: 1.789 g, 78%. UV-Vis (CH_3OH ; λ_{max} , nm): 237.0, 273.0. ^1H NMR (500 MHz, CDCl_3) [δ , ppm]: 8.60 (d of q, $J = 5.0$, 2H, H_a), 8.35 (s, 2H, H_e), 8.03 (d, $J = 7.9$, 2H, H_d), 7.68 (t of d, $J = 7.7$, 1.6, 2H, H_c), 7.27 (m, 2H, H_b), 3.71 (m, 2H, H_f), 2.11 (m, 2H, H_g), 2.04 (m, 2H, H_h), 1.77 (m, 2H, H_g), 1.60 (m, 2H, H_h). ^{13}C NMR (125 MHz, CDCl_3) [δ , ppm]: 166.0 (C_i), 155.1 (C_p), 149.1 (C_a), 136.4 (C_c), 124.4 (C_b), 121.2 (C_d), 70.0 (C_f), 30.9 (C_g), 22.9 (C_h). IR $\nu(\text{cm}^{-1})$: 3059, 3012, 2957, 2925, 2898, 2854, 1649, 1638, 1585, 1563, 1467, 1445, 1435, 1379, 1336, 1327, 1316, 1288, 1226, 1194, 1147, 1138, 1131, 1071, 1042, 992, 978, 967, 931, 895, 875, 856, 819, 790, 772, 747, 740, 686, 666, 648, 621, 617, 596, 516, 484, 448, 409. HR-ESI-MS: m/z 315.1587 [$\text{M}+\text{Na}$] $^+$ calculated for $\text{C}_{18}\text{H}_{20}\text{N}_4\text{Na}$ 315.1586.

2.3.2 Synthesis of *N,N*-bis[(pyridin-2-yl)methylene] 1,3-diaminopropan-2-ol (L3)¹²⁶

To a stirred solution of 2-pyridinecarboxaldehyde (1.00 mL, 10.5 mmol) in acetonitrile (20 mL), was added dropwise 1,3-diaminopropan-2-ol (0.47 mL, 5.30 mmol). The resulting solution was heated to 40 °C for an hour and then left to stir at room temperature for 72 hours. The solution was concentrated yielding a dark-yellow oil. Several aliquots of ether were used to extract a clean yellow oil, leaving behind a dirty green residue. The ether was evaporated and the yellow oil was collected.

Yield: 1.391g, 98%. *UV-Vis* (CH_3OH ; λ_{max} , nm): 237.0, 267.0, 280.5 (sh), 272.0. 1H NMR (400 MHz, $CDCl_3$) [δ , ppm]: 8.63 (ddd, 2H, $J = 4.8, 1.8, 0.9$, H_a), 8.48 (s, 2H, H_e), 7.99 (ddd, $J = 8.0, 1.3, 0.9$, 2H, H_d), 7.72 (m, 2H, H_c), 7.30 (m, 2H, H_b), 5.18 (s, O-H), 4.29 (m, 1H, H_g), 3.90 (ddd, $J = 12.4, 4.7, 1.5$, 2H, H_f), 3.85 (ddd, $J = 12.4, 6.7, 1.5$, 2H, H_f). ^{13}C NMR (125 MHz, $CDCl_3$) [δ , ppm]: 163.9 (C_i), 154.3 (C_p), 149.5 (C_a), 136.6 (C_c), 124.9 (C_b), 121.4 (C_d), 70.8 (C_g), 64.6 (C_f). *IR* $\nu(cm^{-1})$: 3336, 3316, 3308, 3295, 3290, 3282, 3275, 3014, 2908, 2896, 1711, 1649, 1590, 1568, 1471, 1437, 1366, 1301, 1228, 1150, 1088, 1028, 999, 860, 772, 743, 662, 624, 501, 405. *HR-ESI-MS*: m/z 269.1404 [M]⁺ calculated for $C_{15}H_{17}N_4O$ 169.1402.

2.3.3 Synthesis of *N,N*-bis[(pyridin-2-yl)methylene]1,3-diamino-2,2-dimethylpropane (L4)¹⁴⁹

To a stirred solution of 2-pyridinecarboxaldehyde (1.50 mL, 15.8 mmol) in 2-propanol (10 mL), was added dropwise 1,3-diamino-2,2-dimethylpropane (0.66 mL, 7.90 mmol) dissolved in 2-propanol (10 mL). The resulting solution was then stirred at room temperature for 24 hours. The solution was concentrated and the resulting dark orange oil solidified into a low melting dark orange solid on standing.

Yield: 1.511 g, 68%. *UV-Vis* (CH_3OH ; λ_{max} , nm): 236.5, 272.0. 1H NMR (500 MHz, $CDCl_3$) [δ , ppm]: 8.52 (d of q, $J = 5.0$, 2H, H_a), 8.31 (s, 2H, H_e), 7.98 (d of t, $J = 8.1$, 2H, H_d), 7.63 (t of d, $J = 7.8, 1.6$, 2H, H_c), 7.19 (m, 2H, H_b), 3.52 (d, $J = 1.4$, 4H, H_f), 0.98 (s, 6H, H_h). ^{13}C NMR (125 MHz, $CDCl_3$) [δ , ppm]: 162.0 (C_i), 154.6 (C_p), 149.0 (C_a), 136.3 (C_c), 124.4 (C_b), 120.8 (C_d), 69.8 (C_f), 36.9 (C_g), 24.4 (C_h). *IR* $\nu(cm^{-1})$: 3275, 3046, 3004, 2957, 2937, 2900, 2879, 2866, 2833, 1645, 1585, 1566, 1466, 1436, 1384,

1365, 1331, 1290, 1255, 1227, 1188, 1166, 1144, 1096, 1056, 1041, 1024, 990, 958, 948, 920, 895, 857, 847, 775, 758, 745, 668, 618, 503, 492, 431, 408. *HR-ESI-MS*: m/z 303.1578 $[M+Na]^+$ calculated for $C_{17}H_{20}N_4Na$ 303.1586.

2.3.4 Synthesis of *N,N*-bis[(pyridin-2-yl)methylene]1,2-diaminophenylene (**L6**)¹⁶²

To a solution of 2-pyridinecarboxaldehyde (0.72 mL, 7.61 mmol) in acetonitrile (20 mL), was added dropwise a solution of 1,2-diaminophenylene (0.37 g, 3.38 mmol) in acetonitrile (10 mL). The resulting solution was heated to 40 °C for 1 hour and thereafter left to stir at room temperature for a period of 72 hours. The solution was filtered to remove a fluffy pale orange solid that had formed.* The filtrate evaporated and gave a yellow powder found to contain

Yield: ~ 0.2 g, ~ 19%. *UV-Vis* (CH_3OH ; λ_{max} , nm): 214.0 (sh), 239.5, 264.0, 309.0, 322.0 (sh). *IR* $\nu(cm^{-1})$: 3294, 3112, 3051, 2166, 2151, 2001, 1714, 1675, 1588, 1569, 1524, 1438, 1314, 1279, 996, 797, 740, 702, 692, 677, 614, 542, 499, 429, 420, 403. *LR-ESI-MS*: m/z 309.11 $[M+Na]^+$ $C_{18}H_{14}N_4Na$ and 218.06 $[M+Na]^+$ $C_{12}H_9N_3Na$.

2.3.5 Synthesis of *N,N*-bis[(pyridin-2-yl)ethylene]diamine

Where diamine = 1,2-diaminoethane (**L1m**),¹³⁸ 1,3-diaminopropane (**L2m**)¹⁴⁶ or *cis*-1,2-diaminocyclohexane (**L5m**).

To a solution of 2-acetylpyridine (3.35 mL, 29.9 mmol (**L1m**); 2.69 mL, 24.0 mmol (**L2m**); 0.76 mL, 6.80 mmol (**L5m**)) in absolute ethanol (20 mL), was added dropwise a solution of the corresponding diamine (1.00 mL, 14.9 mmol (**L1m**); 10.0 mL, 11.2 mmol (**L2m**); 0.40 mL, 3.40 mmol (**L5m**)) in ethanol (10 mL). The resulting solution was heated at reflux for a period of 23 hours.† The solution was then cooled to room temperature and passed through a column of aluminium oxide with DCM as the eluting solvent to remove any traces of starting material. The low melting solids were collected and weighed.

* This pale orange solid was found to be the cyclised imidazole-containing bidentate ligand: **L6h**. See 2.3.13 b) for characterisation details.

† 2-Acetylpyridine (0.50 mL, 4.50 mmol) was added to the reaction mixture of **L5m** after 15 hours at reflux.

L1m: Yield: 2.862 g, 72%. UV-Vis (CH_3OH ; λ_{max} , nm): 231.0, 262.0, 268.0 (sh). $^1\text{H NMR}$ (500 MHz, CDCl_3) [δ , ppm]: 8.54 (d, 2H, H_a), 7.97 (d, 2H, H_d), 7.57 (m, 2H, H_c), 7.12 (m, 2H, H_b), 3.86 (s, 4H, H_f), 2.35 (s, 6H, H_e). $^{13}\text{C NMR}$ (125 MHz, CDCl_3) [δ , ppm]: 167.4 (C_i), 157.7 (C_p), 148.5 (C_a), 136.4 (C_c), 122.1 (C_b), 120.9 (C_d), 52.8 (C_f), 14.9 (C_e). IR $\nu(\text{cm}^{-1})$: 3356, 3324, 3297, 3051, 3002, 2972, 2929, 2872, 1697, 1638, 1585, 1566, 1465, 1430, 1357, 1344, 1297, 1282, 1238, 1149, 1135, 1083, 1045, 993, 957, 779, 745, 700, 620, 588, 550, 403. LR-ESI-MS: m/z 289.12 $[\text{M}+\text{Na}]^+$ $\text{C}_{16}\text{H}_{18}\text{N}_4\text{Na}$.

L2m: Yield: 2.600 g, 83%. UV-Vis (CH_3OH ; λ_{max} , nm): 231.0, 261.0, 264.5 (sh). $^1\text{H NMR}$ (500 MHz, CDCl_3) [δ , ppm]: 8.52 (d, 2H, H_a), 7.96 (d, 2H, H_d), 7.58 (m, 2H, H_c), 7.15 (m, 2H, H_b), 3.69 (t, 4H, H_f), 3.42 (pent, 2H, H_g), 2.34 (m, 6H, H_e). $^{13}\text{C NMR}$ (125 MHz, CDCl_3) [δ , ppm]: 166.9 (C_i), 157.4 (C_p), 148.7 (C_a), 136.3 (C_c), 122.1 (C_b), 121.1 (C_d), 50.2 (C_f), 37.8 (C_g), 13.7 (C_e). IR $\nu(\text{cm}^{-1})$: 3372, 3350, 3325, 3308, 3052, 3002, 2930, 2866, 1698, 1637, 1585, 1565, 1464, 1431, 1355, 1298, 1283, 1239, 1203, 1150, 1117, 1091, 1044, 993, 975, 900, 782, 744, 719, 589, 576, 542, 499, 461, 405. LR-ESI-MS: m/z 303.14 $[\text{M}+\text{Na}]^+$ $\text{C}_{17}\text{H}_{20}\text{N}_4\text{Na}$.

L5m: Yield: 0.975 g, 89%. UV-Vis (CH_3OH ; λ_{max} , nm): 220.0 (sh), 262.0, 268.0 (sh), 299.0. $^1\text{H NMR}$ (400 MHz, CDCl_3) [δ , ppm]: 8.56 (d, 2H, H_a), 7.97 (d, 2H, H_d), 7.56 (t, 2H, H_c), 7.16 (m, 2H, H_b), 3.87 (m, 2H, H_f), 2.37 (m, 6H, H_e), 1.94 and 1.72 (m, 4H and 4H, H_g and H_h). IR $\nu(\text{cm}^{-1})$: 3053, 3005, 2930, 2857, 1698, 1666, 1584, 1567, 1465, 1434, 1357, 1296, 1282, 1238, 1149, 1100, 1043, 995, 954, 897, 778, 732, 701, 622, 589, 404. HR-ESI-MS: m/z 319.1919 $[\text{M}]^+$ calculated for $\text{C}_{20}\text{H}_{23}\text{N}_4$ 319.1923.

2.3.6 Synthesis of *N,N*-bis[(pyridin-2-yl)ethylene] 1,3-diaminopropan-2-ol (L3m)

To a solution of 2-acetylpyridine (0.75 mL, 6.66 mmol) in absolute ethanol (10 mL), was added dropwise 1,3-diaminopropan-2-ol (0.30 g, 3.33 mmol) in absolute ethanol (10 mL). The resulting solution was heated at reflux for a period of 9 hours and thereafter cooled to room temperature. The cooled solution was passed through a column of aluminium oxide with DCM as the eluting solvent to remove any traces of starting material. The solvent was removed and the resulting yellow-brown oil was collected.

Yield: 0.611 g, 62%. *UV-Vis* (CH_3OH ; λ_{max} , nm): 231.0, 261.0, 266. (sh). $^1\text{H NMR}$ (400 MHz, CDCl_3) [δ , ppm]: 8.58 (d, 2H, H_a), 7.80 (d, 2H, H_d), 7.67 (t, 2H, H_c), 7.16 (m, 2H, H_b), 5.46 (s, O-H), 4.37 (m, 1H, H_g), 3.71 (m, 4H, H_f), 2.40 (s, 6H, H_e). *IR* $\nu(\text{cm}^{-1})$: 3291, 3051, 3003, 2974, 2924, 2870, 1697, 1637, 1586, 1566, 1465, 1430, 1358, 1283, 1239, 1174, 1152, 1093, 1044, 993, 957, 897, 857, 827, 782, 732, 700, 621, 547, 493, 404. *LR-ESI-MS*: m/z 319.13 [$\text{M}+\text{Na}$] $^+$ $\text{C}_{17}\text{H}_{20}\text{N}_4\text{ONa}$.

2.3.7 Synthesis of *N,N*-bis[(pyridin-2-yl)ethylene]1,3-diamino-2,2-dimethylpropane (L4m)¹⁷⁵

To a solution of 2-acetylpyridine (2.25 mL, 20 mmol) in methanol (20 mL), was added dropwise 1,3-diamino-2,2-dimethylpropane (0.84 g, 10 mmol) in methanol (20 mL). The resulting solution was heated at reflux for a period of 8 hours and thereafter cooled to room temperature. The solution was dried by the addition of anhydrous MgSO_4 , which was subsequently removed by filtration, washing with dichloromethane (~ 10 mL). When solvent was removed from the filtrate an orange oil was obtained.

Yield: 2.723 g, 89%. *UV-Vis* (CH_3OH ; λ_{max} , nm): 259.0 (sh), 266.0, 280.0 (sh), 299.0. $^1\text{H NMR}$ (500 MHz, CDCl_3) [δ , ppm]: 8.56 (d, $J = 4.5$, 2H, H_a), 7.73 (d, $J = 7.9$, 2H, H_d), 7.65 (t of d, $J = 7.5$, 1.8, 2H, H_c), 7.14 (t of d, $J = 6.1$, 1.3, 2H, H_b), 2.52 (d, $J = 13.1$, 2H, H_f), 2.38 (d, $J = 13.0$, 2H, H_i), 1.38 (s, 6H, H_e), 1.11 (s, 6H, H_h). $^{13}\text{C NMR}$ (125 MHz, CDCl_3) [δ , ppm]: 163.6 (C_i), 155.7 (C_p), 148.9 (C_a), 136.6 (C_c), 127.0 (C_b), 121.6 (C_d), 71.0 (C_g), 53.2 (C_f), 31.6 (C_e), 23.5 (C_h). *IR* $\nu(\text{cm}^{-1})$: 3323, 3315, 3052, 3004, 2950, 2924, 2902, 2864, 1699, 1641, 1587, 1567, 1465, 1429, 1384, 1365, 1297, 1283, 1239, 1201, 1150, 1097, 1045, 993, 953, 909, 865, 834, 781, 743, 719, 645, 621, 574, 509, 491, 420, 404. *HR-ESI-MS*: m/z 309.2076 [M] $^+$ calculated for $\text{C}_{19}\text{H}_{25}\text{N}_4$ 309.2079.

2.3.8 Synthesis of *N,N*-bis[(pyridin-2-yl)methylene]1,2-diaminophenylene (L6m)

To a solution of 2-acetylpyridine (1.04 mL, 9.25 mmol) dissolved in absolute ethanol (20 mL), was added dropwise a solution of 1,2-diaminophenylene (0.50 g, 4.62 mmol) in absolute ethanol (10 mL). The resulting solution was heated at reflux for a period of 7 hours and thereafter cooled to room temperature. The solution was dried by the addition

of anhydrous MgSO_4 , which was subsequently removed by filtration. The filtrate was concentrated to afford an orange-yellow oil which was redissolved in diethyl ether. 2-Aethylpyridine (0.425 mL, 3.80 mmol) was added to the reaction mixture which was then heated to reflux for a further 14 hours. A dark, shiny mass was collected by evaporation.

Yield: 1.297 g, 89%. *UV-Vis* (CH_3OH ; λ_{max} , nm): 255.0, 331.0 (sh), 426.0 (sh). $^1\text{H NMR}$ (500 MHz, CDCl_3) [δ , ppm]: 8.79 (d, $J = 4.4$, 2H, H_a), 8.60 (d, $J = 8.0$, 2H, H_d), 8.16 (m, 2H, H_g), 7.90 (t of d, $J = 7.7$, 1.8, 2H, H_c), 7.79 (m, 2H, H_h), 7.41 (t of d, $J = 4.8$, 1.1, 2H, H_b), 2.63 (s, 2H, H_e). $^{13}\text{C NMR}$ (125 MHz, CDCl_3) [δ , ppm]: 163.7 (C_i), 154.6 (C_p), 149.4 (C_a), 141.8 (C_f), 137.2 (C_c), 130.1 (C_h), 129.7 (C_g), 124.6 (C_b), 122.1 (C_d), 26.4 (C_e). *IR* $\nu(\text{cm}^{-1})$: 3352, 3064, 2973, 2926, 2893, 1696, 1649, 1613, 1587, 1569, 1467, 1452, 1437, 1359, 1299, 1283, 1239, 1151, 1087, 1045, 995, 956, 879, 804, 780, 743, 623, 590, 495, 430, 395. *HR-ESI-MS*: m/z 337.1427 $[\text{M}+\text{Na}]^+$ calculated for $\text{C}_{20}\text{H}_{18}\text{N}_4\text{Na}$ 337.1429.

2.3.9 Synthesis of *N,N*-bis[phenyl(pyridin-2-yl)methylene]diamine

Where diamine = 1,2-diaminoethane (**L1b**)¹⁸⁹ or 1,3-diaminopropane (**L2b**).¹⁸⁹

A solution of 2-benzoylpyridine (1.00 g, 5.46 mmol) was stirred with the respective diamine (2.73 mmol) in absolute ethanol (15 mL). The resulting mixture was heated at reflux for 7 hours and thereafter cooled to room temperature. On prolonged standing the solutions both produced white precipitates which were filtered and washed with diethyl ether (**L1b** and **L2b**).[‡] The white crystals isolated from the reaction mixture of **L1b** contained a mixture of **L1b** and **L1bh**.

L1b: Yield: 0.537 g, 50%. *UV-Vis* (CH_3OH ; λ_{max} , nm): 248.0. $^1\text{H NMR}$ (500 MHz, $\text{DMSO}-d_6$) [δ , ppm]: 8.47 (d, $J = 4.5$ 2H, H_a), 8.10 (d, $J = 7.8$, 2H, H_d), 7.89 t, $J = 7.8$, 2H, H_c), 7.46 (m, 6H, $\text{H}_{e3,4,5}$), 7.41 (q, $J = 6.2$, 2H, H_b), 7.17 (d, $J = 8.0$, 4H, $\text{H}_{e2,6}$), 3.74 (s, 4H, H_f). $^{13}\text{C NMR}$ (125 MHz, $\text{DMSO}-d_6$) [δ , ppm]: 168.9 (C_i), 157.4 (C_p), 148.8 (C_a), 137.2 (C_{e1}), 137.0 (C_c), 128.7 ($\text{C}_{e3,4,5}$), 128.5 (C_b), 128.4 ($\text{C}_{e2,6}$), 122.1 (C_d), 54.9 (C_f). *IR* $\nu(\text{cm}^{-1})$: 3079, 3052, 3025, 3007, 2940, 2908, 2831, 1665, 1623, 1583, 1465, 1442, 1434, 1280, 1247, 1180, 1153, 1075, 1047, 1017, 992, 954, 914, 902, 800, 777, 760, 741, 727, 703,

[‡] The ether filtrates produced the cyclised imidazole- or hexahydropyrimidine-containing bidentate ligands on standing. See 2.3.13 c) for characterisation details.

685, 664, 622, 568, 496, 461, 409. *HR-ESI-MS*: m/z 413.1734 $[M+Na]^+$ calculated for $C_{26}H_{22}N_4Na$ 413.1742.

L2b: *Yield*: 0.067 g, 6%. *UV-Vis* (CH_3OH ; λ_{max} , nm): 250.0. 1H NMR (500 MHz, $CDCl_3$) [δ , ppm]: 8.57 (d, $J = 3.8$, 2H, H_a), 8.09 (d, $J = 7.6$, 2H, H_d), 7.92 (t, $J = 8.1$, 2H, H_c), 7.42 (m, 6H, $H_{e3,4,5}$), 7.25 (m, 2H, H_b), 7.18 (d, $J = 7.0$, 4H, $H_{e2,6}$), 3.57 and 3.49 (m, 4H, H_f), 2.13 (m, 2H, H_g). ^{13}C NMR (125 MHz, $CDCl_3$) [δ , ppm]: 168.3 (C_i), 157.6 (C_p), 149.0 (C_a), 136.7 (C_c), 136.4 (C_{e1}), 128.3 ($C_{e3,4,5}$), 123.8 (C_b), 122.0 ($C_{e2,6}$), 122.8 (C_d), 52.2 and 51.5 (C_f), 32.7 (C_g). *IR* $\nu(cm^{-1})$: 3051, 3023, 3005, 2984, 2926, 2896, 2878, 2861, 1662, 1627, 1582, 1567, 1462, 1446, 1431, 1379, 1353, 1308, 1282, 1245, 1157, 1131, 1105, 1092, 1074, 1046, 1028, 1009, 981, 939, 909, 859, 818, 772, 744, 698, 650, 626, 599, 584, 516, 401. *HR-ESI-MS*: m/z 427.1900 $[M+Na]^+$ calculated for $C_{27}H_{24}N_4Na$ 427.1899.

2.3.10 Synthesis of *N,N*-bis[phenyl(pyridin-2-yl)methylene] diamine

Where diamine = 1,3-diaminopropan-2-ol (**L3b**) or 1,3-diamino-2,2-dimethylpropane (**L4b**).

A solution of 2-benzoylpyridine (1.00 g, 5.46 mmol) was stirred with the respective diamine (1,3-diaminopropan-2-ol (0.25 g, 2.73 mmol) or 2-dimethyl-1,3-propanediamine (0.28 g, 2.73 mmol)) in absolute ethanol (10 mL). The resulting mixture was heated at reflux for 7 hours and thereafter cooled to room temperature. The solvent was removed from the **L3b** reaction mixture and the resulting oil was redissolved in DCM and cold hexane was added. The resulting mixture was decanted leaving the residue (found to contain mostly the cyclised hexahydropyrimidine-containing bidentate ligand) behind. The dichloromethane was evaporated and the yellow oil was collected and weighed. On standing the solution of **L4b** produced a white crystalline solid that was filtered off.[§] The remaining solution was collected and additional 2-benzoylpyridine (0.41 g, 2.24 mmol) was added. The mixture was heated at reflux in absolute ethanol (15 mL) for 13 hours. A crystalline pale yellow solid was collected by filtration and washed with diethyl ether.

[§] The white crystals were the cyclised hexahydropyrimidine-containing bidentate ligand (**L4bh**). See 2.3.13 d) for characterisation details.

L3b: Yield: ~ 0.8 g, ~ 70%. *UV-Vis* (CH_3OH ; λ_{max} , nm): 255.0. $^1\text{H NMR}$ (500 MHz, CDCl_3) [δ , ppm]: 8.56 (d, $J = 4.8$ 2H, H_a), 8.01 (d, $J = 7.8$, 2H, H_d), 7.70 (t, $J = 7.9$, 2H, H_c), 7.39 (m, 6H, $\text{H}_{e3,4,5}$), 7.29 (t, $J = 7.2$, 2H, H_b), 7.07 (m, $J = 8.0$, 4H, $\text{H}_{e2,6}$), 5.88 (s, 1H, O-H), 4.48 (m, 1H, H_g), 3.48 and 3.18 (m, 3.4, 4H, H_f). $^{13}\text{C NMR}$ (125 MHz, CDCl_3) [δ , ppm]: 167.6 (C_i), 157.3 (C_p), 148.9 (C_a), 136.3 (C_c), 136.1 (C_{e1}), 128.2 ($\text{C}_{e3,4,5}$), 123.9 (C_b), 122.6 ($\text{C}_{e2,6}$), 122.5 (C_d), 77.5 (C_g), 57.8 (C_f). *IR* $\nu(\text{cm}^{-1})$: 3308, 3298, 3055, 3005, 2924, 1662, 1630, 1583, 1567, 1466, 1447, 1432, 1302, 1282, 1245, 1157, 1093, 1047, 1028, 993, 940, 823, 798, 770, 746, 697, 651, 616, 571, 535, 402. *HR-ESI-MS*: m/z 443.1853 $[\text{M}+\text{Na}]^+$ calculated for $\text{C}_{27}\text{H}_{24}\text{N}_4\text{ONa}$ 443.1848.

L4b: Yield: 0.425 g, 36%. *UV-Vis* (CH_3OH ; λ_{max} , nm): 251.0. $^1\text{H NMR}$ (500 MHz, CDCl_3) [δ , ppm]: 8.52 (d, $J = 4.5$ 2H, H_a), 8.07 (d, $J = 7.7$, 2H, H_d), 7.71 (m, 2H, H_c), 7.41 (m, 6H, $\text{H}_{e3,4,5}$), 7.23 (t, $J = 6.8$, 2H, H_b), 7.16 (m, 4H, $\text{H}_{e2,6}$), 3.41 (d, $J = 1.6$, 4H, H_f), 1.04 (s, 6H, H_h). $^{13}\text{C NMR}$ (125 MHz, CDCl_3) [δ , ppm]: 168.0 (C_i), 158.0 (C_p), 148.7 (C_a), 136.3 (C_{e1}), 136.0 (C_c), 128.0 ($\text{C}_{e2,3,4,5,6}$), 123.7 (C_b), 122.1 (C_d), 62.2 (C_f), 37.8 (C_g), 24.7 (C_h). *IR* $\nu(\text{cm}^{-1})$: 3080, 3057, 3045, 3021, 3000, 2972, 2949, 2897, 2876, 2831, 1626, 1583, 1564, 1490, 1465, 1447, 1425, 1381, 1351, 1314, 1296, 1281, 1243, 1211, 1176, 1149, 1092, 1076, 1047, 1024, 992, 961, 942, 890, 846, 793, 777, 749, 694, 649, 616, 602, 509, 463, 433, 400. *HR-ESI-MS*: m/z 455.2214 $[\text{M}+\text{Na}]^+$ calculated for $\text{C}_{29}\text{H}_{28}\text{N}_4\text{Na}$ 455.2212.

2.3.11 Synthesis of *N,N'*-bis[phenyl(pyridin-2-yl)methylene]-1,2-diaminocyclohexane (L5b)

A solution of 2-benzoylpyridine (1.24 g, 6.8 mmol) and *cis*-1,2-diaminocyclohexane (0.40 mL, 3.40 mmol) were stirred in absolute ethanol (10 mL). The resulting mixture was heated at reflux for 29 hours. After being cooled to room temperature fluffy pale brown needles were collected and washed with diethyl ether.** The filtrate was analysed and found to contain trace amounts of **L5b**.

LR-ESI-MS: m/z 467.21 $[\text{M}+\text{Na}]^+$ $\text{C}_{30}\text{H}_{28}\text{N}_4\text{Na}$.

** The pale brown crystals were found to be the cyclised imidazole-containing bidentate ligand, **L5bh**. See 2.3.13 e) for characterisation details.

2.3.12 Synthesis of *N,N'*-bis[phenyl(pyridin-2-yl)methylene]-1,2-diaminophenylene (L6b)

A solution of 2-benzoylpyridine (1.69 g, 9.25 mmol) was stirred with 1,2-diaminophenylene (0.50 g, 4.62 mmol) in absolute ethanol (20 mL). The resulting mixture was heated at reflux for 7 hours and thereafter cooled to room temperature. The solution was dried by the addition of anhydrous MgSO_4 , which was subsequently removed by filtration. The concentrated orange-red oil was redissolved in diethyl ether and on standing it produced a yellow solid which was collected.^{††} 2-Benzoylpyridine (0.25 g, 1.36 mmol) was added to the filtrate and then heated at reflux for a further 20 hours. A single product has not yet been isolated.

LR-ESI-MS: m/z (majority) 296.11 $[\text{M}+\text{Na}]^+$ $\text{C}_{18}\text{H}_{15}\text{N}_3\text{Na}$ (**L6bh**); (small amount) 461.17 $[\text{M}+\text{Na}]^+$ $\text{C}_{30}\text{H}_{22}\text{N}_4\text{Na}$ (**L6b**).

2.3.13 Characterisation data for the cyclised hexahydro-pyrimidine- and imidazole-containing bidentate ligands

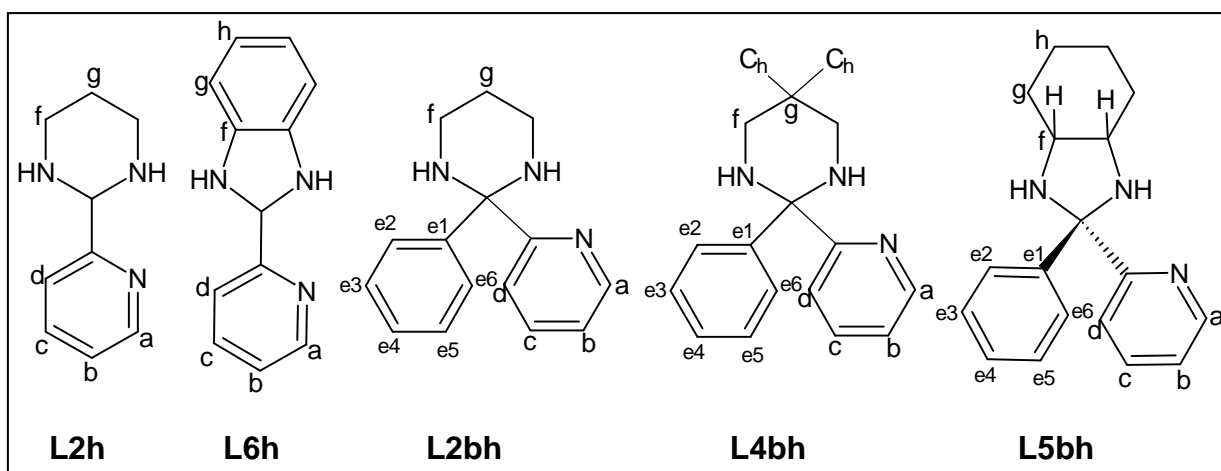


Figure 2.2: Labeled structures of the cyclised hexahydropyrimidine- and imidazole-containing bidentate ligands.

^{††} The yellow powder was found to be majority phenylenediamine with trace amounts of **L6bh**.

a) 2-pyridin-2-yl-1,4,5,6-tetrahydropyrimidine (L2h)

Pale yellow crystals formed on standing of the orange oil of **L2**. Yield: ~ 5%. UV-Vis (CH_3OH ; λ_{max} , nm): 259.0, 346.0. 1H NMR (500 MHz, $CDCl_3$) [δ , ppm]: 8.57 (d, J = 5.0, 1H, H_a), 7.75 (d of t, J = 7.9, 1.1, 1H, H_d), 7.69 (t of d, J = 7.7, 1.9, 1H, H_c), 7.15 (t of d, J = 6.2, 1.2, 1H, H_b), 2.53 (d, J = 13.0, 2H, H_f), 2.40 (d, J = 13.0, 2H, H_f), 1.12 (m, 1H, N-H), 1.41 (m, 2H, H_g). ^{13}C NMR (125 MHz, $CDCl_3$) [δ , ppm]: 163.6 (C_p), 153.6 (C_i), 149.0 (C_a), 136.6 (C_c), 121.8 (C_b), 121.5 (C_d), 53.3 (C_f), 31.6 (C_g). IR $\nu(cm^{-1})$: 3336, 3265, 2946, 2867, 1647, 1596, 1572, 1462, 1435, 1359, 1317, 1229, 1192, 1152, 1104, 1012, 1001, 958, 883, 819, 767, 622, 502, 465, 402. LR-ESI-MS: m/z 186.12 [$M+Na$] $^+$ $C_9H_{13}N_3Na$.

b) 2-pyridin-2-yl-1H-benzimidazole (L6h)

White crystalline material formed on the sides of the flask from the reaction mixture of **L6**. Yield: 0.349 g, 47%. UV-Vis (CH_3OH ; λ_{max} , nm): 220.0 (sh), 239.5, 309.5, 322.0 (sh). 1H NMR (500 MHz, $CDCl_3$) [δ , ppm]: 10.87 (s, 1H, N-H), 8.64 (d, J = 5.0, 1H, H_a), 8.47 (d, J = 7.9, 1H, H_d), 7.87 (t of d, J = 7.7, 1.6, 1H, H_c), 7.67 (s, 2H, H_f), 7.37 (t of d, J = 6.2, 1.1, 1H), 7.30 (m, 2H, H_g). ^{13}C NMR (125 MHz, $CDCl_3$) [δ , ppm]: 150.7 (C_e), 149.1 (C_a), 148.2 (C_p), 137.3 (C_c), 124.6 (C_b), 123.5 ($C_{f,g}$), 121.7 (C_d). IR $\nu(cm^{-1})$: 3064, 3047, 2965, 2891, 2774, 2609, 2511, 2349, 1594, 1568, 1443, 1401, 1315, 1280, 1103, 995, 961, 745, 702, 666, 426. HR-ESI-MS: m/z 218.0695 [$M+Na$] $^+$ calculated for $C_{12}H_9N_4Na$ 218.0694.

c) 2-phenyl-2-pyridin-2-ylhexahydropyrimidine (L2bh)

A white crystalline solid precipitated out of the filtrate for **L2b** on standing. Yield: 0.210 g, 32%. UV-Vis (CH_3OH ; λ_{max} , nm): 250. 1H NMR (500 MHz, $CDCl_3$) [δ , ppm]: 8.55 (d of q, J = 4.8, 0.9, 1H, H_a), 7.72 (d of d, J = 8.5, 1.3, 2H, $H_{e2,6}$), 7.56 (t of d, J = 7.8, 1.8, 1H, H_c), 7.37 (d, J = 8.1, 1H, H_d), 7.34 (t of d, J = 6.8, 1.6, 2H, $H_{e3,5}$), 7.22 (t, J = 7.3, 1H, H_{e4}), 7.08 (q of d, J = 6.1, 2.7, 1.1, 1H, H_b), 3.01 (m, 4H, H_f), 2.60 (s, 2H, N-H), 1.58 (m, 1H, H_g), 1.49 (m, 1H, H_g). ^{13}C NMR (125 MHz, $CDCl_3$) [δ , ppm]: 163.8 (C_p), 148.9 (C_a), 143.7 (C_{e1}), 136.7 (C_c), 128.5 ($C_{e3,5}$), 127.6 ($C_{e2,6}$), 127.1 (C_{e4}), 121.9 (C_b), 121.7 (C_d), 75.3 (C_i), 41.3 (C_f), 27.5 (C_g). IR $\nu(cm^{-1})$: 3308, 3086 3044 2995, 2939 2921 2903 2862 2833 2791, 2690, 1585, 1569, 1456, 1355, 1220, 1187, 1105, 1074, 1015, 994, 963,

918, 897, 821, 787, 743, 715, 699, 654, 624, 605, 551, 520, 454, 408. *HR-ESI-MS*: m/z 240.1502 $[M]^+$ calculated for $C_{15}H_{19}N_3$ 240.1501.

d) 5,5-dimethyl-2-phenyl-2-pyridin-2-ylhexahydropyrimidine (L4bh)

A white crystalline solid precipitated out of the reaction mixture for **L4b** on standing. *Yield*: 0.111 g, 15%. *UV-Vis* (CH_3OH ; λ_{max} , nm): 203, 254. 1H NMR (500 MHz, $CDCl_3$) [δ , ppm]: 8.56 (d, $J = 4.8$, 1H, H_a), 7.79 (d, $J = 7.2$, 2H, $H_{e2,6}$), 7.53 (t, $J = 7.8$, 1H, H_c), 7.34 (t, $J = 7.6$, 2H, $H_{e3,5}$), 7.26 (t, $J = 7.3$, 1H, H_{e4}), 7.19 (d, $J = 7.7$, 1H, H_d), 7.10 (t of d, $J = 6.1$, 1.1, 1H, H_b), 2.71, (d, $J = 13.4$, 2H, H_f), 2.62, (d, $J = 13.5$, 2H, H_f), 2.76 (s, 2H, N-H), 1.04 (s, 3H, H_h), 0.80 (s, 3H, H_h). ^{13}C NMR (125 MHz, $CDCl_3$) [δ , ppm]: 163.1 (C_p), 148.8 (C_a), 143.7 (C_{e1}), 136.6 (C_c), 128.4 ($C_{e3,5}$), 128.2 ($C_{e2,6}$), 127.2 (C_{e4}), 121.0 ($C_{b,d}$), 75.2 (C_i), 53.3 (C_f), 27.8 (C_g), 23.9 (C_h). *IR* $\nu(cm^{-1})$: 3320, 3059, 3045, 2996, 2975, 2946, 2860, 2831, 1583, 1565, 1491, 1454, 1385, 1365, 1317, 1277, 1226, 1195, 1142, 1106, 1090, 1080, 1029, 994, 947, 913, 900, 843, 788, 753, 712, 702, 668, 622, 598, 575, 516, 491, 468, 424, 412, 838. *HR-ESI-MS*: m/z 268.1812 $[M]^+$ calculated for $C_{17}H_{22}N_3$ 268.1814.

e) 2-phenyl-2-pyridin-2-yloctahydro-1-benzimidazole (L5bh)

Pale brown, fine needles formed on evaporation of the filtrate of the **L5b** solution. *Yield*: 0.490 g, 56%. *UV-Vis* (CH_3OH ; λ_{max} , nm): 252.0. 1H NMR (500 MHz, $CDCl_3$) [δ , ppm]: 8.53 (d, $J = 4.9$, 1H, H_a), 8.48 (d, $J = 4.8$, 1H, H_a'), 7.94 (d, $J = 7.8$, 1H, H_d), 7.91 (d, $J = 7.7$, 1H, H_d'), 7.71 (t, $J = 7.7$, 4H, $H_{e2,6}$), 7.64 (t, $J = 7.7$, 1H, H_c), 7.59 (t, $J = 6.5$, 1H, H_c'), 7.30 (q, $J = 7.7$, 7.4, 4H, $H_{e3,5}$), 7.20 (q, $J = 6.5$, 5.7, 4H, H_{e4}), 7.12 (d, $J = 6.0$, 1H, H_b), 7.08 (d, $J = 6.0$, 1H, H_b'), 3.23 (m, 2H, H_f), 3.15 (m, 2H, H_f'), 2.54 (s, 4H, N-H), 1.69 (m, 4H, H_g), 1.62 (m, 4H, H_g'), 1.47 (m, 4H, H_h), 1.32 (m, 4H, H_h'). ^{13}C NMR (125 MHz, $CDCl_3$) [δ , ppm]: 166.6 (C_i), 165.3 (C_i'), 156.1 (C_{p1}), 155.2 (C_{p2}), 148.4 (C_a'), 147.5 (C_a), 138.9 (C_{e1}), 136.9 (C_c), 136.3 (C_{e1}'), 128.3 ($C_{e3,5}$), 127.0 (C_4), 126.4 ($C_{e2,6}$), 122.0 (C_b), 121.5 (C_b'), 120.1 (C_d), 57.6 (C_f), 56.8 (C_f'), 28.6 (C_g), 27.6 (C_g'), 21.9 (C_h), 21.7 (C_h'). *IR* $\nu(cm^{-1})$: 3346, 3311, 3051, 3043, 3029, 3002, 2935, 2925, 2884, 2852, 1583, 1567, 1488, 1431, 1394, 1351, 1310, 1240, 1213, 1156, 1133, 1100, 1083, 1059, 1026, 993, 963, 935, 927, 915, 891, 859, 847, 814, 781, 757, 748, 723, 702, 672, 627, 606, 530, 481, 452, 400. *HR-ESI-MS*: m/z 280.1808 $[M]^+$ calculated for $C_{18}H_{22}N_3$ 280.1814.

2.4 Platinum Group Metal complexes

2.4.1 Metallation with PGMs:

The ligand (0.3 mmol) was dissolved in 1 mL acetonitrile and a metal salt (either $K_2[PtCl_4]$ or $K_2[PdCl_4]$) solution dissolved in 1.5 mL of distilled water (1:1 ratio with the ligand) was added dropwise. $AgSbF_6$, $AgBF_4$ or $AgPF_6$ (1.2 mmol) was added dropwise to the solution as a suspension in acetonitrile (5 mL). The mixture was heated at reflux for more than 30 hours. After cooling to room temperature overnight the solution was removed from the silver chloride solid by cannula transfer. The solution was either left to slowly evaporate or was put into test tubes and layered with ethanol. Solid that precipitated that was not crystalline was redissolved in 2-methoxy ethanol and put in test tubes layering with ether.

2.4.2 Template Metallation:

The metal salt (0.51 mmol, either $K_2[PtCl_4]$ or $K_2[PdCl_4]$) was dissolved in 1–2 mL distilled water and 3 mL acetonitrile. The diamine (0.46 mmol) was dissolved in 4 mL acetonitrile and added dropwise to the metal solution. The reaction mixture was then heated at reflux for a period of 2 hours. LC-MS was used to confirm synthesis of the desired product. The aldehyde (0.92 mmol) was added and reflux was continued for a further 6 hours. It was sometimes necessary for additional aldehyde to be added and subsequently additional reflux.

2.4.3 Characterisation of the metal complexes

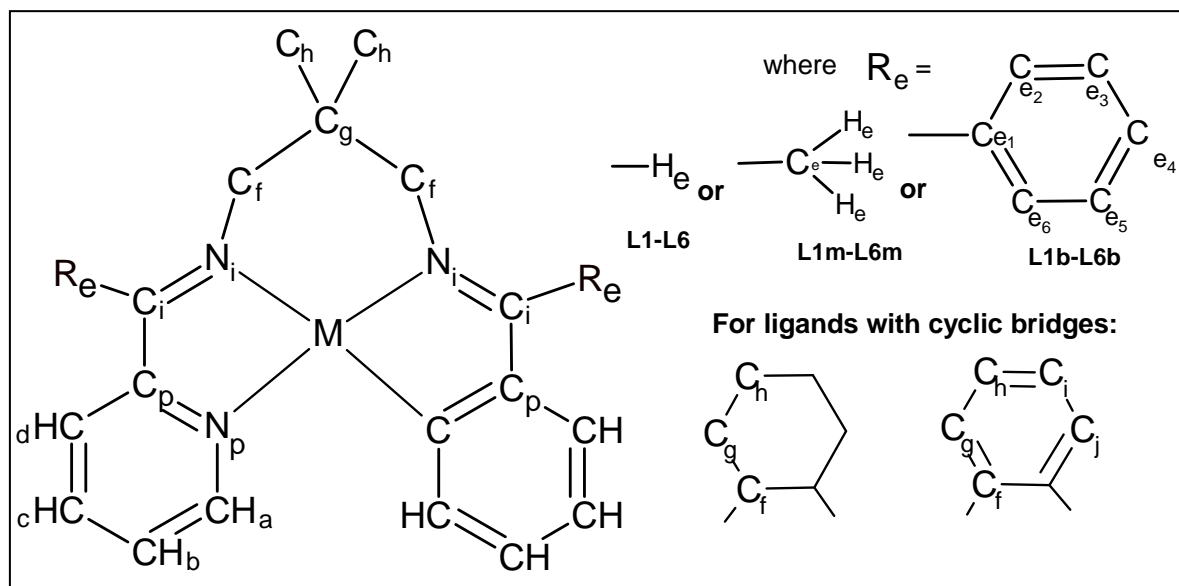


Figure 2.3: The basic metal complex structure showing the notation used for labelling the atoms, where M = Pt(II) or Pd(II).

PtL1 [Pt{N,N'-bis[(pyridin-2-yl)methylene]1,2-diaminoethane}](PF₆)₂

UV-vis (CH₃CN) [λ_{max} , nm (ϵ , M⁻¹cm⁻¹): 200 (14.6 × 10³), 263 (3.8 × 10³), 306 (2.3 × 10³), 365 (1.1 × 10³), 394 (0.8 × 10³), 404 (sh). ¹H NMR (500 MHz, DMSO-d₆) [δ , ppm]: 9.46 (s, 2H, H_e), 8.89 (d, J = 5.5, 2H, H_a), 8.45 (t, J = 7.5, 2H, H_c), 8.25 (d, J = 7.5, 2H, H_d), 8.04 (t, J = 6.9, 2H, H_b), 4.23 (t, J = 5.8, 4H, H_f). ¹³C NMR (125 MHz, DMSO-d₆) [δ , ppm]: 166.3 (C_i), 160.8 (C_p), 150.1 (C_a), 142.2 (C_c), 130.1 (C_b), 129.4 (C_d), 59.7 (C_f). IR ν (cm⁻¹): 3277, 3171, 3085, 3002, 2924, 2856, 1722, 1632, 1603, 1519, 1441, 1365, 1329, 1294, 1239, 1055, 878, 836, 764, 696, 682, 627, 556, 520, 472, 435, 422.

PdL1 [Pd{N,N'-bis[(pyridin-2-yl)methylene]1,2-diaminoethane}](PF₆)₂

UV-Vis (CH₃CN) [λ_{max} , nm (ϵ , M⁻¹cm⁻¹): 200 (4.7 × 10³), 270 (sh), 344 (0.8 × 10³), 418 (0.4 × 10³). ¹H NMR (500 MHz, DMSO-d₆) [δ , ppm]: 8.99 (d, J = 5.3, 2H, H_a), 8.70 (s, 2H, H_e), 8.31 (t, J = 7.7, 2H, H_c), 8.11 (d, J = 7.6, 2H, H_d), 7.88 (t, J = 6.8, 2H, H_b), 4.17 (s, 4H, H_f). ¹³C NMR (125 MHz, DMSO-d₆) [δ , ppm]: 168.1 (C_i), 156.3 (C_p), 150.5 (C_a), 142.1 (C_c), 129.4 (C_b), 129.1 (C_d), 58.4 (C_f). IR ν (cm⁻¹): 3307, 3116, 2916, 2849, 1718, 1664, 1619, 1606, 1535, 1463, 1425, 1329, 973, 883, 849, 760, 719, 681, 625, 518, 469, 400, 381.

PtL2 [Pt{N,N'-bis[(pyridin-2-yl)methylene]1,3-diaminopropane}](PF₆)₂

UV-Vis (CH₃CN) [λ_{max} , nm (ϵ , M⁻¹cm⁻¹): 202.0, 224.0 (sh), 273.5 (7.1 × 10³), 284.5 (5.6 × 10³), 306.5 (4.4 × 10³), 324.0 (3.6 × 10³), 346.5 (2.3 × 10³), 371.0 (2.2 × 10³). ¹H NMR (500 MHz, CD₃CN) [δ , ppm]: 9.04 (t, *J* = 1.9, 2H, H_e), 8.92 (d, *J* = 5.6, 2H, H_a), 8.50 (t of d, *J* = 7.7, 1.3, 2H, H_c), 8.27 (d, *J* = 7.7, 2H, H_d), 8.07 (t of d, *J* = 6.7, 1.6, 2H, H_b), 4.11 (t of d, *J* = 5.3, 1.9, 4H, H_f), 2.34 (m, 2H, H_g). ¹³C NMR (125 MHz, CD₃CN) [δ , ppm]: 173.8 (C_i), 156.4 (C_p), 153.1 (C_a), 144.8 (C_c), 131.1 (C_b), 130.9 (C_d), 57.3 (C_f), 29.9 (C_g). ¹⁹⁵Pt NMR (107 MHz at 11.7 T, DMSO-*d*₆) [δ , ppm]: -2810. IR ν (cm⁻¹): 3366, 3269, 3117, 3090, 2946, 2907, 1632, 1605, 1486, 1447, 1405, 1354, 1316, 1238, 1166, 1128, 1054, 1032, 967, 950, 899, 878, 823, 773, 740, 688, 666, 652, 554, 513, 468, 442, 423, 414, 399.

PdL2 [Pd{N,N'-bis[(pyridin-2-yl)methylene]1,3-diaminopropane}](PF₆)₂

UV-Vis (CH₃CN) [λ_{max} , nm (ϵ , M⁻¹cm⁻¹): 200.0, 215.0, 237.0 (3.0 × 10³), 286.5 (6.5 × 10³), 305.0 (6.8 × 10³). ¹H NMR (500 MHz, CD₃CN) [δ , ppm]: 8.70 (d of d, *J* = 5.6, 1.4, 2H, H_a), 8.61 (t, *J* = 2.0, 2H, H_e), 8.45 (t of d, *J* = 7.8, 1.4, 2H, H_c), 8.19 (d of d, *J* = 7.7, 1.4, 2H, H_d), 7.99 (t of d, *J* = 6.8, 1.5, 2H, H_b), 3.86 (t of d, *J* = 5.5, 2.1, 4H, H_f), 2.27 (m, 2H, H_g). ¹³C NMR (125 MHz, CD₃CN) [δ , ppm]: 173.8 (C_i), 155.7 (C_p), 152.5 (C_a), 144.6 (C_c), 130.9 (C_{b,d}), 56.3 (C_f), 29.6 (C_g). IR ν (cm⁻¹): 3091, 3074, 3057, 3024, 2981, 2947, 1642, 1604, 1485, 1446, 1352, 1316, 1287, 1237, 1202, 1166, 1050, 1027, 970, 957, 903, 878, 826, 775, 740, 650, 555, 511, 485, 469, 451, 428.

PtL4 [Pt{N,N'-bis[(pyridin-2-yl)methylene]1,3-diamino-2,2-dimethylpropane}](PF₆)₂

UV-Vis (CH₃CN) [λ_{max} , nm (ϵ , M⁻¹cm⁻¹): 207.0 (19.3 × 10³), 225.5 (15.5 × 10³), 274.0 (4.0 × 10³), 285.0 (4.2 × 10³), 307.5 (4.5 × 10³), 324.0 (2.9 × 10³), 346.5 (2.9 × 10³), 375.5 (3.7 × 10³). ¹H NMR (400 MHz, D₂O) [δ , ppm]: 9.31 (s, 2H, H_e), 9.14 (d, 2H, *J* = 5.7, H_a), 8.58 (t, *J* = 7.7, 2H, H_c), 8.38 (d, *J* = 7.5, 2H, H_d), 8.16 (t, *J* = 6.4, 2H, H_b), 4.03 (s, 4H, H_f), 1.31 (s, 6H, H_h). ¹³C NMR (125 MHz, D₂O) [δ , ppm]: 173.5 (C_i), 155.7 (C_p), 151.6 (C_a), 143.5 (C_c), 129.6 (C_{b,d}), 65.9 (C_f), 38.1 (C_g), 22.7 (C_h). ¹⁹⁵Pt NMR (107 MHz at 11.7 T, DMSO-*d*₆) [δ , ppm]: -2807. IR ν (cm⁻¹): 3306, 3271, 3089, 2967, 2880, 1604, 1592, 1480, 1463, 1442, 1386, 1338, 1297, 1234, 1169, 1117, 1080, 1060, 1035, 1003, 948, 903, 830, 785, 740, 664, 556, 522, 478, 456, 441, 432, 412.

PdL4 [Pd{N,N'-bis[(pyridin-2-yl)methylene]1,3-diamino-2,2-dimethylpropane}}](PF₆)₂

UV-Vis (CH₃CN) [λ_{max} , nm (ϵ , M⁻¹cm⁻¹): 206.0 (23.1 × 10³), 281.0 (3.0 × 10³), 310.5 (2.7 × 10³). ¹H NMR (500 MHz, D₂O) [δ , ppm]: 8.89 (d, 2H, J = 5.6, H_a), 8.86 (s, 2H, H_e), 8.52 (t, J = 7.8, 2H, H_c), 8.29 (d, J = 7.7, 2H, H_d), 8.07 (t, J = 6.7, 2H, H_b), 3.77 (s, 4H, H_f), 1.27 (s, 6H, H_h). ¹³C NMR (125 MHz, D₂O) [δ , ppm]: 173.4 (C_i), 155.0 (C_p), 150.9 (C_a), 143.2 (C_c), 129.5 (C_{b,d}), 65.0 (C_f), 37.9 (C_g), 22.7 (C_h). *IR* ν (cm⁻¹): 3296, 3253, 3163, 3080, 2962, 2933, 2909, 2877, 1629, 1598, 1568, 1476, 1458, 1439, 1424, 1408, 1384, 1370, 1342, 1330, 1297, 1230, 1194, 1161, 1028, 942, 911, 886, 871, 850, 790, 766, 738, 710, 677, 666, 659, 617, 580, 562, 518, 466, 446, 424.

PtL5 [Pt{N,N'-bis[pyridin-2-yl)methylene]1,2-diaminocyclohexane}}](PF₆)₂

UV-Vis (CH₃CN; λ_{max} , nm): 263.5. *IR* ν (cm⁻¹): 3367, 3261, 2955, 1721, 1634, 1600, 1573, 1470, 1378, 1327, 1295, 1223, 1162, 1096, 1064, 1035, 676, 604, 521, 472.

PdL5 [Pd{N,N'-bis[pyridin-2-yl)methylene]1,2-diaminocyclohexane}}](PF₆)₂

UV-Vis (CH₃CN; λ_{max} , nm): 269.5, 277.0, 306.0, 361.5, 404.5, 434.5. *IR* ν (cm⁻¹): 3332, 3314, 3179, 3098, 3055, 3036, 2984, 2948, 1642, 1604, 1572, 1534, 1509, 1476, 1424, 1322, 1278, 1266, 1195, 1148, 1092, 1058, 857, 817, 758, 718, 683, 670, 624, 569, 560, 522, 473, 425, 411.

Pt(L6h)₂ [Pt{2-pyridin-2-yl-1H-benzimidazole}₂]}](PF₆)₂

UV-Vis (CH₃CN) [λ_{max} , nm (ϵ , M⁻¹cm⁻¹): 206 (2.9 × 10³), 239 (4.2 × 10³), 307 (3.1 × 10³). ¹H NMR (400 MHz, DMSO-d₆) [δ , ppm]: 8.80 (d, 2H, J = 4.8, H_a), 8.35 (d, J = 7.9, 2H, H_d), 8.07 (t of d, J = 7.7, 1.6, 2H, H_c), 7.69 (q, J = 3.2, 2.7, 4H, H_g), 7.60 (t, J = 6.1, 2H, H_b), 7.34 (q, J = 3.1, 4H, H_h). ¹³C NMR (125 MHz, DMSO-d₆) [δ , ppm]: 171.9 (C_p), 150.3 (C_a), 138.5 (C_c), 133.3 (C_f), 126.1 (C_b), 122.6 (C_d), 124.2 (C_h), 115.9 (C_g). *IR* ν (cm⁻¹): 3048, 3011, 3005, 2943, 2907, 2860, 2833, 2778, 2756, 1651, 1614, 1569, 1520, 1489, 1458, 1423, 1404, 1329, 1312, 1257, 1226, 1153, 1108, 1096, 1053, 1096, 1053, 992, 966, 832, 788, 737, 689, 617, 556, 532, 481, 455, 398.

PdL6h' [Pd{N-(pyridin-2-yl)methylene)benzene-1,2-diamine}}](PF₆)₂

UV-Vis (CH₃CN) [λ_{max} , nm (ϵ , M⁻¹cm⁻¹): 200 (4.1 × 10³), 305 (sh), 331 (1.0 × 10³), 341 (0.9 × 10³), 417 (sh). ¹H NMR (400 MHz, DMSO-d₆) [δ , ppm]: 9.09 (d, 1H, J = 5.7, H_a), 8.68 (d, J = 8.4, 1H, H_i), 8.54 (d, J = 6.9, 2H, H_d, H_e), 8.39 (t of d, J = 7.8, 1.5, 1H, H_c), 7.79 (m, 1H, H_b), 7.73 (d, J = 8.3, 1H, H_g), 7.49 (m, 1H, H_h), 7.38 (m, 1H, H_i). ¹³C NMR

(125 MHz, DMSO- d_6) [δ , ppm]: 152.7 (C_p), 150.6 (C_a), 148.1 (C_i), 141.8 (C_c), 133.5 (C_f), 128.0 (C_j), 127.6 (C_b), 126.0 (C_h), 123.8 (C_d), 119.2 (C_j), 113.8 (C_g). IR ν (cm^{-1}): 3066, 3054, 3012, 3005, 2974, 2946, 2902, 2840, 2782, 2750, 1611, 1594, 1583, 1487, 1449, 1440, 1367, 1292, 1270, 1241, 1215, 1189, 1170, 1156, 1111, 1097, 1026, 961, 919, 8353, 780, 768, 740, 665, 618, 554, 544, 509, 467, 422, 393.

PdL4m [Pd{N,N'-bis[(pyridin-2-yl)ethylene]1,3-diamino-2,2-dimethylpropane}}](PF₆)₂

UV-Vis (CH₃CN) [λ_{max} , nm (ϵ , M⁻¹cm⁻¹): 202.5, 217.0, 266.0 (3.8 × 10³), 286.0 (4.1 × 10³), 300.0 (4.1 × 10³). ¹H NMR (400 MHz, CD₃CN) [δ , ppm]: 8.66 (d, 2H, J = 5.6, H_a), 8.45 (t, J = 7.8, 1.4, 2H, H_c), 8.22 (d of d, J = 8.1, 1.2, 2H, H_d), 7.98 (t of d, J = 6.6, 1.4, 2H, H_b), 3.52 (s, 4H, H_f), 2.69 (s, 6H, H_e) 1.26 (s, 6H, H_h). ¹³C NMR (125 MHz, CD₃CN) [δ , ppm]: 182.7 (C_i), 158.1 (C_p), 152.1 (C_a), 144.2 (C_c), 130.9 (C_b), 129.4 (C_d), 61.4 (C_f), 39.8 (C_g), 24.5 (C_h), 18.5 (C_e). IR ν (cm^{-1}): 3099, 3079, 2981, 2975, 2943, 2934, 1623, 1600, 1575, 1467, 1381, 1344, 1264, 1170, 1107, 1029, 877, 823, 780, 745, 664, 652, 585, 555, 466, 422, 389, 383.

PtL1b [Pt{N,N'-bis[phenyl(pyridin-2-yl)methylene]1,2-diaminoethane}}](PF₆)₂

UV-Vis (CH₃CN) [λ_{max} , nm (ϵ , M⁻¹cm⁻¹): 200 (0.8 × 10³), 354 (3.0 × 10³), 368 (2.8 × 10³), 388 (3.3 × 10³). ¹H NMR (400 MHz, DMSO- d_6) [δ , ppm]: 9.36 (d, 2H, J = 5.2, H_a), 8.52 (t of d, J = 7.9, 1.3, 2H, H_c), 8.26 (t of d, J = 6.8, 1.3, 2H, H_b), 7.99 (m, 6H, H_{e,3,4,5}), 7.77 (d, J = 7.6, 2H, H_d), 7.55 (m, 4H, H_{e,2,6}), 4.55 (s, 4H, H_f). ¹³C NMR (125 MHz, DMSO- d_6) [δ , ppm]: 176.5 (C_i), 161.0 (C_p), 153.7 (C_a), 144.1 (C_c), 136.5 (C_{e1}), 131.1 (C_{e,3,4,5}), 130.8 (C_b), 129.9 (C_d), 128.7 (C_{e,2,6}), 60.5 (C_f). IR ν (cm^{-1}): 3094, 3072, 3002, 2960, 2919, 2841, 1667, 1630, 1597, 1579, 1473, 1448, 1362, 1338, 1320, 1284, 1244, 1212, 1173, 1162, 1067, 1028, 1001, 939, 829, 776, 757, 741, 701, 650, 555, 493, 469, 439, 432, 399.

PtL2b [Pt{N,N'-bis[phenyl(pyridin-2-yl)methylene]1,3-diaminopropane}}](PF₆)₂

UV-Vis (CH₃CN) [λ_{max} , nm (ϵ , M⁻¹cm⁻¹): 212 (6.0 × 10³), 235 (sh), 288 (6.0 × 10³), 310 (6.3 × 10³), 354 (5.0 × 10³), 383 (6.1 × 10³). ¹H NMR (400 MHz, CD₃CN) [δ , ppm]: 9.02 (d, 2H, J = 5.8, H_a), 8.40 (t of d, 2H, J = 7.8, 1.3, H_c), 8.11 (t of d, J = 6.8, 1.5, 2H, H_b), 7.77 (m, 6H, H_{e,3,4,5}), 7.62 (d, J = 7.2, 2H, H_d), 7.58 (d, J = 8.2, 4H, H_{e,2,6}), 3.83 (t, J = 5.3, 4H, H_f), 2.19 (m, 2H, H_g). ¹³C NMR (125 MHz, CD₃CN) [δ , ppm]: 180.4 (C_i), 157.4 (C_p), 151.9 (C_a), 143.4 (C_c), 137.6 (C_e), 131.3 (C_d), 129.7 (C_{b,e,3,4,5}), 128.0 (C_{e,2,6}), 54.2 (C_f), 30.1 (C_g). ¹⁹⁵Pt NMR (107 MHz at 11.7 T, CD₃CN) [δ , ppm]: -2825. IR ν (cm^{-1}): 3116, 3101, 3079, 2979, 2918, 1660, 1604, 1575, 1492, 1474, 1441, 1432, 1349, 1318, 1272,

1206, 1171, 1128, 1075, 1035, 1000, 972, 907, 878, 827, 755, 743, 702, 680, 663, 621, 555, 489, 430, 406.

PtL4b [*Pt*{*N,N'*-bis[phenyl(pyridin-2-yl)methylene]1,3-diamino-2,2-dimethylpropane}](PF₆)₂
UV-Vis (CH₃CN) [λ_{max} , nm (ϵ , M⁻¹cm⁻¹): 238 (2.2 × 10³), 243 (sh), 285 (11.0 × 10³), 309 (9.7 × 10³), 354 (4.5 × 10³), 383 (5.9 × 10³). ¹H NMR (400 MHz, CD₃CN) [δ , ppm]: 8.77 (d, 2H, *J* = 4.8, H_a), 8.06 (m, 6H, H_{e,3,4,5}), 7.98 (t, 2H, *J* = 7.6, H_c), 7.62 (d, *J* = 7.3, 2H, H_d), 7.56 (t, *J* = 5.8, 2H, H_b), 7.50 (m, 4H, H_{e2,6}), 2.03 (s, 4H, H_f), 1.27 (s, 6H, H_h). *IR* ν (cm⁻¹): 3283, 3247, 3118, 3067, 2975, 2917, 2850, 1670, 1609, 1534, 1462, 1451, 1426, 1377, 1318, 1293, 1239, 1163, 1099, 1043, 999, 953, 814, 767, 741, 722, 692, 644, 554, 471, 436, 391, 380.

PdL4b [*Pd*{*N,N'*-bis[phenyl(pyridin-2-yl)methylene]1,3-diamino-2,2-dimethylpropane}](PF₆)₂
UV-Vis (CH₃CN) [λ_{max} , nm (ϵ , M⁻¹cm⁻¹): 212 (3.7 × 10³), 270 (sh), 289 (4.2 × 10³). ¹H NMR (400 MHz, CD₃CN) [δ , ppm]: 8.81 (d, 2H, *J* = 5.7, H_a), 8.33 (t of d, *J* = 7.8, 1.3, 2H, H_c), 8.04 (t of d, *J* = 6.7, 1.5, 2H, H_b), 7.77 (m, 6H, H_{e,3,4,5}), 7.53 (d, *J* = 7.3, 2H, H_d), 7.50 (m, 4H, H_{e2,6}), 3.39 (s, 4H, H_f), 1.04 (s, 6H, H_h). ¹³C NMR (125 MHz, CD₃CN) [δ , ppm]: 182.4 (C_i), 158.4 (C_p), 152.4 (C_a), 144.2 (C_c), 133.2 (C_e), 131.1 (C_d), 129.9 (C_{b,e3,4,5}), 128.7 (C_{e2,6}), 63.1 (C_f), 39.8 (C_g), 24.1 (C_h). *IR* ν (cm⁻¹): 3298, 3211, 3110, 2915, 1664, 1585, 1493, 1475, 1446, 1405, 1377, 1345, 1266, 1218, 1164, 1033, 999, 916, 903, 877, 827, 793, 774, 752, 739, 702, 680, 659, 647, 626, 620, 555, 518, 479, 425.

2.5 Discussion of the methods and characterisation

The synthesis of Schiff base ligands is generally a simple procedure, with either only one or very few steps necessary. The methods used to synthesise most of the ligands in this work were adapted from the literature. The original six ligands were chosen due to the availability of their synthons as well as for their similarities and differences in structure. The first and second ligands (**L1** and **L2**, respectively) form the basic structures for the other four ligands by having direct 2-carbon and 3-carbon bridging groups. This is extended by adding a hydroxyl group (**L3**), two methyl groups (**L4**) or a cyclic ring system (**L5** and **L6**). The effect of the added bulk on these bridges can be observed, as well as the consequence of having the 2- or the 3-carbon bridging link.

From here the range was extended by adding groups onto the imine carbon, first a methyl and then a phenyl. The effect that these groups will have on the structure, reactivity and the activity of the ligands was of interest. NMR for the original ligands were all assigned except for **L6**, for which only trace amounts were obtained. Despite obtaining relatively clean LC-MS data for the methyl-substituted ligands (with the ligand being the prominent peak) the NMR data were not as straightforward. It seems that the methyl-ligands generally behaved differently in solution which caused difficulty for the assignment of the NMR data. In the case of **L3m** and **L5m** ^{13}C NMR spectra were not obtained due to poor resolution; however, the assigned ^1H NMR data is presented. The phenyl-substituted ligands showed clean LC-MS spectra and NMR data was assigned for all four of the synthesised phenyl-substituted ligands (**L1b–L4b**), as well as for the cyclised imidazole-containing bidentate ligand **L5bh**. Only trace amounts of the ‘fully-reacted’ bis(imine) ligand (**L5b**) were found in the reaction mixture which could not be isolated. The ligand **L6b** has not been synthesised in this work.

Yields of more than 60% were obtained for all the original six ligands (except for **L6** formed in trace amounts only). The methyl-ligands all had high yields, while the phenyl-ligands did not. This may be explained by the mere bulk of the phenyl-ligands and the presence of unreacted starting material in the methyl-ligand samples. It may also be due to the fact that the phenyl-ligand reactions had a greater tendency to form the cyclised hexahydropyrimidine- or imidazole-containing bidentate ligands. This was also seen for **L2** and **L6** of the original ligands; **L2h** and **L6h**. Crystal structures have been obtained for these cyclised bidentate ligands: **L2h**, **L6h**, **L1bh** and **L2bh** (see Chapter 3), which formed during the syntheses of the full ligands. Once one equivalent of aldehyde was added to the diamine it cyclised before another equivalent of the aldehyde could be added. There seemed little would break the new C–N bond making it a stable (and crystalline) product of some of the reactions. The acyclic single condensation intermediate was not stable and subsequently the equilibrium shifted towards the cyclic structure forming a hexahydropyrimidine or imidazole ring.¹⁷⁵

In an endeavour to avoid these 1:1 ratio bidentate ligands and their subsequent cyclisation another method was attempted, particularly for **PtL6** and **PdL6**. The first involved the formation of $[\text{M}(\text{br})\text{Cl}_2]$ (where M = Pt or Pd and br = bridging diamine) and then the subsequent addition of the pyridine rings along with the formation of the imine

bonds. Unfortunately this mostly yielded a complex with one addition of the pyridine-2-carboxaldehyde and was not successful in obtaining any tetradentate metal complexes.

Metallations of the other synthesised ligands were performed using methods altered from literature. The first complexes synthesised had a chloride counter ion from the metal salt. This produced mainly powder and therefore SbF_6^- was introduced in order to form high quality crystals suitable for X-ray diffraction and spectroscopic characterisation. Limited success was observed for SbF_6^- and therefore BF_4^- and PF_6^- were introduced as far more suitable counter ions. This resulted in a total of eight novel metal complexes producing X-ray quality crystals. Despite identical methods with equal conditions being used not all of the thirty attempted metal complexes could be synthesised. However, five other metal complexes, which produced powder, have been spectroscopically characterised where possible. The yields for the metal complexes were not calculated due to the bulk material not being pure.

The metal complexes did not give uncontaminated or even identifiable LC-MS spectra despite many of the samples being crystalline and clean; as seen in the ^1H NMR spectra. The samples were even run in different solvents, but similar results were obtained, ruling out solvent effects. Thus the use of LC-MS has not been implemented to characterise the metal complexes.^{‡‡} The UV-Vis spectra gave the expected bands for the non planar free ligands. For the metal complexes, intraligand π - π^* transition bands were observed as well as the MLCT bands (in the range of 320–380 nm for Pt(II) complexes and around 300 nm for Pd(II)). Extinction coefficients were determined for the novel metal complexes in acetonitrile, where possible. Despite numerous attempts it was observed that Beer's Law was not obeyed in the region 200–220 nm for **PtL2**, **PdL2** and **PdL4m**.

There is an obvious change in the shift of the ^1H NMR peaks for the metallated derivatives from the spectra of the free ligands. These shifts take place downfield from the respective free ligands ranging from 0.1 to 0.8 ppm for the palladium complexes or 0.4 to 0.9 ppm for the platinum complexes. This is due to the electron donating/accepting ability of the metal centre causing a redistribution of the electron density in the ligand and

^{‡‡} Some samples were submitted for elemental analysis to the University of KwaZulu Natal in Westville, but no meaningful data has been presented due to inconsistencies in the results obtained, which were attributed to instrument failure. In lieu of this samples have been prepared for submission to Galbraith Laboratories in the USA.

hence changes the resonance values for its protons. The ^{195}Pt NMR spectra were obtained for **PtL2** and **PtL4**, as well as a much weaker signal for **PtL2b** (Figure 2.4); however, no data is presented for the other platinum complexes as the peaks could not be observed despite numerous attempts.

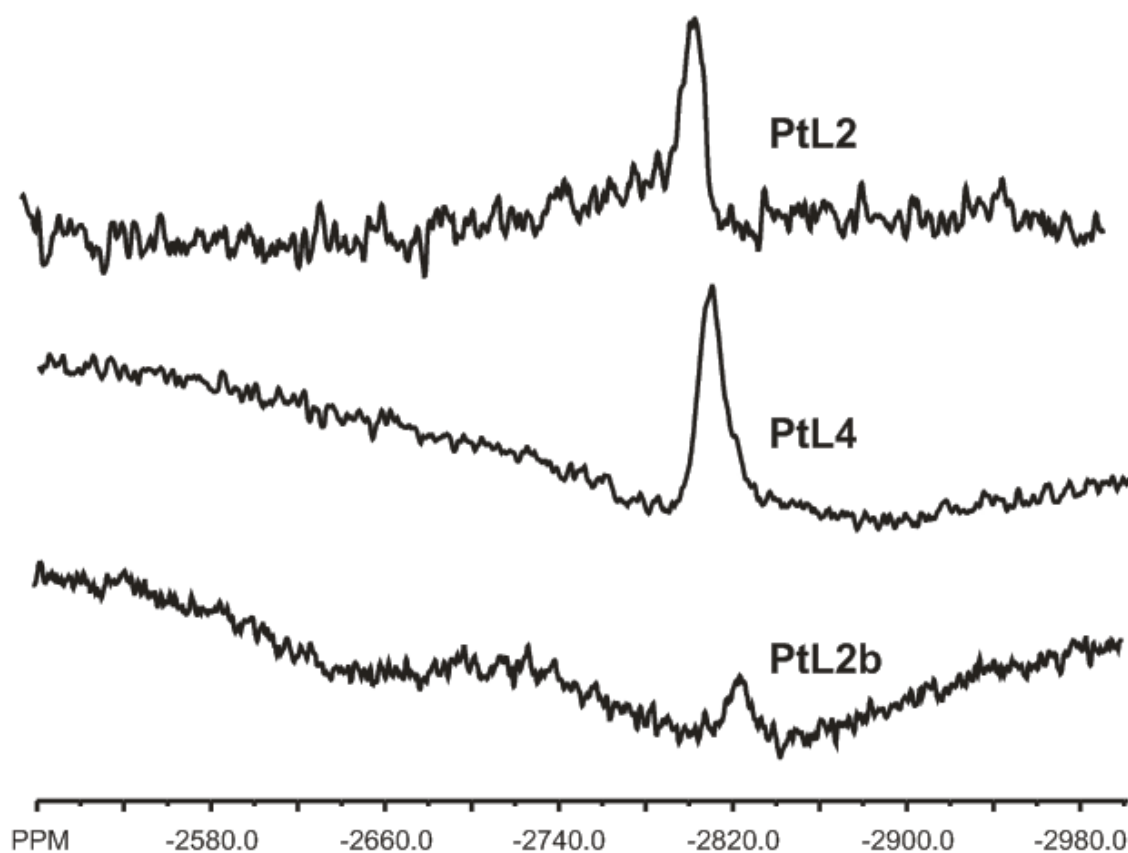


Figure 2.4: The 107 MHz ^{195}Pt NMR spectra at 11.7 T recorded at room temperature for **PtL2**, **PtL4** and **PtL2b**.

CHAPTER 3 – X-ray Crystallography

3.1 Introduction

The determination of a crystal structure using X-ray diffraction half a century ago was a monumental experimental undertaking; however, modern day advances have vastly improved the methodology. X-ray structure determinations may be used in the proof of synthesis and to show exact stereochemistry. The measurement of three dimensional geometries provides important and invaluable information about the properties of molecular or network compounds. This information may assist in explaining activity or applications of these compounds as well as allowing comparisons to be made to the theoretically calculated structural data (see Chapter 4). Studies of Schiff Base ligands and their metal complexes have slowly moved towards those of biological importance. Interest has therefore grown in this important class of compounds, in particular the metallated Schiff bases, so that they may be designed to produce species with particular properties.

The Cambridge Structural Database (CSD)²⁴⁶ shows the popularity of Schiff base derivatives and their metal complexes as a search for the basic structure of a Schiff base gave more than 80 000 results. Searches for Schiff base ligands containing the double imine functionality, $R-C=N-R-N=C-R$, gave more than 30 000 results, of which only slightly more than 2 500 had alkyl groups as the bridging agents and only a few hundred had four nitrogen donors present. Numerous metallated Schiff base complexes were found in the CSD with a range of different metals; including copper, nickel, silver, manganese, cobalt, zinc, ruthenium, samarium, gadolinium, ytterbium and lanthanum.²⁴⁶

Although tetradentate Schiff base ligands comprising two pyrrole groups bridged by a synthetically variable bridging group have been known for several decades,²⁴⁷ there is limited literature available for the ligands in this work (with *pyridine* rings on either side of the bridge). No crystal structures could be found in the CSD for any of the six original free ligands synthesised in this work. There are, however, crystal structures for other derivatives of ligands **L1**, **L2**, **L5** and **L6**. Some examples of these are shown in Figure 3.1. This includes slight differences to the bridging group (e.g. *trans* instead of *cis*

orientation for **L5**), additional ring structures (e.g. quinoline rings instead of a pyridine ring for **L1** and **L5**) or extended ligands linked by extra groups. No results were found for free ligand structural derivatives of either **L3** or **L4**.

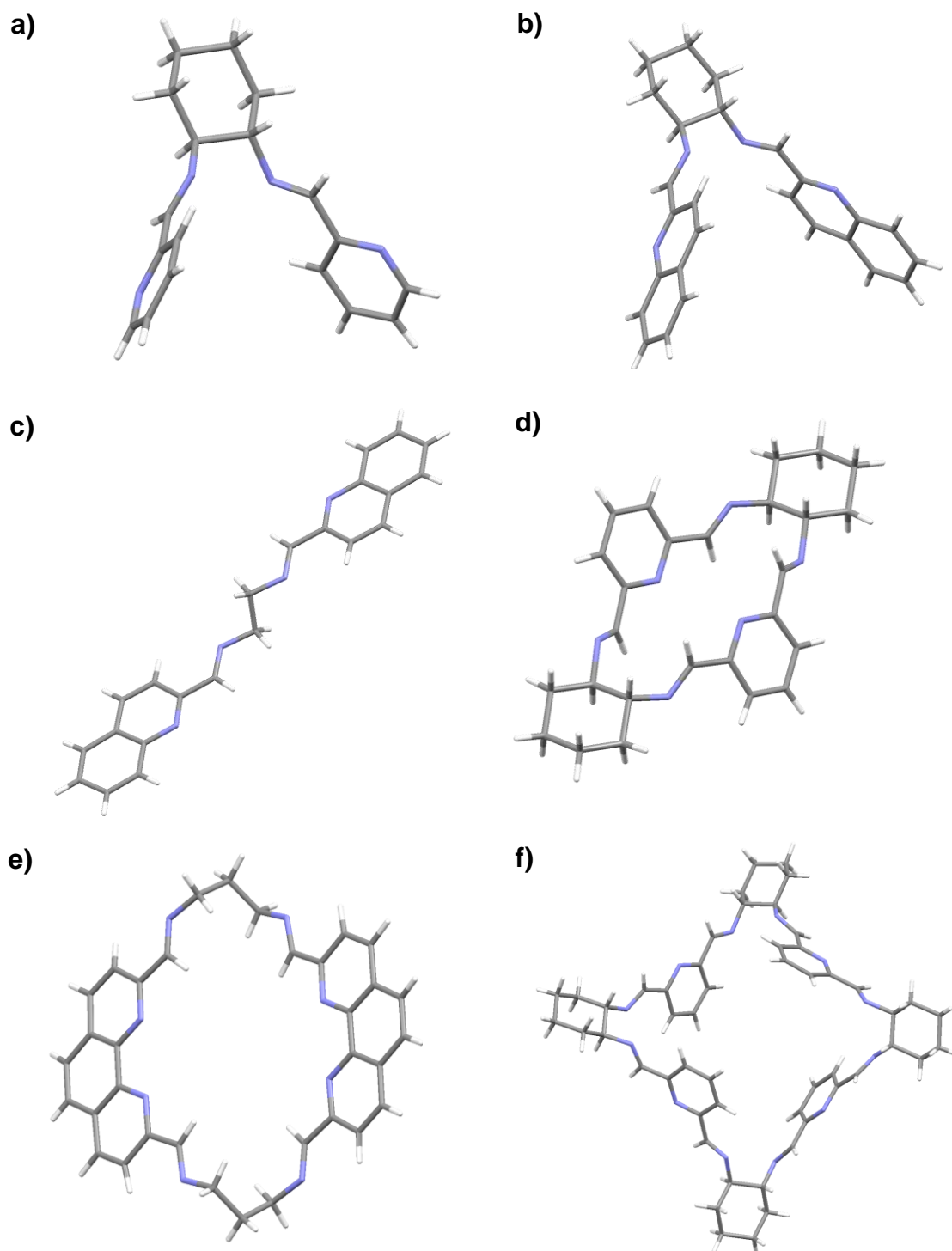


Figure 3.1: Some examples of pyridyl-imine Schiff base ligands similar to those described in this work found in the Cambridge Structural database and their CSD codes: a) MEQFEU²⁴⁸ or SISCEK²⁴⁹, b) ROHBOF²⁵⁰, c) KAGROA²⁵¹, d) JAXHUM²⁵² e) GIWJAY²⁵³ or SISJOA²⁵⁴ and f) JAXJAU.²⁵²

During the synthesis of these novel free ligands some cyclised “half-ligands” were synthesised. These products were formed when the aldehyde and diamine reacted in an unexpected 1:1 ratio and the diamine bridge subsequently cyclised at the imine carbon. The acyclic single condensation intermediate will not be stable and thus equilibrium will be shifted towards the cyclic aminal form. This resulted in a very stable, geometrically planar self-condensation product that was an N₂ donor rather than the expected tetradentate version. Structures of some cyclised 1:1 self-condensation products have been previously reported in the literature, e.g. 2-(4,5-dihydro-1*H*-imidazol-2-yl)pyridine (**L1h**)²⁵⁵ and 2-pyridin-2-yl-1*H*-benzimidazole (**L6h**)^{256,257} (Figure 3.2), but not for any of the other four cyclisation products.

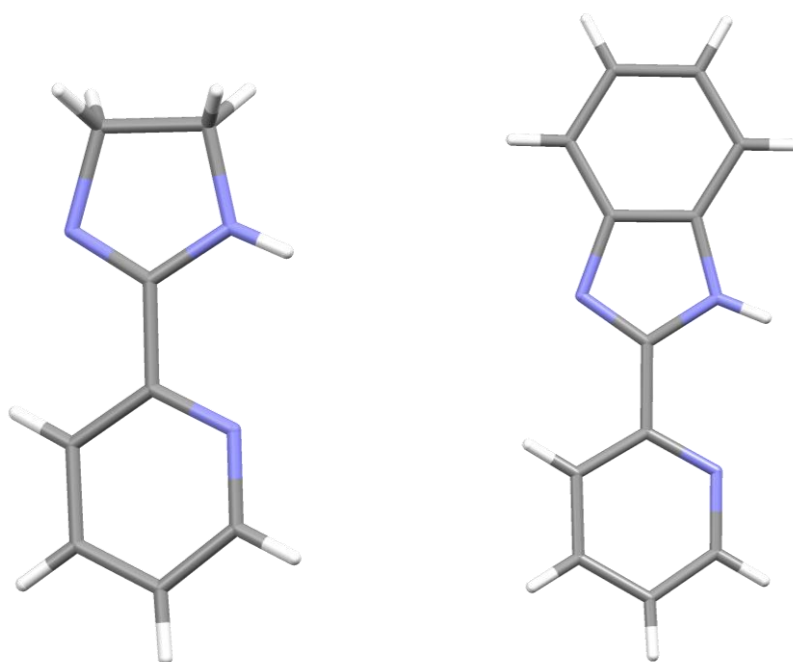


Figure 3.2: Structures of 2-(4,5-dihydro-1*H*-imidazol-2-yl)pyridine, **L1h** (LORPUE)²⁵⁵ and 2-pyridin-2-yl-1*H*-benzimidazole, **L6h** (AJOPOE)²⁵⁶.

Metal complexes that coordinate the tetradentate (N₄ donor) ligands do exist in the literature for four of these ligands, as shown in Table 3.1. No structures were found for **L4** and only dinuclear complexes for **L5** have been described (platinum⁴² and silver²⁵⁸). Most of these metal complexes have been produced and characterised on purely synthetic and structural grounds without any definitive applications. Some of these complexes have, however, exhibited good conductivities in the solid state on doping with iodine.²⁵⁹ Other complexes have also been studied as possible starting materials for the synthesis of oxo/hydroxo coordinated polynuclear metal species²⁶⁰ or to assemble novel end-to-end thiocyanato-bridged infinite 1D polymeric heptacoordinated metal chains.⁴¹

Table 3.1: Summary of available CSD²⁴⁶ reference codes for some of the metal complexes of ligands **L1**, **L2**, **L3** and **L6**.

	L1	L2	L3	L6
Manganese(II)		FIHQES, ¹²⁸ ROPBIH, ROPBON, ROPBUT ²⁶¹	FIHCAA, ¹²⁸ FIHPIV, ¹²⁸ ROPBED ²⁶¹	
Cobalt(II)		MAJDEG ²⁶²		
Nickel(II)		CABSII, ²⁶³ UDESOM ²⁶⁴		WIQFIL ¹⁶¹
Copper(II)		HUWTOI, ²⁶⁵ MAJDIK, ²⁶² VEHJUN ²⁶⁶		
Zinc(II)		MAJDOQ ²⁶²		
Ruthenium(II)		RUXFOF ¹³³		
Cadmium(II)	NEDWAV ¹⁴⁰			
Rhenium(III)	QOLQAJ ²⁶⁷			
Lanthanides	GAJXOF etc. ¹³²	GAKBAW ²⁶⁸		LUHFEZ ²⁶⁹

Not one of these complexes has a square planar geometry; however, the ligands mostly coordinate in the equatorial plane in a flat or near-planar orientation around the metal centres. This octahedral geometry (tetragonally distorted) was preferred for the copper complex of **L2**, whereas square planar geometry was found for a similar mixed ligand.¹⁹³ Karmakar *et al.* showed that with complexes of **L2** the Ni(II) ion constantly formed the *trans* isomer, while the Mn(II) ion gives the *cis* isomer.¹²⁹ The tetradentate ligand is more planar when the additional non-chelating ligands are at 180° to each other (axial) than in the *cis* isomer.

The structures for the nickel(II) complexes in Table 3.1 are of particular interest as nickel is also a group 10 transition metal. Nickel(II) has a d⁸ configuration and forms octahedral complexes with a planar coordination of the tetradentate Schiff base ligands in the equatorial positions leaving the two axial trans positions to be coordinated by other ligands. Nickel(II) complexes from the literature of **L2** and **L6** are shown in Figure 3.3. The only distortion for **L2** from the predominantly flat N₄ plane of the ligand (formed by the two imine (N_i) and two pyridine (N_p) nitrogen atoms) is for the bridging propyl group. The central CH₂ is pushed up between the other two CH₂ groups (which lie in the plane)

in an envelope conformation. The phenyl ring in the **L6** ligand lies in the N_4 plane creating an almost perfectly flat ligand structure around the metal centre.

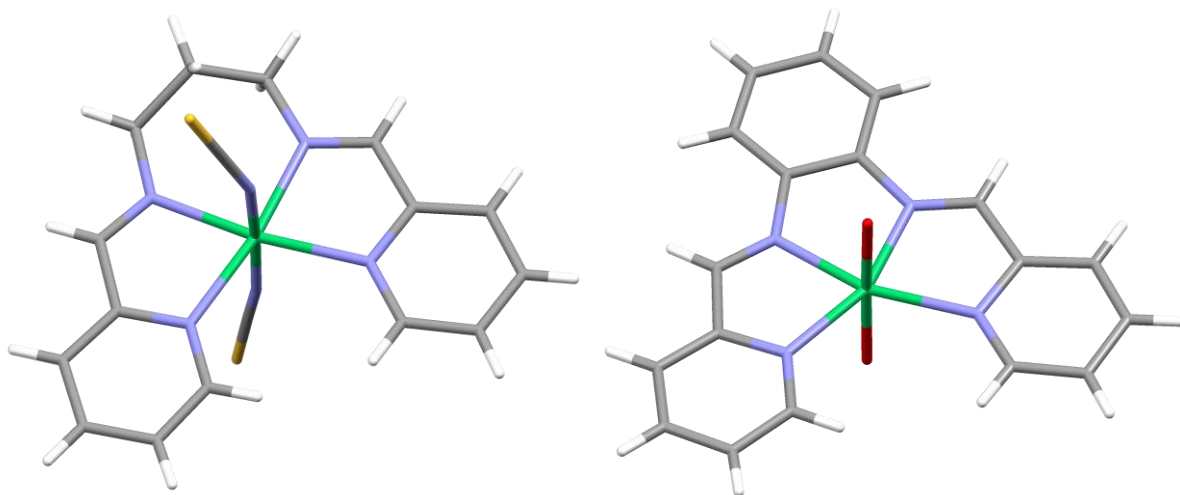


Figure 3.3: The nickel(II) complexes of **L2** (left) and **L6** (right), CSD reference codes: UDESOM²⁶⁴ and WIQFIL,¹⁶¹ respectively.

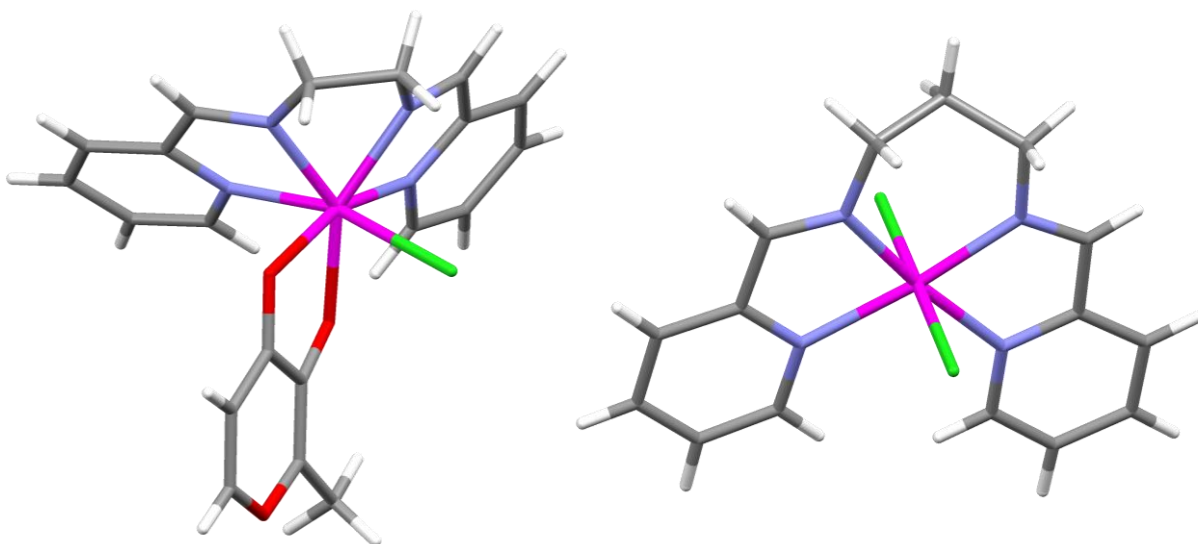


Figure 3.4: The *cis* rhenium(III) 7-coordinate complex of **L1** (left)²⁶⁴ and *trans* ruthenium(II) tetragonally distorted octahedral complex of **L2** (right).¹³³

Also of interest are the two PGM complexes: QOLQAJ²⁶⁴ and RUXFOF¹³³ (Figure 3.4 above), which have 7-coordinate and tetragonally distorted octahedral geometry, respectively. The tetradentate ligand lies flat in the equatorial plane for the ruthenium complex; however, for the rhenium complex the axial ligands form the *cis* isomer. This causes distortions in the symmetry which are reflected by the considerable variation of bond lengths and angles about the rhenium atom. This results in a distortion from planarity in the ligand conformation and four different metal-nitrogen bond lengths. In the

ruthenium complex there is asymmetry with the axial ligand angle being almost 180° and each type of metal-nitrogen bond ($M-N_i$ and $M-N_p$) is the same.

In this work, the above range of ligands has been expanded by adding steric bulk to the imine bond; this has been accomplished in the form of a methyl group on the imine carbon. For this second group of ligands synthesised only one free ligand was found in the CSD: **L1m**¹⁷⁴ (Figure 3.5). An interesting and important feature of this structure is the *trans* arrangement of the pyridyl-rings relative to the bridging group. The bridging alkyl chain has a staggered conformation between the two imine bonds. The methyl groups also display a *trans* configuration relative to these imine double bonds (and are subsequently *trans* to the pyridine rings).

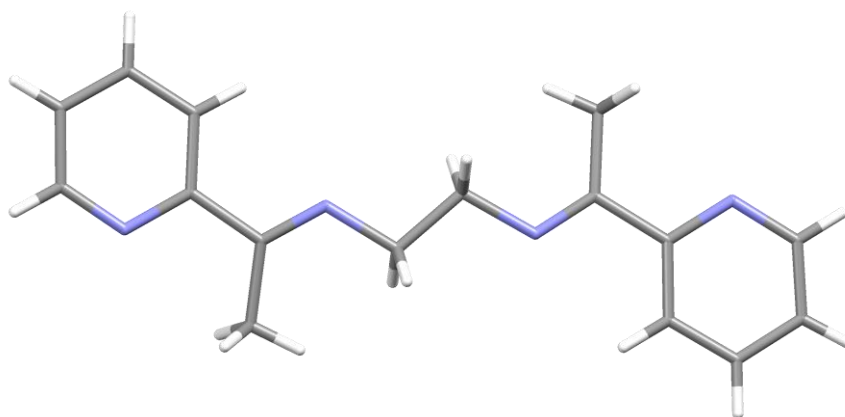


Figure 3.5: The structure of the free ligand **L1m** (NISWES),¹⁷⁴ $R_{int} = 0.105$.

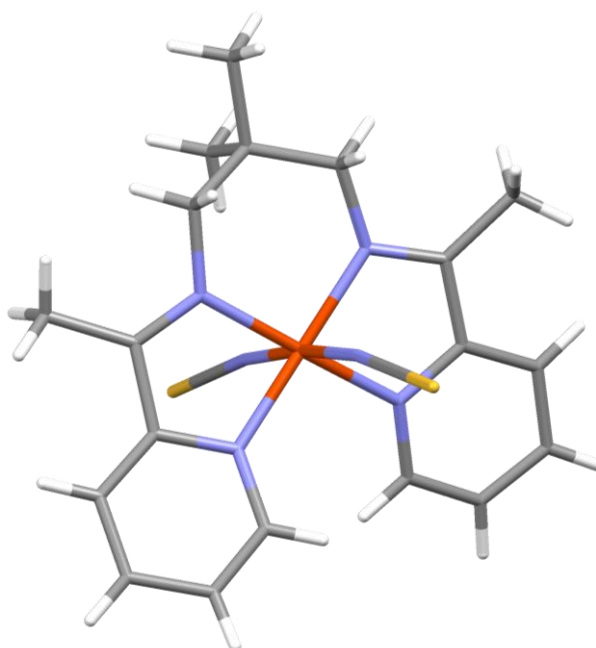


Figure 3.6: The metallated structure of **L4m** with iron(II) and two NCS^- axial ligands (HIDFUW).²⁷⁰

A range of metal complexes, including the metals nickel(II), copper(II) and cadmium(II) have been reported in the literature for **L1m** and **L2m**.^{167,168,172,177,178} Only one metal complex has been described by other workers for **L4m** (Figure 3.6)²⁷⁰ and for **L5m**²⁷¹ only a derivative of the structure is known. The few structures that contained **L3m** and **L6m** were found to have more than one metal atom present. Structures for the cyclised “half-ligands” of two methyl-substituted imine ligands; namely **L2mh**²⁷² and **L3mh**,²⁷³ are available in the literature.

The metal complexes of these ligands have similar coordination geometries (tetragonally distorted octahedral) to those described for the original range of ligands. The Schiff base ligand is predominantly flat on coordination in the *trans* isomer, which is again more common than the *cis* isomer. This has been explained by Banerjee and co-workers to be due to the better degree of metal-N_i backbonding that takes place when a stronger σ -donor N_p atom is in the *trans* position resulting in the sharing of the same d-orbital.²⁷⁴ Apart from these electronic factors, steric factors will always play a role as the *trans* isomer has far less steric repulsion by having the axial moieties located away from each other.¹⁷⁸

Deviations from the plane for the bridging group of **NiL1m** are relatively small (mean deviation 0.08 Å), even in comparison to the limited deviation of the individual π -conjugated chelate rings (mean deviation: 0.01 Å).²⁷⁴ The equatorial plane of **NiL2m** has a higher distortion (mean deviation, 0.021 Å) and the bridging group is puckered into an envelope conformation (as seen for **NiL2**).¹⁷⁸ The iron(II) complex of **L4m** shows a far more distorted planarity for the tetradentate Schiff base ligand that encapsulates the equatorial plane with a similar envelope conformation for the bridging group of the metal complexes of **L2** and **L2m**. The increased length and subsequent increase in bulk for the bridging group chains has a distorting effect on the N₄ plane of the Schiff base ligand.

In this work, we have also synthesised phenyl-substituted imine derivatives of the polydentate bis-(pyridyl-imine) ligands for chelation of Pd(II) and Pt(II). Such ligand derivatives are known to coordinate a range of metal ions. For example, metallated derivatives with manganese (**L1b**¹⁷³ and **L2b**²⁷⁵), cadmium (**L2b**¹⁴⁶), copper (**L2b**^{146,192,276}) and nickel (**L2b**¹⁴⁶ and **L6b**²⁷⁷) (see Figure 3.7 for examples) have been reported. X-ray structures of **L3b** and **L4b** have not been determined either as metal-free ligands or as chelates of metal ions, despite the relatively simple synthetic procedure for

their preparation. The same is true for **L5b**; however, for this ligand the synthesis is far more challenging. **L1bh** is the only cyclised “half-ligand” for which a structure has been reported.²⁷⁸

The overall coordination geometry for this range of complexes is also octahedral (tetragonally distorted), with the ligated atoms equatorially around the metal centre and the remaining two axial coordination sites occupied by other ligands (e.g. NCS^- or Cl^-). The four nitrogen atoms of the ligand form an essentially planar arrangement in all structures of the more common *trans* isomers. This has been observed for a nickel complex where all four nitrogen donor atoms of the ligand are almost planar with a maximum deviation from the equatorial plane being 0.16 Å.²⁵⁹

The prominent difference here is that the imine groups are no longer lying in the plane (like the hydrogen and methyl substituents). The pyridine and phenyl rings are themselves planar; however, they are twisted out of coplanarity relative to each other. It is not possible for these rings to exist in the same plane due to steric hindrance,²⁷⁶ but the pyridine rings have limited rotation due to their coordination to the metal. Therefore, this steric hindrance can only be relieved by the phenyl rings tilting relative to the main N_4 plane (see Figure 3.7). This distortion of the phenyl rings’ orientation takes place to varying extents, and subsequently results in reduced planarity of the structures. For a copper structure these angles between the phenyl ring and pyridyl ring were found to be 140.1°, 109.4° and 135.1°, 91.1°, respectively for two independent cations.²⁷⁶

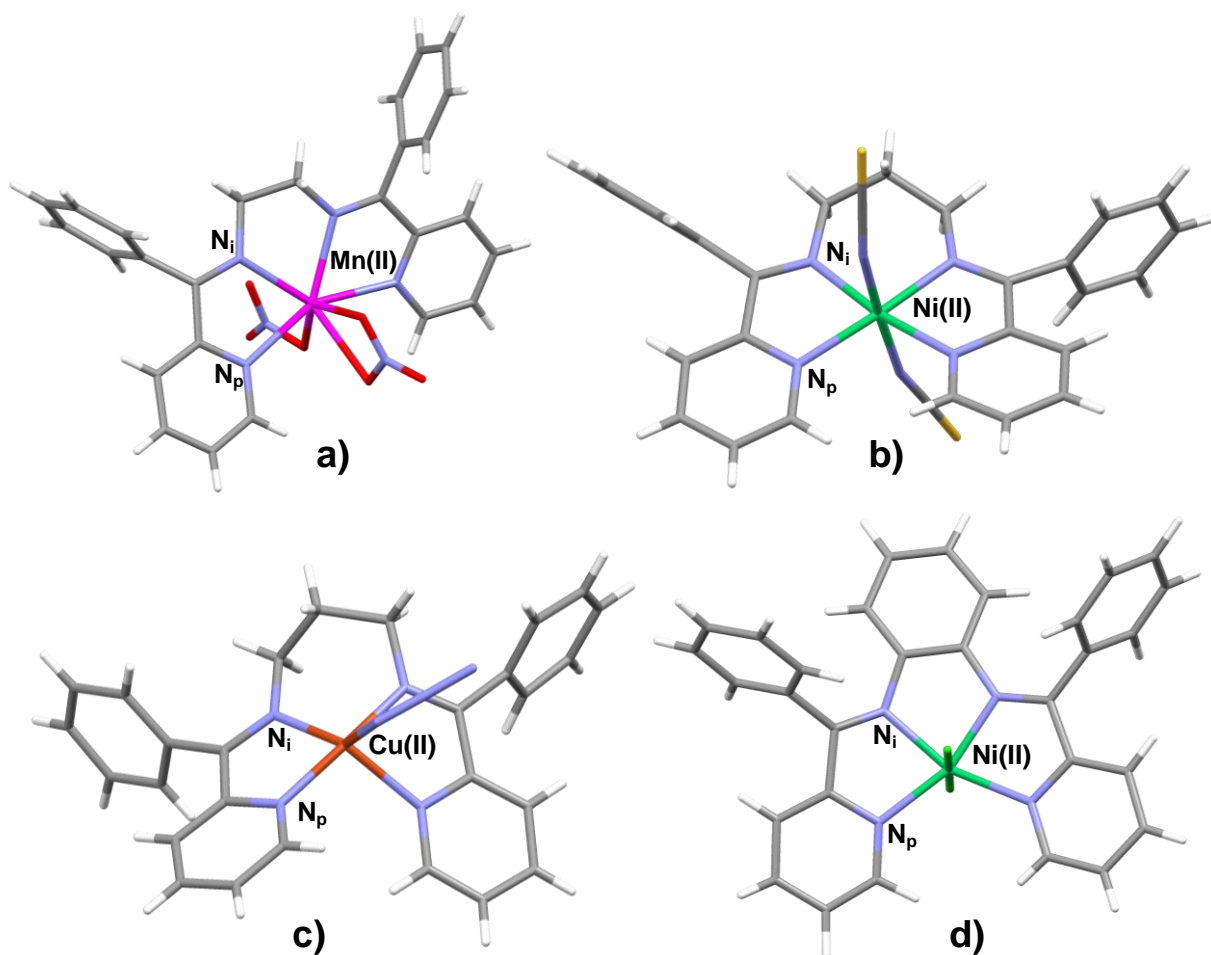


Figure 3.7: Metal complexes of the phenyl-substituted ligands **L1b**, **L2b** and **L6b**: a) $[\text{Mn}(\text{L1b})(\text{NO}_3)_2]$ (KAHHOQ),¹⁷³ b) $[\text{Ni}(\text{L2b})(\text{NCS})_2]$ (UDESUS),¹²⁹ c) $[\text{Cu}(\text{L2b})\text{N}_3]$ (TAYMIQ)¹⁴⁶ and d) $[\text{Ni}(\text{L6b})\text{Cl}_2]$ (XACGAJ).²⁷⁷ Counterions have been omitted for clarity.

Inspection of the literature for ligands with the same or a similar structure to those synthesised in this work, indicates that complexes of copper, nickel, manganese and some lanthanides are the most abundant.²⁴⁶ Although platinum and palladium do not appear to be popular metals for this class of Schiff bases, some literature relating to coordination complexes of PGMs with bis(pyridyl-imine) ligands exists. Structures of platinum and palladium complexes with N_4 chelating Schiff base ligands (with similar bridging groups *trans*-**L5**) have been found in the CSD. They are, however, slightly different in structure having pyrrole rings rather than pyridine rings.^{279,280} Platinum and palladium complexes have also been observed for one of the ligands in this work (Figure 3.8), **L5**,²⁸¹ and for similarly structured ligands thereof (*trans*-configuration^{281,282} of **L5** and **L5** with quinoline rather than pyridine²⁸¹).

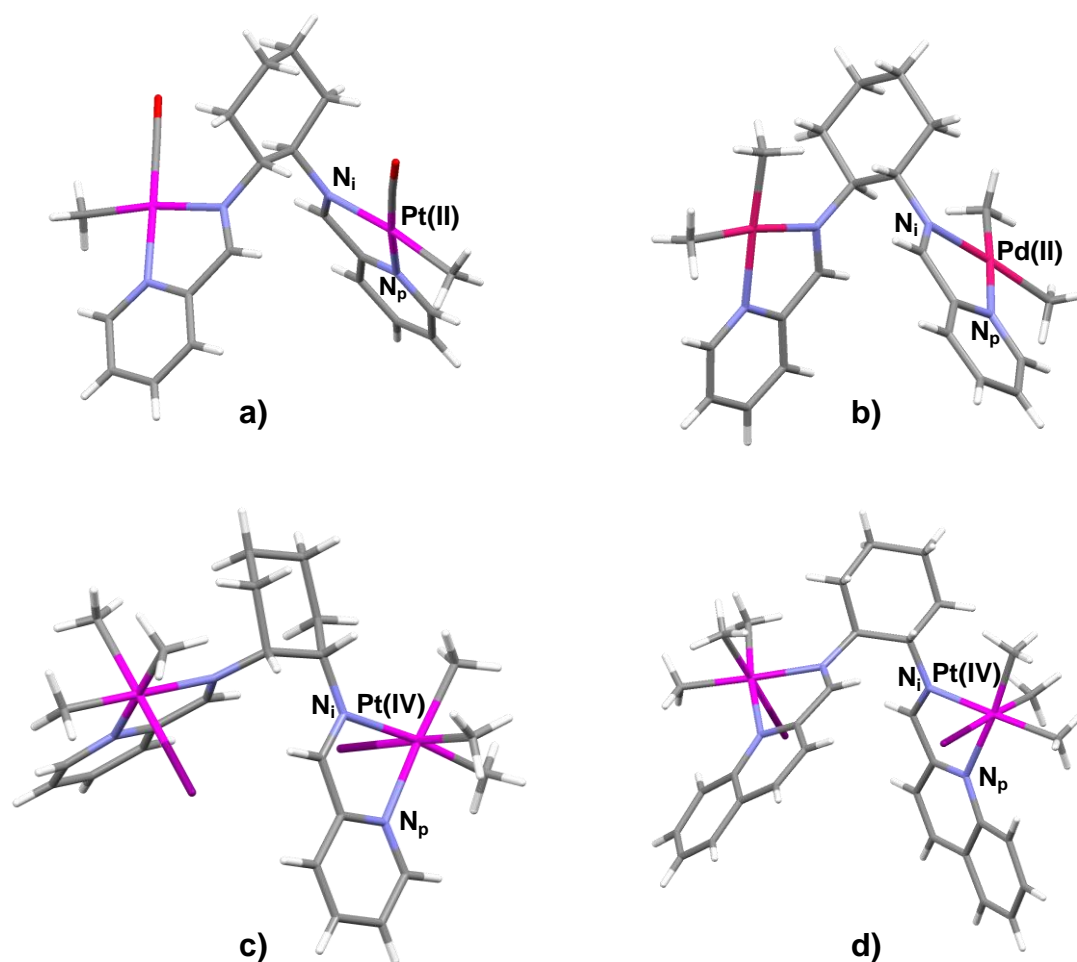


Figure 3.8: Some of the platinum(II/IV) and palladium(II) structures of **L5** and similar ligands found in the CSD: a) HOZLOX,²⁸² b) XIXGEQ,²⁸¹ c) UBAQAP²⁸¹ and d) UBAQOD.²⁸¹ Counterions have been omitted for clarity.

The most notable difference between these PGM complexes (Figure 3.8) and those in Figures 3.3 and 3.7 is the presence of two metal atoms bonded to only one ligand. Each of the metals is bonded to one imine-nitrogen (N_i) and one pyridine-nitrogen (N_p) with various ligands coordinating in the other two (or four, in the case of octahedral platinum) available positions on the metal. Despite the fact that most of these reactions took place with a 1:1 ligand to metal ratio the final product had a 1:2 ratio.^{281,282} Some examples of these are shown in Figure 3.8 above.

When only one metal atom coordinates all four nitrogen atoms of the tetradentate ligand they are all required to be in close proximity. These four nitrogen-donor atoms subsequently form a plane around the central metal atom. Distortions from this plane are possible, but the general arrangement is constant during this chelation as there is limited movement for the groups around the metal. From the structures in Figure 3.8 it is

obvious that this is not the case. The coordination of only two nitrogen atoms to each of the two different metal atoms allows the two pyridyl-imine arms to twist away from each other to resist steric hindrance.²⁸¹ There is nothing forcing the two pyridyl-imine arms towards each other (as in the mononuclear complexes) and therefore due to each side of the molecule twisting individually there is a lack of planarity for these structures. This will not be true for the metal complexes synthesised in this work as they are expected to be mononuclear.

There was one mononuclear square planar palladium(II) complex with an N_4 donor ligand (Figure 3.9).¹⁹⁵ This bis(pyridyl-imine) ligand had *N,N'*-(6,6'-dimethylbiphenyl-2,2'-diyl)diamine as the bridging group and a hydrogen on the imine carbon. The palladium centre of the molecule formed an almost C_2 -symmetric seven-membered chelate ring with this bridge and a five-membered chelating ring on either side with each of the pyridyl-imine moieties. The Pd-N bond lengths were within the expected range¹⁹⁵ and the two planes on either side of the metal spanned an angle of $12.9(5)^\circ$. The bridging group itself was nonplanar due to the twisting of the phenyl rings to reduce the steric strain between the two methyl groups.

A distortion from planarity is also observed for mononuclear complexes of salen ligands which have N_2O_2 donors. When comparing the nickel complexes of **L2**²⁶³ and **L2-salen**²⁸³ it is obvious that there is a large discrepancy in their planarity (Figure 3.10). The Schiff base ligand is almost completely flat (except for the propyl bridging group) for the complex with **L2**, while it is greatly distorted for **L2-salen**. These complexes have the same metal centre and bridging group, but differ for the axial ligands and coordinated rings. Coordination to the metal for the salen-complex still takes place through the two N_i atoms, but now it coordinates through two oxygen atoms and not the N_p atoms.²⁸³ This means that the chelating chains are now extended from 5-membered to 6-membered rings, which allows for greater freedom around the metal.²⁸³ Coupled with the differences in the donor atom to metal bond lengths, this may therefore account for the non-planarity of the ligand. In macrocyclic (closed type) N_4 tetradentate ligands the deviation from the plane is less than for either of these “open-type” ligands (salen or for the ligands in this work). These “open-type” ligands have far less opportunity for the ligand to distort as there are no free ends that may provide the freedom for the distortion.¹⁶¹

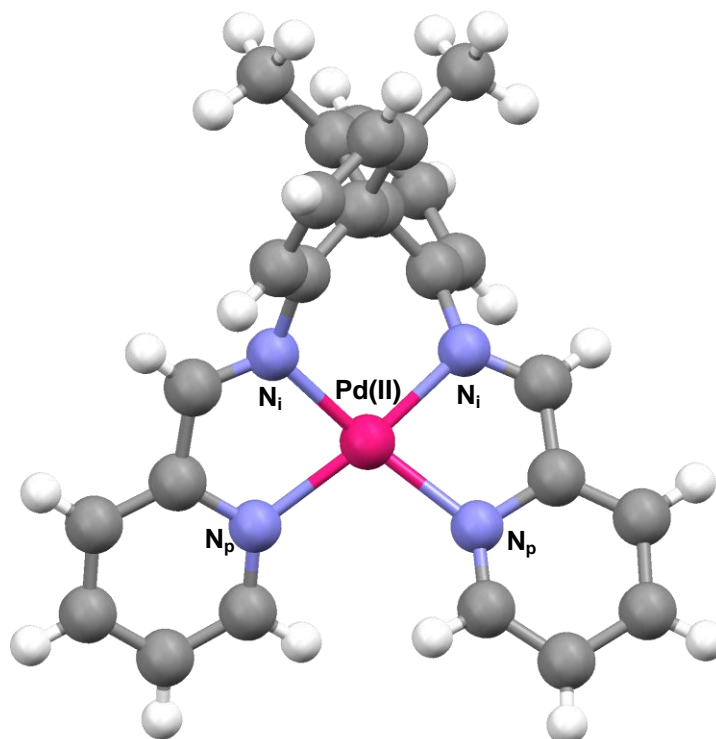


Figure 3.9: The structure of the palladium(II) N_4 donor Schiff base complex with square planar geometry, PAKLOD.¹⁹⁵ Counterions have been omitted for clarity.

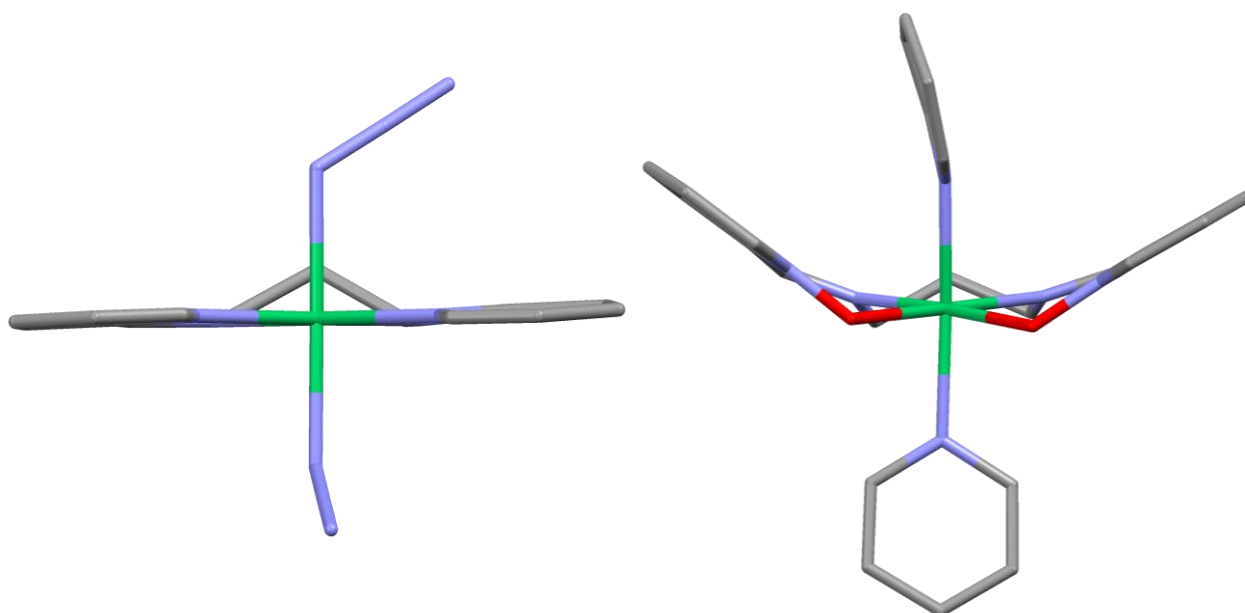


Figure 3.10: The nickel complexes of **L2** (N_4 donor, left) and **L2-salen** (ONNO donor, right) viewed side on to show the variation in planarity (hydrogen atoms have been omitted for clarity).

When this type of tetradentate ligand coordinates to the metal atom then all four nitrogen atoms of the bis(pyridyl-imine) ligand form a plane around that central metal atom. Large distortions from this plane are possible when the coordination number of the metal is

high, particularly for the *cis* isomers, e.g. ten-coordinate lanthanides with **L1** or **L2**,¹³² in order to reduce the steric bulk. The smaller six-coordinate geometries mostly only allow minimal distortions from the plane for the *trans* octahedral structures (these distortions are greater in the case of the *cis* isomer). Manganese has a tendency to form the *cis* isomer of the octahedral structure for **L2**¹²⁹ and **L3**,¹²⁸ while most other metals favour the *trans* isomer.

The metal complexes of methyl-substituted ligands mostly show tetragonally distorted octahedral geometry, which is most often the slightly distorted *trans* isomer (**NiL1m**,²⁷⁴ **CuL1m**,²⁸⁴ **CdL1m**,¹⁶⁸ **MnL1m**¹⁷³ and **FeL4m**¹⁷⁵). There are also some higher coordination numbers: 7 and 10; including the lower coordination number of 5 for copper with **L2m**.¹⁷⁷ The presence of only one axial ligand causes a fair distortion for the tetradentate ligand. Distortion of the N₄ plane is also observed for the higher coordination numbers. The phenyl-substituted ligands generally coordinate in a tetragonally distorted octahedral geometry (*trans* for **CuL2b**,¹⁹⁰ **NiL2b**¹⁴⁶ and **NiL6b**;²⁵⁹ *cis* for **MnL2b** and **CdL2b**) with some 5-coordinate (**CuL2b**)^{146,192} and 7-coordinate structures (**MnL2b**).¹⁷³ Due to the greater steric bulk in these structures there is rotation of the phenyl substituents relative to the plane formed by the four coordinating nitrogen atoms. This plane may also be distorted by the tilting of the pyridine rings to a much greater extent than seen for the original ligands.¹⁹⁰

When keeping the metal centre (copper(II)) and axial ligands (ClO₄⁻) the same, differences in the planarity may then be accounted for by variations in the ligand on the equatorial plane for different complexes. The distortions for three copper complexes with the propyl bridging group are presented in Figure 3.11. The ligands increase in steric bulk on the imine carbon: hydrogen < methyl < phenyl. It is obvious that the smallest distortions are observed for the complex with the “smallest” ligand, **CuL2**,¹⁹³ with only slightly tilted pyridine rings (either side of the N₄ plane). The distortions are much larger for **CuL2m**¹⁷⁷ and **CuL2b**¹⁹⁰ and are visually rather similar. In both structures the phenyl rings are twisted out of the plane, one above the plane and the other below. The same is true for the imine groups, but on each side in the opposite direction to the closest pyridine ring. Figure 3.11 therefore suggests that alkyl and aryl groups appended to the imine carbon permit larger distortions from planarity for the ligand.

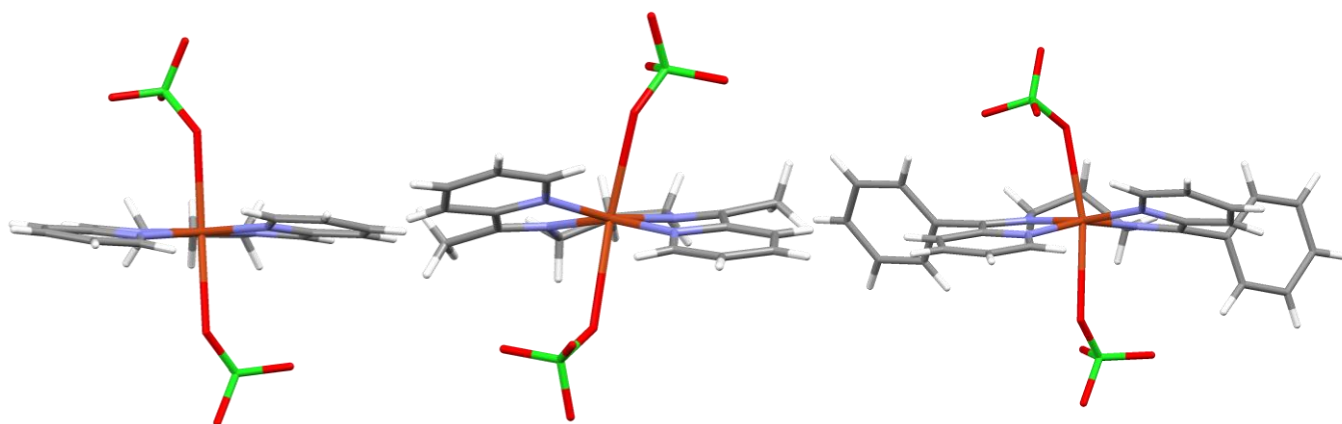


Figure 3.11: The variations in the distortions from planarity for the tetradentate Schiff base copper complexes with varying imine-substituent steric bulk.

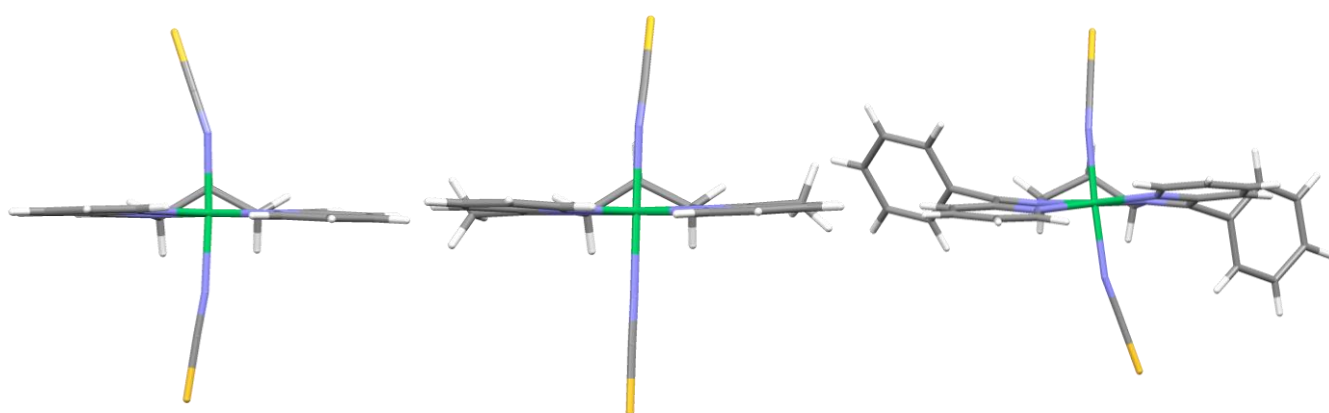


Figure 3.12: The variations in the distortions from planarity for the tetradentate Schiff base nickel complexes with varying imine-substituent steric bulk.

For d^8 nickel(II) complexes of varying ligand steric bulk the distortions from planarity are visually far smaller with **NiL2**²⁶⁴ and **NiL2m**¹⁷⁸ being almost identical (only a slight distortion for **NiL2m** with tilted pyridine rings). The larger steric bulk of **NiL2b**²⁶⁴ shows greater nonplanarity with the phenyl rings tilted out of the plane and in different directions (one up, one down) as well as a greater tilting of the pyridine rings. The methyl group therefore doesn't have much effect for the nickel complexes, whereas the phenyl ring causes fair distortion. There is an obvious distinction between the range of copper complexes and the range of complexes with the smaller Ni(II) ion.

The effects of the different types of metals may be clearly observed when keeping the ligands constant. The nickel (**NiL2**^{263,264}) complexes of **L2** are almost perfectly planar, while the copper (**CuL2**²⁶⁵) complex of the same ligand is far more distorted. The copper member of this series is distorted more strongly than the nickel structures because of the

Jahn-Teller effect.²⁸⁵ This distortion is often observed for $3d^9$ Cu(II) structures due to the degeneracy of the d states in an ideal octahedral field. There will be no resistance to perturbing fields which lower the degeneracy due to a single d electron or d vacancy being unstable.²⁸⁶ The same is true for complexes with the methyl-substituted ligands: **NiL2m**¹⁷⁸ and **CuL2m**,¹⁷⁷ and the phenyl-substituted ligands: **NiL2b**²⁶⁴ and **CuL2b**.²⁷⁶ There is slight distortion for the nickel **L2b** complex, but this may be explained by steric bulk and it is still far less than the distortion seen for the copper complex.

The angles around the central metal atom associated with five-membered chelate rings are invariably smaller than those associated with six-membered rings.¹⁹³ For example; the corresponding values observed for the angle formed by N_i -Cu- N_i for **CuL1m**²⁸⁴ is almost 15° smaller than the same angle for the 6-membered ring in **CuL2m**.¹⁷⁷ The angles formed by N_i -Cu- N_p in five-membered chelate rings are both around 81° for each of these two complexes. The same is observed for N_i -Cu- N_i for **NiL1m**²⁷⁴ and **NiL2m**,¹⁷⁸ which differ by slightly less than 13° . The N_i -Ni- N_p angles are of similar size to each other and to those observed for the copper complexes; however, slightly smaller to accommodate the increased N_i -Cu- N_i for angle. The N_i -metal- N_i angles for the 5-membered chelate rings for copper are slightly larger than for nickel (differ by 0.3°), the same is true for the 6-membered chelate rings (differ by 1.7°). This may be attributed to the different size in the metal ions. The bond lengths will also be slightly affected by the changes in bite angles for each complex; however, the M- N_i bond is always expected to be slightly shorter than that of the M- N_p bonds due to the difference in basicity.²⁸⁷

3.2 Objectives

The main goals of this chapter were to:

- 1) determine and report the crystal structures of each of the four novel 'fully-reacted' bis(imine) and five mono(imine) Schiff Base ligands synthesised in this work;
- 2) determine and report the crystal structures of eight metallated tetradentate chelates;
- 3) report and analyse relevant bond lengths, angles, packing and other interesting features to establish correlations between the ligands themselves and the metal complexes. This incorporates exploring the similarities and the differences between platinum(II) and palladium(II) as metal centres;

- 4) determine whether it is likely that predominantly planar conformations (with only slight deviations from the plane) will be observed for the mononuclear structures synthesised in this work and thus compare and analyse any distortions from the N_4 plane; and
- 5) imbue the disparity seen in the literature thus far as all the structures have been refined to an internal R -factor lower than 10%.

3.3 Methodology

Single crystals of the free ligands were grown by slow evaporation of the solvent. Single crystals of the metal complexes were also obtained by slow evaporation of the solvent or by solvent diffusion. Intensity measurements were carried out on the crystals (which were all air stable) using two diffractometers and standard procedures.

Oxford Diffraction Xcalibur2 CCD 4-circle diffractometer

X-ray diffraction data were collected on an Oxford Diffraction Xcalibur2 CCD 4-circle diffractometer equipped with an Oxford Instruments Cryojet operating at 100(2) or 298(2) K. The data were collected at a crystal-to-detector distance of 50 mm using omega scans at $\theta = 29.389^\circ$ with 10 to 35 s exposures taken at ~ 2 kW X-ray power with 0.75° frame widths. The data were reduced with the program *CrysAlis RED*²⁸⁸ using outlier rejection, scan speed scaling, as well as standard Lorentz and polarisation correction factors. Direct methods (SHELXS-97, WinGX32)^{289,290} were used to solve the structures. All non-H atoms were located in the E-map and refined anisotropically with SHELXL-97.²⁹¹ The hydrogen atoms in each of the structures were included as idealised contributors in the least-squares process with standard SHELXL-97²⁹¹ parameters.

Bruker Apex II Duo instrument

Crystal intensity data were collected on a BRUKER SMART APEX or a BRUKER APEX-II DUO CCD (Charge Coupled Device) Single Crystal X-ray Diffractometer, using graphite-monochromated $MoK\alpha$ radiation ($\lambda = 0.71073 \text{ \AA}$). The generator was operated at 50 kV and 100 mA for the Bruker APEX-II DUO and 50 kV and 30 mA in the case of the SMART-APEX. All data were collected using ϕ and ω scans. Frame widths were 0.3° on the SMART-APEX and 0.5° on the APEX-II DUO. Unit cell determinations and data were measured at 100(2) K. The low temperatures were maintained by cooling the crystals with a constant stream of N_2 gas at a flow rate of $15 \text{ cm}^3 \text{ min}^{-1}$ with the aid of a

Cryostream cooler (Oxford Cryosystems UK). Data were corrected for Lorentz-polarisation effects; unit cell refinement and data-reduction were performed using the program Bruker Saint. All data were subjected to absorption correction using the program multi-scanSADABS.²⁹² Space group determinations were carried out by examining the systematic absences and matching the observed conditions to a known space group.²⁹³ These assignments were confirmed by running the data through the program Xprep.²⁹⁴ SHELXS-97²⁸⁹ input files were generated with Xprep. All structures were refined with SHELXL-97²⁹¹ operating through the interface X-seed.²⁹⁵

3.4 Results and Discussion

3.4.1 General

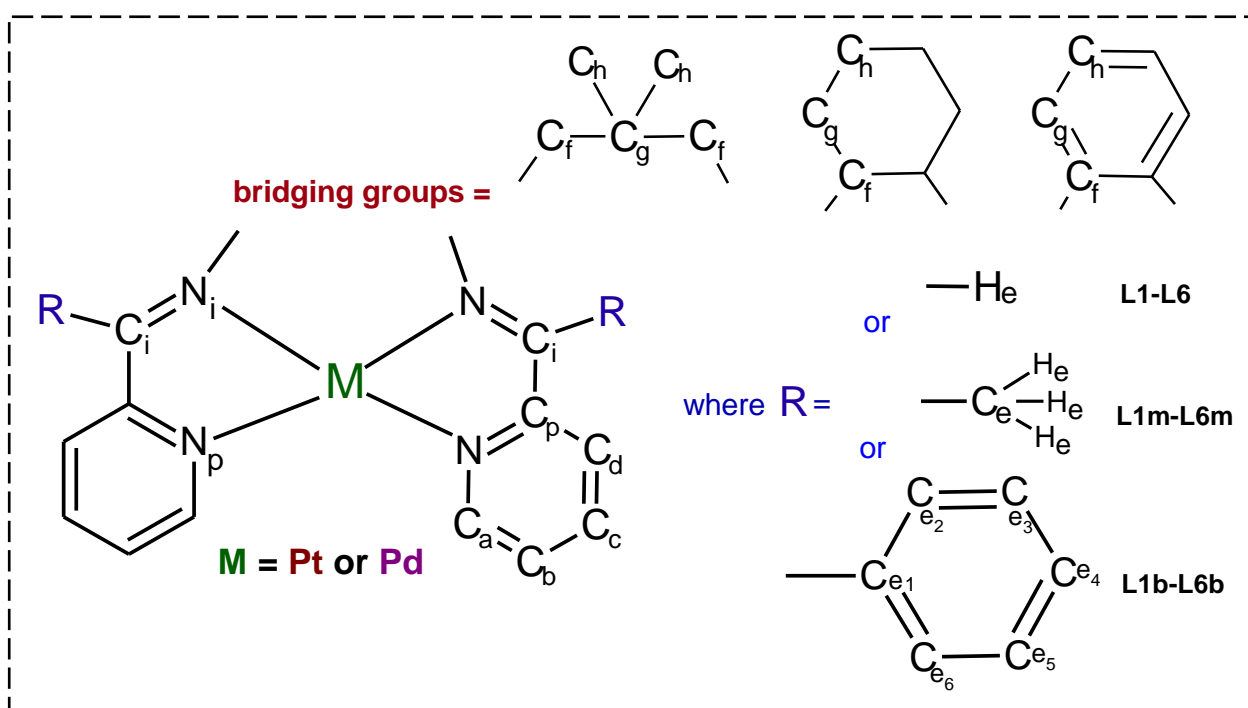


Figure 3.13: The notation used for labelling the chemically unique atoms in the basic framework of the Schiff base ligands and complexes.

Figure 3.13 shows the notation that has been used to label the atom framework of the structures throughout this work. C_f , C_g , C_h etc. are used to denote the bridging group carbon atoms, while C_{a-d} denotes the carbon atoms in the pyridine ring. C_i and C_p refer to the carbon atoms involved in the imine bond and the quaternary carbon in the pyridine ring, respectively. The hydrogen atoms will be named according to the atom to which

they are bonded, except for the hydrogen on the imine group which is labelled H_e . When there is a methyl group on C_i the atoms are labelled C_e and H_e and when it is a phenyl ring the carbons are labelled C_{e1} , C_{e2} etc. (and consequently, H_{e1} , H_{e2} etc.). The nitrogen atoms involved in the *imine* bond are labelled N_i and those in the *pyridine* ring, N_p .

Mononuclear and dinuclear complexes have been reported for many metal complexes of these types of ligands (as discussed earlier). The complexes in this work are expected to be mononuclear by design. Platinum(II) and palladium(II) are considered isoelectronic and isosymmetric²⁹⁶ and we therefore expect to see similarities in the conformation of the ligands around these metal centres, as well as for the bond lengths and angles. The main difference in comparison to the literature structures presented here will be that platinum and palladium form four-coordinate square planar complexes rather than six-coordinate octahedral complexes.

The preferred geometry is correlated to the electronic configuration. A square planar configuration will be imposed not only by the ligand, but as a result of additional splitting of the orbital levels due to lack of z-axis ligands. This additional splitting is most advantageous as it allows for the pairing of all electrons (the value of Δ_o is sufficiently high).²⁹⁷ Four ligands that each donate a pair of electrons to the central metal will fill the sigma bonding MOs (molecular orbitals) and subsequently the *d* electrons must be divided between the e_g , b_{1g} and b_{1g}^* MOs. This reduced symmetry results in no unique energy splitting analogous to Δ_o or Δ_t . The four approximately nonbonding MOs lie much lower in energy than b_{1g}^* and therefore this d^8 system will be more stable as four-coordinate square planar than in an octahedral complex where two electrons will be in the e_g^* MOs.²⁹⁸

The crystal field stabilisation energy (in terms of Δ_o) is therefore much greater for square planar coordination than for octahedral coordination. The *d*-orbital splitting generally increases per period down a group with around 30–50% going from one transition series to the next.²⁹⁹ This subsequently promotes the square planar geometry for complexes of the 5th and 6th period (e.g., Pt and Pd, respectively) transition metals. The loss in bond energy caused by an octahedral complex being transformed to a square planar complex may be made up by this greater energy difference for platinum and palladium; however, it is not usually enough to ensure square planar complexes for nickel. Overall, square planar complexes are far less common than those of octahedral geometry. The ligand

configuration in this work is likely to be square planar (similar to the configuration of the ligand seen for the *trans* isomers of the tetragonally distorted octahedral structures reviewed earlier) with the use of platinum(II) and palladium(II) as the coordinating metals. An important objective of this work is therefore to describe the structures and properties of square planar d^8 PGM complexes of this group of ligands.

Despite the predominantly planar tendency of the tetradentate chelating ligands in this work some distortions from the N_4 plane (formed by the two imine (N_i) and two pyridine (N_p) nitrogen atoms) are to be expected. The bonded central metal ion will resist undue radial expansion or contraction but it can readily distort from a planar geometry; it has been known to be quite flexible toward out-of-plane deformation.³⁰⁰ Consequently, the central metal ion may be easily displaced in a direction perpendicular to the mean plane; however, this is not necessarily the case. The metal may lie in the N_4 plane causing the distortion elsewhere in the structure. This has been observed for the *trans* isomer copper complexes presented from the literature.^{193,177,190}

Distortions may also be due to packing effects in the crystal lattice or an attempt to reduce the strain in the bonding network around the metal. Electrostatic repulsion of the inner hydrogen atoms on the pyridine ring, which applies to solution as well as solid state species, may cause the pyridine rings to tilt out of the N_4 plane created by the ligand and metal centre.²⁴⁹ The pyridine ring subunits are themselves always planar but can be tilted in order to reduce steric strain. Structures with larger substituents on the imine carbon are likely to have a greater tendency towards this type of distortion. This reduction of steric crowding may cause substantial nonplanarity for the structures. Thus it is possible for either or both of these factors to play a role in the out-of-plane deviations for the structures presented in this work.

Lastly, altering the length of the carbon bridge between the imine groups in these complexes not only allows change in the molecular conformation, but also facilitates different crystal packing architectures for each derivative. Thus the distortion from the plane and the nonplanarity of the bridging group are complimentary to each other. The chelating ligand makes an arc around the metal centre in order to offer the four nitrogen atoms for bonding, resulting in limited space available for the other atoms linking these nitrogen atoms. The more atoms in this space, i.e. the larger the bridging group, the greater the extent of distortion of the chelate. This will result in the bridging group being

pulled out of the N_4 plane. The extent to which it is removed from the plane will depend on the nonplanarity seen around the metal and the size and bulk of the bridging group.

3.4.2 X-ray data for the free ligands

***N,N'*-bis[(pyridin-2-yl)methylene]ethane-1,2-diamine (L1)**

$C_{14}H_{14}N_4$, fw = 238.29 amu, $a = 18.9472(19)$ Å, $b = 5.8207(4)$ Å, $c = 13.0548(15)$ Å, $\beta = 121.851(15)^\circ$, $V = 1223.0(2)$ Å³, monoclinic, $C2/c$, $Z = 4$, $D_c = 1.294$ g cm⁻³, $\mu = 0.081$ mm⁻¹, $T = 102(2)$ K, $R_1 (wR_2) = 0.0461 (0.1188)$, for 1374 unique data with $I > 2\sigma(I)$, $R_1 (wR_2) = 0.0570 (0.1253)$ for all 2163 data ($R_{int} = 0.0187$).

X-Ray diffraction data from a colourless rectangular crystal with the approximate dimensions 0.2 x 0.4 x 0.5 mm³ gave a four-molecule monoclinic unit cell. The final R_1 was 0.0461 and wR_2 was 0.1188. A semi-empirical absorption correction was applied to the data using CrysAlis RED 170.²⁸⁸ The maximum and minimum electron densities on the Fourier map were 0.18 e/Å³ (0.73 Å from H7A) and -0.26 e/Å³ (1.37 Å from C3). Atomic coordinates, crystal data and structure refinement tables as well as the IUCR³⁰¹ CIF check report are available in **Appendix A**. Full crystallographic data tables can be found in **Appendix E**.

***N,N'*-bis[(pyridin-2-yl)methylene] 2,2-dimethyl-propane-1,3-diamine (L4)**

$C_{17}H_{20}N_4$, fw = 280.37 amu, $a = 5.8140(14)$ Å, $b = 11.526(3)$ Å, $c = 12.033(3)$ Å, $\alpha = 101.812(2)^\circ$, $\beta = 97.454(3)^\circ$, $\gamma = 93.603(3)^\circ$, $V = 779.3(3)$ Å³, triclinic, $P\bar{1}$, $Z = 2$, $D_c = 1.195$ g cm⁻³, $\mu = 0.073$ mm⁻¹, $T = 100(2)$ K, $R_1 (wR_2) = 0.0414 (0.1054)$, for 3641 unique data with $I > 2\sigma(I)$, $R_1 (wR_2) = 0.0476 (0.1103)$ for all 8755 data ($R_{int} = 0.0220$).

A two-molecule triclinic unit cell was obtained from the colourless shard with the approximate dimensions 0.40 x 0.25 x 0.14 mm³. The final R_1 was 0.0414 and wR_2 was 0.1054. The maximum electron density on the Fourier map was 0.368 e/Å³ (0.75 Å from C8), while the minimum electron density was -0.215 e/Å³ (1.25 Å from C1). Atomic coordinates, crystal data and structure refinement tables as well as the IUCR³⁰¹ CIF check report are available in **Appendix A**. Full crystallographic data tables can be found in **Appendix E**.

***N,N'*-bis[(pyridin-2-yl)methylene]cyclohexane-1,2-diamine (L5)**

$C_{18}H_{20}N_4$, fw = 292.38 amu, $a = 10.8006(6)$ Å, $b = 9.7411(5)$ Å, $c = 15.4012(8)$ Å, $\beta = 96.412(5)^\circ$, $V = 1610.22(15)$ Å³, monoclinic, $P2_1/n$, $Z = 4$, $D_c = 1.206$ g cm⁻³, $\mu = 0.074$ mm⁻¹, $T = 102(2)$ K, $R_1 (wR_2) = 0.0430 (0.1034)$, for 3607 unique data with $I > 2\sigma(I)$, $R_1 (wR_2) = 0.0593 (0.1086)$ for all 6230 data ($R_{int} = 0.0299$).

A colourless crystal with the approximate dimensions 0.4 x 0.4 x 0.55 mm³ gave a four-molecule monoclinic unit cell. The final R_1 was 0.0430 and wR_2 was 0.1034. A semi-empirical absorption correction was applied to the data using CrysAlis RED 170.²⁸⁸ The maximum electron density on the Fourier map was 0.17 e/Å³ (1.43 Å from H15), while the minimum electron density was -0.28 e/Å³ (0.85 Å from C14). Atomic coordinates, crystal data and structure refinement tables as well as the IUCR³⁰¹ CIF check report is available in **Appendix A**. Full crystallographic data tables can be found in **Appendix E**.

2-pyridin-2-yl-1,4,5,6-tetrahydropyrimidinium hydrochloride (L2h)

$C_{18}H_{26}Cl_2N_6O$, fw = 413.35 amu, $a = 14.8632(4)$ Å, $b = 7.6289(2)$ Å, $c = 17.8066(5)$ Å, $V = 2019.09(9)$ Å³, orthorhombic, $Pbcn$, $Z = 8$, $D_c = 1.360$ g cm⁻³, $\mu = 3.062$ mm⁻¹, $T = 100(2)$ K, $R_1 (wR_2) = 0.0350 (0.0948)$, for 1788 unique data with $I > 2\sigma(I)$, $R_1 (wR_2) = 0.0380 (0.0970)$ for all 5131 data ($R_{int} = 0.0271$).

X-Ray diffraction data from a rhombic, pale yellow crystal with the approximate dimensions 0.30 x 0.20 x 0.10 mm³ gave an eight-molecule monoclinic unit cell. This ligand crystallises with a water molecule and a chloride ion as counter ions. The final R_1 was 0.0350 and wR_2 was 0.0948. An analytical absorption correction was applied to the data using CrysAlis RED 170.²⁸⁸ The maximum electron density on the Fourier map was 0.221 e/Å³ (1.09 Å from Cl1), while the minimum electron density was -0.318 e/Å³ (0.44 Å from Cl1). Atomic coordinates, crystal data and structure refinement tables as well as the IUCR³⁰¹ CIF check report are available in **Appendix A**. Full crystallographic data tables can be found in **Appendix E**.

2-pyridin-2-yl-1H-benzimidazole (L6h)

$C_{12}H_9N_3$, fw = 195.22 amu, $a = 18.5652(15)$ Å, $b = 10.7552(11)$ Å, $c = 10.1767(9)$ Å, $V = 2032.0(3)$ Å³, orthorhombic, $Pbna$, $Z = 8$, $D_c = 1.22$ g cm⁻³, $\mu = 0.077$ mm⁻¹, $T = 296(2)$ K, $R_1 (wR_2) = 0.0566 (0.1005)$, for 1405 unique data with $I > 2\sigma(I)$, $R_1 (wR_2) = 0.2037 (0.1341)$ for all 2374 data ($R_{int} = 0.0972$).

X-Ray diffraction data from a colourless crystal with the approximate dimensions 0.35 x 0.30 x 0.25 mm³ gave an eight-molecule orthorhombic unit cell. The final R_1 was 0.0566 and wR_2 was 0.1005. An analytical absorption correction was applied to the data using CrysAlis RED 170.²⁸⁸ The maximum electron density on the Fourier map was 0.155 e/Å³ (0.03 Å from N2), while the minimum electron density was -0.151 e/Å³ (1.52 Å from C12). Crystallographic data tables can be found in **Appendix E**.

***N,N'*-bis[phenyl(pyridin-2-yl)methylene] 2,2-dimethyl-propane-1,3-diamine (L4b)**

C₂₉H₂₈N₄, fw = 432.55 amu, $a = 10.0325(15)$ Å, $b = 24.790(4)$ Å, $c = 10.0691(15)$ Å, $\beta = 112.559(2)^\circ$, $V = 2312.7(6)$ Å³, monoclinic, $P2_1/c$, $Z = 4$, $D_c = 1.242$ g cm⁻³, $\mu = 0.074$ mm⁻¹, $T = 100(2)$ K, $R_1 (wR_2) = 0.0539 (0.1419)$, for 5397 unique data with $I > 2\sigma(I)$, $R_1 (wR_2) = 0.0663 (0.1509)$ for all 13631 data ($R_{int} = 0.0299$).

A four-molecule monoclinic unit cell was obtained from the colourless shard with the approximate dimensions 0.43 x 0.30 x 0.25 mm³. The final R_1 was 0.0539 and wR_2 was 0.1419. The maximum electron density on the Fourier map was 0.573 e/Å³ (1.01 Å from N3), while the minimum electron density was -0.430 e/Å³ (0.53 Å from N3). Atomic coordinates, crystal data and structure refinement tables as well as the IUCR³⁰¹ CIF check report are available in **Appendix A**. Full crystallographic data tables can be found in **Appendix E**.

2-(2-phenylimidazolidin-2-yl)pyridine (L1bh)

C₁₄H₁₅N₃, fw = 225.29 amu, $a = 16.727(2)$ Å, $b = 5.8039(5)$ Å, $c = 24.4882(17)$ Å, $\beta = 95.320(7)^\circ$, $V = 2367.1(4)$ Å³, monoclinic, $C2/c$, $Z = 8$, $D_c = 1.264$ g cm⁻³, $\mu = 0.077$ mm⁻¹, $T = 296(2)$ K, $R_1 (wR_2) = 0.0467 (0.1158)$, for 2872 unique data with $I > 2\sigma(I)$, $R_1 (wR_2) = 0.0555 (0.1192)$ for all 19111 data ($R_{int} = 0.0426$).

The small, white, almost colourless crystal with the approximate dimensions 0.55 x 0.45 x 0.35 mm³ gave X-ray diffraction data consistent with an eight-molecule monoclinic unit cell. The final R_1 was 0.0467 and wR_2 was 0.1158. A semi-empirical absorption correction was applied to the data using CrysAlis RED 170.²⁸⁸ The maximum and minimum electron densities on the Fourier map were 0.21 e/Å³ (0.75 Å from C9) and -0.19 e/Å³ (0.78 Å from C7). Atomic coordinates, crystal data and structure refinement tables as well as the IUCR³⁰¹ CIF check report are available in **Appendix A**. Full crystallographic data tables can be found in **Appendix E**.

2-phenyl-2-pyridin-2-ylhexahydropyrimidine (L2bh)

$C_{15}H_{17}N_3$, fw = 239.32 amu, $a = 8.2380(9)$ Å, $b = 9.0960(8)$ Å, $c = 9.2759(8)$ Å, $\alpha = 97.310(7)^\circ$, $\beta = 94.450(8)^\circ$, $\gamma = 111.855(9)^\circ$, $V = 633.95(10)$ Å³, triclinic, $P\bar{1}$, $Z = 2$, $D_c = 1.254$ g cm⁻³, $\mu = 0.076$ mm⁻¹, $T = 296(2)$ K, $R_1 (wR_2) = 0.0484 (0.1200)$, for 2495 unique data with $I > 2\sigma(I)$, $R_1 (wR_2) = 0.0766 (0.1329)$ for all 7440 data ($R_{int} = 0.0624$).

The X-ray diffraction data for a colorless rectangular crystal of **L2bh** (0.45 x 0.35 x 0.20 mm³) were consistent with a two-molecule triclinic unit cell. The final R_1 was 0.0484 and wR_2 was 0.1200. A semi-empirical absorption correction was applied to the data using CrysAlis RED 170.²⁸⁸ The maximum electron density on the Fourier map was 0.169 e/Å³ (0.85 Å from H9B), while the minimum electron density was -0.201 e/Å³ (1.12 Å from C6). Atomic coordinates, crystal data and structure refinement tables as well as the IUCR³⁰¹ CIF check report is available in **Appendix A**. Full crystallographic data tables can be found in **Appendix E**.

5,5-dimethyl-2-phenyl-2-pyridin-2-ylhexahydropyrimidine (L4bh)

$C_{17}H_{21}N_3$, fw = 267.37 amu, $a = 14.7533(6)$ Å, $b = 6.0380(2)$ Å, $c = 16.4381(6)$ Å, $\beta = 90.923(2)^\circ$, $V = 1464.12(9)$ Å³, monoclinic, $P2_1/c$, $Z = 4$, $D_c = 1.213$ g cm⁻³, $\mu = 0.073$ mm⁻¹, $T = 100(2)$ K, $R_1 (wR_2) = 0.0436 (0.1152)$, for 4128 unique data with $I > 2\sigma(I)$, $R_1 (wR_2) = 0.0598 (0.1216)$ for all 50915 data ($R_{int} = 0.0887$).

A colourless, prism (approximate dimensions 0.125 x 0.08 x 0.025 mm³) gave X-Ray diffraction data yielding a four-molecule monoclinic unit cell. The final R_1 was 0.0436 and wR_2 was 0.1152. The maximum electron density on the Fourier map was 0.334 e/Å³ (0.76 Å from C13), while the minimum electron density was -0.237 e/Å³ (0.61 Å from C5). Atomic coordinates, crystal data and structure refinement tables as well as the IUCR³⁰¹ CIF check report are available in **Appendix A**. Full crystallographic data tables can be found in **Appendix E**.

3.4.3 X-ray structures of the Schiff base ligands

All the above ligands gave white or colourless crystals suitable for X-ray diffraction studies. Some of the single crystals were grown by allowing slow evaporation, undisturbed for a few days, from diethyl ether (**L1**, **L4** and **L5**). Others were formed from the reaction mixture on standing (**L2h**, **L6h** and **L4bh**) or were a minor product which

precipitated out in a crystalline form along with the powder of the major product (**L1bh** and **L2bh**). All of the ligands that crystallised were found to be of either the monoclinic or orthorhombic systems, with the exception of **L4** and **L2bh**, which crystallised in the triclinic crystal system ($P\bar{1}$). All nonhydrogen atoms were refined anisotropically. Hydrogen atoms were inserted with standard SHELXL²⁹¹ idealisation parameters in their geometrically idealised positions for **L4b** and constrained to ride on their parent atoms, with distances in the range 0.95–1.00 Å. Hydrogen atoms for **L1**, **L5** and **L4** were located by difference Fourier synthesis and refined isotropically.

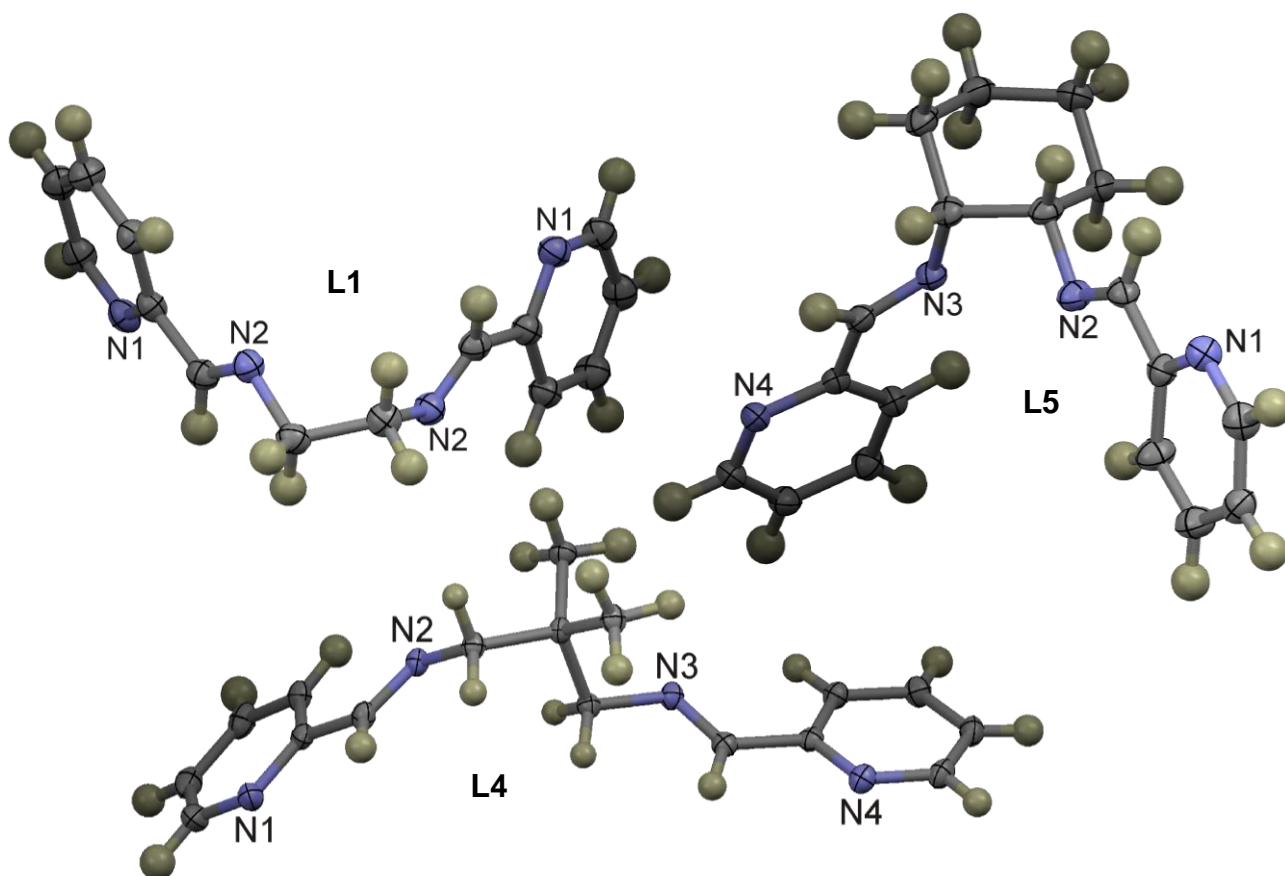


Figure 3.14: Thermal ellipsoid views (with the nitrogen atoms labelled) of the X-ray structures of **L1**, **L4** and **L5** (50% probability displacement ellipsoids), showing the overall molecular conformations. (Hydrogen atoms have been calculated for **L1** and **L5** and located for **L4**.)

L1, **L4** and **L5** are novel examples of structurally characterised N_4 -donor Schiff base ligands; their molecular structures are shown in the thermal ellipsoid plots in Figure 3.14. Due to the *cis*-configuration of the cyclohexane bridge there is no centre of inversion for **L5** and all the nitrogen atoms are unique. However, **L1** has inversion symmetry due to its symmetrical ethyl bridge and hence the ligand contains two identical halves. Although inversion symmetry would be expected for **L4**, such symmetry is absent due to the way

that the bridging group has been distorted. Selected bond lengths and angles are shown in Table 3.2. The *standard uncertainty* (estimated standard deviation) is given in parenthesis. Note that for bonds to differ by a statistically significant amount, the difference must be $> 4 \times$ the esd (estimated standard deviation). The lengths of the C=N bonds are experimentally equivalent: 1.267(2) (**L1**), 1.267(2) (**L4**) and 1.268(2) (**L5**) Å. These lengths fall within the expected range for imine bonds: 1.250 to 1.270 Å.^{158,302}

Table 3.2: Selected average bond lengths (Å) and angles (°) of the free Schiff base ligands.

	L1	L4	L5
N_i=C_i	1.267(2)	1.267(2)	1.268(2)
N_p-C_p	1.342(2)	1.347(2)	1.348(2)
C_f-C_g	1.519(3)	1.539(2)	1.533(2)
C_i-H_e	0.981(1)	0.989(2)	0.994(2)
C_i=N_i-C_f	117.0(1)	116.9(1)	116.5(1)
N_i-C_f-C_g	111.5(1)	112.2(1)	110.7(1)
N_p-C_p-C_i	115.3(1)	114.9(1)	115.0(1)
C_p-C_i-N_i	121.9(1)	121.8(1)	122.6(1)

There is no indication of π - π stacking for the pyridine rings in these ligand structures, even though such interactions might be expected to occur due to their abundance in heteroaromatic systems.³⁰³ Complementary short contacts are seen for all three of these ligands (as shown in Figure 3.15). Short intermolecular contacts have been observed between two neighbouring Schiff base units for the ligand **L5** (C_a-H_a...N_p and N_p...H_a-C_a). A similar contact involving the pyridine-nitrogen takes place in **L1** between C_i-H_e...N_p and N_p...H_e-C_i for adjacent molecules. Because the imine C-H group functions similarly to an aromatic C-H group as a known unconventional H-bond donor³⁰⁴, the pair of C-H...N interactions between neighbouring molecules is consistent with complementary H-bonding. Meanwhile, **L4** has a complementary relationship between the bridging hydrogens of one molecule with the pyridyl carbon atoms from another molecule. There is also a second set of complementary short contacts observed for **L5** involving the imine-nitrogen, C_c-H_c...N_i.

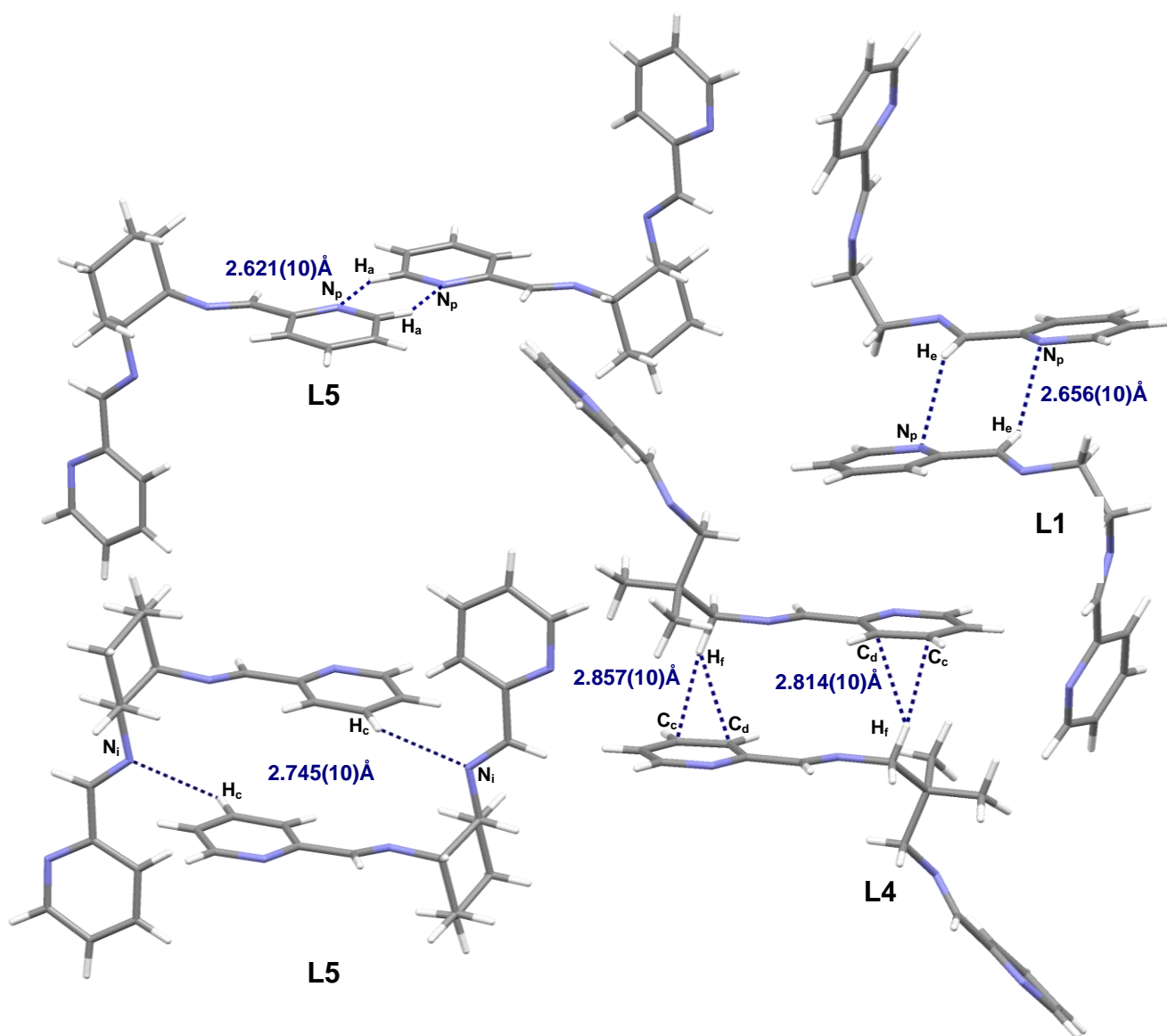


Figure 3.15: Complimentary short intermolecular contacts of **L5** ($2.621(10)$ and $2.745(10) \text{ \AA}$), **L1** ($2.656(10) \text{ \AA}$) and **L4** ($2.857(10) \text{ \AA}$ and $2.814(10) \text{ \AA}$).

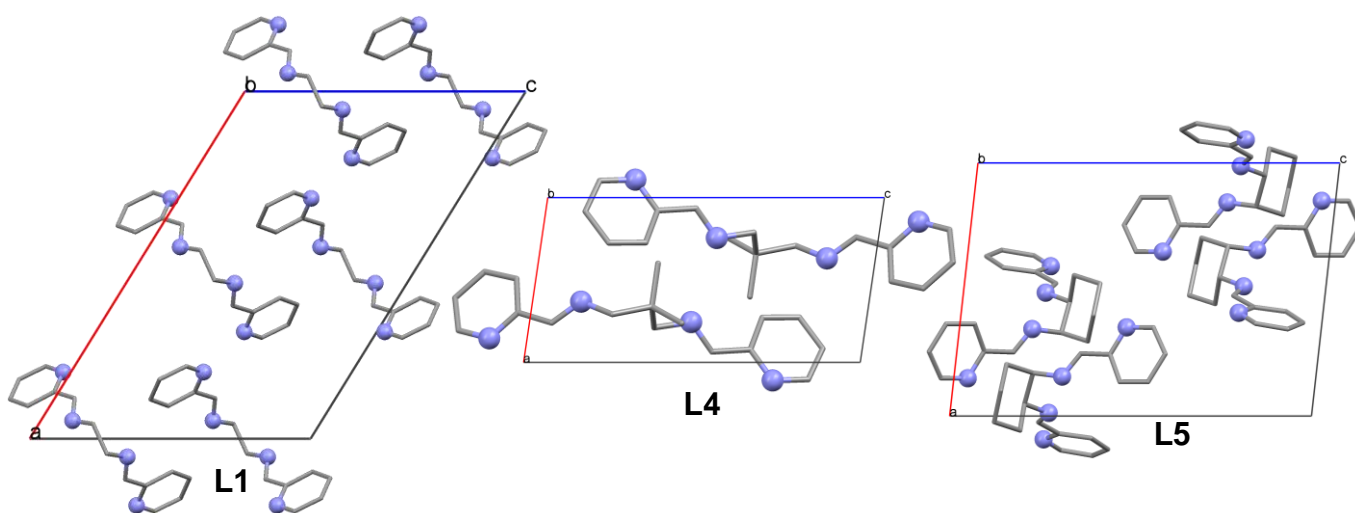


Figure 3.16: Crystal packing diagrams of the unit-cell for **L1** ($Z = 4$), **L4** ($Z = 2$) and **L5** ($Z = 4$), as viewed down the b -axis.

Thus, **L1** and **L5** represent systems with unconventional complementary (sp^2) C-H...N hydrogen bonding, while **L4** simply has a pair of molecules related by inversion with some short non-bonded contacts. The latter are not in any way stabilising, in contrast to the former H-bonded dimers. The unit-cell packing diagrams for each of the ligands are depicted in Figures 3.16 and display the patterns in which the molecules are located in the solid state. They reveal the infinite two-dimensional network structure for each of the compounds.

The ligands with the larger steric bulk on the imine carbon have more difficulty in crystallising. None of the methyl-substituted ligands have thus far produced X-ray quality crystals and only one structure has been obtained for the phenyl-substituted ligands; **L4b**. The structure of this ligand is shown in Figure 3.17 along with its complementary short contacts between $C_h-H_h \cdots C_{e2}$ and $C_{e2} \cdots H_h-C_h$. This space-filling model clearly shows the extra bulk on this ligand.

The other ligands that have formed X-ray quality crystals are mono(imine) ligands (1:1 ratio of aldehyde to diamine) resulting in an N_3 Schiff base ligand. This structure then cyclises intramolecularly at the imine carbon atom to produce an imidazole-containing or hexahydropyrimidine-containing bidentate ligand. X-ray quality crystals have been obtained for: **L2h**, **L6h**, **L1bh**, **L2bh** and **L4bh**. Not much success has thus far been had in obtaining crystals from their fully reacted ligands (2:1 ratio of aldehyde to diamine). Most of these ligands are viscous oils, except for **L4b**, for which the data has been presented here. These bidentate imidazole- or hexahydropyrimidine-containing ligands present the possibility of metallation in a 2:1 ligand to metal ratio. This has been attempted for **L6h** with Pt(II) and Pd(II), where metallated adducts in powder form have been obtained (see Chapter 2 – Experimental).

The imidazoline derivative, **L1bh**³⁰⁵, has been reported in the literature with the same space group as in this work. **L1bh** crystallises in the monoclinic space group $C2/c$ and displays an interesting supramolecular structure – a “zip” – that involves corresponding hydrogen bonding between neighbouring molecules (Figure 3.18). A similar interlocking hydrogen-bonded polymer has been seen by Munro and co-workers for a novel crystalline steroidal sapogenin³⁰⁶ and Barboiu *et al.* have reported metallosupramolecular zippers stabilised by strong π - π stacking interactions.³⁰⁷

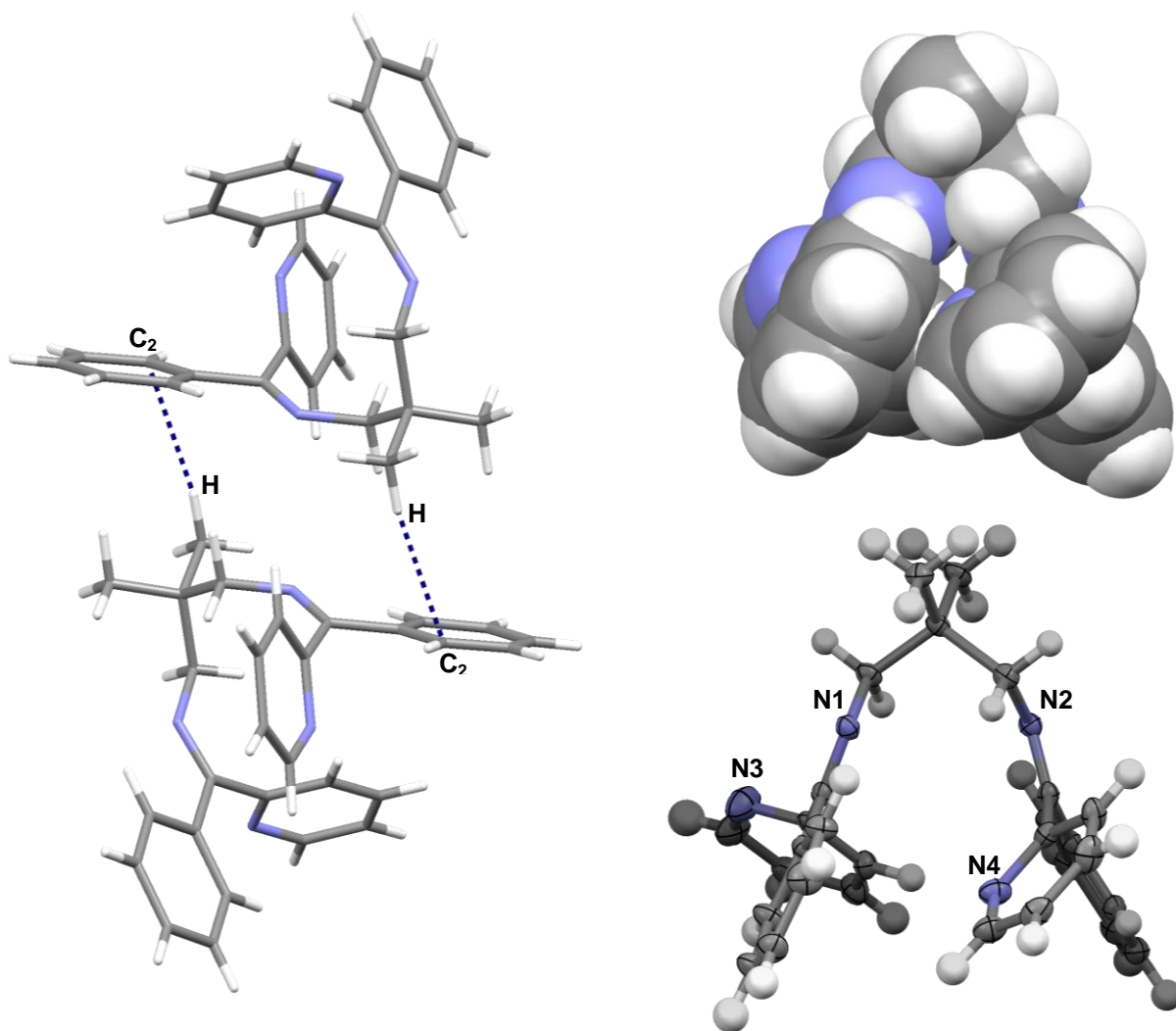


Figure 3.17: *Left:* The complementary short contacts of 2.842 Å for **L4b**. *Right:* The space filling model of **L4b** (top) and a thermal ellipsoid view of the X-ray structure of **L4b** (50% probability displacement ellipsoids), showing the overall molecular conformation where hydrogen atoms are rendered with arbitrary radii (bottom).

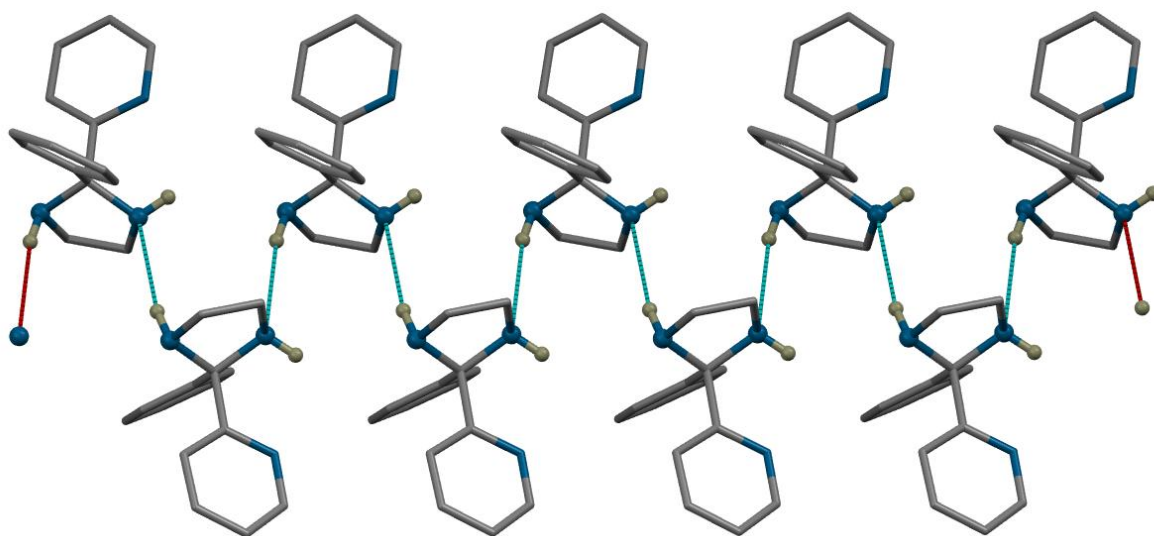


Figure 3.18: The packing “zip” of the imidazoline derivative, **L1bh**, showing short contacts between neighbouring Schiff base molecules. The N-H...N contact measures 2.733 Å.

Although **L6h** has also been synthesised before, it has been reported with space groups of *Pbca*³⁰⁸ and *P2/c*³⁰⁹. Here our space group setting for **L6h** is *Pbna* albeit with a slightly higher *R*-factor ($R_{\text{int}} = 0.0972$) than those reported for the *Pbca* and *P2/c* polymorphs. **L2h** and **L2bh** are both novel structures, with the only difference between them being either a hydrogen atom or a phenyl ring. These structures were synthesised when the aldehyde and diamine starting materials reacted in a 1:1 ratio (see page 41). The bulk of this group clearly has an effect on the structure as the two molecules show very different crystallographic arrangements. **L2h** has interesting hydrogen bonding which involves the water and chloride counter ions. The π – π stacking seen for this molecule is at a distance of 3.355 Å which presumably stabilises the crystal structure (Figure 3.19). **L2bh** does not possess this π – π stacking and the molecules pack in an alternating pattern (zig-zag structure) using hydrogen bonding to stabilise them (Figure 3.20). C_{α} -H $_{\alpha}$...N $_{\text{p}}$ complementary hydrogen bonding favours the formation of one-dimensional chains; this repeated packing chain of these molecules can be seen in Figure 3.21.

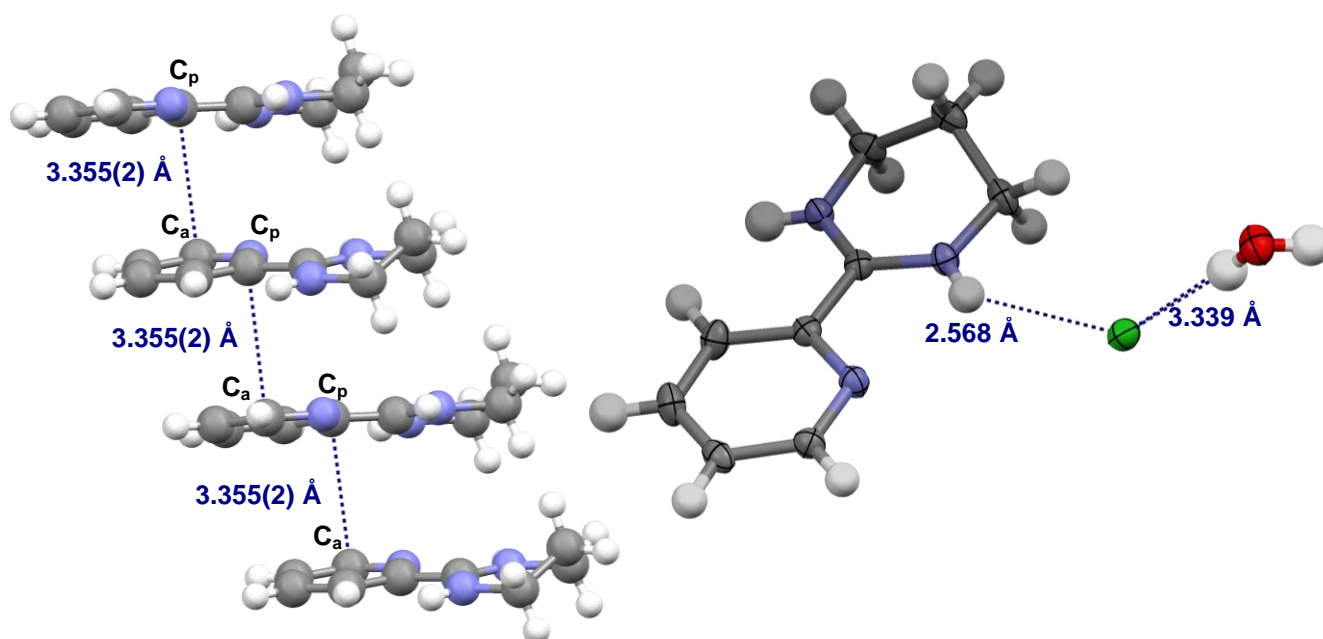


Figure 3.19: Ball and stick model to show the π – π stacking interactions (left) and a thermal ellipsoid view (at 50% probability) of the hydrogen bonding (right) for **L2h**.

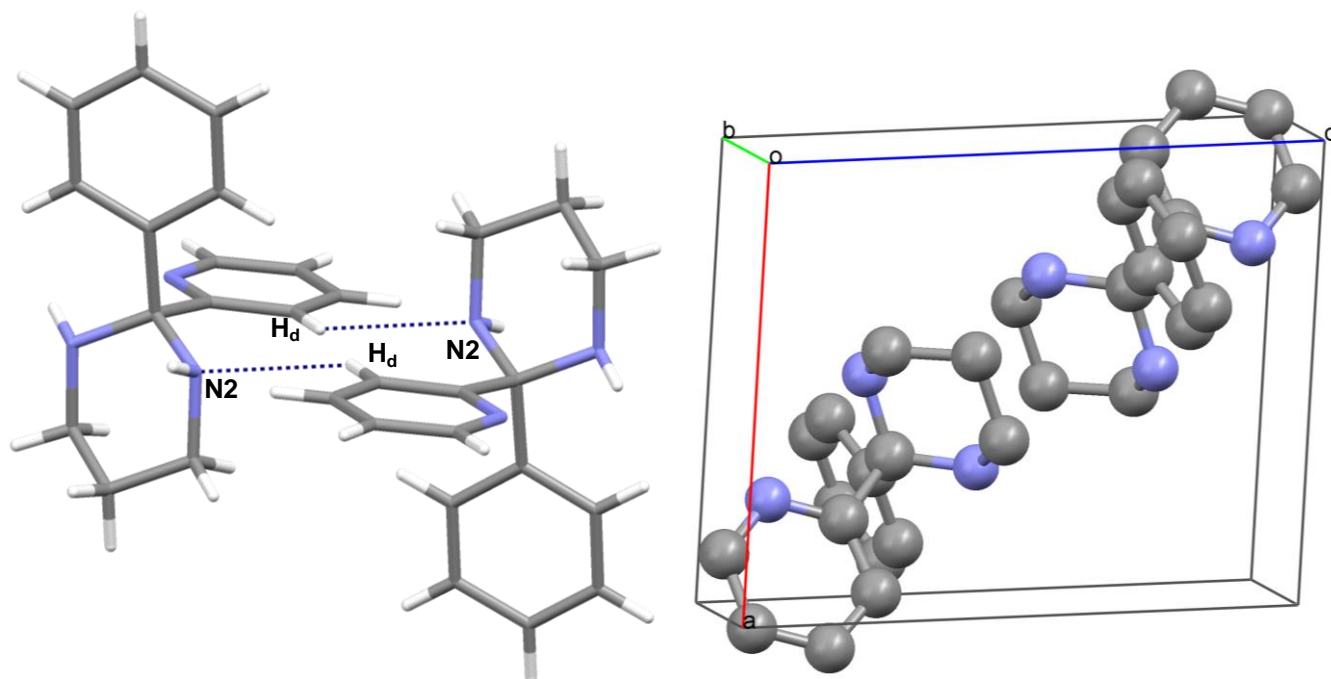


Figure 3.20: The complimentary short contacts of 2.722 Å between neighbouring molecules (left) and the packing diagram for the unit cell of **L2bh**, hydrogen atoms have been omitted for clarity (right).

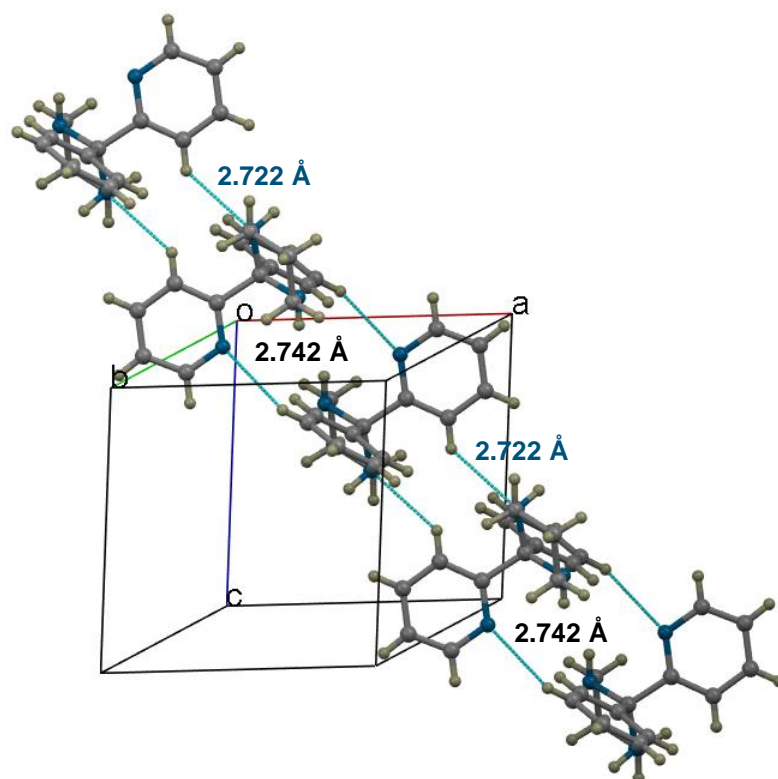


Figure 3.21: The hydrogen-bonded chain of **L2bh** with two alternating intermolecular separations: 2.742 and 2.722 Å.

The structure of **L4bh** is rather similar to that of **L2bh**, differing only by the dimethyl substitution of the central carbon of the propyl bridge of the diamine starting material. This results in greater bulk on the cyclised hexahydropyrimidine ring and subsequently very different packing to that of the triclinic **L2bh**. There are no complimentary short contacts for **L4bh**; but rather a “circular” arrangement of four molecules (Figure 3.22). These four molecules are connected to each other to form a symmetrical pattern, with $H_f \cdots H_3$ and $C_3/C_4 \cdots H_b$ short contacts on either side. Chains of these circular four molecules are then linked to other chains through $H_h \cdots H_h$ (2.2563 Å) short contacts. There is no π – π stacking observed for **L4bh**, as in **L2bh**.

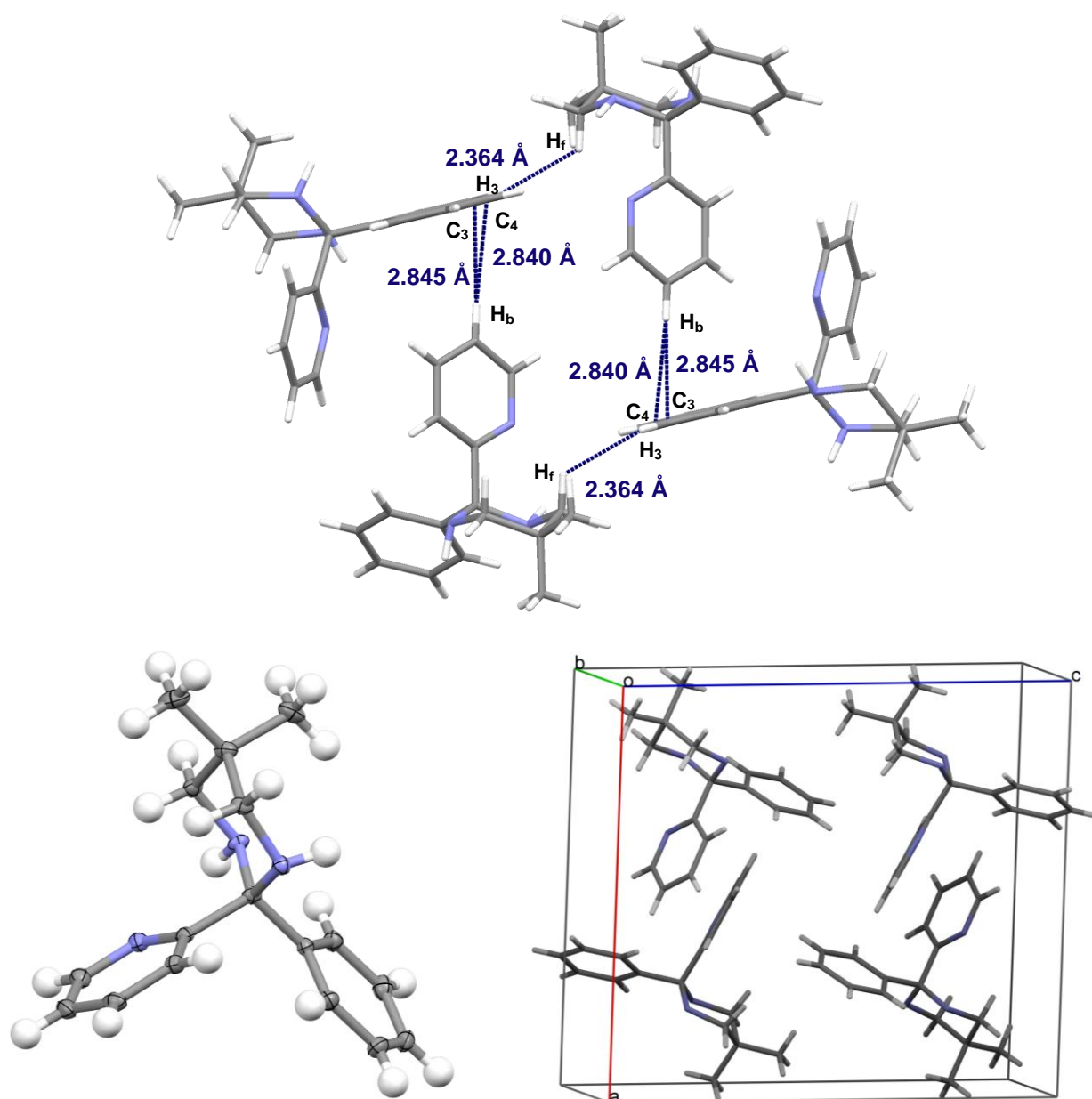


Figure 3.22: Top: The intermolecular short contacts between neighbouring molecules of **L4bh**. Bottom left: a thermal ellipsoid view (at 50% probability). Bottom right: the packing diagram for the monoclinic unit cell of **L4bh**.

3.4.4 X-ray data for the platinum(II) and palladium(II) complexes

***N,N'*-bis[(pyridin-2-yl)methylene]ethane-1,2-diamine platinum(II) hexafluorophosphate(V) (PtL1)**

$C_{14}H_{14}N_4F_{12}P_2Pt$, fw = 723.31 amu, $a = 15.0250(19)$ Å, $b = 10.4150(11)$ Å, $c = 13.0220(10)$ Å, $\beta = 99.285(9)^\circ$, $V = 2011.1(4)$ Å³, monoclinic, $C2/c$, $Z = 4$, $D_c = 2.389$ g cm⁻³, $\mu = 7.257$ mm⁻¹, $T = 100(2)$ K, $R_1 (wR_2) = 0.0483 (0.1017)$, for 3278 unique data with $I > 2\sigma(I)$, $R_1 (wR_2) = 0.0710 (0.1086)$ for all 10150 data ($R_{int} = 0.0622$).

A yellow-orange needle with the approximate dimensions 0.40 x 0.20 x 0.04 mm³ had X-ray diffraction data consistent with a four-molecule monoclinic unit cell. The final R_1 was 0.0483 and wR_2 was 0.1017. A semi-empirical absorption correction was applied to the data using CrysAlis RED 170.²⁸⁸ The maximum and minimum electron densities on the Fourier map were 4.000 e/Å³ (0.86 Å from Pt1) and -1.325 e/Å³ (0.77 Å from Pt1). Atomic coordinates, crystal data and structure refinement tables as well as the IUCR³⁰¹ CIF check report are available in **Appendix B**. Full crystallographic data tables can be found in **Appendix E**.

***N,N'*-bis[(pyridin-2-yl)methylene]ethane-1,2-diamine palladium(II) hexafluorophosphate(V) (PdL1)**

$C_{14}H_{14}N_4F_{12}P_2Pd$, fw = 634.6 amu, $a = 14.8209(19)$ Å, $b = 10.3056(10)$ Å, $c = 13.1386(17)$ Å, $\beta = 100.091(13)^\circ$, $V = 1975.7(4)$ Å³, monoclinic, $C2/c$, $Z = 4$, $D_c = 2.134$ g cm⁻³, $\mu = 1.224$ mm⁻¹, $T = 100(2)$ K, $R_1 (wR_2) = 0.0389 (0.0870)$, for 2110 unique data with $I > 2\sigma(I)$, $R_1 (wR_2) = 0.0663 (0.0984)$ for all 3756 data ($R_{int} = 0.0347$).

X-ray diffraction data from a small, yellow crystal with the approximate dimensions 0.10 x 0.15 x 0.20 mm³ gave a four-molecule monoclinic unit cell. The final R_1 was 0.0389 and wR_2 was 0.0870. A semi-empirical absorption correction was applied to the data using CrysAlis RED 170.²⁸⁸ The maximum and minimum electron densities on the Fourier map were 0.39 e/Å³ (1.04 Å from F1) and -0.51 e/Å³ (0.97 Å from Pd). Atomic coordinates, crystal data and structure refinement tables as well as the IUCR³⁰¹ CIF check report are available in **Appendix B**. Full crystallographic data tables can be found in **Appendix E**.

***N,N'*-bis[(pyridin-2-yl)methylene]propane-1,3-diamine platinum(II) hexafluorophosphate(V) (PtL2)**

$C_{15}H_{16}N_4F_{12}P_2Pt$, fw = 737.35 amu, $a = 13.134(5)$ Å, $b = 10.611(5)$ Å, $c = 15.103(5)$ Å, $\beta = 101.142(5)^\circ$, $V = 2065.2(14)$ Å³, monoclinic, $P2_1/n$, $Z = 4$, $D_c = 2.372$ g cm⁻³, $\mu = 7.069$ mm⁻¹, $T = 100(2)$ K, $R_1 (wR_2) = 0.0476 (0.1339)$, for 6656 unique data with $I > 2\sigma(I)$, $R_1 (wR_2) = 0.0687 (0.1414)$ for all 19521 data ($R_{int} = 0.0415$).

A four-molecule monoclinic unit cell was obtained for the X-ray diffraction data from a yellow crystal with the approximate dimensions 0.50 x 0.40 x 0.20 mm³. The final R_1 was 0.0476 and wR_2 was 0.1339. A semi-empirical absorption correction was applied to the data using CrysAlis RED 170.²⁸⁸ The maximum and minimum electron densities on the Fourier map were 3.113 e/Å³ (0.69 Å from Pt1) and -3.837 e/Å³ (0.71 Å from Pt1). Atomic coordinates, crystal data and structure refinement tables as well as the IUCR³⁰¹ CIF check report are available in **Appendix B**. Full crystallographic data tables can be found in **Appendix E**.

***N,N'*-bis[(pyridin-2-yl)methylene]propane-1,3-diamine palladium(II) hexafluorophosphate(V) (PdL2)**

$C_{15}H_{16}N_4F_{12}P_2Pd$, fw = 648.66 amu, $a = 13.443(5)$ Å, $b = 10.513(5)$ Å, $c = 14.905(5)$ Å, $\beta = 102.674(5)^\circ$, $V = 2055.1(14)$ Å³, monoclinic, $P2_1/n$, $Z = 4$, $D_c = 2.096$ g cm⁻³, $\mu = 1.179$ mm⁻¹, $T = 100(2)$ K, $R_1 (wR_2) = 0.0282 (0.0797)$, for 6638 unique data with $I > 2\sigma(I)$, $R_1 (wR_2) = 0.0327 (0.0814)$ for all 19654 data ($R_{int} = 0.0196$).

X-ray diffraction data from a yellow crystal with the approximate dimensions 0.60 x 0.50 x 0.40 mm³ gave a four-molecule monoclinic unit cell. The final R_1 was 0.0282 and wR_2 was 0.0797. The maximum and minimum electron densities on the Fourier map were 0.842 e/Å³ (0.68 Å from F1) and -1.435 e/Å³ (0.68 Å from Pd1). Atomic coordinates, crystal data and structure refinement tables as well as the IUCR³⁰¹ CIF check report are available **Appendix B**. Full crystallographic data tables can be found in **Appendix E**.

***N,N'*-bis[(pyridin-2-yl)methylene]2,2-dimethyl-propane-1,3-diamine platinum(II) hexafluorophosphate(V) (PtL4)**

$C_{34}H_{40}N_4F_{24}P_4Pt_2$, fw = 1530.72 amu, $a = 10.62600(10)$ Å, $b = 26.9950(3)$ Å, $c = 16.2420(2)$ Å, $\beta = 995.1930(10)^\circ$, $V = 4640(3)$ Å³, monoclinic, $P2_1/c$, $Z = 8$, $D_c = 2.191$ g

cm^{-3} , $\mu = 0.630 \text{ mm}^{-1}$, $T = 100(2) \text{ K}$, $R_1 (wR_2) = 0.0545 (0.1386)$, for 17394 unique data with $I > 2\sigma(I)$, $R_1 (wR_2) = 0.0686 (0.1472)$ for all 2927 data ($R_{\text{int}} = 0.0554$).

A yellow, plate-shaped crystal with the approximate dimensions $0.60 \times 0.40 \times 0.20 \text{ mm}^3$ gave X-ray diffraction data consistent with an eight-molecule unit cell comprising two independent molecules in the asymmetric unit. The final R_1 was 0.0545 and wR_2 was 0.1386. A semi-empirical absorption correction was applied to the data using CrysAlis RED 170.²⁸⁸ The maximum and minimum electron densities on the Fourier map were $1.711 \text{ e}/\text{\AA}^3$ (1.08 \AA from Pt1) and $-2.687 \text{ e}/\text{\AA}^3$ (1.22 \AA from Pt1). Atomic coordinates, crystal data and structure refinement tables as well as the IUCR³⁰¹ CIF check report are available in **Appendix B**. Full crystallographic data tables can be found in **Appendix E**.

***N,N'*-bis[(pyridin-2-yl)methylene]2,2-dimethyl-propane-1,3-diamine palladium(II) hexafluorophosphate(V) (PdL4)**

$\text{C}_{34}\text{H}_{40}\text{N}_4\text{F}_{24}\text{P}_4\text{Pd}_2$, fw = 1353.40 amu, $a = 10.5160(2) \text{ \AA}$, $b = 27.1650(5) \text{ \AA}$, $c = 16.2810(3) \text{ \AA}$, $\beta = 93.884(2)^\circ$, $V = 4640.26(15) \text{ \AA}^3$, monoclinic, $P2_1/c$, $Z = 8$, $D_c = 1.937 \text{ g cm}^{-3}$, $\mu = 0.105 \text{ mm}^{-1}$, $T = 293(2) \text{ K}$, $R_1 (wR_2) = 0.0729 (0.1876)$, for 17470 unique data with $I > 2\sigma(I)$, $R_1 (wR_2) = 0.1103 (0.2047)$ for all 74682 data ($R_{\text{int}} = 0.0730$).

X-ray diffraction data from a yellow crystal with the approximate dimensions $0.30 \times 0.30 \times 0.20 \text{ mm}^3$ were consistent with an eight-molecule unit cell comprising two independent molecules in the asymmetric unit. The final R_1 was 0.0729 and wR_2 was 0.1876. A semi-empirical absorption correction was applied to the data using CrysAlis RED 170.²⁸⁸ The maximum and minimum electron densities on the Fourier map were $6.609 \text{ e}/\text{\AA}^3$ (0.76 \AA from Pd2) and $-3.924 \text{ e}/\text{\AA}^3$ (0.77 \AA from Pd1). Atomic coordinates, crystal data and structure refinement tables as well as the IUCR³⁰¹ CIF check report are available in **Appendix B**. Full crystallographic data tables can be found in **Appendix E**.

***N,N'*- bis[(pyridin-2-yl)ethylene] 2,2-dimethyl- propane-1,3- diamine palladium(II) hexafluorophosphate(V) (PdL4m)**

$\text{C}_{19}\text{H}_{24}\text{N}_4\text{F}_{12}\text{P}_2\text{Pd}$, fw = 704.76 amu, $a = 8.262(5) \text{ \AA}$, $b = 13.068(5) \text{ \AA}$, $c = 23.981(5) \text{ \AA}$, $\beta = 98.914(5)^\circ$, $V = 2557.9(19) \text{ \AA}^3$, monoclinic, $P2_1/n$, $Z = 4$, $D_c = 1.830 \text{ g cm}^{-3}$, $\mu = 0.955 \text{ mm}^{-1}$, $T = 296(2) \text{ K}$, $R_1 (wR_2) = 0.0477 (0.1296)$, for 6099 unique data with $I > 2\sigma(I)$, $R_1 (wR_2) = 0.0614 (0.1355)$ for all 32956 data ($R_{\text{int}} = 0.0555$).

X-ray diffraction data from a yellow-brown crystal with the approximate dimensions 0.55 x 0.45 x 0.35 mm³ gave a four-molecule monoclinic unit cell. The final R_1 was 0.0477 and wR_2 was 0.1296. A semi-empirical absorption correction was applied to the data using CrysAlis RED 170.²⁸⁸ The maximum and minimum electron densities on the Fourier map were 0.791 e/Å³ (1.32 Å from F11) and -0.747 e/Å³ (0.75 Å from Pd1). Atomic coordinates, crystal data and structure refinement tables as well as the IUCR³⁰¹ CIF check report are available in **Appendix B**. Full crystallographic data tables can be found in **Appendix E**.

***N,N'*-bis[phenyl(pyridin-2-yl)methylene]2,2-dimethyl-propane-1,3-diamine palladium(II) hexafluorophosphate(V) (PdL4b)**

C₂₉H₂₈N₄F₁₂P₂Pd, fw = 828.89 amu, $a = 18.294(4)$ Å, $b = 10.329(2)$ Å, $c = 17.997(4)$ Å, $\beta = 97.109(3)^\circ$, $V = 3374.6(12)$ Å³, monoclinic, $P2_1/c$, $Z = 4$, $D_c = 1.631$ g cm⁻³, $\mu = 0.738$ mm⁻¹, $T = 100(2)$ K, $R_1 (wR_2) = 0.0415 (0.0997)$, for 8098 unique data with $I > 2\sigma(I)$, $R_1 (wR_2) = 0.0490 (0.1029)$ for all 21245 data ($R_{int} = 0.1028$).

X-ray diffraction data from a yellow crystal of **PdL4b** (0.1 x 0.1 x 0.1 mm³) were consistent with a four-molecule monoclinic unit cell. The final R_1 was 0.0415 and wR_2 was 0.1029. The maximum and minimum electron densities on the Fourier map were 0.851 e/Å³ (0.78 Å from N1) and -0.860 e/Å³ (0.77 Å from Pd1). Atomic coordinates, crystal data and structure refinement tables as well as the IUCR³⁰¹ CIF check report are available in **Appendix B**. Full crystallographic data tables can be found in **Appendix E**.

3.4.5 X-ray structures of the metal complexes

Despite the similar coordination geometries offered by this range of ligands with the two chosen metals, only eight complexes belonging to this group of compounds were structurally characterised in this work, namely **PtL1**, **PdL1**, **PtL2**, **PdL2**, **PtL4**, **PdL4**, **PdL4m** and **PdL4b**. We encountered problems growing X-ray quality crystals of some of the complexes due to the difficulty involved in obtaining bulk material for some of the metal complexes. For the first few crystals amenable to X-ray analysis, room temperature data collections were employed; however, these structures were redetermined at low temperature and better data sets were obtained. Hence, data were collected from all other crystals thereafter at 100(2) K. The structures were solved using direct methods in WinGX's implementation of SHELXS-97²⁸⁹ and refined to R -values all

smaller than 8%. All non-H atoms were located in the E-map and refined anisotropically with SHELXL-97.²⁹¹ Hydrogen atoms were located for **PdL2**, but ‘added’ (coordinates of the calculated positions were refined using a riding model)²⁹¹ for the other structures.

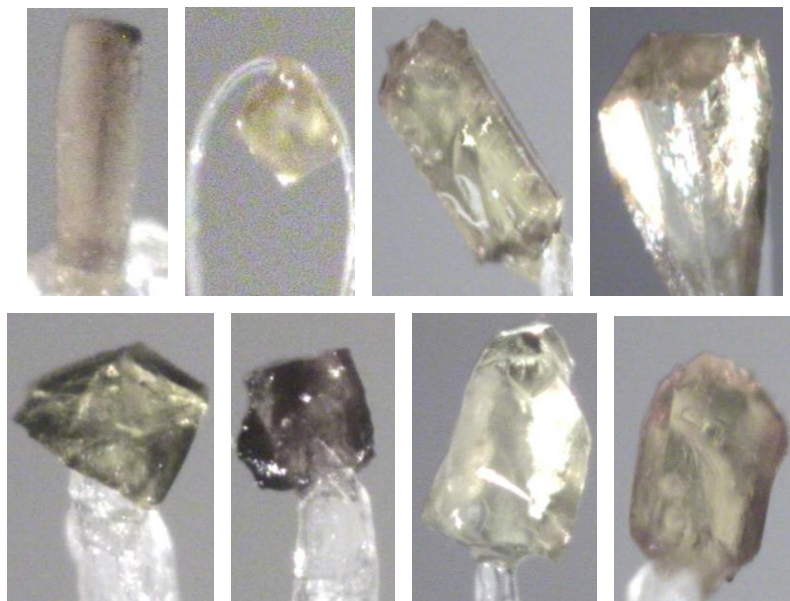


Figure 3.23: Photographs of the different crystal fragments used for data collection for the metal complexes. *Top:* **PtL1**, **PdL1**, **PtL2**, **PdL2**, and *bottom:* **PtL4**, **PdL4**, **PdL4m** and **PdL4b**, respectively.

The seven metal complexes presented here were yellow, orange or red in solution and the crystals were yellow, brown or orange (Figure 3.23). The crystals for these metal complexes were grown either by slow evaporation of acetonitrile (**PtL2**, **PdL2**, **PdL4m**) or solvent diffusion in test tubes (**PtL1**, **PdL1**, **PtL4**, **PdL4**, **PdL4b**). Different solvent systems were used including: acetonitrile/ethanol, 2-methoxy ethanol/ether and distilled water/ethanol.

3.4.5.1 Molecular structures

It is well known that relatively small structural modifications in a multidentate ligand may cause significant changes in the reactivity of the complexes. Platinum is a softer centre than palladium and subsequently it is more sensitive to electronic communication with the chelate ring than palladium. The reactivity of palladium(II) complexes is mostly reported to be a factor of 10^5 – 10^6 faster than that of the corresponding platinum(II) complexes (dependent on the ligands attached).²⁹⁹ Studies of the favoured conformations (in the solid state), as discovered by X-ray analysis, provide useful

insights into the differences and similarities in structural conformations and possible reactivity. The structures of the seven metal complexes synthesised in this work are represented in Figures 3.24 and 3.25.

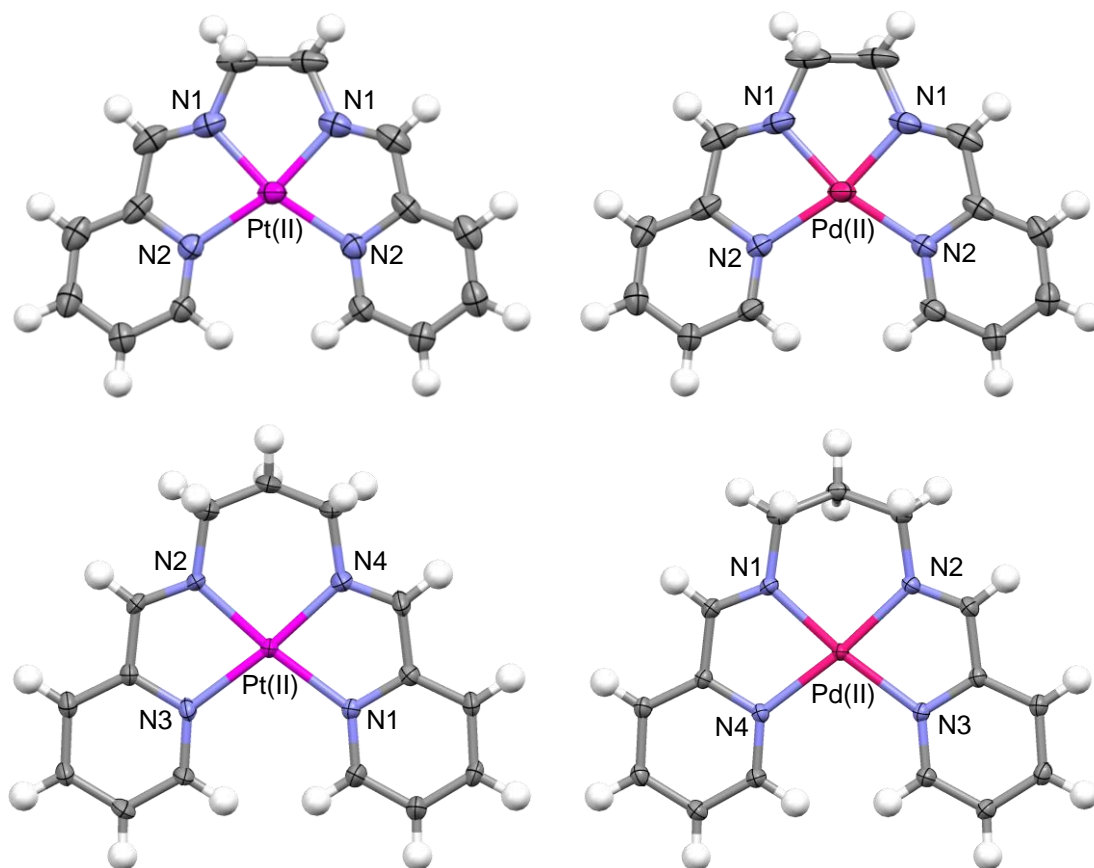


Figure 3.24: Thermal ellipsoid views (50% probability displacement ellipsoids) for four of the metal cations with the nitrogen atoms labelled. *Top: PtL1 and PdL1, and bottom: PtL2 and PdL2.* Counter ions have been omitted for clarity.

The cation chelates synthesised and structurally characterised in this work exhibit the approximately square planar geometry expected for this type of metal and ligand combination (as discussed previously). The hydrogen atoms have been calculated for most of the complexes and are therefore drawn as fixed-sized spheres in all the structures. The structures all display the same general orientation of chemically equivalent atoms around the metal centres and differ only by the nature of bridging diamine or by the group attached to the imine carbons (Figure 3.25: methyl groups for **PdL4m** and phenyl rings for **PdL4b**). Distortions from the N_4 plane (formed by the two imine (N_i) and two pyridine (N_p) nitrogen atoms) that may be observed are discussed in detail below.

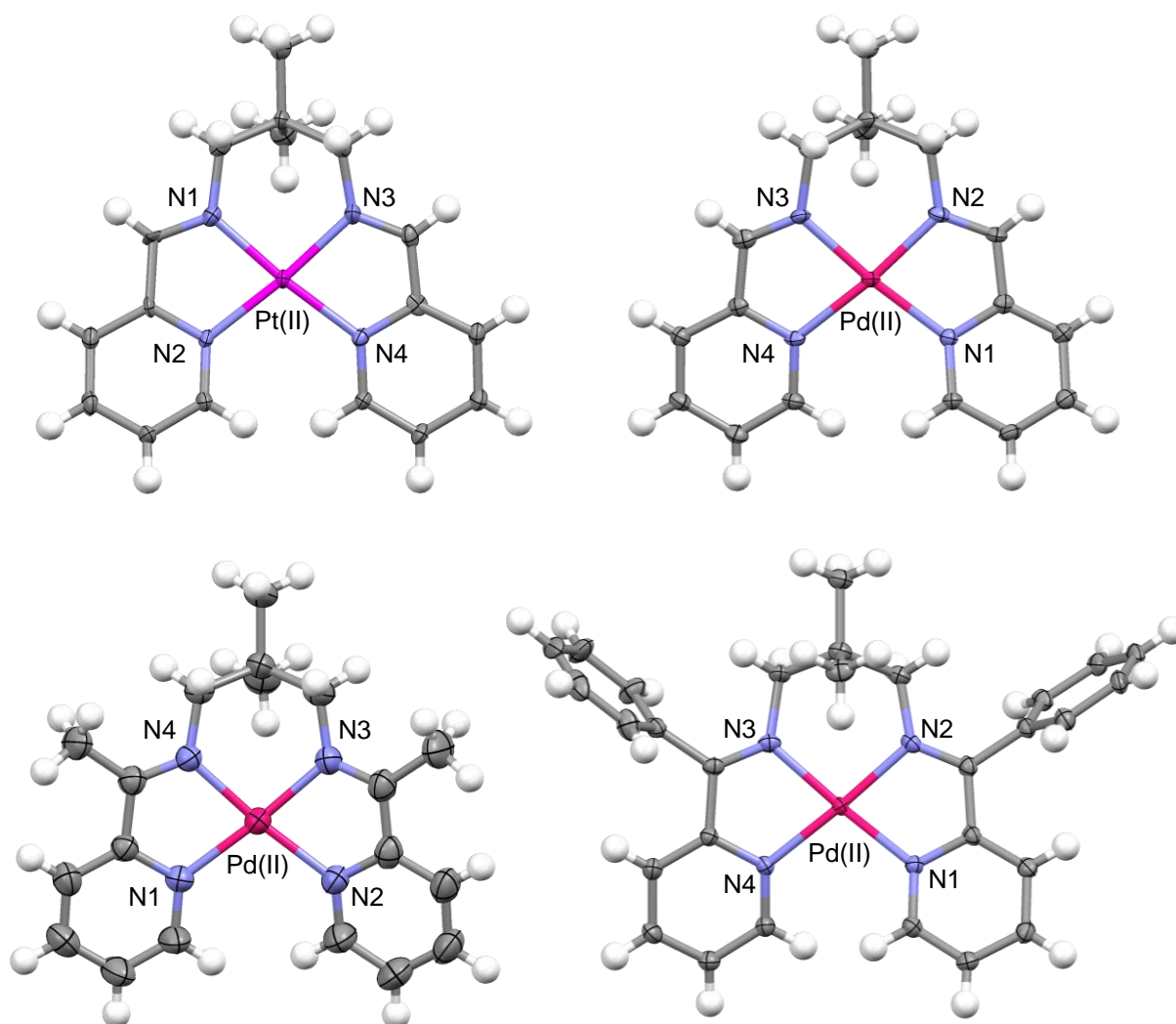


Figure 3.25: Thermal ellipsoid views (50% probability displacement ellipsoids) for four of the metal cations with the nitrogen atoms labelled. *Top: PtL4, PdL4, and bottom: PdL4m and PdL4b.* Counter ions have been omitted for clarity.

The Pt(II) and Pd(II) ions exhibit the expected four-coordinate, square planar geometry within each of the tetradentate chelates crystallised. These Pt(II) and Pd(II) complexes of the same ligands with essentially planar core conformations are isoelectronic, but not necessarily isomorphous. From the selected data in Table 3.3 it is noteworthy that the distance between the two imine-nitrogen atoms increases substantially from the ethyl-bridged to the propyl-bridged ligands, ~ 2.6 to ~ 2.9 Å. Due to this additional distance between the imine-nitrogen atoms the angle N_i-M-N_i also increases from ~ 85 to $\sim 95^\circ$. Hence, there is also a noticeable decrease in the angle N_p-M-N_p from ~ 113 to $\sim 105^\circ$ as we move from the 2-carbon bridging group to the 3-carbon bridging group. This is due to the greater chain length in the central chelate ring of the complex causing the pyridyl groups to be pushed further around the metal on each side, closing the gap at the end and hence reducing the size of the angle. The angles of N_i-M-N_p stay relatively constant

as the atoms in the vicinity that form the structure of these 5-membered chelates do not change, nor does their position. This therefore means that the difference in bite angle has to affect the structure by causing a change in the N_p -M- N_p angles.

Table 3.3: Selected averaged bond lengths (Å) and angles (°) for the metal complexes (esd given in parentheses).

	M- N_i	M- N_p	C _i = N_i	N_i to N_i ^a	N_i -M- N_i	N_i -M- N_p	N_p -M- N_p
PtL1	1.953(5)	2.051(5)	1.261(9)	2.652(8)	85.6(3)	80.8(2)	112.9(3)
PdL1	1.942(4)	2.046(3)	1.261(7)	2.628(5)	85.2(2)	80.7(2)	113.4(2)
PtL2	1.988(6)	2.060(5)	1.278(8)	2.936(8)	95.2(2)	79.4(2)	106.2(2)
PdL2	1.998(2)	2.073(2)	1.278(2)	2.922(2)	94.0(7)	80.2 (7)	105.3(3)
PtL4	1.986(7)	2.038(6)	1.298(10)	2.941(9)	95.6(3)	79.7(3)	106.5(2)
PdL4	1.992(4)	2.057(4)	1.280(6)	2.927(5)	94.3(2)	80.1(2)	105.5(2)
PdL4m	1.998(3)	2.056(3)	1.284(5)	2.946(5)	95.0(1)	79.5(1)	105.6(1)
PdL4b	2.002(5)	2.034(7)	1.291(8)	2.532(8)	96.9(2)	79.9(2)	103.9(2)

^a Chelate ring "width" measured as the N_i ... N_i distance in Mercury 2.4.³¹⁰

It may therefore be concluded that as the mean M- N_i distance decreases due to a change in metal ion radius or alkyl bridge length in the central chelate ring, the N_p -M- N_p and N_i -M- N_i angles concomitantly become progressively more obtuse and acute, respectively. When changing the size of the metal ion and/or the chelate ring the combined structural response of the metal ion coordination geometry is presented in Figure 3.26. A perturbation of one coordination group parameter (e.g. the M- N_i bond length) modulates (increases or decreases) the level of chelate ring strain in the complex. Increases in chelate ring strain are evidently alleviated through changes in the N_p -M- N_p and N_i -M- N_i angles with a decrease in one angular variable requiring a concomitant increase in the opposite angular variable. This means that the N_p -M- N_p and N_i -M- N_i angles will have opposite and linearly correlated "motion" in this category of metal chelates; this is confirmed by the graph in Figure 3.27.

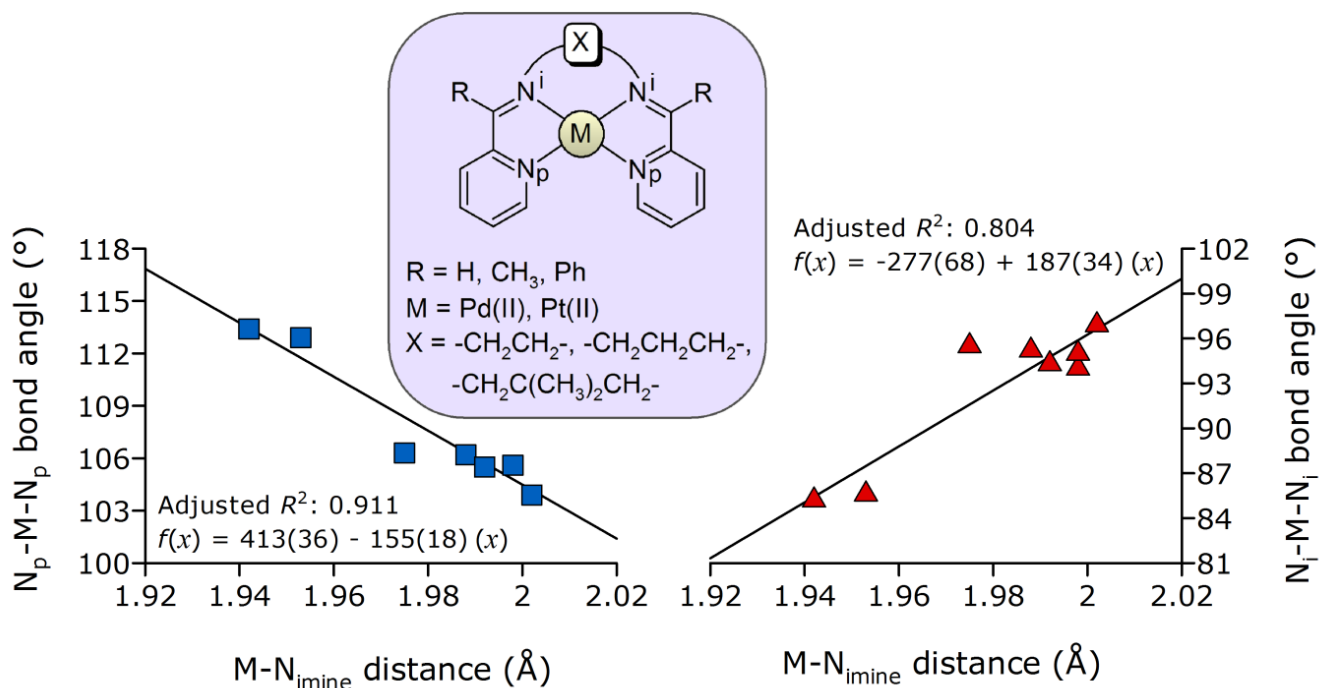


Figure 3.26: Graphs of the variation of N_p-M-N_p bond angle (left) and N_i-M-N_i bond angle (right) with the change in M-N_{imine} bond distance for eight crystallographically characterised square planar Pt(II) and Pd(II) bis(pyridine-imine) chelates. Key: N_p, pyridine nitrogen atom; N_i or N_i, imine nitrogen atom. The straight lines are linear least-squares fits of the data in each case.

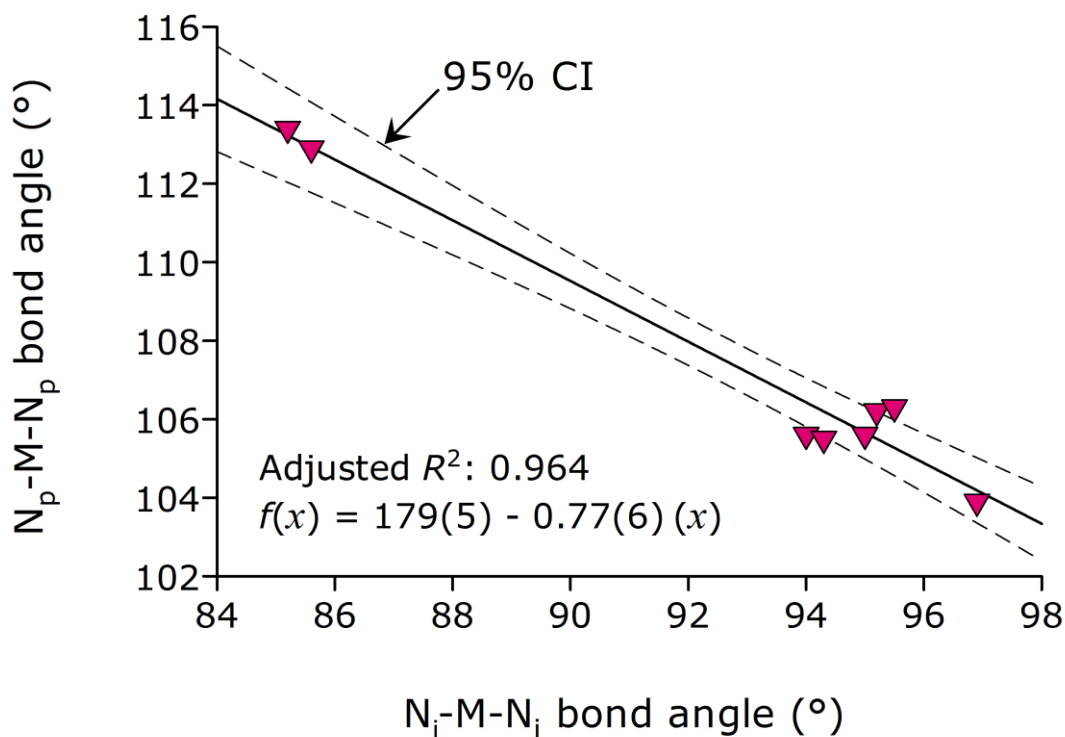


Figure 3.27: Linear least-squares fit of the variation of the N_p-M-N_p angle with the N_i-M-N_i angle. The regression function, correlation coefficient, and 95% confidence interval are shown.

Structural changes in the metal ion coordination geometry and central chelate ring are also accompanied by structural perturbations of the two imine groups of the complex. The relationship between the mean C=N distance of the complex and the mean M-N_i bond length is nonlinear (Figure 3.28) and is well fit by a standard quadratic function. The minimum in the function is observed at a M-N_i distance of 1.949 Å. The C=N_i distance measures 1.261 Å at the turning point and is slightly compressed relative to the ideal strain-free distance of 1.266 Å calculated for methanimine in the gas phase. The relationship may be interpreted in purely classical terms akin to Hooke's Law used to describe the deformation of bonds and angles in molecular mechanics force fields.³¹¹

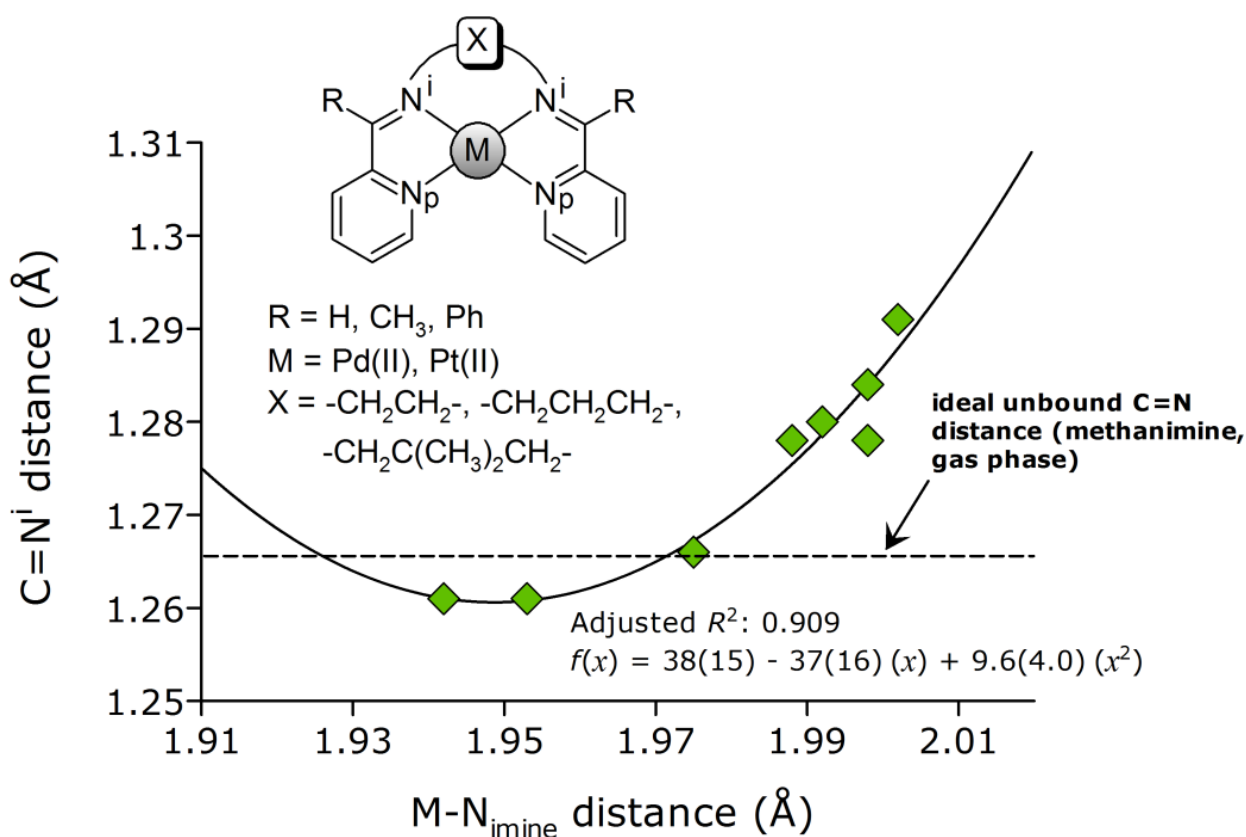


Figure 3.28: Plot of the variation in C=N_i bond distance with M-N_i bond distance for eight crystallographically characterised square planar Pt(II) and Pd(II) bis(pyridine-imine) chelates. The solid line is a nonlinear fit of a quadratic function to the experimental data. The dashed linear line marks the ideal (strain-free) distance for the C=N bond length of methanimine (H₂C=NH) computed at the B3LYP/6-311G** level of theory in the gas phase.

Compression of the M-N_i bonds from values > 2 Å to values around 1.95 Å requires concomitant compression of the C=N_i bonds for optimal C=N_i bonding to be maintained in the ligand as it adjusts to fit the changing coordination requirements of the chelated metal ion. Compression of the M-N_i bonds to mean distances shorter than 1.949 Å,

however, causes undue strain in the two five-membered chelate rings of the complex. This perturbation is marked by an increase in the C=N_i bond lengths as the imine nitrogen atoms maintain dative covalent bonding to the metal ion and the five-membered chelate rings structurally adjust to the increasingly “miss-fitting” metal ion. One caveat with the above interpretation is that additional data points for M-N_i distances <1.95 Å would be required to fully confirm the quadratic relationship shown in Figure 3.28. Despite this limitation, the relationship evident from the graph in Figure 3.28 and its interpretation is reasonable particularly since it gauges the perturbation of a key bond in the organic ligand and organic bonds are the least likely to depart from Morse- or Hooke-type deformation functions.

As the size of a chelate ring increases there is an increase in stability to a point after which the stability starts to decrease (3-membered < 4-membered, 5-membered ~ 6-membered > 7-membered > 8-membered).³¹² Therefore as the size of the chelate ligand increases there must be an effect on the structure of the chelate ring. The angle between the metal and two neighbouring donor atoms of a chelate is called the bite angle. It would be more energy taxing to alter the organic framework of the chelate than to change the bonds and angles around the metal, hence the bite angle and metal bonds are affected. This bite angle has been shown to increase with the size of the chelating ring. This may be explained by the need to accommodate the longer hydrocarbon chain which then forces the two donor atoms further apart. Different metal ions will also affect the size of the bite angle due to the different sizes of their preferred bond lengths.³¹² The smaller metal ions will be able to get closer to the 5-membered chelate rings due to the smaller bond length; however, the bite angle would also need to be favourable towards smaller metals.

A decrease in bite angle with decreasing ring size (6-membered to 5-membered chelate) has been observed for a platinum complex with a bidentate (N₂ donor) ligand,³¹³ as well as for nickel complexes with a tetradentate (N₄ donor) ligand.³¹⁴ The greater thermodynamic stability of 6-membered rings over 5-membered rings has also been shown by Crouch *et al.* for nitrogen donor ligands with a selection of transition metals.³¹⁵ The use of propyl and ethyl bridges and their resulting effects on the complex structure have been compared by Shimazaki and co-workers for a salen ligand (N₂O₂ donor) complexed to Ni(II), Pd(II) and Pt(II).³¹⁶ A greater distortion of the coordination plane was observed for the 1,3-diaminopropane backbone causing slightly longer coordination

sphere bond lengths. Similar results have been obtained for the palladium(II) complexes of bis(pyrrole-imine) ligands; the angle of the 5-membered chelate bite is $83.9(1)^\circ$ while the angle of the 6-membered chelate ring ranges between $94.7(2)$ and $95.9(2)^\circ$.

A chelate ring may not necessarily be the ideal size to “fit” the metal. This is true for both 5-membered and 6-membered chelate rings and may consequently cause internal strain.³¹² This potential mismatch involves the adjustment of metal-donor distances and subsequently the angles around the metal. For multidentate ligands there is more than just one chelate ring size to be taken into account. The combination of chelate ring sizes may increase or decrease the strain on the structure. For tridentate N_3 platinum chelates the presence of a 6-membered ring between two 5-membered rings was found to reduce the strain.³¹⁷ It is also possible for the structure of the chelate to pucker causing a tilt out of the plane and subsequently a smaller bite angle than if it were flat.³¹²

On careful inspection of the structures presented in Figures 3.24 and 3.25 it may be noted that the bridging groups are not completely planar. Distortion from the plane is observed for the ethyl bridging group of **PtL1** and **PdL1**. The ethyl bridge is completely distorted from planarity resulting in one CH_2 below the plane and one above. This reduces the strain on the metal and subsequently allows for a smaller bite angle. Distortion is also observed for the propyl bridging group of **PtL2** and **PdL2**, but to a lesser extent. The three carbon atoms form an envelope shape with the central CH_2 orientated out of the plane and each CH_2 on either side in the plane. With the limited distortion seen for this bridge it is understandable that it possesses a larger bite angle than the ethyl derivatives in order to accommodate the two in-plane CH_2 groups. This may therefore account for the difference of 10° seen between the bite angles of these two chelating groups. There is also a slight inconsistency in the bite angles for metal complexes that have the same sized chelating ring. Although the difference is equal within the esd of the angle determinations it is noteworthy that the bite angles for the platinum complexes are consistently larger than those of the palladium complexes. For the complexes of **L1** this difference is 0.4° , and 1.2° for the complexes of both **L2** and **L4**. This is similar to the increase in the bite angle from the palladium to platinum complexes of a salen ligand (with a propyl bridge) which was shown to be $\sim 1^\circ$.³¹⁶

Another important factor contributing to the size of the angle is the length of the bonds that form this angle. As mentioned, it is not energetically favourable to change the bonds

or angles of the organic component of the chelate ring. Consequently, the changes in bite angle that occur to accommodate the chelates of different lengths must cause some changes to bond lengths. The observed change in the M-N_i bond, when moving from the shorter to longer chelate chain, is an increase in length. This increase is 0.035 Å for the platinum complexes (**PtL1** → **PtL2**) and 0.056 Å for the palladium complexes (**PdL1** → **PdL2**). This somewhat lengthened bond (more than 4 x the esd) therefore helps to accommodate the slightly larger bite angle (Figure 3.26).

There is very little difference between **PdL4** and **PdL4m** which differ by the group on the imine carbon (–H for **PdL4** and –CH₃ for **PdL4m**). Most of the bonds differ by less than 4 times the esd and these discrepancies are therefore not remarkable. The same is generally true for **PdL4b**, which has a phenyl ring on the imine carbon. The most noticeable difference between **PdL4**, **PdL4m** and **PdL4b** is for the distance between the two N_i atoms. This distance reduces markedly for **PdL4b** in comparison to any of the other structures. The main reason for this can be attributed to the larger distortions from planarity observed for this structure, caused by the greater steric bulk present in this complex cation. More data and structures would be required to obtain valid trends and draw conclusions about the presence of greater steric bulk on the imine carbon. See Chapter 4.

It is important to note the differences or similarities between the central metal atoms. Platinum(II) and palladium(II) have already been noted as being isoelectronic and isostructural; however, they do have different electron configurations: 5d⁸ and 4d⁸ respectively. If we compare the elements in group 10 we can say that the ionic radius of Pd will be larger than Ni due to the valence electrons being in a higher orbital shell. Due to the added f electrons between Pd and Pt there is not sufficient shielding for the added nuclear charge and hence the outer shell electrons feel a greater attraction to the nucleus. This *lanthanide contraction* therefore plays a role in the size of the ionic radii for platinum atoms and ions. The Shannon and Prewit ionic radii[#] for the Pt(II) and Pd(II) square planar atoms are given as 0.60 and 0.64 Å, respectively.³¹⁸ Platinum and palladium have almost the same ionic radii and therefore we expect to see only slight differences for the platinum and palladium coordination group geometries.

[#] Effective ionic radii based on $r(\text{VI O}_2) = 1.40 \text{ \AA}$ by Shannon and Prewit.

Platinum-nitrogen bonds will normally average around 2.028(10) Å in the range of square-planar Pt(II)³¹⁹ and some similar Pt-N_p bonds have been reported as 2.03(1)³²⁰ and 2.015(4)³²¹. Thus the Pt-N_p bonds reported here for the platinum structures of these bis(pyridyl-imine) chelates (2.036(7)–2.060(5) Å) are slightly longer than expected; and the Pt-N_i bonds are slightly shorter (1.953(5)–1.988(6) Å). The average of all these bonds, 2.011 Å, is however close to the expected range. The metal-nitrogen bonds are decidedly larger (~ 0.1 Å) for the bond to the pyridine-nitrogen than the bond to the imine-nitrogen. This may be attributed to the imine nitrogen being a stronger base when compared with the pyridyl nitrogen³²² as well as differences in the C=N-C bond angles for the two donor atom types.

There are no Schiff base ligands of this type with Pt(II) or Pd(II) in the literature; however, some platinum and palladium complexes of structurally similar bis(pyrrole-imine) tetradentate N₄ chelates do exist (Figure 3.29). These complexes are expected to have very similar M-N_i bonds with slightly shorter M-N_p bonds than those observed for M-N_p in this work. Platinum(II) complexes have been synthesised with a *trans*-cyclohexyl bridging group forming three five-membered chelate rings around the square planar platinum centre. The Pt-N_i bonds, averaging 1.947(7) Å, are shorter than the Pt-N_p bonds, averaging 2.021(6) Å. These values are both slightly shorter than those reported in this work; however, considering the reported errors these values are within range of each other.

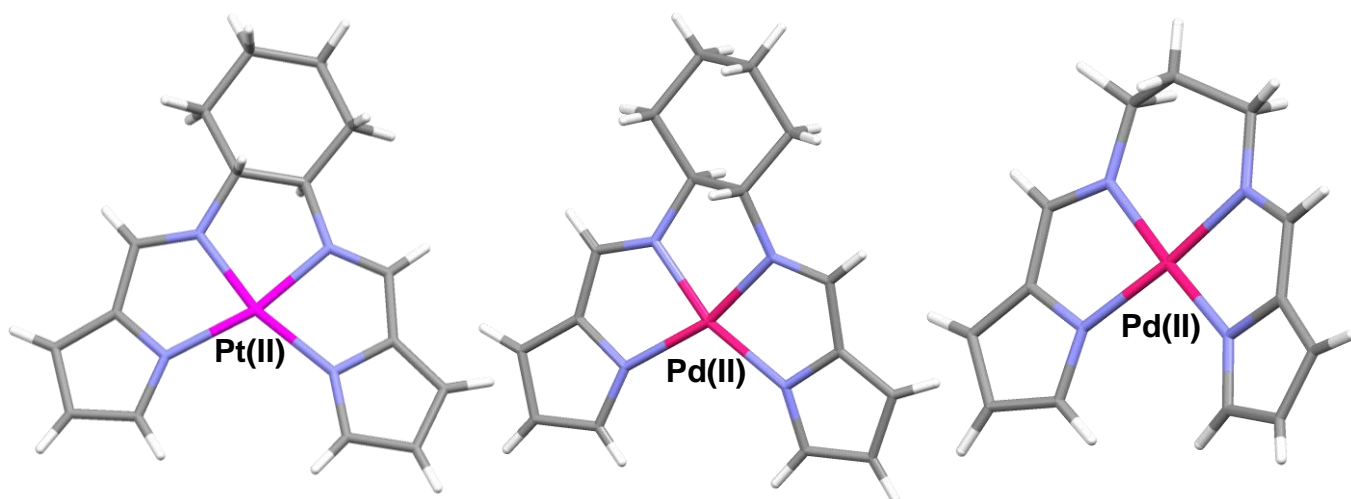


Figure 3.29: The structures of Pt(II) and Pd(II) bis(pyrrole-imine) Schiff base ligands: SOGJOO,²⁷⁹ XUVQEK and XUVQIO.³²³

Palladium complexes of bis(pyrrole-imine) ligands with propyl and *trans*-cyclohexane bridges have been synthesised by Bacchi *et al.*³²³ The Pd-N_i bonds for the propyl bridged complex, averaged between the four crystallographically independent molecules, measure 2.006(7) Å, while for the *trans*-cyclohexane bridged complex they average 1.961(3) Å. The Pd-N_{pyrrole} bonds are longer than those for Pd-N_i: 2.046(3) Å (*trans*-cyclohexane bridge) and 2.012(2) Å (propyl bridge), as is observed for the complexes in this work. The Pd-N_i bonds for the complexes presented here range from 1.942–1.998(4) Å and the Pd-N_p bonds from 2.046–2.073(4) Å. Once again, with errors accounted for, these values are comparable.

The Pd-N_i and Pd-N_p bond distances for PAKLOD (palladium complex of a butyl-bridged bis(pyridyl-imine) chelate: Figure 3.9)¹⁹⁵ average ~ 2.015(7) and ~ 2.033(7) Å, respectively. The Pd-N_i bond lengths are shorter for the palladium complexes in this work, while the Pd-N_p bond lengths are longer. This may be explained by the difference in geometry between the square planar complexes in this work and the tetrahedral distortion seen for the Pd atom in PAKLOD. This distortion was caused by the large deformation in the 2,2'-dimethyl-substituted biphenyl backbone of the bridging group. Another distorted tetrahedral palladium(II) complex is observed when two pyridine-2-carbaldoxime ligands are coordinated (TIQZEZ).³²⁴ These two bidentate ligands allow the structure to distort from the expected square planar conformation of the tetradentate complexes seen in this work. The donor-acceptor Pd-N distances vary for TIQZEZ between 1.9891 Å and 2.074 Å, which agree reasonably well with those recorded here.

The bite angle of N_i-M-N_i for PAKLOD is larger (99.0(3)^o) than those observed in this work (~ 85–95^o).¹⁹⁵ This can be easily accounted for by the difference in the size of the chelate rings. As discussed, we expect the bite angle to increase with increasing chain length of the chelate and hence this 7-membered ring would be expected to have a larger bite angle than those for the 5- and 6-membered chelate rings. This same angle in TIQZEZ does not form a chelate ring; however, it has a magnitude of 94.68(9)^o. This is much larger than the bite angles for the palladium complexes with both the 5- and 6-membered chelate rings. This therefore lends support to our argument that the size and type of the chelate ring has an effect on the size of the angle, as does the difference in bite angles observed for the palladium(II) bis(pyrrole-imine) derivatives (83.9(1)^o for the 5-membered chelate and between 94.7(2) and 95.9(2)^o for the 6-membered chelate).

It may be noted from Table 3.3 that the Pt(II) and Pd(II) coordination group distances are equal within the esd values of the distance determinations. This is expected due to the *lanthanide contraction*, as mentioned above. Equivalent bonds are therefore quite similar for the different ligands as well as for both the platinum and palladium derivatives. The imine bonds are relatively consistent throughout and rather similar for both the Pt and Pd derivatives of the same ligand, but do offer an interesting trend (Figure 3.28). The chelate ring strain and its alleviation through structural adjustments leads to measurable changes in the C=N bonds. The C_i=N_i bond lengths range from 1.261(9)–1.291(5) Å for these metal complexes and this is within the range of previously reported values observed for imine bonds.^{323,325}

We have investigated the structures, conformations, and electronic properties of several new bis(pyridine-imine) chelates of Pt(II) and Pd(II) in an effort to understand the coordination chemistry displayed by them. Single-crystal XRD data at low temperature reveal the complexes to be mainly planar around the four nitrogen atoms, with barely any or very little distortion. The distortion of these square planar complexes out of the plane has been measured for the metal, C_a of the pyridine rings and the central CH₂ of the bridging group (Table 3.4). The four nitrogen donor atoms are taken to lie exactly on the mean plane of the molecule and measurements are made from there.

The metal lies in the N₄ plane for the complexes of **L1**, but is slightly displaced (perpendicular to the plane) for the complexes of **L2**, **L4** **L4m** and **L4b**. There is no obvious trend in the distortion of the metal for the complexes of these ligands. There is, however, a notable change in the distortion of the metal from the plane from the ligand with the 2-carbon bridge to the 3-carbon bridge. The metal is in the N₄ plane for the ethyl bridge and then moves out of the plane for the longer propyl bridge. This is supported by the lengthening of the M-N bonds moving from complexes of **L1** to **L2**. The ethyl bridging groups show slight distortion from the plane, which increases for the central carbon of the propyl bridges. The palladium complex is distorted slightly more than its platinum counterpart in each case. This is also true for the distortion of the pyridine rings from the N₄ plane, except for the complexes of **L1**. The structure of **PdL4b** shows the greatest distortions from planarity; this may be explained by the increased steric bulk this ligand possesses.

Table 3.4: The conformations around the metal centre for each complex and their distortions from the N₄ plane (Å).

	Conformation shape	Pyridine rings tilted out of plane ^a		CH ₂ of bridging group from plane	Metal from plane
PtL1	planar	-0.012	0.012	0.251 ^b	0
PdL1	planar	-0.004	0.004	0.230 ^b	0
PtL2	planar	-0.049	0.037	0.280 ^c	-0.007
PdL2	moderate nonplanarity	-0.086	0.061	0.661 ^c	-0.017
PtL4	saddled or twisted with moderate nonplanarity	-0.121 / 0.231	-0.233 / -0.374	0.427 / 0.519 ^c	-0.061 / -0.015
PdL4	saddled or twisted with moderate nonplanarity	-0.187 / -0.236	-0.139 / 0.366	0.460 / 0.552 ^c	-0.079 / -0.025
PdL4m	saddled with moderate nonplanarity	+0.239	+0.067	0.879 ^c	0.082
PdL4b	twisted with increased nonplanarity	-0.521	+0.414	0.646	0.038

^a Distance measured from the plane to C_a in Mercury.³¹⁰

^b C_f for **L1** complexes.

^c C_g for **L2**, **L4**, **L4m** and **L4b** complexes.

3.4.5.2 Crystal Packing

Complexes of L1 and L2:

Both the complexes of **L1** crystallise in the same space group: monoclinic, *C2/c*; and the complexes of **L2** also crystallise in the equivalent space group: monoclinic, *P2₁/n*. The only short contacts seen for **PtL1**, **PdL1** and **PtL2** are those to the PF₆⁻ counter ions which pack in-between the cations as seen in Figures 3.30 and 3.31. The F...H intermolecular contacts observed here allow for the formation of relatively stable crystal lattices. The strange behaviour of fluorine in non-bonded interactions has been recognised in the literature.³²⁶ Mostly, fluorine will rarely form hydrogen bonds, which is explained by many electrostatic and steric factors (e.g. its low polarisability and tightly contracted lone pairs).³²⁷ Despite these interactions involving fluorine being much

weaker than conventional hydrogen bonds the role which they play in molecular packing cannot be ignored.³²⁷ A search of the CSD reveals the common occurrence of C–H...F interactions in organic crystals. Althoff *et al.* have shown that even a single C–H...F–C contact may be strong enough to pair two molecules.³²⁸

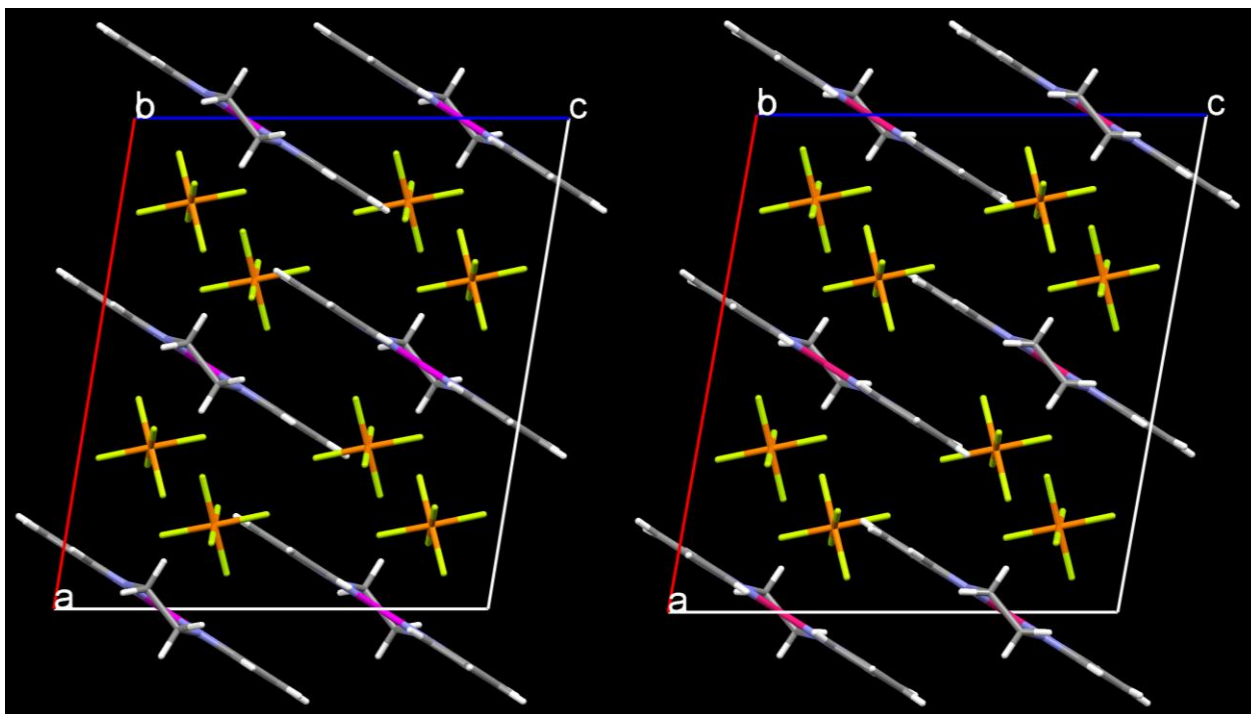


Figure 3.30: Crystal packing viewed down the *b*-axis for **PtL1** ($Z = 4$) and **PdL1** ($Z = 4$).

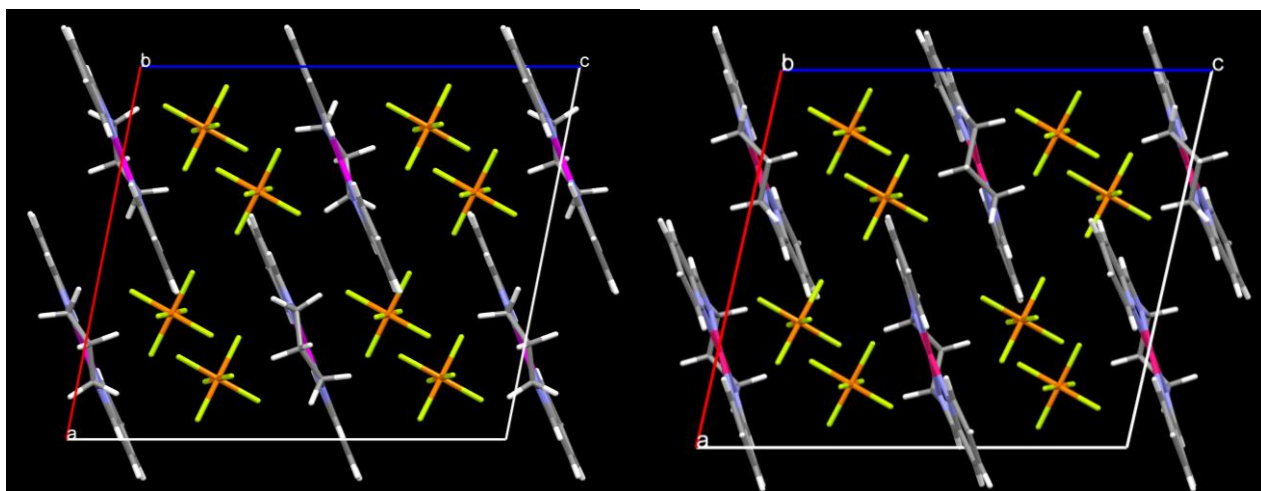


Figure 3.31: Crystal packing viewed down the *b*-axis for **PtL2** ($Z = 4$) and **PdL2** ($Z = 4$).

The metal cations and hexafluorophosphate ions of **PtL1**, **PdL1** and **PtL2** are connected via C–H...F hydrogen bonding with H...F distances ranging from 2.200 to 2.628 Å. These short C–H...F contacts are presented in Table 3.5 and are consistent with relatively strong hydrogen bonds between the hydrogen atoms of the cationic metal chelates and

the fluorine atoms of the anions. A three-dimensional hydrogen-bonded network is created between the interacting cations and anions. Crystal structures were not obtained for most of these metal complexes with smaller or different anions (Cl^- or SbF_6^-). This fact alone clearly suggests the importance of these particular counter ions and their intermolecular interactions that evidently allow the formation of these crystals.

Table 3.5: Selected C–H...F interaction distances (Å) observed for **PtL1**, **PdL1**, **PtL2** and **PdL2**.

Hydrogen atom involved in the interaction	PtL1	PdL1	PtL2	PdL2
H_a	2.594	2.650(40)	–	–
H_c	2.421	2.559(40)	2.435	2.459
	2.488	2.536(40)	2.504	2.516
H_d	–	–	2.619	2.603
H_e	2.437	2.379(40)	2.373	2.436
	2.318	2.195(40)	2.399	2.417
H_f	2.649	–	2.618	2.600
	2.521	–	–	2.658
H_g	–	–	2.642	2.517
	–	–	2.469	2.631

For **PdL2** there are complementary short contacts of 2.848 Å between $\text{C}_f\text{-H}_f\cdots\text{C}_c$. Once more, as seen for the respective ligands, there is no experimentally significant π - π stacking involving the pyridine rings of adjacent molecules. One important reason for this, despite the aromatic nature of the pyridyl groups and the fact that they are well known to π -stack,³⁰³ is that the cationic chelates in the present salts are divalent. Hunter and Sanders have shown that π - π interactions occur when attractive contacts that take place between π -electrons and the σ -framework prevail over unfavourable contributions, e.g. π -electron repulsion.³²⁹ Thus the complexes in this work possess significant Coulombic repulsion which is likely between cations in the lattice³²⁰ and these forces of repulsion presumably outweigh any attractive London/dispersion forces that contribute to π - π stacking.

The observed short contacts may be explained for the **L1** complexes by the size of the bridging group. Due to the bridging group being rather small the cation is mostly flat and hence there is barely any out-of-plane tilting of the pyridyl groups. Thus there is not much contact between the cations themselves, but somewhat more between the cations and their PF_6^- counter ions. These anions are positioned between the metal complexes in the horizontal plane as well as in the vertical plane between the cations. The conformation of the propyl bridge linking the two pyridyl groups is not the regular staggered arrangement for an aliphatic chain. It is clear that the bridging group adopts a more curved conformation, which allows the two imine nitrogen atoms to point towards the metal centre. The structure of **PtL2** is nonetheless predominantly flat with only minor distortions from the N_4 plane.

For **PdL2** the distortion out of the N_4 plane is slightly greater (visible in the packing in Figure 3.31). This is due to the difference in size between the metal centres as the ligand has to slightly ruffle in order to fit around the smaller palladium atom. This therefore allows the complimentary short contact observed between two cations for $\text{C}_r\text{-H}_r\cdots\text{C}_c$.

Due to the similarities between platinum(II) and palladium(II) it is obvious that these two metals are likely to have similar preferences with respect to their ligand selectivity and the symmetry of their coordination compounds.³³⁰ Each divalent metal centre is encircled by a distorted square planar array of four nitrogen atoms with the metal ion located in the mean square plane formed by these four ligating atoms (**PtL1** and **PdL1**) or only slightly distorted from it (**PtL2** and **PdL2**). The two complexes of each ligand are therefore isomorphous; they have the same space group, and remarkably similar bond distances and angles as well as similar unit cell parameters. This can be easily observed from their packing arrangements which are almost identical for each group of complexes. The only difference between them is the position of the cations of the Pd(II) chelates. For the Pd(II) chelates, the alkyl bridges of the cations point along a negative b -axis direction, while those of the Pt(II) chelates point along the positive b -axis direction. In effect, the cation orientations differ about an axis that lies in the ac plane and bisects the a - O - c angle (where O is the cell origin) for the Pt(II) and Pd(II) salts, by a 180° rotation.

Complexes of **L4**, **L4m** and **L4b**:

PtL4 and **PdL4** each have two molecules with different conformations, one saddled and the other 'twisted'. This out-of-plane tilt of the pyridine rings (relative to the N_4 plane) may

be accredited to alleviation of unfavourable steric interactions between the adjacent pyridine rings. These molecules crystallise in alternating layers of the two types of cations (saddled and twisted) with the anions forming a barrier between them. Both **PtL4** and **PdL4** crystallise in the monoclinic space group $P2_1/c$. Their short contacts (not including those to the counter ions, PF_6^-) are shown in Figure 3.32. For **PtL4** there is again no π - π stacking; however, the structure of **PdL4** is loosely stabilised by π - π interactions between pyridine rings of adjacent molecules along the stack. Since the complexes **PtL4** and **PdL4** do not have isomorphous structures, the packing is distinct in the two salts. This leads to different cation-cation interactions for each complex.

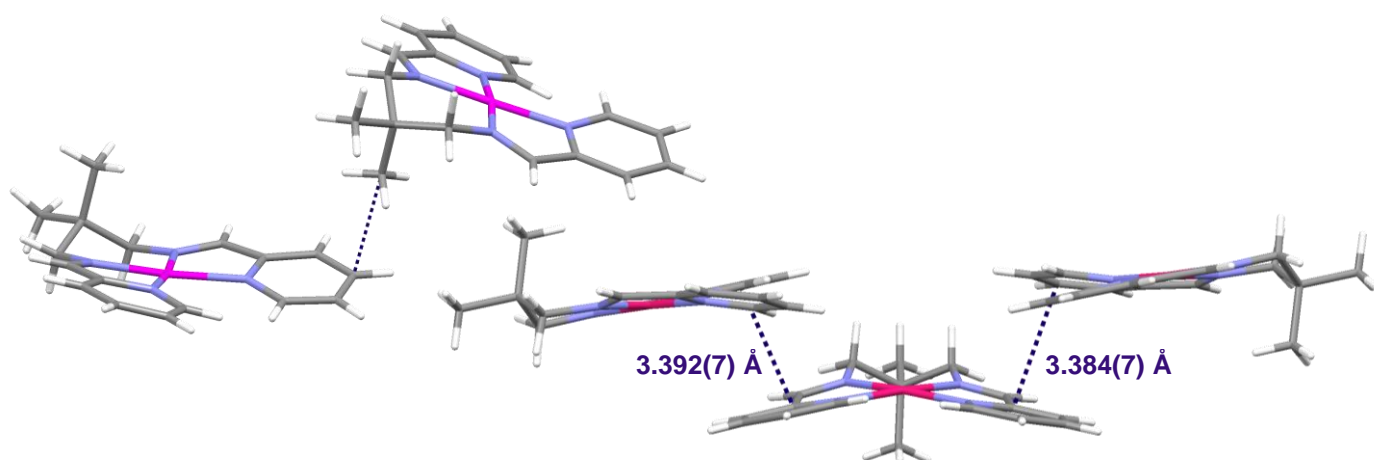


Figure 3.32: Illustration of the short intermolecular contacts for **PtL4** (top left) and **PdL4** (right).

The π - π stacking observed for **PdL4** will be rather weak due to the lack of significant ring-ring overlap. This is, however, consistent with the 2+ charge on each cation and the significant Coulombic repulsion between these cations. An offset overlap of two pyridine rings (Figure 3.33) is more common than complete overlap; complete overlap is indeed considered to be a rather rare phenomenon.³⁰³ The distances for the C_p - C_c short contacts are 3.384(7) and 3.392(7) Å due to the tilted orientation of the two **PdL4** cations towards each other. For the complexes with the 2,-2-dimethylpropane bridge the greater steric bulk causes a much greater distortion from a planar chelate geometry. This allows the molecules to be tilted enough for the short C-C contacts observed. Finally, due to this more distorted conformation and less-ordered packing some π - π interactions are possible. This has also been identified for **PdL4m**.

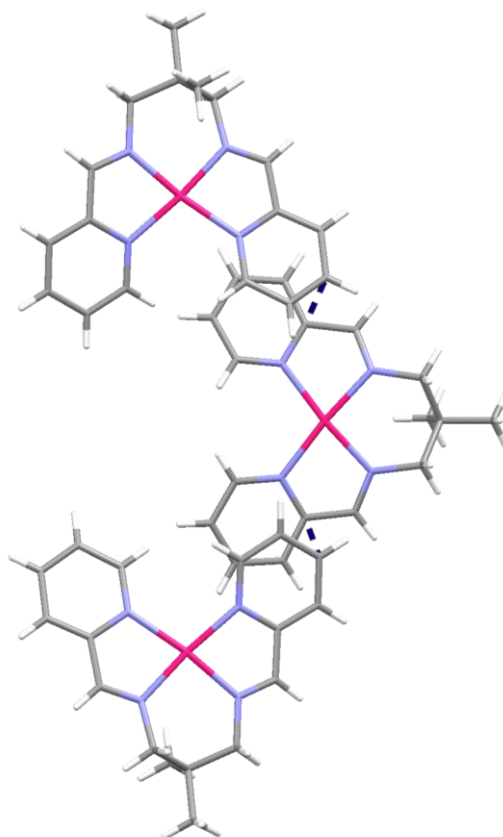


Figure 3.33: The overlap of the observed π - π stack in **PdL4** as viewed down the c -axis.

PdL4m only has a saddled structure (unlike **PtL4** and **PdL4**) which crystallises in the monoclinic, $P2_1/n$ space group. The cations form an interesting alternating conformation as shown in Figure 3.34, which demonstrates an inversion pair. The centre of inversion exists halfway between the two Pd(II) ions in the dimer. The complementary π - π stacking of the pyridine rings of neighbouring cations is also slightly offset, as observed for **PdL4**. Short contacts are present between the pyridine carbon atoms of neighbouring molecules with a $C_c \cdots C_c$ distance of 3.353(8) Å. The perpendicular distance between the mean planes calculated for the four nitrogen atoms of adjacent molecules is measured as 3.938(10) Å.

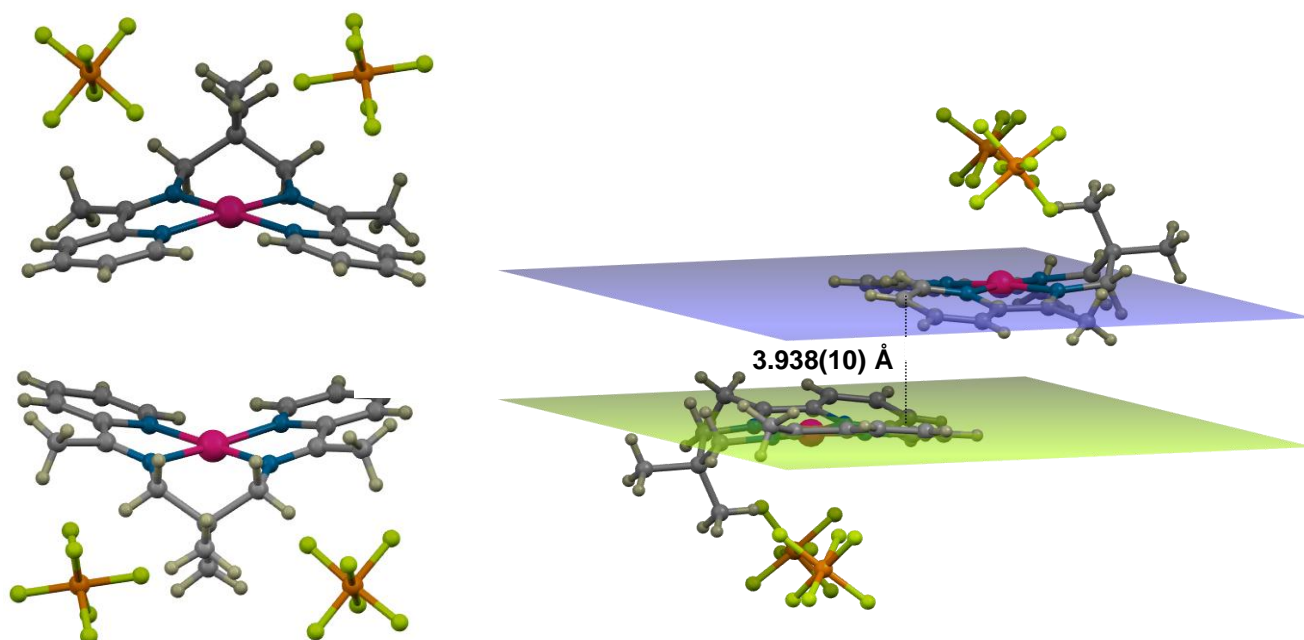


Figure 3.34: Illustration of the alternating packing for **PdL4m** (left) with a view of the π - π stacking and the overall interplanar distance (right).

The larger, more bulky structure of **PdL4b** shown in Figure 3.35 exhibits no π - π stacking. The alkyl C-H groups are not good H-bond donors so C-H \cdots π interactions between cations, which are weakly stabilising, are unlikely. Here, the only short contacts observed between the metal cations are: C₃ \cdots H_h-C_h (2.826 Å) and C₄ \cdots H_h-C_h (2.714 Å). These short, nonbonded contacts between cations form a crystallographically-generated chain of cations along a 2-fold screw axis in the unit cell. These chains are in turn held in position by short contacts to the PF₆⁻ anions present in the crystal. This is a very different packing to either that of **PdL4** or **PdL4m**, which have the same bridging groups. It therefore seems that the change in bulk of the group on the imine carbon and the subsequent distortion from planarity cause great changes in the way these cations stack in the crystal lattice.

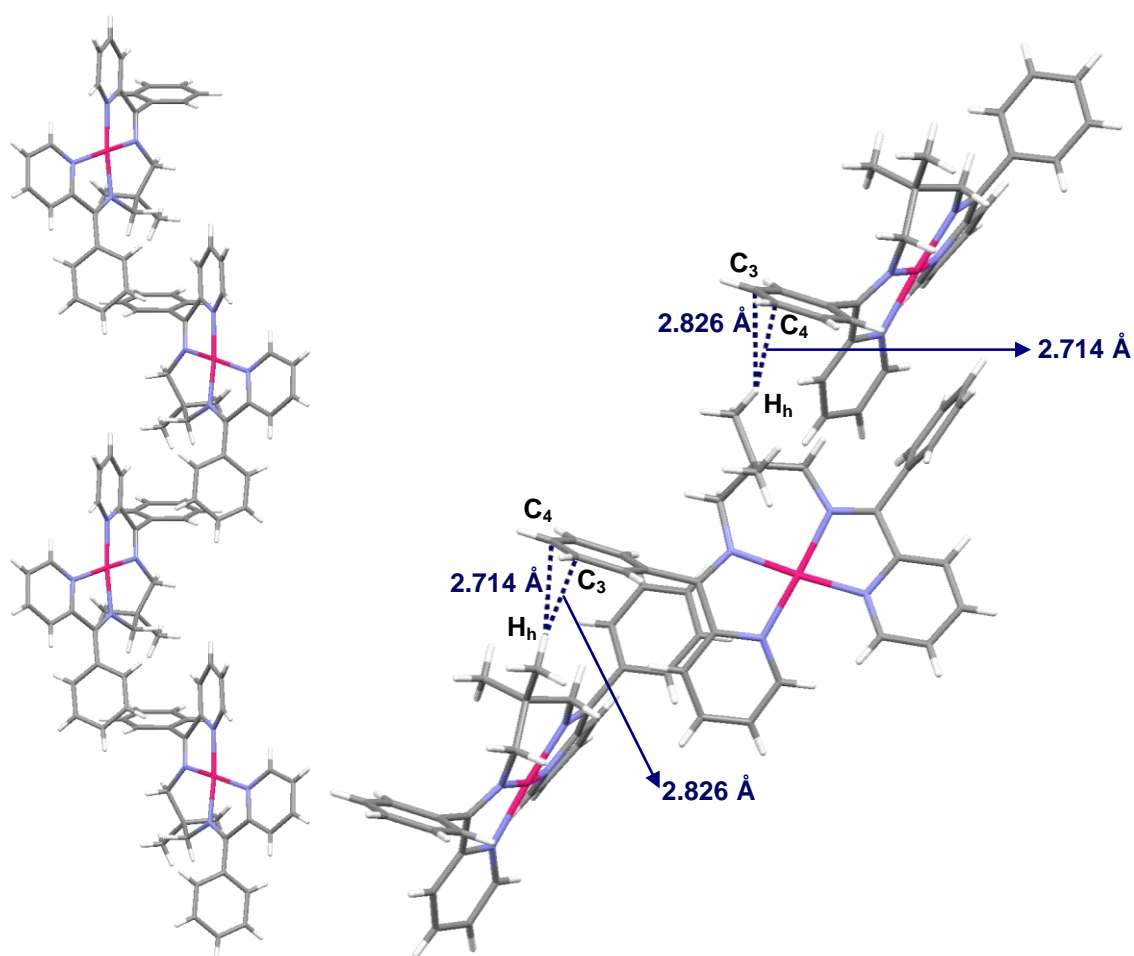


Figure 3.35: Illustration of the one-dimensional chains formed for **PdL4b**, as viewed down the *b*-axis (left) and the short contacts between cations within a chain (right).

CHAPTER 4 – Density Functional Theory

4.1 Introduction

Computational chemistry uses the fundamental laws of physics (either wholly or only partially) as its basis to predict chemical structures and reactions numerically. This then allows the study of chemical phenomena of these compounds and reactions by performing calculations instead of merely using experimental examinations. Thus computational chemistry can be used, not only as an independent study method, but also in conjunction with experimental investigations to further broaden experimental knowledge.³³¹ Molecular simulations are also useful because they do not merely help calculate the properties of synthesised compounds, but they can also predict the structures, energies and other features of unknown molecules.³³² These chemical calculation techniques are therefore significant applications that have often been used in chemical research.

There is an elementary distinction between experimental techniques and the calculations performed (quantum-mechanical or force field), because calculations can also be carried out on molecules that have no real existence; molecules that can either not exist under normal conditions or compounds that have yet to be synthesised.³³² Quantum chemical techniques are therefore especially useful when studying unstable species as these are not easily examined by conventional structure determination procedures; examples include reactive intermediates, excited states, transition states, etc.³³³

These types of calculations can provide extraordinary amounts of information compared with what chemists obtain from experimental techniques. For example, modern DFT calculations can give the molecular structure, heat of formation, dipole moment, ionisation potentials, charge densities, bond orders and spin densities in one experiment. There is still, unfortunately, the possibility that these results obtained from calculations may be unreliable. However, for the most common methods, the advantages and disadvantages have already been established and thus the probable accuracies can be sensibly predicted.³³²

There are two broad methodologies within computational chemistry; *molecular mechanics* and *electronic structure theory*, and both are primarily dedicated to the structure and reactivity of compounds. They both perform the same basic types of calculations: geometry optimisations, and computing the energy and vibrational frequencies. Molecular mechanics uses the laws of classical physics, while electronic structure methods use the laws of quantum mechanics. There are two major classes of electronic structure methods:³³¹

Semi-empirical methods: e.g. AM1, PM3,³³¹ used in programmes like HyperChem and Gaussian, which use parameters already obtained from experimental data in order to simplify the calculation. They solve an approximate form of the Schrödinger equation according to their possession of suitable parameters for that specific system. They are largely characterised by their differing parameter sets.³³¹

Ab initio methods: these use no experimental parameters in computations; rather, computations are founded exclusively on the laws of quantum mechanics—the name *ab initio* means “first principles”—and on a few physical constants (Planck’s constant, speed of light, masses and charges of electrons and nuclei).³³¹ There are a few simplifying assumptions involved in *ab initio* theory, but the calculations are more comprehensive (and therefore computationally more expensive) than those of semi-empirical methods.³³²

The *ab initio* procedure generally searches for exact solutions; all quantities in the calculation are computed as precisely as is numerically possible. The semi-empirical procedure seeks, from the beginning, only approximate solutions. Often the simplifications used may be quite radical, but they are nonetheless required to always be physically justified.³³⁴ The basic steps for the execution of a typical *ab initio* or semi-empirical calculation are very similar.³³⁵ Lately, a third class of electronic structure methods has been used in computations: Density Functional Theory (DFT). Density Functional Theory is not much different from the *ab initio* methods and the calculations need about the same total of computation resources as the Hartree-Fock theory (the least expensive *ab initio* method).³³¹ DFT methods are more appealing due to their inclusion of the effects of electron correlation, whereas Hartree-Fock (HF) calculations regard this effect only in an average sense, which causes less accuracy for some

systems. Therefore using DFT has the advantage and benefits of more expensive methods, but at the performance cost of Hartree-Fock theory.³³¹

DFT based techniques draw from the quantum mechanics research of the 1920s (especially the Thomas-Fermi-Dirac model), and also from fundamental work in quantum chemistry done by Slater in the 1950s.³³⁵ The approach of these DFT methods is founded on a strategy of modelling electron correlation using functionals of the density of the electrons.³³¹ In the last decade, methods based on DFT have gained steadily in popularity. In recent years, DFT has proved to be extremely useful and has been applied to a variety of problems that occur in Schiff base chemistry. DFT can take electron correlation into account in a computationally efficient manner and hence provides practical results.³³³ The best DFT methods achieve considerably better accuracy than Hartree-Fock methods with only a small increase in computational cost. DFT methods aim at providing, in one batch of self-consistent field (SCF) iterations, the real density distribution of correlated electrons in the ground state and the associated energy.³³⁶

Another role played by these theoretical studies is their usefulness in helping to understand structural details in the crystalline solid state. This has been seen for geometrical and structural optimisations of free Schiff base ligands in the recent past.^{337,338,339} There is also an interest in whether the observed structural packing is indeed a fundamental property of the molecule or merely a result of crystal packing forces. This is important particularly in the case of nonplanarity in the structures. It is possible for quantum chemistry to readily distinguish between such intramolecular and intermolecular effects. It has been shown that crystal **packing effects** are partially responsible for the planarity seen for an important class of diorganotin (IV) complexes derived from Schiff bases, as shown by DFT calculations.³⁴⁰ As a final point, quantum chemical computations supply us with the information to be able to understand molecular energetics or thermochemistry in terms of structural properties and molecular structure in terms of electronic structure.³³³

The foundation for DFT (as it is known today) was created in 1964 when a landmark paper appeared in the journal *Physical Review*.³⁴¹ All modern day density functional theories are based on the main theoretical support of the theorems that Hohenberg and Kohn proved in this publication.³³⁵ This publication demonstrated the existence of a unique functional which can determine the ground state energy and density exactly.^{331,342}

It also showed that the ground state electronic energy is determined by the electron density, ρ ,³⁴² implying then that there exists a one-to-one correspondence between the electron density of a system and any property of the system in its ground state, including energy.³³⁶ This is different to using the wave function approach, where the number of coordinates is $3N$ in an N -electron system (3 for each electron and 4 including spin).³⁴² Squaring the wave function and integrating over the $N-1$ electron coordinates gives the electron density; it depends on three coordinates and is independent of the number of electrons.³⁴² Thus, while the complexity of a wave function increases according to the number of electrons, the electron density, independent of the system size, has the same number of variables.³⁴² There is, however, a problem. Although each different density produces a different ground state energy, which has been proven, the connecting functional of these two is not known.³⁴² The objective of DFT methods is to devise functionals connecting the electron density with the energy.³⁴³

There is a difference between a function and a functional; a function is a prescription for generating a number from a set of variables (coordinates) and a functional produces a number from a function (which in turn depends on variables).³⁴² In mathematics, functionals are defined as a function of a function. An energy that depends on an electron density or a wave function is a functional; and the electron density or wave function is a function.³⁴² DFT methods use general functionals of the electron density to compute electron correlation.³³¹

In DFT, functionals are functions of the electron density which is itself a function of coordinates in real space. These functionals divide the electronic energy into several components which are each computed separately. In comparison with the wave mechanics method, it is evident that the energy functional may be divided into three parts. These three parts are kinetic energy, $T[\rho]$; attraction between the nuclei and electrons, $E_{ne}[\rho]$; repulsion between electrons, $E_{ee}[\rho]$ (in the Born-Oppenheimer approximation the nuclear-nuclear repulsion is a constant);³⁴² and then there is also an exchange-correlation term to account for the remainder electron-electron interactions, $E_{xc}[\rho]$, (in most actual DFT formulations it is divided into separate exchange and correlation components).³³¹ A general equation for the energy functional is shown below:

$$E_{\text{DFT}} = T[\rho] + E_{ne}[\rho] + E_{ee}[\rho] + E_{xc}[\rho] \quad (1)$$

The second major paper of modern DFT, written by Kohn and Sham,³⁴⁴ appeared about a year after that of Hohenberg and Kohn. This report proposed how the universal functional, which was unheard of up until then, could easily be handled. Their basic idea was to split the kinetic energy functional into two parts. One would be calculated exactly, while the other would be a small correction term. Their proposal was based on the acknowledgement of a common problem with direct density functionals (e.g. the Thomas-Fermi method) being associated with the way the kinetic energy is established.³³⁵ Kohn and Sham therefore launched the idea of a non-interacting reference system made from a collection of orbitals; one electron functions. It had also been noted that orbital-based approaches such as the Hartree-Fock method performed a lot better in this respect. It permits the exact treatment of the majority of the contributions to the electronic energy of an atomic or molecular system, thus allowing the major part of the kinetic energy to be computed more accurately.³³⁵

In reality, however, the electrons are interacting and therefore the total kinetic energy is not provided, but the difference between the exact kinetic energy and that which is calculated, assuming non-interacting orbitals, is small.³⁴² The remainder is absorbed into an exchange-correlation term; it is merged with the non-classical contributions to the electron-electron repulsion. These are typically also small and include the non-classical fraction of the electron-electron interaction accompanied by the correction for the self-interaction and the component of the kinetic energy that is not included in the non-interacting reference system.³³⁵ This method allows the maximum amount of information to be computed exactly so that only a small part need be calculated from an approximate functional.³³⁵

A few procedures have been promoted to deal with the Kohn-Sham equations: (1) the “scattered wave” (SW) or “multiple scattering” (MS) technique (founded on the so-called “muffin-tin” approximate potential); (2) the discrete variational method (DVM) (relying on the numerical sampling of Slater orbitals; and (3) as standard molecular orbitals, the expansion as linear combinations of Gaussian atomic functions.³³⁶ After the work done by Kohn and Sham, the approximate functionals used by present DFT methods divide the electronic energy into several terms, shown in the general expression:^{331,342}

$$E_{\text{DFT}} = T_{\text{s}}[\rho] + E_{\text{ne}}[\rho] + J[\rho] + E_{\text{xc}}[\rho] \quad (2)$$

where $T_s[\rho]$ is the term for kinetic energy (from the motions of the electrons), $E_{ne}[\rho]$ includes terms for the repulsion between pairs of nuclei and the potential energy for the nuclear-electron attraction, $J[\rho]$ represents the electron-electron repulsion (also known as the Coulomb electron density self-interaction). The term $E_{xc}[\rho]$ represents exchange-correlation and also comprises the leftover components of the electron-electron interactions. These include exchange energy evolving from the anti-symmetry of the quantum mechanical wavefunction, and dynamic correlation in the movement of individual electrons.^{331,342}

If E_{DFT} is equated to the exact energy then it may be seen as the definition of E_{xc} ; the portion which is left over after taking away the non-interacting kinetic energy, and the E_{ne} and J potential energy terms:³⁴²

$$E_{xc}[\rho] = (T[\rho] - T_s[\rho]) + (E_{ee}[\rho] - J[\rho]) \quad (3)$$

The kinetic correlation energy is shown in the first parenthesis and the second contains both the exchange and potential correlation energy.³⁴² This equation may be rewritten as:³³¹

$$E_{xc}[\rho] = E^X[\rho] + E^C[\rho] \quad (4)$$

E_{xc} is determined entirely by the electron density and is usually divided into two parts. These are the exchange and correlation parts, which actually respectively correspond to the same-spin and mixed-spin interactions.³³¹ All three of the equation components are functionals of the electron density; the two terms on the right hand side are the exchange and correlation functionals, respectively. Both of these can be of two distinct types (1) local functionals (which depend only on ρ); and (2) gradient-corrected functionals which depend on ρ as well as its gradient.³³¹

The advantage of DFT is that only the total density needs to be taken into account. However, to accurately calculate the kinetic energy, it is necessary that orbitals be reintroduced. Nonetheless, as previously mentioned, DFT has a computational cost which is similar to that of the least expensive *ab initio* method, Hartree-Fock theory, but it also has the advantage of possibly yielding more accurate results.^{331,342} Despite the similarities, there is one important difference between *ab initio* methods, wave mechanics

Hartree-Fock theory and DFT. DFT methods could give the exact total energy (including electron correlation) if the exact $E_{xc}[\rho]$ was known.^{331,342} DFT methods are popular due to their inclusion of the effects of electron correlation in their model. These effects refer to the reality that electrons in a molecular system react to each other's motion and will try to stay out of the other's way. Therefore DFT methods have the ability to offer the benefits usually associated with more expensive *ab initio* methods at a Hartree-Fock cost.³³¹ Hartree-Fock theory considers this method as an average only (causing less accurate results for some types of systems) while methods that include electron correlation account for the instantaneous interactions of electron pairs with opposite spin.³³¹

The reliable prediction and simulation of molecular structures is one of the most important applications of computational chemistry. A great deal of experience and knowledge has been gathered regarding the functioning and performance of each of the methods that have been employed. Therefore, as opposed to the early days of computational chemistry, it is now rather simple and easy to perform geometry optimisations on systems of more than 50 atoms. Most of these techniques generally have an accuracy performance of about 0.02 Å; this often improves bond lengths where molecules that contain main group elements are involved.³³¹ It is now acknowledged (and has been for a long time) that bond lengths are predicted shorter than they actually are by Hartree-Fock theory. Owing to the neglect of electron correlation, simulating multiple bonds is inclined to be complicated.³³¹ The precision of the bond energies acquired from the use of DFT calculations has been significantly enhanced by taking into account the nonuniformity of the electron density in the exchange and correlation functionals.³³⁶

Rather than restricted Hartree-Fock (RHF), Car-Parinello molecular dynamics and quantum chemical simulations have shown the DFT approach to be more suitable to describe rotational strength (RS) spectral dependences.³⁴⁵ Conversely, the regularly cited main shortfall of DFT is the official incapability to methodically progress the accuracy of quantitative predictions. There are a few key difficulties with DFT, which are clearly documented (weak interactions, excited states and highly degenerate systems). However, to forecast any other possible errors in DFT *a priori* is not possible without a thorough understanding of the fundamental aspects of the theory. Additionally, it has repeatedly been stated that when density functional methods do not succeed in a particular situation, then there is no exact course of action that may be followed to

correct the imperfections, in view of the fact that the underlying reasons for the limitations in the theory are a long way from being understood. This is true when the reason for failure is not the selection of the functional, integration grid, or basis set.³³⁵

DFT methods account reasonably well for hydrogen bonding, which is mainly electrostatic. There are, however, indications that DFT methods less accurately predict relative energies and inadequately portray transition structures. Nevertheless, it must be remembered that for DFT methods the number of systems for which it has been calibrated is still somewhat undersized.³⁴² DFT methods differ according to the choice of the functional form of the exchange-correlation energy. The most preferable DFT method was found to be the gradient functional method of Becke.³⁴⁶ Theory gives rather little guidance about how such functionals should be chosen and therefore many different potentials have been put forward. A variety of functionals has been defined in computational chemistry history and they are characterised by the means by which they deal with the exchange and correlation components.³³¹

4.2 Functionals

4.2.1 Local Density Methods

Local exchange and correlation functionals engage only the values of the electron spin densities.³³¹ The Local Density Approximation (LDA) assumes the electron density is a slowly varying function, i.e. that the electron density locally can be treated as a hypothetical uniform electron gas.^{335,342} The number of electrons and the gas volume are thought to move toward infinity at the same time as the electron density remains finite and reaches a stable value.³³⁵ LDA has been extended to the *Local Spin Density Approximation* (LSDA),³³⁵ which is the unrestricted case where the spin densities, α and β , are not equal. It is also possible to write LSDA in terms of the total density and spin polarisation. This LSDA will be equal to LDA for closed shell systems.³⁴²

For a number of different densities, by using Monte Carlo methods, the correlation energy of a uniform electron gas has been established.^{335,342} It is necessary to have an appropriate analytic interpolation formula to use these results in DFT computations; similarly to that constructed by Vosko, Wilk and Nusair in 1980 (VWN),³⁴⁷ which is a widely-used functional.³⁴² Often, instead of LDA defining the model of local density

approximation, the acronym SVWN is used. The LSDA method does, unfortunately, have limitations. Although its results are mostly superior to that of the Hartree-Fock method, it has a tendency to overestimate outcomes.³³⁵ This LSDA approximation, unfortunately, has a tendency to underestimate the exchange energy by about 10%, which in turn causes errors larger than the whole correlation energy, which is itself overestimated (regularly by a factor close to 2). Consequently, the bond strengths will also be overestimated.³⁴² LSDA techniques may offer outcomes with comparable accuracy to those acquired from Hartree-Fock methods, in spite of the simplicity of their fundamental assumptions.^{331,342}

4.2.2 Gradient Methods

In the early eighties, the first successful expansions to the purely local approximations were developed.³³⁵ To improve on the LSDA approach, a non-uniform electron gas needs to be considered. One way to do this is to make the correlation and exchange energies dependent on electron density *and* derivatives of the density; thus gradient-corrected functionals will entail electron spin densities as well as their gradients.^{331,342} The name given to these processes is *Gradient Corrected or Generalised Gradient Approximation* (GGA) methods (also sometimes called *non-local* functionals in the literature, which is somewhat misleading).³⁴²

In 1986, Perdew and Wang (PW86)³⁴⁸ suggested altering the existing LSDA exchange expression. And in 1988 Becke³⁴⁹ proposed a gradient-corrected correlation functional (B or B88) which became rather popular, followed by another widely-used functional (not a correction) by Lee, Yang and Parr (LYP) in the same year.³⁵⁰ (These two forms were also combined to make the B-LYP method.) There is one empirical parameter in the LYP functional and it differs from other GGA functionals because it includes a few local components.³³⁵ Another functional, with a correction to the LSDA energy, was proposed by Perdew and Wang in 1991,^{331,342} PW91.³⁵¹ It should, however, be noted that quite a few of these proposed functionals defied fundamental restrictions. P86 and PW91, for example, predict correlation energies for one-electron systems and for others, the exchange energy may be unsuccessful in cancelling the Coulomb self-repulsion.³⁴²

4.2.3 Hybrid Functionals

Generally, the exchange contributions are considerably larger in absolute numbers than the analogous correlation effects. Therefore, a prerequisite for acquiring useful outcomes from DFT is a precise expression for the exchange functional specifically.³³⁵ A precise link can be made between the exchange-correlation energy and the corresponding potential connecting the non-interacting reference and actual system using the Hamiltonian and the definition of the exchange-correlation energy.³⁴² The resulting equation involves integration over a parameter that allows for the electron-electron interaction. This equation is known as the Adiabatic Connection Formula (ACF).³⁴²

The Half-and-Half method may be described by writing the exchange energy as a blend of LSDA, a gradient correction term and exact exchange. *Hybrid* methods frequently refer to models that include exact exchange. The *Adiabatic Connection Model* (ACM) and *Becke 3 parameter functional* (B3)³⁵² are therefore examples of hybrid models. These functionals operate well and thus the Half-and-Half model is hardly ever used.³⁴⁴ Several hybrid functionals define the exchange functionals as a linear combination of Hartree-Fock, local, and gradient-corrected exchange terms. This exchange functional is then joined with a local and/or gradient-corrected correlation functional.³³¹ Becke's three-parameter formulation, B3 (B3LYP),³⁵² is the best known of these hybrid functionals and these Becke-style hybrid functionals have been found to be superior to the conventional functionals defined thus far.³³¹

From the time of their manifestation in the early nineties these hybrid functionals have experienced unparalleled success.³³⁵ In particular, the B3LYP functional has become a well known and extremely useful functional, due to its surprisingly good performance in many chemical applications.³³⁵ It was suggested by Stevens *et al.* in 1994³⁵³ and has an unsigned error of only slightly above 2 kcal/mol (with respect to the G2 data base). It is related to that originally suggested by Becke (using B88 and PW91); however, the PW91 correlation functional has been exchanged for the LYP functional.³³⁵

In 1996 Becke made further progress by dropping the number of parameters to one where the amount of exact exchange was empirically ascertained. This resulted in the B1B95 functional.³⁵⁴ Becke presented a new type of exchange-correlation functional, founded on an intricate fitting procedure, in the closing stages of his string of papers on

density functional thermochemistry. It was aptly labelled B97.³⁵⁵ Together, Schmider and Becke, then reparameterised this functional (with respect to the extended G2 set)³⁵⁶ and the ensuing B98 functional preserves the good absolute average and low maximum errors (11.9 kcal/mol and 9.1 kcal/mol, respectively). Additional development was also carried out in the same year on the original B97 functional by Hamprecht *et al.*; they called their result B97-1.³³⁵ The year 1998 also saw van Voorhis and Scuseria³⁵⁷ offer a new exchange-correlation functional known as VSXC; it was dependent on the non-interacting kinetic energy density, as well as on ρ and its gradient, $\Delta\rho$.³³⁵

Development and research into the discovery of new and improved functionals continues. Some of the current functionals do have the ability to yield energy related results approaching alleged “chemical accuracy”. This means that the results are within less than 2 kcal/mol of experimentally determined energies, which is very high accuracy. There are many literature records showing high accuracy obtained by means of modern functionals, and more are being published each year.³³⁵ Theory does not provide much assistance in choosing functionals, thus numerous different potentials have been suggested. To determine the best performing functional involves a comparison with experiments of high-level wave mechanics calculations or with functionals known to have been successful for similar compounds in the past.

4.3 Performing a calculation

In order to meet the requirements of accuracy as well as computing economy, both the theoretical method and the type of basis set need to be taken into account. Over the years it has been found that density functional theory (DFT) is extremely useful in predicting and discussing electronic structures of molecules. The important requirement of a DFT method is the selection of an appropriate structure for the exchange and correlation energies.³⁴² It is possible to use a combination for the exchange and correlation energies; a LSDA form for one and a gradient form for the other. However, this is not actually uniform. The Dirac-Slater expression gives the exchange within the LSDA approximation, thus the only distinction is the interpolation function which is used in the reproduction of (very good) Monte Carlo results for the correlation.³⁴² The term LSDA is generally connected to the acronym SVWN, because the VWN formula is considered to be such a good interpolation function. Gradient corrected methods will typically use the B88 exchange functional or the B3/ACM hybrid, and this will be coupled

with the LYP, P86 or PW91 correlation functional. Other related acronyms are BLYP, BP86, BPW91, **B3LYP**, B3P86, and B3PW91.³⁴²

Current functionals inadequately describe weak interactions due to dispersion (van der Waals type interactions).³⁵⁸ LDA predicts for example (though not very precisely) an attraction between rare gas atoms, whereas all gradient methods foretell a purely repulsive interaction (at least in the case of correction for basis set superposition error).³⁴² LSDA methods do not usually perform as well as gradient corrected methods. There is a notable improvement attained by the addition of gradient terms and hybrid methods operate almost as well as the complex G2 model for some test situations.³⁴² Using the GGA methods for stable molecules usually presents geometries and vibrational frequencies of better or similar quality to those from perturbation methods like MP2 and the computational cost is analogous to that of Hartree-Fock.³⁴²

Lastly, DFT methods at the moment are poorly matched for excited states that possess the same symmetry as the ground state. It is not easy to guarantee orthogonality between excited and ground states due to the deficiency of a wave function.³⁴² Results of DFT procedures have, however, been shown to produce outcomes that are as good as those of coupled cluster methods in multi-reference character systems, where MP2 generally does not succeed. DFT methods founded on unrestricted determinants for open shell systems have another advantage in that they are not as sensitive to “spin contamination”.³⁴²

4.4 DFT and Schiff Base Ligands

High-quality geometry optimisations of large polycyclic molecules are a somewhat more recent advance in computational chemistry. These calculations were originally thought to be a technical feat; however, in this day and age they are routinely possible with the use of DFT methods.³⁵⁹ Density functional theory is nowadays the accepted method (the post-HF approach) for the computation of molecular structure, vibrational frequencies and energies of molecules, resulting in a detailed quantum chemical study. There are methods, especially nonlocal DFT (NLDF) methods that yield structural information that is of such high quality that it is able to rival experimental data, like that acquired from high-quality crystallographic measurements.

In the literature there are more than a hundred cases of DFT being used to analyse free Schiff base compounds, with around a hundred more examining various metal complexes of Schiff base ligands. Although no DFT studies for this particular range of ligands can be found (due to their limited literature), it is possible to find DFT work that has been performed on the pyrrole analogues of our ligands. Much of the literature is focused on Salen-type ligands (ONNO donor ligands synthesised from diamines and aromatic *o*-hydroxyaldehydes).

Many of the papers apply restricted Hartree–Fock (RHF) and several DFT quantum chemical approaches in order to clarify the experimental data available for the studied molecules. However, to our knowledge, complete vibrational studies of the Schiff base ligands discussed herein and their metallated counterparts have not been reported. In most cases in the literature, where DFT computations have been used to compute data about Schiff base ligands, Beke's 3 parameter hybrid functional (B3LYP) is commonly used. The choice of basis sets does however differ according to the type of compound and desired results. Although the basis sets are mostly those from the Pople split valence basis set group, they vary according to the extent of the polarisation function (*, **, (d) or (d,p)) and the diffuse function (+ or ++).

DFT computations (B3LYP/6-31+G* level of theory) were performed in 2003 by Salva and co-workers to study a Schiff base formation of vitamin B6 analogues and to study the topology of the charge density function of the optimised structures. These calculations gave the description for the geometries of all intermediates and transition structures in the reaction pathway.³⁶⁰ DFT has also been used in conjunction with X-ray studies to compare the molecular conformation of some Schiff bases between optimised quantum mechanical calculations and crystal structures. Structures from both methods, theoretical and experimental, were shown to be very similar and compared well.^{361,362}

There has been much discussion about the tautomeric forms of some Schiff base ligands involving different configurations of enol-, keto- and zwitterionic structures.^{339,361,362,363,364,365,366,367} DFT has played a large role in elucidating the structures of many of these ligands. Recently Dziembowska *et al.* considered solvent effects on the tautomeric equilibrium of a Schiff base derived from 2-hydroxy-1-naphthaldehyde and methylamine. Gaussian 03 was used with the functional B3LYP and basis set 6-31G(d,p) to determine the structure in five different solvents.³⁶³

In the last decade, researchers have used DFT to determine, assign and compare vibrational frequencies in Schiff base ligands.^{367,368} Thube and co-workers used Hartree-Fock to calculate vibrational frequencies and obtained results that compared favourably to their experimental work.³⁶⁸ Nowadays, DFT is accepted as a popular post-HF approach in order to compute molecular structure, energies of molecules and vibrational frequencies. In 2007 Pajak *et al.* optimised structures and determined IR and Raman frequencies and intensities using the DFT method with the hybrid B3LYP functional and the 6-31++G(d,p) basis set. After scaling the frequencies, these density functional calculations made interpretation of the experimental spectra far simpler.³⁶⁷ Theoretical harmonic frequencies derived using DFT were also found to be in good agreement with their observed spectral values by Sun *et al.*³⁶⁹

There has also been a great deal of computational work dedicated to metallated Schiff bases. DFT work with metallated Schiff base ligands has involved, amongst other things, the theoretical calculations for the interaction with an anion, e.g. BF_4^- ,³⁷⁰ crystal packing effects³⁴⁰ and absorption spectra³⁷¹.

DFT calculations have been reported for a pyrrole analogue of the ligands presented in this work; this particular analogue is complexed to nickel.³⁷² The results obtained from the B3LYP/6-31G(d) level of theory agree well with the experimental X-ray values and provide insight about the frontier molecular orbitals. In 2004 Rogachev and co-workers reported on the combination of theoretical methods (ROHF for geometry optimisation and DFT/B3LYP for energy calculation) used to obtain geometry parameters for heterobimetallic complexes. The data showed remarkable agreement with the experimental X-ray results and the bonding energy corresponded precisely with the experimental mass-spectroscopy data.³⁷³

Using DFT B3LYP/6-311G(d,p) level calculations the equilibrium geometries, vibrational frequencies and related intensities were determined and analysed for metal complexes of Schiff base ligands.¹⁵ In these complexes the metal is coordinated to salicylic oxygen and azomethine nitrogen atoms for Fe(III), Co(II) and Ni(II), and to salicylic and carbonyl oxygen and azomethine nitrogen atoms for Cu(II) and Zn(II). From this work and the comparison between theoretical and experimental data, Serbest *et al.* concluded that this level of theory is reliable for the prediction of data for these complexes.

Chen *et al.*³⁷² have spectroscopically and theoretically studied the effects of axial coordination for metal-salen complexes in order to try and link axial coordination with catalytic properties of the complexes. This, in turn, will then help with the design and development of new, improved catalysts. Barone *et al.* showed that the DFT-B3LYP method is able to correctly compute (in agreement with the experimental data) the stability predictions of the different spin states of Fe-Salen derivatives. The DFT computations also gave dependable results for the complexes' structure, energetic and magnetic properties.³⁷⁴ Kwit and co-workers used CD spectroscopy combined with DFT calculations (B3LYP/6-31G*) to study structural changes of macrocyclic salen molecules.³⁷⁵

Overall we see good correlation between computational DFT work and experimental values obtained in numerous studies performed for Schiff base ligands and their complexes. The chosen levels of theory presented here gave results that compared well to the experimentally obtained figures. It is therefore clear that DFT is an extremely useful tool for amongst other things: the elucidation of structures, spectral data assignment and determination of energies of molecules.

4.4.1 Choosing the Functionals and Basis Sets

The two variable parameters in DFT methods are the basis set and the variety of exchange-correlation potentials.³⁴² In chemistry a commonly used functional is BLYP, made up of Becke's 1988 functional (incorporates the Slater exchange and corrections involving the gradient of the density)³⁴⁹ and the correlation functional of Lee, Yang, and Parr (includes both local and non-local terms).³⁵⁰ Even more widely used is B3LYP; a hybrid functional in which the exchange energy (from Becke's exchange functional) is combined with the exact energy from Hartree-Fock theory. There are three parameters that define the hybrid functional and specify how much of the exact exchange is mixed in. The B3LYP scheme is often considered to be the most suitable method for structure calculations. Density functional theory has shown good results for the treatment of electronic structures of molecules containing transition metals.

Efficient quantum chemical calculations require the foundation of modern electronic structure theory; basis sets. Throughout the years, many basis sets have been generated in the context of wave function-based approaches to quantum chemistry.³³⁵ A

basis set is defined as the mathematical description of the orbitals in a molecule (which in turn combine to approximate the total electronic wavefunction) used to carry out the theoretical calculation. The basis set thus restricts each electron to an exacting area of space; therefore the more accurate approximations are made by larger basis sets because they impose fewer restrictions on the locations in space.^{331,342} The larger the basis set, however, the more computational resources required.³³¹ Therefore it is necessary to find the largest basis set possible, that will accomplish the job with the best results, without calling for unmanageably large computational resources. Minimal basis sets are the fastest – but the least accurate – in common use. A simple basis set with added flexibility and polarisation functions on atoms heavier than Ne gives reasonable results.

Density functional theory is an extremely popular choice for the study of many systems using first-principles approaches at a similar computational cost to calculations at the Hartree-Fock level. The reliability of this method has now been established for small organic molecules; however, results for compounds that contain transition metals are less developed. For meeting the needs of both computing economy and accuracy, the choice of theoretical methods, as well as basis sets, should be taken into account. The basis set to be used must therefore be a balance between the required accuracy and a realistic amount of computing time. There are no set rules regarding which methods give the best results for which systems. The best starting place is to ascertain whether any successful (or unsuccessful, in the case of elimination) calculations have been performed previously on similar systems. Once it has been established that there have been successful DFT methods on related systems then the pros and cons of the different accessible basis sets have to be inspected. Therefore it is easy to use experimental data to guide the choices of the computational type.

For free Schiff base ligands with similar structure to those in this work, there are a number of DFT computations. Chatziefthimiou and co-workers have used DFT in order to differentiate between the consequences of intermolecular interactions and the position of a methoxy group in stabilising the keto form in a range of planar salicylalideneimine(amine) moieties in the crystalline state.³⁶¹ To accomplish this the B3LYP21 and B3P8621 functionals were used in conjunction with the cc-pVDZ, aug-cc-pVDZ, and aug-cc-pVTZ correlation consistent basis sets of Dunning³⁷⁶ (which

accurately describe core-core and core-valence correlation effects for second row atoms and molecules).

The 6-31G(d,p) basis set was used to study solvent effects on tautomeric equilibrium by Dziembowska *et al.* in 2009.³⁶³ While in 2004, Krygowski and co-workers carried out calculations in order to connect structures to common tautomeric forms. Using 6-3G(d,p), the C=N bond length was in good agreement 5 B3LYP has also been used to examine tautomeric forms of an ortho-hydroxy Schiff base (in conjunction with 6-311+G**),³⁶⁶ for pyridoxal-50-phosphate methylamine Schiff bases (in conjunction with 6-31G*)³⁶⁴ and for sterically hindered Schiff bases (in conjunction with 6-31++G(d,p)).³⁶⁷

Ab initio calculations at the level of B3LYP/6-31G** were performed for three ortho-hydroxy Schiff bases with methyl and ethyl substituents in order to compare with experimental data.³⁷⁷ Bond lengths were mostly overestimated, but valence angles were relatively well predicted. DFT computations (6-31+G(d,p) and 6-11+G(d,p) basis sets) were used to favourably compare the structure, proton transfer, and vibrational dynamics of a selected ortho-hydroxy Schiff base type compound containing a low-barrier hydrogen bond.³³⁷

Munro *et al.* showed that DFT calculations at the B3LYP/6-31G** level of theory appropriately predict the chief geometrical attributes of a dimer structure; while the differences show the function that crystal packing plays in the geometry of the structure.³⁷⁸ Comparison with crystallographic data showed that B3LYP in combination with the 6-31G* or 6-311G* split valence basis set accurately predicts the conformations of some N-benzylideneanilines.³⁷⁹

Hydrogen bond geometries have been calculated for a series of Schiff bases, N-(R1-salicylidene)-alkyl(R2)amines, using B3LYP functional, combined with the standard basis set 6-31++G(d). An estimated margin of error was found to be 5% between the crystallographic data and that computed by DFT.³⁸⁰ Accurately predicted results for the geometry and vibrational frequencies were obtained for some antipyrine derivatives when using B3LYP in conjunction with 6-31G(d).³⁶⁹

In each of the papers that was examined the functional used was always B3LYP and the basis sets were mostly split-valence basis sets. B3LYP is a thoroughly tested method

and therefore it stands to reason why it is so often chosen. It is particularly good for so-called "short range" correlation effects and offers good reliability and electron correlation treatment. The split-valence 6-31G basis set and versions thereof are used for compounds containing: C, H, N and O. Polarisation functions are added when there are heavy atoms (first row and up) and diffuse functions are used when there are non-bonding interactions or anions. For the study of fairly large organic molecules the basis set 6-31G(d) has shown promise due to its acceptable accuracy and economical computational cost.³⁶⁹ The difference between the basis set 6-31G(d) and the basis set 6-31G(d,p) is that the former adds polarisation functions to heavy atoms and the latter to hydrogen atoms as well. Both basis sets have 15 basis functions for first row atoms, but 6-31G(d,p) has 5 for hydrogen atoms whereas 6-31G(d) has only 2.³³¹

These methods presented above, based on the hybrid density functionals (especially B3LYP), predict structures and vibrational spectra of organic molecules very accurately. We are therefore justified in choosing B3LYP as the basic functional for analysis of our free base ligands. For our ligands we do not require any diffuse functions and therefore 6-31+G(d) or 6-31++G(d) would not be essential options. Thus the most obvious choice, and one that has shown accurate and well predicted information for other Schiff base ligands as shown above, is that of 6-31G(d,p).

An excess of basis sets are therefore on hand when working with light elements; however, a much smaller choice is available when incorporating the heavier elements or all the elements. Basis sets like TZVP72 and 6-31G(d) are only parametrised to Kr and therefore effective core potential basis sets need to be used for heavier elements like Pd and Pt. The Effective Core Potential (ECP) basis sets that are defined for all the elements include: LANL2DZ, CEP-121G and SDD.³⁸¹ Although the results from all three are relatively equal, SDD (stands for Stuttgart-Dresden, the cities of the inventors) is somewhat better and has – in some cases – now replaced the LANL2DZ and CEP-121 basis sets. These particular basis sets are valuable because they are quicker (core-electrons replaced by a potential function representing the effective nuclear charge), are available for all elements and can be "quasirelativistic" (specified in parameters). They are, however, not appropriate for the computations of NMR shifts but this is not within the scope of this work.

In the case of DFT calculations, there is evidence of its success for many different relevant metal Schiff base complexes. A problem sometimes experienced with DFT is its failure to predict the asymmetric Metal-O bonds observed experimentally due to the affinity of DFT to prefer delocalised, higher symmetry structures.³⁸² This should, however, not be a factor in our work as there are only metal-N bonds.

In order to correctly compute data for some elements e.g. Hg, Au and Pt, it is important to take relativistic effects into account. When using the SDD basis set for gold it will reproduce relativistic effects without using an explicit relativistic calculation.³⁸¹ When heavy metals like Zn, Cd and Hg are metallated with Schiff ligands then SBKJC pseudopotentials have been used as they include relativistic correction for heavy elements.³⁸³ Qualitative agreement has been found for data computed for lead Schiff complexes using the LanL2DZ valence set.³⁸⁴ Other researchers obtained results from optimisations done at the PBE0 level with SDD and LANL2DZ basis sets for Schiff complexes containing Ir and Hg. It was noted that the larger basis set, SDD, gave structural parameters that were closer to the crystal data than those computed by the LANL2DZ basis set for these particular complexes.³⁸⁵ However, those of particular interest in order to choose the level of theory for this work are Schiff base complexes that involve platinum(II) and palladium(II). There are relatively fewer DFT studies reported concerning platinum group metals (PGM).

In 2006 Liu and co-workers successfully used the B3LYP method with the LanL2DZ basis set (containing effective core potential (ECP) representations of electrons near the nuclei) for palladium and platinum Schiff base complexes.³⁸⁶ Shimazaki *et al.* also performed computations on Schiff complexes containing platinum and palladium; however, they used the PBE0 functional and the SDDAll basis set.³⁸⁷ (They chose the PBE0 functional due to work done by Poverenov and co-workers³⁸⁸ on a series of Pt pincer complexes that showed the ability of this functional in accurately simulating coordination sphere geometries.) The computed results at this level of theory compared reasonably well with those obtained from the X-ray data. Perez and co-workers used the B3LYP functional with the LANL2DZ basis set for novel five-membered pallada- and platinacycles (with terdentate ligands)³⁸⁹ and for new palladium(II)-allyl complexes³⁹⁰. In both cases reasonably good agreement was found between the optimised data and the experimental information, even allowing the assignment of main UV-Vis bands for the pallada- and platinacycles.³⁸⁹ B3LYP/LANL2DZ was used to rationalise observed results

obtained by Arnais and co-workers in 2007 for terdentate Schiff base NNO-coordinated ligands bonded to palladium with nitromethane. This level was used to optimise the structures and transition states were reinforced by a vibrational analysis (including one imaginary frequency) and IRC calculations.³⁹¹

The work discussed above on metallated Schiff Base ligands used the B3LYP or the PBE0 functional in the computations performed. The basis sets varied according to the type of metals in the complexes: SBKJC, LanL2DZ and SDD. In particular, the work for platinum and palladium complexes used either the B3LYP or PBE0 functional with either the LanL2DZ or SDD basis set. The results in all cases were noted to be reliable and correlated well with the experimental data obtained. Thus, there seems to be reasonable competition between these functionals and basis sets for the best results, depending on the actual complexes for which information is being computed. It is therefore necessary to decide which of these functionals and basis sets will be the best method for obtaining the most correct and accurate predictions for the complexes presented in this work. Due to the superiority of the SDD basis set in computing geometrical parameters closer to experimental values for various metal complexes (including carboplatin),³⁹² it was decided that the B3LYP functional would be used in conjunction with this basis set.

4.4.2 Computational Methods

DFT calculations (B3LYP functional,³⁵² 6-31G**³³¹ or SDD basis set, coarse/medium grid) were performed with Gaussian 03W³⁹³ V 6.1, Rev. C.02 running on an Intel dual core or AMD Athlon 64-bit machine under Windows XP-64. We have chosen the functional and basis set to be used to perform all geometry optimisations and data computations due to the literature reviewed above. The 6-31G** basis set is a split valence basis set; it has two (or more) sizes of basis function for each valence orbital. It also adds polarisation functions to the hydrogen atoms as well as all non-H atoms.³³¹ The SDD basis set has been chosen as it employs a double-zeta treatment to the valence shell, so it is not overly expensive in terms of computational cost and it includes relativistic effects to the heavier atoms.

The input files for the free ligands were generated in Gaussian and optimised by PM3 where no X-ray structure has been determined. Otherwise the CIF file created from the X-ray crystallography data was used as the starting point for these ligands. Seven of the

metal complexes used input files that contained coordinates from the X-ray structures of the synthesised compound, again using the CIF file created from the X-ray crystallography data. In the case where a crystal structure was not obtained, the complex was either generated in Gaussian or modified from another similar crystal structure.

All input files contained the full structure of each compound so that any effect that the varying bridge substituents may have on the structure was factored into all the computations performed. Each of the structures was symmetrised in order to make use of molecular point group symmetry and to reduce the number of basis functions in the calculation. Once the geometries had been optimised, frequency jobs were run on each structure to obtain the theoretical IR frequencies for each type of vibrational stretch or bend in the free ligand or metal complex.

4.5 Objectives

The goal of this work was to carry out modern level quantum mechanical calculations on all the free Schiff base ligands and their respective metal complexes. The aim was to determine the stable configurations, relative energies, and structural and spectral features of different variations of bis(pyridine-imine) chelates of PGMs. The results of this spectroscopic and theoretical study will then be used to derive trends and for the prediction of geometries of the investigated compounds.

The main objectives of this chapter were to:

- 1) optimise the geometries of the Schiff base ligands and their metal complexes;
- 2) compare the results for the metal complexes with those observed in the solid state;
- 3) study the predicted geometrical parameters for the complexes that have not been synthesised and compare to those that have;
- 4) characterise the molecular orbitals of this series of metallated Schiff compounds;
- 5) compute the frequencies for each ligand and complex to enable comparison of the theoretical and experimental IR spectra for the imine bond as well as determining the lowest energy vibrations; and
- 6) determine the difference between the free ligands and their respective metal complexes.

4.6 Results and Discussion

4.6.1 Introductory remarks

1970 saw the introduction of the first programme in the GAUSSIAN series; and in 1971 it was made available via QCPE.³⁹⁴ It was called GAUSSIAN70 and was capable of performing single-point calculations or optimisations (using Gaussian basis sets containing *s*- and *p*-orbitals) by cyclic variation of all parameters. This was the first *ab initio* program that found extensive approval. The basis sets, STO-3G and 4-31G, were the two most well-known to be built into the programme. This programme was subsequently used expansively externally to the laboratory in which it was produced, due to the simplicity of the input structure and GAUSSIAN70's swiftness.³³²

The Gaussian 03W version was used for this work.³⁹³ This is a very user-friendly version compared to earlier versions; all of the standard input is free-format and mnemonic with reasonable default settings. The output files are simply laid out and are self-explanatory. This version of Gaussian (and others) have found application by chemists, chemical engineers, biochemists, physicists and others where research is being carried out in other chemical interest areas.³⁹⁵

Gaussian 03W³⁹³ is capable of predicting the energies, molecular structures, absorption bands and vibrational frequencies of molecular systems. It is then also viable for numerous molecular properties to be derived from these basic computation types. These computations can help in the analysis of compounds that may be difficult or impractical to examine experimentally and it is possible for the conditions of the studies to be altered, e.g. properties can be computed in the presence of particular solvents.³⁹⁵

In this work, DFT calculations that were performed³⁹³ were executed in order to acquire a correlation between the theory and the practically collected data. DFT simulations were performed for the fifteen synthesised ligands, three putative ligands, and a total of thirty six putative and synthesised metal complexes. The metallated structures of these complexes are shown in Chart 4.1. All the values ascertained from these computations can be compared to experimental values; any possible discrepancies can then be investigated and their causes examined. These calculations can help in the understanding of many different concepts related to the properties observed for the

Schiff base in question, due to the vast quantity of information that is obtainable from these types of computations. This included IR frequency bands, NBO energies, molecular orbitals and possible conformations for each of our synthesised ligands and metal complexes. Not only do such simulations help in the understanding of the specific data of the particular compound for which the calculations were carried out, but simulations at this level of theory facilitate the discovery of trends that may well occur in similar compounds.

For the notation used to denote the different atoms in the structures please refer to Figure 3.13 (Chapter 3 – X-ray Crystallography, page 60).

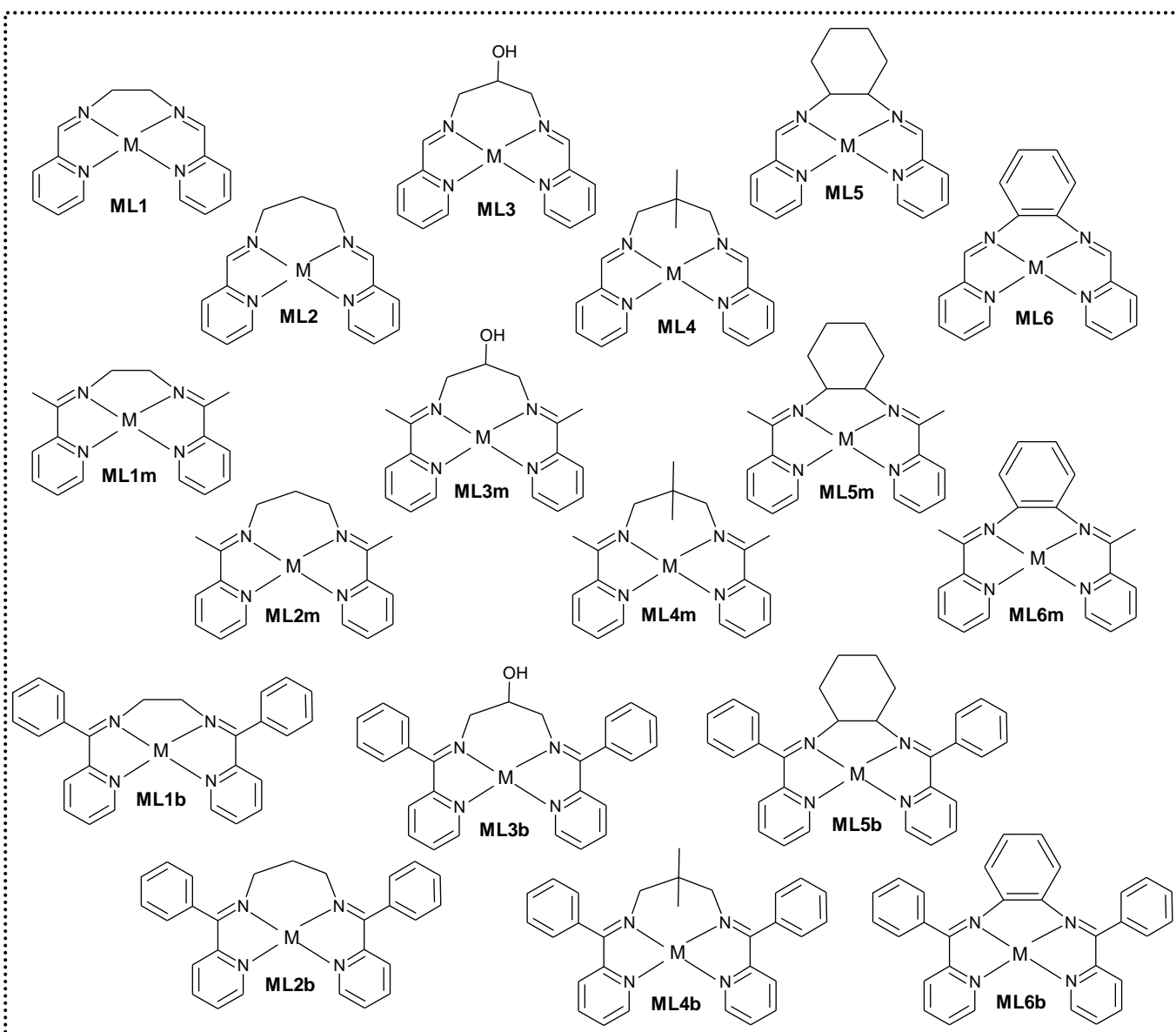


Chart 4.1: The thirty-six metal complexes studied in this work, where M = Pt(II) or Pd(II).

4.6.2 Geometry Optimisations

The DFT-optimised coordination geometries and those obtained from X-ray crystallography in the solid state may be compared. There may be some notable differences between the final structures determined by these two techniques; both small and large conformational deviations may often be attributed to structural deformations brought about by crystal packing interactions in the solid state. The structures determined by X-ray diffraction will include lattice-induced molecular distortions; however, the computations are for the free structure in the gas phase (where possible packing effects are absent). Crystal packing can result in either the flattening of the structure (planarity) or a distortion that pushes the structure out of its planar position (nonplanarity). Thus the observed difference between the two structures (DFT and X-ray) is likely to be merely the level of this distortion from planarity. A simple, yet effective way to explore these differences is by superimposing the DFT-calculated and X-ray determined structures using Mercury software.³¹⁰

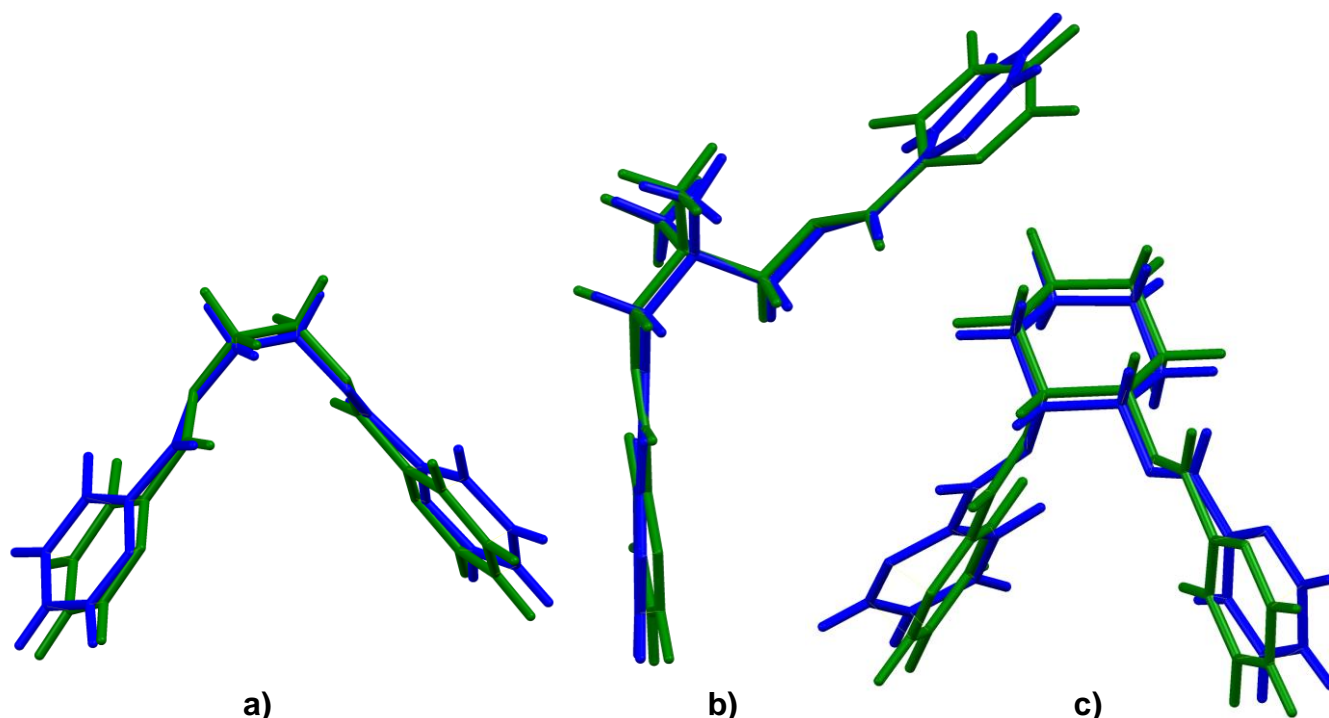


Figure 4.1: Least-squares fit of the DFT-calculated (from the X-ray CIF files) (green) and experimental (blue) structures of a) **L1** (RMSD = 0.357 Å), b) **L4** (RMSD = 0.293 Å) and c) **L5** (RMSD = 0.488 Å) for all non-H atoms.

Optimisations at the B3LYP/6-31G** level of theory were performed for all eighteen ligands. The CIF files created from the X-ray crystallography data were used as input files for the three ligands, **L1**, **L4** and **L5**. The DFT optimises the conformation for the

structure with the lowest energy in the gas phase. Subsequently the optimised forms of these gas-phase X-ray structures differ from the solid-phase structures. This difference is mainly for the position of the pyridyl-imine "arms" of the ligands as there is good correlation between the two structures for each ligand for the bridging groups (Figure 4.1). These differences between the two sets of data can be explained by the different states in which the data has been obtained. For the gas phase structure (DFT-computed) there is freedom of rotation around the bonds, allowing for different forms and subsequently an ideal conformation representing a lowest-energy geometry of all these possibilities is acquired. There are also no counter ions or other molecules and therefore intermolecular interactions are not taken into account by the DFT computations. In the solid state, however, there are forces experienced by the molecules due to crystal packing.

There are short contacts between the molecules in the solid state crystal structures (Figure 3.15) that cause these deviations of the peripheral groups from the predicted idealised geometries by DFT. For **L1** nonbonded short contacts between the imine hydrogen to a neighbouring N_p (2.656(10) Å) will cause the pyridyl-imine "arms" to start to bend away from their predicted ideal gas phase orientations (for which these gas phase interactions are absent). In addition, there are also short contacts between some of the pyridine carbon atoms which will subsequently draw the pyridine rings towards neighbouring molecules. This will tilt the pyridine rings away from their expected orientation due to the forces brought about by the other molecules in the crystal lattice which are not accounted for in the gas-phase computation.

L5 has a short contact between the N_i and a neighbouring molecule (2.745(10) Å), as well as between C_i and a neighbouring molecule (2.392(10) Å). This causes the same type of bending of the pyridyl-imine "arms" for this structure. The pyridine rings are also tilted away from their expected positions due to short contacts between pyridine carbons of one molecule and N_p of another. For **L4** there are short contacts between pyridine carbon atoms and neighbouring molecules which will then result in the same tilting of the pyridine rings. The fit for **L4** is slightly better than for **L1** and **L5** as it shows no short contacts between the imine bond and neighbouring molecules. This results in greater correlation between the position of the imine bonds for this ligand between the DFT-computed and experimentally determined X-ray structures. The resulting deviations

between these structures will therefore be predominantly for the tilting of the pyridine rings. This can be clearly seen in Figure 4.1.

Lui *et al.* have shown that a similar ligand demonstrates a crystal structure with similarly tilted pyridine rings.¹⁵³ The enantiomer of this ligand was shown to also have these slightly twisted pyridine rings in the solid state.¹⁵⁸ We can therefore conclude that the absence of intramolecular interactions in the gas phase clearly accounts for the conformational differences between the two structures.

Data have also been obtained for **L4b** which differs by the much bulkier group on the imine. The presence of this phenyl group causes considerable alteration to the structure compared to **L4**, although now the bridging group agrees almost perfectly with that of the X-ray structure (RMSD = 0.00652 Å for the four carbon bridge). The differences between the computed and experimental structures are again seen for the orientation of the pyridyl-imine "arms" of the bridge (Figure 4.2). Again the CIF file for the X-ray data was optimised and good agreement between the experimental and DFT-computed structures is observed (RMSD = 0.252 Å for all non-H atoms in the structure).

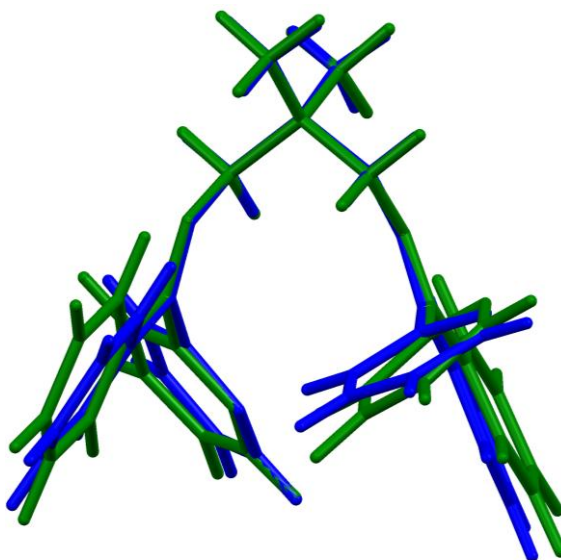


Figure 4.2: Least-squares fit of the DFT-optimised (green) and X-ray (blue) structures of **L4b**. The DFT structure was generated with Gaussian³⁹³ as an optimisation of the CIF file from the X-ray data.

In particular, the deviations between the two structures are for the pyridine and phenyl rings. This may again be explained by the nonbonded short contacts observed for the X-ray structure (Figure 4.3). There are short contacts between a carbon atom of the

pyridine ring of one molecule with its associate carbon atom in a neighbouring molecule (3.339 Å). An H...H short contact (2.349 Å) exists between the pyridine and phenyl rings of adjacent molecules, as well as an H...C (2.796 Å) short contact. There are no intramolecular interactions and therefore these intermolecular contacts that involve the aromatic rings are likely to justify their changes in orientation.

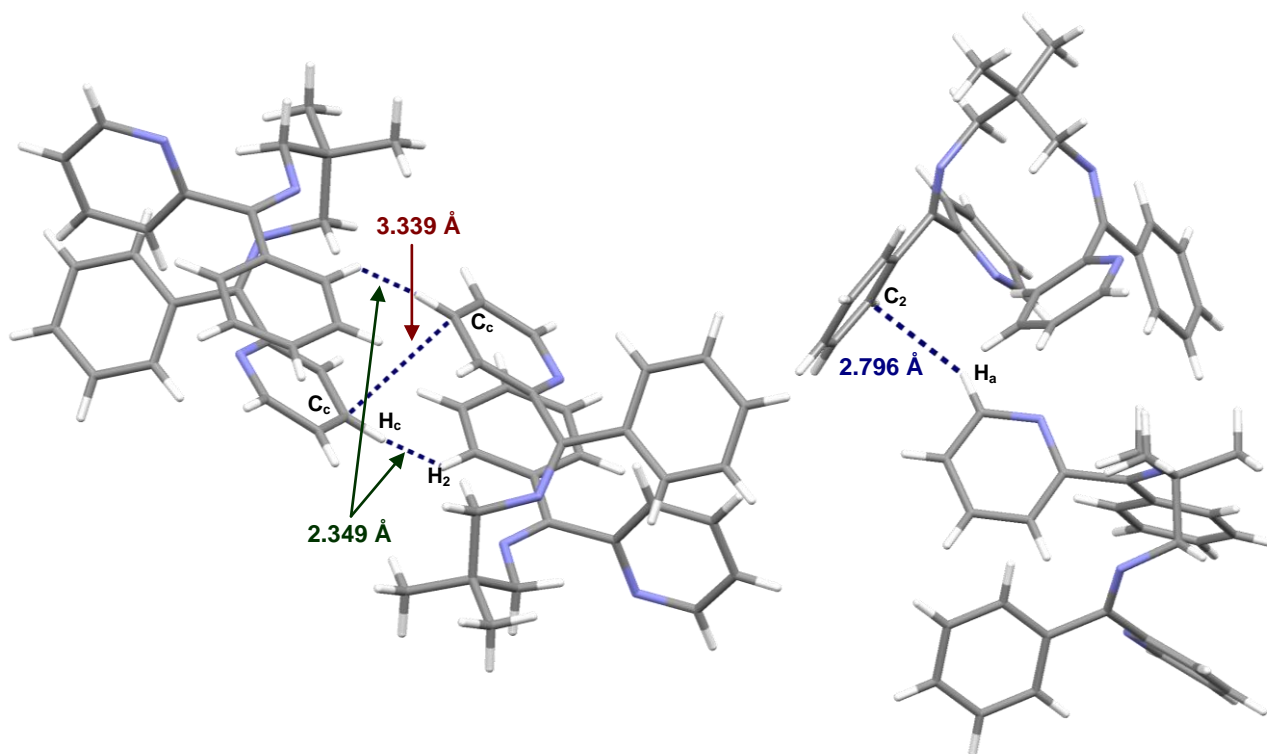


Figure 4.3: Illustration of significantly short H...C and H...H contacts observed in the X-ray structure of **L4b** between neighbouring molecules. Such interactions are absent for DFT-calculated structures in the gas phase.

Overall, when the differences between the two states for which the structures are obtained are taken into account, there is very good correlation between the theoretical and experimental data. This can further be shown by the molecular geometry measurements for the structures, as given in Table 4.1. Not only do the angles of the conformations agree to within 0.2 to 2.0°, but the bond lengths deviate by less than 1% (except for the Cf-Cf' bonds for **L1** and **L5** which deviate by 1.1 and 1.5%, respectively). This shows an excellent relationship between the predicted and determined structures for these four ligands. Given the above degree of similitude between the calculated and experimental data, structural and conformational parameters computed at this level of theory (B3LYP 631G**) are likely to be of acceptable accuracy, particularly for similar structures. Hence the data obtained for the other ligands, putative and synthesised, may be considered good approximations of reality.

Table 4.1: Average selected bond lengths (Å) and angles (°) for the free ligands calculated by DFT simulations (top) and determined from the X-ray structures (*bottom*).

	L1	L4	L5	L4b
N_i=C_i	1.274	1.273	1.273	1.280
	1.267(2)	1.267(2)	1.268(2)	1.278(2)
C_i-C_p	1.479	1.4879	1.479	1.493
	1.474(2)	1.481(2)	1.474(2)	1.496(2)
N_i-C_f	1.451	1.451	1.453	1.455
	1.457(2)	1.463(2)	1.464(2)	1.465(2)
C_f-C_g	1.537*	1.55	1.556*	1.548
	1.519(3)*	1.539(2)	1.533(2)*	1.540(2)
C_f-C_g-C_f	–	108.1	–	109.8
	–	108.3(9)	–	110.2(1)
C_i-N_i-C_f	118.0	118.4	118.2	121.4
	117.0(1)	116.9(1)	116.5(1)	120.0(1)
C_p-C_i-N_i	122.3	122.4	122.4	123.4
	121.9(1)	121.8(1)	122.6(1)	125.0(1)
N_i-C_i-He or N_i-C_i-Ce	123.6	123.5	123.6	118.8
	122.3(9)	122.2(9)	122.7(8)	118.4(1)

*For these ligands the distance Cf-Cf' is given (where ' designates a symmetry related atom).

Similarly, the theoretically and experimentally determined conformations for each of the metal complexes of these ligands are almost identical. The calculated geometries for the metal complexes are therefore also acceptable, given the degree of similitude between the X-ray and DFT-calculated structures. Small differences seen between the calculated and observed geometrical parameters may be attributed to experimental values corresponding to structures in the crystalline state while theoretical calculations have been performed on single molecules in the gaseous phase. However, there is also the possibility that these differences may be due to under- or overestimated parameters arising from inherent shortfalls in the DFT method used.

Metallation of the ligands forces the four N-donor atoms from their various positions into a plane around the metal centre which becomes the basic outline for each of the conformations. Each of the metal complexes has these four N-donor atoms and therefore

the only differences in the metallated structures are expected to be distortions from this plane. The extent of these deviations will therefore reflect the geometric constraints now imposed by the presence of the metal.

In each conformation the deviation may be seen by the slight tilting (out of the N_4 plane) of the pyridine rings. Usually one pyridine ring is tilted slightly above the plane and the other slightly below. The distance between the central carbon atom of the pyridine ring (C_a) and the plane formed by the four nitrogen atoms (N_4 plane) is measured; this may be used to effectively gauge the extent of the tilting taking place in each structure (Figure 4.4).

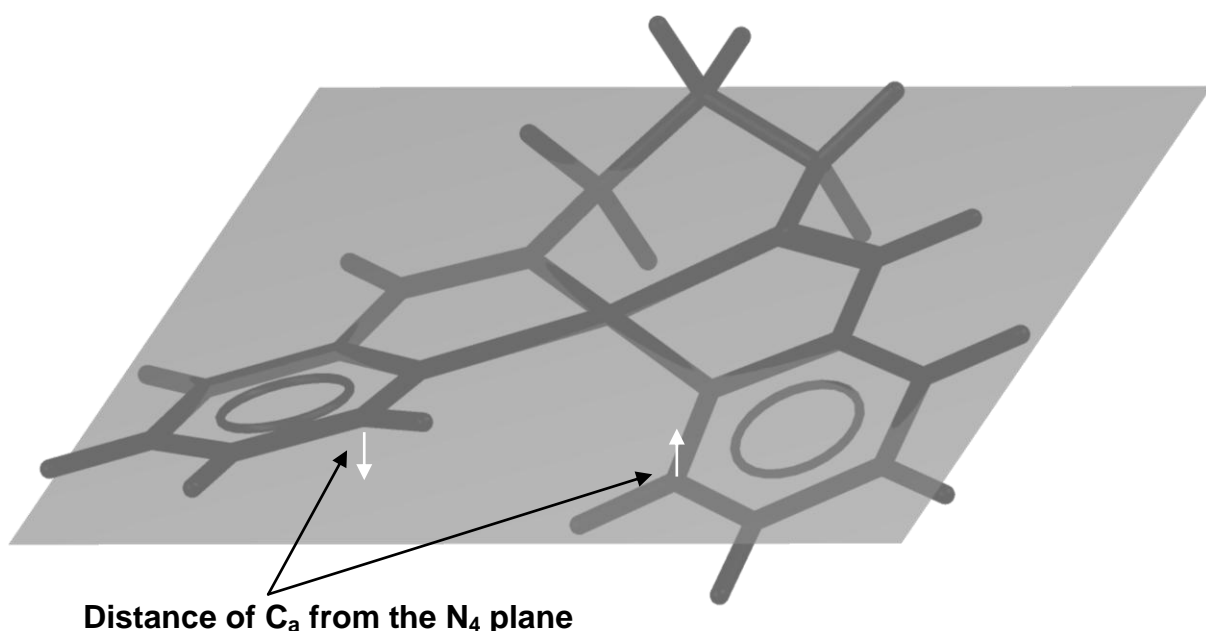


Figure 4.4: The structure of **PdL2** to illustrate the distance measured to determine distortion of the molecule from the N_4 plane.

These distances are mostly calculated to be larger than those observed for the X-ray structures as displayed in Chart 4.2. (For **PtL4** and **PdL4** only the twisted X-ray structures were compared to the DFT-computed structures.) The flatter geometries for the X-ray structures may therefore reflect the intermolecular interactions present in the crystal lattice making the structure less twisted than in the DFT-calculated conformation (gas phase). As the counter ions (PF_6^-) are not taken into account in the DFT computations, the prominent short interactions involving them in the crystallographically observed structures do not play a role in the computed structures. These crystal packing interactions may modulate the observed solid state conformation by flattening the chelate structure beyond that predicted in the absence of such lattice interactions.

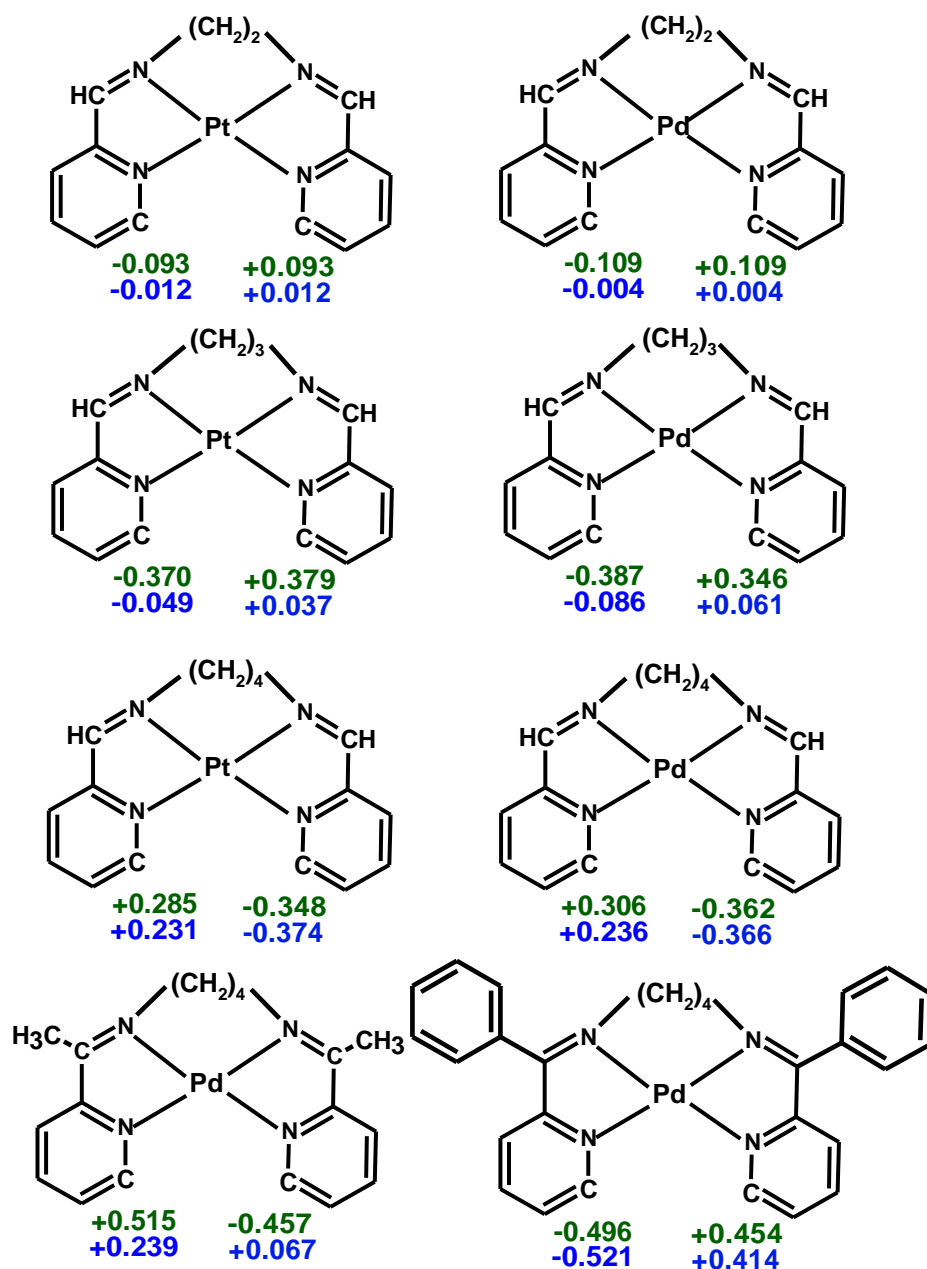


Chart 4.2: Distance (Å) that the central pyridine hydrogen atoms (C_a) are distorted from the N_4 plane for each structure. DFT-computed values in green and X-ray measured distances in blue.

The least-squares fits of the N_4 plane for the platinum complexes of **L1**, **L2** and **L4** are shown in Figure 4.5. The RMSD for each complex is given in Table 4.2. The most noticeable differences (if any) from the overlaying of the X-ray structures and the DFT-calculated structures are for the bridges of the chelating ligand structure. As the length of the bridging group increases from a 2-carbon to a 3-carbon bridge, so there is a slight deterioration of the fit between the computed and experimental data (Table 4.2). However, the increase in bulk on the 3-carbon bridge causes a reduction in the RMSD for the fit. This shows that the DFT simulation overestimates the extent to which the

central carbon of the propyl bridge is distorted from the N_4 mean plane; however, when steric bulk is introduced to this carbon the calculated distortion is improved.

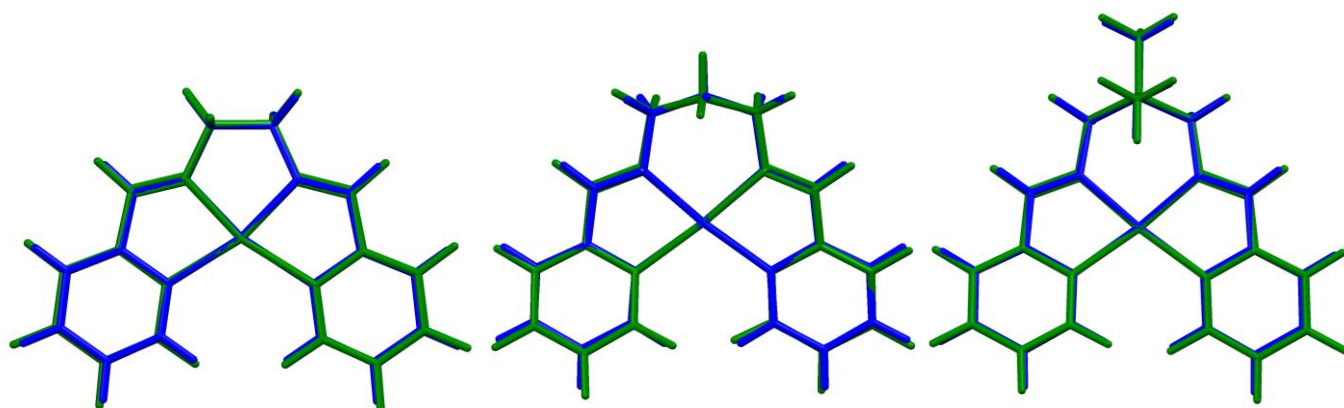


Figure 4.5: Least-squares fit of the DFT-calculated (green) and experimental (blue) structures of the platinum complexes of **L1**, **L2** and **L4** (RMSD = 0.0537, 0.0820 and 0.0546 Å, respectively) for the N_4 plane. Counter ions have been omitted for the sake of clarity.

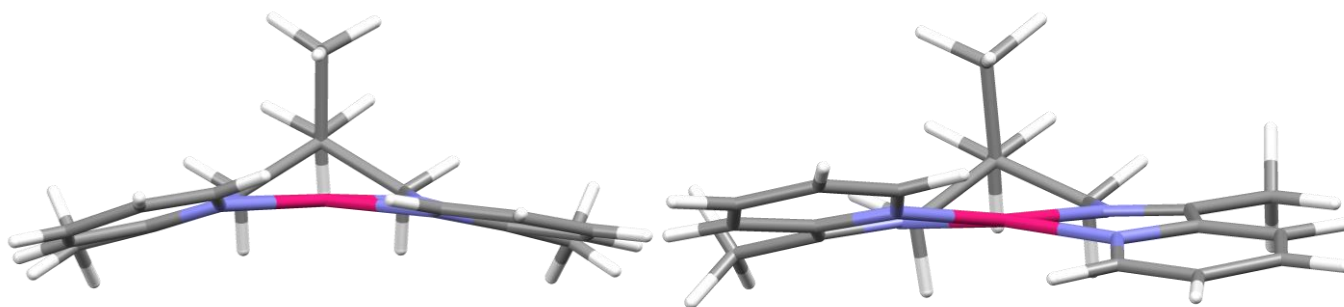


Figure 4.6: The different conformations of the X-ray structure (left) and computed DFT structure (right) for **PdL4m**.

The fit has also been performed for all the non-H atoms in the structure (excluding the metal) as shown in Table 4.2. In each case there is an increase of the RMSD when including *all* the non-H atoms in the least-square fit rather than just the N_4 plane. This shows relatively good agreement between the calculated and experimental nitrogen atom planes for each of the complexes; however, larger deviations are present for the bridging groups (as discussed above) and pyridine rings. In particular, the RMSD for the fit of **PdL4m** increases 3-fold from the N_4 plane when including all non-H atoms. This can be explained by the very different structures for the theoretical and experimental orientations of the pyridine rings. In the crystal structure the pyridine rings are both tilted out of the plane in the same direction causing a saddling type of structure (Figure 4.6), while the DFT method used computes a structure similar to the others with one pyridine tilted on either side of the N_4 plane. The differences for the other structures can be

explained by the larger deviations calculated by the DFT method as it does not take crystal packing interactions into account.

A relatively high RMSD is observed for the least-square fit for all the non-H atoms of **PdL4b**, although lower than that of **PdL4m**. In this case both structures have the same conformation so the better fit is expected. There is a more than 5-fold increase from the least-square fit for the N₄ plane of **PdL4b** which shows that most of the deviations between the structures are not from the plane around the metal, but rather for the bulky substituents. This sort of deviation between the two conformations has been noted for the other structures that have been compared. These discrepancies may therefore also be explained by crystal packing interactions which cause tilting of the aromatic rings.

Table 4.2: The RMSD values (Å) for each of the least-squares fits for the metal complexes.

	PtL1	PdL1	PtL2	PdL2	PtL4	PdL4	PdL4m	PdL4b
RMSD – fit based on the N ₄ plane	0.0537	0.0651	0.0820	0.0835	0.0546	0.0386	0.121	0.0419
RMSD – fit based on all non-H atoms*	0.0876	0.104	0.208	0.180	0.0814	0.0672	0.367	0.222

*Least-squares fit on all non-H atoms excludes the metal atom.

Although the ligands **L1–L4b** are slightly different in each case, the basic structures are comparable and therefore some similarities between the bond lengths and bond angles of the structures will be expected. Structural parameters have been obtained for the X-ray structures (Chapter 3 – X-ray Crystallography) and these values, along with those calculated by DFT, are given in Tables 4.3 and 4.5. Chemically equivalent bond lengths are, as expected, very similar to one another; there are no significant outliers and most differ only in the third decimal place.

In order to compare and obtain trends from these measurements DFT computations were performed for theoretical platinum(II) and palladium(II) complexes of bis(pyridyl-imine) Schiff base ligands with methylene and butyl bridges. This allows us to compare the differences in bond lengths and angles caused by the size of the bridging group and analyse whether the deviations are a definite trend. The data for these computed values are presented in Table 4.4 and 4.6.

Table 4.3: Average bond lengths (Å) calculated by the DFT simulations and observed in the X-ray structures (*in italics*), where possible, for selected bonds.

	M–N_i	M–N_p	C_i=N_i	C_i–C_p	N_i–C_f
PtL1	1.984(0)	2.099(0)	1.303(0)	1.468(0)	1.498(0)
	<i>1.953(5)</i>	<i>2.051(5)</i>	<i>1.261(9)</i>	<i>1.464(10)</i>	<i>1.475(8)</i>
PdL1	1.980(0)	2.101(0)	1.301(0)	1.468(0)	1.495(0)
	<i>1.942(4)</i>	<i>2.046(3)</i>	<i>1.261(7)</i>	<i>1.467(6)</i>	<i>1.494(6)</i>
PtL2	2.034(4)	2.093(1)	1.305(1)	1.458(0)	1.491(1)
	<i>1.988(6)</i>	<i>2.060(5)</i>	<i>1.278(8)</i>	<i>1.444(9)</i>	<i>1.479(10)</i>
PdL2	2.035(4)	2.094(2)	1.303(1)	1.460 (0)	1.488(2)
	<i>1.998(2)</i>	<i>2.073(2)</i>	<i>1.278(2)</i>	<i>1.451(3)</i>	<i>1.475(2)</i>
PtL3	2.033(4)	2.090(1)	1.304(1)	1.458(1)	1.484(3)
PdL3	2.033(8)	2.092(1)	1.302(1)	1.459(1)	1.481(3)
PtL4	2.033(1)	2.095(2)	1.305(1)	1.457(1)	1.490(2)
	<i>1.986(7)</i>	<i>2.038(6)</i>	<i>1.298(10)</i>	<i>1.441(11)</i>	<i>1.478(11)</i>
PdL4	2.032(3)	2.096(3)	1.303(1)	1.460(0)	1.487(2)
	<i>1.992(4)</i>	<i>2.057(4)</i>	<i>1.280(6)</i>	<i>1.457(6)</i>	<i>1.472(6)</i>
PtL5	1.986(2)	2.099(2)	1.302(0)	1.469(0)	1.510(9)
PdL5	1.981(2)	2.101(3)	1.299	1.469	1.506(9)
PtL6	1.993(0)	2.088(0)	1.311(0)	1.461(0)	1.433(0)
PdL6	1.988(0)	2.090(0)	1.309(0)	1.461(0)	1.429(0)
PtL1m	1.987(0)	2.089(0)	1.312(0)	1.488(0)	1.497(0)
PdL1m	1.981(0)	2.090(0)	1.310(0)	1.489(0)	1.494(0)
PtL2m	2.041(1)	2.076(1)	1.318(1)	1.480(0)	1.490(0)
PdL2m	2.038(1)	2.075(1)	1.316(2)	1.482(0)	1.487(2)
PtL3m	2.039(1)	2.076(1)	1.318(1)	1.479(0)	1.484(1)
PdL3m	2.036(0)	2.075(1)	1.316(2)	1.481(0)	1.481(1)
PtL4m	2.026(0)	2.080(0)	1.315(2)	1.483(0)	1.490(0)
PdL4m	2.035(0)	2.074(2)	1.313(0)	1.483(0)	1.486(2)
	<i>1.998(3)</i>	<i>2.056(3)</i>	<i>1.284(5)</i>	<i>1.457(6)</i>	<i>1.461(5)</i>
PtL5m	1.994(15)	2.082(8)	1.313(3)	1.490(4)	1.512(19)
PdL5m	1.987(17)	2.082(10)	1.311(3)	1.492(4)	1.508(17)

PtL6m	1.999(0)	2.073(0)	1.324(0)	1.485(0)	1.440(0)
PdL6m	1.992(0)	2.073(0)	1.322(0)	1.486(0)	1.436(0)
PtL1b	1.985(0)	2.088(0)	1.318(0)	1.493(0)	1.494(0)
PdL1b	1.978(0)	2.089(0)	1.316(0)	1.493(0)	1.491(0)
PtL2b	2.041(6)	2.076(2)	1.322(1)	1.481(1)	1.488(2)
PdL2b	2.039(8)	2.075(2)	1.320(1)	1.483(1)	1.486(3)
PtL3b	2.040(6)	2.075(2)	1.323(1)	1.481(1)	1.482(1)
PdL3b	2.037(8)	2.074(4)	1.322(1)	1.483(1)	1.480(2)
PtL4b	2.024(0)	2.076(0)	1.322(0)	1.484(0)	1.490(0)
PdL4b	2.018(0)	2.074(0)	1.320(0)	1.487(0)	1.487(0)
	2.002(5)	2.034(7)	1.291(8)	1.477(7)	1.465(7)
PtL5b	1.992(14)	2.085(6)	1.316(0)	1.491(2)	1.514(17)
PdL5b	1.985(16)	2.085(9)	1.314(0)	1.491(0)	1.510(17)
PtL6b	1.999(0)	2.075(0)	1.326(0)	1.484(0)	1.441(0)
PdL6b	1.992(0)	2.075(0)	1.324(0)	1.485(0)	1.437(0)

Table 4.4: Average bond lengths (Å) calculated by DFT simulations for selected bonds of platinum and palladium complexes with methylene (Mbridge) or butyl bridges (Bbridge).

	M–N_i	M–N_p	C_i=N_i	C_i–C_p	N_i–C_f
Pt_Mbridge	1.957(0)	2.123(0)	1.315(2)	1.483(0)	1.486(2)
Pd_Mbridge	1.957(0)	2.123(0)	1.297(0)	1.481(0)	1.513(0)
Pt_Bbridge	2.059(7)	2.082(0)	1.307(1)	1.456(0)	1.495(7)
Pd_Bbridge	2.060(11)	2.082(1)	1.304(1)	1.459(0)	1.493(8)

Table 4.5: Average bond angles ($^{\circ}$) calculated by the DFT simulations and observed in the X-ray structures (*in italics*), where possible, for selected angles.

	N_i-M-N_p	N_i-M-N_i	N_p-M-N_p	$C_p-C_i-N_i$
PtL1	80.0(0)	85.1(0)	115.2(0)	115.7(0)
	<i>80.8(2)</i>	<i>85.6(3)</i>	<i>112.9(3)</i>	<i>115.9(6)</i>
PdL1	80.5(0)	84.1(0)	115.1(0)	116.4(0)
	80.7(2)	85.2(2)	113.4(2)	<i>115.8(4)</i>
PtL2	79.2(0)	96.4	105.8	117.5(1)
	<i>79.4(2)</i>	<i>95.2(2)</i>	<i>106.2(2)</i>	<i>116.8(6)</i>
PdL2	79.9(0)	95.4	105.2	118.2(1)
	<i>80.2 (7)</i>	<i>94.0(7)</i>	<i>105.6(1)</i>	<i>117.8(2)</i>
PtL3	79.3(0)	96.1(0)	105.8(0)	117.5(1)
PdL3	80.0(0)	95.3(0)	105.3(0)	118.2(2)
PtL4	79.5(3)	95.4(0)	106.3(0)	117.7(1)
	<i>80.1(2)</i>	<i>94.3(2)</i>	<i>105.5(2)</i>	<i>116.8(9)</i>
PdL4	80.1(0)	94.7(0)	105.5(0)	118.4(1)
	<i>80.1(2)</i>	<i>94.3(2)</i>	<i>105.5(2)</i>	<i>117.1(4)</i>
PtL5	80.1(1)	85.0(0)	115.1(0)	115.9(1)
PdL5	80.6(2)	84.1(0)	114.9(0)	116.6(1)
PtL6	80.5(0)	84.2(0)	114.8(0)	115.9(0)
PdL6	81.0(0)	83.5(0)	114.4(0)	116.5(0)
PtL1m	79.7(0)	86.1(0)	114.6(0)	113.5(0)
PdL1m	80.2(0)	85.4(0)	114.4(0)	114.0(0)
PtL2m	78.6(1)	98.5(0)	105.2(0)	114.8(1)
PdL2m	79.3(1)	97.8(0)	104.6(0)	115.3(3)
PtL3m	79.2(6)	98.1(0)	105.4(0)	114.8(1)
PdL3m	79.4(1)	97.5(0)	104.8(0)	115.3(3)
PtL4m	76.2(0)	94.6(0)	109.8(0)	114.3(0)
PdL4m	79.5(1)	97.3(0)	104.7(0)	115.4(2)
	<i>79.5(1)</i>	<i>95.0(1)</i>	<i>105.6(1)</i>	<i>115.8(4)</i>
PtL5m	80.0(5)	86.6(0)	113.8(0)	113.5(3)
PdL5m	80.5(5)	85.8(0)	113.4(0)	114.1(3)

PtL6m	80.4(0)	85.3(0)	113.5(0)	113.6(0)
PdL6m	80.9(0)	84.8(0)	113.1(0)	114.0(0)
PtL1b	79.6(0)	86.0(0)	114.9(0)	113.0(0)
PdL1b	80.1(0)	85.3(0)	114.9(0)	113.5(0)
PtL2b	78.8(2)	98.4(0)	104.9(0)	114.6(1)
PdL2b	79.4(2)	97.9(0)	104.3(0)	115.1(2)
PtL3b	78.8(2)	98.2(0)	105.0(0)	114.6(1)
PdL3b	79.5(2)	99.6(0)	104.4(0)	115.1(2)
PtL4b	79.3(0)	94.7(0)	109.1(0)	114.0(0)
PdL4b	80.0(0)	94.1(0)	108.7(0)	114.4(0)
	79.9(2)	96.9(2)	103.9(2)	115.5(5)
PtL5b	80.0(5)	86.4(0)	113.9(0)	113.6(5)
PdL5b	80.5(6)	85.7(0)	113.6(0)	114.0(6)
PtL6b	80.7(0)	85.4(0)	113.1(0)	113.8(0)
PdL6b	81.2(0)	84.9(0)	112.6(0)	114.2(0)

Table 4.6: Average bond angles ($^{\circ}$) calculated by DFT simulations for selected angles of platinum and palladium complexes with methylene (Mbridge) or butyl bridges (Bbridge).

	N_i-M-N_p	N_i-M-N_i	N_p-M-N_p	C_p-C_i-N_i
Pt_Mbridge	80.4(0)	69.8(0)	129.5(0)	114.1(0)
Pd_Mbridge	80.5(0)	69.3(0)	129.8(0)	114.8(0)
Pt_Bbridge	79.0(1)	101.0(0)	103.1(0)	118.0(3)
Pd_Bbridge	79.8(1)	100.3(0)	102.6(0)	118.6(3)

The differences and similarities between the platinum(II) and palladium(II) centres have been noted in Chapter 3 – X-ray Crystallography. These $5d^8$ and $4d^8$ metals have similar ionic radii and therefore similar geometrical properties. The metal-N_p bond is always slightly longer than that of the M-N_i bond (as was observed for the X-ray data – see Chapter 3) due to the stronger basicity of the imine nitrogen. This DFT-computed bond length (metal-N_p) stays relatively constant throughout the range of metallated structures for both platinum and palladium complexes.²⁸⁷ The environment of the pyridyl-nitrogen

does not change and therefore this is expected due to the similar ionic radii of the metals. The metal-N_i bond shows more variation; however, for platinum and palladium complexes of the same ligand it is mostly quite similar (within experimental error). These differences between ligand structures may be explained by the effect of the change in bridging groups. Little change in bond lengths is noted when varying the group on the imine carbon. Most often, only a very slight increase when moving from the hydrogen to the methyl-group, and barely any change on further increase in bulk to the phenyl-group.

The imine bond distances range from about 1.29 to 1.32 Å and compare favourably with one another; however, they are decidedly longer than those measured for the X-ray structures (~ 1.27 Å). In general, there seems to be slightly better correlation between the X-ray and DFT-calculated data for the C_i-C_p and N_i-C_f bond lengths for the palladium complexes in comparison to the platinum complexes. This difference is, however, very small and therefore the prediction of these geometrical parameters is of acceptable accuracy at this level of theory.

With increasing chain length there is an increase in stability up to a point after which the stability will decrease.³¹² This change is usually seen around the 5-membered and 6-membered rings created by this chelation, as these are the most stable forms. The difference in size between these two bite angles for these different chelate rings has been shown in the literature.^{313,314,315,316} The larger chelate ring has the greater bite angle (as discussed in Chapter 3, pp 85–87). For the X-ray structures in this work an increase in N_i-M-N_i was noted as the length of the bridging group increased; this is also true for the DFT-computed structures (for the methyl-substituted and phenyl-substituted ligands as well).

This trend was also followed by the theoretical structures computed for complexes similar to those in this work, but with methylene and butyl bridges. These different sized bridges illustrate smaller and larger bite angles, relative to the ethyl and propyl bridges, respectively. This trend for the size of these bite angles has been represented pictorially in Figure 4.6: methylene < ethyl < propyl < butyl. The distance between each N_p (pyridyl nitrogen) and its adjoining N_i (imine nitrogen) stays constant therefore there is very little change in these angles. Subsequently the change due to the chain length of the bridge must cause alteration of the bite angle. The planar coordination sphere must always

equal 360° and therefore this in turn causes a change in the $N_p\text{-M-N}_p$ angle – as the bite angle increases so this angle must decrease.

The increase in size of the bite angles can be observed in Figure 4.7. The increase from the methyl to ethyl to propyl chelates is around 15° and 11° , respectively for both metal complexes. The increase from the propyl to butyl bridging chains is however less than 4° . The general trend of increasing angle with increasing length of the chelate is, however, shown to be accurate for this range of metal complexes. There is also a slight discrepancy in the bite angle for metal complexes of the same size chelate ring. With increasing chelate length these discrepancies for the platinum and palladium complexes are 0.5° , 1° , 1° and 0.7° , respectively. This is similar to the increase in the bite angle from the palladium to platinum complexes of a salen ligand (with a propyl bridge) which was shown to be $\sim 1^\circ$.³¹⁶

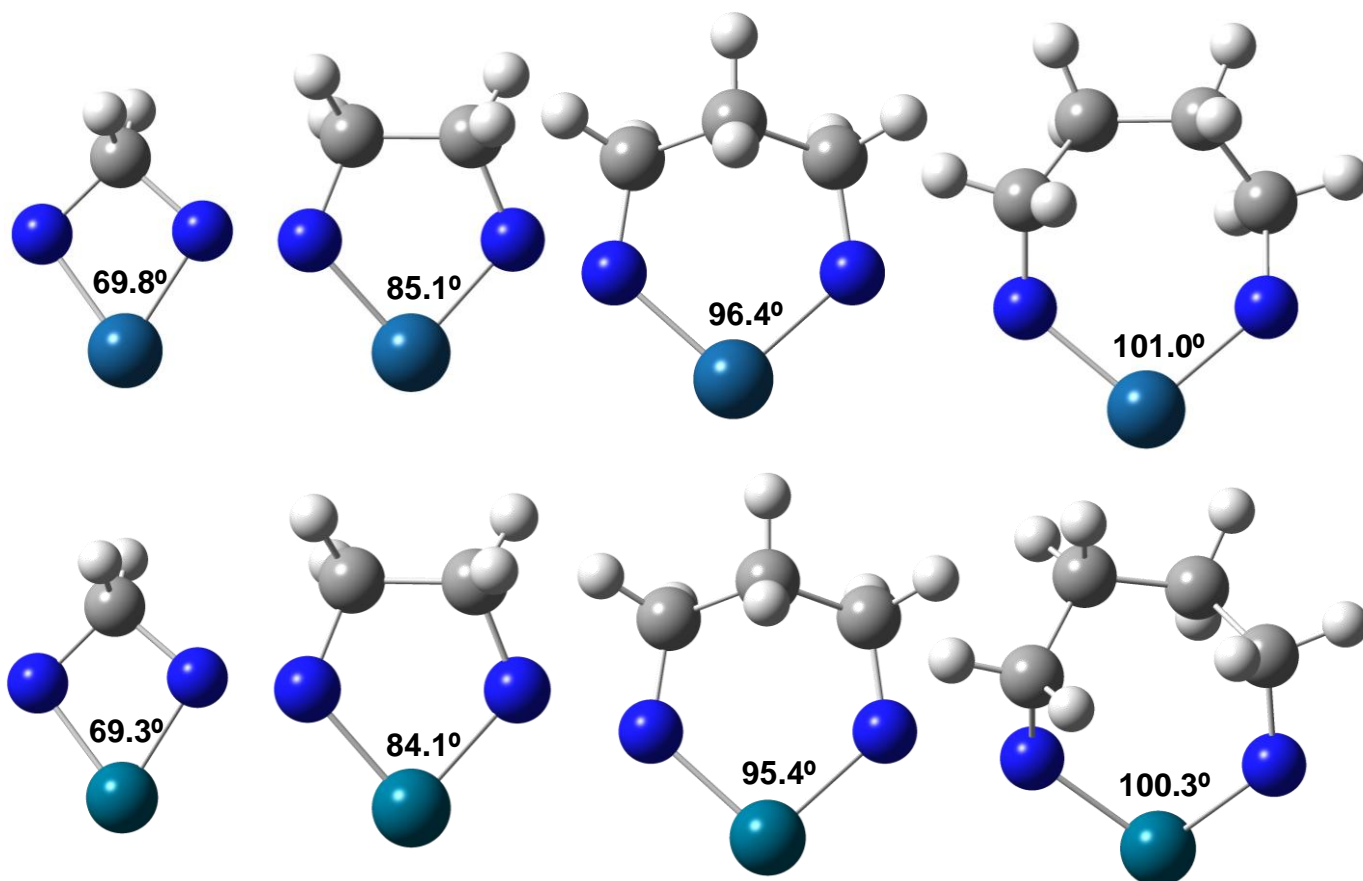


Figure 4.7: Portions of the platinum complexes (top) and palladium complexes (bottom) showing the increasing size of the DFT-computed bite angles for the increasing length of the chelate ring's bridging group.

Distortion from the plane is observed for the ethyl bridging group of **PtL1** and **PdL1**. The ethyl bridge is completely distorted from planarity resulting in one CH_2 below the plane

and one above. This reduces the strain on the metal and subsequently allows for a smaller bite angle. Distortion is also observed for the propyl bridging group of **PtL2** and **PdL2**, but to a lesser extent. The three carbon atoms form an envelope shape with the central CH₂ orientated out of the plane and each CH₂ on either side in the plane. With the limited distortion seen for this bridge it is understandable that it possesses a larger bite angle than the ethyl derivatives, in order to accommodate the two in-plane CH₂ groups.

It has been noted that it would be more energetically favourable for the bonds and angles of the metal centre to change, rather than those of the carbon-chain chelate rings (page 88). We subsequently expect to see some changes in the bond lengths to the metal caused by these changes in bite angles. There is an increase in the length of the M-N_i bond when moving from the ethyl to the propyl bridging groups. This is true for both the DFT-computed and the X-ray data for both the platinum and palladium complexes. The same trend has been observed for the methylene and butyl bridging groups. The methylene bridge has shorter M-N_i bond lengths than for the ethyl bridge, while for the butyl derivative they are marginally longer than for all the others. This increase therefore helps to assist the increase in the bite angle with increasing chelate length.

A moderate change in bite angle has also been noted for the different groups of ligands. When moving from the original set of ligands to the methyl-substituted ligands, there is now an increased bite angle; e.g. the bite angle is 85.1° for **PtL1** and 86.1° for **PtL1m**. This is true for both platinum and palladium complexes and the difference ranges from 1 to 3°. Bayat *et al.* also observed this change when moving from H to the electron donating methyl group.²⁸⁷ A similar trend is seen for the phenyl-substituted ligands with very little difference in bite angles between them and the methyl-substituted ligands. These small differences may therefore be attributed to the presence of the methyl or phenyl groups attached to the imine carbon.

4.6.3 Molecular Orbitals

Also determined from the computations were the four frontier molecular orbitals (FMOs) for each of the metal complexes. Although these orbitals may be useful in the qualitative understanding of some molecules, they are merely mathematical functions that represent solutions to the Hartree-Fock equations for that molecule. It is possible for other orbitals

to exist, which look quite different, yet produce the same energy and properties. There is no physical reality that can be connected with these images; individual orbitals are mathematical not physical constructs.³³¹

Here, we are mainly interested in determining to what degree the different bridging groups and metals may or may not perturb the frontier MOs of the complex. GaussView 3.09³⁹⁶ was used to compute the surfaces for the four frontier molecular orbitals of the thirty-six metal complexes. These four frontier molecular orbitals include the highest and second-highest occupied molecular orbitals and the lowest and second-lowest unoccupied molecular orbitals. These are denoted HOMO, HOMO-1, LUMO, LUMO+1, respectively. Given that the frontier molecular orbitals for each range of metal complexes are all rather similar, for brevity we shall present the discussion for the metal complexes of one ligand from each group. The wavefunctions for the molecular orbitals of platinum and palladium complexes of **L2**, **L2m** and **L2b** are shown pictorially in Figures 4.8, 4.9 and 4.10, respectively.

Molecular orbitals can be useful in identifying the orbitals involved in electronic excitations. The frontier molecular orbitals play an important role in electric, optical and spectroscopic properties, as well as chemical reactivity. These orbitals have been generated using an isovalue for the surfaces of 0.02 (smaller isosurface values produce larger orbitals). The red and green colours of the orbitals represent different phases of the wavefunction. Sometimes molecular orbitals are consistent with our ideas of bonding and anti-bonding, sometimes they are delocalised.

There is impressive similarity observed for the corresponding molecular orbitals for the platinum and palladium complexes of **L2**, as seen in Figure 4.8. This is also the case for the equivalent MOs of the platinum and palladium complexes of **L2m** and **L2b**. Each of the two HOMO and each of the two LUMO orbitals for all three sets of ligands look almost identical. The HOMO and LUMO levels have π symmetry, with opposite phases below and above the molecular plane.

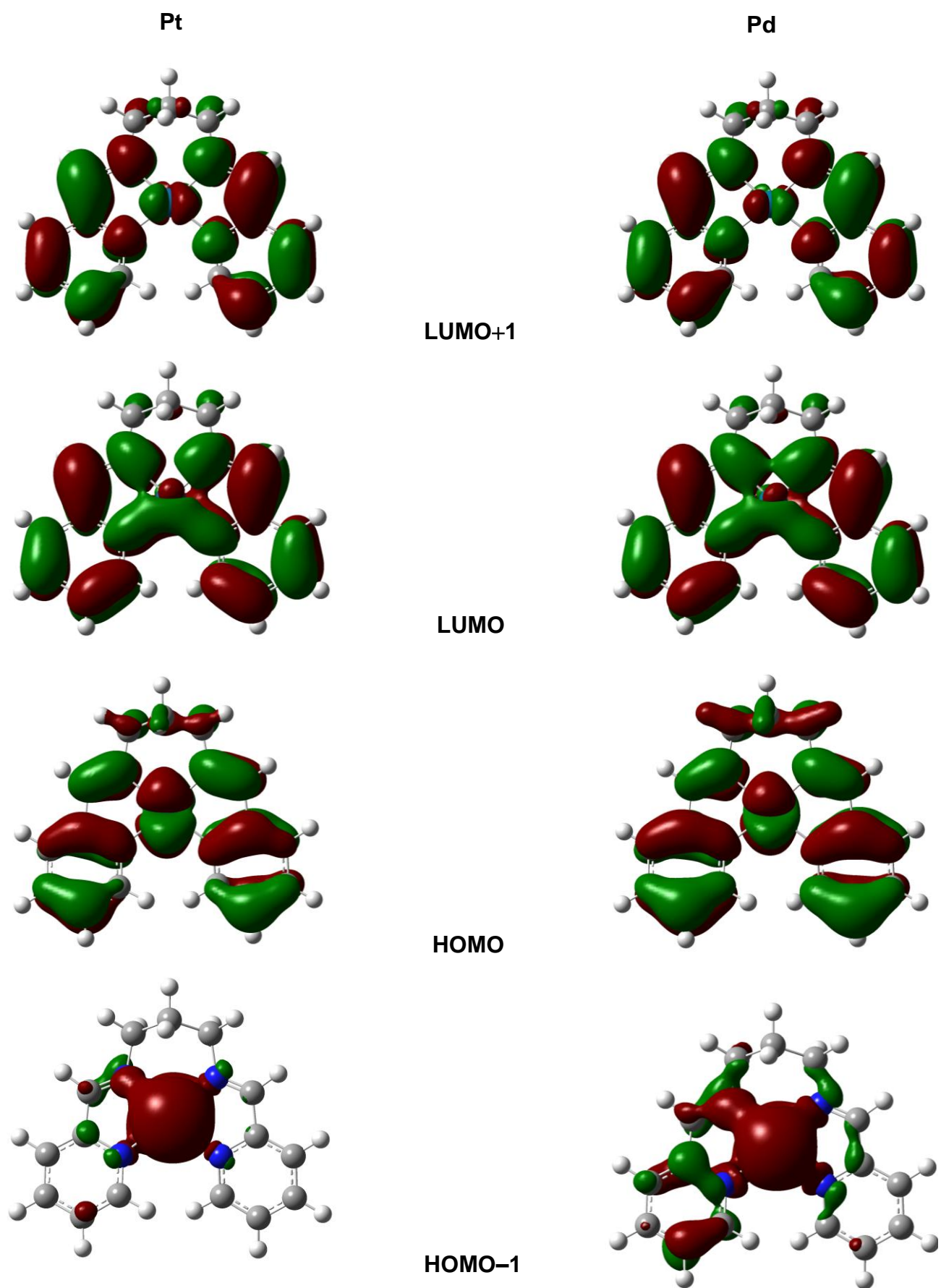


Figure 4.8: LUMOs (top) and HOMOs (bottom) calculated for **PtL2** (left images) and **PdL2** (right images) with GaussView.³⁹⁶

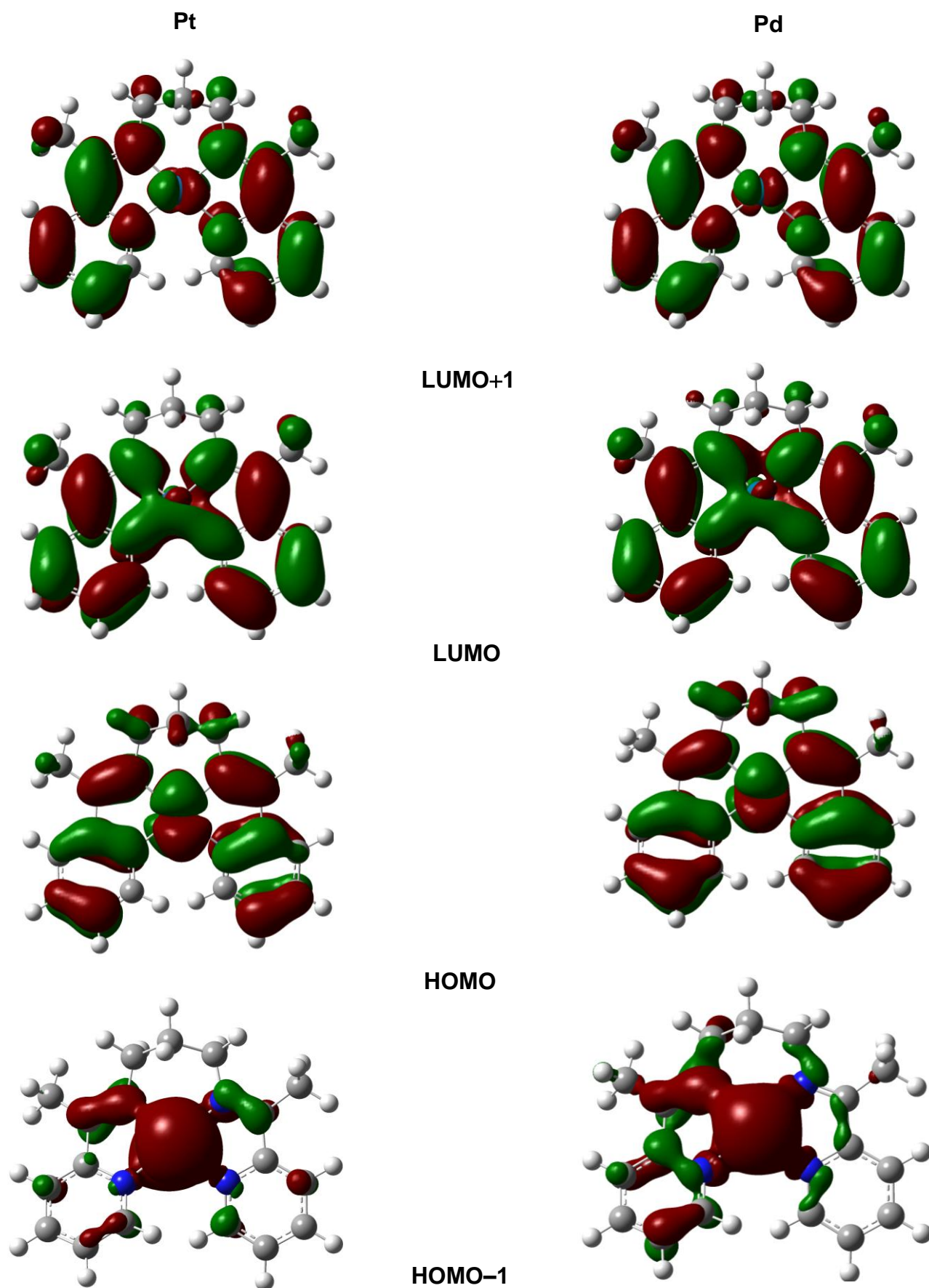


Figure 4.9: LUMOs (top) and HOMOs (bottom) calculated for PtL2m (left images) and PdL2m (right images) with GaussView.³⁹⁶

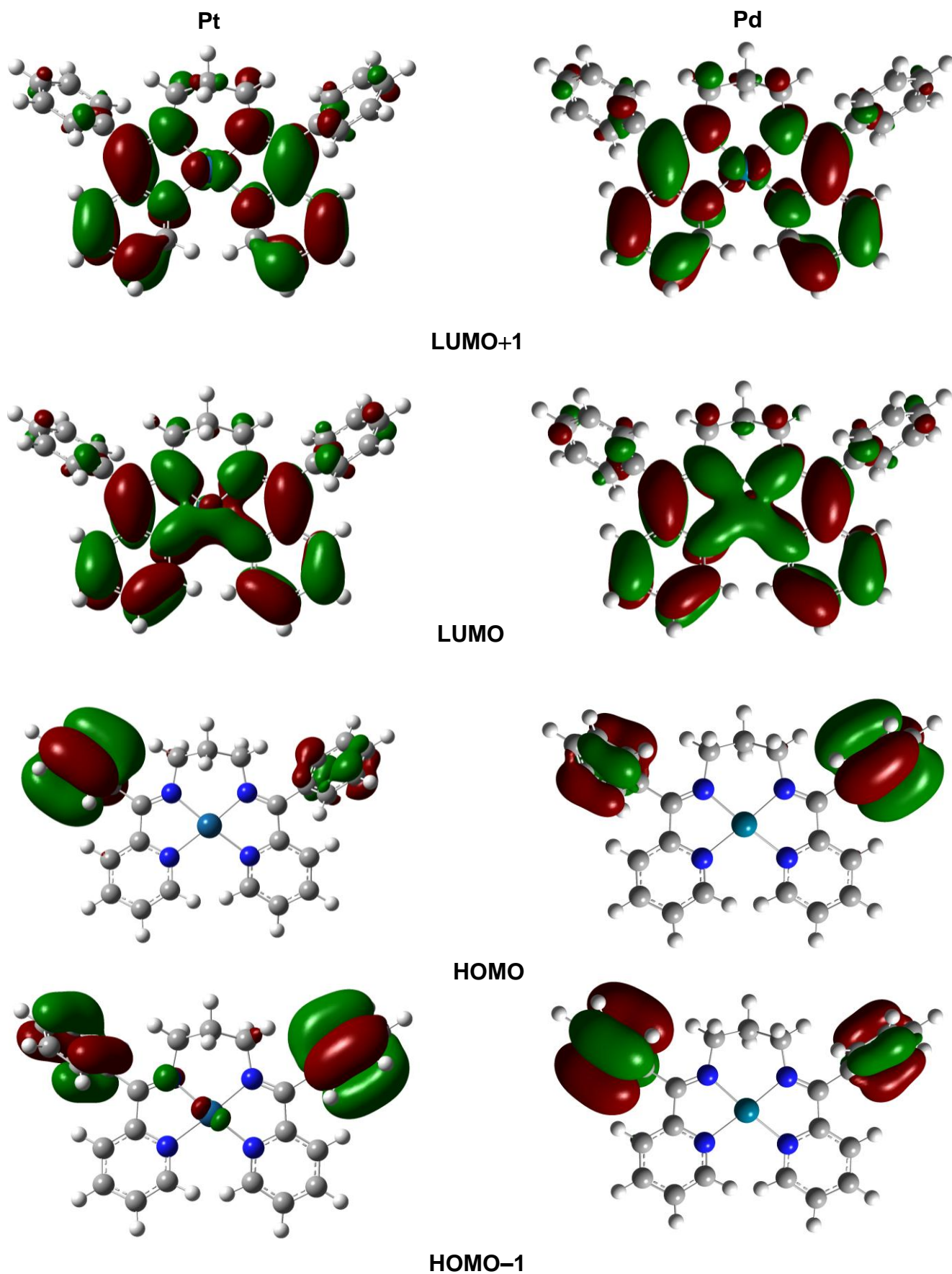


Figure 4.10: LUMOs (top) and HOMOs calculated for **PtL2b** (left images) and **PdL2b** (right images) with GaussView.³⁹⁶

For all six of the complexes they are localised mainly on the central metal and imine/ pyridine ligand structure, with little or no contribution from the bridging groups, depending on the particular complex and orbital. The HOMO-1 orbitals generated for the metal complexes of **L2** and **L2m** seem to be localised metallic orbitals (Pt(II) or Pd(II) dz^2 orbitals); while the HOMOs are π molecular orbitals of mainly pyridine and imine character mixed with a d_{yz} metal-based orbital. The HOMO-1 is therefore mainly the dz^2 orbital that has only partial mixing with the ligand causing them to be close to pure metal atomic orbitals. The HOMO is metal d_{yz} orbital mixed with ligand π -orbital with its main components on the pyridine rings and imine double bonds.

The LUMO and LUMO+1 are mainly composed of the metal centre, pyridine rings and imine, with almost negligible contribution from the bridging fragments. The LUMO is near degenerate with the LUMO+1; this trend is evident for these frontier orbitals for the other complexes as well. There is an interesting inverse symmetry observed for the LUMO+1 and delocalised orbitals across the metal for the LUMOs. The LUMO is essentially a pure ligand π^* molecular orbital, while the LUMO+1 is the metal d_{xz} orbital mixed with the ligand π^* MO.

The LUMOs and LUMO+1 molecular orbitals for the platinum and palladium complexes of **L2b** are quite similar to those of **L2** and **L2m**. They also show negligible contribution from the bridging fragments, as well as from the phenyl groups. Inverse symmetry is also present for the delocalised orbitals across the metal for the LUMOs. The HOMO and HOMO-1 orbitals are very different to those of the **L2** and **L2m** complexes. They are based predominantly on the phenyl substituents with little or no contribution from the rest of the structure. These molecular orbitals are near-degenerate.

The energies of the four frontier molecular orbitals of all thirty-six complexes are given in Table C2.2 in **Appendix C**. Orbital energy level diagrams with structures showing the calculated energy levels of the HOMO-1, HOMO, LUMO, and LUMO+1 orbitals of the complexes are shown in Figures 4.11, 4.12 and 4.13. From the figures, it is clear that the bridge structure affects the HOMO-LUMO gap and energies and that similar trends exist for the Pt(II) and Pd(II) chelates. The HOMO and LUMO energies systematically increase in a similar manner as we move to the bulkier ligands; however, the magnitudes are clearly metal dependent.

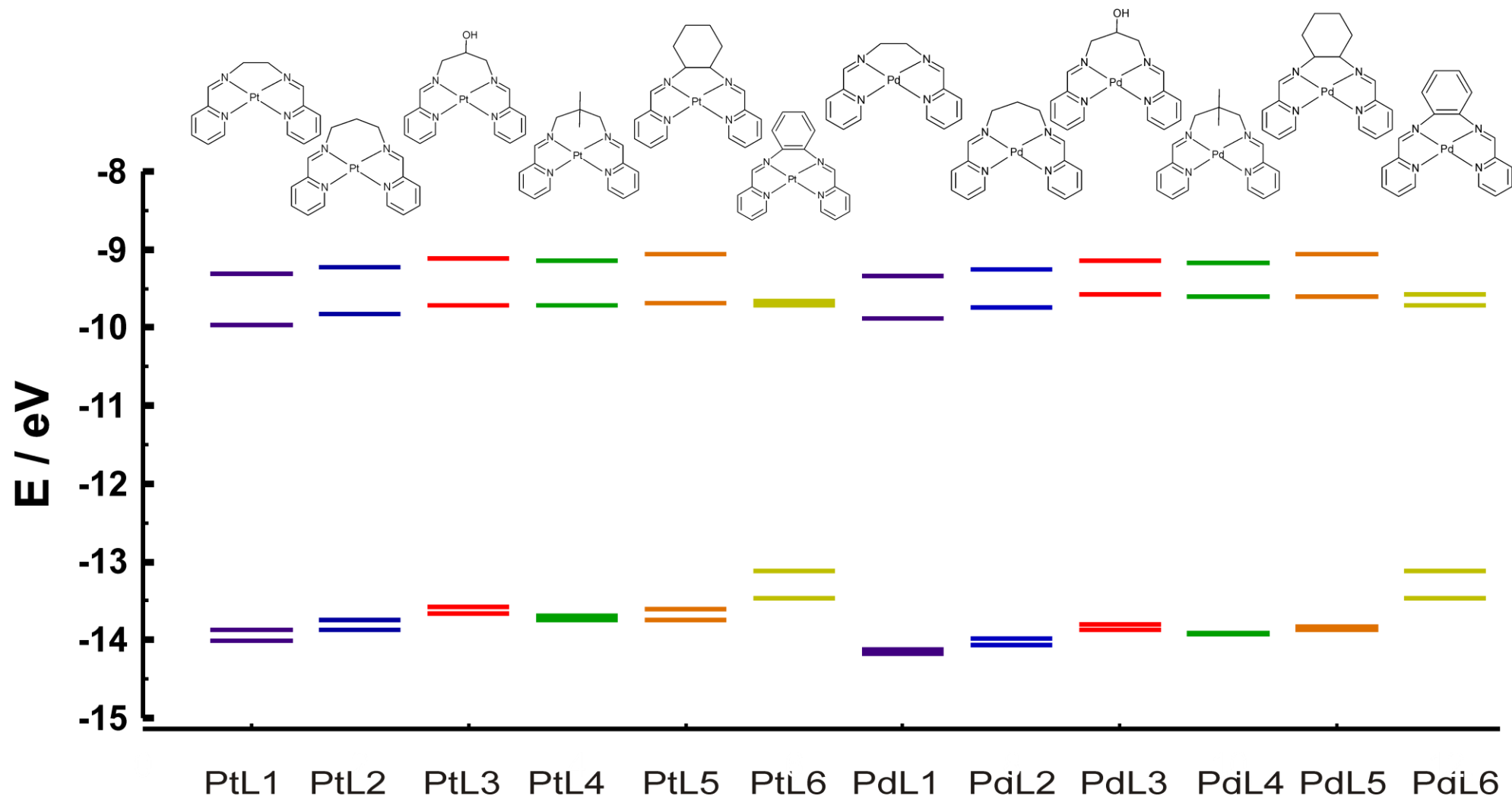


Figure 4.11: The frontier molecular orbitals for the metal complexes of the original ligands: L1 – L6.

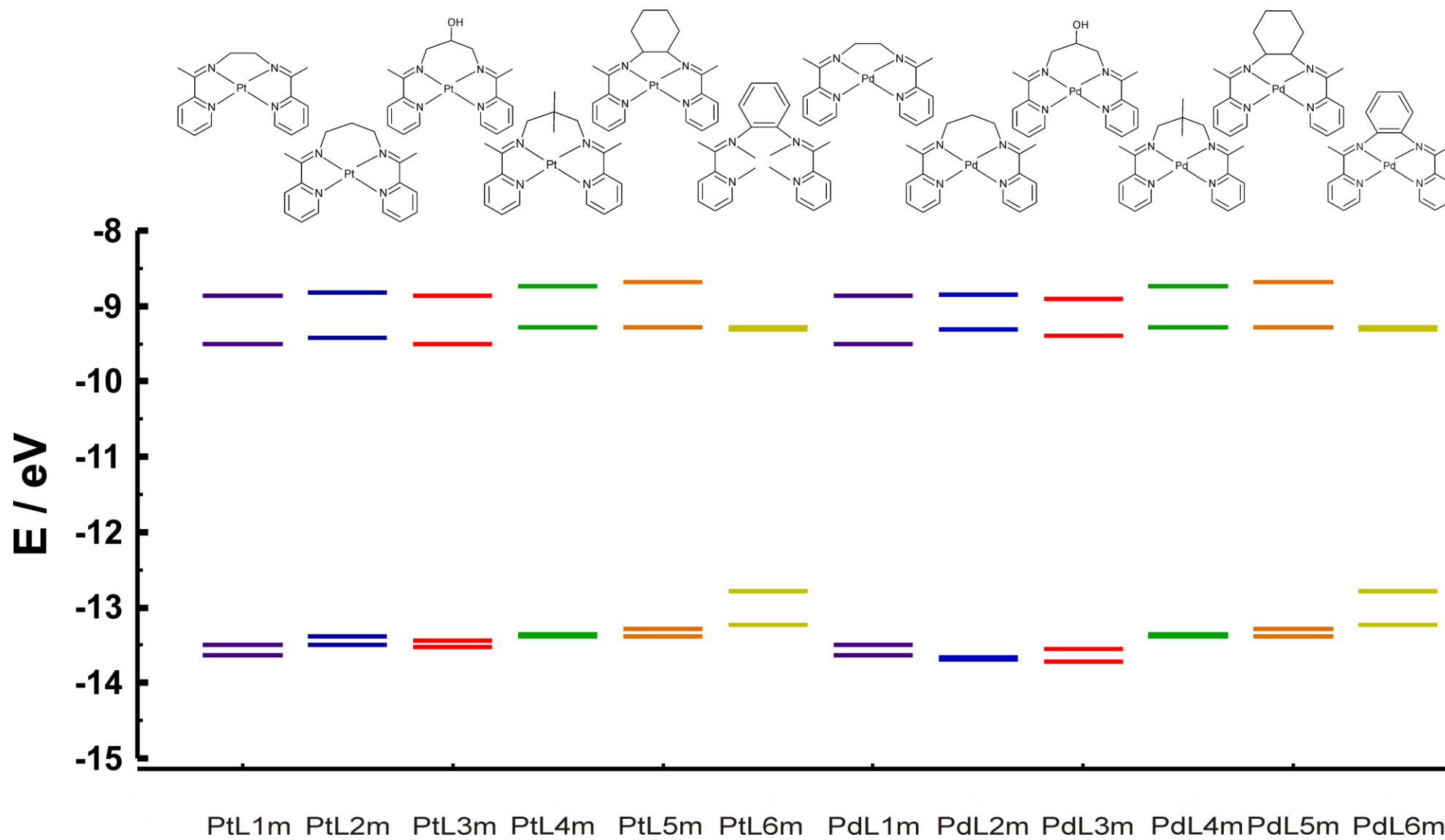


Figure 4.12: The frontier molecular orbitals for the metal complexes of the methyl-substituted ligands: L1m – L6m.

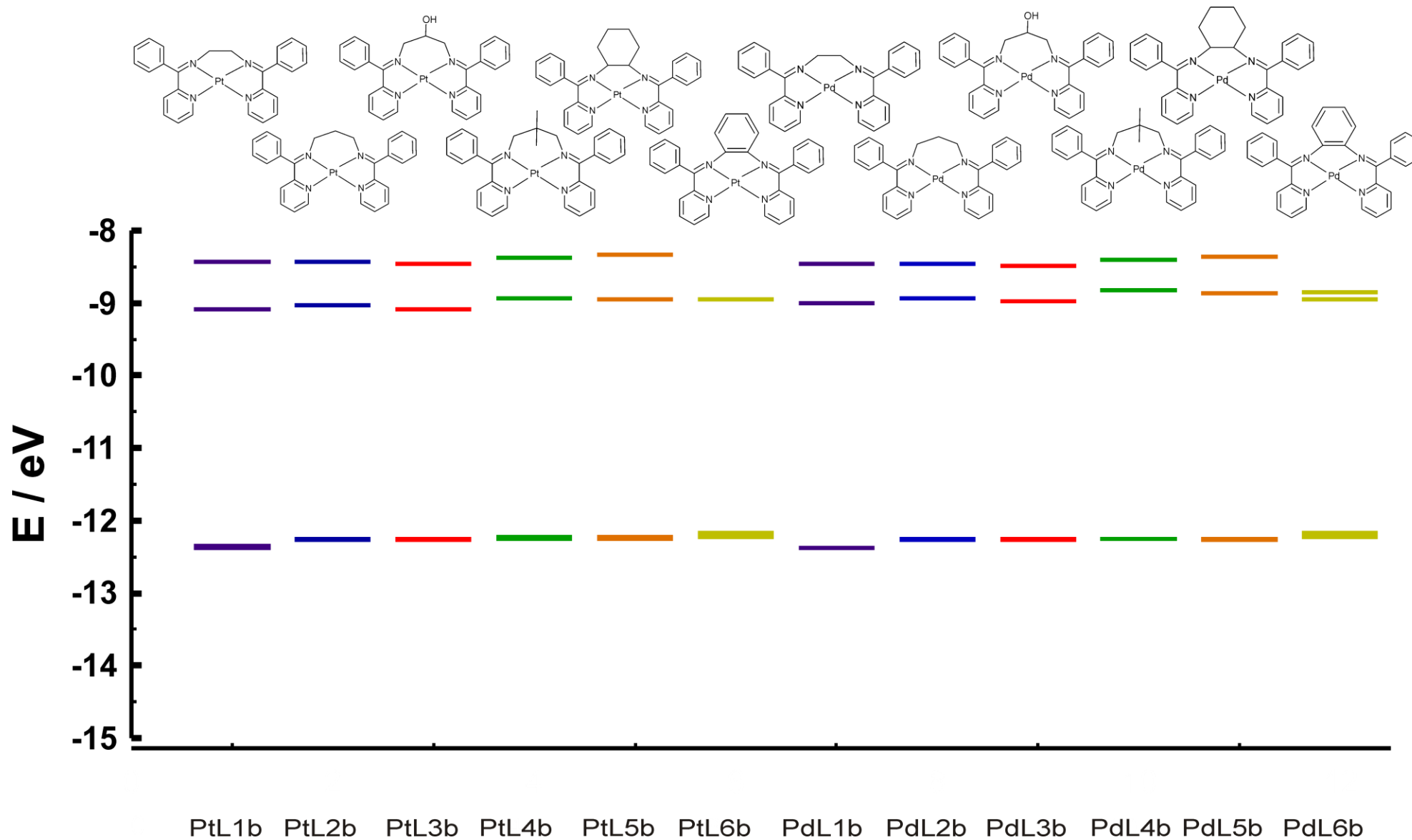


Figure 4.13: The frontier molecular orbitals for the metal complexes of the phenyl-substituted ligands: L1b – L6b.

For the complexes of the original ligands (Figure 4.11) there is a general increase in MO energy with increasing bridge length and/or complexity for both metals. The difference in energy between HOMO-1 and HOMO, as well as the difference between LUMO and LUMO+1, for each metal complex is relatively similar. However, the energies for the LUMOs for the complexes of **L6** are almost identical. This is also seen for the metal complexes of **L6m** (Figure 4.12). The other methyl-substituted ligand complexes (**L1m–L5m**) show a slightly less defined increase with steric bulk; however, there is a definite increase in energies in comparison to Figure 4.11. This may be accounted for by the addition of the electron-donating methyl group. The energies for the metal complexes of the phenyl-substituted ligands increase even further (Figure 4.13). These frontier molecular orbitals are all very similar to each other; the exception once again is for the complexes with the aromatic ring bridging group (**L6b**). The HOMO and HOMO-1 energies are almost identical for each of these metal complexes.

The energy gaps between the HOMO and the LUMO orbitals for each complex are depicted in Table 4.7. The energy of the LUMO is directly related to the electron affinity and the energy of the HOMO is directly related to the ionisation potential. Thus the energy difference between HOMO and LUMO orbitals, the so-called *HOMO-LUMO gap*, is important with regards to the stability of structures.³⁹⁷ The magnitude of this HOMO–LUMO energy gap could then indicate the reactivity pattern of the molecule. According to molecular orbital theory, HOMOs and LUMOs have an important influence on bioactivity.³⁹⁷ The interaction between the receptor of the cancer cell and the complex may be dominated by π – π or hydrophobic interaction amid these frontier molecular orbitals. The positive charges located on the atoms will most likely interact with the negative part of the receptor. In contrast, the most negatively charged parts will interact quite easily with the positively charged part of the receptor. These interactions will subsequently be part of the molecular mechanism of action that may inhibit the growth of cancer cells.

The larger the HOMO-LUMO gap, the higher the kinetic stability as it is energetically unfavourable to extract electrons from a low-lying HOMO or to add them to a high-lying LUMO.³⁹⁸ There is an obvious increase in the HOMO–LUMO gap from the platinum complexes to the palladium complexes. The Pd(II) complexes are harder in Pearson's classification of hard and soft metal ions;³⁹⁹ they are less polarisable than the Pt(II) complexes. The largest HOMO–LUMO energy gap is calculated for **PdL1m** and the

smallest for **PtL3b**. An increase in the metal-ligand interaction energy is noted when the electron donating methyl group is present on the imine carbon and a decrease when this is exchanged for a conjugating phenyl ring.²⁸⁷ This is expected as the energy levels of the occupied orbitals will clearly change due to electrostatic effects caused by these groups.

Table 4.7: The energy difference between the HOMO and the LUMO orbitals for each complex.

Complex	Energy gap / eV	Complex	Energy gap / eV	Complex	Energy gap / eV
PtL1	3.918	PtL1m	4.000	PtL1b	3.265
PdL1	4.245	PdL1m	4.381	PdL1b	3.374
PtL2	3.918	PtL2m	3.973	PtL2b	3.211
PdL2	4.245	PdL2m	4.354	PdL2b	3.320
PtL3	3.864	PtL3m	3.946	PtL3b	3.156
PdL3	4.218	PdL3m	4.163	PdL3b	3.265
PtL4	3.973	PtL4m	4.082	PtL4b	3.292
PdL4	4.299	PdL4m	4.381	PdL4b	3.429
PtL5	3.918	PtL5m	4.000	PtL5b	3.265
PdL5	4.218	PdL5m	4.327	PdL5b	3.374
PtL6	3.401	PtL6m	3.483	PtL6b	3.311
PdL6	3.374	PdL6m	3.456	PdL6b	3.238

The NBO (natural bond orbital) analysis provides accurate representations of the electron density as the orbital details are mathematically chosen. It provides information about interactions in both filled and virtual orbital spaces.³⁹⁷ The metal orbital energies and electron populations are given for each of the metal complexes in Table 4.8. The electron population on each of the metals is more than expected which may be due to σ -donation from the ligand. The partial atomic charges are all very similar for each of the metal atoms; with the platinum derivative of the same ligand having slightly less positive charge than the palladium complex. This is consistent with the Pt(II) ion having a marginally softer character than the Pd(II) ion³⁹⁹ for the same ligand, as evidenced by the smaller HOMO-LUMO gaps for the Pt(II) complexes relative to the Pd(II) complexes.

Table 4.8: Key NBO charge and electron populations for the platinum and palladium atoms calculated at the B3LYP/SDD level of theory.

Complex	Atom	Charge	Core	Valence	Rydberg	Total
PtL1	Pt	0.785	67.989	9.193	0.033	77.215
PdL1	Pd	0.799	35.990	9.178	0.034	45.201
PtL2	Pt	0.727	67.990	9.197	0.036	77.223
PdL2	Pd	0.784	35.990	9.191	0.035	45.216
PtL3	Pt	0.789	67.990	9.186	0.035	77.212
PdL3	Pd	0.811	35.990	9.162	0.037	45.189
PtL4	Pt	0.775	67.989	9.201	0.035	77.225
PdL4	Pd	0.779	35.990	9.195	0.036	45.221
PtL5	Pt	0.781	67.989	9.197	0.033	77.219
PdL5	Pd	0.794	35.990	9.182	0.034	45.206
PtL6	Pt	0.790	67.990	9.188	0.032	77.210
PdL6	Pd	0.806	35.990	9.171	0.033	45.194
PtL1m	Pt	0.775	67.990	9.204	0.032	77.225
PdL1m	Pd	0.791	35.990	9.186	0.033	45.209
PtL2m	Pt	0.767	67.990	9.211	0.032	77.233
PdL2m	Pd	0.790	35.990	9.186	0.034	45.210
PtL3m	Pt	0.766	67.990	9.211	0.033	77.234
PdL3m	Pd	0.789	35.990	9.186	0.034	45.211
PtL4m	Pt	0.770	67.989	9.209	0.032	77.230
PdL4m	Pd	0.790	35.990	9.184	0.035	45.210
PtL5m	Pt	0.771	67.989	9.208	0.033	77.229
PdL5m	Pd	0.786	35.990	9.190	0.034	45.214
PtL6m	Pt	0.778	67.990	9.200	0.032	77.222
PdL6m	Pd	0.797	35.990	9.180	0.033	45.203
PtL1b	Pt	0.772	67.989	9.207	0.032	77.228
PdL1b	Pd	0.787	35.990	9.191	0.033	45.213
PtL2b	Pt	0.766	67.990	9.213	0.032	77.234
PdL2b	Pd	0.787	35.990	9.189	0.033	45.213
PtL3b	Pt	0.765	67.990	9.213	0.032	77.235
PdL3b	Pd	0.786	35.990	9.190	0.034	45.214
PtL4b	Pt	0.768	67.989	9.211	0.032	77.232
PdL4b	Pd	0.787	35.990	9.190	0.033	45.213
PtL5b	Pt	0.768	67.989	9.210	0.032	77.232
PdL5b	Pd	0.782	35.990	9.195	0.033	45.218
PtL6b	Pt	0.774	67.990	9.205	0.032	77.226
PdL6b	Pd	0.791	35.990	9.186	0.032	45.209

4.6.4 IR

Geometry optimisations and energy calculations ignore vibrations in the molecular system; thus calculations are performed using an idealised view of the nuclear positions. In reality the nuclei in molecules are constantly in motion; these vibrations are regular and predictable in equilibrium states and thus can be used to identify molecules from their characteristic spectra. Gaussian 03 computes vibrational spectra for both the excited and ground states. Besides predicting the frequency and intensity of spectral lines, the programme can also depict the displacements undergone by a system in its normal modes. This means it can predict the direction and magnitude of the nuclear displacements that occur when a system absorbs a quantum of energy.³³¹

A significant application for modern quantum chemical methods is the computational prediction of vibrational spectra, since it permits the elucidation and understanding of experimental spectra. This may then be used to assist with identification of unknown compounds or help to clarify the structures of already known compounds. There are two characteristics of vibrational spectra that need to be considered; the frequency of the absorbed incident light and how much is absorbed. To determine the frequency and intensity the harmonic vibrational frequencies of the particular molecule are calculated and accurate intensities must be supplied. For IR spectra, “the intensity is related to the square of the infinitesimal change of the electric dipole moment μ with respect to the normal coordinates”.³³¹ These intensities will be calculated as sharp peaks, not broad bands as for the experimental data.

The crude frequency values calculated using the Hartree-Fock level have systematic errors because electron correlation is ignored and this results in overestimates of around 10-20%. Therefore it is normal for values that have been computed at the Hartree-Fock level to be scaled by an empirical factor of 0.8929.³³¹ It has been found that the use of this factor results in good agreement with experimental values for a broad series of systems. Different factors are required for different method and basis set combinations.⁴⁰⁰ For the particular level of theory used in this work for the ligands, B3LYP/6-31G(d,p), the scale factor to be used is 0.9613 (RMS error = 34 cm^{-1}).³³¹ The scale factor for the metal complexes was taken to be the same despite the different basis set that was used (basis set for the metal complexes: SDD).

The individual values are usually more useful in the qualitative sense, as it is the trends they display that are generally more important than the actual values. The most significant and useful stretching vibration in the compounds investigated in this work is for the imine bonds. Not only does this prominent vibrational mode prove synthesis of these Schiff bases, but it also gives a specific means to characterise and compare these compounds. The corrected DFT data gave relatively good results that matched up to the experimental spectra for all the ligands and complexes, where possible.

Some of the calculated modes show a zero intensity which is due to the fact that there is no change in the dipole moment. Therefore even though the mode has been calculated it will instead be seen in the resonance Raman spectra of the compound. On further inspection, it was clear that when the intensity was zero it was always only the symmetrical stretch; in particular for the ligands with an ethyl bridging group. In the experimental data there is only one peak, which either represents both the symmetrical and asymmetrical stretches, or is an average of the two.

The theoretical and calculated values for the imine vibrational modes for the free ligands are given in Table 4.9. The DFT-calculated frequencies for the C=N bonds of the original free ligands are all around 1660 cm^{-1} , except for **L6** which is about 15 cm^{-1} less. This same trend is observed for the experimental values except at about 10 cm^{-1} less, in the region of 1650 cm^{-1} . The calculated frequency for **L6** is slightly lower by a further 25 cm^{-1} . This may be explained by conjugation effects introduced by the aromatic ring which is the bridging group for this ligand. The aryl bridge will cause the shift to lower frequencies around $1631\text{-}1613\text{ cm}^{-1}$ for compounds of the type $\text{ArCH}=\text{NAr}'$.¹⁶² The DFT computations therefore seem to slightly underestimate the effect of the aromatic group; however, they interpret the nature of effect it will have (reduced frequency) correctly.

All the experimental vibrational modes for the imine bond for the methyl-substituted ligands are just less than 1700 cm^{-1} . This is a substantial increase of about 50 cm^{-1} in comparison to the original ligands. The difference between these two structures is the presence of the electron-donating $-\text{CH}_3$ on the carbon atom of the imine bond. The shift to higher wavenumber for the C=N band suggests an increased bond order, as might be expected if π -overlap was enhanced by an electron-releasing methyl substituent. The phenyl-substituted ligands only show a slightly more than 10 cm^{-1} increase from the original ligands. The phenyl group withdraws electron density from the imine group and

this weakens π -overlap for the C=N bond; the band thus shifts to lower frequency. The effect of the conjugation of the phenyl ring bridging group is not prominent for the methyl-ligands and is unknown for the phenyl-substituted ligands as **L6b** could not be synthesised. The DFT computations consistently calculate the conjugation effects for **L6**, **L6m** and **L6b** (decrease in C=N stretching frequency) in comparison to the other ligands in each group.

Table 4.9: Experimental peaks (where possible) and theoretical peaks (calculated at B3LYP/6-31G(d,p) level of theory) for the imine (N=C) vibrational stretch of the eighteen free ligands.

	$\nu(\text{N}=\text{C})$ (cm^{-1})	$\nu(\text{N}=\text{C})$ (cm^{-1})	$\nu_{\text{s}}(\text{N}=\text{C})$ (cm^{-1})		$\nu_{\text{as}}(\text{N}=\text{C})$ (cm^{-1})		Difference [§] (cm^{-1})
	Experimental value	Literature value	DFT _{corr}	Int.	DFT _{corr}	Int.	
L1	1648	1651 ¹³⁹	1663	0	1662	137.98	-14.5
L2	1647	1590 ¹⁴⁶	1661	46.39	1659	46.16	-13
L3	1649	*	1667	48.51	1663	59.00	-16
L4	1645	*	1662	34.09	1662	79.25	-17
L5	1649	1645 ¹⁵²	1664	53.53	1658	72.40	-12
L6	1625	1618 ¹⁶²	1643	109.64	1646	37.05	30.5
L1m	1697	1680 ¹⁶⁷	1665	0	1663	170.92	33
L2m	1698	1592 ¹⁴⁶	1667	44.56	1665	96.32	32
L3m	1697	*	1671	86.11	1663	85.84	30
L4m	1699	*	1664	68.54	1662	109.45	36
L5m	1698	1638 ¹⁸²	1669	93.73	1660	73.52	33.5
L6m	1696	*	1643	157.38	1642	82.44	53.5
L1b	1665	1665, 1585 ¹⁷⁴	1640	0	1638	226.96	26
L2b	1662	1595 ¹²⁷	1638	33.07	1636	114.18	25
L3b	1662	*	1640	112.79	1631	93.11	26.5
L4b	1626	*	1639	53.79	1637	124.22	-12
L5b	_#	*	1638	93.12	1632	93.38	
L6b	_#	*	1625	141.67	1623	116.41	

DFT_{corr} = corrected value for the DFT calculation using the factor 0.9613.

Int. = the intensity of the DFT calculated values in arbitrary units.

= no experimental value as these ligands could not be synthesised.

* = no literature data available.

§ = the experimental value – average of the DFT values.

Overall the DFT frequencies are calculated to be higher than the experimental values for the original ligands; however, lower for the ligands with substituted groups on the imine (methyl-substituted and phenyl-substituted ligands). There is little difference between the DFT-computed values for the original and methyl-substituted ligands; however, there is $\sim 20 \text{ cm}^{-1}$ decrease for the phenyl-substituted ligands. The literature values for the C=N stretching modes cited for **L1**, **L5**, **L6**, **L1m** and **L1b** compare well (within 1% error) to the experimental values obtained in this work. The values for **L2**, **L2m** and **L2b** all show consistently larger ($\sim 4\text{--}7\%$ higher) vibrational modes than have been recorded in the literature by Rahaman and co-workers.^{127,146} The frequency for **L5m** also differs (60 cm^{-1}) from the value given by Yoshida *et al.*; however, this band has not been definitively assigned by them. Nonetheless, there is good correlation of the experimental values, within each type of ligand. The effect of the type of imine group is consistent for each collection of ligands with little effect from the change in bridging group (except for **L6**).

The C=N stretching frequencies of the platinum and palladium complexes are given in Tables 4.10 and 4.11, respectively. There is a marked difference in frequency between the free ligand and the metal complex. For both the platinum and palladium complexes the experimental values of the frequencies decrease by about $15\text{--}40 \text{ cm}^{-1}$ for ligands **L1**, **L2**, **L4** and **L5**. The DFT-computed values also show this decrease; however, to a much greater extent. The difference in these imine stretching frequencies may confirm the greater electron-withdrawing effect of the chelating Schiff base ligands.¹⁶⁷ When the Schiff base is coordinated to the metal through the N_i atoms then the metal back-donates electron-density into the π^* MO that involves the imine groups (e.g., the LUMO of Figure 4.9). It is likely that some of the π -bond character for the C=N groups will therefore be affected. (Note that the π^* MO or LUMO has nodes at the C=N bonds.) This lower bond order would result in a higher electron density in the antibonding MO which causes the lower stretching value for the metal complexes. For most of the other metal complexes, for which there are no experimental values, the DFT computed frequencies are in the high 1500s. There are a few complexes that have frequencies in the low 1500s which are mostly those with phenyl substituents. These stretching values are this low due to the added effect of the phenyl group as the imine-substituent. It behaves as an electron donating group which would result in a higher electron density for the ligand and in turn for the imine bond which causes the further reduction in the wavenumber.

Table 4.10: Experimental peaks (where possible) and theoretical peaks (calculated at the B3LYP/SDD level of theory) for the imine (N=C) vibrational stretch of the platinum complexes.

Pt	$\nu(\text{N}=\text{C})$ (cm^{-1})	$\nu_s(\text{N}=\text{C})$ (cm^{-1})		$\nu_{as}(\text{N}=\text{C})$ (cm^{-1})		Difference [§] (cm^{-1})
	Experimental value	DFT _{corr}	Int.	DFT _{corr}	Int.	
L1	1632	1595	62.39	1571	70.71	49
L2	1632	1595	32.18	1567	62.96	51
L3		1600	33.00	1568	49.02	
L4	1604	1591	31.95	1569	66.08	24
L5	1634	1591	42.45	1572	78.24	52.5
L6		1551	9.50	1569	87.97	
L1m		1593	9.97	1587	86.75	
L2m		1562	42.03	1551	45.34	
L3m		1561	40.60	1551	47.08	
L4m		1571	6.66	1570	122.20	
L5m		1588	37.90	1561	63.49	
L6m		1522	3.36	1565	129.43	
L1b	1667	1559	14.27	1555	131.25	110
L2b	1660	1522	105.45	1517	183.44	140.5
L3b		1519	109.83	1514	214.05	
L4b	1670	1547	1.50	1525	246.30	134
L5b		1534	75.10	1545	117.54	
L6b		1508	3.51	1505	86.33	

DFT_{corr} = corrected value for the DFT calculation using the factor 0.9613.

Int. = the intensity of the DFT calculated values in arbitrary units.

[§] = the experimental value – average of the DFT values.

Table 4.11: Experimental peaks (where possible) and theoretical peaks (calculated at the B3LYP/SDD level of theory) for the imine (N=C) vibrational stretch of the palladium complexes.

Pd	$\nu(\text{N}=\text{C})$ (cm^{-1})	$\nu_s(\text{N}=\text{C})$ (cm^{-1})		$\nu_{as}(\text{N}=\text{C})$ (cm^{-1})		Difference [§] (cm^{-1})
	Experimental value	DFT _{corr}	Int.	DFT _{corr}	Int.	
L1	1644	1603	70.94	1597	90.28	64
L2	1642	1527	27.45	1505	53.75	126
L3		1608	49.40	1568	50.41	
L4	1629	1595	42.83	1593	26.20	35
L5	1642	1599	51.58	1593	60.76	76
L6		1572	7.60	1566	70.39	
L1m		1597	13.44	1591	157.36	
L2m		1565	68.31	1553	66.66	
L3m		1564	68.07	1553	66.24	
L4m	1623	1580	11.17	1570	108.01	48
L5m		1590	66.96	1565	109.30	
L6m		1556	11.44	1564	162.19	
L1b		1574	38.29	1555	212.32	
L2b		1526	123.34	1521	265.77	
L3b		1523	130.99	1517	291.74	
L4b	1664	1547	1.34	1529	336.98	126
L5b		1538	36.02	1537	141.35	
L6b		1508	5.90	1505	114.32	

DFT_{corr} = corrected value for the DFT calculation using the factor 0.9613.

Int. = the intensity of the DFT calculated values in arbitrary units.

§ = the experimental value – average of the DFT values.

One important frequency in the calculated output of the DFT calculations is the value for the lowest energy vibration determined for each ligand and complex. If this value is negative, then the geometry optimisation has located a transition state instead of a local minimum. For each of our computations, the lowest energy vibrations were above zero (the smallest being around 4 cm^{-1}) and thus stable minimum energy conformations were computed in all cases. These values and their respective assignments are shown in Table 4.12.

Table 4.12: The lowest energy DFT-computed vibration for each of the Schiff base ligands and their metal complexes.

	Free ligands			Platinum complexes			Palladium complexes		
	$\bar{\nu}_{\text{corr}}$ (cm^{-1})	Intensity	Distortion mode	$\bar{\nu}_{\text{corr}}$ (cm^{-1})	Intensity	Distortion mode	$\bar{\nu}_{\text{corr}}$ (cm^{-1})	Intensity	Distortion mode
L1	6.7	3.47	eclipsed	48.3	10.11	saddled	48.4	7.09	saddled
L2	11.5	1.48	eclipsed	45.9	5.70	saddled	51.1	1.36	saddled
L3	10.1	1.60	eclipsed	41.2	2.04	saddled twisting	40.0	1.22	saddled twisting
L4	9.2	1.33	eclipsed	36.5	0.22	saddled	35.1	1.36	saddled
L5	12.7	1.04	eclipsed	44.5	0.41	twisting	44.7	0.04	saddled
L6	23.4	0.25	eclipsed	46.0	0.00	twisting	46.9	0.00	twisting
L1m	9.1	3.11	eclipsed	37.0	0.00	twisting	37.3	0.00	twisting
L2m	6.0	1.32	eclipsed	34.8	2.55	saddled	28.8	0.21	saddled
L3m	10.3	1.44	eclipsed	34.9	2.76	saddled	27.9	0.43	saddled
L4m	10.5	1.57	eclipsed	32.6	1.35	saddled	31.6	0.84	saddled
L5m	9.1	0.35	staggered	28.5	2.82	saddled	29.6	2.45	saddled
L6m	21.9	0.44	eclipsed staggered	27.7	0.01	twisting	28.4	0.01	twisting
L1b	3.9	1.72	twisting	18.0	0.01	twisting	16.7	0.01	twisting
L2b	6.8	0.39	twisting	17.7	0.69	saddled	17.4	0.32	saddled
L3b	8.3	0.07	twisting	16.9	0.92	saddled	16.6	0.53	saddled
L4b	8.3	0.87	twisting	17.9	0.43	saddled	18.8	0.21	saddled
L5b	4.6	0.35	twisting	17.7	0.56	saddled	17.5	0.32	saddled
L6b	16.0	0.04	eclipsed staggered	11.7	0.05	twisting	13.5	0.09	twisting

These lowest vibrations have rather small intensities for the free ligands (all below 4 units) and metal complexes (except for **PtL1**: 10.11 and **PdL1**: 7.09). The vibration associated with each of these values according to the DFT computation is caused by the distorted motion of the bridge and its pyridine ring substituents. The trend seen for the free ligands is an *eclipsed* conformation with each pyridyl-imine “arm” hanging down on either side of the bridging group. As more steric bulk is added to the group on the imine carbon and to the alkyl bridge this conformation changes to having one “arm” up and one “arm” down. For all the phenyl-substituted free ligands this *staggered* conformation is observed. Figure 4.14 shows an example of these eclipsed (**L2**) and staggered (**L2b**) free ligands.

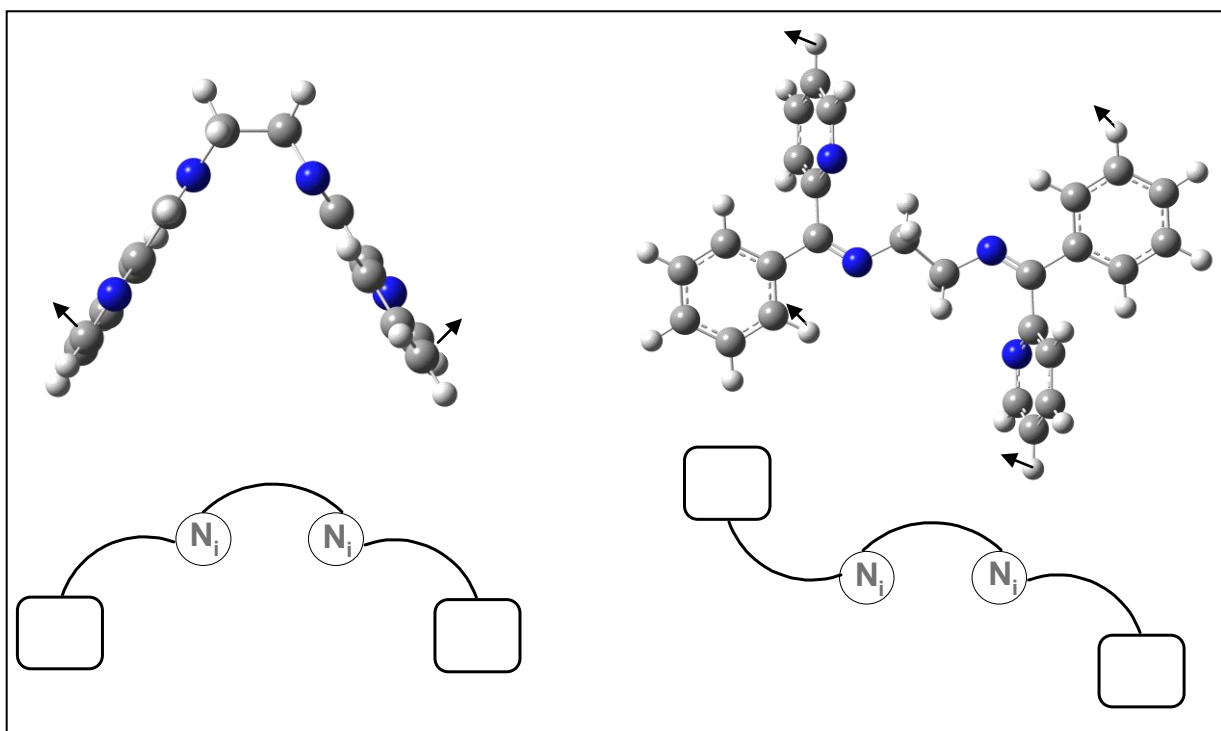


Figure 4.12: Schematic diagrams and examples of the eclipsed (left) and staggered (right) geometries observed for the lowest vibrational modes for the free ligands. The terms "eclipsed" and "staggered" refer to the relative orientations of the C-N bonds in three-dimensional space.

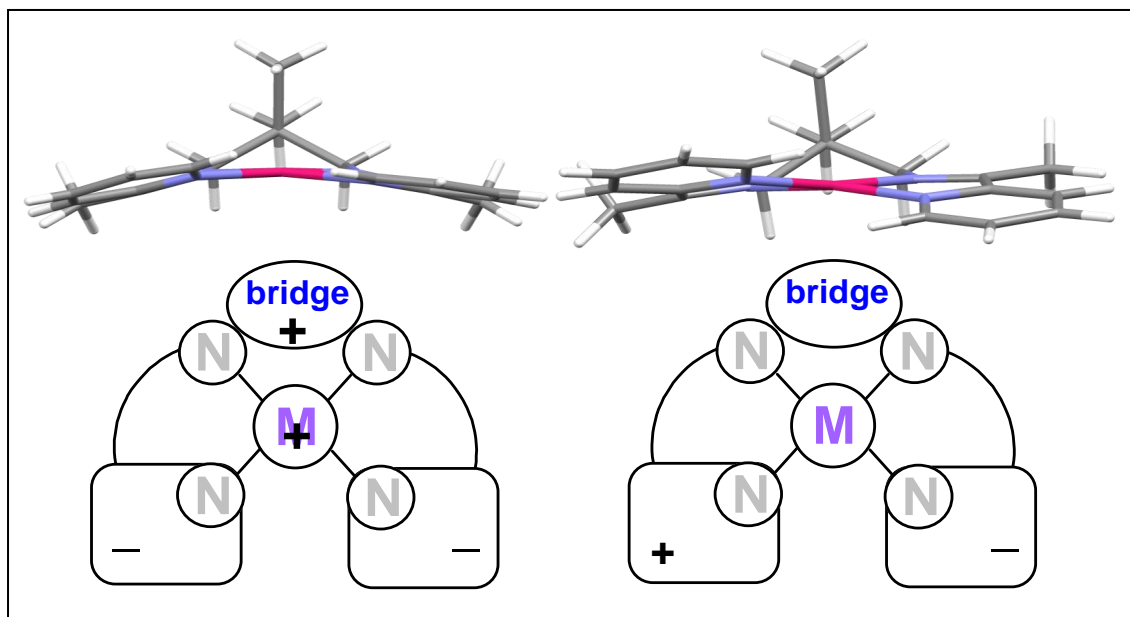


Figure 4.15: The general distortions associated with saddling (left) and twisting (right) of the metal complexes observed for the lowest vibrational modes for the free ligands. The N_4 atoms form the plane from which distortion is observed.

The platinum(II) and palladium(II) complexes mostly maintain the general conformation seen for their respective free ligands; but there are a few exceptions, notably **L6**, **L1m**,

L5m, L2b, L3b, L4b and **L5b**. The frequency of these lowest-energy vibrations computed for each metal complex is on average 2–4 times larger than that of the free ligands. This presumably reflects a stiffer chelate conformation that is less amenable to distortion as a result of coordination of the metal ion. The largest frequencies are generally observed for the twisting distortion rather than for the saddling motion. In general, a twisting distortion is observed for the complexes of the ligands with ethyl and phenyl bridging groups (except for **L1**).

CHAPTER 5 – DNA Binding Studies

5.1 Introduction

DNA is the intracellular target of anticancer metallodrugs, making metal complexes that can bind to specific nucleotides of DNA immensely significant.⁴⁰¹ The interaction of small molecules with DNA is vital in the design of new pharmaceutical molecules, which makes it one of the major challenges in the field of molecular recognition. An understanding of how DNA sites can be targeted with specificity will make it possible to design and synthesise new chemotherapeutics. This will also allow DNA to be probed for the subsequent development of highly receptive diagnostic agents.⁴⁰² The binding affinities of small molecules to DNA is thus useful and important for understanding the individual molecule's behaviour; as well as for the further design and development of DNA molecular probes and novel therapeutic reagents.⁴⁰³

After the discovery of the chemical nuclease activity of transition metal complexes in the 1980s, interest in the interaction and mechanism of these complexes with DNA grew markedly. Their applications in antineoplastic medication, molecular biology and bioengineering were also of significance.⁴⁰⁴ Complexes containing metal centres may be useful as investigative tools in biological systems if they are spectroscopically active, water-soluble, stable and inert.⁴⁰² Metal centres in complexes also have different redox and spectral properties, as well as versatile coordination environments. All of this provides the capacity to design new species that are able to bind and cleave DNA.⁴⁰⁵

Some of the first compounds discovered to be active against deoxyribonucleic acid (DNA) were sulfur mustards; however, their high toxicity resulted in the search for other, possibly more efficient compounds, but with less toxicity.⁴⁰⁶ Reports on the occurrence of a non-covalent interaction between acridine and DNA gave grounds to the idea that anticancer agents worked by interacting with DNA.⁴⁰⁷ The prerequisites for an anticancer drug are inhibition of DNA replication and transcription. This is achieved by the drugs either distorting the double-helix structure, alkylating or even cleaving a DNA strand.²⁰⁸ The antitumour drugs and many antiviral and antibacterial therapies developed and discovered that target DNA can be grouped according to their mode of action.

The different ways in which metal complexes can interact non-covalently with DNA include external binding, groove binding and intercalation⁴⁰⁸ (as illustrated in Figure 5.1). External binding refers to binding that takes place on the surface of the DNA, often occurring by means of the ionic atmosphere of the biopolymer capturing the complex. A stronger interaction takes place if the molecule is a suitable size and shape to fit into a groove of DNA. If the molecule is predominantly planar and aromatic then it may be able to intercalate between two adjacent bases at the core of the macromolecule. This means that square planar molecules are usually capable of this insertion and will, in principle at least, almost certainly be intercalators.⁴⁰⁹ Complexes with tetrahedral or octahedral coordination, however, are therefore unlikely to be able to insert themselves between the two adjacent base pairs of DNA and hence normally bind externally.

Intercalation is a useful mode by which many molecules interact with the base pairs of double-stranded DNA. The drug forces the sequential base pairs apart; this increases the helix's length and stiffness, which subsequently prevents the transcription and replication of DNA.⁴¹⁰ These intercalators often have antitumour properties associated with them (e.g. doxorubicin⁴¹¹ and daunomycin^{411,412}) or may find application as structural and functional probes for nucleic acids (ethidium and a variety of metal complexes).⁴¹³ Intercalation does not necessarily imply the whole molecule. The original design of an intercalator⁴¹⁴ was that the entire molecule would fit in between the base pairs; however, since then partial intercalation has also been reported.⁴⁰⁸ The expected intercalation mode of a flat molecule may be disrupted by distortions from planarity or also by bulky substituents attached to this predominantly planar molecule. This may then allow for partial intercalation or be able to change the mode completely to external binding.

For an aromatic complex it has been found that perfect coplanarity of the rings present is unnecessary. Either the twist of DNA base pairs is complemented or enhanced by some distortion in the bonds joining the aromatic rings or it may open up to lodge the skewed group.⁴⁰⁸ Thus, deviation from planarity does not necessarily destroy the intercalating ability of a complex, but may in fact play a role in improving it. Cusumano *et al.* have shown an out of plane phenyl group to largely increase the complex's binding affinity for DNA.⁴⁰⁸

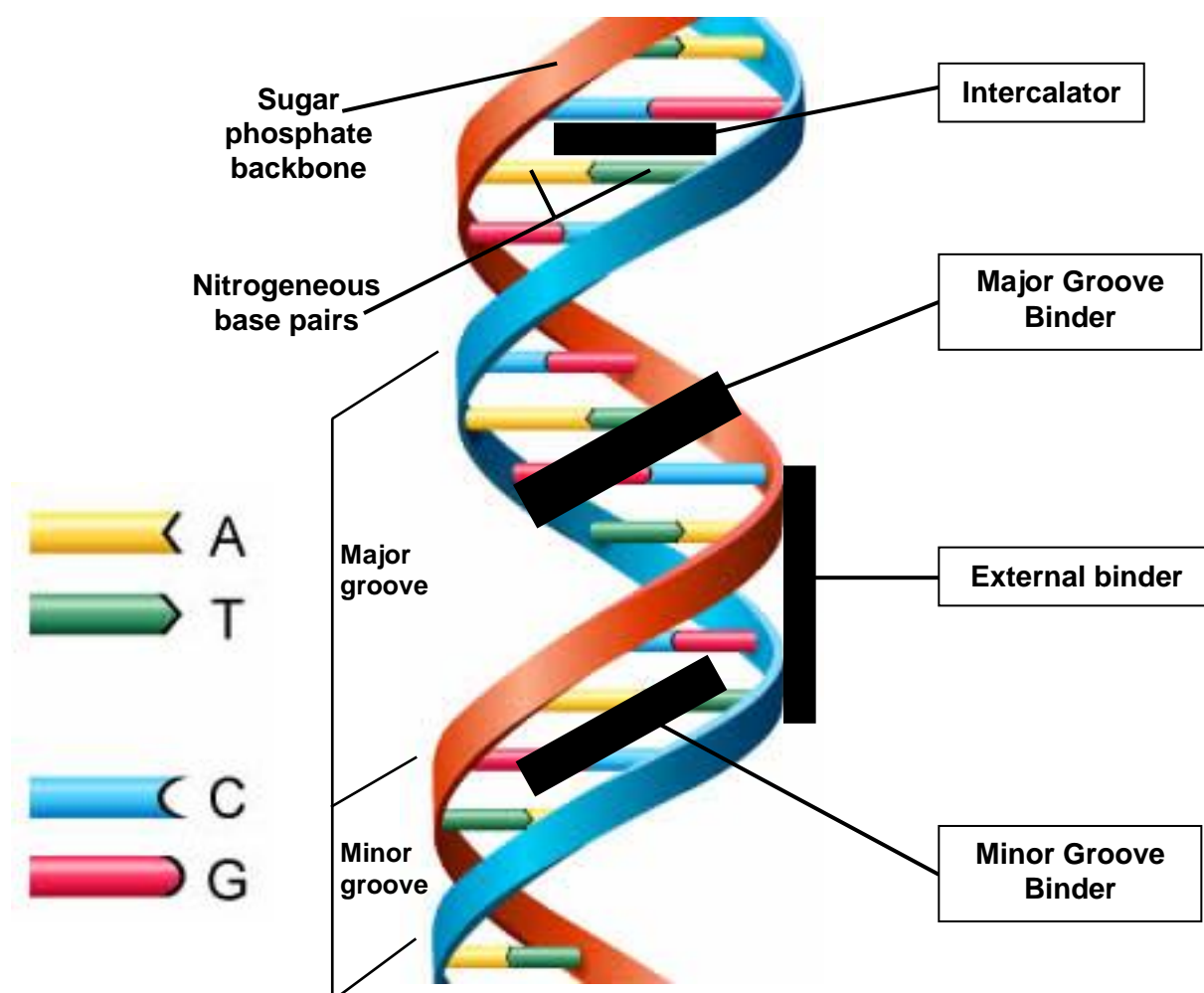


Figure 5.1: The structure of the DNA double helix; colour-coded by nucleotides: adenine (A), thymine (T), cytosine (C) and guanine (G).⁴¹⁵ The positions of the black blocks represent the three types of non-covalent binding modes possible between metal complexes and DNA.

A driving force may be provided by the different hydrophilic and hydrophobic interactions between an intercalator and the nucleobases and phosphate groups. If the intercalator has a positive charge then the interaction with the negatively charged DNA phosphate backbone also contributes electrostatically. The presence of aromatic ring stacking between nucleobases and intercalators is also thought to be a chief structural and mechanistic requirement leading to binding.⁴¹⁶ All substances that incorporate aromatic coplanar rings may be possible DNA intercalators; however, *noncoplanar-aromatic* and *planar-nonaromatic* complexes are not.^{417,418}

The quality of the toxicity of a possible drug (its cytotoxicity) does not depend entirely on its interaction with DNA. In order for a drug to be biologically active it is necessary for it to target DNA; however, this is not the only criterion. There are some intercalators that do not function as cytotoxic agents, thus a drug must be capable of overcoming different

obstacles in order to be completely effective. This may include metabolic pathways, and nuclear and cytoplasmic membranes.⁴¹⁹ The drug needs to be capable of achieving entry into the nucleus and of forming a stable complex with the DNA (with a relatively long half-life). Cytotoxicity is a consequence when important enzymes such as DNA topoisomerases⁴²⁰ are poisoned. These enzymes are involved in the fundamental steps of cellular growth (DNA replication), DNA recognition, and the S- and M-phases of the cell cycle. Once poisoning has taken place the ternary DNA-drug-topoisomerase cleavage complex will be detected as damaged, which starts a sequence of events; almost certainly the most important being cell apoptosis (programmed cell death).⁴²⁰

In clinical trials, cytotoxicity is used to measure a drug's ability to function as an antitumour agent. The assessment of a new compound as a cytotoxic agent may be done either *in vitro* or *in vivo*. *In vitro* studies are the more common choice and the most accepted method is the one used by the National Cancer Institute (NCI).⁴²¹ A group of cells is incubated with the potential drugs in different concentrations (< 100 μM) and with reference compounds.⁴²² If the IC_{50} is less than 100 μM then other probes and concentrations will be evaluated. The activity of a compound is determined by the goal of the study and is therefore dependent on design and synthesis.⁴²³

Once the ability of the drug to function as an antitumour agent has been established it is important to try and determine the mode of action associated with it. Due to the interaction taking place between the drug and DNA, it is expected that there will be some sort of relationship between the drug's cytotoxicity and its DNA affinity constant. Other studies have suggested that the efficiency of the drug seems to be dependent on the binding character and mode of the drug, as well as nucleobase selectivity and the kinetic mechanism when it reacts with DNA.^{424,425} Studies on DNA binding therefore help in determining the applications of these complexes as gene regulators or as chemotherapeutic agents.

It is not always the case that direct structural analogues of known DNA intercalator drugs will show comparable or improved clinical efficacy in relation to the parent drug. A possible explanation is that if the test drug does bind DNA, then it will be with an identical mode and thus produce the same biological mode of action.⁴²⁶ Therefore, although it is necessary to take inspiration from known drugs, it is equally important to look beyond those structure-activity relationships and attempt to identify novel materials as potential

anticancer agents. This may also provide an answer to drug-resistance if their DNA binding modes or molecular mechanisms of action are different.

Positively charged metalointercalators are of particular interest, with how they interact with the base-pair stack of DNA being highly desirable for delineating their molecular mechanism of action.⁴²⁷ Metal complexes with square planar coordinating multidentate aromatic ligands (N_4 or N_2O_2) have, in particular, been significant in these studies due to their DNA-binding affinity and cytostatic properties.⁴²⁸

Numerous reviews have shown that the activity of the anticancer drug cisplatin is due to it binding directly to DNA.⁴²⁹ Cisplatin's cytotoxicity stems from its role in interstrand cross-linking⁴³⁰ and this mode of binding deactivates the DNA as a template for replication and probably transcription as well. Research in the area of inorganic antitumour agents has largely been inspired by the considerable success of cisplatin in the clinical treatment of human malignancies.⁴³¹ Intercalating drugs containing platinum have subsequently been extensively investigated in binding studies.^{432,433,434} It has been determined that N7 atoms of guanine and adenine are the primary binding sites of platinum complexes, found in the major groove of DNA.⁴³⁵ Non-covalent intercalation is dependent on numerous factors, including aromaticity, planarity and surface size and expansion. Platinum(II) complexes have been studied as intercalators due to their appropriate geometry, high electron density and inertness toward possible competitive covalent processes.⁴³⁶

The literature shows that square-planar complexes of Pt(II) containing aromatic ligands in particular, are good intercalators.⁴³⁷ Such complexes possess the correct geometry and are inert towards possible competitive covalent processes. Several investigators have shown that the role of platinum may consist largely of imposing this appropriate geometry and positive charge to the complexes.⁴¹³ There is also the wide choice of ligands that may be used which can modify the electronic and steric properties of the complexes. The efficacy of the intercalation event may be fundamentally influenced by the electronic and steric properties of non-interacting ligands. The remarkable similarity between Pt(II) and Pd(II) coordination stereochemistry has encouraged studies of palladium(II) compounds as anticancer drugs.⁴³¹ The intercalation of Pd(II) and Pt(II) complexes between DNA base pairs causing detrimental changes to the DNA has been acknowledged in the literature.⁴²⁶ It has been reported that some palladium complexes

bind DNA through π - π interactions, as well as covalent binding and may promote DNA cleavage.^{438,439,440}

In 1974, Jennette and co-workers identified a square planar platinum(II) complex that would bind to DNA by intercalation; the complex had an aromatic heterocyclic ligand.⁴¹⁹ Four years later a square planar platinum complex, bound within a dinucleotide duplex, reported by Wang and co-workers, also showed intercalation.⁴⁴¹ Interest in DNA-intercalators that bind tightly but reversibly to DNA between the base pairs has since grown,⁴⁴² which includes work on platinum(II) and palladium(II) complexes which can have potential antitumour activity.^{443,444} It has been shown that the binding of platinum complexes to DNA can start the apoptotic processes in tumour cells.^{445,446} Palladium complexes have been chosen in this work due to the remarkable analogy between the coordination stereochemistry of Pt(II) and Pd(II). It is also an advantage that palladium(II) chelates have a high solubility in water and are cheaper than platinum.^{447,448}

The most common way to investigate the interactions of complexes with DNA is to use electronic absorption spectroscopy.^{449,450,451,452} A compound binding to DNA through intercalation usually results in hypochromism due to the intercalation mode involving a strong π - π stacking interaction between the aromatic chromophore and the DNA base pairs.⁴⁵³ It seems to be generally accepted that the extent of the hypochromism in the UV-vis band is consistent with the strength of intercalative interaction.⁴⁴⁹ Van der Waals forces, as well as hydrogen bonding and/or charge transfer forces stabilise the complexes of DNA intercalators. These processes are all reversible and subsequently there must be an equilibrium constant related to them.

A range of platinum(II) and palladium(II) cytotoxic agents with nitrogen donor ligands are shown in Table 5.1. Their structures and binding constants as well as their binding modes are given. Platinum complexes with a rigid aromatic bidentate ligand and either a non-aromatic bidentate ligand or a monodentate ligand may be potent DNA intercalators. These additional ligands can determine the efficacy of the interaction according to their electronic and steric properties.⁴¹³ Higher binding affinities may be attributed to larger stacking surfaces, e.g. the presence of additional phenyl rings.⁴⁰⁸ Enhanced cytotoxicity of an intercalator may indirectly reflect the extent to which the compound may intercalate DNA in a chromatin setting (i.e., within a cell's nucleus). It has been revealed that there is a direct relationship between binding affinity and electron density of the intercalating

moiety. (K_b values increase with increasing σ - donor power of pyridine nitrogens). This may imply that van der Waals interactions are more important than CT interactions.⁴⁰⁸

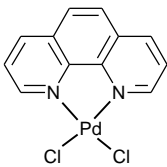
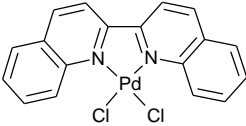
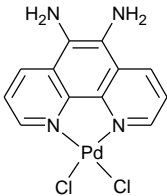
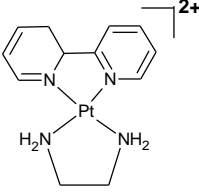
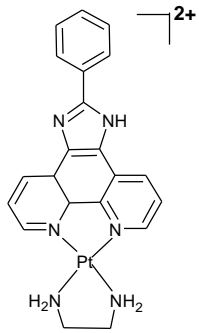
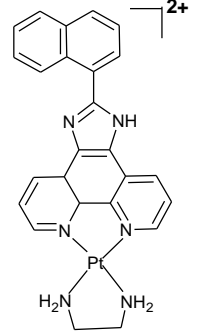
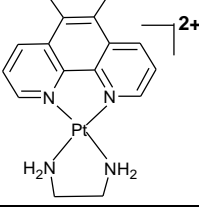
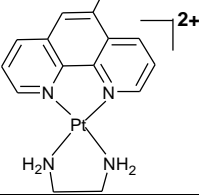
The palladium structure $[\text{Pd}(\text{L})_2\text{Cl}_2]\cdot\text{DMF}$ has no chelating ligands and has a mixed binding mode between covalent interaction and intercalation.⁴²⁶ Platinum- and palladium-intercalators containing bipyridyl or other bidentate aromatic ligands have binding constant values of the order 10^3 – 10^7 M^{-1} . In particular, those with two bidentate ligands seem to have the higher binding constants^{413,427,434,454,455} relative to those that have only one bidentate chelate.^{451,456,457} There are, however, exceptions to this, e.g. $[\text{Pd}(\text{phen})(\text{L-asp})]\cdot 3\text{H}_2\text{O}$ ⁴⁴² and 56MEEN ⁴⁵⁵ (2 bidentate chelates) have binding constants $\sim 10^4$ while $[\text{Pt}(\text{bipy})(\text{py})_2]^{2+}$ (only one bidentate chelate) has a binding constant $\sim 10^5$ (or higher, 10^7 , for the extended structure of $[\text{Pt}(4,4'\text{-Ph}_2\text{bipy})(\text{py})_2]^{2+}$).

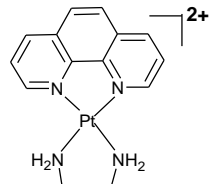
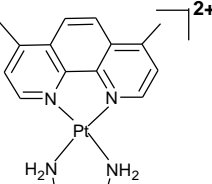
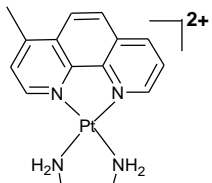
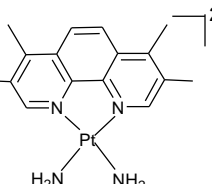
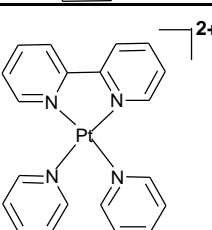
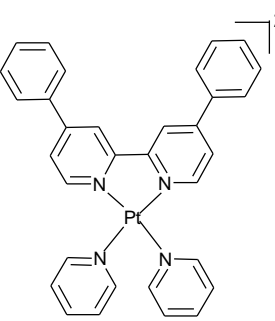
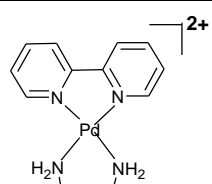
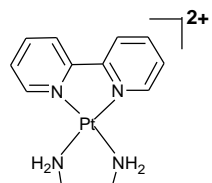
Moderate binding to CT-DNA (calf thymus DNA) through an intercalative mode has been observed for platinum complexes with two bidentate (N_2) ligands (Figure 5.1). Hypochromicity of up to more than 40% accompanied by large shifts in the $\pi \rightarrow \pi^*$ bands have been observed.⁴³⁴ Unusual spectral changes have been observed for platinum(II) complexes with thioureas on addition of CT-DNA. After the addition of a small amount there is an increase in the absorption peak at 300–500 nm; however, upon further additions the expected hypochromic shifts are observed. This implies intercalation of the complex into the DNA.⁴⁵⁸

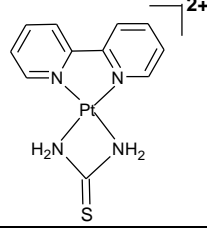
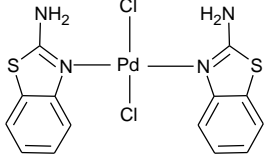
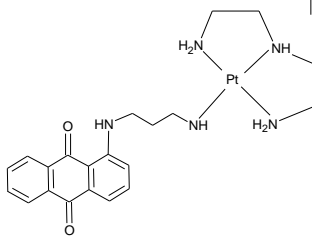
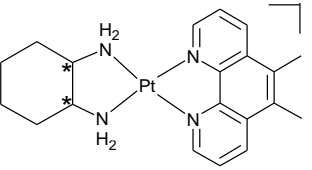
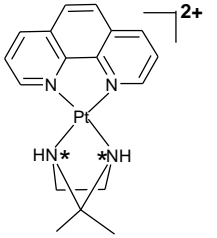
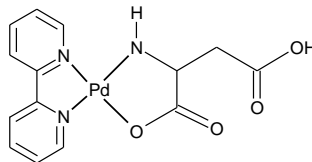
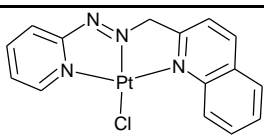
The binding constant for Pt(II) complexes may sometimes be much greater than that of Pd(II) complexes; however, a palladium complex with a N_3 tridentate ligand showed hyperchromism with blue shift in the absorption band at ~ 400 nm and was found to have an intercalating binding mode ($K_b = 1.47 \times 10^5$ M^{-1}).⁴⁵³ The two tridentate platinum complexes represented here have comparable binding constants and intercalation. The only complex shown in the table with a tetradentate chelate is a platinum complex that binds to DNA externally by stacking, with a binding constant of the order 10^5 .⁴⁷⁴

Table 5.1: Binding constants, sites per nucleotide (where given) and mode of binding for some platinum(II) and palladium(II) cytotoxic complexes.

Complex formula / code	K_b ($\text{dm}^3 \text{mol}^{-1}$)	S (binding sites per DNA base pair)	Structure	Mode of binding	Ref.
[Pt(bpy)(cbdca)]	2×10^4	0.011		Coordinate covalent	459
[Pd(bpy)(cbdca)]	1×10^4	0.045			
PdCl ₂ (LL)	2.69×10^3	–		Partial intercalation	451
[Pt(terpy)(SCH ₂ CH ₂ OH)] ⁺	1.2×10^6	0.20		Intercalation	417
[Pd(phen)(L-asp)]·3H ₂ O	3.18×10^4	–		Intercalation	452
[Pt(L ³)]	$1.72(26) \times 10^5$	–		Stacking mode	460
[PtCl(CG [#])(en)]	$11.2(4) \times 10^3$	0.121(2)		Intercalation	456
[Pt(CG [#]) ₂ (en)]	$9.2(7) \times 10^3$	0.098(2)		Electrostatic interaction	

[PdCl ₂ (phen)]•H ₂ O	3.5(7) x 10 ⁴	–		Electrostatic interactions – groove binding	457
[PdCl ₂ (biquinoline)] • 1/2H ₂ O	4.1(5) x 10 ⁴	–			
[PdCl ₂ (phendiamine)] • 1/2H ₂ O	2.8(9) x 10 ⁴	–			
[Pt(en)(bipyridine)] ²⁺	1.00 x 10 ⁴	–		Intercalation	434
[Pt(en)(phenylphen)] ²⁺	1.65 x 10 ⁵	–			
[Pt(en)(naphphen)] ²⁺	2.80 x 10 ⁵	–			
[Pt(en)(5,6-Me ₂ phen)] ²⁺	1.5(1.1) x 10 ⁶	–			
[Pt(en)(5-Mephen)] ²⁺	0.7(2) x 10 ⁶	–		Intercalation	454

$[\text{Pt}(\text{en})(\text{phen})]^{2+}$	$2.2(5) \times 10^6$	—		Intercalation	454
$[\text{Pt}(\text{en})(4,7\text{-Me}_2\text{phen})]^{2+}$	$1.3(4) \times 10^6$	—			
$[\text{Pt}(\text{en})(4\text{-Mephen})]^{2+}$	$1.2(4) \times 10^6$	—			
$[\text{Pt}(\text{en})(3,4,7,8\text{-Me}_4\text{phen})]^{2+}$	$0.7(3) \times 10^6$	—			
$[\text{Pt}(\text{bipy})(\text{py})_2]^{2+}$	$1.62(2) \times 10^5$	—		Intercalation	408
$[\text{Pt}(4,4'\text{-Ph}_2\text{bipy})(\text{py})_2]^{2+}$	$1.67(2) \times 10^7$	—			
$[\text{Pd}(\text{bpy})\text{en}]^{2+}$	$2.13(5) \times 10^5$	—		Intercalation	416
$[\text{Pt}(\text{bpy})\text{en}]^{2+}$	$1.52(1) \times 10^5$	—			

$[\text{Pt}(\text{bpy})(\text{H}_2\text{NCSNH}_2)_2]^{2+}$	$17(1) \times 10^5$	2.4(1)		Partial intercalation	413
$[\text{Pd}(\text{L})_2\text{Cl}_2] \cdot \text{DMF}$	11.0×10^5	0.196(1)		Intercalation and covalent	426
$[\text{Pt}(\text{1C3})(\text{dien})]^{2+}$	3.7×10^5			Intercalation and covalent	461
56MESS	5.9×10^4	–		Intercalation	455
56MERR	4.1×10^4	–			
56MEEN	5.2×10^4	–			
$[\text{Pt}(\text{R,S-tmcp})(\text{phen})]\text{Cl}_2$	$11.0(1) \times 10^5$	2.0(1)		Intercalation	427
$[\text{Pt}(\text{S,R-tmcp})(\text{phen})]\text{Cl}_2$	$8.6(2) \times 10^5$	8.6(2)			
$\text{Pd}(\text{bipy})(\text{L-asp})$	2.62×10^6	–		Intercalation	462
$[\text{Pd}(\text{L})\text{Cl}]$	1.47×10^5	–		Intercalation	453

CG = cholyglycinate

5.2 Objectives

The principal aims of this chapter were to:

- 1) test several new Pt(II) and Pd(II) complexes for cytotoxicity against cancer cell lines;
- 2) obtain equilibrium constants for DNA binding using electronic absorption spectroscopy; and
- 3) characterise the mode of interaction observed for these complexes with CT-DNA.

Here we report the experimental findings of the biological testing and the results of an investigation of the interaction of six metal complexes with CT-DNA. These binding constants are expected to provide a basis for understanding how these N_4 square planar platinum group metal complexes interact with DNA. Comparisons to literature binding constants have been used when warranted to help to characterise the mode of action of these complexes. This data may also help in clarifying the results obtained for the cytotoxicity screening of these platinum group metal complexes.

5.3 Experimental

5.3.1 Materials and Chemicals

5.3.1.1 Biological screening

Cell Line: A549/ATCC (Non-small lung cancerous cell line), *Control:* $Au(dppe)_2Cl$.

Cell Line: U251 (Central Nervous System (CNS) cancerous cell line) *Control:* $Au(dppe)_2Cl$.

MTS (Celltiter One Solution, Promega, USA).

5.3.1.2 DNA Binding

Ultra pure water was used in all experiments. Calf thymus DNA (CT-DNA) was purchased from Sigma-Aldrich and stored in the fridge until use. The phosphate buffer solution (0.0580 M Na_2HPO_4 , 0.0420 M NaH_2PO_4 , pH ~ 7.0) was prepared using de-ionised water.^{401,463}

A solution of CT-DNA in the buffer gave a ratio of UV-visible absorbance at 260 and 280 nm of 1.7:1, indicating that the DNA was sufficiently free of protein.⁴⁰¹ The concentration of the CT-DNA base pairs was determined by using absorption spectroscopy and the molar absorptivity per base pair ($6600 \text{ M}^{-1} \text{ cm}^{-1}$) at 260 nm.⁴⁰¹

All reagents and solvents were purchased commercially and used without purification.

5.3.1.3 Topoisomerase II kinetoplast DNA (kDNA) decatenation assay

Purified topoisomerase II (8 U Topo II) was used for these studies. Kinetoplast DNA (200 ng) was used as the substrate in these experiments, and the control was VP-16 (etoposide).

5.3.2 Physical Measurements

5.3.2.1 Biological screening

In vitro cytotoxicity studies were carried out at Mintek, Johannesburg, SA by a standard method.

Cells were trypsinised on day one, distributed in a flat bottomed 96 well plate to have a final concentration of 2×10^5 cells/mL, and left to adhere overnight. On day two the compounds were administered at a final starting concentration of 100 μM per well with subsequent serial dilutions (eight in total). $\text{Au}(\text{dppe})_2\text{Cl}$ was started at a final concentration of 12 μM per well. On day four (72 hours after compound administration), MTS was added and a reading taken after a good colour change was observed. Concentrations were duplicated per plate and experiments were repeated three times. Sigmoidal curves were fitted to the results using Origin 6.1 to calculate the IC_{50} value.

5.3.2.2 DNA Binding

UV-visible spectra were recorded on a Perkin Elmer Lambda 45 double beam scanning spectrophotometer using 1.0 cm path length quartz cuvettes at room temperature. The absorption titrations of the complexes were carried out in the pH 7 phosphate buffer using a fixed complex concentration to which aliquots of the DNA stock solution were added. A concentration of 50 to 150 μM was used for the complexes.

Initially, 3000 μL of the buffer only was placed in the reference cuvette and 3000 μL of the complex in the buffer solution was placed in the second cuvette. The spectra were recorded between the 250 and 650 nm range. Gradually aliquots (10–100 μL) of the DNA stock solution were added to the complex and to the blank, so as to eliminate the absorbance of DNA itself. The solutions were mixed by repeated inversion and then allowed to incubate for 5 minutes before recording the electronic absorption spectra.

The titration was repeated until binding saturation was achieved. This was indicated when there was no further change in the spectra for at least four DNA aliquot additions. Absorbance values were corrected for dilution.

5.3.2.3 Topoisomerase II kinetoplast DNA (kDNA) decatenation assay

The titration of **PdL2** was performed by Alex Fageson (Prof. Mark T. Muller's group, College of Medicine, University of Central Florida, USA).

For a typical *in vitro* decatenation assay, 10^7 fibroblasts were fractionated. Nuclear extracts were assayed for decatenatory activity using the TopoGEN Eukaryotic Topoll Assay kit (TopoGEN, Inc., Port Orange, FL). The standard assay was performed following the method published by TopoGen.⁴⁶⁴

5.4 Results and Discussion

The results of the growth inhibition assays of the platinum and palladium complexes against the L1210 mouse Leukaemia cell lines are presented in Table 5.2. None of the tested complexes, nor their free ligands, inhibited the growth of the selected cancer cell lines. This suggests that the compounds do not reach nuclear DNA in living cells or that such compounds are possibly substrates for efflux transporters. This was an unfortunate result; however, it does not rule out interaction of the complexes with DNA. Only two cell lines have been used in the testing of cytotoxicity for our metal complexes which means activity for other cell lines may still be possible. Subsequently these complexes may also have some kind of interaction with DNA even if their cytotoxicity is not particularly high. The type and extent of this interaction therefore needs to be assessed. Thus we have studied the interactions of the complexes with calf thymus (CT) DNA, using an absorption technique to obtain the binding constants. This may allow us to characterise

the drug binding mode as the observed changes in the absorption spectrum of the complex caused by the presence of DNA are commonly used to assist in the determination of its binding mode and binding affinity.⁴³⁴

Table 5.2: Results of the growth inhibition assays of our new Pt(II) and Pd(II) complexes against the L1210 mouse Leukaemia cell lines.

Compound	A549 IC ₅₀ (μM)	U251 IC ₅₀ (μM)
L2	> 100	> 100
L4m	> 100	> 100
PdL2	> 100	> 100
PtL2	> 100	> 100
PdL4	> 100	> 100
PtL4	> 100	> 100
PdL4m	> 100	> 100

The different ways in which drugs may bind are dependent on the site in the DNA duplex where they bind: between two base pairs, major or minor grooves, on the outside of the helix or electrostatically.⁴⁶⁵ The binding of these drugs to double-stranded DNA may be characterised through absorption spectral titrations and the binding constants (with binding sites) may be determined. Generally, DNA intercalators demonstrate hypochromism and broadening of the absorption maximum and a shift in wavelength (red shift) when they bind to DNA.^{442,465,466,467} This red shift has been associated with the decrease in the energy gap between the HOMO and LUMO after binding of the complex to DNA.⁴⁶⁸ The magnitude of the intercalative interaction determines the degree of hypochromism in the UV–vis band. Groove binders will also show spectral changes, but these are likely to be less pronounced than for intercalators. They have been found to cause hyperchromism and small red shifts.^{469,470} Substantial increases in intensity (absorbance) may be attributed to electrostatic interaction between the complex and the phosphate backbone of the DNA.⁴⁷¹ This may decrease the repulsion between the negatively charged phosphate moieties and subsequently cause the stabilisation of the DNA double helix.⁴⁷²

The binding constant, K_b , was calculated using the following equations:^{452,463}

$$\frac{(\varepsilon_a - \varepsilon_f)}{(\varepsilon_b - \varepsilon_f)} = \frac{\left(b - \left(b^2 - \frac{2K_b^2 C_t [DNA]}{s}\right)^{\frac{1}{2}}\right)}{2K_b C_t} \quad \dots \text{equation 1}$$

$$b = 1 + K_b C_t + K_b [DNA]/2s \quad \dots \text{equation 2}$$

Where [DNA] is the concentration of DNA in base pairs, ε_a is the extinction coefficient ($A_{\text{obs}}/[\text{complex}]$), ε_f and ε_b are the free extinction coefficients for the free metal complex and the extinction coefficient for the metal complex in the fully bound form, respectively. K_b is the equilibrium binding constant, C_t is the total metal complex concentration and s is the binding site size.

Owing to their design, which includes coplanar aromatic rings and planarity, all of these complexes have the ability to behave as intercalators.⁴¹⁶ They also have an acceptable size, shape and charge to allow these complexes to slip easily between adjacent base pairs of the biopolymer, giving rise to potentially efficient intercalative interaction. The differences between these complexes are the metal centres and the substituents on the imine nitrogen. These variations may be used to observe if, and to what extent, these differences are reflected in the DNA binding ability of the complexes.

For brevity, examples of the data obtained for the metal complexes during the CT-DNA titrations will be discussed. Spectra for the other metal complexes may be found in **Appendix D** and full listings of DNA titration data are included in **Appendix E**. The platinum and palladium complexes of the ligand **2** will be presented. Treatment of **PtL2** with calf thymus DNA resulted in spectral changes characterised by hypochromicity. Although no obvious bathochromic or hypsochromic effects have been noted for the bands seen in Figure 5.2, there is the characteristic hypochromism for each of the five bands. The bands at 282 and 307 nm may be those of intraligand π - π^* transitions, while the bands at 325, 346 and 376 nm are tentatively assigned to MLCT. These MLCT bands arise due to the transfer of charge from a d -orbital of the Pt(II) ion to the π^* orbital of the ligand. The intensity of the peak at 307 nm was reduced by 14.1% upon addition of DNA. No other peaks are prominent in this spectrum, nor were any obvious isosbestic

points observed. The spectral data does however suggest binding to the biopolymer by this metal complex through a noncovalent intercalative mode.⁴³²

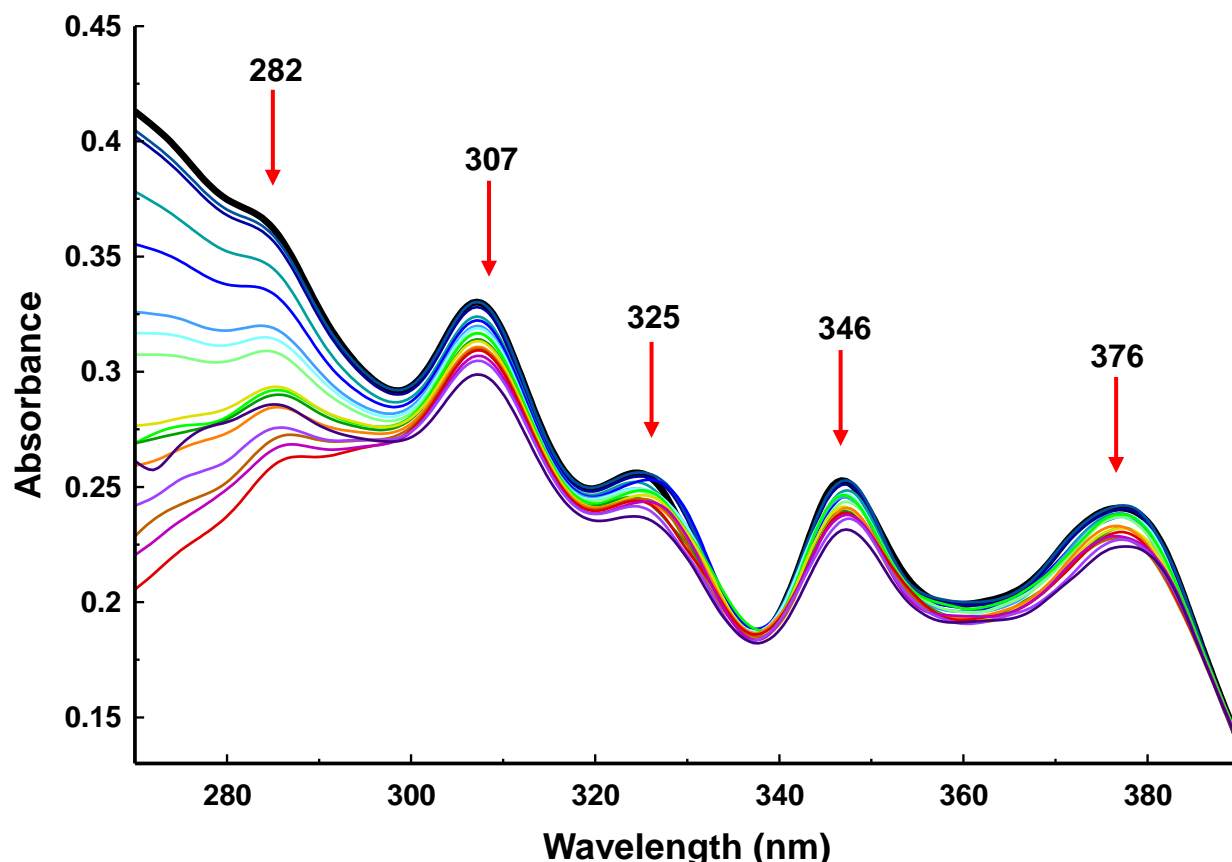


Figure 5.2: The absorption spectra for **PtL2** (where — denotes the starting spectrum) in a phosphate buffer (pH = 7.1) at 298 K with subsequent CT-DNA additions; from 270 to 390 nm. All the spectra have been corrected for dilution.

The absorption spectrum for **PdL2** is shown for the ultraviolet region in Figure 5.3. In this part of the spectrum there are two clearly visible peaks at 289 nm and 306 nm; both show decreasing absorption intensity on addition of the CT-DNA. The spectral variation for the band at 286 nm, however, takes place as a three-step function. First, there is a slight decrease in absorbance, then a slightly bigger increase and finally hypochromism for the last additions of DNA. These absorption bands appear to correspond to intraligand π - π^* transitions, but may also have some charge-transfer character (Pd(II) $d\pi$ - π^* metal-to-ligand, MLCT). Fewer and further blue shifted MLCT bands, in comparison to the platinum complex, are in agreement with other spectral data observed for palladium complexes.^{452,465} Palladium(II) is a weaker electron donor than platinum(II) and thus the MLCT transition should occur at higher energies (shorter wavelengths) when compared to platinum complexes.^{473,474}

Although the exact assignment of this band is uncertain, the spectral perturbation may show an interaction taking place between the metal complex and DNA bases.⁴⁶⁰ As this band at 306 nm is the absorption maximum this characteristic hypochromism may demonstrate intercalation of the complex with DNA;^{452,465,466} however, the lack of isosbestic points may disprove intercalation.

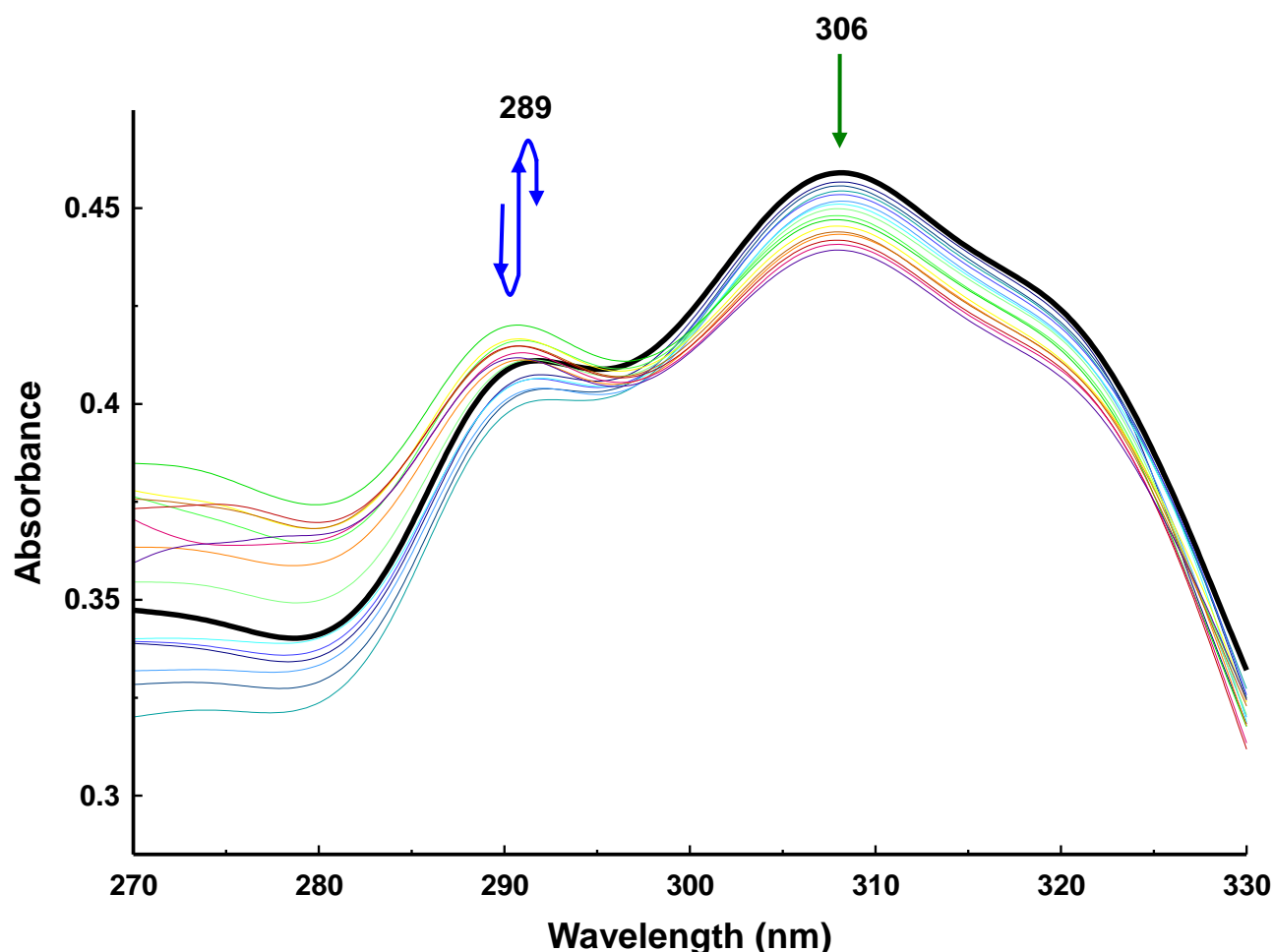


Figure 5.3: Absorption spectra for **PdL2** (where — denotes the starting spectrum) in a phosphate buffer (pH = 7.1) at 298 K with subsequent CT-DNA additions; 270 to 330 nm region. All the spectra have been corrected for dilution.

Slight bathochromic and then hypsochromic effects (red and blue shifts, respectively) are seen for the band at 289 nm. The occurrence of isosbestic points for the duration of the titration of the metal complexes with DNA may assist in proving the existence of only the free and intercalated complex. Furthermore, it also denotes equilibrium between the free and bound metal complex. There are no isosbestic points visible for either **PtL2** or **PdL2**, and this lack of isosbestic points suggests that the chromophore environment was not altered after the interaction, which in turn implies multiple equilibria more consistent with

ion associations than intercalation.⁴⁶⁸ The intensity of the peak at 306 nm decreased by around 6.5% when the concentration of the DNA reached $\sim 3.0 \times 10^{-4}$ M.

The binding constant for the binding taking place between the metal complexes and DNA is determined from the fits for the variation of $(\epsilon_a - \epsilon_f)/(\epsilon_b - \epsilon_f)$ with increasing [DNA]. These plots are shown for **PtL2** and **PdL2** in Figures 5.4 and 5.5, respectively. It was noted that the data obtained for the series of palladium complexes were rather similar to each other, as were the data for the platinum complexes (**Appendix D2**). It was also noted that the non-linear equation fitted the data for the palladium complexes slightly better than for those of the platinum complexes. This may show a difference in their mode of interaction with the DNA dependent on the metal centre.

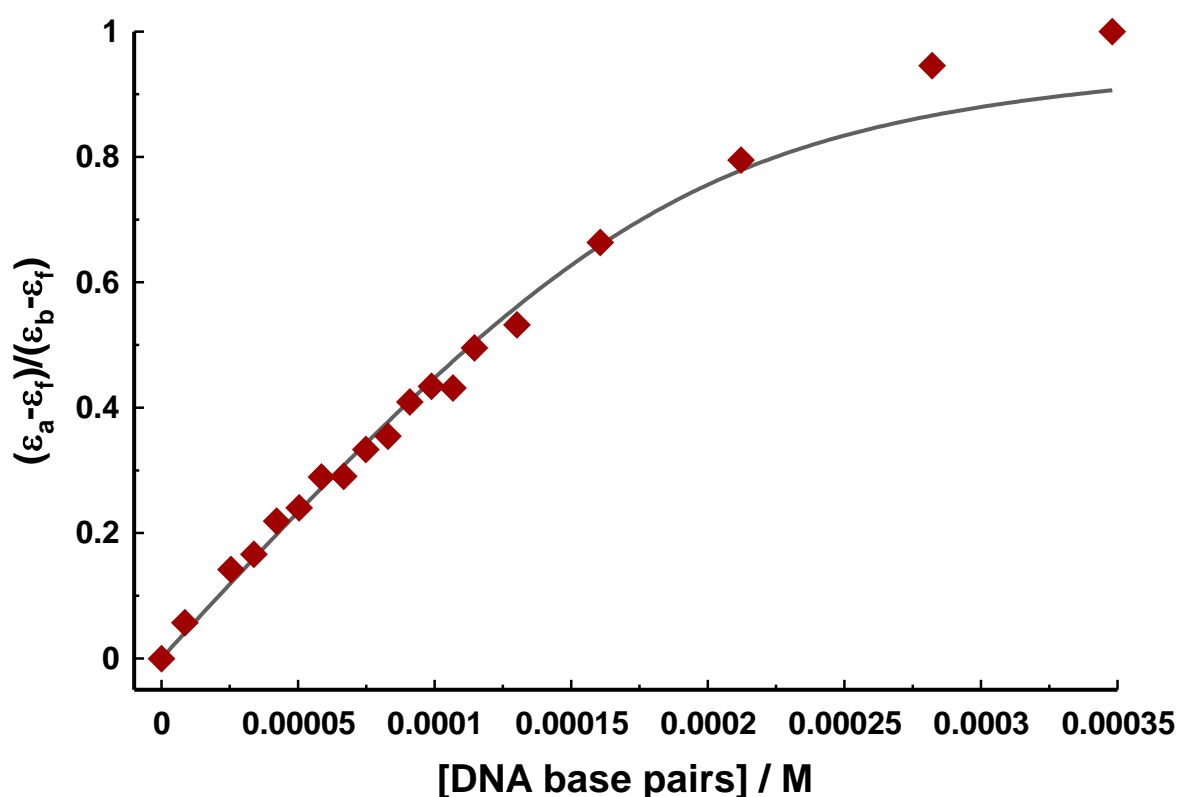


Figure 5.4: The non-linear fit for the plot of $(\epsilon_a - \epsilon_f)/(\epsilon_b - \epsilon_f)$ against [DNA base pairs] for the titration of **PtL2** with CT-DNA.

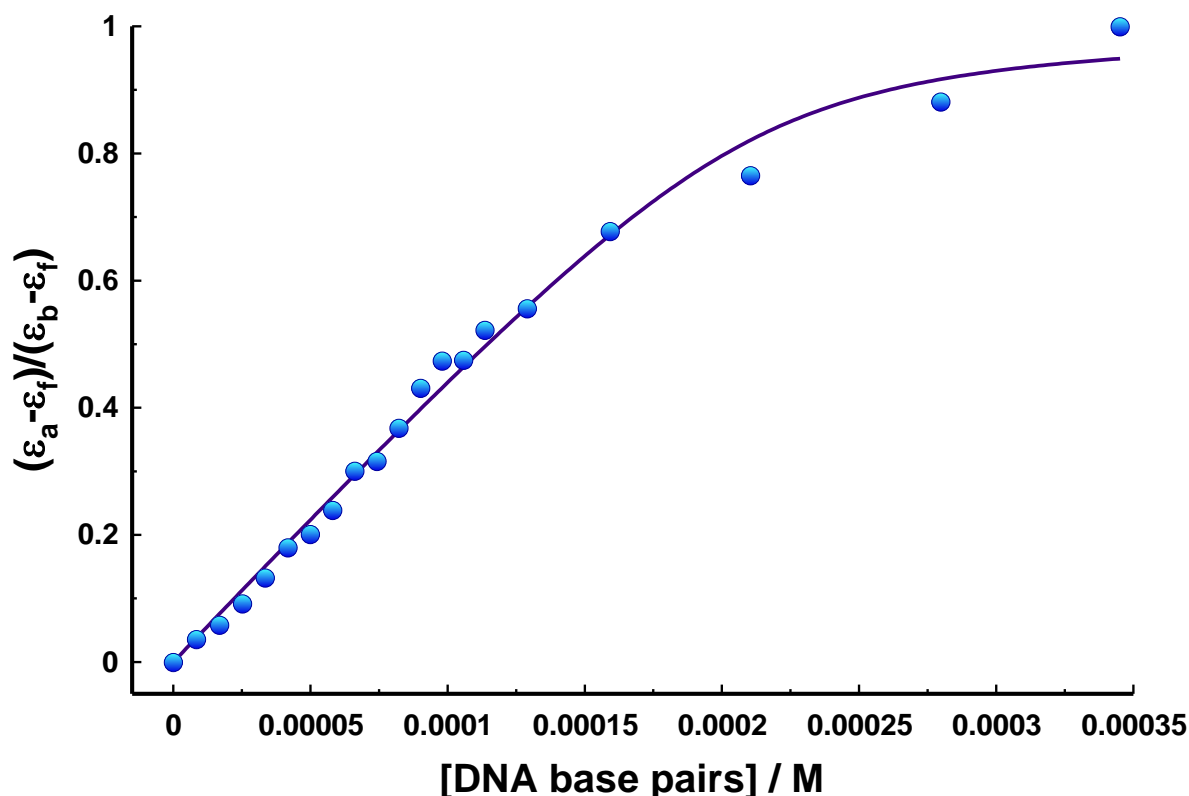


Figure 5.5: The non-linear fit for the plot of $(\epsilon_a - \epsilon_f) / (\epsilon_b - \epsilon_f)$ against [DNA base pairs] for the titration of **PdL2** with CT-DNA.

The binding constants (K_b) for the platinum(II) and palladium(II) complexes in this work towards CT-DNA are of the order of $10^5 \text{ dm}^3 \text{ mol}^{-1}$ as estimated by using UV/vis absorption spectroscopy. Comparatively, these experimentally determined binding abilities are in the average scope of many reported platinum and palladium complexes (as presented in Table 5.1). The results for the binding constants, binding sites and % hypochromicity for each of the metal complexes tested are shown in Table 5.3. The palladium and platinum complexes in this work have a similar DNA binding affinity to known intercalators such as ethidium bromide (EB-DNA, $3.3 \times 10^5 \text{ M}^{-1}$ in 50 mmol L^{-1} Tris-HCl/ 1.0 mol L^{-1} NaCl buffer, pH 7.5).⁴⁷⁵ This may be accredited to the 2+ charge that each metal cation possesses which would favour strong electrostatic binding. This could even be strong enough to compete with an intercalator that has only a single positive charge and therefore explains the comparatively similar values.

Table 5.3: Binding parameters and details for the effect of CT-DNA on the metal complexes.

Complex	K_b ($\text{dm}^3\text{mol}^{-1}$)	s (number of binding sites per DNA base pair)	Wavelength (nm)	% Change in absorption [#]
PtL2	$1.6(5) \times 10^5$	1.30(8)	307	14.1%
PdL2	$4.5(8) \times 10^5$	1.72(6)	306	6.5%
PtL4	$2.1(8) \times 10^5$	0.79(7)	326	7.7%
PdL4	$1.1(6) \times 10^5$	0.47(4)	323	6.3%
PdL4m	$0.9(2) \times 10^5$	1.05(5)	312	4.4%
PdL4b	$2.2(3) \times 10^5$	0.138(3)	315	29.8%

The % change in the absorption at the given wavelength upon binding of the complex with [DNA] = $\sim 3.0 \times 10^{-4}$ M.

Binding constants for N_4 chelates with platinum and palladium could not be found in the literature; however, the binding constants found for N-donor Pt(II) and Pd(II) complexes compare well to the literature values of these complexes with bidentate ligands (see Table 5.1). Many of these complexes have shown an intercalating mode of action with a few acting as groove binders. The spectral changes on addition of CT-DNA are all rather similar for the complexes in this work; except for **PdL4b**.

If the mode of action of the complexes in this work were to be considered as intercalation then there are certain factors to consider. From X-ray data (**Chapter 3**) and DFT computations (**Chapter 4**) it is obvious that these complexes show only minor distortions from being perfectly planar. Thus all the complexes have the correct charge, size and geometry to allow for intercalation. It must, however, be noted that these characteristics are also appropriate for groove-binders. The binding constant of an intercalator is dependent on the planar aromatic surface of the complex to accommodate it between the nucleobases and to allow for stacking.⁴³⁶ As no steric limitations seem to exist for the intercalation of **PtL2**, **PdL2**, **PtL4** and **PdL4**, it seems the whole surface is potentially available for intercalation. The slightly lower binding constant for **PdL4m** may then be attributed to the minimal steric interference by the methyl groups on the imine carbon. The similarity in the data may, however, reflect similar interactions for the metal complexes.

The only predicament with the assignment of a purely intercalated mode of action is the spectral changes observed for the absorbance spectra on addition of CT-DNA. All the complexes have the same skeletal design with isoelectronic metal centres. This explains the analogous results for each complex as it is expected that they will all bind in a similar manner. Similar effects and changes are observed in the UV-Vis spectra for both the Pt(II) and Pd(II) cations of **L2** when CT-DNA is added. Hypochromism and bathochromism are associated with intercalation, therefore the lack of shift in the wavelength and small changes in intensity for the metal complexes in this work are more indicative of weak electrostatic interactions. This would be consistent with non-intercalative binding; either simple electrostatic adduct formation or major/minor groove binding.

Norden *et al.* have described some platinum complexes that seem to initially intercalate but then coordinate to vertically-positioned nitrogens on adjacent bases on one of the DNA strands.⁴⁷⁶ This is unlikely for our complexes as a tetradentate chelate should resist base dissociation for a kinetically inert d^8 metal chelate. In order for the complexes in this work to show either groove binding or electrostatic association we would expect hyperchromism of the spectrum of the drug on the addition of CT-DNA.⁴⁶⁹ However, groove binders may also show slight changes in the spectrum (either increasing or decreasing absorption) depending on the type and strength of the groove binding that is taking place which is dependent on the structure of the drug being tested. Some platinum complexes have however been identified as nonintercalating when hypochromicity and no obvious red shift were observed.⁴⁵⁷ Our complexes show exactly these results which therefore raises the question – if the mode of action for the complexes in this work is not intercalation, then what is causing the spectral changes on addition of DNA? When the ionic atmosphere around the chromophore is changed, even for only weak interactions with DNA, the transition dipoles responsible for the MLCT bands are likely to be affected. Thus if the chromophore is bound electrostatically to the negatively charged DNA poly-anion a loss of intensity is consistent with a weaker oscillation of the electric dipole involved in the transition.

Although these changes are not as intense as expected nor are these variations typical of intercalating drugs, they can most likely not be attributed to covalent interactions.⁴⁷⁵ Small changes are often more likely to reflect groove binding; however, the decrease in the absorption intensity of our group of metal chelates is definitely true, and hence intercalation cannot yet be ruled out. There are also no observed bathochromic shifts;

however, there are some drugs that have been diagnosed as intercalators even without significant bathochromic spectral shift in the UV-Vis spectra.⁴⁷⁷ The absorption for the complexes in this work do show the expected hypochromism for intercalators; but very weakly in comparison to some well known intercalators. The best way to confirm the mode of interaction would therefore be to compare the data to a known intercalator. Ethidium bromide (EB) was chosen for its known intercalative mechanism. The absorption spectra for EB and the changes in these absorptions on addition of CT-DNA are presented in Figure 5.6.

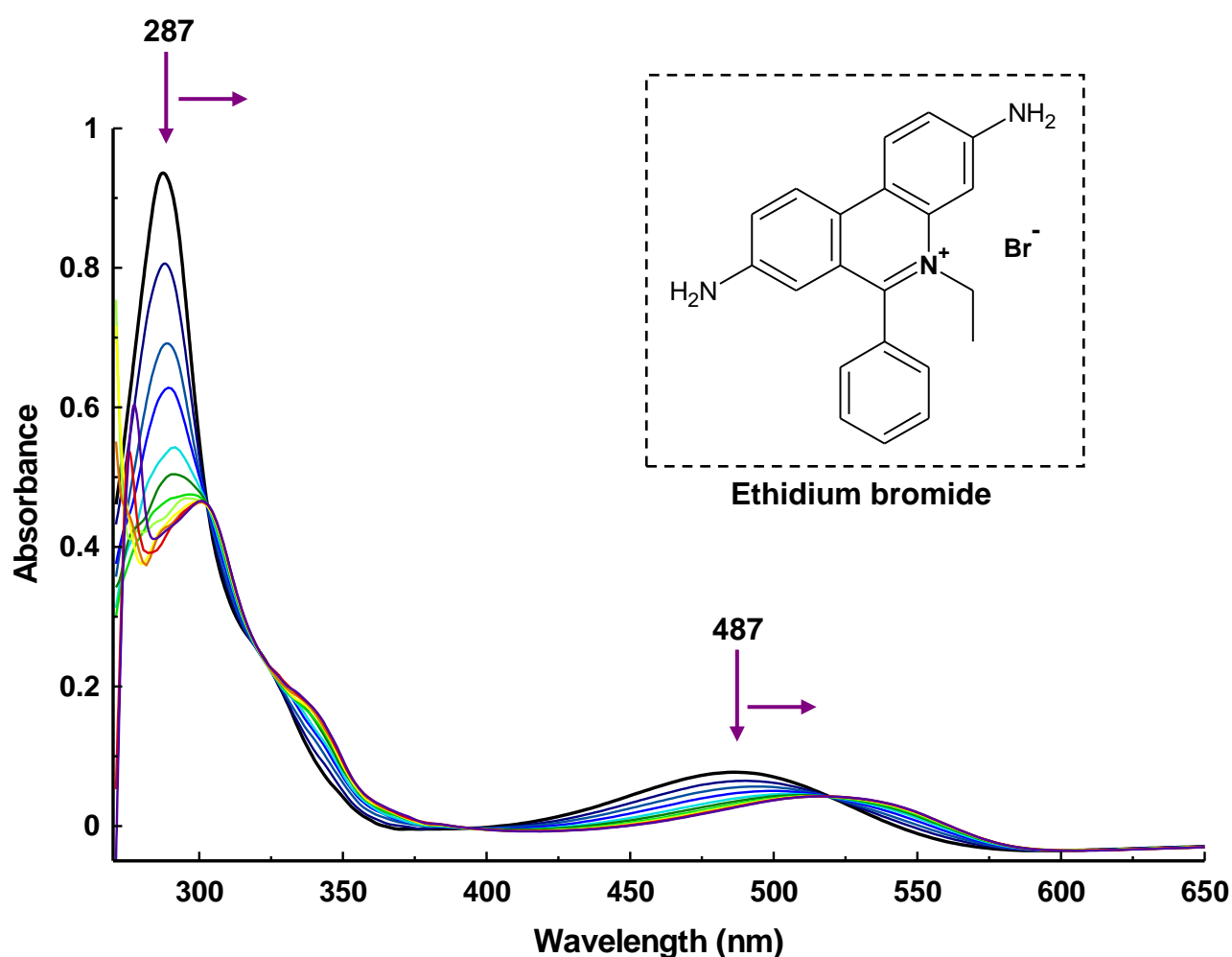


Figure 5.6: Absorption spectra for ethidium bromide (where — denotes the starting spectrum) in a phosphate buffer (pH = 7.1) at 298 K with subsequent CT-DNA additions; 270 to 650 nm region. All the spectra have been corrected for dilution.

The addition of CT-DNA to EB, at pH ~ 7, causes immediate spectral changes characterised by strong hypochromicity and a significant red shift of the absorption maxima. These changes adequately indicate the intercalative binding of EB as does the presence of the isosbestic points at 302, 321, 394 and 519 nm. These points are

consistent and conserved throughout the titration and show the presence of only two absorbing species; free EB and bound EB. The absorption maximum is shifted by 1 nm on the first addition of CT-DNA and finally ends up red shifted by 14 nm, while the band at 487 nm shifts to 522 nm. The intensity is decreased by 13.2% and 16.4% after the first addition of CT-DNA for the bands at 287 and 487 nm, respectively. These absorbance changes are very different to those observed for the metal complexes in this work and it is now possible to exclude intercalation as a possible mode of interaction for these Pt(II) and Pd(II) chelates.

The binding constant for EB acquired from the plot of $(\epsilon_a - \epsilon_f)/(\epsilon_b - \epsilon_f)$ versus [DNA] is 7.1×10^5 (Figure 5.7) and the number of binding sites per DNA base pair is $s = 0.0046(1)$. These values compare well to those in this work; however, there is a considerable difference in the shape of the plots. When comparing the plot for EB with those of **PtL2** and **PdL 2** (Figures 5.4 and 5.5, respectively) it is evident that there is a much “flatter” curve observed for the complexes in this work in comparison to EB. This may also establish the difference in the modes of action and hence substantiate the idea that **PtL2**, **PdL2**, **PtL4**, **PdL4** and **PdL4m** do not behave as DNA intercalators.

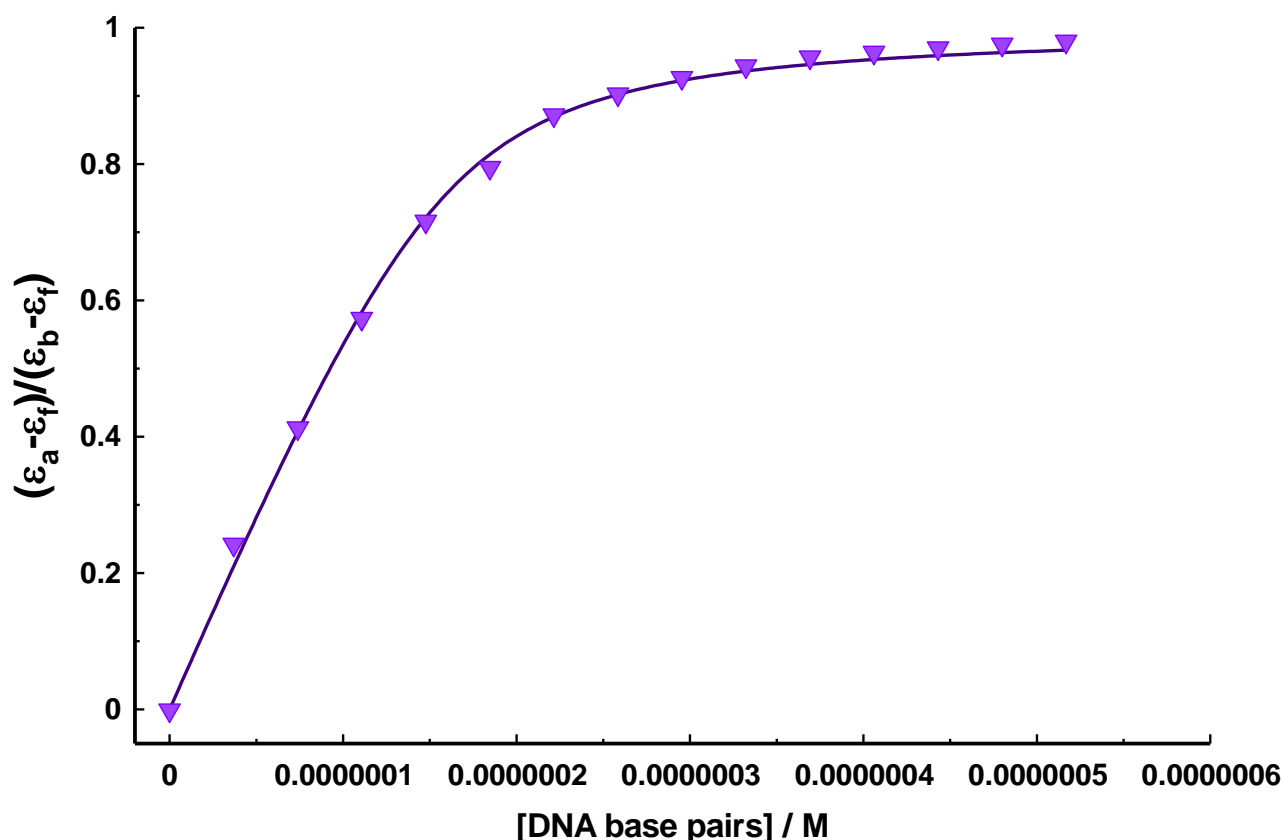


Figure 5.7: The non-linear fit for ethidium bromide for the titration with CT-DNA.

The data for **PdL4b** (Figure 5.8) are quite different from that observed for the other complexes, despite having a similar binding constant. The absorption spectra show hyperchromism (band at 277 nm) and hypochromism (band at 213 nm) as well as isosbestic points at 248 and 289 nm. There are also shifts observed for the two main bands; the band at 213 nm shows a bathochromic shift to 220 nm and the band at 277 is blue shifted by 3 nm. Hyperchromism and hypochromism are spectral features concerning the double-helix structure of DNA and are indicative of the interaction occurring between the metal complex and DNA. Enhanced absorption intensity can be caused by a distortion in the coordination sphere due to electrostatic binding on the DNA surface.⁴⁷⁸

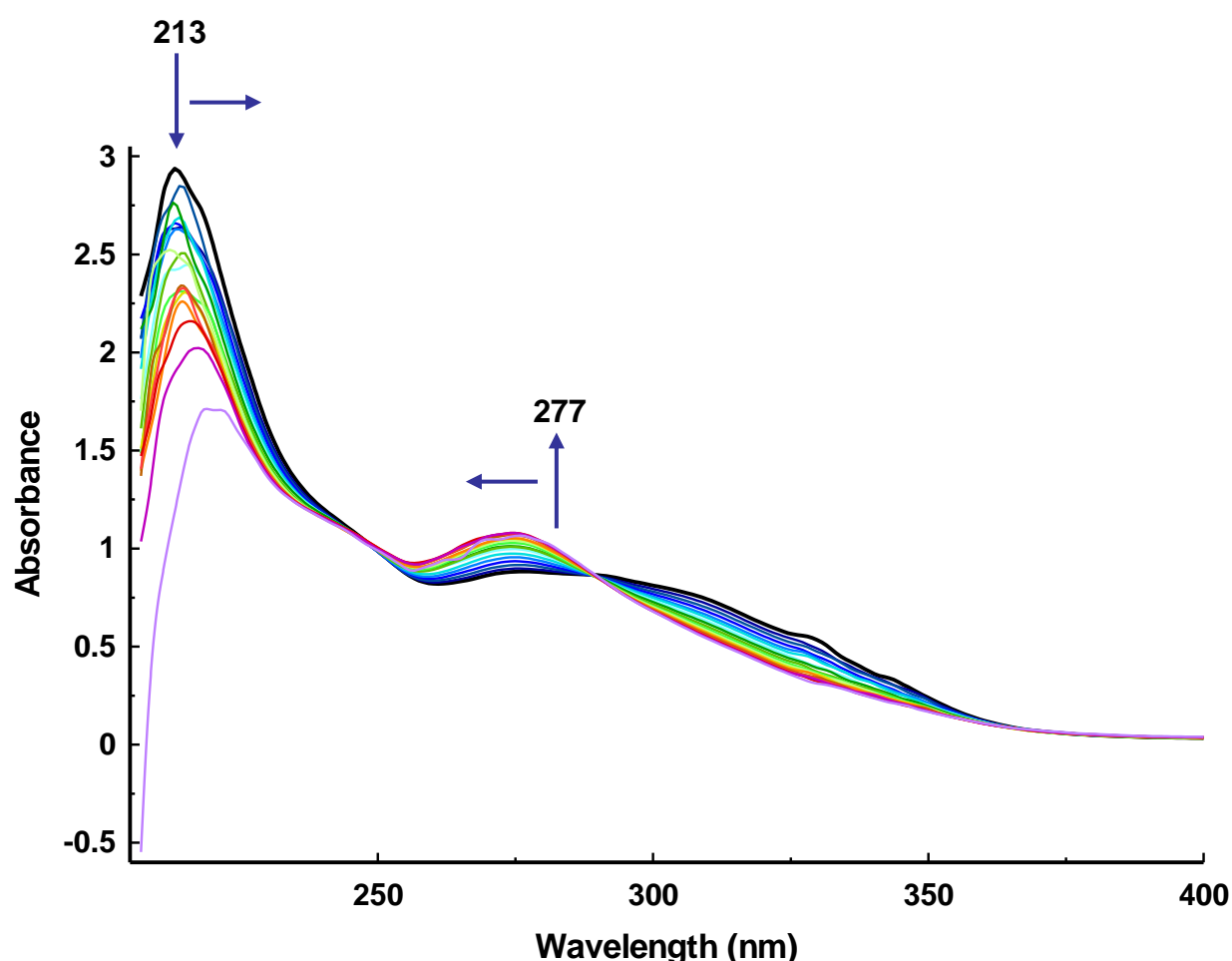


Figure 5.8: Absorption spectra for **PdL4b** (where — denotes the starting spectrum) in a phosphate buffer (pH = 7.1) at 298 K with subsequent CT-DNA additions; 205 to 400 nm region. All the spectra have been corrected for dilution.

It has therefore been suggested that enhancement in absorption intensity and hyperchromism in absorption spectra may be due to a mixed mode of intercalation and surface binding.⁴⁷⁹ Pure intercalation is unlikely for this metal complex due to the large steric bulk; however, if a planar ring was to insert into the helix then the other rings would

extend away from the plane due to stereochemical constraints on binding. Subsequently, some of the planar aromatic rings may be available for electrostatic binding. It is expected that this complex will interact with DNA in a similar manner to the other complexes in this work, therefore, the observed spectral changes for **PdL4b** may be rationalised in terms of electrostatic binding *and* partial intercalation.

More evidence of a non-intercalative mode is obtained from the decatenation assay by Topo II (Topoisomerase II) for **PdL2** (Figure 5.9). The control used, VP-16 (etoposide), is a Topo II poison and blocks re-ligation of cleaved double-stranded DNA. Linear DNA is thus detected on the gel. A catalytic inhibitor of Topo II should bind DNA if it does not target the ATPase domain of the enzyme. Non-specific inhibition is normal for most salts at a high enough concentration as seen in the gel. **PdL2** was not a Topoisomerase II poison and is also not a catalytic inhibitor of the enzyme.

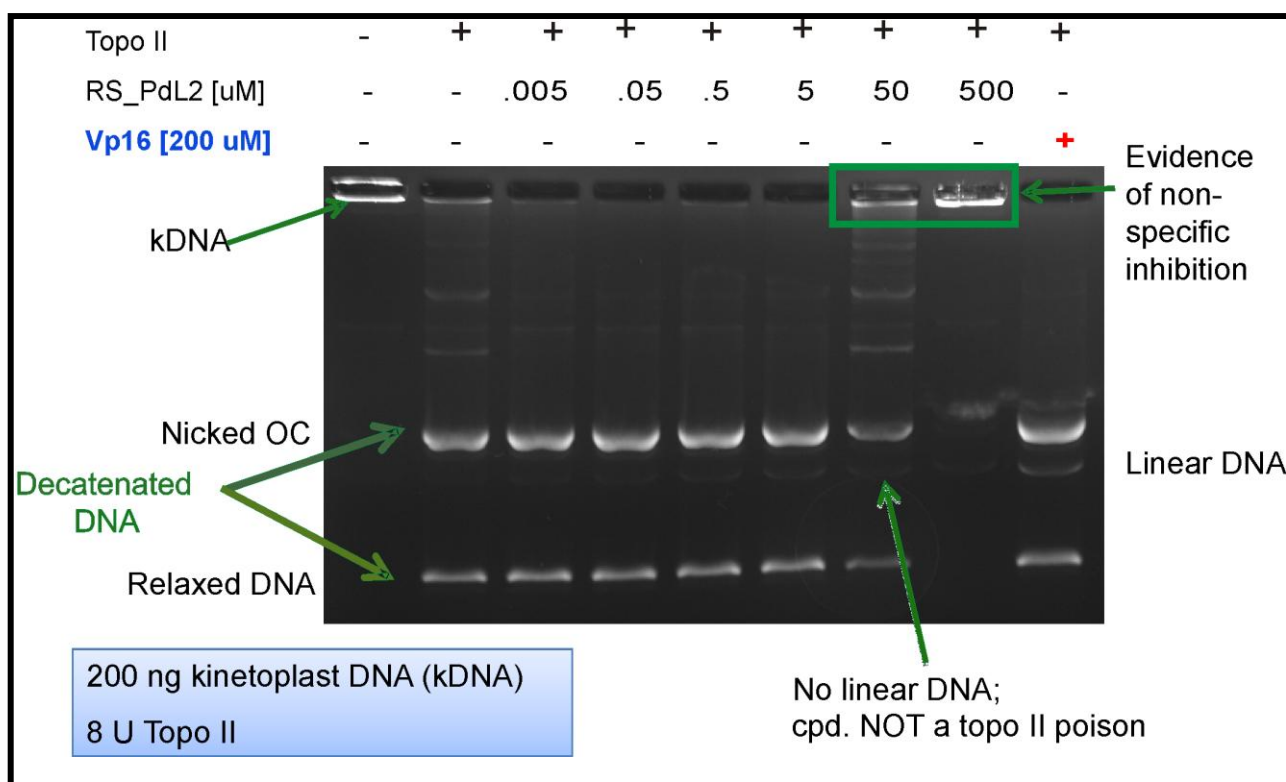


Figure 5.9: Decatenation assay by Topo II employing kinetoplast DNA as the substrate and different concentrations of **PdL2**.

If these complexes are not intercalators then it accounts for their lack of cytotoxicity. A complex cation that binds electrostatically to the outside of the sugar-phosphate backbone would only show a weak spectral change as it enters the ion cloud of the DNA duplex. It would not disrupt DNA topoisomerases and is thus likely not to be cytotoxic

(assuming efflux pumps are inoperative). This lends support to the idea that our complexes may, in fact, not be DNA intercalators despite showing high binding constants to DNA. It is more likely that there is electrostatic non-intercalative binding to DNA.

CHAPTER 6 – Conclusion

The primary objective of this work was to synthesise and characterise a range of tetradentate bis(pyridyl-imine) ligands for the chelation of selected Platinum Group Metals (PGMs) and to explore the chemotherapeutic potential of the metal complexes which, by design, have the potential to bind to DNA. A total of eight metal complexes (tetradentate bis(pyridyl-imine) chelates of Pd(II) or Pt(II)) have been characterised by X-ray diffraction, as well as four metal-free tetradentate bis(pyridyl-imine) ligands and five cyclised hexahydropyrimidine- or imidazole-containing bidentate ligands. A further eleven metal-free ligands and five metal complexes have been synthesised and characterised making a total of fifteen ligands (three novel) and thirteen metal complexes (all novel) that are presented and established in this work.

Due to their configurations the X-ray structures obtained for the free ligands generally did not possess inversion symmetry, except for **L1**. This resulted in all four nitrogen atoms being unique for these structures. No π - π stacking for the pyridine rings was observed in the ligand structures, except for the cyclised structure of **L2h**. Short intermolecular contacts have been examined between neighbouring Schiff base units for all the free ligands; however, no hydrogen bonding has been observed.

All metal chelates had the expected nominal square planar coordination geometry for Pd(II) and Pt(II) and approximate or exact C_2 molecular symmetry. Distortions were observed for the metal complexes from the N_4 plane formed by the two imine (N_i) and two pyridine (N_p) nitrogen atoms around the metal centre. These distortions were mostly observed for the pyridine rings and the bridging groups of the metal chelates. Pt(II) complexes with propyl bridging groups exhibited the most significant nonplanar conformations. The length of the bridging group was observed to have an effect on the bite angle of the chelate as well as the mean M- N_i distance, while the N_p -M- N_p and N_i -M- N_i angles had opposite and linearly correlated “motion”. It was discovered that structural changes in the metal ion coordination geometry and central chelate ring were also accompanied by structural perturbations of the two imine groups of the complex. The relationship between the mean C=N distance of the complex and the mean M- N_i bond length was found to be nonlinear. The metal-nitrogen bonds observed for the metal

complexes were all consistent with the normal ranges for Pt-N and Pd-N bonds reported in the literature.

Short intermolecular nonbonded contacts were observed for the metal complexes **PtL1**, **PdL1** and **PtL2**; these occurred primarily between the PGM cations and the adjacent layers of PF_6^- ions in the crystal lattice. The observed F...H intermolecular contacts allow for the formation of relatively stable crystal lattices. **PtL4** also shows no π - π stacking; however, the structure of **PdL4** is loosely stabilised by π - π interactions between pyridine rings of adjacent molecules along the stack. This is also true for **PdL4m**, which has π - π stacking; however, similar interactions were not observed for **PdL4b**.

DFT geometry optimisations at the B3LYP/6-31G** level of theory were performed for all eighteen ligands and at the B3LYP/SDD level of theory for the thirty-six metal complexes. More specifically, the simulations (a) delineated key differences between gas-phase and solid state (X-ray) structures, (b) probed the effect of the structural variations of the bridging and imine substituent groups and (c) offered insights as to the preferred conformational isomers as well as their electronic structures (including FMO symmetries).

Structures were determined for the lowest energy in the gas phase during DFT computations which differed from the solid-phase structures. The main difference for the structures of the free ligands was the position of the pyridyl-imine "arms" as there was good correlation for the bridging groups. No intermolecular interactions nor forces experienced by the molecules due to crystal packing deviations were taken into account by the DFT computations; this may explain the deviations of the peripheral groups from the predicted idealised geometries by DFT. Thus structures computed at this level of theory (B3LYP 631G**), putative and synthesised, were likely to be of acceptable accuracy, particularly for similar structures.

The structures of the metal complexes determined by X-ray diffraction included lattice-induced molecular distortions; however, the computations were for the free structure (gas phase) with no counter ions, absent of possible packing effects. As the counter ions (PF_6^-) were not taken into account in the DFT computations the prominent short interactions involving them in the crystallographically observed structures did not play a role in the computed structures. The most noticeable differences between the X-ray

structures and the DFT-calculated structures were for the bridges of the chelating ligand structure. Bond distances were mostly calculated to be slightly larger than those observed for the X-ray structures. Generally, there seems to be slightly better agreement between the calculated and observed bond distances of C_i-C_p and N_i-C_f for the palladium complexes in comparison to the platinum complexes. The DFT-computed structures also predicted an increase in N_i-M-N_i angle and the length of the $M-N_i$ bond as the length of the bridging group increased. The calculated geometries for the metal complexes were therefore of acceptable accuracy at this level of theory.

The four frontier molecular orbitals for all the metal complexes were calculated using DFT. Metal complexes of the original (H-atom appended to the imine carbon atom) and methyl-substituted ligands (methyl group appended to the imine carbon atom) were found to have very similar molecular orbitals. The HOMO and HOMO-1 orbitals of the phenyl-substituted ligands (phenyl group appended to the imine carbon atom) were very different and based predominantly on the phenyl substituents with little or no contribution from the rest of the structure. The DFT-calculations predicted a significant increase in the HOMO–LUMO gap for the Pd(II) chelates relative to the Pt(II) chelates, consistent with the softer character of the latter metal ion.

The DFT-computed frequencies were calculated to be higher than the experimental values for the ligands with H-atom substituents on their imine units; however, lower for the ligands with substituted groups on the imine carbon atoms (methyl-substituted and phenyl-substituted ligands). The DFT-computed values for the $C=N$ modes showed the expected frequency decrease from the free ligands to the metal complexes observed for the experimental data. The frequency of the lowest-energy vibrations were computed for each ligand and metal complex. The distortional mode characteristic of these vibrations was related to the energy; larger frequencies were generally observed for a twisting distortion mode rather than a saddle-like distortion mode of the metal chelate.

Finally, the resulting metal complexes were evaluated for their cytotoxicity against a range of cancer cell lines. None of the tested complexes showed inhibition of growth of the selected cancer cell lines. Association constants for the binding of the metal complexes to calf thymus DNA (CT-DNA) were determined spectroscopically. The Pt(II) and Pd(II) complexes tested in this work have not shown spectral evidence that they bind by intercalation to DNA; the data were consistent with the proposal that the complexes

interact electrostatically with DNA and may possibly be groove-binders. Additional research, for example molecular simulations, to obtain the exact binding mode of these complexes is necessary. Selective interaction may occur with particular DNA sequences and therefore a better understanding of the binding mode is necessary. Proposed methods to further elucidate the mode of action may include viscosity measurements, circular dichroism (CD) spectral studies or even thermal denaturation; which are currently not within the scope of this work.

References

1. SAinfo reporter: www.southafrica.info "Mining and minerals in South Africa" Article last updated May 2008.
2. AllAfrica Global Media, Business Day: <http://allafrica.com/stories/201001080090.html> "South Africa: Palladium, Platinum On Road to Recovery" Article January 2010 from AllAfrica Global Media (allafrica.com).
3. Schiff, H. *Ann. Suppl.* 1864, 3, 343–70.
4. Tidwell, T. T. *An. Chem. Int. Ed.* 2008, 47, 1016–20.
5. Holm, R. H.; Everett Jr., G. W.; Chakravorty, A. *Prog. Inorg. Chem.* 1966, 7, 83–214.
6. Chattopadhyay, B.; Basu, S.; Chakraborty, P.; Choudhuri, S. K.; Mukherjee, A. K.; Mukherjee, M. J. *Molec. Struct.* 2009, 932, 90–6.
7. Holanda, M. I. D.; Krumholz, P.; Chum, H. L. *Inorg. Chem.* 1976, 15, 890–3.
8. Toda, F.; Imai, M. *J. Chem. Soc. Perkin Trans. 1* 1994, 19, 2673–4.
9. Lydon, D. P.; Cave, G. W. V.; Rourke, J. P. J. *Mater. Chem.* 1997, 7, 403–6.
10. Cave, G. W. V.; Lydon, D. P.; Rourke, J. P. J. *Organomet. Chem.* 1998, 555, 81–8.
11. Saccomando, D. J.; Black, C.; Cave, G. W. V.; Lydon, D. P.; Rourke, J. P. J. *Organomet. Chem.* 2000, 601, 305–10.
12. Schmeyers, J.; Toda, F.; Boy, J.; Kaupp, G. J. *J. Chem. Soc. Perkin Trans. 2* 1998, 4, 989–93.
13. Correa, W. H.; Papadopoulos, S.; Radnidge, P.; Roberts, B. A.; Scott, J. L. *Green Chem.* 2002, 4, 245–51.
14. van den Ancker, T. R.; Cave, G. W. V.; Raston, C. L. *Green Chem.* 2006, 8, 50–3.
15. Serbest, K.; Özen, A.; Ünver, Y.; Er, M.; Değirmencioğlu, I.; Sancak, K. J. *Molec. Struct.* 2009, 922, 1–10.
16. Chatterjee, D.; Basak, S.; Riahi, A.; Muzart, J. J. *Mol. Catal. A Chem.* 2006, 255, 283–9.
17. Chatterjee, D.; Basak, S.; Mitra, A.; Sengupta, A.; Le Bras, J.; Muzart, J. *Inorg. Chim. Acta.* 2006, 359, 1325–8.
18. Drozdak, R.; Allaert, B.; Ledoux, N.; Dragutan, I.; Dragutan, V.; Verpoort, F. *Coord. Chem. Rev.* 2005, 249, 3055–74.
19. Holland, D.; Laidler, D. A.; Milner, D. J. *J. Mol. Catal.* 1981, 11, 119–27.
20. M. Diéguez, M.; Pàmies, O.; Ruis, A.; Díaz, Y.; Castellón, S.; Claver, C. *Coord. Chem. Rev.* 2004, 248, 2165–92.
21. Borriello, C.; Del Litto, R.; Panunzi, A.; Ruffo, F. *Tetrahedron: Asymmet.* 2004, 15, 681–6.
22. Sessler, J. L.; Melfi, P. J.; Pantos, G. D. *Coord. Chem. Rev.* 2006, 250, 816–43.
23. Koola, J.; Kochi, J. K. *Inorg. Chem.* 1987, 26, 908–16.

24. Querci, C.; Strologo, S.; Ricci, M. *Tetrahedron Lett.* 1990, 31, 6577–80.
25. Chellamani, A.; Alhaji, N. M. I.; Rajagopal, S. J. *Chem. Soc. Perkin Trans. 2* 1997, 2, 299–302.
26. Bernardo, K.; Seppard, S.; Robert, A.; Commenges, G.; Daha, F.; Meunier, B. *Inorg. Chem.* 1996, 35, 387–96.
27. Fukata, T.; Katsuki, T. *Synlett* 1995, 825–9.
28. Kim, S. K.; Jacobsen, E. N. *Angew. Chem., Int. Ed.* 2004, 43, 3952–4.
29. Schans, S. E.; Branalt, J.; Jacobsen, E. N. *J. Org. Chem.* 1998, 63, 403–7.
30. Cozzi, P. G. *Chem. Soc. Rev.* 2004, 33, 410–21.
31. Kaya, I. Vilayetoglu, A. R.; Mart, H. *Polymer* 2001, 42, 4859–65.
32. Esteban-Gómez, D.; Ferreirós, R.; Fernández-Martínez, S.; Avecilla, F.; Platas-Iglesias, C.; de Blas, A.; Rodríguez-Blas, T. *Inorg. Chem.* 2005, 44, 5428–36.
33. Esteban-Gómez, D.; Platas-Iglesias, C.; Avecilla, F.; de Blas, A.; Rodríguez-Blas, T. *Eur. J. Inorg. Chem.* 2007, 12, 1635–43.
34. Li C.; Zhang, W.; Gao, G.; Xie, Y. *Wuli Huaxue Xuebao* 1994, 10(3), 230–4.
35. Evans, O. R.; Lin, W. *Acc. Chem. Res.* 2002, 35, 511–22.
36. Herchel, R.; Boča, R.; Gembický, M.; Falk, K.; Fuess, H.; Haase, W.; Svoboda, I. *Inorg. Chem.* 2007, 46, 1544–6.
37. Maldhure, K. A.; Aswar, S. A. *World J. Chem.* 2009, 4, 207–9.
38. Feringa, B. L.; Jager, W. F.; de Lange, B. *Tetrahedron* 1993, 49, 8267–310.
39. Trivedi, R. Sen, P.; Dutta, P. K.; Sen, P. K. *Nonlinear Optics* 2002, 29, 51–9.
40. Karakas, A.; Elmali, A.; Ünver, H.; Svoboda, I. *J. Mol. Struct.* 2004, 702, 103–10.
41. Rahaman, S. H.; Ghosh, R.; Mostafa, G.; Ghosh, B. K. *Inorg. Chem. Comm.* 2005, 8, 1137–40.
42. Baar, C. R.; Jennings, M. C.; Puddephatt, R. J. *Organometallics* 1999, 18, 4373–9.
43. Toyota, E.; Ng, K. K. S.; Sekisaki, H.; Itoh, K.; Tanisawa, K.; James, M. N. G. *J. Mol. Biol.* 2001, 305, 471–9.
44. Lien, E.J. *Prog. Drug Res.* 1993, 40, 163–89.
45. Shelley, M. D.; Hartley, L.; Paul, P. W.; Fish, R. G. *Anticancer Drug* 2000, 11, 209–16.
46. Baumgrass, R.; Weivad, M.; Erdmann, F. J. *Biol. Chem.* 2001, 276, 47914–21.
47. Ying, F.; Yi, L.; Changli, X.; Songsheg, Q.; Zhifeng, L.; Haoyu, S.; Maosheng, D.; Xiangcai, Z. *Thermochim. Acta* 1996, 285, 181–9.
48. Brown, L. S.; Gat, Y.; Sheves, M.; Yamazaki, Y.; Maeda, A.; Needleman, R.; Lanyi, J. K. *Biochemistry* 1994, 33, 12001–11.
49. Ul-Hassan, M.; Scozzafava, A.; Chohan, Z. H.; Supuran, C. T. *J. Enzyme Inhib.* 2001, 16, 499–505.

50. Ahmed, Z.; Ravandi, A.; Maguire, G. F.; Kuksis, A.; Connelly, P. W. *Cardiovasc. Res.* 2003, 58, 712–20.
51. Toyota, E.; Sekisaki, H.; Takahashi, Y.; Itoh, K.; Tanisawa, K. *Chem. Pharm. Bull.* 2005, 53, 22–6.
52. Mure, M.; Brown, D. E.; Saysell, C.; Rogers, M. S.; Wilmot, C. M.; Kurtis, C. R.; McPherson, M. J.; Phillips, S. E. V.; Knowles, P. F.; Dooley, D. M. *Biochemistry* 2005, 44, 1568–82.
53. Puccetti, L.; Fasoils, G.; Vullo, D.; Chohan, Z. H.; Scozzafava, A.; Supuran, C. T. *Bioorg. Med. Chem. Lett.* 2005, 15, 3096–101.
54. Bieschke, J.; Zhang, Q.; Powers, E. T.; Lerner, R. A.; Kelly, J. W. *Biochemistry*, 2005, 44, 4977–3.
55. Fishkin, N. E.; Sparrow, J. R.; Allikmets, R.; Nakanishi, K. *Proc. Natl. Acad. Sci. USA* 2005, 102, 7091–6.
56. Majumder, S.; Dutta, P.; Mukherjee, P.; Datta, E. R.; Efferth, T.; Bhattacharya, S.; Choudhuri, S. K. *Can. Lett.* 2006, 244, 16–23.
57. Mookerjee, A.; Mookerjee Basu, J.; Dutta, P.; Majumder, S.; Bhattacharyya, S.; Biswas, J.; Pal, S.; Mukherjee, P.; Raha, S.; Baral, R. N.; Das, T.; Efferth, T. Sa, G.; Roy, S.; Choudhuri, S. K. *Clin. Can. Res.* 2006, 12, 4339–49.
58. Pignatello, R.; Panico, A.; Mazzone, P.; Piniszotto, M. R.; Garozzo, A.; Furneri, P. M. *Eur. J. Med. Chem.* 1994, 29, 781–5.
59. Ravoof, T. B. S. A.; Crouse, K. A.; Tahir, M. I. M.; Cowley, A. R.; Ali, M. A. *Polyhedron* 2007, 26, 1159–65.
60. Shanker, K.; Rohini, R.; Ravinder, V.; Reddy, P. M.; Ho, Y.-P. *Spectrochim. Acta Part A* 2009, 73, 205–21.
61. Ali, M. A.; Mirza, A. H.; Butcher, R. J.; Tarafder, M. T. H.; Ali, M. A. *Inorg. Chim. Acta* 2001, 320, 1–6.
62. Ali, M. A.; Mirza, A. H.; Butcher, R. J.; Tarafder, M. T. H.; Keat, T. B.; Ali, A. M. *J. Inorg. Biochem.* 2002, 92, 141–8.
63. Ambike, V.; Adsule, S.; Ahmed, F.; Wang, Z.; Afrasiabi, Z.; Sinn, E.; Sarkar, F.; Padhye, S. J. *Inorg. Biochem.* 2007, 101, 1517–24.
64. Barve, V.; Ahmed, F.; Adsule, S.; Banerjee, S.; Kulkarni, S.; Katiyar, P.; Anson, C. E.; Powell, A. K.; Padhye, S.; Sarkar, F. H. *J. Med. Chem.* 2006, 49, 3800–8.
65. González, A.; Gómez, E.; Cortés-Lozada, A.; Hernández, S.; Ramírez-Apan, T.; Nieto-Camacho, A. *Chem. Pharm. Bull.* 2009, 57(1), 5–15.
66. da Silveira, V. C.; Luz, J. S.; Oliveira, C. C.; Graziani, I.; Ciriolo, M. R.; da Costa Ferreira, A. M. *J. Inorg. Biochem.* 2008, 102, 1090–103.
67. Sathisha, M. P.; Revankar, V. K.; Pai, K. S. R. *Met. Based Drugs* 2008, 362105.

68. Boualam, M.; Biesemans, M.; Meunier-Piret, J.; Willem, R.; Gielen, M. *Appl. Organomet. Chem.* 1992, 6, 197–205.
69. Danish, M.; Alt, H. G.; Badshah, A.; Ali, S.; Mazhar, M.; Islam, N. J. *Organomet. Chem.* 1995, 486, 51–6.
70. Gielen, M.; Dalil, H.; Biesemans, M.; Mahieu, B.; de Vos, D.; Willem, R. *Appl. Organomet. Chem.* 1999, 13, 515–20.
71. Gielen, M. *J. Braz. Chem. Soc.* 2003, 14, 870–7.
72. Razakantoanina, V.; Phung, N. K. P.; Jaureguiberry, G. *Parasitol. Res.* 2000, 86, 665–8.
73. Li, Q. X.; Tang, H. A.; Li, Y. Z.; Wang, M.; Wang, L. F.; Xia, C. G. *J. Inorg. Biochem.* 2000, 78, 167–74.
74. Bayly, S. R.; Fisher, C. L.; Storr, T.; Adam, M. J. *Ch. Orvig, Bioconjugate Chem.* 2004, 15, 923–6.
75. Hansen, P. E.; Filarowski, A.; *J. Molec. Struct.* 2004, 707, 69–75.
76. Dziembowska, T. *Pol. J. Chem.* 1998, 72, 151–484.
77. Sobczyk, L.; *Khim. Phys.* 2005, 24, 31–8.
78. Sobczyk, L.; Grabowski, S.J.; Krygowski, T.M. *Chem. Rev.* 2005, 105, 3513–60.
79. Hall, D.; Rae, A. D.; Waters, T. N. *J. Chem. Soc.* 1963, 5897–901.
80. Cariati, F.; Morazzoni, F.; Busetto, C.; Del Piero, G.; Zazzetta, A. *J. Chem. Soc., Dalton Trans.* 1976, 4, 342–7.
81. Lin, Ch.-Ch.; Liu, Sh.-X.; Shi, S.; You, X.; Wang, X.; Zeng, S. *Jiegou Huaxue (Chinese J. Struct. Chem.)* 1990, 9, 133–6.
82. Girichev, G. V.; Giricheva, N. I.; Kuzmina, N. P.; Medvedeva, Y. S.; Rogachev, A. Y. *J. Struct. Chem.* 2008, 49, 837–49.
83. Rigamonti, L.; Demartin, F.; Forni, A.; Righetto, S.; Pasini, A. *Inorg. Chem.* 2006, 45, 10976–89.
84. Henson, N. J.; Hay, P. J.; Redondo, A. *Inorg. Chem.* 1999, 38, 1618–26.
85. Combes, A. C. *R. Acad. Fr.* 1889, 108, 1252.
86. Zhang, W.; Leoback, J. L.; Jacobsen, E. N. *J. Am. Chem. Soc.* 1990, 112, 2801–3.
87. Irie, R.; Noda, K.; Ito, Y.; Katsuki, T.; *Tet. Lett.* 1990, 31, 7345–8.
88. Emregul, K. C.; Duzgun, E.; Atakol, O. *Corros. Sci.* 2006, 48, 3243–60.
89. Behpour, M.; Ghoreishi, S. M.; Soltani, N.; Salavati-Niasari, M.; Hamadani, M.; Gandomi, A. *Corros. Sci.* 2008, 50, 2172–81.
90. Chatziefthimiou, S. D.; Lazarou, Y. G.; Hadjoudis, E.; Dziembowska, T.; Mavridis, I. M. *J. Phys. Chem. B* 2006, 110, 23701–9.
91. Filarowski, A.; Głowiaka, T.; Koll, A. *J. Molec. Struct.* 1999, 484, 75–89.
92. Hadjoudis, E. *Mol. Eng.* 1995, 5, 301–37.

93. Hadjoudis, E.; Mavridis, I. M. *Chem. Soc. Rev.* 2004, 33, 579–88.
94. Moustakali-Mavridis, L.; Hadjoudis, E.; Mavridis, A. *Acta Crystallogr. B* 1978, 34, 3709–15.
95. Kabak, M.; Elmali, A.; Elerman, Y.; Durlu, T. N. *J. Mol. Struct.* 2000, 553, 187–92.
96. Fernández-G, J. M.; del Rio-Portilla, F.; Quiroz-García, B.; Toscano, R. A.; Salcedo, R. J. *Mol. Struct.* 2001, 561, 197–207.
97. Hadjoudis, E.; Vittorakis, M.; Moustakali-Mavridis, L. *Tetrahedron* 1987, 43, 1345–60.
98. Sato, K.; Chikira, M.; Fujii, Y.; Komatsu, A. *J. Chem. Soc. Chem. Commun.* 1994, 5, 625–6.
99. Shrivastava, H. Y.; Devaraj, S. N.; Nair, B. U. *J. Inorg. Biochem.* 2004, 98, 387–92.
100. Scheringer, C.; Hinkler, K.; van Stackelberg, M. Z. *Anorg. Chem.* 1960, 306, 35–8.
101. Gerloch, M.; Mabbs, F. E. *J. Chem. Soc. A* 1967, 10, 1598–608.
102. Gerloch, M.; Mabbs, F. E. *J. Chem. Soc. A* 1967, 11, 1900–8.
103. Bancroft, G. M.; Maddock, A. G.; Randl, R. P. *J. Chem. Soc. A* 1968, 12, 2939–44.
104. Gerloch, M.; Lewis, J.; Mabbs, F. E.; Richards, A. J. *J. Chem. Soc. A* 1968, 1, 112–6.
105. Gullotti, M.; Casella, L.; Pasini, A.; Ugo, R. *J. Chem. Soc. Dalton Trans.* 1977, 4, 339–45.
106. Lloret, F.; Moratal, J.; Faus, J. J. *J. Chem. Soc. Dalton Trans.* 1983, 8, 1743–8.
107. Böttcher, A.; Grinstaff, M. W.; Labinger, J. A.; Gray, H. B. *J. Mol. Catal. A: Chem.* 1996, 113, 191–200.
108. Liou, Y. W.; Wang, C. M. *J. Electroanal. Chem.* 2000, 481, 102–9.
109. Silvestri, A.; Barone, G.; Ruisi, G.; Giudice, M. T. L.; Tumminello, S. J. *Inorg. Biochem.* 2004, 98, 589–94.
110. Germain, M. E.; Vargo, T. R.; Khalifah, P. G.; Knapp, M. J. *Inorg. Chem.* 2007, 46, 4422–9.
111. Cano, M.; Rodríguez, L.; Lima, J. C.; Pina, F.; Cort, A. D.; Pasquini, Ch.; Schiffanio, L. *Inorg. Chem.* 2009, 48, 6229–35.
112. Vladimirova, K. G.; Freidzon, A. Y.; Kotova, O. V.; Vaschenko, A. A.; Lepnev, L. S.; Bagatur'yants, A. A.; Vitukhnovskiy, A. G.; Stepanov, N. F.; Alfimov, M. V. *Inorg. Chem.* 2009, 48, 11123–30.
113. Wezenberg, S. J.; Kleij, A. W. *Angew. Chem., Int. Ed.* 2008, 47, 2354–64.
114. Kleij, A. W. *Dalton Trans.* 2009, 24, 4635–9.
115. Krause, R. A.; Busch, D. H. *J. Am. Chem. Soc.* 1960, 82, 4830–4.
116. Robinson, M. A.; Busch, D. H. *Inorg. Chem.* 1963, 2, 1171–7.
117. Stratton, W. J.; Busch, D. H. *J. Am. Chem. Soc.* 1958, 80, 1286–9.
118. Stratton, W. J.; Busch, D. H. *J. Am. Chem. Soc.* 1958, 80, 3191–5.
119. Stratton, W. J.; Busch, D. H. *J. Am. Chem. Soc.* 1960, 82, 4834–9.
120. Zhou, X.-H.; Wu, T.; Li, D. *Inorg. Chim. Acta.* 2006, 359, 1442–8.
121. Cressey, M.; McKenzie, E. D.; Yates, S. J. *J. Am. Chem. Soc.* 1971, 93, 2677–84.
122. Goodwin, H. A.; Lions, F. J. *J. Am. Chem. Soc.* 1960, 82, 5013–23.

123. Braithwaite, A. C.; Rickard, C. E. F.; Waters, T. N. *J. Chem. Soc. Dalton Trans.* 1975, 21, 2149–53.
124. McKenzie, E. D.; Harris, C. M. *J. Chem. Soc.* 1969, 5, 746–53.
125. Habib, M.; Karmakar, T. K.; Aromi, G.; Ribas-Arin, J.; Fun, H.-K.; Chantrapromma, S.; Chandra, S.K. *Inorg. Chem.* 2008, 47, 4109–17.
126. Campbell, T. G.; Urbach, F.L. *Inorg. Chem.* 1973, 12, 1836–40.
127. Rahaman, S. H.; Chowdhury, H.; Bose, D.; Ghosh, R. Hung, C.-H.; Ghosh, B. K. *Polyhedron* 2005, 24, 1755–63.
128. Mikuriya, M.; Hatano, Y.; Asato, E. *Bull. Chem. Soc. Jpn.* 1997, 70, 2495–507.
129. Karmakar, T. K.; Aromi, G.; Ghosh, B. K.; Usman, A.; Fun, H.-K.; Mallah, T.; Behrens, U.; Solansf, X.; Chandra, S. K. *J. Mater. Chem.* 2006, 16, 278–85.
130. Busch, D. H.; Bailar Jr. J.C. *J. Am. Chem. Soc.* 1956, 78, 1137–42.
131. Mirkhani, V.; Tangestaninejad, S.; Moghadamb, M.; Moghbel, M. *Bioorg. Med. Chem.* 2004, 12, 4673–7.
132. Drew, M. G. B.; Foreman, M. R. StJ.; Hudson, M. J.; Kennedy, K. F. *Inorg. Chim. Acta.* 2004, 357, 4102–12.
133. Pal, S.; Pal, S. *Polyhedron* 2003, 22, 867–73.
134. Harries, C. Lenart, G.H. *Ann.* 1915, 410, 101–3.
135. deVos, D. E.; Feigen, E. J. P.; Jacobs, P. A. *J. Am. Chem. Soc.* 1994, 116, 4746–52.
136. Ebralidze, I. I.; Leitus, G.; Shimon, L. J. W.; Neumann, R. *J. Molec. Struct.* 2008, 891, 491–7.
137. Habermehl, N. C.; Angus, P. M.; Kilah, N. L.; Norn, L.; Rae, A. D.; Willis, A. C.; Wild, S. B. *Inorg. Chem.* 2006, 45, 1445–62.
138. Oshima, S.; Hirayama, N.; Kubono, K.; Kokusen, H.; Honjo, T. *Annal. Chim. Acta.* 2001, 441, 157–64.
139. Pal, P. K.; Chowdhury, S.; Purkayastha, P.; Tocher, D. A.; Datta, D. *Inorg. Chem. Comm.* 2000, 3, 585–9.
140. Rahaman, S. H.; Ghosh, R.; Ghosh, B. K. *Inorg. Chem. Comm.* 2006, 9, 1011–4.
141. Stoufer, R. C.; Busch, D. H. *J. Am. Chem. Soc.* 1960, 82, 3491–5.
142. Wagner, J.; Pielichowski, J.; Honsch, A.; Pielichowski, K.; Bogdal, D.; Pajda, M.; Kurek, S. S.; Burczyk, A. *Synth. Metals* 2004, 146, 159–65.
143. Zhou, X.-H.; Wu, T.; Li, D. *Inorg. Chim. Acta.* 2006, 359, 1442–8.
144. Che, C.-M.; Tang, W.-T.; Li, C.-K. *J. Chem. Soc. Dalton Trans.* 1990, 12, 3735–9.
145. Mondal, N.; Mitra, S.; Rosair, G. *Polyhedron* 2001, 20, 2473–6.
146. Rahaman, S. H.; Ghosh, R. Lu, T.-H.; Ghosh, B. K. *Polyhedron* 2005, 24, 1525–32.
147. Mazurek, W.; Berry, K. J.; Murray, K. S.; O'Connor, M. J.; Snow, M. R.; Wedd, A. G. *Inorg. Chem.* 1982, 21, 3071–80.

148. Striegler, S.; Dittel, M. J. *Am. Chem. Soc.* 2003, 125, 11518–24.
149. Oshima, S.; Hirayama, N.; Kubono, K.; Kokusen, H.; Honjo, T. *Japan Soc. Anal. Chem.*, 2002, 18, 1351–5.
150. Baar, C. R.; Jennings, M. C.; Puddephatt, R. J. *Organometallics* 1999, 18, 4373–9.
151. Cristau, H.-J.; Cellier, P. P.; Hamada, S. Spindler, J.-F.; Taillefer, M. *Org. Lett.*, 2004, 6, 913–6.
152. Lu, X.-H.; Xia, Q.-H.; Zhan, H.-J.; Yuan, H.-X.; Ye, C.-P.; Su, K.-X.; Xu, G. *J. Molec. Cat. A* 2006, 250, 62–9.
153. Liu, B.; Zhang, M.-J.; Cui, J.; Zhu, J. *Acta Cryst.* 2006, E62, o5359–60.
154. Nguyen, Q. T.; Jeong, J. H. *Polyhedron*, 2006, 25, 1787–90.
155. Schoumacker, S.; Hamelin, O.; Pécaut, J.; Fontecave, M. *Inorg. Chem.* 2003, 42, 8110–6.
156. Soundiressane, T.; Selvakumar, S.; Menage, S.; Hamelin, O.; Fontecave, M. Singh, A. P. *J. Molec. Cat. A* 2007, 270, 132–43.
157. van Stein, G. C.; van Koten, G.; Vrieze, K.; Brevard, C.; Spek, A. L. *J. Am. Chem. Soc.* 1984, 106, 4486–92.
158. Zhang, Y.; Xiang, L.; Wang, Q.; Duan, X. -F.; Zi, G. *Inorg. Chim. Acta.* 2008, 361, 1246–54.
159. Basheer, C.; Vetrichelvan, M.; Perera, A. P.; Valiyaveettil, S.; Lee, H. K. *Int. J. Nanoscience* 2005, 4, 599–606.
160. Basheer, C.; Vetrichelvan, M.; Perera, A. P.; Valiyaveettil, S.; Lee, H. K. *Tet. Lett.* 2006, 47, 957–61.
161. Garoufis, A.; Kasselouri, S.; Mitsopoulou, C.-A.; Sletten, J.; Papadimitriou, C.; Hadjiliadis, N. *Polyhedron* 1999, 18, 39–47.
162. Kasselouri, S.; Garoufis, A.; Kalkanis, G.; Perlepes, S. P.; Hadjiliadis, N. *Trans. Met. Chem.* 1993, 18, 531–6.
163. Knödler, A.; Hübler, K.; Sixt, T.; Kaim, W. *Inorg. Chem. Comm.* 2000, 3, 182–4.
164. Mishra, D.; Naskar, S.; Butcher, R. J.; Chattopadhyay, S. K. *Inorg. Chim. Acta.* 2005, 358, 3115–21.
165. Shakir, M.; Azam, M.; Azim, Y.; Parveen, S.; Khan, U. *Polyhedron* 2007, 26, 5513–8.
166. Tsiouri, M.; Plakatouras, J. C.; Garoufis, A.; Nastopoulos, V.; Hadjiliadis, N. *Inorg. Chem. Comm.* 2002, 5, 844–7.
167. Banjeer, S.; Gangopadhyay, J.; Lu, C.-Z.; Chen, J.-T.; Ghosh, A. *Eur. J. Inorg. Chem.* 2004, 2533–41.
168. Banerjee, S.; Ghosh, A.; Wu, B.; Lassahn, P.-G.; Janiak, C. *Polyhedron* 2005, 24, 593–9.
169. Banerjee, S.; Lassahn, P.-G.; Janiak, C.; Ghosh, A. *Polyhedron* 2005, 24, 2963–71.
170. Chattopadhyay, S.; Ray, M. S.; Drew, M. G. B.; Figuerola, A.; Diaz, C.; Ghosh, A. *Polyhedron* 2006, 25, 2241–53.

171. Gourbatsis, S.; Plakatouras, J. C.; Nastopoulos, V.; Cardin, C. J.; Hadjiliadis, N. *Inorg. Chem. Comm.* 1999, 2, 468–71.
172. Gourbatsis S.; Perlepes, S. P.; Hadjiliadis, N. *Trans. Met. Chem.* 1990, 15, 300–8.
173. Louloudi, M.; Nastopoulos, V.; Gourbatsis, S.; Perlepes, S. P.; Hadjiliadis, N. *Inorg. Chem. Comm.* 1999, 2, 479–83.
174. Mentés, A.; Sezek, S.; Hanhan, M. E.; Büyükgüngör, O. *Turk. J. Chem.* 2007, 31, 667–76.
175. Bréfuel, N.; Shova, S.; Tuchagues, J.-P. *Eur. J. Inorg. Chem.* 2007, 27, 4326–34.
176. Chattopadhyay, S.; Drew, M. G. B.; Diaz, C.; Ghosh, A. *Dalton. Trans.* 2007, 24, 2492–4.
177. Chattopadhyay, S.; Drew, M. G. B.; Ghosh, A. *Inorg. Chim. Acta.* 2006, 359, 4519–25.
178. Chattopadhyay, S.; Drew, M. G. B.; Ghosh, A. *Polyhedron* 2007, 26, 3513–22.
179. Shen, L.; Zhang, H.-Y.; Ji, H.-F. *J. Mol. Struct. Theochem* 2007, 817, 161–2.
180. Psomas, G.; Bréfuel, N.; Dahan, F.; Tuchagues, J.-P. *Inorg. Chem.* 2004, 43, 4590–4.
181. Bréfuel, N.; Vang, I.; Shova, S.; Dahan, F.; Costes, J.-P.; Tuchagues, J.-P. *Polyhedron* 2007, 26, 1745–57.
182. Yoshida, S.; Fukui, K.; Kikuchi, S.; Yamada, T. *J. Am. Chem. Soc.* 2010, 132, 4072–3.
183. Chattopadhyay, S.; Bhar, K.; Das, S.; Satapathi, S.; Fun, H.-K.; Mitra, P.; Ghosh, B. K. *Polyhedron* 2010, 29, 1667–75.
184. Chowdhury, H.; Ghosh, R.; Rahaman, Sk. H.; Ghosh, B. K. *Polyhedron* 2007, 26, 5023–9.
185. Deoghoria, S.; Sain, S.; Soler, M.; Wong, W. T.; Christou, G.; Bera, S. K.; Chandra, S. K. *Polyhedron* 2003, 22, 257–62.
186. Ghosh, R.; Rahaman, Sk. H.; Rosair, G. M.; Ghosh, B. K. *Inorg. Chem. Comm.* 2007, 10, 61–5.
187. Gourbatsis, S.; Perlepes, S. P.; Butler, I. S.; Hadjiliadis, N. *Polyhedron*, 1999, 18, 2369–75.
188. Karmakar, T. K.; Chandra, S. K.; Ribas, J.; Mostafa, G.; Lu, T. H.; Ghosh, B. K. *Chem. Comm.* 2002, 20, 2364–5.
189. Karmakar, T. K.; Ghosh, B. K.; Usman, A.; Fun, H.-K.; Riviere, E.; Mallah, T.; Arom, G.; Chandra, S. K. *Inorg. Chem.* 2005, 44, 2391–9.
190. Liu, C.-M.; Xiong, R.-G.; You, X.-Z.; Liu, Y.-J.; *Polyhedron* 1996, 24, 4565–71.
191. Liu, C.-M.; Xiong, R.-G.; You, X.-Z. *Polyhedron* 1997, 16, 119–23.
192. Rahaman, Sk. H.; Fun, H.-K.; Ghosh, B. K. *Polyhedron* 2005, 24, 3091–7.
193. Ray, M. S.; Bhattacharya, R.; Chaudhuri, S.; Righi, L.; Bocelli, G.; Mukhopadhyay, G.; Ghosh, A. *Polyhedron*, 2003, 22, 617–24.
194. Cambridge Crystallographic Data Centre, CSDS 2006 release. 12 Union Rd, Cambridge CB21EZ, UK.
195. Kettunen, M.; Vedder, C.; Brintzinger, H.-H.; Mutikainen, I.; Leskelä, M.; Repo, T. *Eur. J. Inorg. Chem.* 2005, 6, 1081–9.

- ^{196.} Orvig, C.; Abrams, M. J. *Med. Inorg. Chem. Intro. Chem. Rev.* 1999, 99, 2201–3.
- ^{197.} Figueroa-Quintanilla, D.; Salazar-Lindo, E.; Sack, R. B.; Leon-Barua, R.; Sarabia-Arce, S.; Campos-Sanchez, M.; Eyzaguirre-Maccan, E. *New Engl. J. Med.* 1993, 328, 1653–8.
- ^{198.} Wadhera, A.; Fung, M. *Dermatology Online J.* 2005, 11(1), 12–5.
- ^{199.} Copper Development Association: <http://www.copper.org/publications/newsletters/innovations/2000/06/medicine-chest.html> Affiliated with the International Copper Association, LTD. "Copper Connects Life" Written June 2000.
- ^{200.} Caravan, P.; Ellison, J. F.; McMurry, T. J.; Lauffer, R. B. *Chem. Rev.* 1999, 99, 2293–352.
- ^{201.} Champion, G.D.; Graham, G.G.; Ziegler, J.B. *Ballieres Clin. Rheumatol.* 1990, 4, 491–534.
- ^{202.} Watson, J. D.; Crick, F. H. C. *Nature* 1953, 171, 737–8.
- ^{203.} Zhang, C. X.; Lippard, S.J. *Curr. Opinion Chem. Bio.* 2003, 7, 481–9.
- ^{204.} Kostova, I. *Rec. Pat. Anti-Cancer Drug Disc.* 2006, 1, 1–22.
- ^{205.} A. P. John Institute for Cancer Research: <http://www.apjohncancerinstitute.org/cancer/brain.htm> Cancer Treatment - Prevention - Research - A. P. John Cancer Institute, 2009.
- ^{206.} Virtual Chembook: <http://www.elmhurst.edu/~chm/vchembook/650drugs.html> Charles E Ophardt, Elmhurst College, 2003.
- ^{207.} Richards A. D.; Rodger, A. *Chem. Soc. Rev.* 2007, 36, 471–83.
- ^{208.} Voet, D.; Voet, J. G. *Biochemistry*, 2nd Ed., John Wiley & Sons, New York, 1995; pp 1020–65.
- ^{209.} Moran, L.; Mirault, M.-E.; Tissières, A.; Lis, J.; Schedl, P.; Artavanis-Tsakonas, S.; Gehring, W. *Cell* 1979, 17, 1–8.
- ^{210.} EzineArticles: <http://ezinearticles.com/?Platinum-And-Its-Uses&id=794819> "Platinum And Its Uses" 2010.
- ^{211.} eBullionGuide: <http://www.ebullionguide.com/platinum-uses.aspx> "Uses of Platinum" 2009.
- ^{212.} United States Geological Survey: <http://minerals.usgs.gov/minerals/pubs/commodity/platinum/myb1-2006-plati.pdf>. "Mineral Yearbook 2006: Platinum-Group Metals" George, Micheal W. 2006.
- ^{213.} Wilkinson, R.G. *Plat. Met. Rev.* 1961, 5, 128–31.
- ^{214.} Rosenberg, B.; Van Camp, L.; Trosko, J. E.; Mansour, V. H. *Nature*, 1969, 222, 385–6.
- ^{215.} Sedivy, D.; Keck, M. V.; Gerasimchuk, N.; Ratcliff, Abstracts, 42nd Midwest Regional Meeting of the American Chemical Society, 2007, 416.
- ^{216.} Dodd, D. W.; Toews, H. E.; Trevail, M. J.; Jennings, M. C.; Hudson, R. H. E.; Jones, N. D. *Can. J. Chem.* 2009, 87, 321–7.
- ^{217.} Durham, P.; Sedivy, D.; Keck, M. V.; Ratcliff, J.; Gerasimchuk, N. N. Abstracts of Papers, 232nd ACS National Meeting, 2006.
- ^{218.} Griffith, B. *Chem. World* 2005, 2, 50–3.

- ²¹⁹. Northwest Territorial Mint: http://bullion.nwtmint.com/palladium_uses.php "Uses of Palladium" 2010.
- ²²⁰. Gao, E.; Liu, C.; Zhu, M.; Lin, H.; Wu, Q.; Liu, I. *Anti-Cancer Agents Med. Chem.* 2009, 9, 356–68.
- ²²¹. Kirschner, S.; Maurer, A.; Dragulescu, C. *Clin. Hematol. Oncol.* 1977, 7, 190–6.
- ²²². Pneumatikakis, G.; Hadjiliadis, N.; Theophanides, T. *Inorg. Chem.* 1978, 17, 915–22.
- ²²³. Soenmez, M.; Celebi, M.; Yardim, Y.; Sentuerk, Z. *Eur. J. Med. Chem.* 2010, 45, 4215–20.
- ²²⁴. Gonzalez, M. L.; Tercero, J. M.; Matilla, A.; Niclos-Gutierrez, J.; Fernandez, M. T.; Lopez, M. C.; Alonso, C.; Gonzalez, S. *Inorg. Chem.* 1997, 36, 1806–12.
- ²²⁵. Peyrone, M., *Ann. Chem Liebigs*, 1845, 51, 15.
- ²²⁶. Jamieson, E.R.; Lippard, S. *J. Chem. Rev.* 1999, 99, 2467–98.
- ²²⁷. Ishida, S.; Lee, J.; Thiele, D. J.; Herskowitz, I. *Proc. Natl. Acad. Sci. USA* 2002, 99, 14298–302.
- ²²⁸. Lin, X.; Okuda, T.; Holzer, A.; Howell, S. B. *Mol. Pharmacol.* 2002, 62, 1154–9.
- ²²⁹. Lippert, B. *Cisplatin. The Chemistry and Biochemistry of a Leading Anticancer Drug*, Wiley-VCH, Weinheim, 1999; pp 3, 6–8, 12–58, 112–115, 183–196, 339–359.
- ²³⁰. Gray, H. B.; Ballhausen, C. J. *J. Am. Chem. Soc.* 1963, 85, 260–5.; Costa, L. A. S.; Rocha, W. R.; De Almeida, W. B.; Dos Santos, H. F. *J. Inorg. Biochem.* 2005, 99, 575–83.; Connors, T. A.; Jones, M.; Ross, W. C.; Braddock, P. D.; Khokhar, A. R.; Tobe, M. L. *Chem. Biol. Interact.* 1972, 5, 415–24.
- ²³¹. Raudaschl, G.; Lippert, B.; Hoeschele, J. D.; Howard-Lock, H. E.; Lock, C. J. L.; Pilon, P. *Inorg. Chim. Acta*, 1985, 106, 141–4.
- ²³². U.S. Food and Drug Administration • 10903 New Hampshire Ave. Silver Spring, MD 20993 • 1-888-INFO-FDA (1-888-463-6332)
- ²³³. Curt, G. A.; Grygiel, J. J.; Corden, B. J.; Ozols, R. F.; Weiss, R. B.; Tell, D. T.; Myers, C. E.; Collins, J. M. *Can. Res.* 1983, 43, 4470–3. Boven, E.; van der Vijgh, W. J. F.; Nauta, M. M.; Schlüper, H. M. M.; Pinedo, H. M. *Can. Res.* 1985, 45, 86–90.
- ²³⁴. Latif, L.; Wood, T.; Connell, C.; Smith, D. C.; Vaughn, D.; Lebwohl, D.; Peereboom, D. *Investigational New Drugs* 2005, 23, 79–84.
- ²³⁵. Ulrich-Pur, H.; Fiebiger, W. C. C.; Schüll, B.; Kornek, G. V.; Scheithauer, W.; Raderer, M. *Oncology* 2000, 59, 187–9. Hejna, M.; K"ostler, W. J.; Raderer, M.; Tomek, S.; Brodowicz, T.; Scheithauer, W.; Wiltshcke, C.; Zielinski, C. C. *Anti-Cancer Drugs* 2000, 11, 629–34.
- ²³⁶. Kelland, L. *Expert Op. Investig. Drugs* 2007, 16, 1009–21.
- ²³⁷. National Cancer Institute: <http://www.cancer.gov/newscenter/benchmarks-vol2-issue12/page2> A Service of the National Cancer Institute, 2010.
- ²³⁸. RxList, The Internet Drug Index: <http://www.rxlist.com/> by RxList Inc. Copyright © 2011.

239. Drugs.com: <http://www.drugs.com/> Copyright © 2000–2011.
240. Jakupec, M. A.; Keppler, B. K. *Curr. Topics Med. Chem.* 2004, 4, 1575–83.
241. The University of Sydney: <http://www.usyd.edu.au/research/opportunities/opportunities/141> “Design of new metal-based anti-cancer drugs”, © 2002–2009.
242. Sun, R. W.-Y.; Li, C. K.-L.; Ma, D.-L.; Yan, J. J.; Lok, C. N.; Leung, C.-H.; Zhu, N.; Che, C.-M. *Chem. Eur. J.* 2010, 16, 3097–113.
243. Hasegawa, K.; Mori, K.; Ishii, N.; Aoki, Y.: CA 2478640 2003.; Essigmann, J. M., Croy, R. G., Yarema, K. J., Morningstar, M.: US6500669 2002.
244. Gümüş, F.; Eren, G.; Açıık, L.; Celebi, A.; Öztürk, F.; Yılmaz, S.; Sağkan, R. I.; Gür, S.; Özkul, A.; Elmalı, A.; Elerman, Y. *J. Med. Chem.* 2009, 52, 1345–57.
245. Marat, K. SpinWorks, Version 2.5.5, Copyright 1999–2006 and Version 2.4 PL2, Copyright 1999–2004.
246. Cambridge Crystallographic Data Centre, CSDS 2006 release. 12 Union Rd, Cambridge CB21EZ, UK.
247. Weber, J. H. *Inorg. Chem.* 1967, 6, 258–62.
248. Liu, B.; Zhang, M.-J.; Cui, J.; Zhu, J. *Acta Crystallogr., Sect. E: Struct. Rep. Online* 2006, 62, o5359–60.
249. Zhang, Y.; Xiang, L.; Wang, Q.; Duan, X.-F.; Zi, G. *Inorg. Chim. Acta.* 2008, 361, 1246–54.
250. Abu-Surrah, A.S.; Laine, T.V.; Repo, T.; Fawzi, R.; Steimann, M.; Rieger, B. *Acta Crystallogr., Sect. C: Cryst. Struct. Commun.* 1997, 53, 1458–9.
251. Patra, G. K.; Goldberg, I. *New J. Chem.* 2003, 27, 1124–31.
252. Gregoliński, J.; Lisowski, J.; Lis, T. *Org. Biomol. Chem.* 2005, 3, 3161–6.
253. Tsukuda, T.; Maeda, S.; Yasui, M.; Tamane, T.; Tsubomura, T. *Bull. Chem. Soc. Jpn.* 2008, 81, 358–60.
254. Krakowiak, K.E.; Bradshaw, J.S.; Jiang, W.; Dalley, N.K.; Wu, G.; Isatt, R.M. *J. Org. Chem.* 1991, 56, 2675–80.
255. Kia, R.; Fun, H.-K.; Kargar, H. *Acta Crystallogr., Sect. E: Struct. Rep. Online* 2009, 65, o780.
256. Yue, S.-M.; Su, Z.-M.; Ma, J.-F.; Liao, Y.; Kan, Y.-H.; Zhang, H.-J. *Jiegou Huaxue (Chin. J. Struct. Chem.)* 2003, 22, 174–8.
257. Guo, Y.-C.; Zhuo, L.-H.; Zhao, Y.-Y.; Yao, X.-Z.; Huang, Q.-Z.; *Jiegou Huaxue (Chin. J. Struct. Chem.)* 2008, 27, 1333–8.
258. Bowyer, P. K.; Porter, K. A.; Rae, A. D.; Willis, A. C.; Wild, S. B. *Chem. Commun.* 1998, 10, 1153–4.
259. Garoufis, A.; Kasselouri, S.; Mitsopoulou, C.-A.; Sletten, J.; Papadimitriou, C.; Hadjiliadis N. *Polyhedron* 1999, 18, 39–47.
260. Pal, S.; Pal, S. *Polyhedron* 2003, 22, 867–73.

261. Mikuriya, M.; Hatano, Y.; Asato, E. *Chem. Lett.* 1996, 849.
262. Jantti, A.; Rissanen, K.; Valkonen, J. *Acta Chem. Scand.* 1998, 52, 1010–6.
263. Niu, D.-Z.; Sun, B.-W.; Lu, Z.-S.; Wang, Z.-M.; Yan, C.-H. *Acta Cryst. E: Struct. Rep. Online* 2001, 57, m589–90.
264. Karmakar, T.K.; Ghosh, B. K.; Usman, A.; Fun, H.-K.; Chandra, S. K. *Indian J. Chem. A: Inorg. Bio-inorg. Phys. Theor. Anal. Chem.* 2006, 45, 1356–61.
265. Ray, M. S.; Bhattacharya, R.; Chaudhuri, S.; Righi, L.; Bocelli, G.; Mukhopadhyay, G.; Ghosh, A. *Polyhedron* 2003, 22, 617–24.
266. Zang, Y.; Lu, Q.; Yin, Z.; Zeng, C.; Dai, A.; Zhou, Z. *Gaodeng Xuexiao Huaxue Xuebao (Chem. J. Chin. Univ.)* 1989, 10, 1–5.
267. Xu, L.; Pierrero, J.; Patrick, B. O.; Orvig, C. *Inorg. Chem.* 2001, 40, 2005–10.
268. Drew, M. G. B.; Foreman, M. R. StJ.; Hudson, M. J.; Kennedy, K. F. *Inorg. Chim. Acta* 2004, 357, 4102–12.
269. Tsiouri, M.; Plakatouras, J. C.; Garoufis, A.; Nastopoulos, V.; Hadjiliadis, N. *Inorg. Chem. Comm.* 2002, 5, 844–7.
270. Bréfuel, N.; Vang, I.; Shova, S.; Dahan, F.; Costes, J.-P.; Tuchagues, J.-P. *Polyhedron* 2007, 26, 1745–57.
271. Bligh, S. W. A.; Choi, N.; Cummins, W. J.; Evagorou, E. G.; Kelly, J. D.; McPartlin, M. J. *Chem. Soc. Dalton Trans.* 1994, 23, 3369–76.
272. Al-Resayes, S. *Acta Cryst. E: Struct. Rep. Online* 2009, 65, o1874.
273. Fenton, D. E.; Moody, R.; Casellato, U.; Vigato, P. A.; Graziani, R. J. *Heterocyclic Chem.* 1985, 22, 1639–42.
274. Banerjee, S.; Gangopadhyay, J.; Lu, C.-Z.; Chen, J.-T.; Ghosh, A. *Eur. J. Inorg. Chem.* 2004, 12, 2533–41.
275. Karmakar, T. K.; Ghosh, B. K.; Chandra S. K. *Ind. J. Chem. Sect. A Inorg. Bio-inorg. Phys. Theor. Anal. Chem.* 2006, 45, 1121–5.
276. Liu, C.-M.; Xiong, R.-G.; You, X.-Z.; Liu, Y.-J.; Cheung, K.-K. *Polyhedron* 1996, 15, 4565–71.
277. Garoufis, A.; Kasselouri, S.; Raptopoulou, C. P.; Terzis, A. *Polyhedron* 1999, 18, 585–91.
278. Emam, S. M.; McArdle, P.; McManus, J.; Mahon, M. *Polyhedron* 2008, 27, 2379–85.
279. Shan, X.-F.; Wang, D.-H.; Tung, C.-H.; Wu, L.-Z. *Tetrahedron* 2008, 64, 5577–82.
280. Bacchi, A.; Carcelli, M.; Gabba, L.; Ianelli, S.; Pelagatti, P.; Peliszi, G.; Rogolino, D. *Inorg. Chim. Acta* 2003, 342, 229–35.
281. Baar, C. R.; Jennings, M. C.; Puddephatt, R. J. *Organometallics* 2001, 20, 3459–65.
282. Baar, C. R.; Jennings, M. C.; Puddephatt, R. J.; Muir, K. W. *Organometallics* 1999, 18, 4373–9.
283. Wang, G.; Lu, Q.; Zeng, C.; Zhou, Z. *Jiegou Huaxue (Chin. J. Struct. Chem.)* 1989, 8, 278–82.

284. Coles, S. J.; Sengul, A.; Kurt, O.; Altin, S. *Acta Cryst.* 2008, E64, m1435.
285. Jahn, H. A. & Teller, E. *Proc. R. Soc. London Ser. A* 1937, 161, 220–35.
286. Maslen, E. N.; Watson, K. J.; Moore, F. H. *Acta Cryst.* 1988, B44, 102–7.
287. Bayat, M.; von Hopffgarten, M.; Salehzadeh, S.; Frenking, G. *J. Organomet. Chem.* 2011, 696, 2976–84.
288. CrysAlis CCD and CrysAlis RED, Version 170, Oxford Diffraction Ltd., Abingdon, UK, 2002.
289. Sheldrick, G.M. *Acta Crystallogr. A* 1990, 46, 467.
290. Farrugia, L. J. *J. Appl. Crystallogr.* 1999, 32, 837–838.
291. Sheldrick, G. M. SHELXL-97, Program for solution of crystal structures, University of Göttingen, Germany, 1997.
292. Sheldrick, G. M. SADABS. University of Göttingen, Germany, 1996.
293. International Tables for Crystallography, Vol. C: Mathematical, Physical and Chemical Tables, Wilson, A.J.C. (ed.), Kluwer Academic Publishers, Dordrecht, 1992, 691.
294. Data Preparation and Reciprocal Space Exploration, Version 5.1, © Bruker Analytical X-ray Systems, 1997.
295. Barbour, L.J. *Supramol. Chem.* 2001, 1, 189–92.
296. Bontemps, S.; Sircoglou, M.; Bouhadir, G.; Puschmann, H.; Howard, J. A. K.; Dyer, P. W.; Miqueu, K.; Bourissou, D. *Chem. Eur. J.* 2008, 14, 731–40.
297. Douglas, B. E.; McDaniel, D. H. *Concepts and Models of Inorganic Chemistry*, Blaisdell Publishing Company, Waltham, 1965; pp 354–6.
298. Porterfield, W. W. *Inorganic Chemistry A Unified Approach*, 2nd Ed., Academic Press Inc., San Diego, California, 1993; pp 548.
299. Cotton, F. A.; Wilkinson, G. *Advanced Inorganic Chemistry*, 3rd Ed., John Wiley & Sons, New York, 1988; pp 536, 1297.
300. Handbook Sheidt, W. R. In *The Porphyrin Handbook*; Kadish, K. M.; Smith, K. M.; Guillard, R., Eds.; Academic: New York, 2000; Vol 1, Chapter 2.
301. International Union of Crystallography, CheckCIF, [online] Available: <http://www.iucr.org/>
302. Abu-Surrah, A. S.; Laine, T. V.; Repo, T.; Fawzi, R.; Steimann, M.; Rieger, B. *Acta. Cryst. C* 1997, C53, 1458–9.
303. Janiak, C. *J. Chem. Soc. Dalton Trans.* 2000, 21, 3885–96.
304. Steiner, T. *Angew. Chem. Int. Ed.* 2002, 41, 48–76.
305. Emam, S. M.; McArdle, P.; McManus, J.; Mahon, M. *Polyhedron* 2008, 27, 2379–85.
306. Munro, O. Q.; du Toit, K.; Drewes, S. E.; Crouch, N. R.; Mulholland, D. A. *New J. Chem.* 2006, 30, 197–207.
307. Barboiu, M.; Petit, E.; Vaughan, G. *Chem. Eur. J.* 2004, 10, 2263–70.

308. Likhanova, N. V.; Veloz, M. A.; Hopfl, H.; Matias, D. J.; Reyes-Cruz, V. E.; Olivares, O.; Martinez-Palou, R. J. *Heterocycl. Chem.* 2007, 44, 145–53.
309. Guo, Y.-C.; Zhuo, L.-H.; Zhao, Y.-Y.; Yao, X.-Z.; Huang, Q.-Z. *Jiegou Huaxue (Chin. J. Struct. Chem.)* 2008, 27, 1333–8.
310. Mercury CSD 2.2 (Build RC5), CCDC Copyright 2001–2008.
311. Jurs, P. C. *Computer Software Applications in Chemistry*, 2nd Ed., John Wiley & Sons, New York, NY. 1996: pp 202–4.
312. Lawrance, G. A. *Introduction to Coordination Chemistry*, 1st Ed., John Wiley & Sons, Chichester, UK. 2009; pp 21–5.
313. Babai, A.; Deacon, G. B.; Erven, A. P.; Meyer, G. Z. *Anorg. Allg. Chem.* 2006, 632, 639–644.
314. Bernard, B. R.; Haines, R. I.; Rowley, J. I. *Trans. Met. Chem.* 2001, 26, 164–9.
315. Crouch, A. M.; Polhuis, M. J. *Molec. Struct. (Theochem)* 2000, 530, 171–6.
316. Shimazaki, Y.; Arai, N.; Dunn, T. J.; Yajima, T.; Tani, F.; Ramogida, C. F.; Storr, T.; Dalton *Trans.* 2011, 40, 2469–79.
317. Garner, K. L.; Parkes, L. F.; Piper, J. D.; Williams, J. A. G. *Inorg. Chem.* 2010, 49, 476–87.
318. Shannon, R. D.; Prewitt, C. T. *Acta Cryst.* 1969, B25, 925–46.
319. Cini, R.; Faniszi, F. P.; Intini, F. P.; Natile, G. J. *Am. Chem. Soc.* 1991, 113, 7805–6.
320. Coyer, M. J.; Herber R. H.; Cohen, S. *Acta Cryst. Sect. C* 1991, C47, 1376–8.
321. Vicente, J.; Chicote, M.-T.; Guerrero, R.; Vicente-Hernández, I. *Inorg. Chem.* 2006, 45, 5201–9.
322. Sreekanth, A.; Kurup, M. R. P. *Polyhedron* 2004, 23, 969–78.
323. Bacchi, A.; Carcelli, M.; Gabba, L.; Ianelli, S.; Pelagatti, P.; Peliszi, G.; Rogolino, D. *Inorg. Chim. Acta*, 2003, 342, 229–35.
324. Torabi, A. A.; Soudozil, A.; Welter, R. Z. *Kristallogr. NCS* 2007, 222, 197–8.
325. Munro, O. Q.; Camp, G. L.; *Acta. Cryst. C.* 2003, 59, o672–5.
326. Dunitz, J. D. *Chem. BioChem.* 2004, 5, 614–21.
327. Howard, J. A. K.; Hoy, V. J.; O' Hagan, D.; Smith, G. T. *Tetrahedron* 1996, 52, 12613–22.
328. Althoff, G.; Ruis, J.; Rodríguez, V.; López, G.; Pérez, J.; Janiak, C. *Cryst. Eng. Comm.* 2006, 8, 662–5.
329. Hunter, C. A.; Sanders, J. K. M. *J. Am. Chem. Soc.* 1990, 112, 5525–34.
330. Hartley, F. R. *Chemistry of Platinum Group Metals*, Elsevier, 1991; pp. 2–10.
331. Foresman, J. B.; Frisch, A. E. In *Exploring Chemistry with Electronic Structure Methods*, 2nd ed.; Gaussian Inc.: Pittsburgh, 1993; pp 6, 9, 21, 61–63, 97, 100–103, 112, 118, 154–160, 272.
332. Clark, T. *A Handbook of Computational Chemistry—A Practical guide to Chemical Structure and Energy Calculations*; John Wiley & Sons: USA, 1999; pp 1, 99, 233, 242.

333. Ghosh, A. In *The Porphyrin Handbook*; Kadish, K. M.; Smith, K. M.; Guillard, R., Eds.; Academic: New York, 2000; Vol 1, Chapter 2.
334. Wagnière, G. H. *Introduction to Elementary Molecular Orbital Theory*; Springer-Verlag: Berlin, 1976; pp 3.
335. Koch, W.; Holthausen, M. C. *A Chemist's Guide to Density Functional Theory*; Wiley-VCH: Weinheim, 2000; pp 30, 41, 70–85, 117–119, 191, 195, 199, 212.
336. Lecomte, C.; Rohmer, M.-M.; Bénard, M. In *The Porphyrin Handbook*; Kadish, K. M.; Smith, K. M.; Guillard, R., Eds.; Academic: New York, 2000; Vol 7, Chapter 48.
337. Jezierska-Mazzarello, A.; Vuilleumier, R.; Panek, J. J.; Ciccotti, G. J. *Phys. Chem. B* 2010, 114, 242–53.
338. Platas-Iglesias, C.; Esteban, D.; Ojea, V.; Avecilla, F.; de Blas, A.; Rodríguez-Blas, T. *Inorg. Chem.* 2003, 42, 4299–307.
339. Upadhyay, K. K.; Kumar, A.; Upadhyay, S.; Mishra, P. C. *J. Molec. Struct.* 2008, 873, 5–16.
340. Reyes, H.; García, C.; Farfán, N.; Santillan, R.; Lacroix, P. G.; Lepetit, C.; Nakatani, K. J. *Organomet. Chem.* 2004, 689, 2303–10.
341. Hohenberg, P.; Kohn, W. *Phys. Rev. B.* 1994, 136, 846–71.
342. Jensen, F. In *Introduction to Computational Chemistry*; John Wiley & Sons: Chichester, 1999; pp 177.
343. Ziegler, T. *Chem. Rev.* 1991, 91, 651–67.
344. Kohn, W.; Sham, L. J. *Phys. Rev. A.* 1965, 140, 1133–8.
345. Car, R.; Parinello, M. *Phys. Rev. Lett.* 1985, 55, 2471–4.
346. Andraud, C.; Kityk, I.V.; Lemercier, G.; Alexandre, M.; Gruhn, W. J. *Phys. B: At. Mol. Opt. Phys.* 2002, 35, 4069–76.
347. Vosko, S. H.; Wilk, L.; Nusair, M. *Can. J. Phys.* 1980, 58, 1200–11.
348. Perdew, J. D.; Wang, Y. *Phys. Rev. B.* 1986, 33, 8800–2.
349. Becke, A. D. *Phys. Rev. B.* 1988, 38, 3098–100.
350. Lee, C.; Yang, W.; Parr, R. G. *Phys. Rev. B.* 1988, 37, 785–9.
351. Perdew, J. P.; Chevary, J. A.; Vosko, S. H. ; Jackson, K. A. ; Pederson, M. R.; Singh, D. J.; Fiolhais, C. *Phys. Rev. B-Cond. Matter.* 1992, 46, 6671–87.
352. Becke, A. D. *J. Chem. Phys.* 1993, 98, 5648–52.
353. Stevens, P. J.; Devlin, J. F.; Chabalowski, C. F.; Frisch, M. J. *J. Phys. Chem.* 1994, 98, 11623–7.
354. Becke, A. D. *J. Chem. Phys.* 1996, 104, 1040–6.
355. Becke, A. D. *J. Chem. Phys.* 1997, 107, 8554–60.
356. Schmider, H. L.; Becke, A. D. *J. Chem. Phys.* 1998, 108, 9624–31.
357. van Voorhis, T.; Scuseria, G. E. *J. Chem. Phys.* 1998, 109, 400–10.

358. Meijer, E. J.; Sprik, M. J. *Chem. Phys.* 1996, 105, 8684–9.
359. Ghosh, A. *Acc. Chem. Res.* 1998, 31, 189–98.
360. Salvà, A.; Donoso, J.; Frau, J.; Muñoz J. *Phys. Chem. A* 2003, 107, 9409–14.
361. Chatziefthimiou, S. D.; Lazarou, Y. G.; Hadjoudis, E.; Dziembowska, T.; Mavridis, I. M. J. *Phys. Chem. B* 2006, 110, 23701–9.
362. Chattopadhyay, B.; Basu, S.; Chakraborty, P.; Choudhuri, S. K.; Mukherjee, A. K.; Mukherjee, M. J. *Molec. Struct.* 2009, 932, 90–6.
363. Dziembowska, T.; Szafran, M.; Katrusiak, A.; Rozwadowski, Z. J. *Molec. Struct.* 2009, 929, 32–42.
364. Kuramshina, G. M.; Takahashi, H. J. *Molec. Struct.* 2005, 735–736, 39–51.
365. Hansen, P. E.; Filarowski, A. J. *Molec. Struct.* 2004, 707, 69–75.
366. Krygowski, T. M.; Zachara, J. E.; Moszyński, R. J. *Chem. Inf. Model.* 2005, 45, 1837–41.
367. Pajak, J.; Maes, G.; De Borggraeve, W. M.; Boens, N.; Filarowski, A. J. *Molec. Struct.* 2007, 844–845, 83–93.
368. Thube, D. R.; Duhmal, N. R.; Rayne, S. Y.; Gejji, S. P. J. *Molec. Struct.* 2002, 579, 139–46.
369. Sun, Y.-X.; Hao, Q.-L.; Wei, W.-X.; Yu, Z.-X.; Lu, L.-D.; Wang, X.; Wang, Y.-S. J. *Molec. Struct. Theochem.* 2009, 904, 74–82.
370. Macchioni, A.; Magistrato, A.; Orabona, I.; Ruffo, F.; Rothlisberger, U.; Zuccaccia, C. *New J. Chem.* 2003, 27, 455–8.
371. Sarkar, S.; Biswas, S.; Liao, M.-S.; Kar, T.; Aydogdu, Y.; Dagdelen, F.; Mostafa, G.; Chattopadhyay, A. P.; Yap, G. P. A.; Xie, R.-H.; Khan, A. T.; Dey, K. *Polyhedron* 2008, 27, 3359–70.
372. Chen, J.-M.; Ruan, W.-J.; Meng, L.; Gao, F.; Zhu, Z.-A. *Spectrochimica Acta Part A* 2008, 71, 191–8.
373. Rogachev, A.; Kuzmina, N.; Nemukhin, A. J. *Alloys Comp.* 2004, 374, 335–8.
374. Barone, G.; Silvestri, A.; La Manna G.; J. *Molec. Struct: Theochem.* 2005, 715, 79–83.
375. Kwit, M.; Zabicka, B.; Gawronski, J. *Dalton Trans.* 2009, 34, 6783–9.
376. Dunning, T. H., Jr. *J. Chem. Phys.* 1989, 90, 1007–23.
377. Filarowski, A.; Głowiaka, T.; Koll, A. J. *Molec. Struct.* 1999, 484, 75–89.
378. Munro, O. Q.; Strydom, S. D.; Grimmer, C. D. *New J. Chem.* 2004, 28, 34–42.
379. Neuvonen, H.; Neuvonen, K.; Koch, A.; Kleinpeter, E. J. *Molec. Struct. Theochem.* 2007, 815, 95–104.
380. Sharif, S.; Denisov, G. S.; Toney, M. D.; Limbach, H. H. *J. Am. Chem. Soc.* 2006, 128, 3375–87.
381. Group Chemistry Fall Term: http://131.104.156.23/Lectures/7113/7113_Computational.html “CHEM 7110 Advanced Main” Michael K. Denk, 2007.

- ³⁸². Cramer, C. J. *Essentials of Computational Chemistry*, 2nd ed.; Wiley:West Sussex, England, 2004.
- ³⁸³. Lo, J. M. H.; Klobukowski, M. *Inorg. Chim. Acta* 2003, 353, 15–21.
- ³⁸⁴. Platas-Iglesias, C.; Esteban-Gómez, D.; Enríquez-Pérez, T.; Avecilla, F.; de Blas, A.; Rodríguez-Blas, T. *Inorg. Chem.* 2005, 44, 2224–33.
- ³⁸⁵. Huang, X.-X.; Xu, X. *Acta Phys. Chim. Sin.* 2009, 25, 1362–6.
- ³⁸⁶. Liu, C.-G.; Qiu, Y.-Q.; Sun, S.-L.; Chen, H.; Li, N.; Su, Z.-M. *Chem. Phys. Lett.* 2006, 429, 570–4.
- ³⁸⁷. Shimazaki, Y.; Stack, T. D. P.; Storr, T. *Inorg. Chem.* 2009, 48, 8383–92.
- ³⁸⁸. Poverenov, E.; Efremenko, I.; Frenkel, A. I.; Ben-David, Y.; Shimon, L. J. W.; Leitun, G.; Konstantinovski, L.; Martin, J. M. L.; Milstein, D. *Nature* 2008, 455, 1093–6.
- ³⁸⁹. Pérez, S.; López, C.; Caubet, A.; Bosque, R.; Solans, X.; Bardía, M. F.; Roig, A.; Molins, E. *Organometallics* 2004, 23, 224–36.
- ³⁹⁰. Pérez, S.; López, C.; Caubet, A.; Bosque, R.; Solans, X.; Bardía, M. F.; Roig, A.; Molins, E.; van Leeuwen, P. W. N. M.; van Strijdonck, G. P. F.; Freixa, Z. *Organometallics* 2008, 27, 4288–99.
- ³⁹¹. Arnais, A. M.; Carbayo, A.; Cuevas, J. V.; Diez, V.; García-Herbosa, G.; González, R.; Martínez, A. Muñoz, A. *Eur. J. Inorg. Chem.* 2007, 29, 4637–44.
- ³⁹². Gao, H. *Spectrochimica Acta A* 2011, 79, 687–93.
- ³⁹³. Gaussian 03W, version 6.1. Gaussian Inc. Carnegie Office Park-Building 6, Pittsburgh, PA 15106, USA. Copyright 1995–2004. M. J. Frisch, G. W. Trucks, H. B. Schlegel, G. E. Scuseria, M. A. Robb, J. R. Cheeseman, J. J. A. Montgomery, T. Vreven, K. N. Kudin, J. C. Burant, J. M. Millam, S. S. Iyengar, J. Tomasi, V. Barone, B. Mennucci, M. Cossi, G. Scalmani, N. Rega, G. A. Petersson, H. Nakatsuji, M. Hada, M. Ehara, K. Toyota, R. Fukuda, J. Hasegawa, M. Ishida, T. Nakajima, Y. Honda, O. Kitao, H. Nakai, M. Klene, X. Li, J. E. Knox, H. P. Hratchian, J. B. Cross, C. Adamo, J. Jaramillo, R. Gomperts, R. E. Stratmann, O. Yazyev, A. J. Austin, R. Cammi, C. Pomelli, J. W. Ochterski, P. Y. Ayala, K. Morokuma, G. A. Voth, P. Salvador, J. J. Dannenberg, V. G. Zakrzewski, S. Dapprich, A. D. Daniels, M. C. Strain, O. Farkas, D. K. Malick, A. D. Rabuck, K. Raghavachari, J. B. Foresman, J. V. Ortiz, Q. Cui, A. G. Baboul, S. Clifford, J. Cioslowski, B. B. Stefanov, G. Liu, A. Liashenko, P. Piskorz, I. Komaromi, R. L. Martin, D. J. Fox, T. Keith, M. A. Al-Laham, C. Y. Peng, A. Nanayakkara, M. Challacombe, P. M. W. Gill, B. Johnson, W. Chen, M. W. Wong, C. Gonzalez, J. A. Pople, Gaussian 03, revision B.04, Gaussian, Inc., Pittsburgh, PA, 2003.
- ³⁹⁴. Hehre, W. J.; Lathan, W. A.; Ditchfield, R.; Newton, M. D.; Pople, J. A. QCPE Program No. 236.

- ³⁹⁵. The official Gaussian website: www.gaussian.com/ Copyright © 2009-2011, Gaussian, Inc. Last update: 13 October 2011.
- ³⁹⁶. GaussView 3.09, Gaussian Inc. Carnegie Office Park-Building 6, Pittsburgh, PA 15106, USA. Copyright 2000–2003.
- ³⁹⁷. Sudha, S.; Sundaraganesan, N.; Kurt, M.; Cinar, M.; Karabacak, M. J. *Molec. Struct.* 2011, 985, 148–56.
- ³⁹⁸. Ren, X. Y.; Liu, Z. Y. *J. Chem. Phys.* 2005, 122, 034306.
- ³⁹⁹. Pearson, R. G. *J. Am. Chem. Soc.* 1963, 85, 3533-9.
- ⁴⁰⁰. Scott, A. P.; Radom, L. *J. Phys. Chem.* 1996, 100(41), 16502–13. Wong, M. W. *Chem. Phys. Lett.* 1996, 256(4,5), 391–9.
- ⁴⁰¹. Zhang, H.; Liu, C. S.; Bu, X. H.; Yang, M. J. *Inorg. Biochem.* 2005, 99, 1119–25.
- ⁴⁰². Erkkila, K. E.; Odom, D. T.; Barton, J. K. *Chem. Rev.* 1999, 99, 2777–95.
- ⁴⁰³. Hall, D. B.; Holmlin, R. E.; Barton, J. K. *Nature* 1996, 382, 731–5. Mishra, L.; Yadaw, A. K.; Srivastava, S.; Patel, A. B. *New J. Chem.* 2000, 24, 505–10. Liu, Y. J.; Chao, H.; Yuan, Y. X.; Yu, H. J.; Ji, L. N. *Inorg. Chim. Acta* 2006, 359, 3807–14.
- ⁴⁰⁴. Raman, N.; Raja, J.; Dhaweethu, S. A. *J. Chem. Sci. (Bangalore, India)* 2007, 119(4), 303–10.
- ⁴⁰⁵. Leelavathy, L.; Anbu, S.; Kandaswamy, M.; Karthikeyan, N.; Mohan, N. *Polyhedron* 2009, 28, 903–10.
- ⁴⁰⁶. Gilman, A. *Am. J. Surg.* 1963, 105(5), 574–8.
- ⁴⁰⁷. Lerman, L. S., *J. Mol. Biol.* 1961, 3, 18–30.
- ⁴⁰⁸. Cusumano, M.; Di Pietro, M. L.; Giannetto, A.; Nicolo, F.; Rotondo, E. *Inorg. Chem.* 1998, 37, 563–8.
- ⁴⁰⁹. Lippard, S. J. *Acc. Chem. Res.* 1978, 11, 211.
- ⁴¹⁰. Kemp, S.; Wheate, N. J.; Wang, S.; Collins, J. G.; Ralph, S. F.; Day, A. I.; Higgins, V. J.; Aldrich-Wright, J. R. *J. Biol. Inorg. Chem.* 2007, 12, 969–79.
- ⁴¹¹. Chaires, J. Molecular basis of specificity, in: Pullman, B.; Jortner, J. (Eds.), *Nucleic Acid–Drug Interaction*, Kluwer Academic Press, Dordrecht, 1990, p. 123.
- ⁴¹². Arcamone, F. *Doxorubicin Anti-Cancer Antibiotics*, Academic Press, New York, 1981.
- ⁴¹³. Cusumano, M.; Di Pietro, M. L.; Giannetto, A.; Vainiglia, P. A. *J. Inorg. Biochem.* 2005, 99, 560–5.
- ⁴¹⁴. Wang, A. H.-J.; Nathans, J.; van der Marel, G. A.; van Boom, J. H.; Rich, A. *Nature* 1978, 276, 471–4.
- ⁴¹⁵. Food, Fashion, and...Science: <http://foodfashionscience.blogspot.com/> “DNA Nanobots and Origami”, 2010.
- ⁴¹⁶. Cusumano, M.; Giannetto, A. *J. Inorg. Biochem.* 1997, 65, 137–44.

417. Jennette, K. W.; Lippard, S. J.; Vassiliades, G. A.; Bauer, W. R. *Proc. Natl. Acad. Sci. U.S.A.* 1974, 71, 3839–43.
418. Howe-Grant, M.; Lippard, S. J. *Biochem.* 1979, 18, 5762–9.
419. Martinez, R.; Chacón-García, L. *Curr.t Med. Chem.* 2005, 12, 127–51.
420. Froelich-Ammon, S. J.; Osheroff, N. J. *Biol. Chem.* 1995, 270, 21429–32.
421. National cancer Institute at the National Institutes of Health, located in Bethesda, Maryland. <http://www.cancer.gov>
422. Monks, A.; Scudiero, D.; Skehan, P.; Shoemaker, R.; Paull, K.; Vistica, D.; Hose, C.; Langley, J.; Cronise, P.; Vaigro-Wolff, A.; Gray-Goodrich, M.; Campbell, H.; Mayo, J.; Boyd, M. J. *Nat. Cancer Inst.*, 1991, 83, 757–66.
423. Boyd, M. R.; Paull, K. D. *Drug. Develop. Res.*, 1995, 34, 91–109.
424. Metcalfe, C.; Thomas, J. A. *Chem. Soc. Rev.* 2003, 32, 215–24.
425. Marcon, G.; Carotti, S.; Coronello, M.; Messori, L.; Mini, E.; Orioli, P.; Mazzei, T.; Cinellu, M. A.; Minghetti, G. *J. Med. Chem.* 2002, 45, 1672–7.
426. Gao, E.; Liu, L.; Zhu, M.; Huang, Y.; Guan, F.; Gao, X.; Zhang, M.; Wang, L.; Zhang, W.; Sun, Y. *Inorg. Chem.* 2011, 50, 4732–41.
427. Jaramillo, D.; Buck, D. P.; Collins, J. G.; Fenton, R. R.; Stootman, F. H.; Wheate, N. J.; Aldrich-Wright, J. R. *Eur. J. Inorg. Chem.* 2006, 4, 839–49.
428. Gao, E.-J.; Wang, L.; Zhu, M.-C.; Liu, L.; Zhang, W.-Z. *Eur. J. Med. Chem.* 2010, 45, 311–6.
429. Sherman, S. E.; Lippard, S. J. *Chem. Rev.* 1987, 87, 1153. Reedijk, J. *Pure Appl. Chem.* 1987, 59, 181. Eastman, A. *Pharmac. Ther.* 1987, 34, 155. Roberts, J. J. *Pontificiae Academiae Scientiarum Scripta Varia* 1988, 70, 464. Pinto, A. L.; Lippard, S. J. *Biochim. Biophys. Acta* 1985, 780, 167.
430. Brabec, V.; Nepelchova, K.; Kasparkova, J.; Farrell, N. J. *Biol. Inorg. Chem.* 2000, 5, 364–8.
431. Zhao, G.; Lin, H.; Zhu, S.; Sun, H.; Chen, Y. J. *Inorg. Biochem.* 1998, 70, 219–26.
432. Che, C. M.; Yang, M.; Wong, K. H.; Chan, H. L.; Lam, W. *Chem. Eur. J.* 1999, 5, 3350–6.
433. Cusumano, M.; Giannetto, A. J. *Inorg. Biochem.* 1997, 65, 137–44.
434. Kieltyka, R.; Fakhoury, J.; Moitessier, N.; Sleiman, H. F. *Chem. Eur. J.* 2008, 14, 1145–54.
435. Whan, R. M.; Messerle, B. A.; Hambley, T. W. *Dalt. Trans.* 2009, 6, 932–9.
436. Cusumano, M.; Di Pietro, M. L.; Giannetto, A. *Inorg. Chem.* 1999, 38, 1754–8.
437. McCoubrey, A.; Latham, H. C.; Cook, P. R.; Rodger, A.; Lowe, G. *FEBS Lett.* 1996, 380, 73–8. Che, C. M. *Chem. Commun.* 1995, 509–10.
438. Gao, E. J.; Sun, Y. G.; Liu, Q. T.; Duan, L. Y. *J. Coord. Chem.* 2006, 59, 1295–300.
439. Gao, E. J.; Liu, Q. T.; Duan, L. Y. *Russ. J. Coord. Chem.* 2007, 33, 120–3.
440. Gao, E. J.; Wang, K. H.; Gu, X. F.; Yu, Y.; Sun, Y. G.; Zhang, W. Z.; Yin, H. X.; Wu, Q.; Zhu, M. C.; Yan, X. M. *J. Inorg. Biochem.* 2007, 101, 1404–9.

441. Wang, A. H. J.; Nathans, J.; van der Marel, G.; van Boom, J. H.; Rich, A. *Nature* 1978, 276, 471–4.
442. Gao, E.-J.; Wu, Q.; Wang, C.-S.; Zhu, M.-C.; Wang, L.; Liu, H.-Y.; Huang, Y.; Sun, Y.-G. *J. Coord. Chem.* 2009, 62, 3425–37.
443. Faraglia, G.; Fregona, D.; Sitran, S.; Giovagnini, L.; Marzano, C.; Baccichetti, F.; Casellato, U.; Graziani, R. *J. Inorg. Biochem.* 2001, 83, 31–40.
444. Gao, E. J.; Zhu, M. C.; Yin, H. X.; Liu, L.; Wu, Q.; Sun, Y. G.; *J. Inorg. Biochem.* 2008, 102, 1958–64.
445. Hambley, T. W. *J. Chem. Soc., Dalton Trans.* 2001, 19, 2711–8.
446. Gonzalez, V. M.; Fuertes, M. A.; Alonso, C.; Perez, J. *Mol. Pharmacol.* 2001, 59, 657–63.
447. Akdi, K.; Vilaplana, R. S.; Kamah, S.; Navarro, J. A. R.; Salas, J. M.; Gonzalez-Vilchez, F. J. *Inorg. Biochem.* 2002, 90, 51–60.
448. Butour, J. L.; Wimmer, S.; Wimmer, F.; Castan, P. *Chem._Biol. Interact.* 1997, 104, 165–78.
449. Zou, X. H.; Ye, B. H.; Li, H.; Liu, J. G.; Xiong, Y.; Ji, L. N. *J. Chem. Soc., Dalton Trans.* 1999, 9, 1423–8.
450. Zhang, Q. L.; Liu, J. G.; Liu, J. Z.; Li, H.; Yang, Y.; Xu, H.; Chao, H.; Ji, L. N. *Inorg. Chim. Acta.* 2002, 339, 34–40.
451. Kashanian, S.; Shahabadi, N.; Roshanfekar, H.; Shalmashi, K.; Omidfar, K. *Biochem. (Moscow)* 2008, 73, 929–36.
452. Gao, E.; Liu, L.; Shi, C.; Yin, H.; Zhu, M.; Wu, Q.; Liu, G. *Chin. J. Chem.* 2009, 27, 1061–6.
453. Mukherjee, S.; Chowdhury, S.; Chattapadhyay, A. P.; Bhattacharya, A. *Inorg. Chim. Acta* 2001, 373, 40–6.
454. Brodie, C. R.; Collins, J. G.; Aldrich-Wright, J. R. *Dalton Trans.* 2004, 1145–52.
455. Krause-Heuer, A. M.; Wheate, N. J.; Tilby, M. J.; Pearson, D. G.; Ottley, C. J.; Aldrich-Wright, J. R. *Inorg. Chem.* 2008, 47, 6880–8.
456. Alonso, A.; Almendral, M. J.; Curto, Y.; Criado, J. J.; Rodríguez, E.; Manzano, J. L. *J. Fluoresc.* 2007, 17, 390–400.
457. Navarro, M.; Betancourt, A.; Hernández, C.; Marchán, E. *J. Braz. Chem. Soc.* 2008, 19, 1355–60.
458. Lu, W.; Vivic, D. A.; Barton, J. K. *Inorg. Chem.* 2005, 44, 7970–80.
459. Mansuri-Torshizi, H.; Ghadimy, S.; Akbarzadeh, N. *Chem. Pharm. Bull.* 2001, 49(12), 1517–20.
460. Wu, P.; Ma, D. L.; Leung, C. H.; Yan, S. C.; Zhu, N.; Abagyan, R.; Che, C. M. *Chem. Eur. J.* 2009, 15, 13008–21.
461. Whan, R. M.; Messerle, B. A.; Hambley, T. W. *Dalton Trans.* 2009, 932–9.
462. Gao, E.-J.; Zhao, S.-M.; Zhang, D.; Liu, Q.-T. *Chin. J. Chem.* 2005, 23, 54–7.

- ⁴⁶³. Chen, L.-M.; Liu, J.; Chen, J.-C.; Tan, C.-P.; Shi, S.; Zheng, K.-C.; Ji, L.-N.; *J. Inorg. Biochem.* 2008, 102, 330–41.
- ⁴⁶⁴. TopoGen A Decatenation-Supercoiling Assay: <http://www.topogen.com/p/methods-protocols.html> TopoGEN, Inc. 108 Aces Alley, Port Orange, Florida 32128, USA.
- ⁴⁶⁵. Kashanian, S.; Dolatabadi, E. N. *Food Chem.* 2009, 116, 743–7.
- ⁴⁶⁶. Barton, J. K.; Danishefsky, A.; Goldberg, J. J. *Am. Chem. Soc.* 1984, 106, 2172–6.
- ⁴⁶⁷. Bloomfield, V. A.; Crothers, D. M.; Tinoco, I. *Physical Chemistry of Nucleic Acids* 1974, Harper and Row, New York, p. 432.
- ⁴⁶⁸. Tan, J. H.; Lu, Y.; Huang, Z. S.; Gu, L. Q.; Wu, J. Y. *Eur. J. Inorg. Chem.* 2007, 42, 1169–75.
- ⁴⁶⁹. Vaidyanathan, V. G.; Nair, B. U. *J. Inorg. Biochem.* 2004, 94, 121.
- ⁴⁷⁰. Ghazaryan, A. A.; Dalyan, Y. B.; Haroutiunian, S. G.; Tikhomirova, A.; Taulier, N.; Wells, J. W.; Chalikian, T. V. *J. Am. Chem. Soc.* 2006, 128, 1914–21.
- ⁴⁷¹. Devi, Ch. V.; Singh, N. R. *Spectrochim. Acta Part A* 2001, 78, 1180–6.
- ⁴⁷². Han, G.; Yang, P. J. *Inorg. Biochem.* 2002, 91, 230–6.
- ⁴⁷³. Gidney, P. M.; Gillard, R. D.; Heaton, B. T. *J. Chem. Soc. Dalton Trans.* 1973, 2, 132–4.
- ⁴⁷⁴. Kunkely, H.; Vogler, A. *Inorg. Chim. Acta* 2001, 319, 183–6.
- ⁴⁷⁵. Long, E. C.; Barton, J. K. *Acc. Chem. Res.* 1990, 23, 271–3.
- ⁴⁷⁶. Norden, B. *Febs Letters*, 1978, 94, 204–6.
- ⁴⁷⁷. Wang, P.; Leung, C.-H.; Ma, D.-L.; Lu, W.; Che, C.-M. *Chem. Asian J.* 2010, 5, 2271–80.
- ⁴⁷⁸. Arjmand, F.; Azis, M. *Eur. J. Med. Chem.* 2009, 44, 834–44.
- ⁴⁷⁹. Mahadevan, S.; Indira, S.; Palaniandavar, M. *Proc. Ind. Acad. Sci.* 1994, 106, 765–6.

APPENDIX A

A1 – Crystallographic data tables for L1

Table A1-1: Crystal data and structure refinement for L1.

Table A1-2: Atomic coordinates ($\times 10^4$) and equivalent isotropic displacement parameters ($\text{\AA}^2 \times 10^3$) for L1. $U(\text{eq})$ is defined as one third of the trace of the orthogonalised U_{ij} tensor.

Table A1-3: IUCR CIF check report for L1.

A2 – Crystallographic data tables for L4

Table A2-1: Crystal data and structure refinement for L4.

Table A2-2: Atomic coordinates ($\times 10^4$) and equivalent isotropic displacement parameters ($\text{\AA}^2 \times 10^3$) for L4. $U(\text{eq})$ is defined as one third of the trace of the orthogonalised U_{ij} tensor.

Table A2-3: IUCR CIF check report for L4.

A3 – Crystallographic data tables for L5

Table A3-1: Crystal data and structure refinement for L5.

Table A3-2: Atomic coordinates ($\times 10^4$) and equivalent isotropic displacement parameters ($\text{\AA}^2 \times 10^3$) for L5. $U(\text{eq})$ is defined as one third of the trace of the orthogonalised U_{ij} tensor.

Table A3-3: IUCR CIF check report for L5.

A4 – Crystallographic data tables for L2h

Table A4-1: Crystal data and structure refinement for L2h.

Table A4-2: Atomic coordinates ($\times 10^4$) and equivalent isotropic displacement parameters ($\text{\AA}^2 \times 10^3$) for L2h. $U(\text{eq})$ is defined as one third of the trace of the orthogonalised U_{ij} tensor.

Table A4-3: IUCR CIF check report for L2h.

A5 – Crystallographic data tables for L1bh

Table A5-1: Crystal data and structure refinement for **L1bh**.

Table A5-2: Atomic coordinates ($\times 10^4$) and equivalent isotropic displacement parameters ($\text{\AA}^2 \times 10^3$) for **L1bh**. $U(\text{eq})$ is defined as one third of the trace of the orthogonalised U_{ij} tensor.

Table A5-3: IUCR CIF check report for **L1bh**.

A6 – Crystallographic data tables for L2bh

Table A6-1: Crystal data and structure refinement for **L2bh**.

Table A6-2: Atomic coordinates ($\times 10^4$) and equivalent isotropic displacement parameters ($\text{\AA}^2 \times 10^3$) for **L2bh**. $U(\text{eq})$ is defined as one third of the trace of the orthogonalised U_{ij} tensor.

Table A6-3: IUCR CIF check report for **L2bh**.

A7 – Crystallographic data tables for L4b

Table A7-1: Crystal data and structure refinement for **L4b**.

Table A7-2: Atomic coordinates ($\times 10^4$) and equivalent isotropic displacement parameters ($\text{\AA}^2 \times 10^3$) for **L4b**. $U(\text{eq})$ is defined as one third of the trace of the orthogonalised U_{ij} tensor.

Table A7-3: IUCR CIF check report for **L4b**.

A8 – Crystallographic data tables for L4bh

Table A8-1: Crystal data and structure refinement for **L4bh**.

Table A8-2: Atomic coordinates ($\times 10^4$) and equivalent isotropic displacement parameters ($\text{\AA}^2 \times 10^3$) for **L4bh**. $U(\text{eq})$ is defined as one third of the trace of the orthogonalised U_{ij} tensor.

Table A8-3: IUCR CIF check report for **L4bh**.

A1 – Crystallographic data tables for L1

Table A1-1: Crystal data and structure refinement for L1.

Identification code	rs_l1	
Empirical formula	C ₁₄ H ₁₄ N ₄	
Formula weight	238.29 amu	
Temperature	102(2) K	
Wavelength	0.71073 Å	
Crystal system	Monoclinic	
Space group	C2/c	
Unit cell dimensions	$a = 18.9472(19)$ Å	$\alpha = 90^\circ$.
	$b = 5.8207(4)$ Å	$\beta = 121.851(15)^\circ$.
	$c = 13.0548(15)$ Å	$\gamma = 90^\circ$.
Volume	1223.0(2) Å ³	
Z	4	
Density (calculated)	1.294 Mg/m ³	
Absorption coefficient	0.081 mm ⁻¹	
F(000)	504	
Crystal size	0.50 x 0.40 x 0.20 mm ³	
Theta range for data collection	3.18 to 28.66°.	
Index ranges	$-25 \leq h \leq 4$	
	$-6 \leq k \leq 7$	
	$-17 \leq l \leq 17$	
Reflections collected	2163	
Independent reflections	1374 [$R_{\text{int}} = 0.0187$]	
Completeness to theta = 25.00°	99.9 %	
Max. and min. transmission	0.9840 and 0.9605	
Refinement method	Full-matrix least-squares on F^2	
Data / restraints / parameters	1374 / 0 / 110	
Goodness-of-fit on F^2	1.064	
Final R indices [$I > 2 \sigma(I)$]	$R_1 = 0.0461$, $wR_2 = 0.1188$	
R indices (all data)	$R_1 = 0.0570$, $wR_2 = 0.1253$	
Largest diff. peak and hole	0.184 and -0.260 e Å ⁻³	

Table A1-2: Atomic coordinates ($\times 10^4$) and equivalent isotropic displacement parameters ($\text{\AA}^2 \times 10^3$) for **L1**. $U(\text{eq})$ is defined as one third of the trace of the orthogonalised U_{ij} tensor.

	x	y	z	$U(\text{eq})$
C(1)	7089(1)	-1876(2)	1028(1)	32(1)
C(2)	6712(1)	-2180(2)	1686(1)	35(1)
C(3)	6134(1)	-580(2)	1567(1)	35(1)
C(4)	5948(1)	1264(2)	797(1)	30(1)
C(5)	6350(1)	1425(2)	159(1)	27(1)
C(6)	6169(1)	3299(2)	-706(1)	28(1)
C(7)	5429(1)	6397(2)	-1929(1)	31(1)
N(1)	6921(1)	-109(2)	278(1)	30(1)
N(2)	5522(1)	4527(2)	-1125(1)	30(1)

Table A1-3: IUCR CIF check report for L1.**IUCR CcheckCIF/PLATON (standard)**

No syntax errors found.

Datablock: rs_I1

Bond precision:	C-C = 0.0019 A	Wavelength=0.71073
Cell:	a=18.9472(19) b=5.8207(4) c=13.0548(15)	
	alpha=90 beta=121.851(15) gamma=90	
Temperature:	102 K	
	Calculated	Reported
Volume	1223.0(3)	1223.0(2)
Space group	C 2/c	C 2/c
Hall group	-C 2yc	-C 2yc
Moiety formula	C14 H14 N4	C14 H14 N4
Sum formula	C14 H14 N4	C14 H14 N4
Mr	238.29	238.29
Dx,g cm-3	1.294	1.294
Z	4	4
Mu (mm-1)	0.081	0.081
F000	504.0	504.0
F000'	504.15	
h,k,lmax	25,7,17	25,7,17
Nref	1577	1374
Tmin,Tmax	0.962,0.984	0.961,0.984
Tmin'	0.960	
Correction method=	MULTI-SCAN	
Data completeness=	0.871	Theta(max)= 28.660
R(reflections)=	0.0461(1095)	wR2(reflections)= 0.1253(1374)
S =	1.064	Npar= 110

The following ALERTS were generated. Each ALERT has the format

test-name_ALERT_alert-type_alert-level.

Click on the hyperlinks for more details of the test.

Alert level C

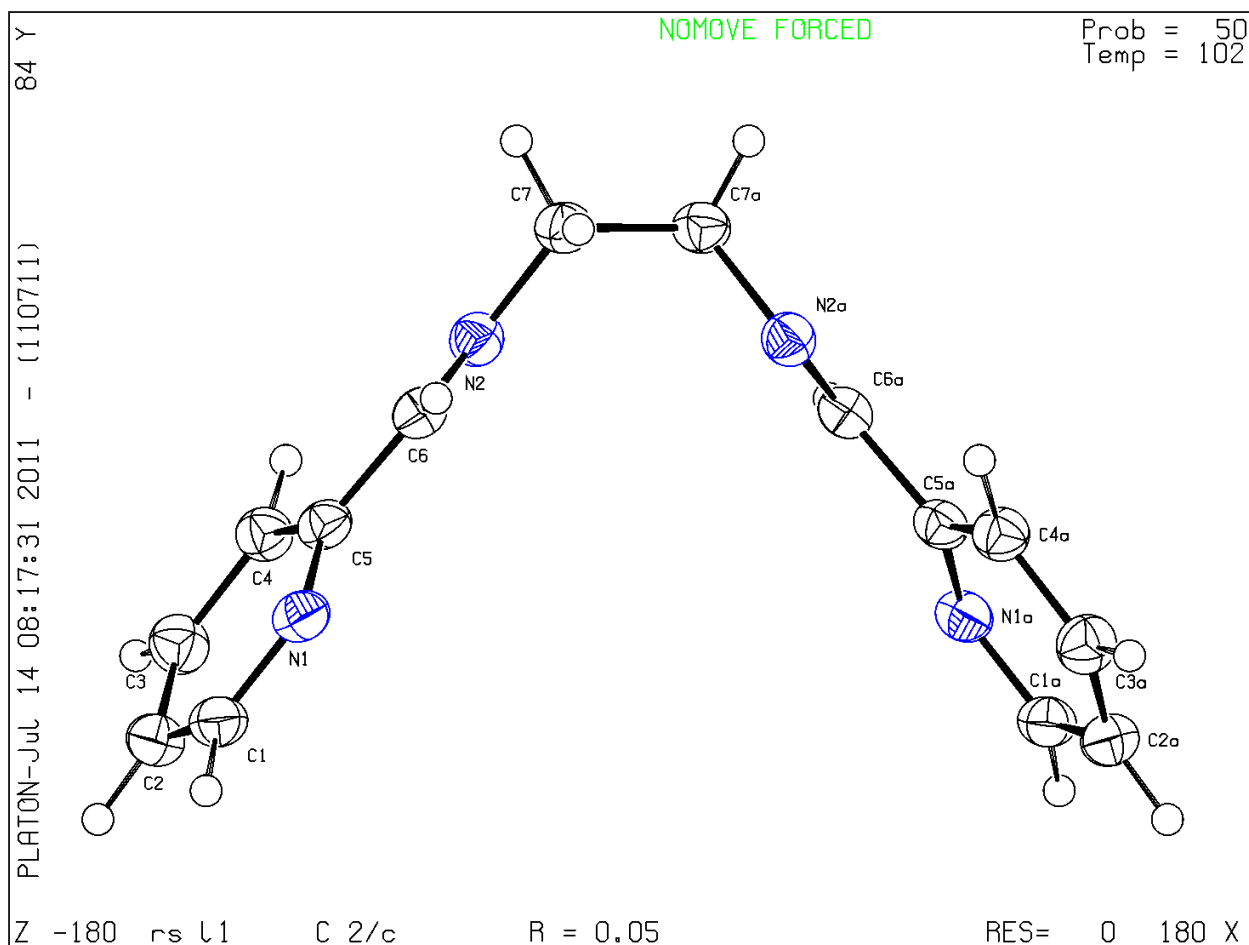
[PLAT790_ALERT_4_C](#) Centre of Gravity not Within Unit Cell: Resd.

Alert level G

PLAT005_ALERT_5_G No _iucr_refine_instructions_details in CIF ?

PLATON version of 11/07/2011; check.def file version of 04/07/2011

Datablock rs_l1 - ellipsoid plot



A2 – Crystallographic data tables for L4

Table A2-1: Crystal data and structure refinement for L4.

Identification code	rs_l4	
Empirical formula	C ₁₇ H ₂₀ N ₄	
Formula weight	280.37 amu	
Temperature	100(2) K	
Wavelength	0.71073 Å	
Crystal system	Triclinic	
Space group	$P\bar{1}$	
Unit cell dimensions	$a = 5.8140(14)$ Å	$\alpha = 101.812(2)^\circ$.
	$b = 11.526(3)$ Å	$\beta = 97.454(3)^\circ$.
	$c = 12.033(3)$ Å	$\gamma = 93.603(3)^\circ$.
Volume	779.3(3) Å ³	
Z	2	
Density (calculated)	1.195 Mg/m ³	
Absorption coefficient	0.073 mm ⁻¹	
F(000)	300	
Crystal size	0.40 x 0.25 x 0.14 mm ³	
Theta range for data collection	2.23 to 28.63°.	
Index ranges	$-7 \leq h \leq 7$	
	$-15 \leq k \leq 14$	
	$-15 \leq l \leq 16$	
Reflections collected	8755	
Independent reflections	3641 [$R_{\text{int}} = 0.0220$]	
Completeness to theta = 25.00°	99.0 %	
Max. and min. transmission	0.9898 and 0.9712	
Refinement method	Full-matrix least-squares on F^2	
Data / restraints / parameters	3641 / 0 / 270	
Goodness-of-fit on F^2	1.060	
Final R indices [$I > 2 \sigma(I)$]	$R_1 = 0.0414$, $wR_2 = 0.1054$	
R indices (all data)	$R_1 = 0.0476$, $wR_2 = 0.1103$	
Largest diff. peak and hole	0.368 and -0.215 e Å ⁻³	

Table A2-2: Atomic coordinates ($\times 10^4$) and equivalent isotropic displacement parameters ($\text{\AA}^2 \times 10^3$) for **L4**. $U(\text{eq})$ is defined as one third of the trace of the orthogonalised U_{ij} tensor.

	x	y	z	$U(\text{eq})$
N(4)	1088(2)	4666(1)	7476(1)	21(1)
N(3)	-2450(2)	3504(1)	4804(1)	19(1)
N(2)	-3688(2)	1228(1)	1443(1)	19(1)
C(10)	-655(2)	3854(1)	5548(1)	18(1)
C(11)	-786(2)	4627(1)	6681(1)	18(1)
C(5)	-3027(2)	1605(1)	-383(1)	19(1)
C(6)	-2407(2)	1136(1)	662(1)	21(1)
C(15)	1024(2)	5320(1)	8529(1)	23(1)
C(16)	-2383(2)	873(1)	4525(1)	21(1)
C(9)	-2115(2)	2722(1)	3725(1)	18(1)
C(4)	-5079(2)	2144(1)	-572(1)	22(1)
C(8)	-3386(2)	1474(1)	3568(1)	16(1)
N(1)	-1465(2)	1479(1)	-1125(1)	26(1)
C(7)	-2920(2)	711(1)	2426(1)	19(1)
C(13)	-2742(2)	5918(1)	7992(1)	23(1)
C(12)	-2726(2)	5244(1)	6896(1)	20(1)
C(3)	-5508(3)	2604(1)	-1549(1)	27(1)
C(1)	-1946(3)	1905(1)	-2075(1)	31(1)
C(2)	-3913(3)	2479(1)	-2320(1)	29(1)
C(17)	-6005(2)	1537(1)	3564(1)	22(1)
C(14)	-838(2)	5954(1)	8826(1)	23(1)

Table A2-3: IUCR CIF check report for L4.**IUCR CheckCIF/PLATON (standard)**

No syntax errors found.

Datablock: rs_I4

Bond precision: C-C = 0.0018 A Wavelength=0.71073

Cell: a=5.8140(14) b=11.526(3) c=12.033(3)
alpha=101.812(2) beta=97.454(3) gamma=93.603(3)

Temperature: 100 K

	Calculated	Reported
Volume	779.3(3)	779.3(3)
Space group	P -1	P -1
Hall group	-P 1	-P 1
Moiety formula	C17 H20 N4	C17 H20 N4
Sum formula	C17 H20 N4	C17 H20 N4
Mr	280.37	280.37
Dx,g cm-3	1.195	1.195
Z	2	2
Mu (mm-1)	0.073	0.073
F000	300.0	300.0
F000'	300.09	
h,k,lmax	7,15,16	7,15,16
Nref	3991	3641
Tmin,Tmax	0.978,0.990	0.971,0.990
Tmin'	0.971	

Correction method= MULTI-SCAN

Data completeness= 0.912 Theta(max)= 28.630

R(reflections)= 0.0414(3157) wR2(reflections)= 0.1103(3641)

S = 1.060 Npar= 270

The following ALERTS were generated. Each ALERT has the format
test-name_ALERT_alert-type_alert-level.

Alert level C

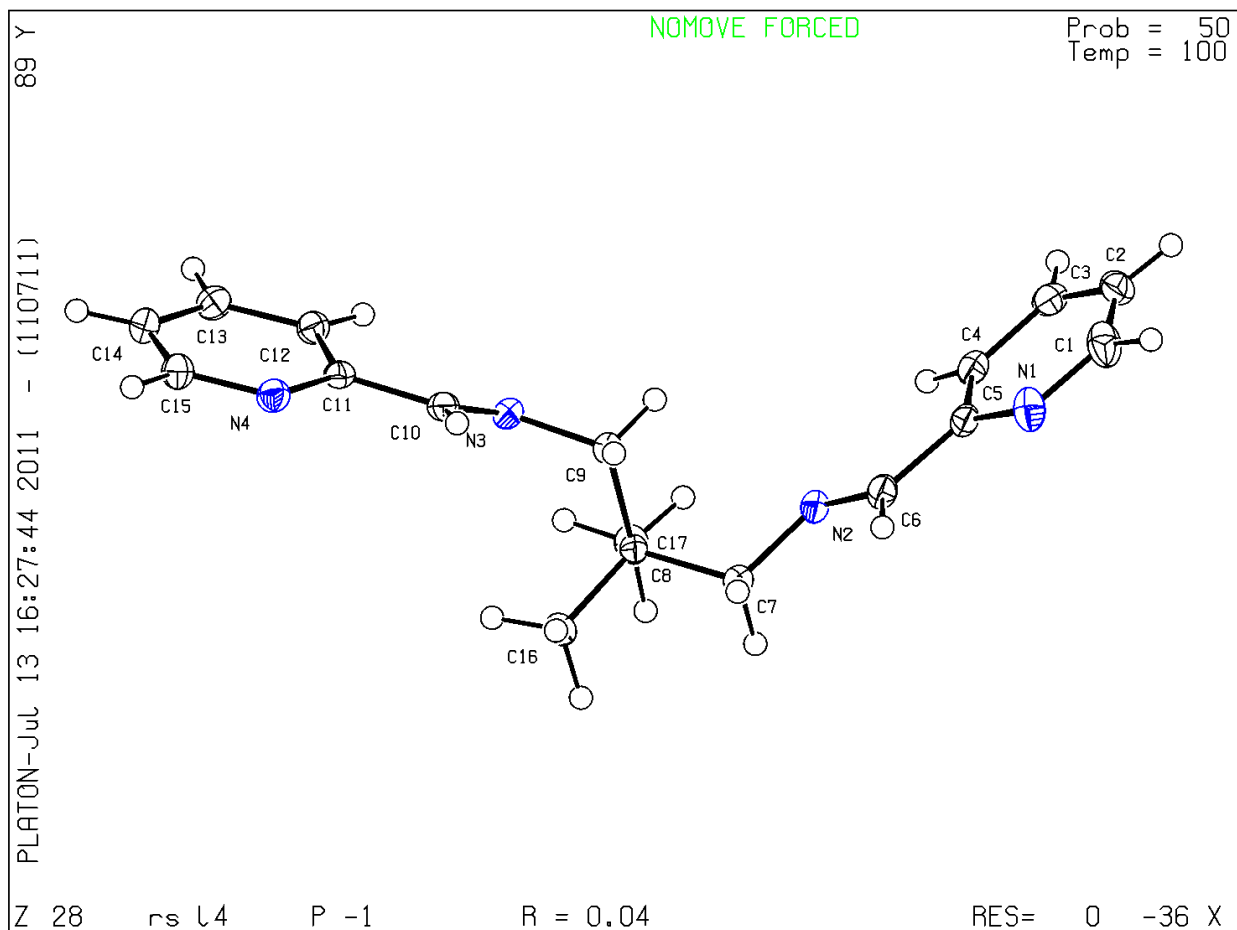
PLAT790_ALERT_4_C Centre of Gravity not Within Unit Cell: Resd

Alert level G

PLAT005_ALERT_5_G No _iucr_refine_instructions_details in CIF ?

PLATON version of 11/07/2011; check.def file version of 04/07/2011

Datablock rs_l4 - ellipsoid plot



A3 – Crystallographic data tables for L5

Table A3-1: Crystal data and structure refinement for L5.

Identification code	rs_I5	
Empirical formula	C ₁₈ H ₂₀ N ₄	
Formula weight	292.38 amu	
Temperature	102(2) K	
Wavelength	0.71073 Å	
Crystal system	Monoclinic	
Space group	<i>P</i> 2 ₁ / <i>n</i>	
Unit cell dimensions	<i>a</i> = 10.8006(6) Å	$\alpha = 90^\circ$.
	<i>b</i> = 9.7411(5) Å	$\beta = 96.412(5)^\circ$.
	<i>c</i> = 15.4012(8) Å	$\gamma = 90^\circ$.
Volume	1610.22(15) Å ³	
<i>Z</i>	4	
Density (calculated)	1.206 Mg/m ³	
Absorption coefficient	0.074 mm ⁻¹	
F(000)	624	
Crystal size	0.55 x 0.40 x 0.40 mm ³	
Theta range for data collection	3.03 to 28.67°.	
Index ranges	-14 ≤ <i>h</i> ≤ 11	
	-13 ≤ <i>k</i> ≤ 10	
	-12 ≤ <i>l</i> ≤ 20	
Reflections collected	6230	
Independent reflections	3607 [<i>R</i> _{int} = 0.0299]	
Completeness to theta = 25.00°	99.8 %	
Max. and min. transmission	0.9710 and 0.9604	
Refinement method	Full-matrix least-squares on <i>F</i> ²	
Data / restraints / parameters	3607 / 0 / 279	
Goodness-of-fit on <i>F</i> ²	0.949	
Final <i>R</i> indices [<i>I</i> > 2 σ (<i>I</i>)]	<i>R</i> ₁ = 0.0430, <i>wR</i> ₂ = 0.1034	
<i>R</i> indices (all data)	<i>R</i> ₁ = 0.0593, <i>wR</i> ₂ = 0.1086	
Largest diff. peak and hole	0.170 and -0.279 e Å ⁻³	

Table A3-2: Atomic coordinates ($\times 10^4$) and equivalent isotropic displacement parameters ($\text{\AA}^2 \times 10^3$) for **L5**. $U(\text{eq})$ is defined as one third of the trace of the orthogonalised U_{ij} tensor.

	x	y	z	U(eq)
C(1)	3654(1)	2685(1)	1829(1)	33(1)
C(2)	3438(1)	2620(1)	929(1)	32(1)
C(3)	3688(1)	1406(2)	525(1)	35(1)
C(4)	4134(1)	303(2)	1027(1)	32(1)
C(5)	4307(1)	449(1)	1931(1)	25(1)
C(6)	4755(1)	-674(1)	2527(1)	25(1)
C(7)	5481(1)	-2828(1)	2968(1)	26(1)
C(8)	4436(1)	-3877(1)	3008(1)	29(1)
C(9)	4768(1)	-4897(2)	3749(1)	34(1)
C(10)	6009(1)	-5611(1)	3663(1)	32(1)
C(11)	7041(1)	-4559(1)	3586(1)	30(1)
C(12)	6706(1)	-3547(1)	2829(1)	26(1)
C(13)	7474(1)	-4347(1)	1565(1)	23(1)
C(14)	7436(1)	-5165(1)	758(1)	22(1)
C(15)	6354(1)	-5830(1)	403(1)	24(1)
C(16)	6356(1)	-6520(1)	-379(1)	27(1)
C(17)	7455(1)	-6572(1)	-768(1)	29(1)
C(18)	8501(1)	-5921(1)	-358(1)	28(1)
N(1)	4080(1)	1636(1)	2332(1)	29(1)
N(2)	5125(1)	-1828(1)	2272(1)	28(1)
N(3)	6562(1)	-4321(1)	2014(1)	24(1)
N(4)	8506(1)	-5204(1)	384(1)	26(1)

Table A3-3: IUCR CIF check report for L5.**IUCR CcheckCIF/PLATON (standard)**

No syntax errors found.

Datablock: rs_I5

Bond precision: C-C = 0.0019 A Wavelength=0.71073

Cell: a=10.8006(6) b=9.7411(5) c=15.4012(8)

alpha=90 beta=96.412(5) gamma=90

Temperature: 102 K

	Calculated	Reported
Volume	1610.22(15)	1610.22(15)
Space group	P 21/n	P 21/n
Hall group	-P 2yn	-P 2yn
Moiety formula	C18 H20 N4	C18 H20 N4
Sum formula	C18 H20 N4	C18 H20 N4
Mr	292.38	292.38
Dx,g cm-3	1.206	1.206
Z	4	4
Mu (mm-1)	0.074	0.074
F000	624.0	624.0
F000'	624.19	
h,k,lmax	14,13,20	14,13,20
Nref	4149	3607
Tmin,Tmax	0.965,0.971	0.960,0.971
Tmin'	0.960	

Correction method= MULTI-SCAN

Data completeness= 0.869 Theta(max)= 28.670

R(reflections)= 0.0430(2637) wR2(reflections)= 0.1086(3607)

S = 0.949 Npar= 279

The following ALERTS were generated. Each ALERT has the format

test-name_ALERT_alert-type_alert-level.**● Alert level C**

PLAT045_ALERT_1_C Calculated and Reported Z Differ by 0.80 Ratio

PLAT790_ALERT_4_C Centre of Gravity not Within Unit Cell: Resd. #1

● Alert level G

FORMU01_ALERT_1_G There is a discrepancy between the atom counts in the
_chemical_formula_sum and _chemical_formula_moiety.

PLAT005_ALERT_5_G No _iucr_refine_instructions_details in CIF ?

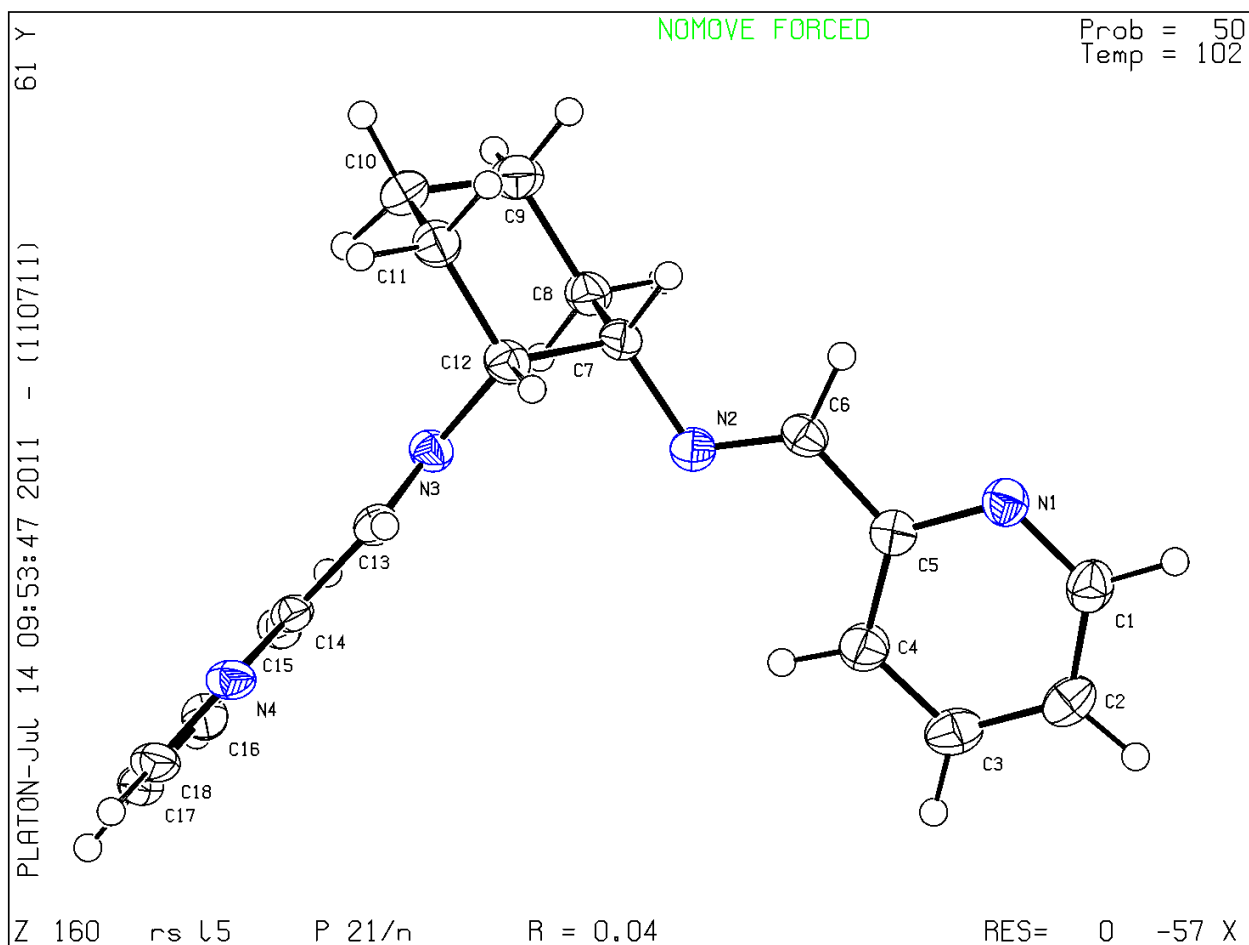
PLAT128_ALERT_4_G Alternate Setting of Space-group P21/c P21/n

PLAT793_ALERT_4_G The Model has Chirality at C7 (Verify) S

PLAT793_ALERT_4_G The Model has Chirality at C12 (Verify) R

PLATON version of 11/07/2011; check.def file version of 04/07/2011

Datablock rs_l5 - ellipsoid plot



A4 – Crystallographic data tables for L2h

Table A4-1: Crystal data and structure refinement for L2h.

Identification code	rs_l2	
Empirical formula	C ₁₈ H ₂₆ Cl ₂ N ₆ O ₁	
Formula weight	413.35 amu	
Temperature	100(2) K	
Wavelength	1.54184 Å	
Crystal system	Orthorhombic	
Space group	<i>Pbcn</i>	
Unit cell dimensions	$a = 14.8632(4)$ Å	$\alpha = 90^\circ$.
	$b = 7.6289(2)$ Å	$\beta = 90^\circ$.
	$c = 17.8066(5)$ Å	$\gamma = 90^\circ$.
Volume	2019.09(9) Å ³	
Z	8	
Density (calculated)	1.360 Mg/m ³	
Absorption coefficient	3.062 mm ⁻¹	
F(000)	872	
Crystal size	0.30 x 0.20 x 0.10 mm ³	
Theta range for data collection	4.97 to 67.21°.	
Index ranges	$-17 \leq h \leq 16$	
	$-8 \leq k \leq 9$	
	$-19 \leq l \leq 21$	
Reflections collected	5131	
Independent reflections	1788 [$R_{\text{int}} = 0.0271$]	
Completeness to theta = 67.21°	99.0 %	
Absorption correction	Analytical	
Max. and min. transmission	0.926 and 0.805	
Refinement method	Full-matrix least-squares on F^2	
Data / restraints / parameters	1788 / 0 / 135	
Goodness-of-fit on F^2	1.064	
Final R indices [$I > 2 \sigma(I)$]	$R_1 = 0.0350$, $wR_2 = 0.0948$	
R indices (all data)	$R_1 = 0.0380$, $wR_2 = 0.0970$	
Largest diff. peak and hole	0.221 and -0.318 e Å ⁻³	

Table A4-2: Atomic coordinates ($\times 10^4$) and equivalent isotropic displacement parameters ($\text{\AA}^2 \times 10^3$) for **L2h**. $U(\text{eq})$ is defined as one third of the trace of the orthogonalised U^{ij} tensor.

	x	y	z	$U(\text{eq})$
C(1)	1528(1)	6922(2)	-83(1)	20(1)
C(2)	1921(1)	6169(2)	-784(1)	20(1)
C(3)	1391(1)	5759(2)	-1397(1)	27(1)
C(4)	1806(1)	5110(2)	-2037(1)	31(1)
C(5)	2722(1)	4871(2)	-2039(1)	26(1)
C(6)	3200(1)	5318(2)	-1401(1)	24(1)
C(7)	1757(1)	7988(2)	1192(1)	26(1)
C(8)	787(1)	7478(2)	1319(1)	26(1)
C(9)	240(1)	7977(2)	630(1)	26(1)
N(1)	663(1)	7239(2)	-43(1)	23(1)
N(2)	2069(1)	7260(2)	480(1)	22(1)
N(3)	2818(1)	5962(2)	-776(1)	24(1)
O(1)	5000	5644(2)	2500	35(1)
Cl(1)	4050(1)	7659(1)	1159(1)	26(1)

Table A4-3: IUCR CIF check report for L2h.**IUCR CcheckCIF/PLATON (standard)**

No syntax errors found.

Datablock: rs_l2h

Bond precision:	C-C = 0.0020 Å	Wavelength=1.54184
Cell:	a=14.8632(4) b=7.6289(2) c=17.8066(5)	
	alpha=90 beta=90 gamma=90	
Temperature:	100 K	
	Calculated	Reported
Volume	2019.09(9)	2019.09(9)
Space group	P b c n	P b c n
Hall group	-P 2n 2ab	-P 2n 2ab
Moiety formula	2(C ₉ H ₁₂ N ₃), H ₂ O, 2(Cl)	C ₇₂ H ₁₀₄ N ₂₄ O ₄ Cl ₈
Sum formula	C ₁₈ H ₂₆ Cl ₂ N ₆ O	C ₁₈ H ₂₆ Cl ₂ N ₆ O
Mr	413.35	413.35
D _x , g cm ⁻³	1.360	1.360
Z	4	8
Mu (mm ⁻¹)	3.062	3.062
F ₀₀₀	872.0	872.0
F ₀₀₀ '	876.99	
h,k,l _{max}	17,9,21	17,9,21
N _{ref}	1805	1788
T _{min} ,T _{max}	0.504,0.736	0.805,0.926
T _{min} '	0.380	
Correction method=	ANALYTICAL	
Data completeness=	0.991	Theta(max)= 67.210
R(reflections)=	0.0350(1604)	wR2(reflections)= 0.0970(1788)
S =	1.064	N _{par} = 135

The following ALERTS were generated. Each ALERT has the format

test-name_ALERT_alert-type_alert-level.**● Alert level C**

ABSTY02_ALERT_1_C An _exptl_absorpt_correction_type has been given without a literature citation.

PLAT042_ALERT_1_C Calc. and Reported MoietyFormula Strings Differ ?

PLAT045_ALERT_1_C Calculated and Reported Z Differ by 0.50 Ratio

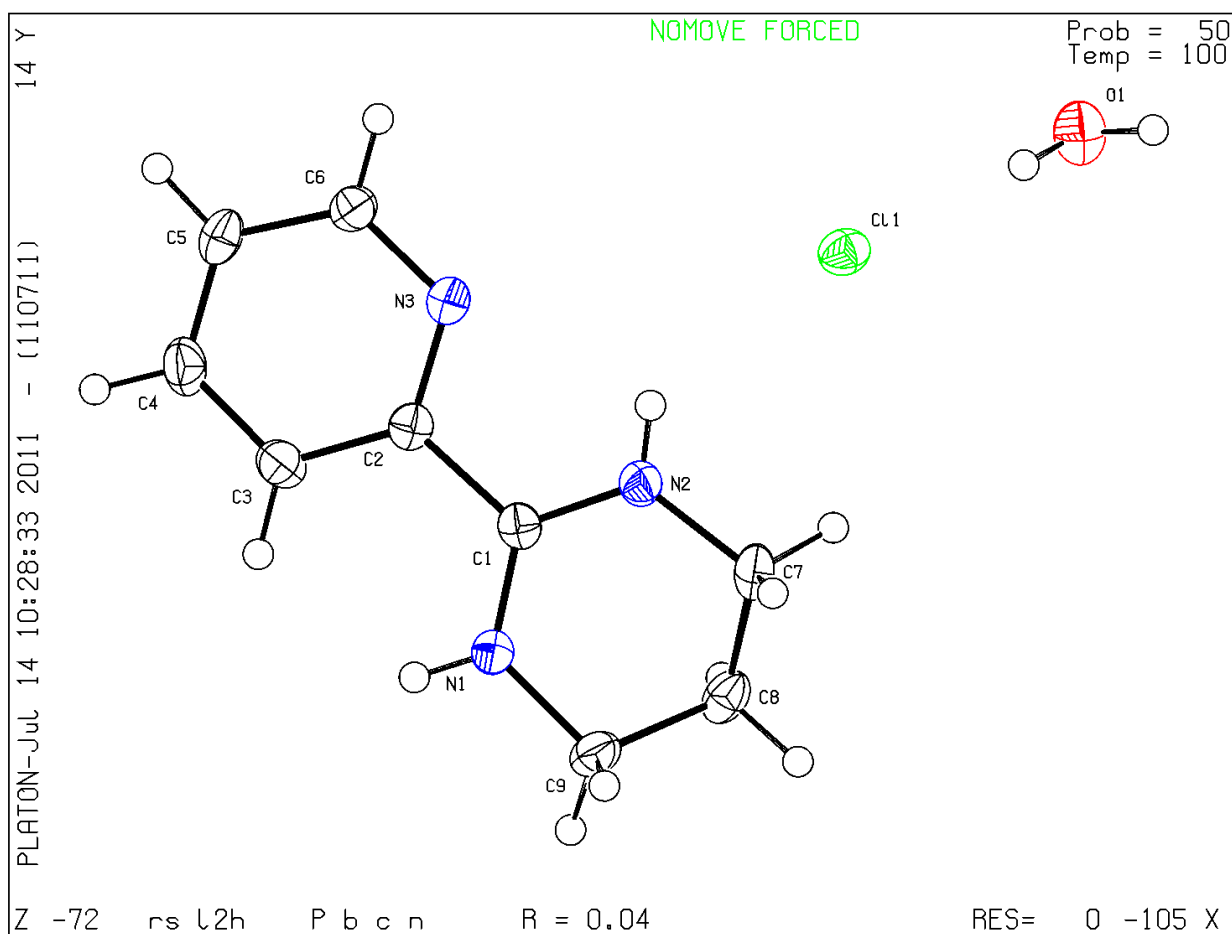
● Alert level G

FORMU01_ALERT_1_G There is a discrepancy between the atom counts in the
_chemical_formula_sum and _chemical_formula_moiety.

PLAT005_ALERT_5_G No _iucr_refine_instructions_details in CIF ?

PLATON version of 11/07/2011; check.def file version of 04/07/2011

Datablock rs_l2h - ellipsoid plot



A5 – Crystallographic data tables for L1bh

Table A5-1: Crystal data and structure refinement for L1bh.

Identification code	rs_l1b	
Empirical formula	C ₁₄ H ₁₅ N ₃	
Formula weight	225.29 amu	
Temperature	296(2) K	
Wavelength	0.71073 Å	
Crystal system	Monoclinic	
Space group	C2/c	
Unit cell dimensions	$a = 16.727(2)$ Å	$\alpha = 90^\circ$.
	$b = 5.8039(5)$ Å	$\beta = 95.320(7)^\circ$.
	$c = 24.4882(17)$ Å	$\gamma = 90^\circ$.
Volume	2367.1(4) Å ³	
Z	8	
Density (calculated)	1.264 Mg/m ³	
Absorption coefficient	0.077 mm ⁻¹	
F(000)	960	
Crystal size	0.55 x 0.45 x 0.35 mm ³	
Theta range for data collection	3.09 to 28.74°.	
Index ranges	$-21 \leq h \leq 22$	
	$-7 \leq k \leq 7$	
	$-32 \leq l \leq 32$	
Reflections collected	19111	
Independent reflections	2872 [$R_{\text{int}} = 0.0426$]	
Completeness to theta = 25.00°	99.9 %	
Max. and min. transmission	0.9734 and 0.9586	
Refinement method	Full-matrix least-squares on F^2	
Data / restraints / parameters	2872 / 0 / 162	
Goodness-of-fit on F^2	1.071	
Final R indices [$I > 2 \sigma(I)$]	$R_1 = 0.0467$, $wR_2 = 0.1158$	
R indices (all data)	$R_1 = 0.0555$, $wR_2 = 0.1192$	
Largest diff. peak and hole	0.207 and -0.192 e Å ⁻³	

Table A5-2: Atomic coordinates ($\times 10^4$) and equivalent isotropic displacement parameters ($\text{\AA}^2 \times 10^3$) for **L1bh**. $U(\text{eq})$ is defined as one third of the trace of the orthogonalised U_{ij} tensor.

	x	y	z	U(eq)
C(1)	8321(1)	4077(3)	304(1)	46(1)
C(2)	8760(1)	2470(3)	46(1)	51(1)
C(3)	8913(1)	382(3)	304(1)	50(1)
C(4)	8613(1)	-28(3)	804(1)	39(1)
C(5)	8183(1)	1702(2)	1036(1)	29(1)
C(6)	7812(1)	1364(2)	1584(1)	29(1)
C(7)	8953(1)	687(3)	2163(1)	49(1)
C(8)	8695(1)	3127(4)	2265(1)	62(1)
C(9)	6930(1)	734(2)	1450(1)	28(1)
C(10)	6724(1)	-1372(2)	1201(1)	37(1)
C(11)	5921(1)	-1951(3)	1078(1)	45(1)
C(12)	5321(1)	-447(3)	1196(1)	49(1)
C(13)	5525(1)	1648(3)	1432(1)	49(1)
C(14)	6325(1)	2248(2)	1558(1)	37(1)
N(1)	8039(1)	3750(2)	793(1)	37(1)
N(2)	8239(1)	-487(2)	1898(1)	39(1)
N(3)	7920(1)	3429(2)	1937(1)	39(1)

Table A5-3: IUCR CIF check report for **Libh**.**IUCR CcheckCIF/PLATON (standard)**

No syntax errors found.

Datablock: rs_I1bh

Bond precision:	C-C = 0.0020 A	Wavelength=0.71073
Cell:	a=16.727(2) b=5.8039(5) c=24.4882(17)	
	alpha=90 beta=95.320(7) gamma=90	
Temperature:	296 K	
	Calculated	Reported
Volume	2367.1(4)	2367.1(4)
Space group	C 2/c	C 2/c
Hall group	-C 2yc	-C 2yc
Moiety formula	C14 H15 N3	C112H120N24
Sum formula	C14 H15 N3	C14 H15 N3
Mr	225.29	225.29
Dx,g cm-3	1.264	1.264
Z	8	8
Mu (mm-1)	0.077	0.077
F000	960.0	960.0
F000'	960.29	
h,k,lmax	22,7,33	22,7,32
Nref	3063	2872
Tmin,Tmax	0.959,0.973	0.959,0.973
Tmin'	0.959	
Correction method=	MULTI-SCAN	
Data completeness=	0.938	Theta(max)= 28.740
R(reflections)=	0.0467(2389)	wR2(reflections)= 0.1192(2872)
S =	1.071	Npar= 162

The following ALERTS were generated. Each ALERT has the format

test-name_ALERT_alert-type_alert-level.**● Alert level C**

PLAT042_ALERT_1_C Calc. and Reported MoietyFormula Strings Differ ?

PLAT045_ALERT_1_C Calculated and Reported Z Differ by 1.60 Ratio

PLAT241_ALERT_2_C Check High Ueq as Compared to Neighbors for C8

PLAT420_ALERT_2_C D-H Without Acceptor N2 - H2A ... ?

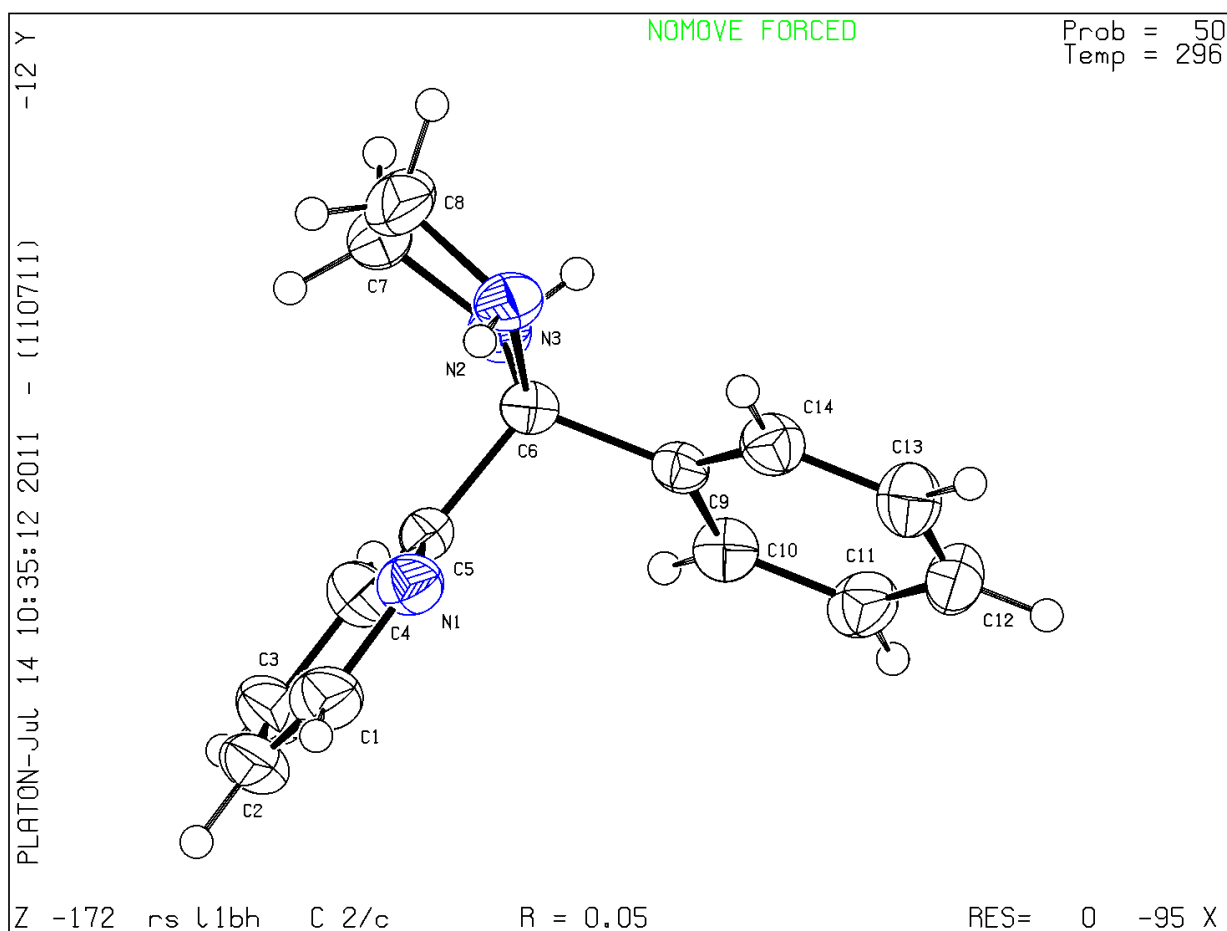
● Alert level G

FORMU01_ALERT_1_G There is a discrepancy between the atom counts in the
_chemical_formula_sum and _chemical_formula_moiety.

PLAT005_ALERT_5_G No _iucr_refine_instructions_details in CIF ?

PLATON version of 11/07/2011; check.def file version of 04/07/2011

Datablock rs_l1bh - ellipsoid plot



A6 – Crystallographic data tables for L2bh

Table A6-1: Crystal data and structure refinement for L2bh.

Identification code	rs_l2bh	
Empirical formula	C ₁₅ H ₁₇ N ₃	
Formula weight	239.32 amu	
Temperature	296(2) K	
Wavelength	0.71073 Å	
Crystal system	Triclinic	
Space group	P $\bar{1}$	
Unit cell dimensions	$a = 8.2380(9)$ Å	$\alpha = 97.310(7)^\circ$.
	$b = 9.0960(8)$ Å	$\beta = 94.450(8)^\circ$.
	$c = 9.2759(8)$ Å	$\gamma = 111.855(9)^\circ$.
Volume	633.95(10) Å ³	
Z	2	
Density (calculated)	1.254 Mg/m ³	
Absorption coefficient	0.076 mm ⁻¹	
F(000)	256	
Crystal size	0.45 x 0.35 x 0.20 mm ³	
Theta range for data collection	2.85 to 26.05°.	
Index ranges	$-10 \leq h \leq 10$	
	$-11 \leq k \leq 11$	
	$-11 \leq l \leq 11$	
Reflections collected	7440	
Independent reflections	2495 [$R_{\text{int}} = 0.0624$]	
Completeness to theta = 25.00°	99.9 %	
Max. and min. transmission	0.9849 and 0.9665	
Refinement method	Full-matrix least-squares on F^2	
Data / restraints / parameters	2495 / 0 / 171	
Goodness-of-fit on F^2	0.948	
Final R indices [$I > 2 \sigma(I)$]	$R_1 = 0.0484$, $wR_2 = 0.1200$	
R indices (all data)	$R_1 = 0.0766$, $wR_2 = 0.1329$	
Largest diff. peak and hole	0.169 and -0.201 e Å ⁻³	

Table A6-2: Atomic coordinates ($\times 10^4$) and equivalent isotropic displacement parameters ($\text{\AA}^2 \times 10^3$) for **L2bh**. $U(\text{eq})$ is defined as one third of the trace of the orthogonalised U_{ij} tensor.

	x	y	z	U(eq)
C(1)	8561(2)	2849(2)	-166(2)	52(1)
C(2)	10193(2)	2966(2)	422(2)	52(1)
C(3)	10719(2)	3540(2)	1894(2)	47(1)
C(4)	9595(2)	3970(2)	2714(2)	39(1)
C(5)	7970(2)	3814(2)	2035(2)	34(1)
C(6)	6680(2)	4360(2)	2857(2)	34(1)
C(7)	6341(2)	2659(2)	4754(2)	52(1)
C(8)	4451(2)	1662(2)	4081(2)	57(1)
C(9)	4261(2)	1723(2)	2464(2)	48(1)
C(10)	7113(2)	6117(2)	2711(2)	34(1)
C(11)	8739(2)	7287(2)	3346(2)	44(1)
C(12)	9184(2)	8873(2)	3202(2)	52(1)
C(13)	8004(3)	9330(2)	2422(2)	56(1)
C(14)	6397(2)	8194(2)	1797(2)	52(1)
C(15)	5942(2)	6599(2)	1933(2)	42(1)
N(1)	7449(2)	3261(2)	605(1)	44(1)
N(2)	6996(2)	4293(2)	4417(1)	41(1)
N(3)	4835(2)	3396(2)	2242(2)	39(1)

Table A6-3: IUCR CIF check report for **L2bh**.**IUCR CcheckCIF/PLATON (standard)**

No syntax errors found.

Datablock: rs_l2bh

Bond precision:	C-C = 0.0024 Å	Wavelength=0.71073
Cell:	a=8.2380(9) b=9.0960(8) c=9.2759(8)	
	alpha=97.310(7) beta=94.450(8) gamma=111.855(9)	
Temperature:	296 K	
	Calculated	Reported
Volume	633.95(11)	633.95(10)
Space group	P -1	P -1
Hall group	-P 1	-P 1
Moiety formula	C15 H17 N3	C15 H17 N3
Sum formula	C15 H17 N3	C15 H17 N3
Mr	239.32	239.32
Dx, g cm ⁻³	1.254	1.254
Z	2	2
Mu (mm ⁻¹)	0.076	0.076
F000	256.0	256.0
F000'	256.08	
h,k,lmax	10,11,11	10,11,11
Nref	2498	2495
Tmin,Tmax	0.969,0.985	0.966,0.985
Tmin'	0.966	
Correction method=	MULTI-SCAN	
Data completeness=	0.999	Theta(max)= 26.050
R(reflections)=	0.0484(1676)	wR2(reflections)= 0.1329(2495)
S =	0.948	Npar= 171

The following ALERTS were generated. Each ALERT has the format
test-name_ALERT_alert-type_alert-level.

● Alert level C

PLAT420_ALERT_2_C D-H Without Acceptor N2 - H2A ... ?

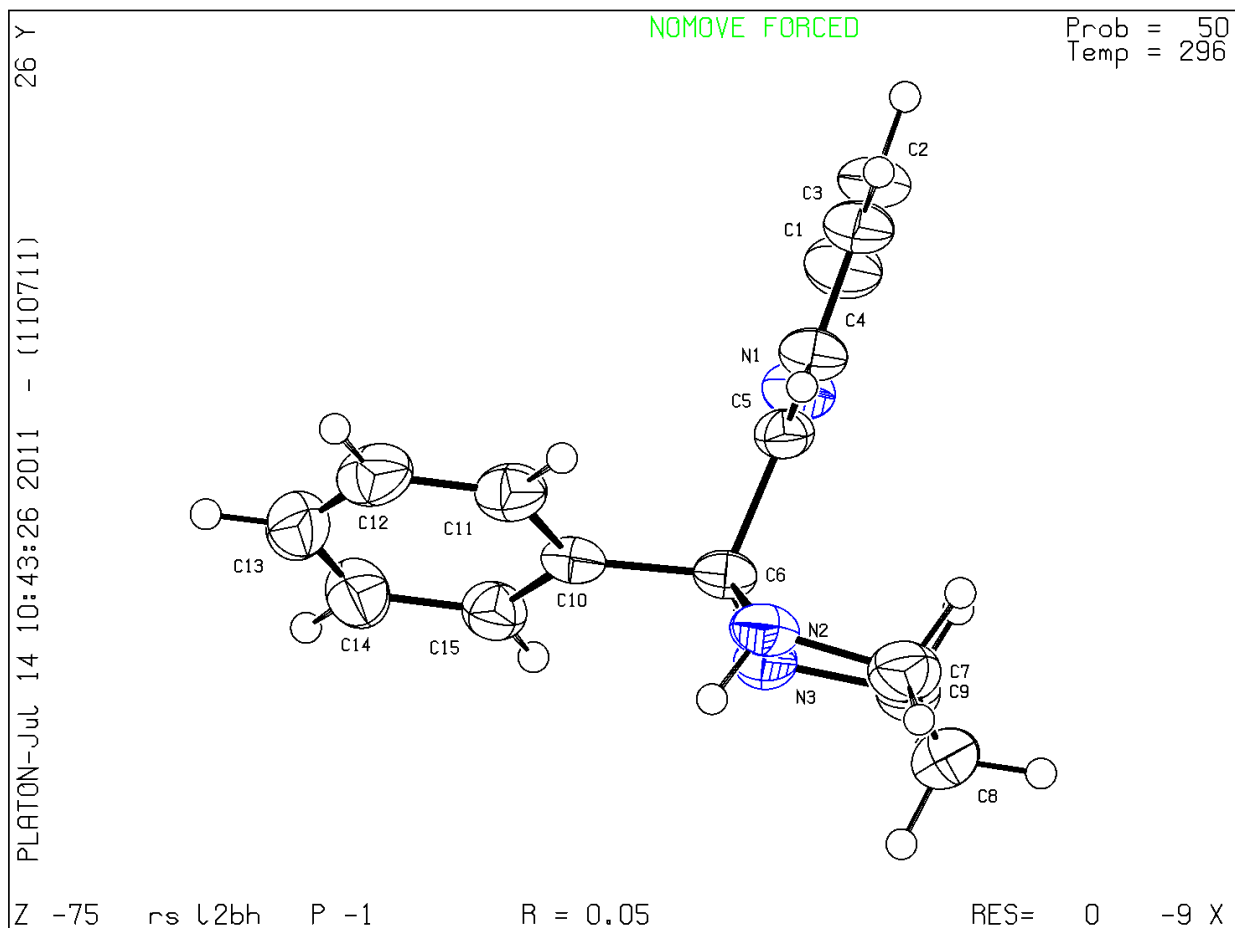
● Alert level G

PLAT005_ALERT_5_G No _iucr_refine_instructions_details in CIF ?

PLAT180_ALERT_4_G Check Cell Rounding: # of Values Ending with 0 = 4

PLATON version of 11/07/2011; check.def file version of 04/07/2011

Datablock rs_l2bh - ellipsoid plot



A7 – Crystallographic data tables for L4b

Table A7-1: Crystal data and structure refinement for L4b.

Identification code	rs_l4b	
Empirical formula	C ₂₉ H ₂₈ N ₄	
Formula weight	432.55 amu	
Temperature	100(2) K	
Wavelength	0.71073 Å	
Crystal system	Monoclinic	
Space group	<i>P</i> 2 ₁ / <i>c</i>	
Unit cell dimensions	<i>a</i> = 10.0325(15) Å	$\alpha = 90^\circ$.
	<i>b</i> = 24.790(4) Å	$\beta = 112.559(2)^\circ$.
	<i>c</i> = 10.0691(15) Å	$\gamma = 90^\circ$.
Volume	2312.7(6) Å ³	
<i>Z</i>	4	
Density (calculated)	1.242 Mg/m ³	
Absorption coefficient	0.074 mm ⁻¹	
F(000)	920	
Crystal size	0.43 x 0.30 x 0.25 mm ³	
Theta range for data collection	1.64 to 28.68°.	
Index ranges	-13 ≤ <i>h</i> ≤ 7	
	-31 ≤ <i>k</i> ≤ 32	
	-13 ≤ <i>l</i> ≤ 13	
Reflections collected	13631	
Independent reflections	5397 [<i>R</i> _{int} = 0.0299]	
Completeness to theta = 25.00°	98.7 %	
Max. and min. transmission	0.9817 and 0.9688	
Refinement method	Full-matrix least-squares on <i>F</i> ²	
Data / restraints / parameters	5397 / 0 / 300	
Goodness-of-fit on <i>F</i> ²	1.031	
Final <i>R</i> indices [<i>I</i> > 2 σ (<i>I</i>)]	<i>R</i> ₁ = 0.0539, <i>wR</i> ₂ = 0.1419	
<i>R</i> indices (all data)	<i>R</i> ₁ = 0.0663, <i>wR</i> ₂ = 0.1509	
Largest diff. peak and hole	0.573 and -0.430 e Å ⁻³	

Table A7-2: Atomic coordinates ($\times 10^4$) and equivalent isotropic displacement parameters ($\text{\AA}^2 \times 10^3$) for **L4b**. $U(\text{eq})$ is defined as one third of the trace of the orthogonalised U_{ij} tensor.

	x	y	z	U(eq)
N(1)	6497(2)	3517(1)	3167(2)	20(1)
N(2)	9311(1)	4384(1)	5144(1)	19(1)
C(1)	6541(2)	3146(1)	4065(2)	19(1)
C(13)	7756(2)	3609(1)	2796(2)	20(1)
C(23)	10616(2)	4279(1)	9012(2)	20(1)
C(16)	9202(2)	4342(1)	6363(2)	18(1)
C(8)	7807(2)	2774(1)	4763(2)	19(1)
C(14)	7941(2)	4213(1)	2535(2)	18(1)
N(4)	7306(2)	3999(1)	7065(2)	28(1)
C(2)	5262(2)	3071(1)	4461(2)	20(1)
C(28)	9305(2)	4270(1)	2210(2)	22(1)
C(15)	8064(2)	4545(1)	3866(2)	19(1)
C(9)	8803(2)	2898(1)	6098(2)	22(1)
C(22)	10507(2)	4168(1)	7629(2)	19(1)
C(27)	11628(2)	3896(1)	7416(2)	24(1)
C(24)	11835(2)	4124(1)	10178(2)	26(1)
C(29)	6640(2)	4426(1)	1258(2)	23(1)
C(17)	7848(2)	4435(1)	6646(2)	19(1)
C(11)	10140(2)	2109(1)	5997(2)	28(1)
C(7)	5212(2)	2646(1)	5335(2)	29(1)
C(26)	12834(2)	3734(1)	8589(2)	29(1)
C(20)	5385(2)	4552(1)	7182(2)	29(1)
C(19)	5969(2)	4993(1)	6768(2)	31(1)
C(18)	7210(2)	4937(1)	6487(2)	26(1)
C(25)	12941(2)	3848(1)	9979(2)	28(1)
C(3)	4131(2)	3435(1)	3979(2)	26(1)
C(12)	9100(2)	1990(1)	4666(2)	37(1)
C(4)	2966(2)	3373(1)	4376(2)	33(1)
C(6)	4033(2)	2587(1)	5720(2)	35(1)
N(3)	7924(2)	2323(1)	4030(2)	41(1)
C(21)	6068(2)	4058(1)	7306(2)	30(1)
C(10)	9974(2)	2565(1)	6711(2)	29(1)
C(5)	2908(2)	2951(1)	5247(2)	31(1)

Table A7-3: IUCR CIF check report for **L4b**.**IUCR CcheckCIF/PLATON (standard)**

No syntax errors found.

Datablock: rs_l4b

Bond precision:	C-C = 0.0027 Å	Wavelength=0.71073
Cell:	a=10.0325(15) b=24.790(4) c=10.0691(15)	
	alpha=90 beta=112.559(2) gamma=90	
Temperature:	100 K	
	Calculated	Reported
Volume	2312.6(6)	2312.7(6)
Space group	P 21/c	P 21/c
Hall group	-P 2ybc	-P 2ybc
Moiety formula	C29 H28 N4	C29 H28 N4
Sum formula	C29 H28 N4	C29 H28 N4
Mr	432.55	432.55
Dx,g cm-3	1.242	1.242
Z	4	4
Mu (mm-1)	0.074	0.074
F000	920.0	920.0
F000'	920.30	
h,k,lmax	13,33,13	13,32,13
Nref	5968	5397
Tmin,Tmax	0.974,0.982	0.969,0.982
Tmin'	0.969	
Correction method=	MULTI-SCAN	
Data completeness=	0.904	Theta(max)= 28.680
R(reflections)=	0.0539(4387)	wR2(reflections)= 0.1509(5397)
S =	1.031	Npar= 300

The following ALERTS were generated. Each ALERT has the format

test-name_ALERT_alert-type_alert-level.**● Alert level C**

DIFMX01_ALERT_2_C The maximum difference density is > 0.1*ZMAX*0.75

DIFMX02_ALERT_1_C The maximum difference density is > 0.1*ZMAX*0.75

PLAT097_ALERT_2_C Large Reported Max. (Positive) Residual Density 0.57 eA-3

PLAT230_ALERT_2_C Hirshfeld Test Diff for N3 -- C8 .. 6.5 su

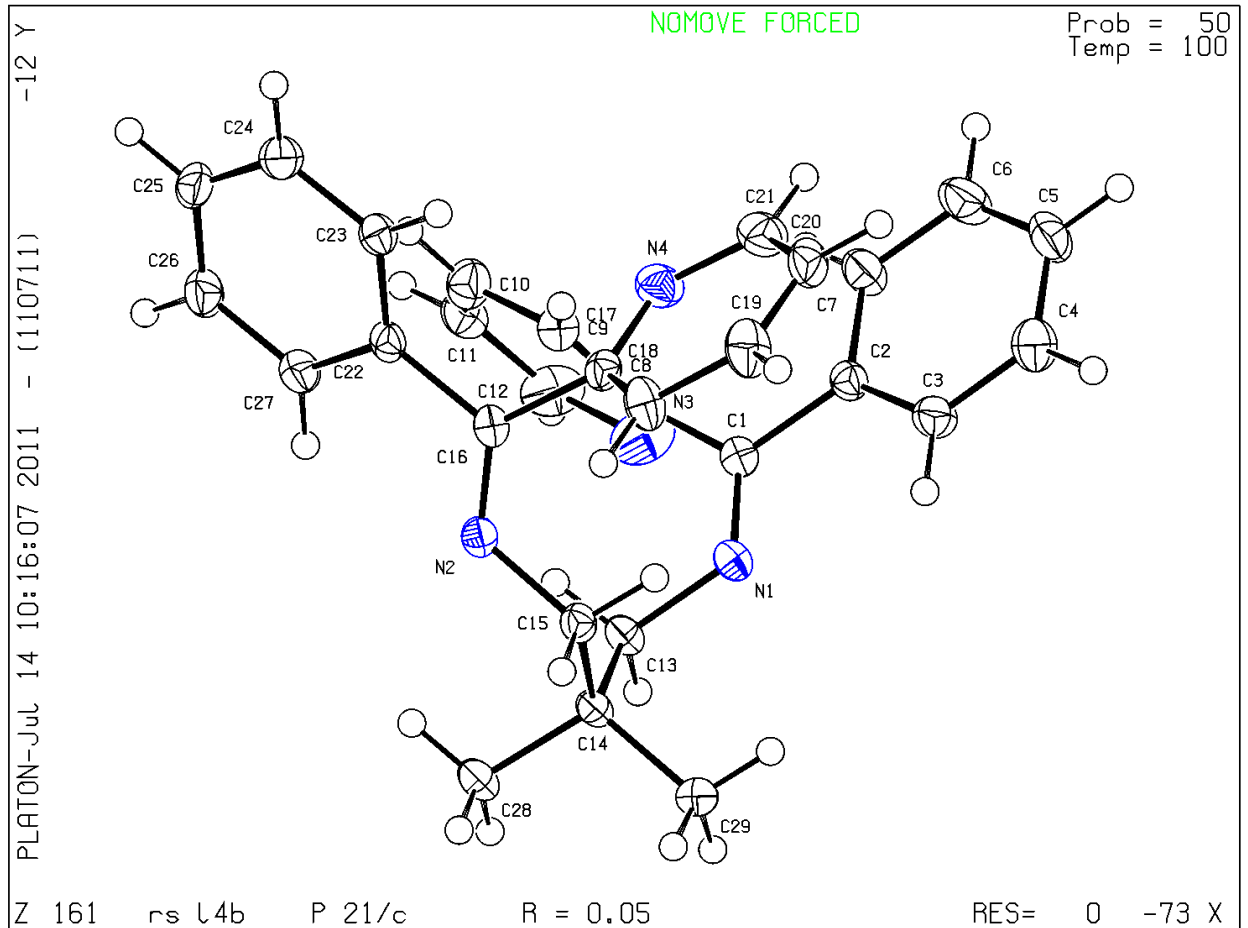
PLAT230_ALERT_2_C Hirshfeld Test Diff for C9 -- C10 .. 5.1 su

● Alert level G

PLAT005_ALERT_5_G No _iucr_refine_instructions_details in CIF ?

PLATON version of 11/07/2011; check.def file version of 04/07/2011

Datablock rs_l4b - ellipsoid plot



A8 – Crystallographic data tables for L4bh

Table A8-1: Crystal data and structure refinement for L4bh.

Identification code	rs_l4bh	
Empirical formula	C ₁₇ H ₂₁ N ₃	
Formula weight	267.37 amu	
Temperature	100(2) K	
Wavelength	0.71073 Å	
Crystal system	Monoclinic	
Space group	<i>P</i> 2 ₁ / <i>c</i>	
Unit cell dimensions	<i>a</i> = 14.7533(6) Å	$\alpha = 90^\circ$.
	<i>b</i> = 6.0380(2) Å	$\beta = 90.923(2)^\circ$.
	<i>c</i> = 16.4381(6) Å	$\gamma = 90^\circ$.
Volume	1464.12(9) Å ³	
<i>Z</i>	4	
Density (calculated)	1.213 Mg/m ³	
Absorption coefficient	0.073 mm ⁻¹	
F(000)	576	
Crystal size	0.125 x 0.08 x 0.025 mm ³	
Theta range for data collection	1.38 to 29.89°.	
Index ranges	-20 ≤ <i>h</i> ≤ 20	
	-8 ≤ <i>k</i> ≤ 8	
	-22 ≤ <i>l</i> ≤ 22	
Reflections collected	50915	
Independent reflections	4118 [<i>R</i> _{int} = 0.0887]	
Completeness to theta = 29.89°	99.5 %	
Refinement method	Full-matrix least-squares on <i>F</i> ²	
Data / restraints / parameters	4118 / 0 / 191	
Goodness-of-fit on <i>F</i> ²	1.040	
Final <i>R</i> indices [<i>I</i> > 2 σ (<i>I</i>)]	<i>R</i> ₁ = 0.0436, <i>wR</i> ₂ = 0.1152	
<i>R</i> indices (all data)	<i>R</i> ₁ = 0.0589, <i>wR</i> ₂ = 0.1216	
Largest diff. peak and hole	0.334 and -0.237 e Å ⁻³	

Table A8-2: Atomic coordinates ($\times 10^4$) and equivalent isotropic displacement parameters ($\text{\AA}^2 \times 10^3$) for **L4bh**. $U(\text{eq})$ is defined as one third of the trace of the orthogonalised U^{ij} tensor.

	x	y	z	$U(\text{eq})$
C(12)	2610(1)	7583(3)	4424(1)	19(1)
C(13)	3314(1)	4071(3)	4700(1)	20(1)
C(9)	4561(1)	4803(3)	1321(1)	19(1)
C(14)	3055(1)	6172(3)	4964(1)	19(1)
C(10)	4601(1)	1044(3)	1758(1)	19(1)
C(11)	5006(1)	2777(3)	1349(1)	20(1)
N(3)	3762(1)	5187(3)	1676(1)	16(1)
C(17)	3766(1)	1392(3)	2118(1)	16(1)
C(15)	2423(1)	6933(3)	3626(1)	16(1)
C(16)	3129(1)	3416(3)	3903(1)	17(1)
N(2)	1962(1)	5782(3)	2047(1)	14(1)
N(1)	1924(1)	2014(2)	2558(1)	14(1)
C(3)	1009(1)	3074(3)	1296(1)	16(1)
C(6)	2466(1)	4044(3)	2487(1)	12(1)
C(7)	2679(1)	4841(3)	3357(1)	13(1)
C(8)	3369(1)	3490(3)	2068(1)	13(1)
C(5)	1523(1)	1277(3)	1777(1)	15(1)
C(4)	1656(1)	5042(3)	1233(1)	15(1)
C(1)	137(1)	3748(4)	1721(1)	23(1)
C(2)	786(2)	2188(4)	447(1)	26(1)

Table A8-3: IUCR CIF check report for **L4bh**.**IUCR CcheckCIF/PLATON (standard)**

No syntax errors found.

Datablock: rs_l4bh

Bond precision:	C-C = 0.0015 A	Wavelength=0.71073
Cell:	a=14.7533(6) b=6.0380(2) c=16.4381(6)	
	alpha=90 beta=90.923(2) gamma=90	
Temperature:	100 K	
	Calculated	Reported
Volume	1464.12(9)	1464.12(9)
Space group	P 21/c	P 21/c
Hall group	-P 2ybc	-P 2ybc
Moiety formula	C17 H21 N3	C17 H21 N3
Sum formula	C17 H21 N3	C17 H21 N3
Mr	267.37	267.37
Dx,g cm-3	1.213	1.213
Z	4	4
Mu (mm-1)	0.073	0.073
F000	576.0	576.0
F000'	576.17	
h,k,lmax	20,8,23	20,8,22
Nref	4240	4118
Tmin,Tmax	0.993,0.998	
Tmin'	0.991	
Correction method=	Not given	
Data completeness=	0.971 Theta(max)= 29.890	
R(reflections)=	0.0436(3130)	wR2(reflections)= 0.1216(4118)
S =	1.040	Npar= 191

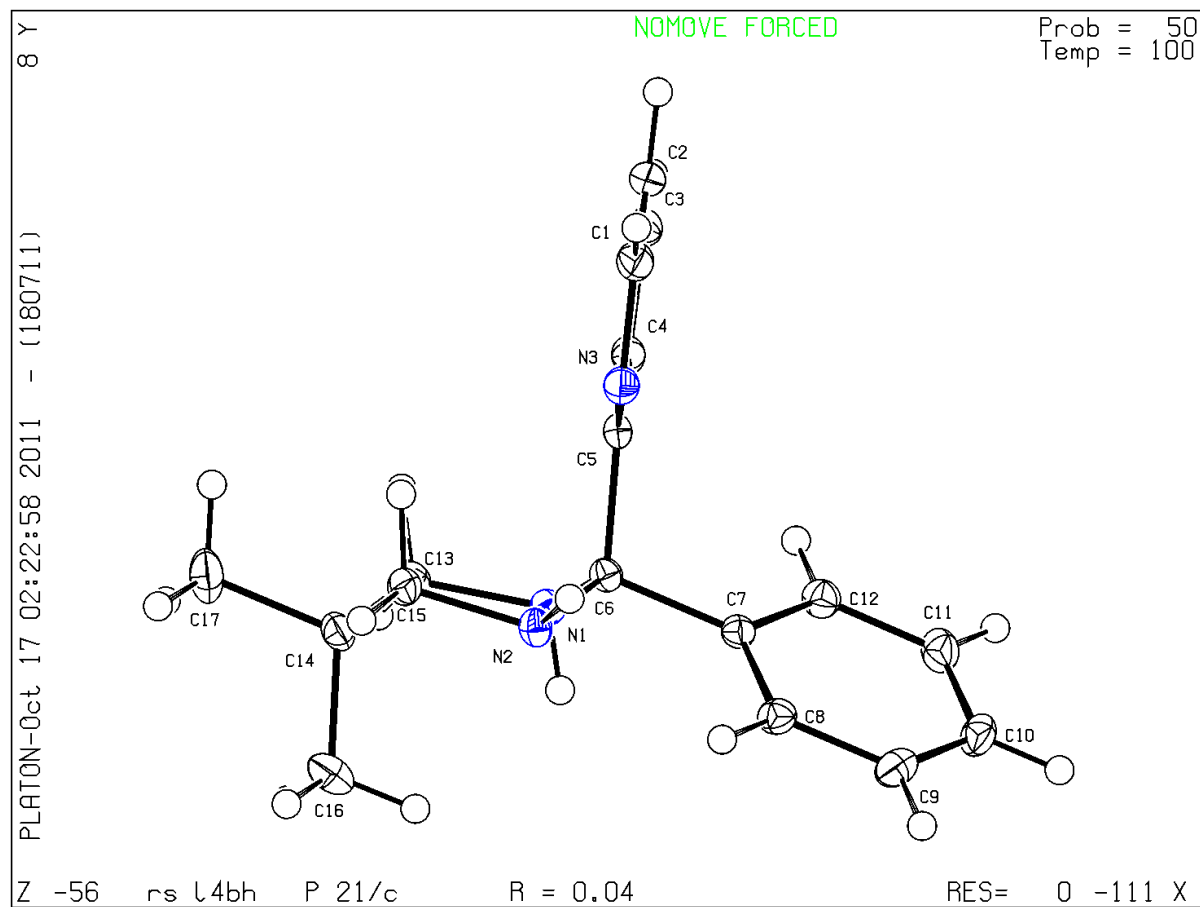
The following ALERTS were generated. Each ALERT has the format

test-name_ALERT_alert-type_alert-level.**● Alert level C**

PLAT420_ALERT_2_C D-H Without Acceptor N1 - H1 ... ?

PLATON version of 18/07/2011; check.def file version of 04/07/2011

Datablock rs_l4bh - ellipsoid plot



APPENDIX B

B1 – Crystallographic data tables for PtL1

Table B1-1: Crystal data and structure refinement for **PtL1**.

Table B1-2: Atomic coordinates ($\times 10^4$) and equivalent isotropic displacement parameters ($\text{\AA}^2 \times 10^3$) for **PtL1**. $U(\text{eq})$ is defined as one third of the trace of the orthogonalised U_{ij} tensor.

Table B1-3: IUCR CIF check report for **PtL1**.

B2 – Crystallographic data tables for PdL1

Table B2-1: Crystal data and structure refinement for **PdL1**.

Table B2-2: Atomic coordinates ($\times 10^4$) and equivalent isotropic displacement parameters ($\text{\AA}^2 \times 10^3$) for **PdL1**. $U(\text{eq})$ is defined as one third of the trace of the orthogonalised U_{ij} tensor.

Table B2-3: IUCR CIF check report for **PdL1**.

B3 – Crystallographic data tables for PtL2

Table B3-1: Crystal data and structure refinement for **PtL2**.

Table B3-2: Atomic coordinates ($\times 10^4$) and equivalent isotropic displacement parameters ($\text{\AA}^2 \times 10^3$) for **PtL2**. $U(\text{eq})$ is defined as one third of the trace of the orthogonalised U_{ij} tensor.

Table B3-3: IUCR CIF check report for **PtL2**.

B4 – Crystallographic data tables for PdL2

Table B4-1: Crystal data and structure refinement for **PdL2**.

Table B4-2: Atomic coordinates ($\times 10^4$) and equivalent isotropic displacement parameters ($\text{\AA}^2 \times 10^3$) for **PdL2**. $U(\text{eq})$ is defined as one third of the trace of the orthogonalised U_{ij} tensor.

Table B4-3: IUCR CIF check report for **PdL2**.

B5 – Crystallographic data tables for PtL4

Table B5-1: Crystal data and structure refinement for **PtL4**.

Table B5-2: Atomic coordinates ($\times 10^4$) and equivalent isotropic displacement parameters ($\text{\AA}^2 \times 10^3$) for **PtL4**. $U(\text{eq})$ is defined as one third of the trace of the orthogonalised U_{ij} tensor.

Table B5-3: IUCR CIF check report for **PtL4**.

B6 – Crystallographic data tables for PdL4

Table B6-1: Crystal data and structure refinement for **PdL4**.

Table B6-2: Atomic coordinates ($\times 10^4$) and equivalent isotropic displacement parameters ($\text{\AA}^2 \times 10^3$) for **PdL4**. $U(\text{eq})$ is defined as one third of the trace of the orthogonalised U_{ij} tensor.

Table B6-3: IUCR CIF check report for **PdL4**.

B7 – Crystallographic data tables for PdL4m

Table B7-1: Crystal data and structure refinement for **PdL4m**.

Table B7-2: Atomic coordinates ($\times 10^4$) and equivalent isotropic displacement parameters ($\text{\AA}^2 \times 10^3$) for **PdL4m**. $U(\text{eq})$ is defined as one third of the trace of the orthogonalised U_{ij} tensor.

Table B7-3: IUCR CIF check report for **PdL4m**.

B8 – Crystallographic data tables for PdL4b

Table B8-1: Crystal data and structure refinement for **PdL4b**.

Table B8-2: Atomic coordinates ($\times 10^4$) and equivalent isotropic displacement parameters ($\text{\AA}^2 \times 10^3$) for **PdL4m**. $U(\text{eq})$ is defined as one third of the trace of the orthogonalised U_{ij} tensor.

Table B8-3: IUCR CIF check report for **PdL4m**.

B1 – Crystallographic data tables for PtL1

Table B1-1: Crystal data and structure refinement for **PtL1**.

Identification code	rs_pt_l1	
Empirical formula	C ₁₄ H ₁₄ F ₁₂ N ₄ P ₂ Pt	
Formula weight	723.31 amu	
Temperature	100(2) K	
Wavelength	0.71073 Å	
Crystal system	Monoclinic	
Space group	C2/c	
Unit cell dimensions	$a = 15.0250(19)$ Å	$\alpha = 90^\circ$.
	$b = 10.4150(11)$ Å	$\beta = 99.285(9)^\circ$.
	$c = 13.0220(10)$ Å	$\gamma = 90^\circ$.
Volume	2011.1(4) Å ³	
Z	4	
Density (calculated)	2.389 Mg/m ³	
Absorption coefficient	7.257 mm ⁻¹	
F(000)	1368	
Crystal size	0.40 x 0.20 x 0.04 mm ³	
Theta range for data collection	2.74 to 32.10°.	
Index ranges	$-15 \leq h \leq 22$	
	$-15 \leq k \leq 15$	
	$-18 \leq l \leq 19$	
Reflections collected	10150	
Independent reflections	3278 [$R_{\text{int}} = 0.0622$]	
Completeness to theta = 25.00°	99.9 %	
Absorption correction	Semi-empirical from equivalents	
Max. and min. transmission	0.9716 and 0.7601	
Refinement method	Full-matrix least-squares on F^2	
Data / restraints / parameters	3278 / 0 / 150	
Goodness-of-fit on F^2	0.957	
Final R indices [$I > 2 \sigma(I)$]	$R_1 = 0.0483$, $wR_2 = 0.1017$	
R indices (all data)	$R_1 = 0.0710$, $wR_2 = 0.1086$	
Largest diff. peak and hole	4.000 and -1.325 e Å ⁻³	

Table B1-2: Atomic coordinates ($\times 10^4$) and equivalent isotropic displacement parameters ($\text{\AA}^2 \times 10^3$) for **PtL1**. $U(\text{eq})$ is defined as one third of the trace of the orthogonalised U_{ij} tensor.

	x	y	z	$U(\text{eq})$
C(3)	3968(4)	5047(7)	5475(5)	40(1)
C(4)	3499(5)	4537(7)	4567(5)	46(2)
C(5)	3434(4)	3207(7)	4461(5)	46(2)
C(6)	3837(4)	2433(7)	5257(5)	42(1)
C(7)	4299(4)	3013(6)	6164(5)	35(1)
C(8)	4055(5)	6425(7)	5690(6)	46(2)
C(10)	4590(5)	8006(6)	7061(6)	53(2)
N(2)	4380(3)	4266(5)	6278(4)	34(1)
N(9)	4498(4)	6730(5)	6564(5)	42(1)
F(12)	1339(3)	7344(4)	6623(3)	57(1)
F(13)	1926(3)	6089(5)	5463(3)	60(1)
F(14)	1501(3)	5705(4)	7781(3)	60(1)
F(15)	2684(3)	6394(6)	7078(4)	76(2)
F(16)	2065(5)	4478(4)	6614(4)	76(2)
F(17)	725(4)	5425(5)	6157(5)	83(2)
P(11)	1704(1)	5899(2)	6619(1)	35(1)
Pt(1)	5000	5354(1)	7500	33(1)

Table B1-3: IUCR CIF check report for **PtL1**.**IUCR CcheckCIF/PLATON (standard)**

No syntax errors found.

Datablock: rs_pt_I1

Bond precision:	C-C = 0.0097 A	Wavelength=0.71073
Cell:	a=15.0250(19) b=10.4150(11) c=13.022(1)	
	alpha=90 beta=99.285(9) gamma=90	
Temperature:	100 K	
	Calculated	Reported
Volume	2011.1(4)	2011.1(4)
Space group	C 2/c	C 2/c
Hall group	-C 2yc	-C 2yc
Moiety formula	C14 H14 N4 Pt, 2(F6 P)	C14 H14 N4 Pt, 2(F6 P)
Sum formula	C14 H14 F12 N4 P2 Pt	C14 H14 F12 N4 P2 Pt
Mr	723.31	723.31
Dx,g cm-3	2.389	2.389
Z	4	4
Mu (mm-1)	7.257	7.257
F000	1368.0	1368.0
F000'	1363.20	
h,k,lmax	22,15,19	22,15,19
Nref	3528	3278
Tmin,Tmax	0.191,0.748	0.760,0.972
Tmin'	0.050	
Correction method=	MULTI-SCAN	
Data completeness=	0.929	Theta(max)= 32.100
R(reflections)=	0.0483(2506)	wR2(reflections)= 0.1086(3278)
S =	0.957	Npar= 150

The following ALERTS were generated. Each ALERT has the format

test-name_ALERT_alert-type_alert-level.**● Alert level C**

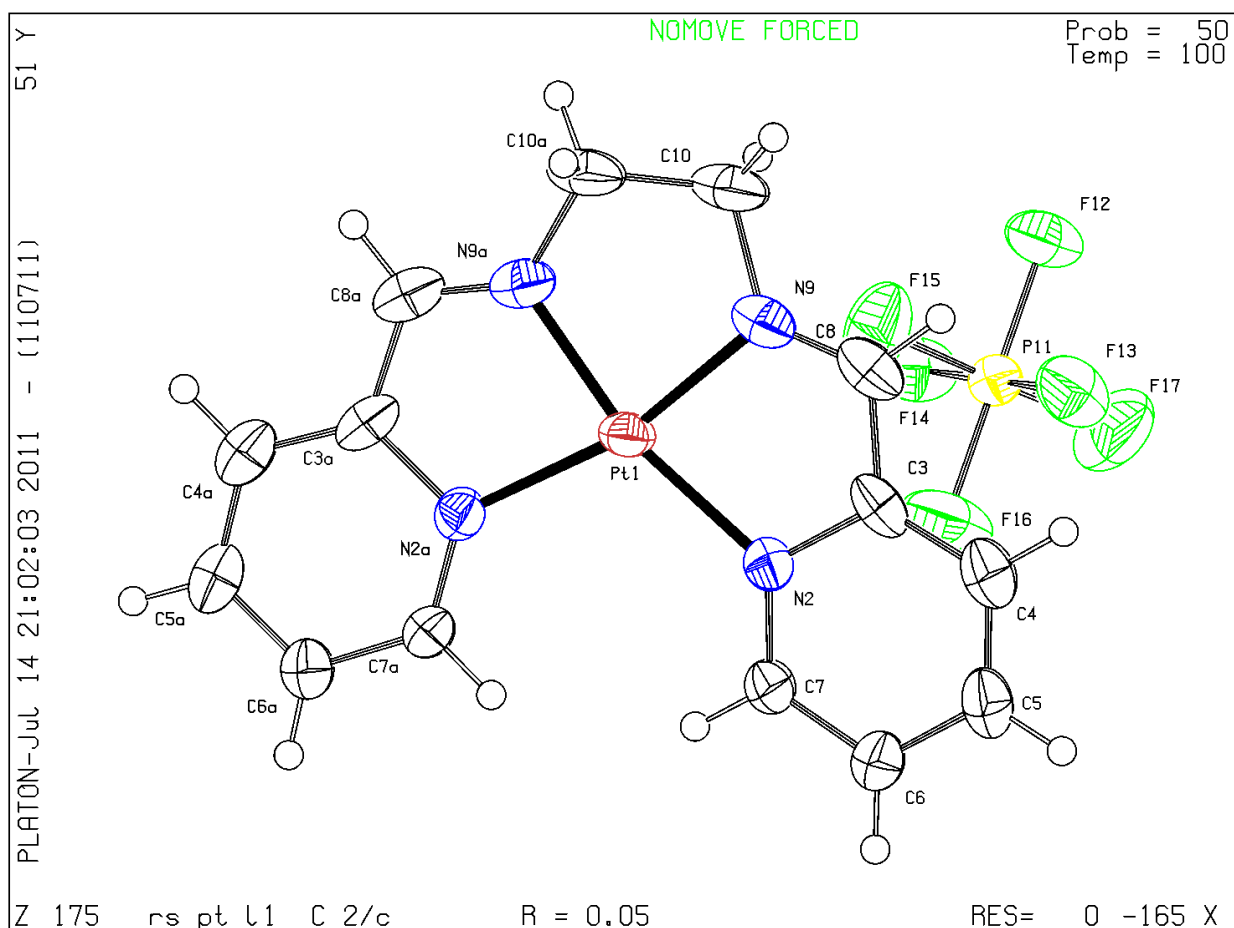
PLAT094_ALERT_2_C Ratio of Maximum / Minimum Residual Density 3.02
 PLAT244_ALERT_4_C Low 'Solvent' Ueq as Compared to Neighbors of P11
 PLAT342_ALERT_3_C Low Bond Precision on C-C Bonds 0.0097 Ang

● Alert level G

PLAT005_ALERT_5_G No _iucr_refine_instructions_details in CIF ?
 PLAT432_ALERT_2_G Short Inter X...Y Contact F15 .. C8 .. 2.95 Ang.
 PLAT710_ALERT_4_G Delete 1-2-3 or 2-3-4 Linear Torsion Angle ... # 45
 PLAT764_ALERT_4_G Overcomplete CIF Bond List Detected (Rep/Expd) 1.20 Ratio
 PLAT779_ALERT_4_G Suspect or Irrelevant (Bond) Angle in CIF # 5
 PLAT779_ALERT_4_G Suspect or Irrelevant (Bond) Angle in CIF # 20

PLATON version of 11/07/2011; check.def file version of 04/07/2011

Datablock rs_pt_l1 - ellipsoid plot



B2 – Crystallographic data tables for PdL1

Table B2-1: Crystal data and structure refinement for PdL1.

Identification code	rs_pd_l1	
Empirical formula	C ₁₄ H ₁₄ F ₁₂ N ₄ P ₂ Pd	
Formula weight	634.63 amu	
Temperature	100(2) K	
Wavelength	0.71073 Å	
Crystal system	Monoclinic	
Space group	C2/c	
Unit cell dimensions	$a = 14.8209(19)$ Å	$\alpha = 90^\circ$.
	$b = 10.3056(10)$ Å	$\beta = 100.091(13)^\circ$.
	$c = 13.1386(17)$ Å	$\gamma = 90^\circ$.
Volume	1975.7(4) Å ³	
Z	4	
Density (calculated)	2.134 Mg/m ³	
Absorption coefficient	1.224 mm ⁻¹	
F(000)	1240	
Crystal size	0.20 x 0.15 x 0.10 mm ³	
Theta range for data collection	3.15 to 29.34°.	
Index ranges	$-18 \leq h \leq 19$	
	$-9 \leq k \leq 13$	
	$-18 \leq l \leq 12$	
Reflections collected	3756	
Independent reflections	2110 [$R_{\text{int}} = 0.0347$]	
Completeness to theta = 25.00°	92.1 %	
Refinement method	Full-matrix least-squares on F^2	
Data / restraints / parameters	2110 / 0 / 173	
Goodness-of-fit on F^2	0.762	
Final R indices [$I > 2 \sigma(I)$]	$R_1 = 0.0389$, $wR_2 = 0.0870$	
R indices (all data)	$R_1 = 0.0663$, $wR_2 = 0.0984$	
Largest diff. peak and hole	0.627 and -0.650 e.Å ⁻³	

Table B2-2: Atomic coordinates ($\times 10^4$) and equivalent isotropic displacement parameters ($\text{\AA}^2 \times 10^3$) for **PdL1**. $U(\text{eq})$ is defined as one third of the trace of the orthogonalised U_{ij} tensor.

	x	y	z	U(eq)
Pd(1)	0	369(1)	2500	32(1)
P(2)	-1713(1)	4107(1)	-1642(1)	33(1)
F(2)	-1496(2)	4285(3)	-2774(2)	50(1)
F(3)	-1391(2)	2628(2)	-1644(2)	50(1)
F(6)	-1934(2)	3914(3)	-505(2)	51(1)
F(5)	-699(2)	4514(3)	-1162(3)	69(1)
F(4)	-2722(2)	3679(3)	-2110(2)	62(1)
F(1)	-2029(3)	5565(3)	-1628(2)	66(1)
N(1)	-624(2)	-721(3)	1274(3)	29(1)
C(2)	-1162(3)	-2555(5)	247(3)	37(1)
N(2)	-494(3)	1756(3)	1566(3)	41(1)
C(5)	-1023(3)	58(4)	470(3)	34(1)
C(3)	-1561(3)	-1772(5)	-536(4)	41(1)
C(4)	-1498(3)	-446(5)	-420(4)	40(1)
C(1)	-697(3)	-1998(4)	1145(3)	32(1)
C(6)	-945(3)	1452(4)	693(4)	42(1)
C(9)	-388(4)	3057(5)	2074(5)	53(1)

Table B2-3: IUCR CIF check report for **PdL1**.**IUCR CcheckCIF/PLATON (standard)**

No syntax errors found.

Datablock: rs-pd-l1

Bond precision:	C-C = 0.0053 A	Wavelength=0.71070
Cell:	a=14.8209(19) b=10.3056(10) c=13.1386(17)	
	alpha=90 beta=100.091(13) gamma=90	
Temperature:	115 K	
	Calculated	Reported
Volume	1975.7(4)	1975.7(4)
Space group	C 2/c	C2/c
Hall group	-C 2yc	-C 2yc
Moiety formula	C14 H14 N4 Pd, 2(F6 P)	C14 H14 N4 Pd, 2(F6 P)
Sum formula	C14 H14 F12 N4 P2 Pd	C14 H14 F12 N4 P2 Pd
Mr	634.63	634.63
Dx,g cm-3	2.134	2.134
Z	4	4
Mu (mm-1)	1.224	1.224
F000	1240.0	1240.0
F000'	1237.77	
h,k,lmax	20,14,18	19,13,18
Nref	2720	2095
Tmin,Tmax	0.791,0.874	0.981,1.000
Tmin'	0.773	
Correction method=	MULTI-SCAN	
Data completeness=	0.770 Theta(max)= 29.340	
R(reflections)= 0.0373(1460)	wR2(reflections)= 0.0659(2095)	
S = 0.885	Npar= 150	

The following ALERTS were generated. Each ALERT has the format

test-name_ALERT_alert-type_alert-level.**● Alert level C**

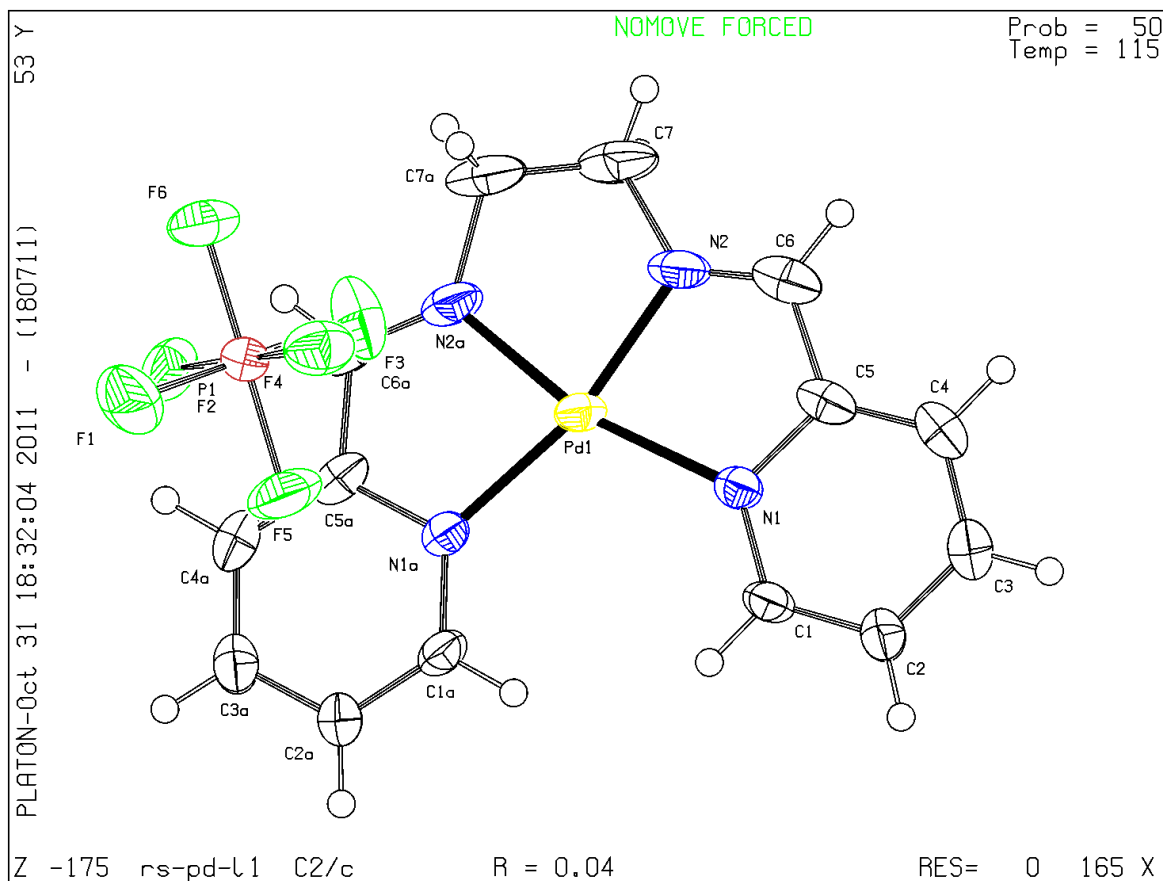
PLAT244_ALERT_4_C Low 'Solvent' Ueq as Compared to Neighbors of P1
 PLAT431_ALERT_2_C Short Inter HL..A Contact F3 .. N2 .. 2.89 Ang.

● Alert level G

PLAT003_ALERT_2_G Number of Uiso or Uij Restrained Atom Sites 2
 PLAT005_ALERT_5_G No _iucr_refine_instructions_details in CIF ?
 PLAT432_ALERT_2_G Short Inter X...Y Contact F3 .. 6 2.95 Ang.
 PLAT860_ALERT_3_G Note: Number of Least-Squares Restraints 12

PLATON version of 18/07/2011; check.def file version of 04/07/2011

Datablock rs-pd-l1 - ellipsoid plot



B3 – Crystallographic data tables for PtL2

Table B3-1: Crystal data and structure refinement for **PtL2**.

Identification code	rs_pt_l2	
Empirical formula	C ₁₅ H ₁₆ F ₁₂ N ₄ P ₂ Pt	
Formula weight	737.35 amu	
Temperature	100(2) K	
Wavelength	0.71073 Å	
Crystal system	Monoclinic	
Space group	<i>P2₁/n</i>	
Unit cell dimensions	<i>a</i> = 13.134(5) Å	$\alpha = 90.000(5)^\circ$.
	<i>b</i> = 10.611(5) Å	$\beta = 101.142(5)^\circ$.
	<i>c</i> = 15.103(5) Å	$\gamma = 90.000(5)^\circ$.
Volume	2065.2(14) Å ³	
Z	4	
Density (calculated)	2.372 Mg/m ³	
Absorption coefficient	7.069 mm ⁻¹	
F(000)	1400	
Crystal size	0.50 x 0.40 x 0.20 mm ³	
Theta range for data collection	2.69 to 32.23°.	
Index ranges	-18 ≤ <i>h</i> ≤ 18	
	-14 ≤ <i>k</i> ≤ 15	
	-22 ≤ <i>l</i> ≤ 22	
Reflections collected	19521	
Independent reflections	6656 [<i>R</i> _{int} = 0.0415]	
Completeness to theta = 25.00°	99.9 %	
Max. and min. transmission	0.3321 and 0.1261	
Refinement method	Full-matrix least-squares on <i>F</i> ²	
Data / restraints / parameters	6656 / 0 / 307	
Goodness-of-fit on <i>F</i> ²	1.213	
Final <i>R</i> indices [<i>I</i> > 2 σ (<i>I</i>)]	<i>R</i> ₁ = 0.0476, <i>wR</i> ₂ = 0.1339	
<i>R</i> indices (all data)	<i>R</i> ₁ = 0.0687, <i>wR</i> ₂ = 0.1414	
Largest diff. peak and hole	3.113 and -3.837 e Å ⁻³	

Table B3-2: Atomic coordinates ($\times 10^4$) and equivalent isotropic displacement parameters ($\text{\AA}^2 \times 10^3$) for **PtL2**. $U(\text{eq})$ is defined as one third of the trace of the orthogonalised U_{ij} tensor.

	x	y	z	U(eq)
C(1)	1262(5)	-1983(6)	9325(5)	30(2)
C(2)	394(5)	-2607(7)	8846(5)	30(2)
C(3)	-445(5)	-1936(6)	8416(4)	27(1)
C(4)	-416(5)	-622(7)	8479(4)	27(1)
C(5)	464(5)	-53(6)	8964(4)	22(1)
C(6)	565(5)	1291(6)	9049(4)	25(1)
C(7)	1543(7)	3087(8)	9648(8)	61(3)
C(8)	2555(7)	3533(7)	9914(7)	69(4)
C(9)	3385(7)	3064(7)	10529(9)	66(3)
C(10)	4410(5)	1263(7)	10996(5)	29(1)
C(11)	4529(5)	-97(6)	11043(4)	21(1)
C(12)	5419(5)	-661(6)	11497(4)	24(1)
C(13)	5454(5)	-1975(6)	11524(4)	26(1)
C(14)	4614(5)	-2631(7)	11084(5)	34(2)
C(15)	3749(5)	-1997(7)	10628(5)	30(2)
N(1)	3685(4)	-740(5)	10596(3)	18(1)
N(2)	1416(4)	1706(5)	9515(4)	28(1)
N(3)	1308(4)	-722(5)	9393(3)	21(1)
N(4)	3547(5)	1690(6)	10561(4)	31(1)
F(1)	1697(4)	2485(4)	6534(3)	42(1)
F(2)	2722(3)	768(4)	6544(3)	37(1)
F(3)	2209(3)	1379(5)	7817(3)	47(1)
F(4)	1549(4)	-398(4)	7105(4)	51(1)
F(5)	530(3)	1327(4)	7106(3)	35(1)
F(6)	1034(4)	715(5)	5821(3)	47(1)
F(7)	4450(3)	1268(4)	12954(3)	39(1)
F(8)	3277(3)	2464(4)	13499(3)	41(1)
F(9)	2774(4)	1297(6)	12237(3)	51(1)
F(10)	2255(3)	743(4)	13521(3)	38(1)
F(11)	3430(4)	-445(5)	12991(5)	60(2)
F(12)	3941(4)	721(5)	14253(3)	50(1)
P(1)	1623(1)	1036(2)	6828(1)	26(1)
P(2)	3351(1)	994(2)	13244(1)	28(1)
Pt(1)	2490(1)	435(1)	10021(1)	20(1)

Table B3-3: IUCR CIF check report for **PtL2**.**IUCR CcheckCIF/PLATON (standard)**

No syntax errors found.

Datablock: rs_ptl2

Bond precision:	C-C = 0.0052 Å	Wavelength=0.71073
Cell:	a=15.103(5) b=10.611(5) c=13.134(5)	
	alpha=90 beta=101.142(5) gamma=90	
Temperature:	100 K	
	Calculated	Reported
Volume	2065.2(14)	2065.2(14)
Space group	C 2/c	C2/c
Hall group	-C 2yc	-C 2yc
Moiety formula	C15 H16 N4 Pt, 2(F6 P)	C15 H16 N4 Pt, 2(F6 P)
Sum formula	C15 H16 F12 N4 P2 Pt	C15 H16 F12 N4 P2 Pt
Mr	737.34	737.35
Dx,g cm-3	2.372	2.372
Z	4	4
Mu (mm-1)	7.069	7.069
F000	1400.0	1400.0
F000'	1395.20	
h,k,lmax	22,15,19	22,15,18
Nref	3659	3331
Tmin,Tmax	0.097,0.120	0.171,1.000
Tmin'	0.073	
Correction method=	MULTI-SCAN	
Data completeness=	0.910 Theta(max)= 32.230	
R(reflections)=	0.0321(3088)	wR2(reflections)= 0.0830(3331)
S =	1.097	Npar= 190

The following ALERTS were generated. Each ALERT has the format

test-name_ALERT_alert-type_alert-level.

Click on the hyperlinks for more details of the test.

Alert level B

PLAT410_ALERT_2_B Short Intra H...H Contact H1 .. H1 .. 1.87 Ang.

Alert level C

PLAT244_ALERT_4_C Low 'Solvent' Ueq as Compared to Neighbors of P1

PLAT250_ALERT_2_C Large U3/U1 Ratio for Average U(i,j) Tensor 2.3

PLAT303_ALERT_2_C Full Occupancy H-Atom H7A with # Connections 2

PLAT303_ALERT_2_C Full Occupancy H-Atom H8A with # Connections 2

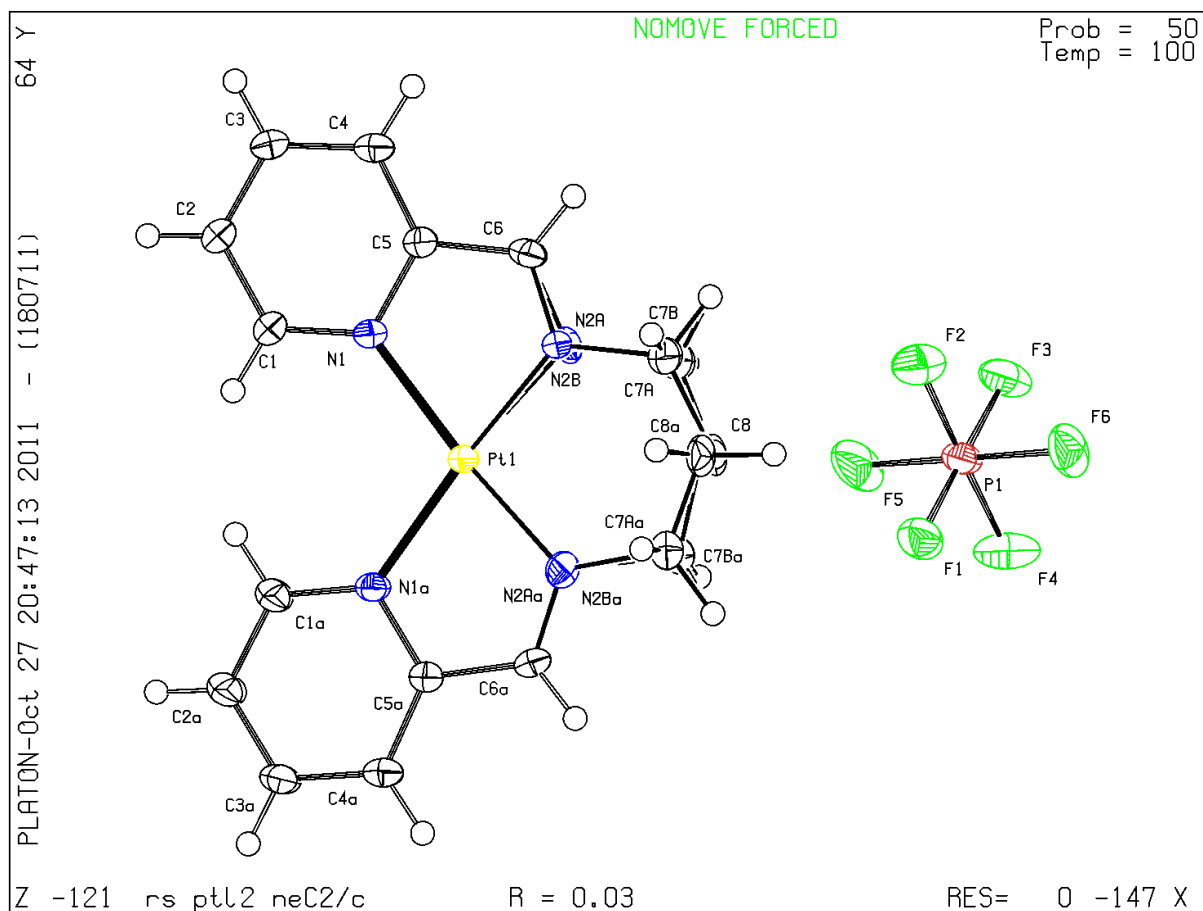
PLAT431_ALERT_2_C Short Inter HL..A Contact F4 .. N2A .. 2.78 Ang.

● Alert level G

PLAT002_ALERT_2_G	Number of Distance or Angle Restraints on AtSite	7
PLAT003_ALERT_2_G	Number of Uiso or Uij Restrained Atom Sites	5
PLAT153_ALERT_1_G	The su's on the Cell Axes are Equal	0.00500 Ang.
PLAT164_ALERT_4_G	Nr. of Refined C-H H-Atoms in Heavy-Atom Struct.	1
PLAT301_ALERT_3_G	Note: Main Residue Disorder	25 Perc.
PLAT432_ALERT_2_G	Short Inter X...Y Contact F3 .. C6 ..	2.94 Ang.
PLAT720_ALERT_4_G	Number of Unusual/Non-Standard Labels	1
PLAT860_ALERT_3_G	Note: Number of Least-Squares Restraints	34

PLATON version of 18/07/2011; check.def file version of 04/07/2011

Datablock rs_ptl2 - ellipsoid plot



B4 – Crystallographic data tables for PdL2

Table B4-1: Crystal data and structure refinement for PdL2.

Identification code	rs_pd_l2	
Empirical formula	C ₁₅ H ₁₆ F ₁₂ N ₄ P ₂ Pd	
Formula weight	648.66 amu	
Temperature	100(2) K	
Wavelength	0.71073 Å	
Crystal system	Monoclinic	
Space group	<i>P2₁/n</i>	
Unit cell dimensions	<i>a</i> = 13.443(5) Å	α = 90.000(5)°.
	<i>b</i> = 10.513(5) Å	β = 102.674(5)°.
	<i>c</i> = 14.905(5) Å	γ = 90.000(5)°.
Volume	2055.1(14) Å ³	
Z	4	
Density (calculated)	2.096 Mg/m ³	
Absorption coefficient	1.179 mm ⁻¹	
F(000)	1272	
Crystal size	0.60 x 0.50 x 0.40 mm ³	
Theta range for data collection	2.68 to 32.18°.	
Index ranges	-19 ≤ <i>h</i> ≤ 17	
	-15 ≤ <i>k</i> ≤ 15	
	-19 ≤ <i>l</i> ≤ 21	
Reflections collected	19654	
Independent reflections	6638 [<i>R</i> _{int} = 0.0196]	
Completeness to theta = 25.00°	99.9 %	
Max. and min. transmission	0.6498 and 0.5380	
Refinement method	Full-matrix least-squares on <i>F</i> ²	
Data / restraints / parameters	6638 / 0 / 307	
Goodness-of-fit on <i>F</i> ²	1.070	
Final <i>R</i> indices [<i>I</i> > 2 σ (<i>I</i>)]	<i>R</i> ₁ = 0.0282, <i>wR</i> ₂ = 0.0797	
<i>R</i> indices (all data)	<i>R</i> ₁ = 0.0327, <i>wR</i> ₂ = 0.0814	
Largest diff. peak and hole	0.842 and -1.435 e Å ⁻³	

Table B4-2: Atomic coordinates ($\times 10^4$) and equivalent isotropic displacement parameters ($\text{\AA}^2 \times 10^3$) for **PdL2**. $U(\text{eq})$ is defined as one third of the trace of the orthogonalised U_{ij} tensor.

	x	y	z	$U(\text{eq})$
Pd(1)	7523(1)	429(1)	4938(1)	15(1)
P(2)	8319(1)	-3997(1)	3259(1)	19(1)
P(1)	8375(1)	1068(1)	8097(1)	18(1)
F(1)	9454(1)	1359(1)	7838(1)	27(1)
F(2)	8958(1)	706(1)	9123(1)	33(1)
F(5)	7298(1)	799(1)	8357(1)	26(1)
F(8)	7252(1)	-4243(1)	3549(1)	29(1)
F(6)	8438(1)	-375(1)	7791(1)	34(1)
F(10)	9386(1)	-3742(1)	2970(1)	31(1)
F(11)	8916(1)	-4243(1)	4299(1)	36(1)
F(7)	8247(1)	-2510(1)	3492(1)	34(1)
F(3)	8320(1)	2526(1)	8411(1)	33(1)
F(12)	7722(1)	-3744(1)	2227(1)	33(1)
F(9)	8392(1)	-5476(1)	3043(1)	37(1)
C(12)	4566(1)	-675(2)	3550(1)	22(1)
F(4)	7801(1)	1438(1)	7074(1)	33(1)
C(5)	9532(1)	-55(2)	6016(1)	18(1)
C(11)	5468(1)	-102(2)	3984(1)	18(1)
N(2)	6471(1)	1715(1)	4388(1)	19(1)
C(10)	6232(1)	-2034(2)	4415(1)	24(1)
C(6)	10402(1)	-605(2)	6544(1)	21(1)
N(3)	6309(1)	-772(1)	4420(1)	17(1)
N(1)	8605(1)	1729(1)	5373(1)	18(1)
C(3)	8492(1)	3106(2)	5193(1)	25(1)
C(9)	8738(1)	-1999(2)	5721(1)	23(1)
C(1)	6644(1)	3099(2)	4359(1)	25(1)
C(4)	9441(1)	1308(2)	5864(1)	21(1)
N(4)	8695(1)	-744(1)	5601(1)	17(1)
C(7)	10427(1)	-1917(2)	6660(1)	21(1)
C(8)	9588(1)	-2619(2)	6239(1)	24(1)
C(13)	4506(1)	-1999(2)	3545(1)	22(1)
C(2)	7426(1)	3563(2)	5184(1)	23(1)
C(15)	5599(1)	1267(2)	3997(1)	22(1)
C(14)	5348(1)	-2681(2)	3988(1)	24(1)

Table B4-3: IUCR CIF check report for **PdL2**.**IUCR CcheckCIF/PLATON (standard)**

No syntax errors found.

Datablock: rs_pd_l2

Bond precision:	C-C = 0.0025 Å	Wavelength=0.71073
Cell:	a=13.443(5) b=10.513(5) c=14.905(5)	
	alpha=90 beta=102.674(5) gamma=90	
Temperature:	100 K	
	Calculated	Reported
Volume	2055.1(14)	2055.1(14)
Space group	P 21/n	P21/n
Hall group	-P 2yn	-P 2yn
Moiety formula	C15 H16 N4 Pd, 2(F6 P)	C15 H16 N4 Pd, 2(F6 P)
Sum formula	C15 H16 F12 N4 P2 Pd	C15 H16 F12 N4 P2 Pd
Mr	648.66	648.66
Dx,g cm-3	2.096	2.096
Z	4	4
Mu (mm-1)	1.179	1.179
F000	1272.0	1272.0
F000'	1269.78	
h,k,lmax	20,15,22	19,15,21
Nref	7257	6625
Tmin,Tmax	0.498,0.624	0.595,1.000
Tmin'	0.488	
Correction method=	MULTI-SCAN	
Data completeness=	0.913 Theta(max)= 32.180	
R(reflections)= 0.0279(5725)	wR2(reflections)= 0.0792(6625)	
S = 1.053	Npar= 307	

The following ALERTS were generated. Each ALERT has the format

test-name_ALERT_alert-type_alert-level.

Click on the hyperlinks for more details of the test.

Alert level B

[PLAT112_ALERT_2_B ADDSYM Detects Additional \(Pseudo\) Symm. Elem...](#) A

Alert level C

[PLAT410_ALERT_2_C Short Intra H...H Contact H9 .. H10 .. 1.91 Ang.](#)
[PLAT431_ALERT_2_C Short Inter HL..A Contact F12 .. N2 .. 2.89 Ang.](#)

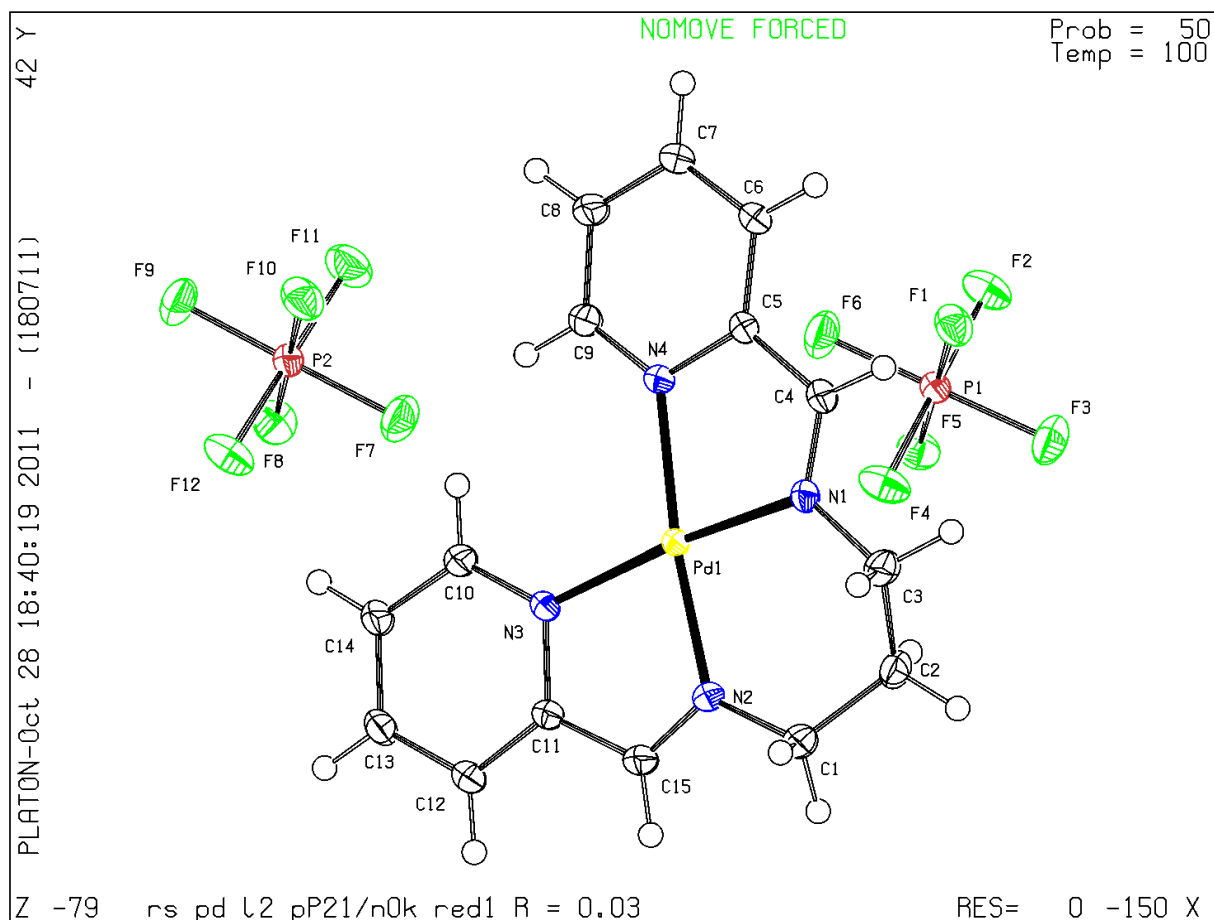
Alert level G

[PLAT128_ALERT_4_G Alternate Setting of Space-group P21/c P21/n](#)
[PLAT153_ALERT_1_G The su's on the Cell Axes are Equal 0.00500 Ang.](#)

PLAT432_ALERT_2_G Short Inter X...Y Contact F1 .. C4 .. 2.94 Ang.
PLAT432_ALERT_2_G Short Inter X...Y Contact F10 .. C15 .. 2.94 Ang.
PLAT790_ALERT_4_G Centre of Gravity not Within Unit Cell: Resd. # 3 F6 P

PLATON version of 18/07/2011; check.def file version of 04/07/2011

Datablock rs_pd_I2 - ellipsoid plot



B5 – Crystallographic data tables for PtL4

Table B5-1: Crystal data and structure refinement for **PtL4**.

Identification code	rs_pt_l4	
Empirical formula	$C_{17.50} H_{17} F_{12} N_4 P_2 Pt$	
Formula weight	768.37 amu	
Temperature	293(2) K	
Wavelength	0.71073 Å	
Crystal system	Monoclinic	
Space group	$C2/m$	
Unit cell dimensions	$a = 16.563(5) \text{ \AA}$	$\alpha = 90.000(5)^\circ$.
	$b = 27.167(5) \text{ \AA}$	$\beta = 96.312(5)^\circ$.
	$c = 10.778(5) \text{ \AA}$	$\gamma = 90.000(5)^\circ$.
Volume	$4820(3) \text{ \AA}^3$	
Z	8	
Density (calculated)	2.118 Mg/m^3	
Absorption coefficient	0.606 mm^{-1}	
F(000)	2927	
Crystal size	$0.60 \times 0.40 \times 0.20 \text{ mm}^3$	
Theta range for data collection	$2.57 \text{ to } 26.14^\circ$.	
Index ranges	$-20 \leq h \leq 20$	
	$-33 \leq k \leq 33$	
	$-13 \leq l \leq 13$	
Reflections collected	25206	
Independent reflections	4891 [$R_{\text{int}} = 0.0858$]	
Completeness to theta = 25.00°	99.8 %	
Refinement method	Full-matrix least-squares on F^2	
Data / restraints / parameters	4891 / 0 / 346	
Goodness-of-fit on F^2	1.039	
Final R indices [$I > 2 \sigma(I)$]	$R_1 = 0.0545$, $wR_2 = 0.1386$	
R indices (all data)	$R_1 = 0.0686$, $wR_2 = 0.1472$	
Largest diff. peak and hole	1.711 and $-2.687 \text{ e \AA}^{-3}$	

Table B5-2: Atomic coordinates ($\times 10^4$) and equivalent isotropic displacement parameters ($\text{\AA}^2 \times 10^3$) for **PtL4**. $U(\text{eq})$ is defined as one third of the trace of the orthogonalised U_{ij} tensor.

	x	y	z	$U(\text{eq})$
Pt(1)	2604(1)	0	1187(1)	38(1)
N(1A)	2657(4)	-600(2)	2326(7)	41(2)
C(5A)	2469(5)	-1030(3)	1698(8)	45(2)
C(4A)	2429(6)	-1478(3)	2287(10)	57(2)
C(3A)	2612(7)	-1502(4)	3554(11)	63(3)
C(2A)	2827(8)	-1084(4)	4187(10)	71(3)
C(1A)	2833(7)	-638(4)	3559(9)	60(3)
C(6A)	2382(6)	-969(3)	358(9)	52(2)
N(2A)	2477(4)	-538(2)	-50(7)	43(2)
Pt(10)	5000	7590(1)	5000	55(1)
N(11)	4743(4)	8046(3)	3497(6)	40(2)
C(5B)	4462(5)	7792(3)	2451(7)	41(2)
C(4B)	4278(6)	8024(4)	1319(8)	53(2)
C(1B)	4868(6)	8525(4)	3386(8)	50(2)
C(2B)	4684(7)	8773(4)	2294(9)	57(2)
N(16)	5310(8)	7096(3)	6327(9)	87(4)
P(17)	5000	0	0	44(1)
F(18)	5262(18)	0	1382(12)	217(11)
F(19)	4358(6)	-412(3)	61(15)	173(6)
P(20)	5000	0	5000	54(1)
F(21)	5549(7)	0	6301(9)	94(3)
F(22)	5567(6)	404(3)	4512(9)	120(3)
P(23)	7087(2)	8012(1)	2427(2)	53(1)
F(24)	6422(6)	7606(3)	2202(12)	136(4)
F(25)	6682(7)	8194(5)	3554(9)	150(4)
F(26)	7744(5)	8426(3)	2659(9)	117(3)
F(27)	7654(6)	7671(4)	3269(13)	154(5)
F(28)	7480(8)	7831(7)	1301(12)	206(7)
F(29)	6544(6)	8364(4)	1561(9)	137(4)
P(1)	5000	6236(2)	0	68(1)
F(1)	4545(7)	6615(6)	-834(16)	222(8)
F(2)	5702(5)	6230(4)	-869(8)	112(3)
C(8A)	2067(8)	0	-1933(12)	51(3)
C(9A)	2170(11)	0	-3353(14)	74(5)

Table B5-2: Continued.

	x	y	z	U(eq)
C(3B)	4385(6)	8523(4)	1240(9)	57(2)
C(7A)	2513(8)	-462(4)	-1399(9)	63(3)
C(10A)	1198(11)	0	-1725(15)	75(5)
F(3)	5463(7)	5826(5)	786(11)	167(5)
C(6B)	5573(6)	7273(4)	7410(9)	53(2)
C(8B)	5000	6356(5)	5000	49(3)
C(9B)	5000	5801(6)	5000	107(8)
C(7B)	5280(20)	6566(5)	6145(17)	239(19)
C(10B)	4108(14)	6429(9)	5400(30)	162(9)

Table B5-3: IUCR CIF check report for **PtL4**.**IUCR CcheckCIF/PLATON (standard)**

No syntax errors found.

Datablock: rs_pt_I4

Bond precision:	C-C = 0.0066 Å	Wavelength=0.71073
Cell:	a=10.6260(1) b=26.9950(3) c=16.2420(2)	
	alpha=90 beta=95.193(1) gamma=90	
Temperature:	100 K	
	Calculated	Reported
Volume	4639.88(9)	4639.88(9)
Space group	P 21/c	P 1 21/c 1
Hall group	-P 2ybc	-P 2ybc
Moiety formula	C17 H20 N4 Pt, 2(F6 P)	C17 H20 N4 Pt, 2(F6 P)
Sum formula	C17 H20 F12 N4 P2 Pt	C17 H20 F12 N4 P2 Pt
Mr	765.39	765.40
Dx,g cm-3	2.191	2.191
Z	8	8
Mu (mm-1)	6.297	6.297
F000	2928.0	2928.0
F000'	2918.41	
h,k,lmax	16,42,25	16,42,24
Nref	19305	17350
Tmin,Tmax	0.240,0.284	0.413,1.000
Tmin'	0.139	
Correction method=	MULTI-SCAN	
Data completeness=	0.899 Theta(max)= 34.260	
R(reflections)=	0.0484(12951)	wR2(reflections)= 0.1262(17350)
S =	0.994	Npar= 666

The following ALERTS were generated. Each ALERT has the format

test-name_ALERT_alert-type_alert-level.**Alert level B**

Crystal system given = monoclinic

PLAT112_ALERT_2_B ADDSYM Detects Additional (Pseudo) Symm. Elem... A

NOTE: this was investigated. The FALSE alert arises because two PF6-counterions in the asymmetric unit are located on centers of inversion in the structure. They exhibit half-occupancy. The remaining three counterions are located at general positions and are fully occupied. Both cations are found at general positions and are fully occupied. Use of PLATON's ADDSYM algorithm clearly reveals that the correct space group choice has been used for the model.

● Alert level C

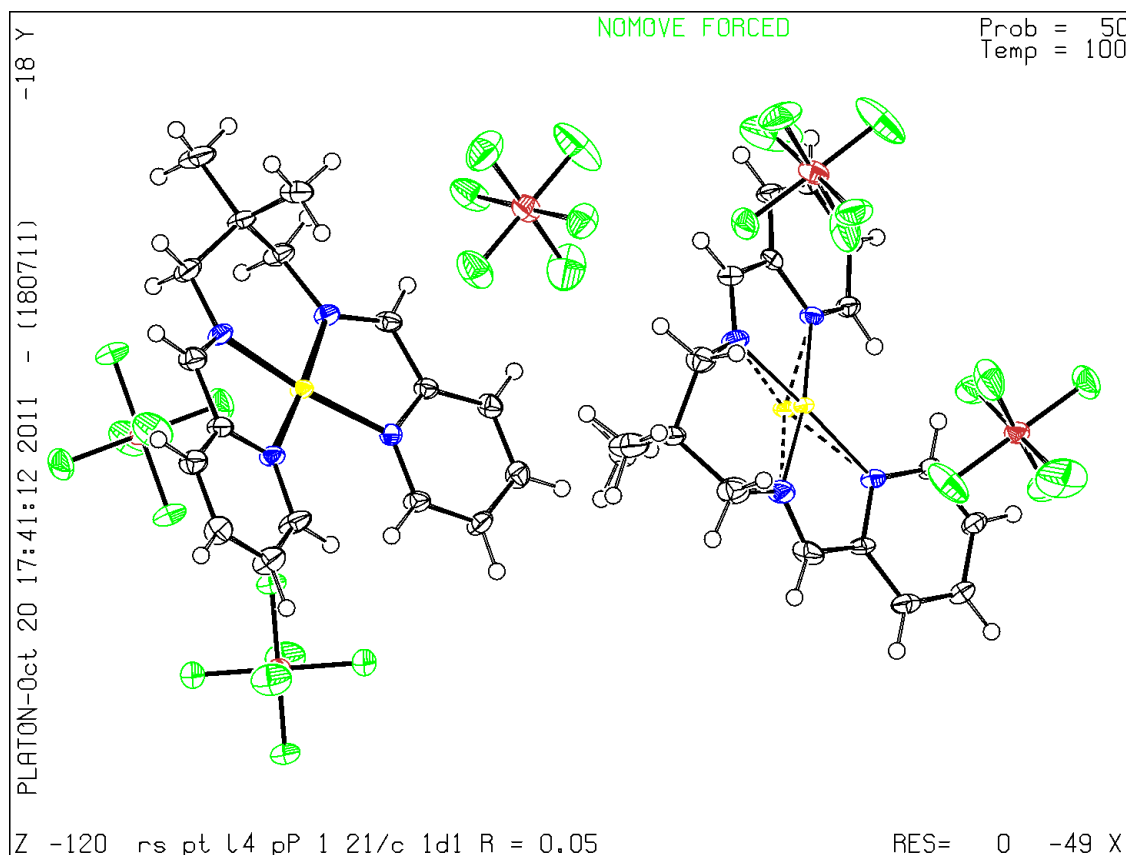
PLAT143_ALERT_4_C su on c - Axis Small or Missing 0.00010 Ang.
 PLAT244_ALERT_4_C Low 'Solvent' Ueq as Compared to Neighbors of P1
 PLAT244_ALERT_4_C Low 'Solvent' Ueq as Compared to Neighbors of P2
 PLAT244_ALERT_4_C Low 'Solvent' Ueq as Compared to Neighbors of P3
 PLAT244_ALERT_4_C Low 'Solvent' Ueq as Compared to Neighbors of P4
 PLAT244_ALERT_4_C Low 'Solvent' Ueq as Compared to Neighbors of P5
 PLAT250_ALERT_2_C Large U3/U1 Ratio for Average U(i,j) Tensor 2.1
 PLAT410_ALERT_2_C Short Intra H...H Contact H1B .. H15B .. 1.97 Ang.
 PLAT410_ALERT_2_C Short Intra H...H Contact H1A .. H15A .. 1.91 Ang.

● Alert level G

PLAT003_ALERT_2_G Number of Uiso or Uij Restrained Atom Sites 2
 PLAT301_ALERT_3_G Note: Main Residue Disorder 2 Perc.
 PLAT432_ALERT_2_G Short Inter X...Y Contact F5 .. C10A .. 2.94 Ang.
 PLAT432_ALERT_2_G Short Inter X...Y Contact F7 .. C7B .. 2.96 Ang.
 PLAT432_ALERT_2_G Short Inter X...Y Contact F10 .. C6B .. 2.92 Ang.
 PLAT432_ALERT_2_G Short Inter X...Y Contact F12 .. C1B .. 2.90 Ang.
 PLAT605_ALERT_4_G Structure Contains Solvent Accessible VOIDS of . 28 Å³
 PLAT720_ALERT_4_G Number of Unusual/Non-Standard Labels 8
 PLAT860_ALERT_3_G Note: Number of Least-Squares Restraints 18
 PLAT869_ALERT_4_G ALERTS Related to the use of SQUEEZE Suppressed !

PLATON version of 18/07/2011; check.def file version of 04/07/2011

Datablock rs_pt_l4 - ellipsoid plot



B6 – Crystallographic data tables for PdL4

Table B6-1: Crystal data and structure refinement for PdL4.

Identification code	rs_pd_l4	
Empirical formula	C ₁₇ H ₂₀ F ₁₂ N ₄ P ₂ Pd	
Formula weight	676.71 amu	
Temperature	100(2) K	
Wavelength	0.71073 Å	
Crystal system	Monoclinic	
Space group	<i>P</i> 2 ₁ / <i>c</i>	
Unit cell dimensions	<i>a</i> = 10.506(5) Å	$\alpha = 90^\circ$.
	<i>b</i> = 27.297(5) Å	$\beta = 94.032(5)^\circ$.
	<i>c</i> = 16.327(5) Å	$\gamma = 90^\circ$.
Volume	4671(3) Å ³	
Z	8	
Density (calculated)	1.925 Mg/m ³	
Absorption coefficient	1.042 mm ⁻¹	
F(000)	2672	
Crystal size	0.40 x 0.40 x 0.40 mm ³	
Theta range for data collection	2.69 to 26.07°.	
Index ranges	-12 ≤ <i>h</i> ≤ 7	
	-33 ≤ <i>k</i> ≤ 33	
	-20 ≤ <i>l</i> ≤ 20	
Reflections collected	32251	
Independent reflections	9184 [<i>R</i> _{int} = 0.0730]	
Completeness to theta = 25.00°	99.6 %	
Refinement method	Full-matrix least-squares on <i>F</i> ²	
Data / restraints / parameters	9184 / 0 / 656	
Goodness-of-fit on <i>F</i> ²	1.054	
Final <i>R</i> indices [<i>I</i> > 2 σ (<i>I</i>)]	<i>R</i> ₁ = 0.0585, <i>wR</i> ₂ = 0.1565	
<i>R</i> indices (all data)	<i>R</i> ₁ = 0.0666, <i>wR</i> ₂ = 0.1606	
Largest diff. peak and hole	2.457 and -1.929 e Å ⁻³	

Table B6-2: Atomic coordinates ($\times 10^4$) and equivalent isotropic displacement parameters ($\text{\AA}^2 \times 10^3$) for **PdL4**. $U(\text{eq})$ is defined as one third of the trace of the orthogonalised U_{ij} tensor.

	x	y	z	U(eq)
C(3)	1412(4)	5609(2)	7181(3)	24(1)
C(4)	757(5)	6050(2)	7216(3)	27(1)
C(5)	1413(5)	6474(2)	7438(3)	24(1)
C(6)	2726(5)	6447(2)	7612(3)	22(1)
C(7)	3326(4)	5992(2)	7557(3)	18(1)
C(8)	4689(4)	5934(2)	7648(3)	21(1)
C(10)	6534(4)	5434(2)	7517(3)	23(1)
C(11)	7037(4)	4960(2)	7929(3)	22(1)
C(12)	8479(5)	4959(2)	7853(4)	34(1)
C(13)	6532(4)	4508(2)	7445(3)	24(1)
C(14)	4716(4)	4000(2)	7610(3)	19(1)
C(16)	3338(4)	3938(2)	7534(3)	17(1)
C(18)	1442(4)	4313(2)	7108(3)	21(1)
C(19)	796(5)	3870(2)	7143(3)	22(1)
C(20)	1452(4)	3453(2)	7399(3)	22(1)
C(21)	2755(5)	3485(2)	7598(3)	21(1)
C(22)	6730(5)	4934(2)	8831(3)	27(1)
C(26)	-2580(4)	2829(2)	4547(3)	18(1)
C(27)	-3679(4)	3082(2)	4288(3)	22(1)
C(28)	-3714(4)	3590(2)	4368(3)	23(1)
C(29)	-2652(4)	3829(2)	4712(3)	22(1)
C(30)	-1567(4)	3558(2)	4952(3)	19(1)
C(31)	-2517(4)	2291(2)	4582(3)	20(1)
C(33)	-1452(5)	1572(2)	5078(3)	24(1)
C(34)	-122(4)	1343(2)	5044(3)	19(1)
C(35)	-268(5)	795(2)	5214(4)	32(1)
C(36)	814(4)	1548(2)	5709(3)	21(1)
C(38)	2297(4)	2217(2)	5765(3)	21(1)
C(39)	2558(4)	2737(2)	5669(2)	17(1)
C(41)	1708(4)	3488(2)	5239(3)	20(1)
C(42)	2892(4)	3718(2)	5385(3)	22(1)
C(43)	3908(4)	3442(2)	5683(3)	22(1)
C(44)	3754(4)	2941(2)	5827(3)	20(1)
C(45)	371(5)	1411(2)	4185(3)	29(1)

Table B6-2: Continued.

	x	y	z	U(eq)
N(2)	2670(4)	5569(1)	7349(2)	19(1)
N(9)	5149(4)	5501(1)	7534(2)	18(1)
N(15)	5151(4)	4429(1)	7485(2)	19(1)
N(17)	2688(4)	4357(1)	7311(2)	18(1)
N(24)	-1513(3)	3067(1)	4858(2)	16(1)
N(32)	-1499(3)	2108(1)	4932(2)	19(1)
N(37)	1164(4)	2064(1)	5580(2)	19(1)
N(40)	1522(3)	3007(1)	5392(2)	16(1)
F(47)	5070(3)	4511(1)	5555(2)	33(1)
F(48)	4337(4)	5284(1)	5713(2)	48(1)
F(49)	6362(4)	5157(2)	5408(2)	47(1)
F(51)	6105(4)	2883(2)	7595(2)	54(1)
F(52)	7751(3)	3388(1)	7859(2)	35(1)
F(53)	8080(4)	2570(1)	7818(2)	46(1)
F(54)	6774(3)	3362(1)	6578(2)	41(1)
F(55)	7103(4)	2536(1)	6537(2)	41(1)
F(56)	8742(3)	3055(2)	6791(2)	41(1)
F(58)	9385(3)	4652(1)	5666(2)	34(1)
F(59)	11326(3)	4997(1)	5546(2)	33(1)
F(60)	9555(3)	5474(1)	5491(2)	39(1)
F(62)	6222(4)	7094(2)	7455(3)	80(2)
F(63)	7754(3)	6535(1)	7637(2)	33(1)
F(64)	6590(4)	6560(2)	6429(2)	58(1)
F(65)	8260(5)	7326(1)	7512(2)	64(1)
F(66)	8636(3)	6796(1)	6489(2)	37(1)
F(67)	7085(6)	7358(2)	6292(3)	82(2)
F(69)	4317(3)	6306(1)	10710(2)	36(1)
F(70)	6173(3)	6132(1)	9256(2)	34(1)
F(71)	4601(4)	6663(2)	9477(2)	53(1)
F(72)	6281(4)	6579(2)	10423(2)	49(1)
F(73)	4233(4)	5852(2)	9548(2)	50(1)
F(74)	5890(4)	5772(1)	10493(2)	47(1)
P(46)	5000	5000	5000	17(1)
P(50)	7436(1)	2961(1)	7196(1)	20(1)
P(57)	10000	5000	5000	21(1)
P(61)	7432(1)	6952(1)	6962(1)	26(1)

Table B6-2: Continued.

	x	y	z	U(eq)
P(68)	5249(1)	6219(1)	9987(1)	24(1)
Pd(1)	3864(1)	4965(1)	7367(1)	16(1)
Pd(23)	-84(1)	2582(1)	5202(1)	16(1)

Table B6-3: IUCR CIF check report for **PdL4**.**IUCR CcheckCIF/PLATON (standard)**

No syntax errors found.

Datablock: rs_pd_I4

Bond precision:	C-C = 0.0071 A	Wavelength=0.71073
Cell:	a=10.506(5) b=27.297(5) c=16.327(5)	
	alpha=90 beta=94.032(5) gamma=90	
Temperature:	100 K	
	Calculated	Reported
Volume	4671(3)	4671(3)
Space group	P 21/c	P21/c
Hall group	-P 2ybc	-P 2ybc
Moiety formula	C17 H20 N4 Pd, 2(F6 P)	C17 H20 N4 Pd, 2(F6 P)
Sum formula	C17 H20 F12 N4 P2 Pd	C17 H20 F12 N4 P2 Pd
Mr	676.71	676.71
Dx,g cm-3	1.925	1.925
Z	8	8
Mu (mm-1)	1.042	1.042
F000	2672.0	2672.0
F000'	2667.59	
h,k,lmax	12,33,20	12,33,20
Nref	9233	9184
Tmin,Tmax	0.666,0.659	0.322,1.000
Tmin'	0.653	
Correction method=	MULTI-SCAN	
Data completeness=	0.995 Theta(max)= 26.070	
R(reflections)=	0.0585(7731)	wR2(reflections)= 0.1606(9184)
S =	1.054	Npar= 656

The following ALERTS were generated. Each ALERT has the format **test-name_ALERT_alert-type_alert-level**.

🟡 Alert level B

PLAT112_ALERT_2_B ADDSYM Detects Additional (Pseudo) Symm. Elem... A

NOTE: this has been inspected. The model is NOT in error; there are two PF6-anions located on special positions with half occupancy that lead to this flag.

● Alert level C

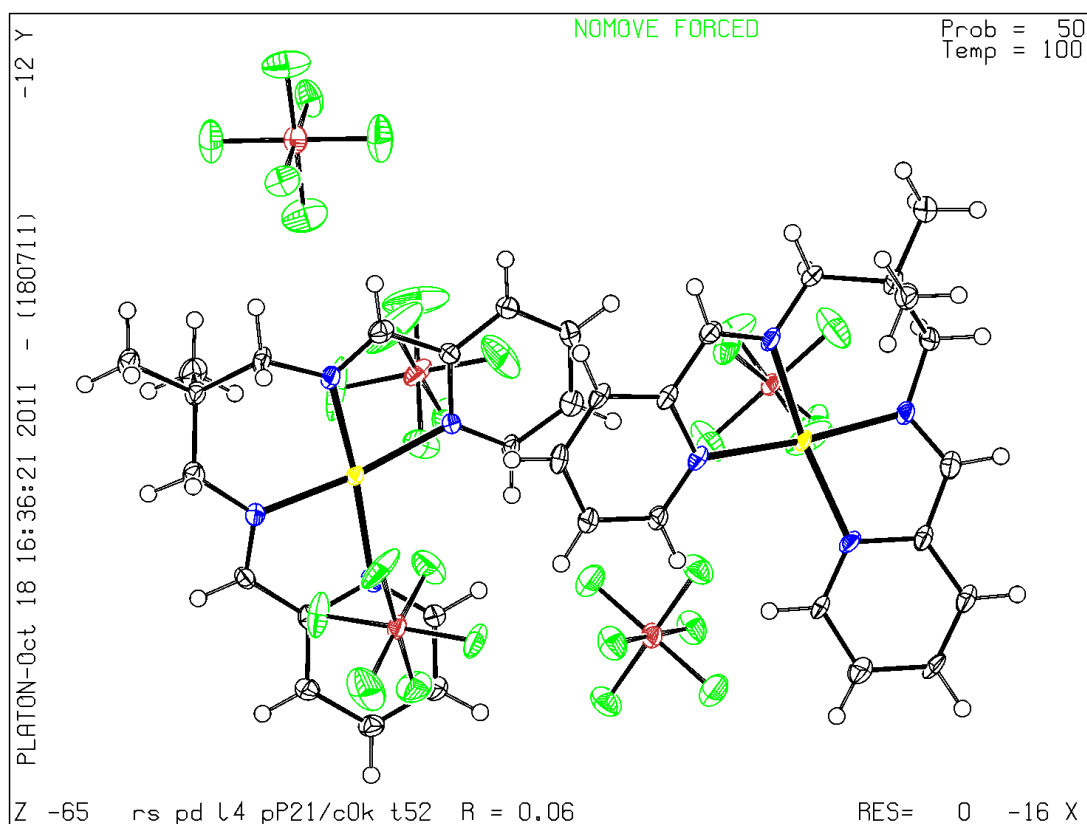
PLAT244_ALERT_4_C Low 'Solvent' Ueq as Compared to Neighbors of P1
 PLAT244_ALERT_4_C Low 'Solvent' Ueq as Compared to Neighbors of P2
 PLAT244_ALERT_4_C Low 'Solvent' Ueq as Compared to Neighbors of P3
 PLAT244_ALERT_4_C Low 'Solvent' Ueq as Compared to Neighbors of P4
 PLAT250_ALERT_2_C Large U3/U1 Ratio for Average U(i,j) Tensor 2.5
 PLAT250_ALERT_2_C Large U3/U1 Ratio for Average U(i,j) Tensor 2.7
 PLAT410_ALERT_2_C Short Intra H...H Contact H1A .. H15A .. 1.98 Ang.
 PLAT410_ALERT_2_C Short Intra H...H Contact H1B .. H15B .. 1.96 Ang.

● Alert level G

PLAT072_ALERT_2_G SHELXL First Parameter in WGHT Unusually Large. 0.11
 PLAT083_ALERT_2_G SHELXL Second Parameter in WGHT Unusually Large. 8.94
 PLAT153_ALERT_1_G Thes'u's on the Cell Axes are Equal 0.00500 Ang.
 PLAT432_ALERT_2_G Short Inter X...Y Contact F14 .. C6A .. 2.97 Ang.
 PLAT432_ALERT_2_G Short Inter X...Y Contact F19 .. C6B .. 2.93 Ang.
 PLAT432_ALERT_2_G Short Inter X...Y Contact F21 .. C1B .. 2.92 Ang.
 PLAT605_ALERT_4_G Structure Contains Solvent Accessible VOIDS of . 30 A**3
 PLAT720_ALERT_4_G Number of Unusual/Non-Standard Labels 8
 PLAT790_ALERT_4_G Centre of Gravity not Within Unit Cell: Resd. # 4 F6 P
 PLAT790_ALERT_4_G Centre of Gravity not Within Unit Cell: Resd. # 6 F6 P
 PLAT869_ALERT_4_G ALERTS Related to the use of SQUEEZE Suppressed !

PLATON version of 18/07/2011; check.def file version of 04/07/2011

Datablock rs_pd_I4 - ellipsoid plot



B7 – Crystallographic data tables for PdL4m

Table B7-1: Crystal data and structure refinement for **PdL4m**.

Identification code	rs_pd_l4m	
Empirical formula	C ₁₉ H ₂₄ F ₁₂ N ₄ P ₂ Pd	
Formula weight	704.76 amu	
Temperature	296(2) K	
Wavelength	0.71073 Å	
Crystal system	Monoclinic	
Space group	<i>P2₁/n</i>	
Unit cell dimensions	<i>a</i> = 8.262(5) Å	$\alpha = 90.000(5)^\circ$.
	<i>b</i> = 13.068(5) Å	$\beta = 98.914(5)^\circ$.
	<i>c</i> = 23.981(5) Å	$\gamma = 90.000(5)^\circ$.
Volume	2557.9(19) Å ³	
Z	4	
Density (calculated)	1.830 Mg/m ³	
Absorption coefficient	0.955 mm ⁻¹	
F(000)	1400	
Crystal size	0.55 x 0.45 x 0.35 mm ³	
Theta range for data collection	3.01 to 28.75°.	
Index ranges	-11 ≤ <i>h</i> ≤ 11	
	-17 ≤ <i>k</i> ≤ 16	
	-31 ≤ <i>l</i> ≤ 32	
Reflections collected	32956	
Independent reflections	6099 [<i>R</i> _{int} = 0.0555]	
Completeness to theta = 25.00°	99.8 %	
Max. and min. transmission	0.7309 and 0.6216	
Refinement method	Full-matrix least-squares on <i>F</i> ²	
Data / restraints / parameters	6099 / 0 / 347	
Goodness-of-fit on <i>F</i> ²	1.023	
Final <i>R</i> indices [<i>I</i> > 2 σ (<i>I</i>)]	<i>R</i> ₁ = 0.0477, <i>wR</i> ₂ = 0.1296	
<i>R</i> indices (all data)	<i>R</i> ₁ = 0.0614, <i>wR</i> ₂ = 0.1355	
Largest diff. peak and hole	0.791 and -0.747 e Å ⁻³	

Table B7-2: Atomic coordinates ($\times 10^4$) and equivalent isotropic displacement parameters ($\text{\AA}^2 \times 10^3$) for **PdL4m**. $U(\text{eq})$ is defined as one third of the trace of the orthogonalised U_{ij} tensor.

	x	y	z	U(eq)
C(1)	2894(7)	382(3)	-246(2)	60(1)
C(2)	3154(8)	161(4)	-783(2)	68(1)
C(3)	3223(7)	942(4)	-1156(2)	61(1)
C(4)	3020(6)	1912(3)	-985(2)	52(1)
C(5)	2783(5)	2115(3)	-439(2)	37(1)
C(6)	2689(5)	3146(3)	-206(2)	40(1)
C(7)	2654(6)	4044(4)	-579(2)	59(1)
C(8)	2686(6)	4182(3)	602(2)	47(1)
C(9)	3181(6)	4154(3)	1244(2)	46(1)
C(10)	3209(7)	5279(3)	1440(2)	63(1)
C(11)	2061(7)	-376(3)	1076(2)	65(1)
C(12)	1520(8)	-1163(4)	1386(2)	73(2)
C(13)	665(7)	-898(4)	1814(2)	64(1)
C(14)	417(6)	114(4)	1923(2)	57(1)
C(15)	1017(5)	855(3)	1598(2)	44(1)
C(16)	985(5)	1941(3)	1718(2)	46(1)
C(17)	206(8)	2325(5)	2201(2)	77(2)
C(18)	1888(6)	3622(3)	1528(2)	55(1)
C(19)	4867(6)	3681(4)	1412(2)	61(1)
N(1)	2726(4)	1335(2)	-61(1)	39(1)
N(2)	1799(4)	600(2)	1157(1)	43(1)
N(3)	1727(4)	2522(2)	1409(1)	41(1)
N(4)	2655(4)	3188(2)	328(1)	36(1)
F(1)	6332(5)	2048(3)	277(3)	161(3)
F(2)	6353(4)	3654(2)	64(2)	84(1)
F(3)	6784(6)	2452(6)	-526(2)	186(3)
F(4)	8840(6)	3445(4)	-167(3)	171(3)
F(5)	8867(4)	1829(2)	65(2)	119(2)
F(6)	8462(7)	3031(5)	652(2)	179(3)
F(7)	4565(7)	36(4)	2364(2)	143(2)
F(8)	4184(7)	1623(5)	2500(3)	166(2)
F(9)	6018(8)	1148(4)	1959(2)	150(2)
F(10)	6852(8)	1868(6)	2767(3)	212(4)
F(11)	7243(8)	222(7)	2588(4)	221(4)

Table B7-2: Continued.

	x	y	z	U(eq)
F(12)	5544(6)	670(7)	3181(2)	201(4)
P(1)	7619(1)	2747(1)	72(1)	55(1)
P(2)	5759(2)	934(1)	2575(1)	63(1)
Pd	2327(1)	1869(1)	714(1)	36(1)

Table B7-3: IUCR CIF check report for **PdL4m**.**IUCR CcheckCIF/PLATON (standard)**

No syntax errors found.

Datablock: rs-pdl4m

Bond precision:	C-C = 0.0066 A	Wavelength=0.71073
Cell:	a=8.262(5) b=13.068(5) c=23.981(5)	
	alpha=90 beta=98.914(5) gamma=90	
Temperature:	296 K	
	Calculated	Reported
Volume	2557.9(19)	2557.9(19)
Space group	P 21/n	P 21/n
Hall group	-P 2yn	?
Moiety formula	C19 H24 N4 Pd, 2(F6 P)	C19 H24 N4 Pd, 2(F6 P)
Sum formula	C19 H24 F12 N4 P2 Pd	C19 H24 F12 N4 P2 Pd
Mr	704.76	704.76
Dx,g cm-3	1.830	1.830
Z	4	4
Mu (mm-1)	0.955	0.955
F000	1400.0	1400.0
F000'	1397.81	
h,k,lmax	11,17,32	11,17,32
Nref	6622	6099
Tmin,Tmax	0.603,0.716	0.622,0.731
Tmin'	0.586	
Correction method=	MULTI-SCAN	
Data completeness=	0.921	Theta(max)= 28.750
R(reflections)=	0.0477(4845)	wR2(reflections)= 0.1355(6099)
S =	1.023	Npar= 347

The following ALERTS were generated. Each ALERT has the format

test-name_ALERT_alert-type_alert-level.**● Alert level C**

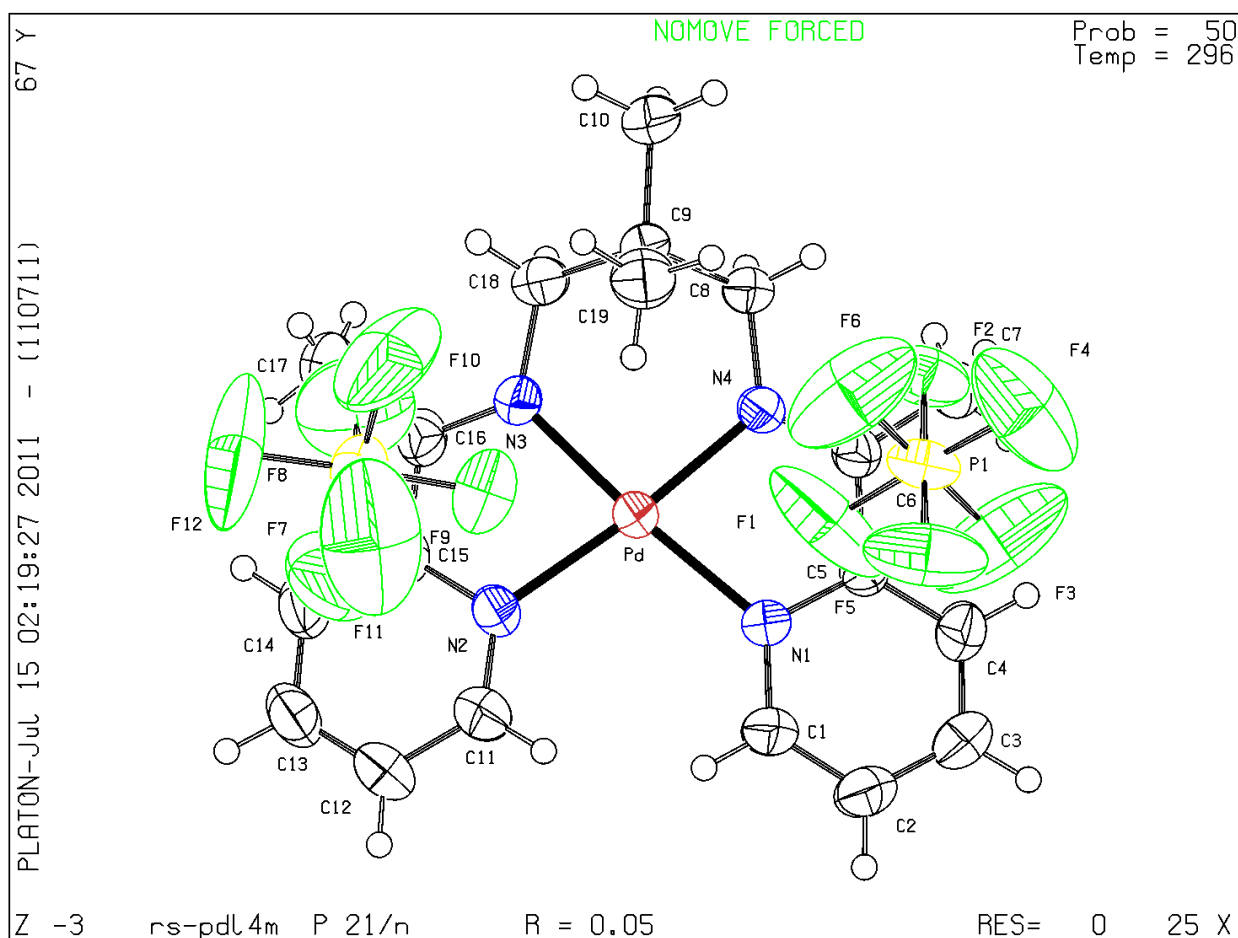
PLAT244_ALERT_4_C Low 'Solvent' Ueq as Compared to Neighbors of P1
 PLAT244_ALERT_4_C Low 'Solvent' Ueq as Compared to Neighbors of P2
 PLAT250_ALERT_2_C Large U3/U1 Ratio for Average U(i,j) Tensor 3.0
 PLAT410_ALERT_2_C Short Intra H...H Contact H1 .. H11 .. 1.98 Ang.

● Alert level G

PLAT005_ALERT_5_G No _iucr_refine_instructions_details in CIF ?
 PLAT128_ALERT_4_G Alternate Setting of Space-group P21/c P21/n
 PLAT153_ALERT_1_G The su's on the Cell Axes are Equal 0.00500 Ang.
 PLAT710_ALERT_4_G Delete 1-2-3 or 2-3-4 Linear Torsion Angle ... # 51
 PLAT710_ALERT_4_G Delete 1-2-3 or 2-3-4 Linear Torsion Angle ... # 52
 PLAT710_ALERT_4_G Delete 1-2-3 or 2-3-4 Linear Torsion Angle ... # 59
 PLAT710_ALERT_4_G Delete 1-2-3 or 2-3-4 Linear Torsion Angle ... # 60
 PLAT710_ALERT_4_G Delete 1-2-3 or 2-3-4 Linear Torsion Angle ... # 61
 PLAT710_ALERT_4_G Delete 1-2-3 or 2-3-4 Linear Torsion Angle ... # 62
 PLAT710_ALERT_4_G Delete 1-2-3 or 2-3-4 Linear Torsion Angle ... # 69
 PLAT710_ALERT_4_G Delete 1-2-3 or 2-3-4 Linear Torsion Angle ... # 70

PLATON version of 11/07/2011; check.def file version of 04/07/2011

Datablock rs-pdl4m - ellipsoid plot



B8 – Crystallographic data tables for PdL4b

Table B8-1: Crystal data and structure refinement for PdL4b.

Identification code	rs_pdl4b	
Empirical formula	C ₂₉ H ₃₆ F ₁₂ N ₄ P ₂ Pd	
Formula weight	828.89 amu	
Temperature	100(2) K	
Wavelength	0.71073 Å	
Crystal system	Monoclinic	
Space group	<i>P</i> 2 ₁ / <i>c</i>	
Unit cell dimensions	<i>a</i> = 18.294(4) Å	$\alpha = 90.000(5)^\circ$.
	<i>b</i> = 10.329(2) Å	$\beta = 97.109(3)^\circ$.
	<i>c</i> = 17.997(4) Å	$\gamma = 90.000(5)^\circ$.
Volume	3374.6(12) Å ³	
Z	4	
Density (calculated)	1.631 Mg/m ³	
Absorption coefficient	0.739 mm ⁻¹	
F(000)	1656	
Crystal size	0.1 x 0.1 x 0.1 mm ³	
Theta range for data collection	2.24 to 28.91°.	
Index ranges	-24 ≤ <i>h</i> ≤ 20	
	-13 ≤ <i>k</i> ≤ 13	
	-24 ≤ <i>l</i> ≤ 22	
Reflections collected	21245	
Independent reflections	8098 [<i>R</i> _{int} = 0.1028]	
Completeness to theta = 25.00°	99.5 %	
Refinement method	Full-matrix least-squares on <i>F</i> ²	
Data / restraints / parameters	8098 / 0 / 434	
Goodness-of-fit on <i>F</i> ²	0.994	
Final <i>R</i> indices [<i>I</i> > 2 σ (<i>I</i>)]	<i>R</i> ₁ = 0.0415, <i>wR</i> ₂ = 0.0997	
<i>R</i> indices (all data)	<i>R</i> ₁ = 0.0490, <i>wR</i> ₂ = 0.1029	
Largest diff. peak and hole	0.851 and -0.860 e Å ⁻³	

Table B8-2: Atomic coordinates ($\times 10^4$) and equivalent isotropic displacement parameters ($\text{\AA}^2 \times 10^3$) for **PdL4b**. $U(\text{eq})$ is defined as one third of the trace of the orthogonalised U_{ij} tensor.

	x	y	z	U(eq)
F(3)	-413(2)	2318(3)	1093(2)	25(1)
F(1)	429(2)	1210(4)	1880(2)	32(1)
F(6)	509(2)	3227(4)	534(2)	30(1)
F(2)	424(2)	1045(3)	623(2)	31(1)
F(4)	1351(2)	2123(4)	1321(2)	34(1)
F(5)	504(2)	3396(4)	1791(2)	33(1)
F(10)	3875(2)	-2000(5)	1828(3)	45(1)
F(8)	2782(2)	-2455(4)	2203(2)	40(1)
F(7)	3214(3)	-423(4)	2317(3)	52(1)
F(11)	3345(3)	-414(4)	1069(3)	54(1)
F(12)	2904(3)	-2452(4)	972(3)	49(1)
F(9)	2249(3)	-902(5)	1462(3)	58(1)
C(20)	1763(3)	5219(5)	2304(3)	19(1)
C(19)	1750(3)	5108(6)	3127(3)	21(1)
C(16)	3788(3)	4789(6)	1864(4)	31(1)
C(13)	3275(3)	2779(5)	1172(3)	23(1)
C(17)	2706(3)	3596(5)	2295(3)	22(1)
C(14)	3419(3)	3472(5)	1933(3)	23(1)
C(18)	1462(3)	4002(6)	3425(3)	23(1)
C(15)	3934(3)	2585(6)	2437(3)	29(1)
C(25)	1288(3)	6168(5)	1867(3)	19(1)
C(29)	983(3)	7045(5)	673(3)	21(1)
C(22)	2026(3)	5996(6)	4370(3)	26(1)
C(23)	1728(3)	4886(7)	4664(3)	28(1)
C(21)	2024(3)	6105(6)	3599(3)	24(1)
C(28)	550(3)	7981(6)	958(3)	23(1)
C(26)	856(3)	7049(6)	2171(3)	22(1)
C(24)	1439(3)	3901(6)	4190(3)	26(1)
C(27)	473(3)	7976(6)	1711(3)	24(1)
Pd(1)	2015(1)	4716(1)	817(1)	16(1)
P(2)	472(1)	2210(1)	1206(1)	19(1)
P(3)	3067(1)	-1433(2)	1643(1)	28(1)
N(2)	2187(3)	4541(4)	1934(2)	19(1)
N(4)	1831(2)	4701(4)	-322(2)	17(1)

Table B8-2: Continued.

	x	y	z	U(eq)
N(3)	2818(2)	3519(4)	591(3)	20(1)
N(1)	1336(2)	6130(4)	1115(2)	18(1)
C(6)	2960(3)	3530(5)	-95(3)	18(1)
C(7)	3604(3)	2870(5)	-352(3)	21(1)
C(2)	1193(3)	5012(6)	-1544(3)	24(1)
C(5)	2399(3)	4176(5)	-635(3)	17(1)
C(4)	2404(3)	4135(5)	-1399(3)	23(1)
C(3)	1793(3)	4576(6)	-1867(3)	25(1)
C(1)	1230(3)	5081(5)	-767(3)	21(1)
C(12)	3639(3)	1525(6)	-358(4)	32(1)
C(9)	4814(4)	2985(9)	-729(4)	41(2)
C(8)	4201(4)	3607(7)	-538(4)	33(1)
C(10)	4857(3)	1643(8)	-731(4)	40(2)
C(11)	4280(4)	941(7)	-546(4)	40(2)

Table B8-3: IUCR CIF check report for **PdL4b**.**IUCR CcheckCIF/PLATON (standard)**

No syntax errors found.

Datablock: rs-pdl4b

Bond precision:	C-C = 0.0041 Å	Wavelength=0.71073
Cell:	a=18.294(4) b=10.329(2) c=17.997(4)	
	alpha=90 beta=97.109(3) gamma=90	
Temperature:	100 K	
	Calculated	Reported
Volume	3374.6(12)	3374.6(12)
Space group	P 21/c	P 21/c
Hall group	-P 2ybc	-P 2ybc
Moiety formula	C ₂₉ H ₂₈ N ₄ Pd, 2(F6 P)	C ₂₉ H ₂₈ N ₄ Pd, 2(F6 P)
Sum formula	C ₂₉ H ₂₈ F ₁₂ N ₄ P ₂ Pd	C ₂₉ H ₂₈ F ₁₂ N ₄ P ₂ Pd
Mr	828.89	828.89
Dx,g cm ⁻³	1.632	1.631
Z	4	4
Mu (mm ⁻¹)	0.738	0.738
F000	1656.0	1656.0
F000'	1653.91	
h,k,lmax	24,14,24	24,13,24
Nref	8892	8098
Tmin,Tmax	0.929,0.929	
Tmin'	0.929	
Correction method=	Not given	
Data completeness=	0.911 Theta(max)= 28.910	
R(reflections)= 0.0415(6725)	wR2(reflections)= 0.1029(8098)	
S = 0.994	Npar= 434	

The following ALERTS were generated. Each ALERT has the format

test-name_ALERT_alert-type_alert-level.

● Alert level C

PLAT244_ALERT_4_C Low 'Solvent' Ueq as Compared to Neighbors of P3

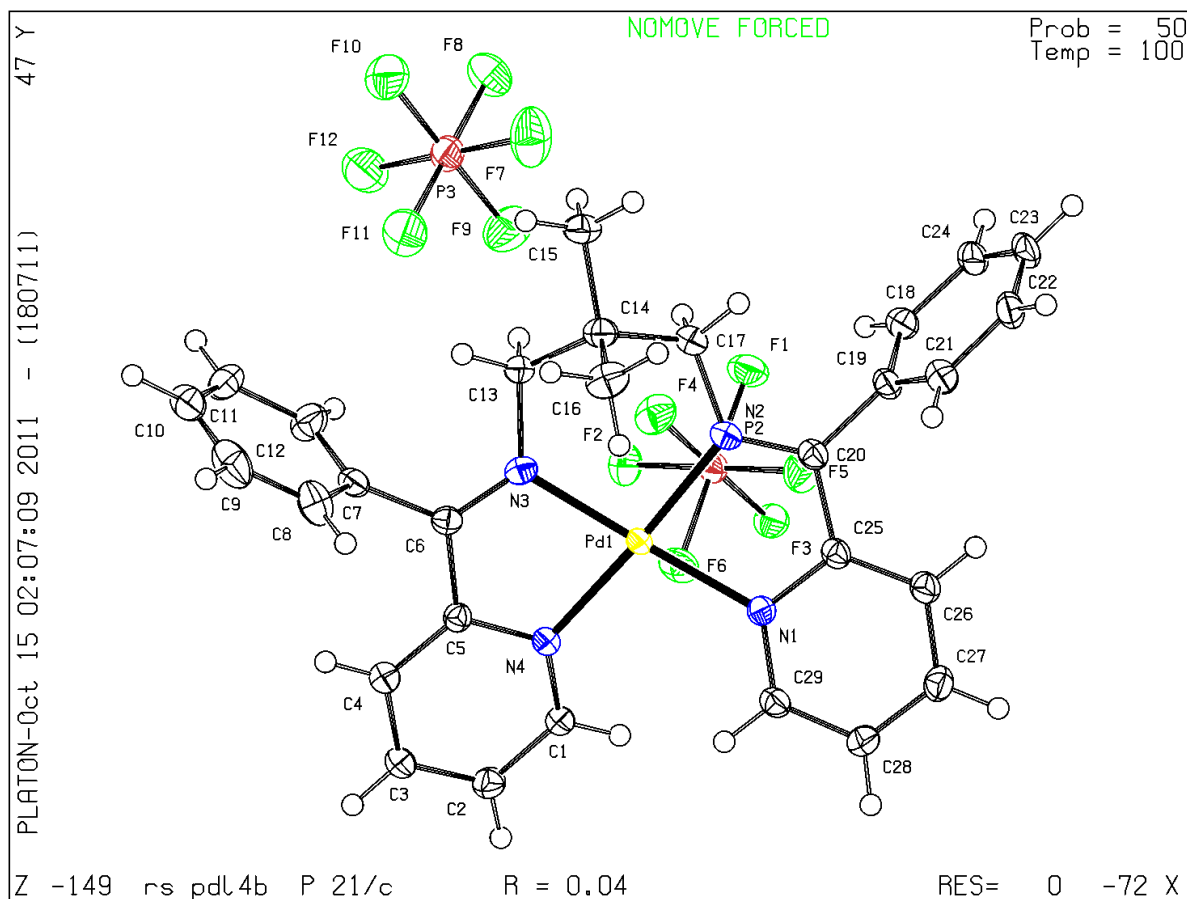
● Alert level G

PLAT605_ALERT_4_G Structure Contains Solvent Accessible VOIDS of 90 Å³

PLAT790_ALERT_4_G Centre of Gravity not Within Unit Cell: Resd. # 3 F6 P
 PLAT869_ALERT_4_G ALERTS Related to the use of SQUEEZE Suppressed !

PLATON version of 18/07/2011; check.def file version of 04/07/2011

Datablock rs_pdl4b - ellipsoid plot



APPENDIX C

C1 – Conversions

Energy conversions:

All DFT-calculated energies are given in Hartrees in the computational output data files. They are then converted to electron volts (eV) by convention.

1 Hartree = 27.211 eV

C2 – Data for the metal complexes computed by DFT

Table C2-1: Distance (Å) that the central pyridine hydrogen atoms (C_a) are distorted from the N_4 plane.

Table C2-2: The MO energies (eV) for each of the orbitals for each complex: LUMO+1, LUMO, HOMO and HOMO-1.

Table C2-1: Distance (Å) that the central pyridine hydrogen atoms (C_a) are distorted from the N_4 plane.

	DFT predictions	X-ray computed
PtL1	-0.093, +0.093	-0.012, +0.012
PdL1	-0.109, +0.109	-0.004, +0.004
PtL2	-0.370, +0.379	-0.049, +0.037
PdL2	-0.387, +0.346	-0.086, +0.061
PtL4	+0.285, -0.348	+0.231, -0.374
PdL4	+0.306, -0.362	+0.236, -0.366
PdL4m	+0.515, -0.457	+0.239, +0.067
PdL4b	-0.496, +0.454	-0.521, +0.414

Table C2-2: The MO energies (eV) for each of the orbitals for each complex: LUMO+1, LUMO, HOMO and HOMO-1.

	PtL1	PtL2	PtL3	PtL4	PtL5	PtL6
LUMO+1	-9.306	-9.224	-9.116	-9.143	-9.061	-9.660
LUMO	-9.959	-9.823	-9.714	-9.714	-9.687	-9.714
HOMO	-13.877	-13.741	-13.578	-13.687	-13.605	-13.116
HOMO-1	-14.014	-13.877	-13.660	-13.741	-13.741	-13.469
	PdL1	PdL2	PdL3	PdL4	PdL5	PdL6
LUMO+1	-9.333	-9.252	-9.143	-9.170	-9.061	-9.578
LUMO	-9.877	-9.741	-9.578	-9.605	-9.605	-9.741
HOMO	-14.122	-13.986	-13.796	-13.905	-13.823	-13.116
HOMO-1	-14.177	-14.068	-13.877	-13.932	-13.877	-13.469
	PtL1m	PtL2m	PtL3m	PtL4m	PtL5m	PtL6m
LUMO+1	-8.871	-8.816	-8.871	-8.735	-8.680	-9.279
LUMO	-9.497	-9.415	-9.497	-9.279	-9.279	-9.306
HOMO	-13.497	-13.388	-13.442	-13.360	-13.279	-12.789
HOMO-1	-13.633	-13.497	-13.524	-13.388	-13.388	-13.224
	PdL1m	PdL2m	PdL3m	PdL4m	PdL5m	PdL6m
LUMO+1	-8.871	-8.843	-8.898	-8.735	-8.680	-9.279
LUMO	-9.497	-9.306	-9.388	-9.279	-9.279	-9.306
HOMO	-13.497	-13.660	-13.551	-13.360	-13.279	-12.789
HOMO-1	-13.633	-13.687	-13.714	-13.388	-13.388	-13.224
	PtL1b	PtL2b	PtL3b	PtL4b	PtL5b	PtL6b
LUMO+1	-8.435	-8.435	-8.463	-8.381	-8.326	-8.952
LUMO	-9.088	-9.034	-9.088	-8.925	-8.952	-8.952
HOMO	-12.354	-12.245	-12.245	-12.218	-12.218	-12.163
HOMO-1	-12.381	-12.272	-12.272	-12.245	-12.245	-12.218
	PdL1b	PdL2b	PdL3b	PdL4b	PdL5b	PdL6b
LUMO+1	-8.463	-8.463	-8.490	-8.408	-8.354	-8.843
LUMO	-9.007	-8.925	-8.980	-8.816	-8.871	-8.980
HOMO	-12.381	-12.245	-12.245	-12.245	-12.245	-12.218
HOMO-1	-12.381	-12.272	-12.272	-12.245	-12.272	-12.218

APPENDIX D

D1 – Absorption spectra of metal complexes with subsequent CT-DNA additions

Figure D1-1: The absorption spectra for **PtL4** (—) in a phosphate buffer (pH = 7.1) at 298 K with subsequent CT-DNA additions; from 270 to 400 nm.

Figure D1-2: The absorption spectra for **PdL4** (—) in a phosphate buffer (pH = 7.1) at 298 K with subsequent CT-DNA additions; from 270 to 340 nm.

Figure D1-3: The absorption spectra for **PdL4m** (—) in a phosphate buffer (pH = 7.1) at 298 K with subsequent CT-DNA additions; from 280 to 325 nm.

D2 – Plots of $(\epsilon_a - \epsilon_f)/(\epsilon_b - \epsilon_f)$ against [DNA base pairs] for the metal complexes

Figure D2-1: The non-linear fit for the plot of $(\epsilon_a - \epsilon_f)/(\epsilon_b - \epsilon_f)$ against [DNA base pairs] for the titration of **PtL4** with CT-DNA.

Figure D2-2: The non-linear fit for the plot of $(\epsilon_a - \epsilon_f)/(\epsilon_b - \epsilon_f)$ against [DNA base pairs] for the titration of **PdL4** with CT-DNA.

Figure D2-3: The non-linear fit for the plot of $(\epsilon_a - \epsilon_f)/(\epsilon_b - \epsilon_f)$ against [DNA base pairs] for the titration of **PdL4m** with CT-DNA.

Figure D2-4: The non-linear fit for the plot of $(\epsilon_a - \epsilon_f)/(\epsilon_b - \epsilon_f)$ against [DNA base pairs] for the titration of **PdL4b** with CT-DNA.

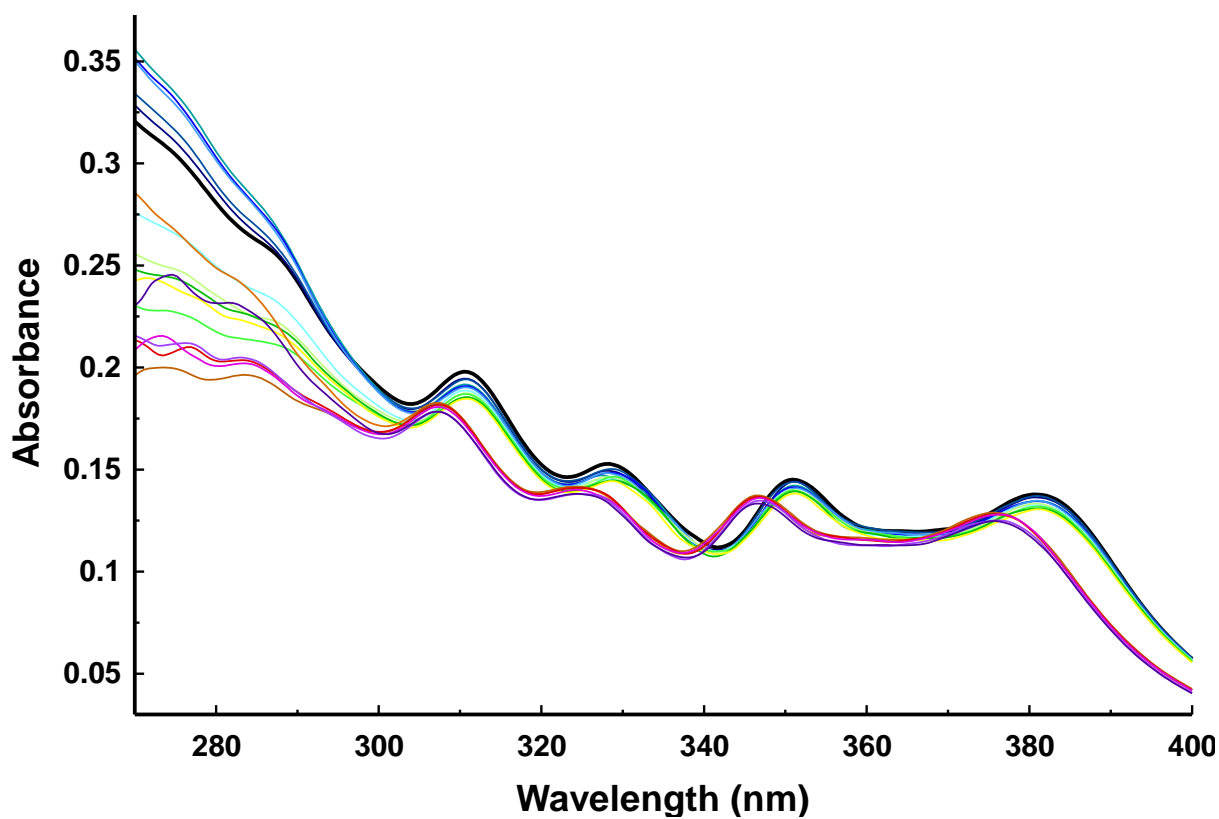


Figure D1-1: The absorption spectra for PtL4 (—) in a phosphate buffer (pH = 7.1) at 298 K with subsequent CT-DNA additions; from 270 to 400 nm.

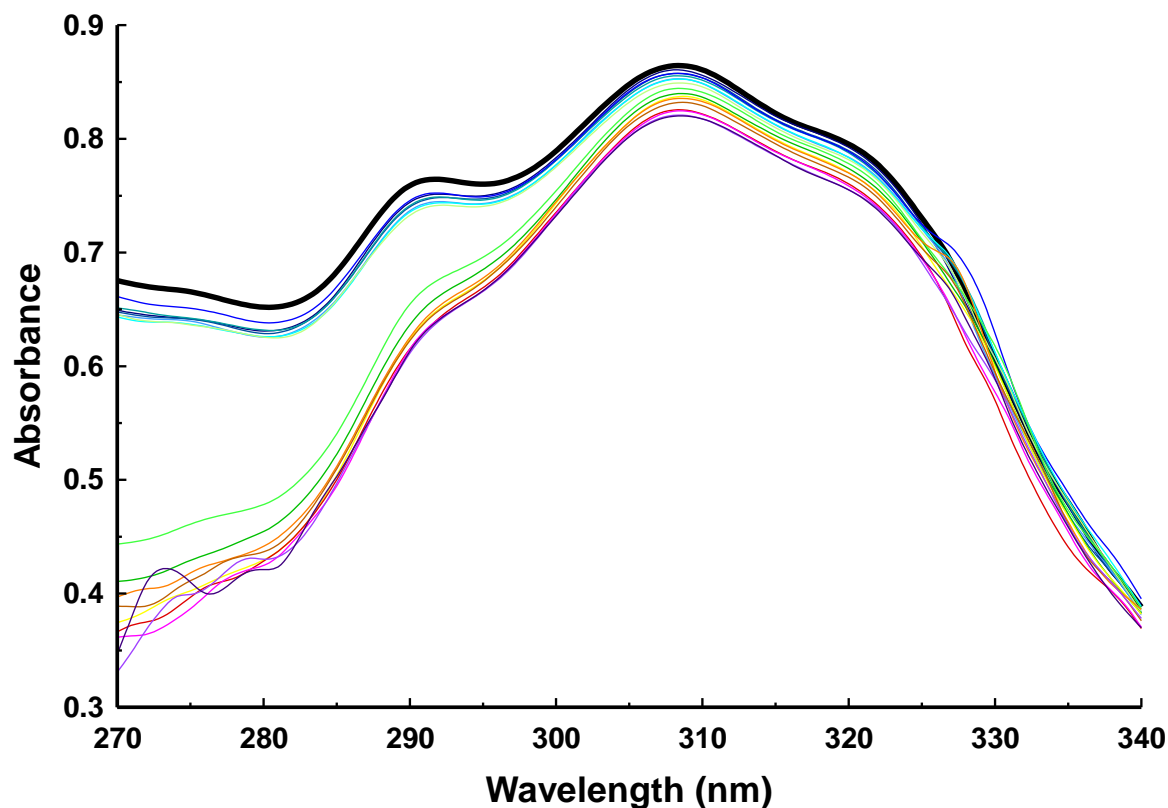


Figure D1-2: The absorption spectra for PdL4 (—) in a phosphate buffer (pH = 7.1) at 298 K with subsequent CT-DNA additions; from 270 to 340 nm.

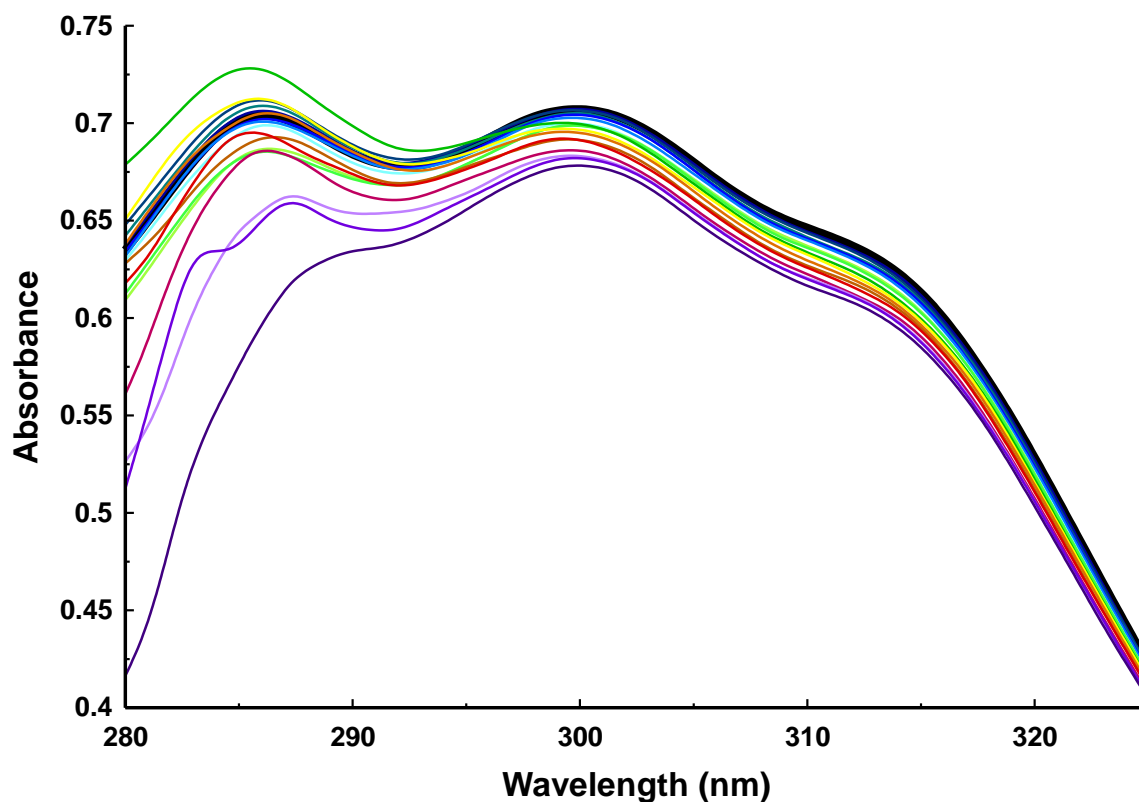


Figure D1-3: The absorption spectra for **PdL4m** (—) in a phosphate buffer (pH = 7.1) at 298 K with subsequent CT-DNA additions; from 280 to 325 nm.

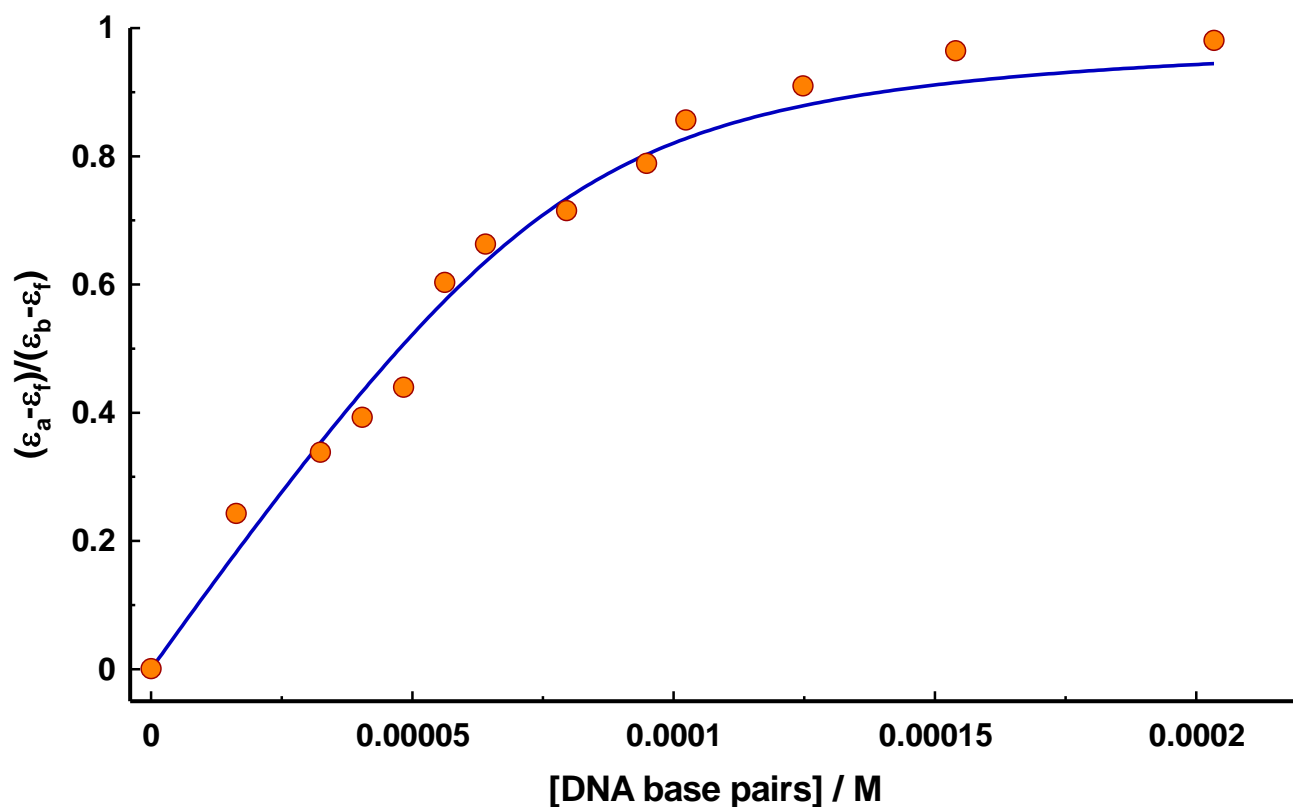


Figure D2-1: The non-linear fit for the plot of $(\epsilon_a - \epsilon_f) / (\epsilon_b - \epsilon_f)$ against [DNA base pairs] for the titration of PtL4 with CT-DNA.

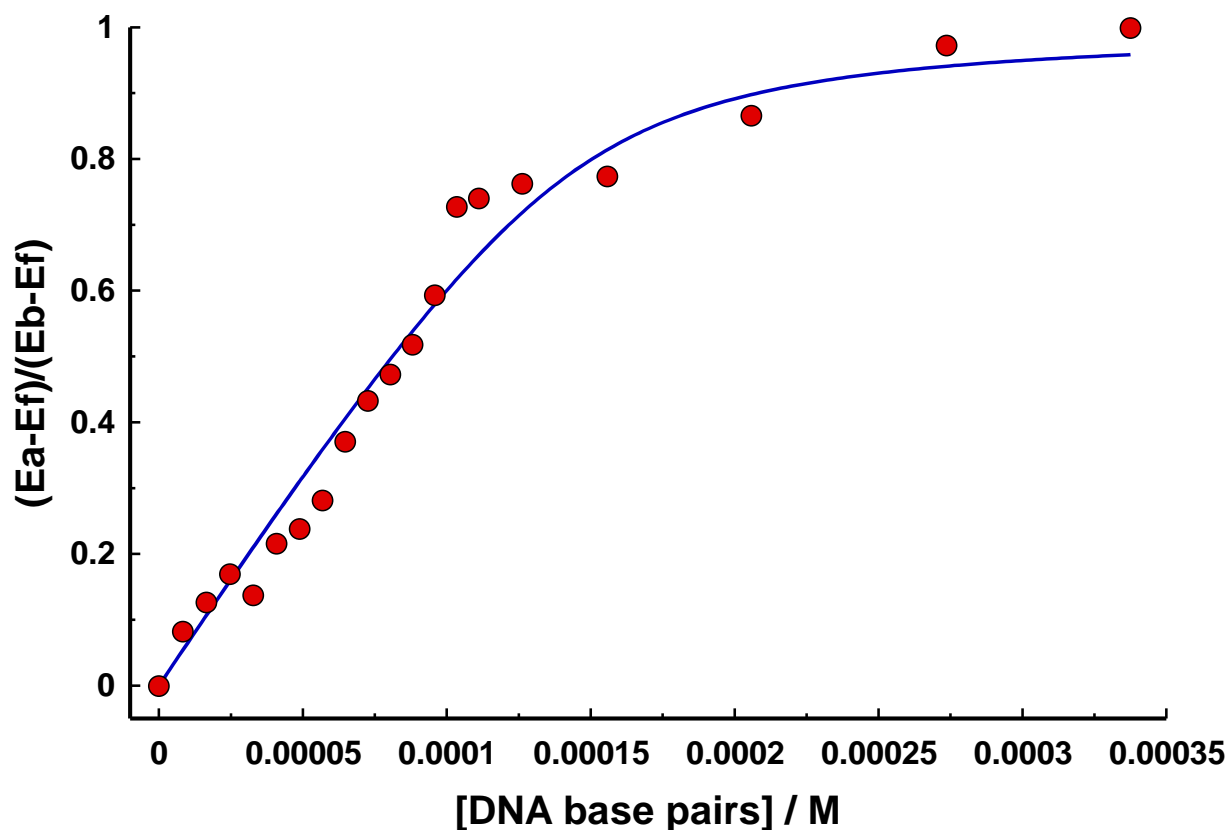


Figure D2-2: The non-linear fit for the plot of $(\epsilon_a - \epsilon_f) / (\epsilon_b - \epsilon_f)$ against [DNA base pairs] for the titration of PdL4 with CT-DNA.

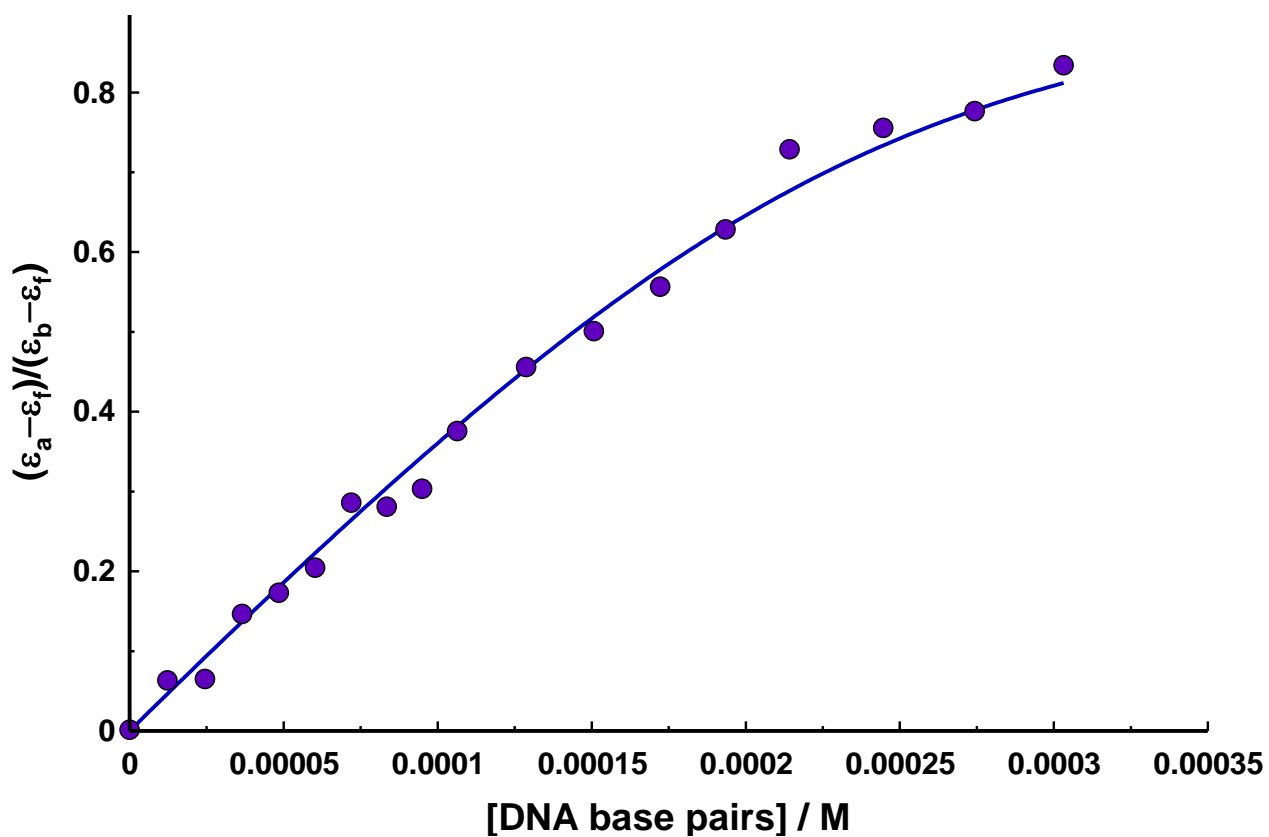


Figure D2-3: The non-linear fit for the plot of $(\epsilon_a - \epsilon_f) / (\epsilon_b - \epsilon_f)$ against [DNA base pairs] for the titration of PdL4m with CT-DNA.

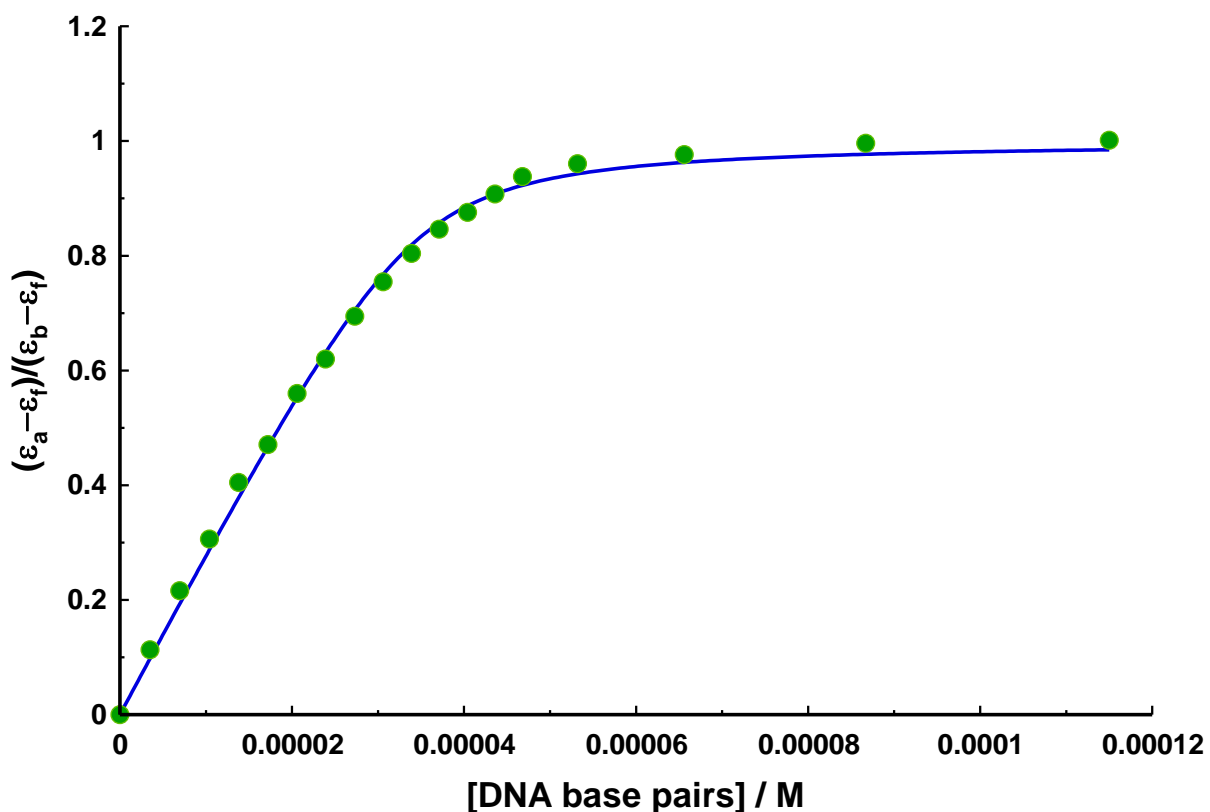


Figure D2-4: The non-linear fit for the plot of $(\epsilon_a - \epsilon_f) / (\epsilon_b - \epsilon_f)$ against [DNA base pairs] for the titration of PdL4b with CT-DNA.